DEVELOPMENT OF SELECTIVE RIBOSOME P-SITE INHIBITORS AND THEIR APPLICATIONS AS NEW ANTITUBERCULAR AGENTS AND EFFORTS TOWARD DEVELOPMENT OF FIRST-IN-CLASS ANTIBIOFILM ANTIBACTERIAL AGENTS

by

Hariprasada Reddy Kanna Reddy

A dissertation submitted to the faculty of
The University of Utah
in partial fulfillment of the requirements for the degree of

Doctor of Philosophy

Department of Chemistry

The University of Utah

December 2017

The University of Utah Graduate School

STATEMENT OF DISSERTATION APPROVAL

The dissertation of **Hariprasada Reddy Kanna Reddy**

has been approved by the following supervisory committee members:

Ryan E. Looper	, Chair	**03.22.2017** Date Approved
Jon D. Rainier	, Member	**03.22.2017** Date Approved
Janis Louie	, Member	**03.22.2017** Date Approved
Peter F. Flynn	, Member	**03.22.2017** Date Approved
David P. Goldenberg	, Member	**03.27.2017** Date Approved

and by **Cynthia J. Burrows**, Chair/Dean of

the Department/College/School of **Chemistry**

and by David B. Kieda, Dean of The Graduate School.

ABSTRACT

The fight against tuberculosis (TB), has been further complicated by both the emergence of multidrug resistant strains of the organism, along with its coinfection with Human Immunodeficiency Virus (HIV). Since current TB regimens reduce the efficacy of highly active antiretroviral therapies (HAART) by cytochrome induction, TB and HIV cannot be treated simultaneously. With mortality rates of TB–HIV coinfected people rising globally, the scientific community has seen renewed vigor in the search for a novel, noncytochrome inducing antitubercular, agent. In a screen conducted at the University of Utah, the natural product amicetin was identified as a potential scaffold with antitubercular activity, noncytotoxicity, and compatibility with HAART.

The first generation of analogs aimed to simultaneously reduce the complexity involved in the synthesis of the disaccharide moiety and replace the acid labile glycosidic linkage. It was shown with analog **CZ–02–023** that despite the removal of eight stereocenters from amicetin, potency (IC_{50} of 0.98 μM against *Mtb*) and on–target selectivity ($SI_{RR/E.coli}$ =111) could be retained.

The crystal structure of Ami bound to the Peptidyl Transferase Center (PTC) of the *T. thermophiles* 70S ribosome elucidated amicetin's important binding interactions, includes a cation–π interaction of its terminal aminosugar with A2450 and a Watson–Crick base pair between its cytosine portion and G2262.

Additionally, hydrogen bonding of amicetin's α–methylserine moiety with the phosphate backbone of G2506 and π– π stacking with the *p*–aminobenzoyl moiety with A2613 were observed. Not only did this data demonstrate amicetin's binding to the therapeutically unexploited PTC, it served to guide intelligent SAR development which led to the synthesis of **CZ–02033** and **CZ–02039** with broad spectrum activity and faded on–target selectivity ($SI_{RR/E.coli}$ < 3).

The loss of on–target selectivity prompted further modifications to the Cytosine–PABA region in a series of third generation analogs based on the knowledge of the crystal structure of the Ami–70S–tRNA ternary complex. The third generation piperazinyl urea analogs including **CZ–02–117**, **CZ–02118**, and **CZ–02–132** increased selectivity ($SI_{RR/E.coli}$ >400). Efforts continue to further the development of amicetin–based broad–spectrum antibiotics.

To my loving parents and my beautiful, caring wife, who has been a constant source of support and encouragement during the challenges of graduate school and life.

TABLE OF CONTENTS

Appendices

LIST OF FIGURES

LIST OF TABLES

LIST OF ABBREVIATIONS

A	adenine
α	alpha
Ac	acetyl
$[\alpha]^{20}_{D}$	specific rotation at wavelength of sodium D line
A_{570}	absorbance at 570 nm
A site	aminoacyl site
AIDS	acquired immune deficiency syndrome
AMK	amikacin
Ar	aryl
ATP	adenosine triphosphate
AZ	Astra Zeneca
β	beta
BCG	Bacille Calmette-Guérin
BIKAKEN	Institute of Microbial Chemistry, Japan
Bn	benzyl
BnOH	benzyl alcohol
Boc	tert-butyloxycarbonyl
2,2'-bipy	2,2'-bipyridine
Bs/brs	broad singlet

^{t}Bu	tert-Butyl
c	concentration for specific rotation measurements
C	cytosine
°C	degrees Celsius
CAMPs	cationic antimicrobial peptides
Cbz	carbobenzyloxy
CDC	Center for Disease Control
CD4	cluster of differentiation antigen 4
CD_{50}	half maximal cytotoxic dose
CM	capreomycin
CFX	ciprofloxacin
CYP	cytochrome p450
CYP2C9	cytochrome p450 isoform 2C9
CYP34A	cytochrome p450 isoform 34A
d	doublet
DCS	D-cycloserine
dd	doublet of doublet
DEPT	Distortionless Enhancement by Polarization Transfer
ddd	doublet of double of doublet
dq	doublet of quartet
DMAP	4-dimethylaminopyridine
dmeda	*N,N'*-dimethylethylenediamine
DMF	*N,N*-dimethylformamide

DMSO	dimethyl sulfoxide
DNA	deoxyribonucleic acid
EC_{50}	50% effective concentration
EMA	European Medicines Association
EMB	ethambutol
equiv	equivalent
ESI	electrospray ionization
Et_3N	trietheylamine
Et_2O	diethylether
ETO	ethionamide
EtOAc	ethyl acetate
EtOH	ethanol
FDA	Food and Drug Administration
G	guanine
g	gram(s)
GSK	Glaxo-Smith-Kline
hr(s)	hour(s)
HAART	highly active antiretroviral therapy
HIV	human immunodeficiency virus
Hm	*Haloarcula marismortuii*
hq	8-hydroxyquinoline;
HRMS	high-resolution mass spectroscopy
Hz	hertz

IC_{50}	half maximal inhibitory concentration
IDRI	Infectious Disease Research Institute
iM4TB	Innovative Medicines for TB
IMM	Institute of Materia Medica
INH	isoniazid
IR	infrared spectroscopy
J	coupling constant
KB	β-keratin
KM	kanamycin
KM-R	kanamycin resistant
L	liter
LD_{50}	half maximal lethal dosage
Leu	leucine
LHMDS	lithium hexamethyldisilazide
LTBI	latent TB infection
LXF	levofloxacin
m	multiplet or milli
μ	micro
M	molar
Me	methyl
MeI	methyl iodide
MEC	minimum effective concentration
MHz	megahertz

MDR-TB	multidrug resistant TB
MIC	minimum inhibitory concentration
min	minute(s)
mol	mole(s)
mp	melting point
Mtb	*Mycobacterium tuberculosis*
m/z	mass to charge ratio
n	nano
NBS	*N*-bromosuccinimide
NBSH	2-Nitrobenzenesulfonylhydrazide
NIAID	National Institute for Infectious Diseases and Allergy
NM-R	neomycin resistant
NMM	*N*-methylmorpholine
NMR	nuclear magnetic resonance
NNRTI	non-nucleotide reverse transcriptase inhibitors
NRTI	nucleoside reverse transcriptase inhibitors
NtRTI	nucleotide reverse transcriptase inhibitors
OD_{600}	optical density at 600 nm
OBz	benzoate
p	para
PAS	*p*-aminosalicylic acid
PC-R	penicillin G resistant
$Pd_2(dba)_3$	Tris(dibenzylideneacetone)dipalladium

P-gp	P-glycoprotein
Ph	phenyl
pH	hydrogen ion concentration in aqueous solution
Phe	phenylalanine
phen	phenanthroline
PhH	benzene
PI	protease inhibitor
PPh_3	triphenyl phospine
ppm	parts per million
p-site	peptidyl site
PTC	peptidyl transeferace center
pyr	pyridine
PZA	pyrazinamide
q	quartet
RMP	rifampicin
RNA	ribonucleic acid
rt	room temperature
Rf	retention factor
RF1	release factor 1
RF2	release factor 2
RNS	reactive nitrogen species
S	Svedberg, sedimentation unit
s	singlet or strong

S. cer.	Saccharomyces cerevisiae
SAR	structure activity relationship
smFRET	single-molecule Förster resonance energy transfer
SM-R	streptomycin resistant
STAND	Shortening Treatments by Advancing Novel Drugs
STM	Streptomycin
t	triplet
TB	tuberculosis
TDR-TB	totally drug-resistant TB
THF	tetrahydrofuran
TMS	trimethylsilyl
THZ	thioacetanone
TNF	tumor necrosis factor
TRD	terizidone
tRNA	transfer RNA
Tth	*Thermus thermophilus*
UIC	University of Illinois, Chicago
UV	ultraviolet
VIM	viomycin
WHO	World Health Organization
XDR-TB	extensively drug-resistant TB
XXDR-TB	extremely drug-resistant TB

CHAPTER 1

INTRODUCTION

Tuberculosis: Cause and Spread

Tuberculosis (TB) is an infectious disease caused by the bacterial pathogen *Mycobacterium tuberculosis* (*Mtb*) and is the leading cause of death among any single infectious pathogen. TB has been known by many aliases throughout history such as Consumption, Phthisis, Scrofula, Pott's disease, and the White Plague.[1, 2, 3] It is also called Koch's disease, which is named after the German scientist Robert Koch who in 1882 first discovered *Mtb* as the etiologic agent.[4, 5] There are three major types of tubercle bacilli that are capable of causing TB: *Mycobacterium tuberculosis*, the most common bacilli which affects humans and is simultaneously spread by humans; *Mycobacterium bovis*, which is spread by infected cattle and has the potential to affect humans as well as other mammals; *Mycobacterium avium–intracellualare* complex (MAC), which is transmitted through infected birds, which can cause infections in birds, pigs, and especially in immunocompromised individuals such as HIV patients.[6] In general, TB is an airborne disease, transmitted from person to person by inhalation of respiratory droplets (coughs or sneezes) of an active TB infected (TB disease) individual. The infection primarily targets the lungs (pulmonary TB); when the air droplets containing *Mtb* bacteria are inhaled, they harbor in the alveoli. The *Mtb* bacteria from lungs can spread

through the blood stream to other organs of the body, including the kidney, spine, brain, lymphatic, and nervous systems (extrapulmonary TB). With the apparent ease of transmission, it is assessed that nearly one-third of the world's population harbors the asymptomatic latent or dormant form of TB.[7, 8, 9, 10, 11]

Not all individuals who are exposed to *Mtb* bacteria become symptomatic, and are able to transmit the disease to others; however, exposure to *Mtb* leads to two–TB related conditions; a) latent TB infection, and b) TB disease.[12]

Latent TB Infection

Latent tuberculosis infection (LTBI) is a condition in which a person's immune system defends the body against the attack by *Mtb* bacteria and takes control over the bacteria to prevent them from developing into the active disease. In the latent infection, an individual is already exposed to bacteria, but it can remain dormant for years by forming a thick waxy coat on its cell wall. Individuals with latent TB infection are asymptomatic, cannot transmit TB to others, and do not fall ill. However, they show positive skin tests, positive blood tests, normal chest x–rays, and negative sputum cultures.[13]

Mantoux Tuberculin Skin Test (TST)

A tuberculin skin test is a standard protocol performed to determine if a person is infected with *Mtb* bacteria. The test is carried out by injecting 0.1 mL of tuberculin purified protein derivatives (PPD) under the epidermal layer of the skin with a syringe having the needle bevel facing upward. The test results are read by measuring the diameter of the indurated area (palpable area) in millimeters. An

induration of 5 mm in diameter is considered positive in Human Immuno–deficiency Virus (HIV) infected persons. An induration of ≥ 10 mm in individuals from high TB burdened countries, persons with known TB risk factors (mycobacteriology lab personnel), and children under 4 years of age is considered positive. An induration of ≥ 15 mm in any individual is considered positive. Often, TST can create false positive reactions in case of infections with nontuberculosis mycobacteria, and in individuals vaccinated with the Bacillus Calmette–Guerin (BCG) vaccine. In addition, the TST will not be able to differentiate between latent and active TB infections.[14]

The TB blood test

The TB blood test also known as interferon–gamma release assay (IGRA) while the QuantiFERON®–TB Gold in–tube test (QFT–GIT) is an alternate method for tuberculin skin testing performed to find out if a person has TB infection. The QFT–GIT measures a cell–mediated immune response using ELISA technology, by adding a cocktail of three mycobacterial proteins (ESAT–6, CFP–10, and TB 7.7)[15] to patients' blood to stimulate T–cell mediate interferon–gamma (INF–γ) release. The TB blood test has improved specificity for *Mtb* bacteria, latent infection, and unaffected by prior BCG vaccination.[16]

TB Disease

Not all latent TB infections develop into TB disease. Individuals with LTBI are at lifetime risk of developing active TB and high risk in HIV patients. If a person's immune system fails to stop *Mtb* bacteria from proliferating, the bacteria

becomes active and starts multiplying leading to TB disease. Among the 2.3 billion LTB infected individuals, approximately 10.4 million people develop active TB symptoms annually, with 1.8 to 2 million cases in due course leading to death. Nearly 60% of 10.4 million new cases are from six high burden countries such as India, China, Russia, Indonesia, Pakistan, and South Africa.[11]

Active TB disease, which is usually pulmonary TB, is accompanied by pertussis, chest pain, and coughing up of blood or sputum (phlegm). Unlike LTB infected persons, individuals with TB disease are able to spread the disease. TB disease can be diagnosed with positive TST, positive sputum or smear culture (samples are examined under a microscope for presence of *Mtb* bacteria), and abnormal chest X–rays (cavities and lesions in lungs).[11, 12, 13]

Treatment Options for TB (LTBI and TB Disease)

Effective antituberculosis chemotherapy was first developed in the 1940s, with the introduction of Streptomycin, an antibiotic from *Streptomyces griseus*. Later in the 1950s, a few other TB drugs (*p*–aminosalicylic acid, isoniazid, pyrazinamide, cycloserine) with different mechanisms of action were introduced into the available therapeutic portfolio. At present, the standard TB drug regimen consists of more than 20 drugs[11] categorized under different groups. Existing chemotherapy for TB heavily depends on drugs that target bacterial metabolism and cell wall synthesis.[17] Based on their mechanism of action, TB drugs (Table 1.1) can be classified as cell wall synthesis inhibitors (isoniazide (INH), ethambutol (EMB), ethionamide, cycloserine), nucleic acid synthesis inhibitors (rifampicin (RIF), quinolones), inhibitors of membrane energy metabolism (pyrazinamide

(PNH)), and protein synthesis inhibitors (streptomycin, kanamycin) which bind to the small 16S rRNA of the 30S subunit of the bacterial ribosome, interfering with the binding of formyl–methionyl–tRNA to the 30S subunit (Table 1.1).[18]

Treatment for LTBI involves two options: a six–month isoniazid regimen, where patients are asked to take isoniazid for the entire duration under the direct observation of a health care worker (DOTS–Directly Observed Therapy, Short course), or a 12–dose once–weekly drug combination of isoniazid and rifampin.

The standard recommended treatment for drug susceptible TB (DS–TB) involves a cocktail of four drugs, also referred to as first line drugs. The treatment for DS–TB involves two phases, the initial two–month treatment phase which involves the administration of a cocktail of four of the first line drugs RIF, INH, PNH, and EMB. The continuation of the second phase involves the administration of RIF, and INH for the next four to seven months. The four–medicine regimen is effective and can cure 85% of drug sensitive TB patients when taken as prescribed. But when treatment is inadequate or intermittent and fails to treat DS–TB, the disease becomes resistant and more difficult to cure.[19]

Recurrent TB and drug resistant strains of Mtb

The incomplete and intermittent TB treatment therapies have resulted in the recurrent TB with *Mtb* resistance, and promoted the development of, multidrug resistant TB (MDR–TB) and extensively drug–resistant TB (XDR–TB). The advent of drug resistant strains of TB is posing a problem for developed countries with successful and highly focused TB treatment strategies.[20, 21, 22]

MDR–TB strains are resistant to rifampicin (RIF) and isoniazid (INH), the

two most important first line anti–TB drugs from the core of standard treatment regimen, which also includes pyrazinamide (PNH), and ethambutol (EMB). XDR are referred to the strains of MDR, which are also resistant to fluoroquinolones and any of the injectable second line of anti–TB drugs like kanamycin, amikacin or capreomycin. In 2009 the term totally drug–resistant TB (TDR–TB) was proposed for the TB strains that are resistant *in vitro* to existing standard treatment regimen including all first and second line drugs.[11]

According to the World Health Organization (WHO) global TB surveillance report 2015, there were about 480,000 reported new cases of MDR–TB.[11] The MDR–TB treatment requires the administration of second line drugs for two years or longer, involving more than 14,000 pills, along with daily injections for a period of six months. Almost all medications are associated with side effects, and TB medication is no exception. Generally, compared to first line anti–TB drugs the second line anti–TB regimen are associated with side effects that are more serious. The first line drugs can cause issues related to gastrointestinal issues, rashes, and drug induced hepatitis, whereas the second line drugs can result in hearing loss, depression, and renal failure. Furthermore, the longer duration, intricacies and unaffordable cost of continuing to treat MDR–TB results in only a 50% success rate in curing MDR–TB patients around the world. The rapid increase in TB disease burden and 50% of the world's MDR–TB cases are accounted for by the two most populous countries in the world, India and China. The immense TB population from these two countries (around 100,000 each) increases the number of estimated MDR–TB cases to 480,000. In a recent report by the World

Health Organization (WHO) on drug resistance surveillance data, an estimated average of around 10% of MDR–TB cases have developed into XDR–TB. The treatment for XDR–TB is more complex, expensive, and lengthier, often impossible to cure and ultimately leads to death.[11, 23, 24]

The XDR–TB patients who have received an erratic, intermittent and incorrect doses have developed TDR–TB often referred to as extremely drug resistant TB (XXDR–TB).[24] The term extremely drug resistant was first used in 2007 by Migliori and co–workers to describe the strains of *Mtb* (cases from Italy) that are resistant to almost all the first line and second line anti–TB drugs.[25] After the initial reports of XXDR–TB strains, two years later in Iran, Velayati co–workers used the term totally drug resistant to describe the similar strains as XXDR–TB that are resistant to all first and second line anti–TB drugs *in vitro*. The patients affected with TDR–TB remained culture and smear positive even after 18 months of treatment with second line drugs.[26] The alarming progress in the emergence of lethal resistant strains of *Mtb* have been reported in at least three countries. Although the term TDR–TB has not yet been accepted by the WHO, in 2012, an article on TDR–TB cases in India authenticating *Mtb* strains exhibiting resistance to every drug available to treat TB gained worldwide attention.[27, 28] In spite of their clinical differentiations in drug–susceptibility test results, the reported cases of TDR–TB or XXDR–TB are officially classified under XDR–TB. While poor clinical and control practices result in the development of TDR–TB strains, the treatment options for TDR–TB remain dismal. Many factors are aggravating the spread of drug resistant TB, including interrupted and ineffective treatment, and inadequate

infection control; however, a key factor is its synergistic relation with HIV.

TB–HIV Co–Infection

Preliminary anecdotal evidence suggests two ways through which the incidence of drug resistant TB increases: acquired resistance and transmitted resistance as in case of HIV coinfection.[29] In persons co–infected with both HIV and either latent or active TB, each disease speeds up the progression of the other. In particular, HIV in particular can facilitate the progression of latent to active TB, and in turn, the TB can worsen the HIV infection. In a deadly synergy of HIV and TB infection, TB remains the leading cause of death among persons with HIV coinfection. The huge upsurge in the prevalence of TB epidemic can be attributed to high incidence of HIV infection, collectively leading to TB–HIV synergistic pandemics.[28] Together, these are the two deadliest infectious diseases worldwide, killing four million people every year. Globally, people with HIV are at higher risk (26 times) to develop active TB than those who are HIV–negative. According to global TB report by WHO in 2016, an estimated 14% (1.4 million) among the 10.4 million people who developed active TB were HIV positive. In 2015, there were 1.8 million deaths from TB, the toll comprised of 0.4 million (~27%) of people who were HIV–positive.[11]

The situation was further complicated by the drug–drug interactions that impede the co–administration of the current regimen for TB along with anti–retroviral therapy. The major concern in confronting global HIV (viral infection) and TB (bacterial infection) epidemics is developing a compatible treatment regimen. The key impediments involve both the unwanted drug–drug interactions between

antiretroviral therapy (ART for HIV) and antibacterial (for TB) drugs, and overlapping adverse side effects. The main issue being the ART and antibacterial treatment regimen compatibility.[30, 31]

The first line anti–TB drug RIF upregulates the expression of the hepatic cytochrome P450 (CYP2C9 (5.6–fold) and CYP3A4 (47–fold) oxidase system responsible for the metabolism of HIV protease inhibitors (PIs), thereby resulting in subtherapeutic plasma levels of ART medication which makes it inefficacious. Even so, the use of CYP450 inhibitors (for example Ritonavir) could not maintain and rescue the therapeutic levels of PIs, thereby impeding the co–administration of PIs, whether boosted or not, along with current regimen for TB (RIF). This situation of drug–drug interactions resulted in the only treatment option for HIV–infected TB patients being the use of non–nucleoside–reverse–transcriptase–inhibitors (NNRTI), leaving none for patients with NNRTI mutations. However, the advances in identifying new RIF analogs with minimal drug–drug interactions (reduced CYP induction), such as rifabutin, were in vain because the presence of the CYP inhibitor ritonavir in PIs cocktail regimen results in increased serum concentration of rifabutin, ultimately increasing its associated toxicity.[32, 33, 34, 35, 36]

TB Pipeline

TB remained a neglected disease for long time, and drug discovery efforts toward developing antitubercular drugs remained unattended. However, significant progress has been made in the TB treatment pipeline with the initiatives taken by WHO, TB Alliance (TBA), and the Bill and Melinda Gates Foundation to fight against TB.

Although, in the last ten years various new drug candidates have progressed to different phases of clinical trials, while in particular, the last year has been a big setback for the development of antitubercular drugs with the discontinuation of AZD–5847 (AstraZeneca–5847), due to its lack of *in vivo* potency against TB, and TBA–354 (signs of neurotoxicity).

The other concerning fact is, the majority of newly approved drug candidates are the analogs of existing TB drugs (known drug resistance) such as, gatifloxacin, and moxifloxacin (fluoroquinolones) for treatment of MDR–TB as second line drugs. Linezolid (oxazolidinone) was introduced into TB treatment therapy for treating MBR and XDR–TB, albeit, it has associated side effects include painful nerve damage. Rifampin analogs such as rifapentine and rifabutin were developed to shorten the treatment for LTBI, and DS–TB in combination with isoniazid (Figure 1.1).[30, 37, 38, 39, 40, 41, 42, 43, 44, 45]

In over 50 years, after the introduction of Rifampin (1966) the two new classes of drugs that were introduced into TB treatment regimen for treating DR–TB are Delamanid and Bedaquiline.

Delamanid (Deltyba®)

Delamanid is a nitro imidazole class of antibiotic developed by Ostuka pharmaceutical company for treating pulmonary MDR–TB in adults in combination with standard drug regimen. Delamanid was approved in early 2014 by the European Medical Agency (EMA), and targets the cell wall by inhibiting mycolic acid synthesis (FDA approval is still pending).[45]

Bedaquiline (SURTURO®)

The FDA approved Bedaquiline, a novel bi–aryl quinolone class of antibiotic developed by Janssen Pharmaceutica, on a fast track basis in late 2012 (in late 2014 by EMA) for the treatment of DR–TB as part of combination therapy in adults. It targets ATP synthase and interferes with bacterial energy metabolism, which is a different mechanism of action from the existing TB drugs.

The WHO, as last resort drugs for treating DR–TB that lacks viable treatment options, placed both Delamanid and Bedaquiline on the list of essential medicines. However, the biggest concern with these drugs is their associated side effects such as prolonging the QT interval (irregular heartbeat), neurological disturbances and hyperuricemia (excess uric acid in blood). In fact, Bedaquiline is marketed with a warning label of potentially increased mortality from life–threatening abnormal heartbeats. The more concerning fact is that just a year after the introduction of these drugs to the TB regimen, acquired resistance was seen in *Mtb* strains causing XXDR–TB in a Tibetan refugee in Switzerland.[44, 45, 46]

Even after the discovery of etiology and half a century of medical advances in the therapeutic area of TB, the global TB epidemic seems persistent. The unabated TB epidemic situation highlights the drawbacks of the existing TB treatment strategies. To control the global epidemic of TB there is a requirement for new TB drugs, which can: 1) shorten and simplify treatment duration 2) are effective against MDR and XDR–TB strains 3) are compatible with antiretroviral therapy 4) are effective against latent or dormant infection 5) minimize resistance, and more importantly 6) contain new scaffolds exhibiting novel methods of action

and fewer or no side effects.[30]

University of Utah Natural Products Screening:

Amicetin as a Viable Lead

In the course of the search for potential TB drugs with new scaffolds possessing the aforementioned requirements, we revisited and screened a small molecule library of natural products and synthetic derivatives at the University of Utah for antitubercular activity and further tested for mammalian toxicity and CYP induction properties, in collaboration with Professor Louis R. Barrow's group (Department of *Pharmacology and Tox*icology University of Utah). Screening has led to the identification of amicetin, an old under explored natural product, as a possible lead compound that potentially suits this profile. This natural product is active against the attenuated mutant strain *Mtb*–H37Ra with an IC_{50} of 0.24 µM.

Amicetin showed limited cytotoxicity when tested against the CEM/TART T–Cell leukemia cell line (IC_{50} of 4.4 µM). In addition, it showed negligible mammalian cytotoxicity: a) against human mammary epithelial cell line MCF–10A (EC_{50} of 74 µM); b) against breast cancer (MCF–7) cell line (EC_{50} of 84 µM); c) against monkey kidney epithelial cells (Vero IC_{50} = >100 µM); d) and against human liver cancer cell line (Hep–G2 IC_{50} = >100 µM). More importantly, it shows no significant activation of hepatic cytochromes (< 2–fold induction of CYP2C9 and CYP3A4) as measured by qPCR in the HepG2 cell line (compatible with HAART) compared to rifampicin (>54–fold induction).[47, 48, 49] All of these properties of amicetin are distinct in comparison to the current drug regimen for TB and the existing pipeline drugs, prompting us to further investigate and re–engineer

amicetin (Figure 1.2).

Literature Reports on Amicetin

Upon exploring literature data on amicetin, it is reported as an amino hexose pyrimidine nucleoside antibiotic isolated by J. Hinman and coworkers in 1953 from fermentation broths of *Streptomyces vinaceusdrappus.*[50] Amicetin was also isolated by various research groups from different *Streptomyces species*.[51, 52, 53] Stereochemistry and specific configuration of the disaccharide portion in the molecule was determined by NMR analysis and synthesis of hydrolysis products.[54, 55, 56, 57, 58, 59, 60, 61] Later in 1981, the crystallographic studies published by Smith et al. confirm the structure of amicetin.[62] In the seminal isolation paper, amicetin was shown to be active against the virulent strain of *Mtb–H37Rv* with an IC_{100} = 0.5 μg/mL (0.81 μM), against *Mtb var. homonis. ATCC 607* with an IC_{100} = 1.0 μg/mL (1.62 μM), and *Staphylococcus aureus* (FDA–209) with an IC_{100} = 2.0 μg/mL. Amicetin showed no significant activity against *Gram* (–) bacteria (Table 1.2). In addition, it was shown to be active *in vivo* against *Mtb–H37Rv* infected mice (details unpublished). Further, the reported systemic toxicity of amicetin was reasonable with LD_{50} = 200 mg/kg in rat when administered intravenously (IV), and the subcutaneous (SC) LD_{50} = 600 mg/kg.[63, 64]

Amicetin–a known protein synthesis inhibitor

Amicetin was known to exhibit its antibiotic activity by functioning as a peptidyl–transferase inhibitor to inhibit protein biosynthesis. In a report by Rychlik and coworkers, translational inhibition activity was measured as a function of

percentage adduct (CACA–AcLeu–puromycin) formation with respect to antibiotic concentration. Plicacetin, cytimidine, and cytosamine (Figure 1.3) were shown to be ten–, fifty– and 100–fold less active than amicetin, respectively, whereas oxamicetin, a close structural analog to amicetin, was shown to be a more potent inhibitor of the overall peptidyl transferase inhibition activity than amicetin. Correlating the decrease in protein synthesis inhibition activity with the absence of certain structural features clearly emphasizes the importance of the presence of the aminoacyl portion, i.e., *L–α–methylserine* portion (Figure 1.3). [65, 66, 67]

Hypothetical binding site of amicetin

While amicetin was shown to inhibit protein synthesis, its exact role in translation inhibition is unknown. In an effort to determine the exact binding site of amicetin to the ribosome, Levive et al. have performed site–directed mutations, and chemical foot printing experiments on the highly conserved 23S rRNA, the secondary structural motif of larger subunit (50S) of ribosome. The results imply a single point mutation in the peptidyl transferase center of domain V, U2547C, has shown to be responsible for resistance and has been suggested as the hypothetical binding site of amicetin. However, the exact working mechanism for amicetin with atomic resolution still remains undefined.[68] Another important outcome of this experiment was that after 100 passages of *H. halobium sp.* over a period of 1.5 months, the resistant bacteria were sensitive to 2X MIC of amicetin (only 2–fold increase in MIC). This result suggests the target mutations at PTC are lethal and antibiotic resistance by amicetin's binding site alterations is slow.

Introduction to the Ribosome

Amicetin has long been known to inhibit protein synthesis.[69] However, the atomic details of the mechanism of action have been unknown. Efforts were also focused on probing the mode of action of amicetin with molecular details by solving their crystal structures bound to the ribosome.[70, 71, 72, 73, 74, 75, 76]

Both the prokaryotic and eukaryotic ribosomes consist of two major subunits, the small ribosomal subunit, and the large ribosomal subunit. However, the prokaryotic and eukaryotic ribosomes differ in their size, structure, and slightly in the translation process. These differences offer an opportunity for selectivity in which drugs can target the prokaryotic bacterial ribosomes over eukaryotic ribosomes. The bacterial 70S ribosomes consists of ~ 54 ribosomal proteins, a larger 50S subunit with two different types of ribosomal RNAs (rRNAs; 23S, 5S) with ribozyme (a sequence of RNA with enzymatic activity), and a smaller 30S subunit comprised of 16S rRNA. The eukaryotic 80S ribosomes composed of ~80 ribosomal proteins and a larger 60S subunit with three rRNAs (28S, 5.8S, and 5S) and a smaller 30S subunit consist of 18S rRNA.[77, 78, 79, 80]

Structure of Ribosome

Until recently, the complexity and dynamic nature of ribosomes made it difficult to understand the relationship between structure (dynamics) and function. Since the 1950s disclosure of the role of the ribosomes in translation a great deal of effort has gone into studying the translational process and how it is hindered by ribosomal antibiotics. The ribosome targeting antibiotics bind to specific regions in the prokaryotic ribosome with specific interactions and hinder the normal ribosomal

functions. These are used both for probing various steps involved in protein translation, and clinically to cure severe infections. Over time bacteria have developed resistance to these antibiotics. Therefore understanding the mechanisms of bacterial resistance is of great importance as the significance of developing potential therapeutics.[81, 82, 83, 84, 85]

Initially, the structure of the ribosome was visualized by electron microscopy (EM) and advanced with cryo–EM techniques that could capture different phases of protein synthesis. At first, the rRNAs were regarded as scaffolding units for the catalytically active r–proteins. Later, the significant contributions from genetic and biochemical approaches have changed the perception of the ribosomal components and their relative roles, in which rRNAs play a vital role in ribosome function, and r–proteins play a supporting role.[84, 85, 86] The intrinsic resolving power of cryo–EM results did not permit the elucidation of the different functional states of translation with minute details of its molecular interactions. However, at the end of the twentieth century, advances in the high–resolution X–ray diffraction studies (X–ray crystallography) of the ribosome have provided compelling pieces of evidence in the translational process. There were no r–proteins closer than 18 Å at the peptidyltransferase center (PTC) on 50S subunit, suggesting that the translational process is RNA–directed and ultimately based on RNA–RNA interactions. Given the significance of the rRNA in translation, it is anticipated that most of the protein synthesis inhibitors target the rRNA rich surfaces on both the ribosomal 30S and 50S subunits. Significant progress towards understanding the detailed mechanism of protein synthesis has been made after initial reports of

ribosomal crystal studies during last two decades.[87, 88, 89, 90, 91, 92]

By the early 2000s, all atom crystal structures of individual small 30S and large 50S ribosomal subunits of bacterial ribosomes had been solved.[92, 93, 94] The crystal structures of individual subunits allow us to infer limited information regarding the translational process. Since the bacteria use full–length tRNA for its protein biosynthesis, the atomic details (crystal structures) of intact 70S ribosome complex with integral tRNAs were also resolved and studied at 5 Å and 3.5 Å resolution.[95, 96] The X–ray crystallographic model of the *Thermus thermophiles (Tth)* entire 70S ribosome embracing tRNA and messenger RNA (mRNA) at 5.5 Å resolution accounts for the electron densities for all the ribonucleoproteins (16S, 23S, and 5S rRNAs and proteins), and the A–, P–, and E– site tRNAs (Figure 1.4). The model also provides a general description of RNA–rich interfacial core between the 30S and 50S ribosomal subunits where the tRNAs are bound and the protein rich interfacial periphery. However, because of its limited resolution, it fails to reveal the significance of particular atoms in ribosomal function. The full atomic crystal structures of the intact 70S ribosome of *Escherichia coli* bacteria at 3.5 Å resolution have provided complete atomic details, and deeper understanding of the interface between intraribosomal subunits, and molecular details of ribosomal conformational flexibility. Furthermore, the reports of X–ray crystal structures of the *Tth* intact 70S ribosome complexed with mRNA and tRNA refined to 2.8 Å emphasizes the fact that, though these complexes are solved in different crystal forms, they all demonstrate conformational similarities of the ribosome and its substrates.[97, 98]

Peptidyl Transferase Center (PTC)

After the advances in high–resolution crystallography, the mechanistic understanding of translation has progressed rapidly. Description of specific structural interactions of the ribosome with mRNA, and tRNA in the P–, and E–sites of the peptidyl transferase center (PTC). The A–site of PTC recognizes the aminoacyl–tRNA, positions it for the peptidyl transferase reaction, and monitors the interaction between codon and anticodon in the 30S subunit-decoding site. The aminoacyl–tRNA in A–site also functions as the acceptor for the growing polypeptide during peptide bond formation. The P–site is responsible for binding the initiator tRNA (fMet–tRNA) during the initiation phase. The P–site role also includes positioning of the translational reading frame and holding onto the nascent polypeptide chain. After peptide bond formation between the two adjacent amino acids on the P–site tRNA and A–site tRNA, the E–site acts as a host for deacetylated tRNA favoring the translocation from P–site to E–site. The E–site also provides free energy change for the exit of deacetylated tRNA out of the 50S P–site. The conformational differences between the vacant and tRNA complexed 70S ribosome, asserts the induced fit model (an active site of the ribosome, when makes contact with substrate, the ribosome itself adopts the shape of the substrate) for the ribosome in response to tRNA binding, accompanied by significant changes in the peptidyl–transferase catalytic site.[80, 85, 99, 100]

The Process of Translation

The prestigious Nobel prize–winning science by Dr. Steitz, Dr. Ramakrishnan, and Dr. Yonath on “studies of the structure and function of

ribosome" have provided unparalleled insights into the mechanism of action of ribosomes and the bacterial translational process. These scientific discoveries have not only helped a great deal in understanding binding, and mode of action of ribosomal antibiotics (natural and semisynthetic), but also bacterial resistance mechanisms, and aided in the design of more efficient ribosomal antibiotics. Each step of the life's core process, translation of DNAs information to functional protein, has been extensively studied over the past decade; however, these studies are by no means exhaustive. [80, 85, 99, 100]

Initiation

A schematic view of protein biosynthesis (translation) is shown in Figure 1.5. Translation can be divided into four steps. First, initiation implicates the assembly of a smaller 30S subunit and larger 50S subunit to form a 70S ribosomal complex. This step also includes precise positioning of N–formyl methionyl (fMet)–tRNA at the ribosomal peptidyl site (P–site) in 50S subunit to the target mRNA start codon (often AUG) on 30S ribosomal subunit. In prokaryotes, the three key initiation factors, IF1, IF2, and IF3, facilitate the efficiency and fidelity of translational initiation process.[80]

Elongation

Elongation is a three–step cyclic process. It begins with the delivery of an aminoacylated tRNA (aa–tRNA), facilitated by Elongation Factor–Tu (EF–Tu) in association with guanosine triphosphate (GTP) and dictated by the nucleotide triplet codon on the mRNA, to the A–site. Next, the formation of the peptide bond

between the two amino acids attached to A– and P–site tRNAs, mediated by peptidyl transferase located on the 50S ribosomal subunit the process of peptide bond formation results in migration of amino acid from P–tRNA to A–tRNA.

Translocation

The next step is translocation facilitated by Elongation Factor–G (EF–G). To accommodate the incoming aa–tRNA in the A–site, the tRNA of the initiator is ejected from the P–site to E–site. The dipeptidyl–tRNA (fMet–aa–tRNA) is moved to the P–site and the mRNA moves relative to the ribosome to expose a new triplet codon in the A–site, allowing the cycle to repeat. The translocation process runs in parallel with elongation of nascent polypeptide chain which exits through an exit tunnel into the cytoplasm and folds into a functionalized protein. In many cases, the protein will fold into its three–dimensional shape as it's released into the cytoplasm.

Termination

During the termination step, the peptide is released when the mRNA terminator codon is read.[79] The elongation cycle continues until a stop codon on the mRNA is recognized by release factors (RF1 and RF2), which then hydrolyzes the peptidyl–tRNA bond. The result is the release of a nascent polypeptide chain. Therefore, recycling the disassembled post–translational complex to be available for the next translational initiation process.

Translation is a multistep process involving complex structures such as ribosomes, and multiple translation factors. The catalytic peptidyl PTC of the

bacterial ribosome is one of the major *in vivo* targets for a number of antibiotics such as purine nucleosides (e.g., puromycin), sparsomycin, chloramphenicol, streptogramins, oxazolidines, lincosamides, tetracyclines, and pyrimidine nucleosides (blasticidin S, gougerotin) among others.[77] Each step of bacterial translation is targeted by at least one ribosomal antibiotic (protein synthesis inhibitors).

Initially, the biochemical information, structural insights, and mode of action of different antibiotics were characterized by crystallizing individual 30S or 50S subunits of the ribosome with antibiotics. However, over the past decade the ability to elucidate the complexes of antibiotics bound to 70S ribosomes with high resolution has resulted in documentation of almost all of the major classes of ribosomal antibiotic complexes with ribosomes. Subsequently, collection and interpretation of highly resolved X–ray diffraction patterns of ribosome–antibiotic complexes have taken place.

The majority of known clinically used antibiotics such as the aminoglycosides, chloramphenicol, fusidic acids, oxazolidinones, streptogramins, and tetracyclines target the elongation cycle of bacterial translation. Several other classes of antibiotics block the initiation, termination, and recycling phases of bacterial protein synthesis. However, the clinical applications of antibiotics targeting the initiation phase such as pactamycin, edeine, evernimicin, and thiopeptides are limited due to specificity (selectivity index), toxicity, and solubility issues associated with them. Notably, the majority of the antibiotics targeting termination and recycling phases of translation, such as fusidic acid, blasticidin S,

chloramphenicol, puromycin, and sparsomycin, exert their significant inhibitory effect on the elongation phase of translation.

Antibiotics Targeting the 30S Subunit of Ribosome

In 2014, Professor Wilson, in his review on "Ribosome–targeting antibiotics and mechanism of bacterial resistance," states that "despite the large size of the ribosome, relatively few sites are targeted by our current arsenal of antibiotics. On the 30S subunit, the antibiotic binding sites are clustered along the path of mRNA and tRNAs." Evidence from several assays[80–84] and structural studies (crystal structures) of these natural product ribosomal antibiotics and their synthetic analogs explain the way these antibiotics interact with ribosomes. They also suggest that antibiotics, despite considerable structural diversity, engage in common and only a few competitive binding sites of the ribosome. The major classes of antibiotics bound to the 30S ribosome subunit are fusidic acid, tetracyclines (tetracycline, oxytetracycline, doxycycline, tigacil, and minocycline), aminoglycosides (gentamycin, amikacin, tobramycin), pactamycin, and edeine (Figure 1.6). [80,85]

Antibiotics Targeting the 50S Subunit of Ribosome

The most common binding sites on the 50S subunit targeted by current antibiotic regimen are grouped around PTC, especially overlaid on A–tRNA (e.g., chloramphenicol, lincosamides, oxazolidines, puromycin, and sparsomycin) and few (e.g., macrolides, and streptogramins) within the exit tunnel. Surprisingly, there are no reported clinically used antibiotics which bind in the p–site. Only, Blasticidin

S (BlaS) was shown to bind at P–tRNA as well as overlapping on A– and P–sites. However, BlaS is a universal antibiotic and is known to inhibit both prokaryotic and eukaryotic translation equally. It was shown to be toxic to bacteria, fungi, and mammals (mice and rat). While BlaS is used to control plant disease (treatment of rice blast disease), its associated toxicity, and lack of species specificity hinders the BlaS clinical use in treating human infections (Figure 1.7).[101, 102, 103]

Blasticidin S

Initially, the molecular details emphasizing the binding of BlaS (belongs to amino hexose–cytosine class of antibiotics) to the larger subunit of ribosome *50S* of *Haloarcula marismortui* (*Hm*) was illustrated by crystallographic studies in Steitz's lab. Strangely, two ligands of BlaS were reported occupying two non–overlapping binding sites with varied strengths (Figure 1.8). First, a high–affinity binding site is characterized by a conserved Watson–Crick base pairing between BlaS cytosine and G2284 (G2251)) [*Hm, (E. coli)*] of the 23S rRNA, and a cation–π interaction with A2472 (A2439). The hydrogen bonding interactions of the *N*–methyl guanidine tail with the phosphates of A2472 (A2439) and A2635 (A2600) further stabilize the interaction. Secondly, there are low–affinity binding interactions involving a W–C base pairing of BlaS cytosine with G2285 (G2252) [*Hm, (E. coli)*]. Since the two bases [G2284, and G2285 (*Hm*)] interacting with two molecules of the BlaS are universally conserved and base pair with the two cytosine residues (C75 and C74, respectively) of the P–tRNA CCA tail, BlaS was thought to inhibit translation by being a competitive inhibitor of P–site binding substrates. [101, 102, 103]

Later, the exact mechanism of action for BlaSwas resolved by X–ray crystallographic studies of BlaS bound to 70S ribosome of *Tth* in presence of *P*–site tRNA.[33] Unlike previously reported crystal structure of the 50S subunit of *Hm* with two BlaS ligands, the 70S–tRNA complex was seen bound with only one BlaS ligand with its cytosine moiety W–C base paired to G2262 (G2251) [*Tth, (E. coli)*]. Moreover, it was shown to inhibit translation by stabilizing distorted P–tRNA on the ribosome, by displacing Watson–Crick base pairing of C75 of 3'CCA tail with G2262 (G2251) [*Tth, (E. coli)*], thereby inhibiting new peptide formation beside release factor–mediated peptidyl–tRNA hydrolysis (Figure 1.9). [101, 102, 103, 104]

Amicetin Binds to P–site of PTC Similar to BlaS

The Looper group has succeded in solving the X–ray crystal structures of the natural product amicetin (Ami) (re–expressed, isolated, and purified from the bacteria *Streptomyces vinaceousdrappus* by Dr. Serrano in Looper lab),[105] in complex with the 70S *Tth* ribosome within 3.5 Å resolution, in collaboration with Dr. Eiler of the Steitz's lab at Yale University.

Molecular mapping of amicetin and its analogs bound to *Tth* 70S ribosome

In the crystal structure, amicetin is seen bound to the P–site of the PTC of 23S rRNA, at the same binding site as BlaS. Critical interactions that highlight the binding of amicetin to the ribosome are: 1) the nucleobase cytosine of amicetin is engaged in a W–C base pair with G2262 (2251) [*Tth (E. coli)* numbering]. 2) *p*–Aminobenzoate portion of amicetin is involved in π–π stacking interaction with

A2613 (2602). 3) The dimethylamine group of the disaccharide portion of amicetin participates in a (cation–π interaction) with A2450 (2439), and the hydroxyl group is engaged in a hydrogen bonding interaction with a phosphate group of C2612(2601). 4) Finally, the amino acid α–methylserine lies in an extremely polar region, exposed to a solvated front, forming a hydrogen bonding interaction with a phosphate group of G2506(2495) via an amine. The hydroxyl group of α–methylserine is in proximity to the glutamate (E80) of L–16 ribosomal proteins, which could result in a possible weak interaction via the terminal hydroxyl group (Figure 1.10). [104, 105]

Amicetin Bound to *Tth* 70S Ribosome in Presence of P–site tRNA

All the binding interactions in Ami–70S complex, except π–π stacking interaction of *p*–aminobenzoate of amicetin with A2613(2602), are also seen in the structure of Ami–70S–P–tRNA ternary complex. Similar to BlaS, the W–C base pairing of the cytosine of Ami with G2262(2251) causes distortion in C75 of 3'–CCA tail of P–tRNA. The phosphate backbone of C75 is shifted by 7Å in BlaS–70S–tRNA ternary complex, whereas the nearby A76 and C74 are shifted by 2Å, 4Å, respectively (Figure 1.11). [101, 102, 103, 104]

Mechanism of Action of Amicetin

The crystallographic studies of amicetin bound to 70S ribosome of *Tth* in the presence of P–site tRNA provide mechanistic insights into the mode of action of amicetin. The studies suggest that amicetin inhibits translation by stabilizing a

deformed conformation of P–site tRNA of the larger ribosomal subunit similar to BlaS. The site where amicetin binds and involves in Watson–Crick (W–C) base pairing of cytosine with G2251 is also a binding site for P–site tRNA, where the C74 and C75 of 3'CCA tail of P–tRNA forms a W–C base pair with G2252, and G2251 (*E. coli* numbering), respectively, and positions itself in the P–site of the ribosome for translational elongation. During the formation of a new peptide bond, hydrogen bonding interactions between rRNA nucleotides constituting the PTC and tRNA nucleotides result in an orientation of acceptor aminoacyl–tRNA (Aa–tRNA) and donor peptidyl–tRNA suitable for peptidyl transfer. This adjustment allows the attack of the α–amino group of the acceptor A–site bound aminoacyl–tRNA on to the carbonyl center of the ester bond of a P–site bound tRNA with the spontaneous transfer of peptidyl residue to the A–site bound aminoacyl–tRNA amino acid to form a new peptide bond.[106, 107, 108] After peptide bond formation the nascent oligopeptide is transported through the exit tunnel and placed below the PTC. Amicetin interrupts this interaction of C75–G2251 by displacing C75 and forming key Watson–Crick base pair of its cytosine with G2262(2251). The displaced C75 results in bending of the P–tRNA toward the A–site creating an unproductive conformation on the ribosome thus inhibiting peptidyl tRNA hydrolysis (Figure 1.12). [101, 102, 103, 104]

Factors Governing the Selectivity of Amicetin Compared to BlaS

While both Ami and BlaS bind at the same site in PTC, unlike BlaS, amicetin selectively inhibits prokaryotic translation over eukaryotic translation.[96] Although

the factors governing amicetin's selectivity are not clear, we anticipate four elements that seem to oversee selectivity. 1) The ability of amicetin to be involved in $\pi-\pi$ stacking interactions (note: BlaS lacks this interaction) with A2613(2602) [*Tth*, (*E. coli*)]. The highly conserved A2602 (*E. coli*) is shown to be critical for RF dependent peptidyl–tRNA hydrolysis.[97] 2) The presence of α–methylserine of amicetin and its interaction with ribosomal protein L16, and the universally conserved phosphate groups might have a part in antibiotic activity and selectivity. 3) The absence of a guanidine moiety in amicetin (instead it has a dimethylamino pyranose). BlaS binds tightly in the binding pocket (Six noncovalent interactions vs Two in Ami) utilizing a guanidine to engage the cation–π interaction and hydrogen bonding interactions with A2439.[98, 99] 4) Lastly, the magnitude of displacement with C75 in presence of Ami compared to BlaS in tRNA stacked 70S ribosome may not be accommodated in eukaryotic 80S ribosomes.[101, 102, 103, 104]

Table 1.1 Clinically used first lineTuberculosis drugs[18]

First-line drugs

Drug (Abbreviation) (year of discovery)	Structure	Mode of action
Isoniazid (INH) (1952)	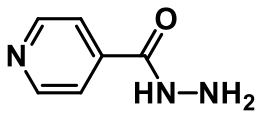	Inhibits mycolic acid (cell wall) synthesis
Rifampin (RIF) (1966)	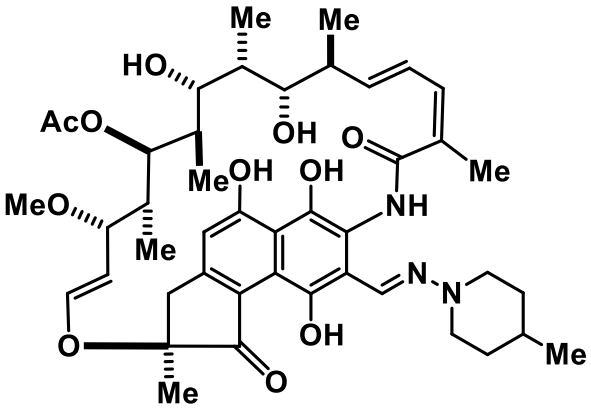	Inhibits transcription
Pyrazinamide (PZA) (1954)	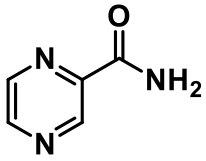	Inhibits translation / Acidifies cytoplasm
Ethambutol (EMB) (1961)	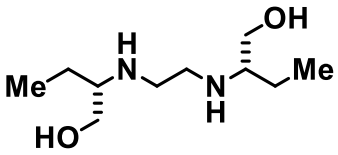	Inhibits arabino galactan synthesis

Table 1.2 Clinically used second lineTuberculosis drugs[18]

Second-line drugs

Drug (Abbreviation) (year of discovery)	Structure	Mode of action
p-amino salicylic acid (PAS) (1948)	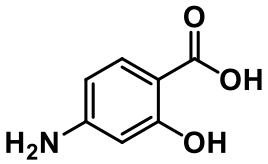	Inhibits folate biosynthesis
D-Cycloserine (DCS) (1955)	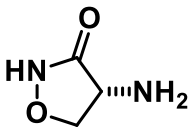	Inhibits peptidoglycan synthesis
Ethionamide (ETO) (1961)	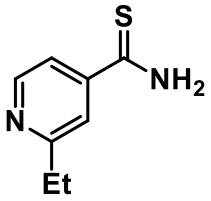	Inhibits mycolic acid biosynthesis
Levofloxacin (LFX) (1989)	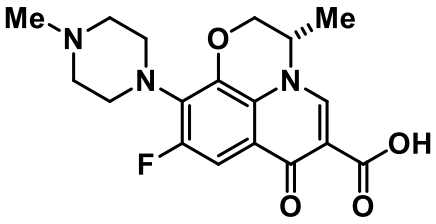	Inhibits DNA super coiling
Levofloxacin (CFX) (1981)	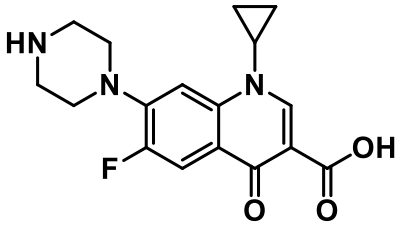	Inhibits DNA replication

Table 1.3 Clinically used second line injectable Tuberculosis drugs[18]

Second-line injectables (amino glycosides)

Drug (Abbreviation) (year of discovery)	Structure	Mode of action
Streptomycin (STM) (1944)	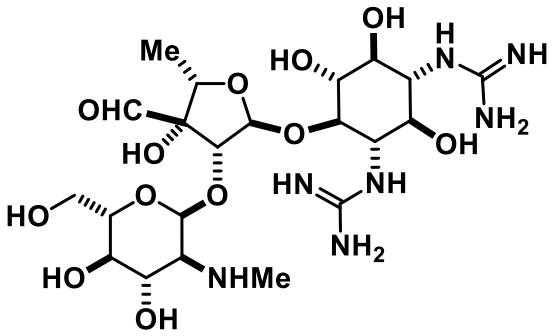	Inhibits translation
Kanamycin (KM) (1957)	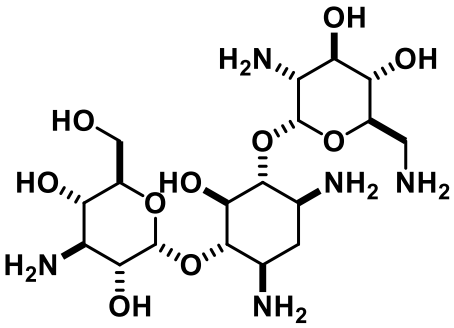	Inhibits translation
Amikacin (AMK) (1972)	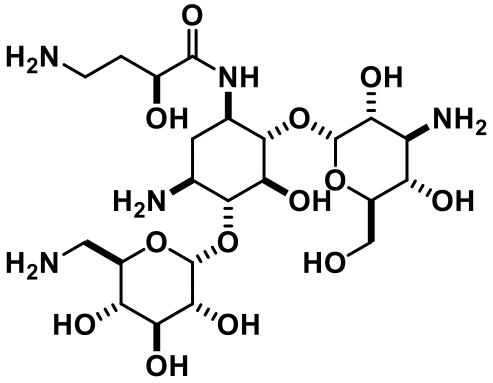	Inhibits translation
Capreomycin (CM) (1963)	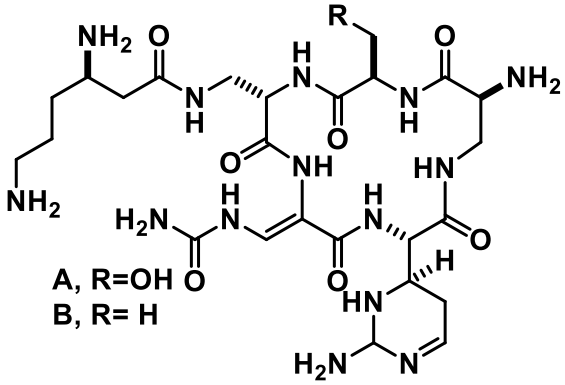	Inhibits translation

Table 1.4 Reported *in vitro* efficacy of amicetin[47]

Test Organism	IC_{100} (μg/mL)
Gram (+)	
Staphylococcus aureus FDA-209	0.2
Bacillus subtilis III	4.0
Acid-fast mycobacterium	
Mycobacterium tuberculosis H37Rv	0.5
Mycobacterium tuberculosis ATCC-607	1.0
Gram (-)	
Klebseilla pneumoniae PCI-602	>20
Escherichia coli ATCC-26	>20

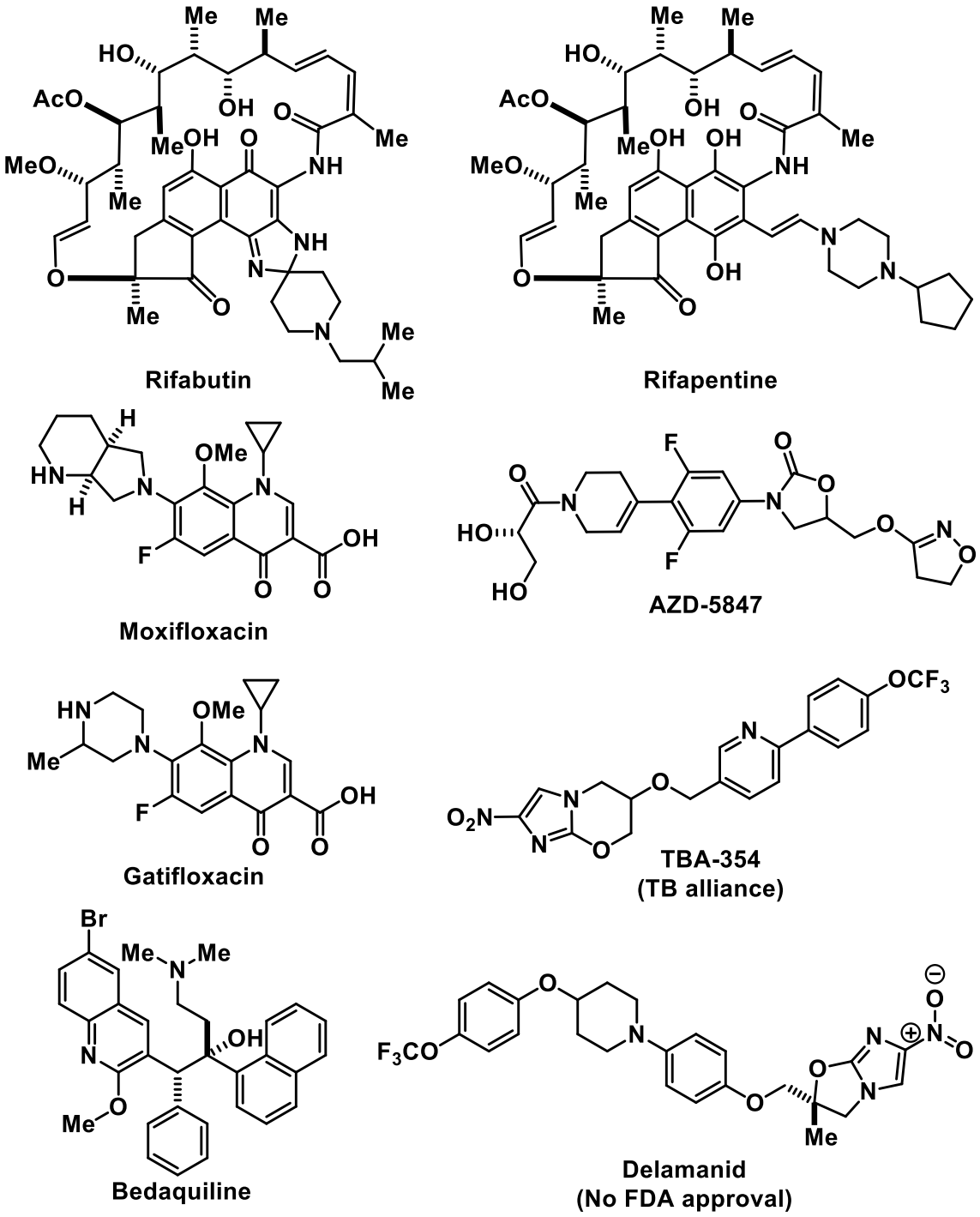

Figure 1.1 TB pipeline

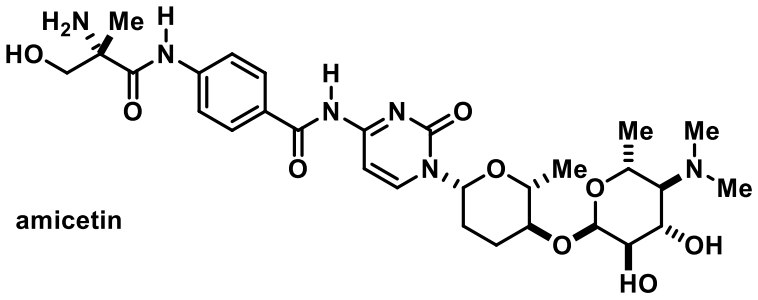

Figure 1.2 Structure of amicetin

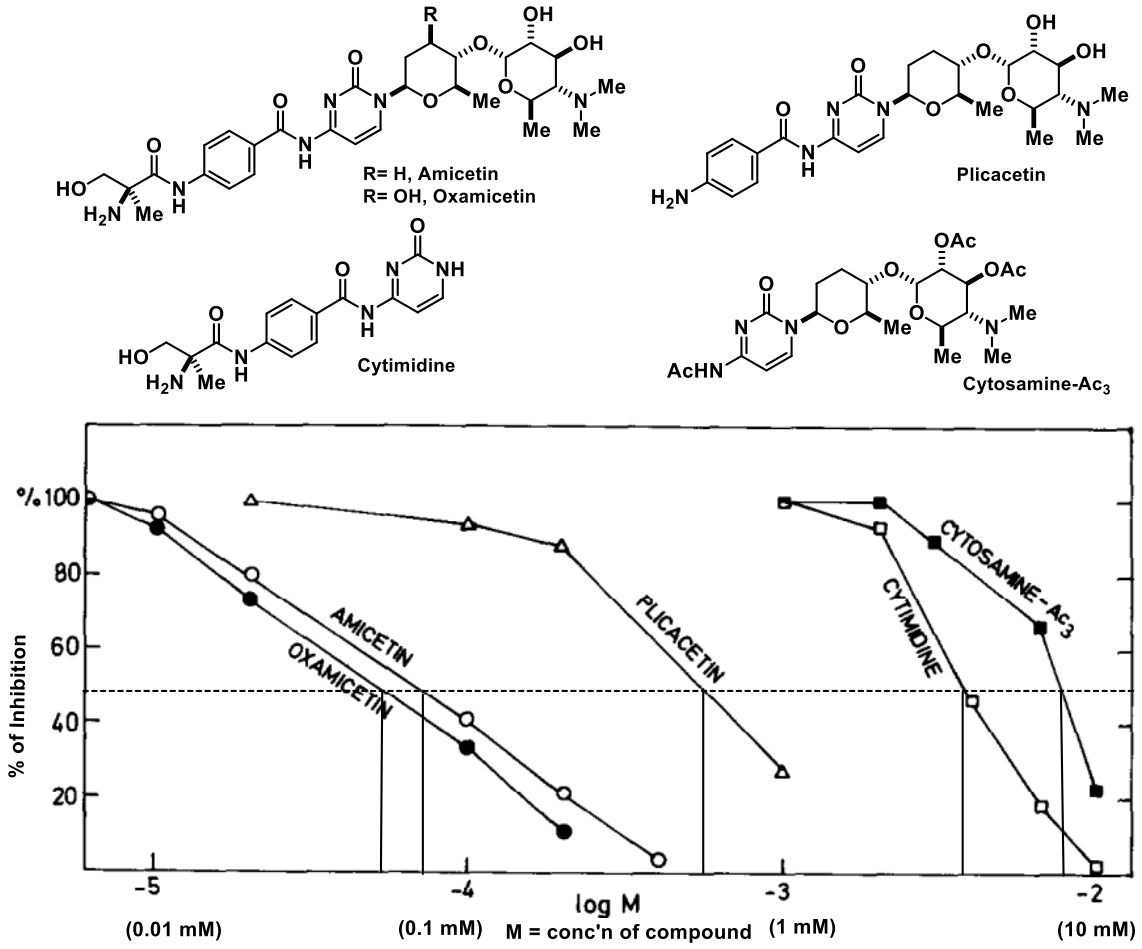

Figure 1.3 Protein synthesis inhibition assay of amicetin and congeners[67] (Adapted from Lichtenhaler, F. W.; Cerna, J.; Rychlik, I. *FEBS Lett.* **1975**, *53*, 184–187.)

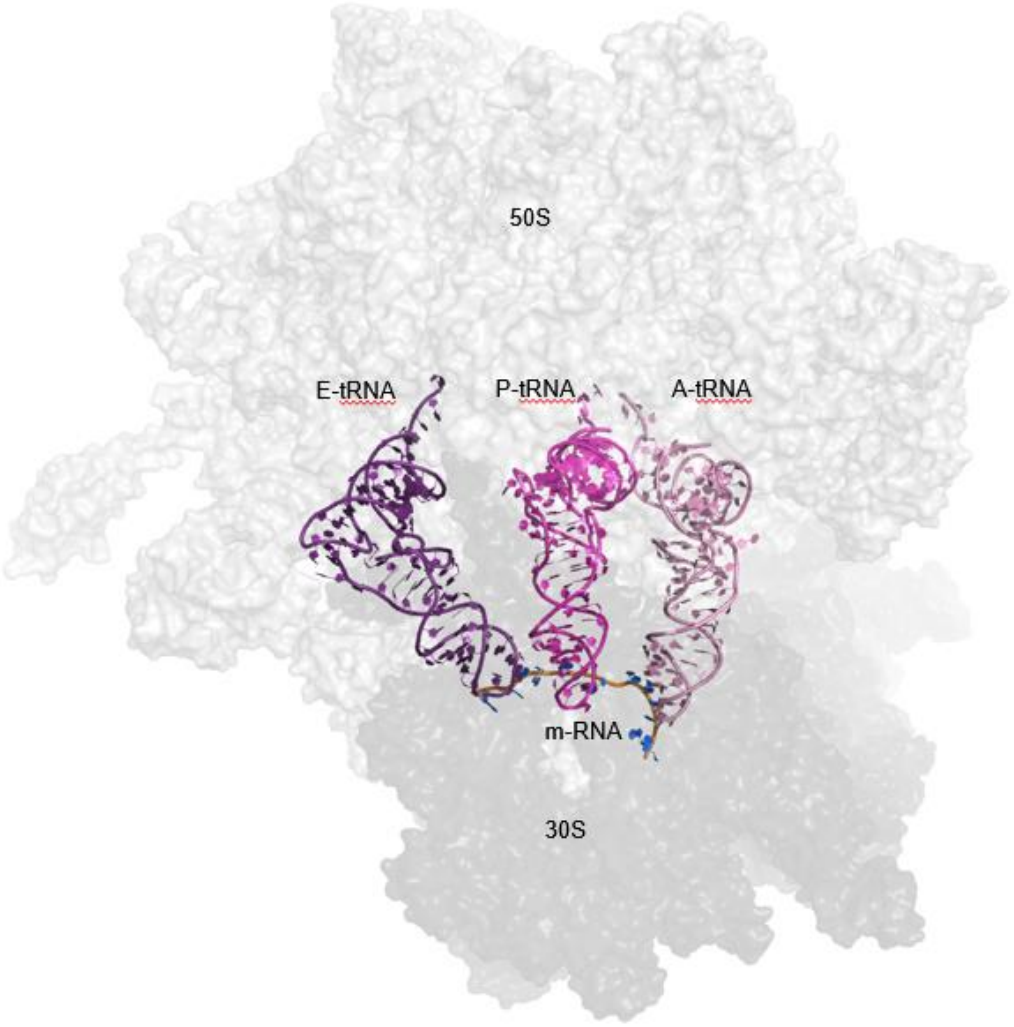

Figure 1.4 Structure of ribosome with two subunits, A, P, and E–site tRNAs and mRNA (orange)

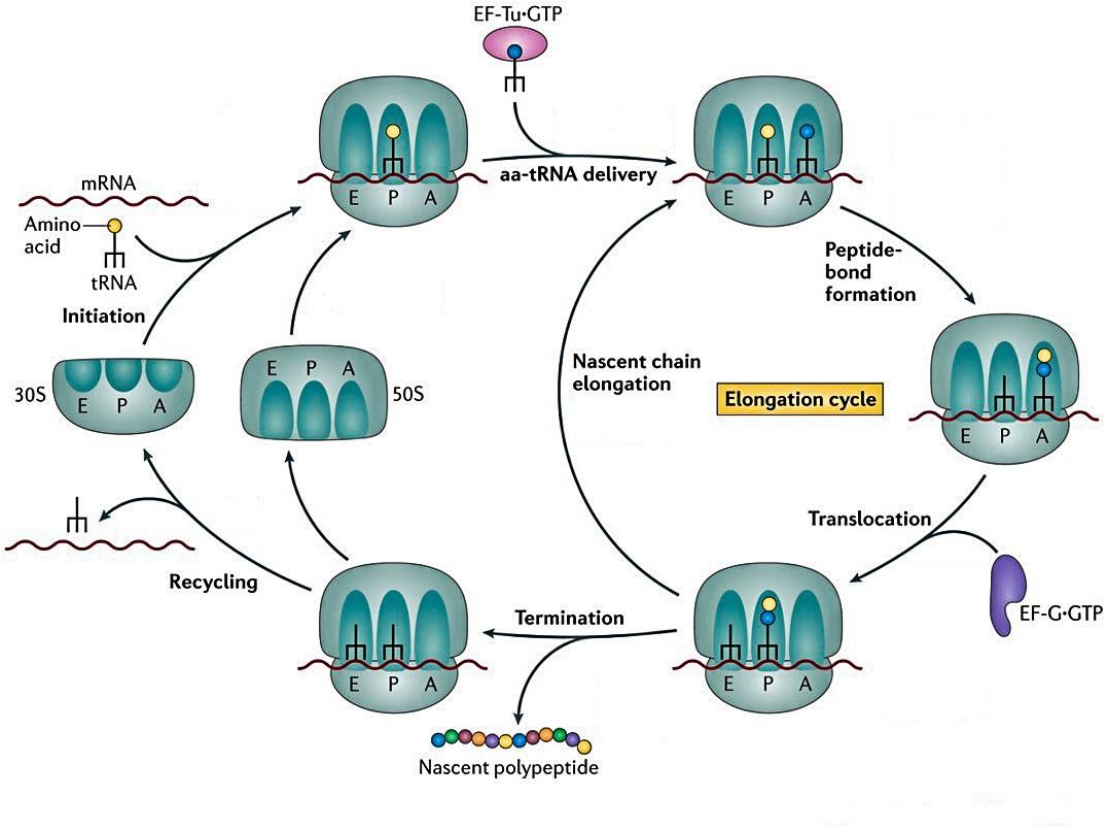

Figure 1.5 Translation and various steps involved in translation (Adapted from *Nature reviews microbiology* **2014**, *12*, 35–48. License # 4003320132514)

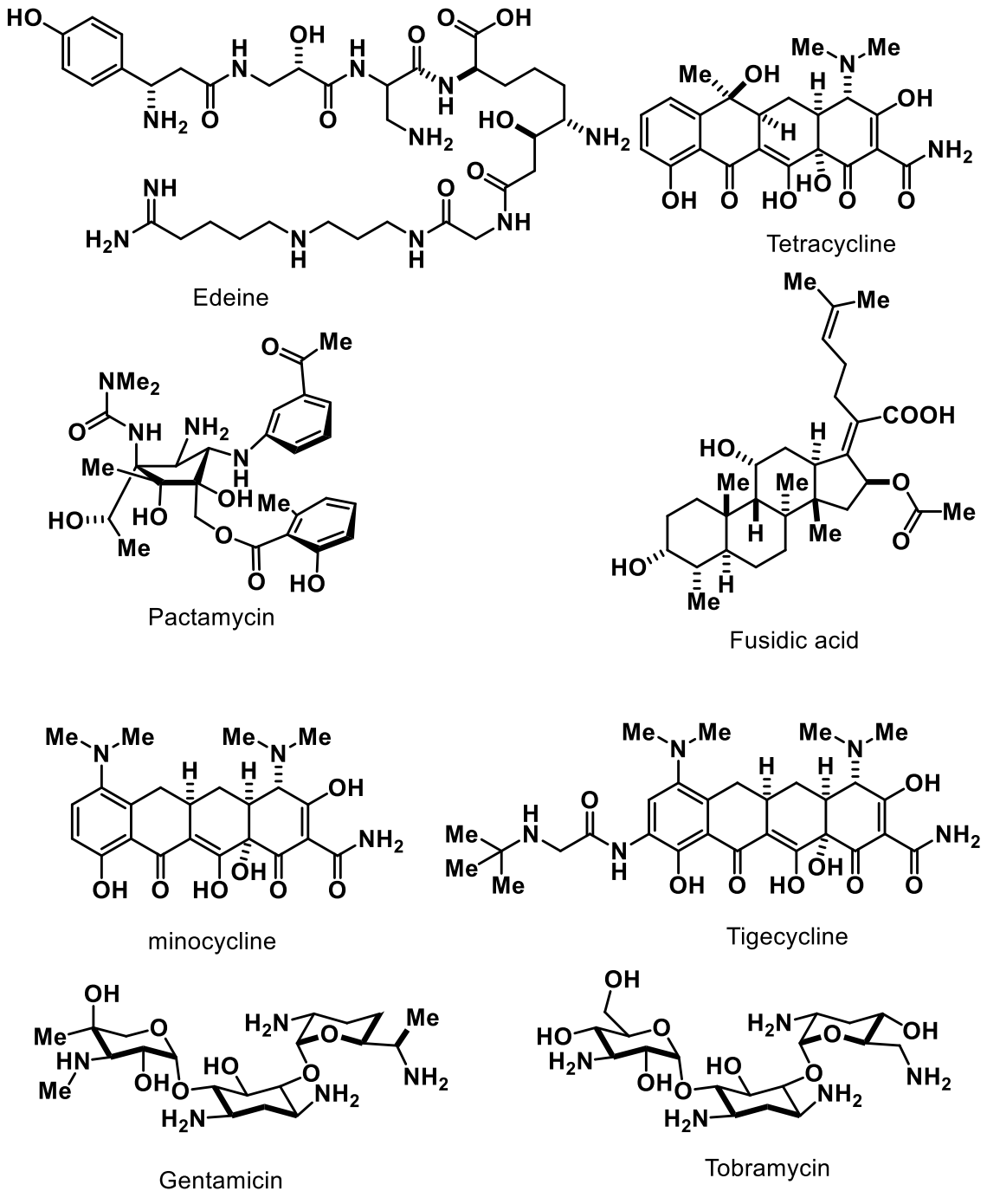

Figure 1.6 Antibiotics targeting 30S subunit of the ribosome

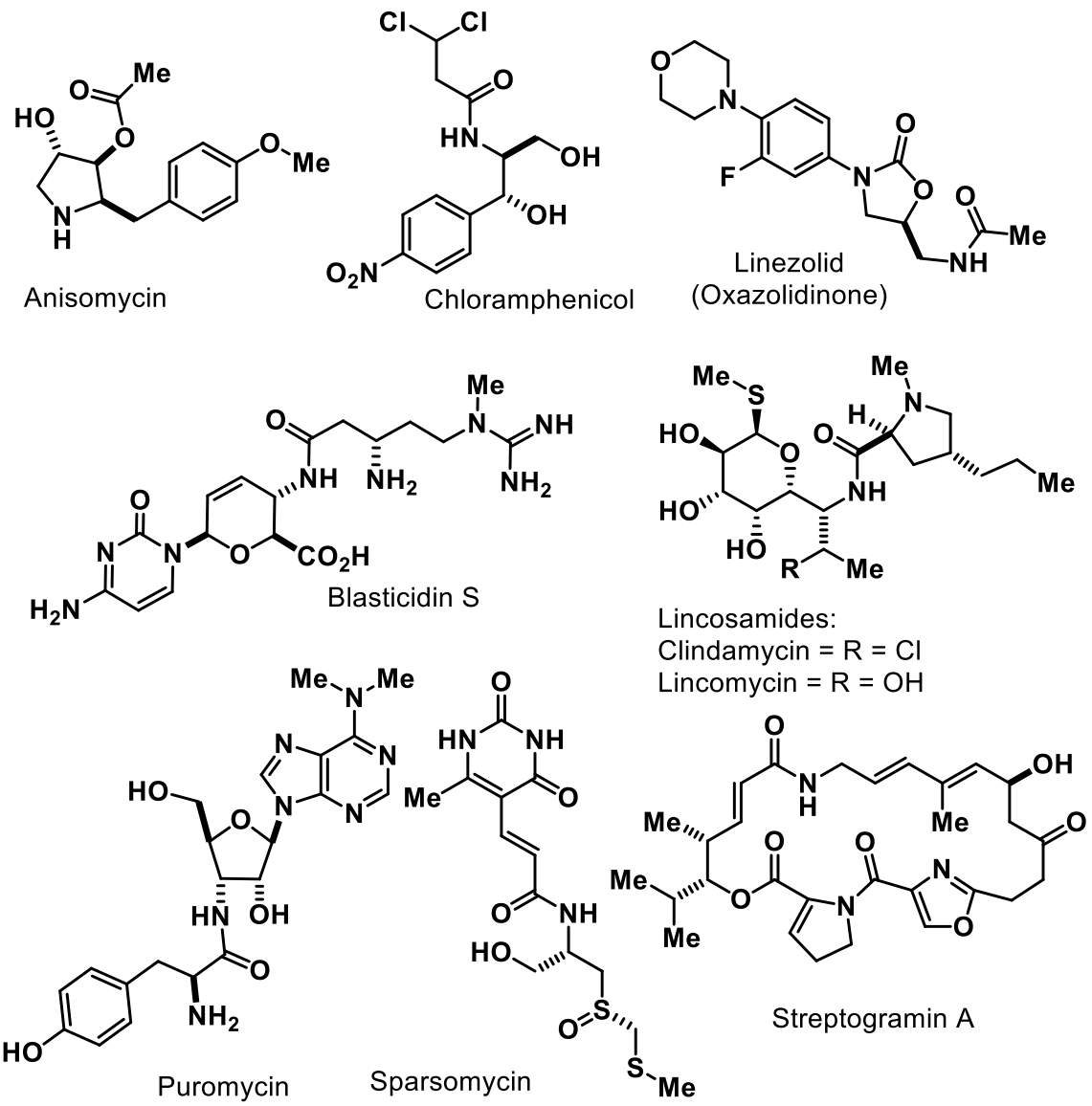

Figure 1.7 Antibiotics targeting 50S subunit of the ribosome

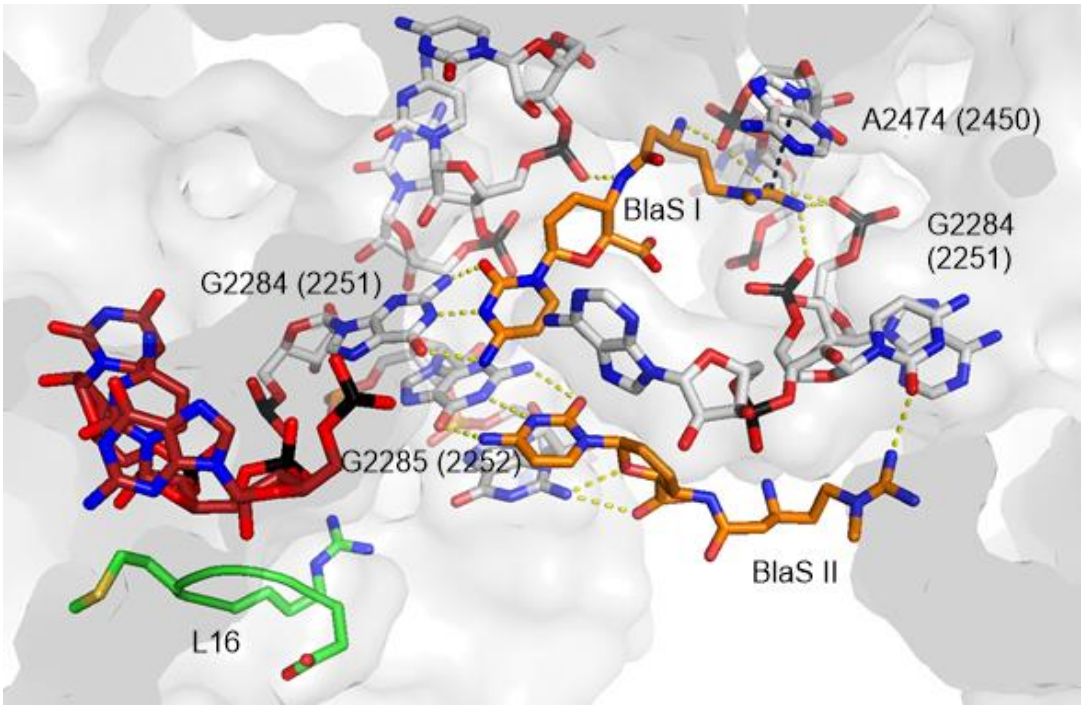

Figure 1.8 BlaS bound to 50S ribosomal subunit of *Haloarcula marismortui*

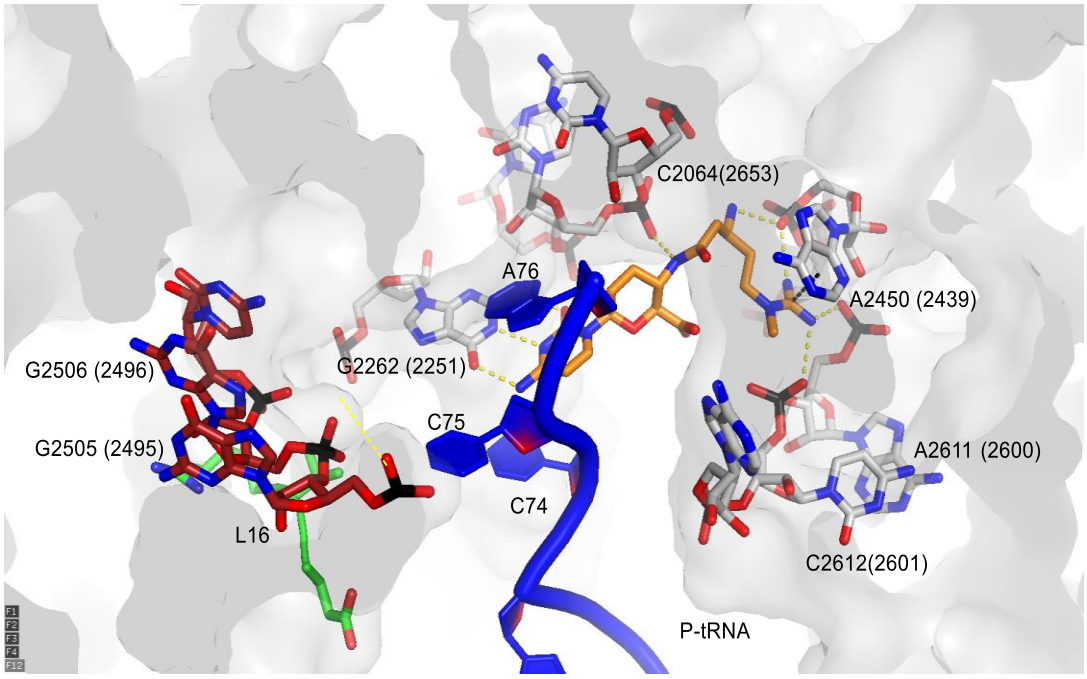

Figure 1.9 BlaS bound to 70S ribosome of *Thermus thermophilus* in the presence of P–tRNA

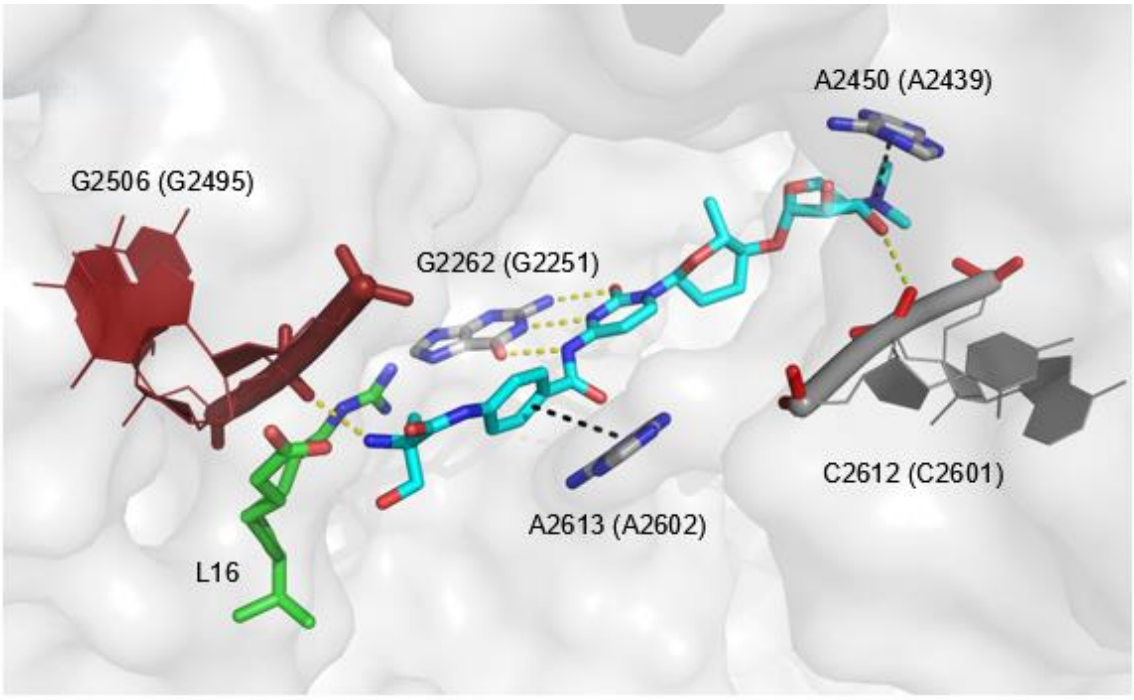

Figure 1.10 Molecular interactions of amicetin bound to 70S *Tth* ribosome

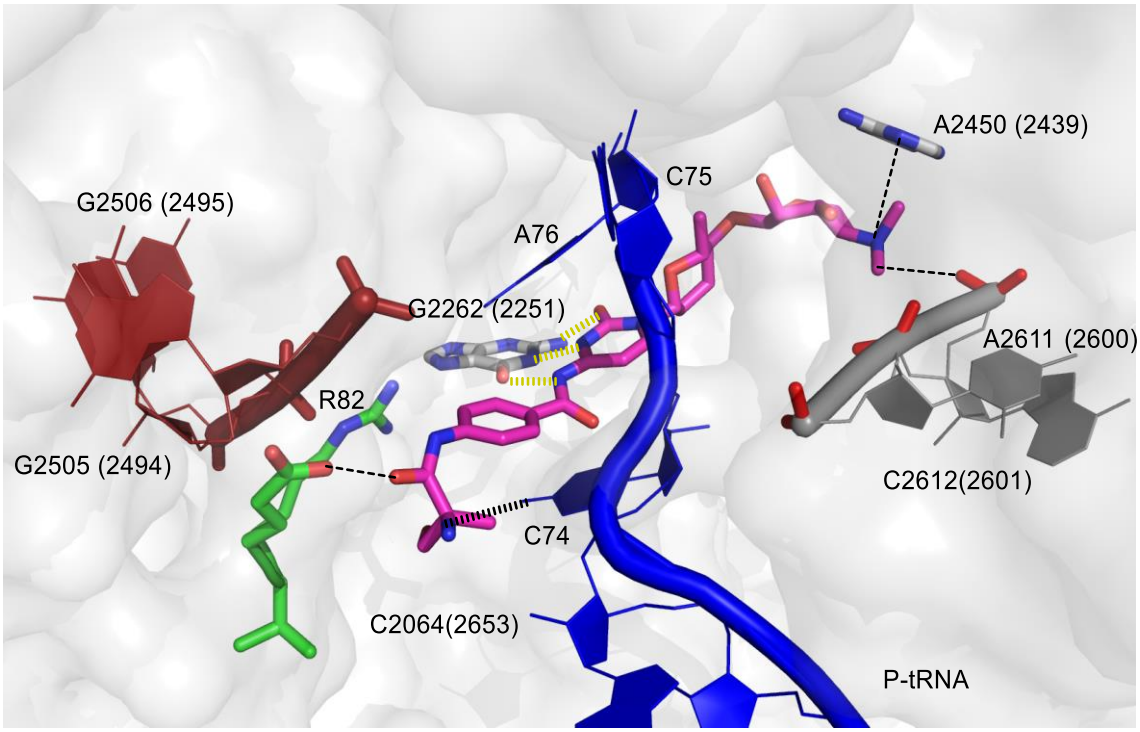

Figure 1.11 Amicetin bound to *Tth* 70S ribosome in the presence of P–tRNA

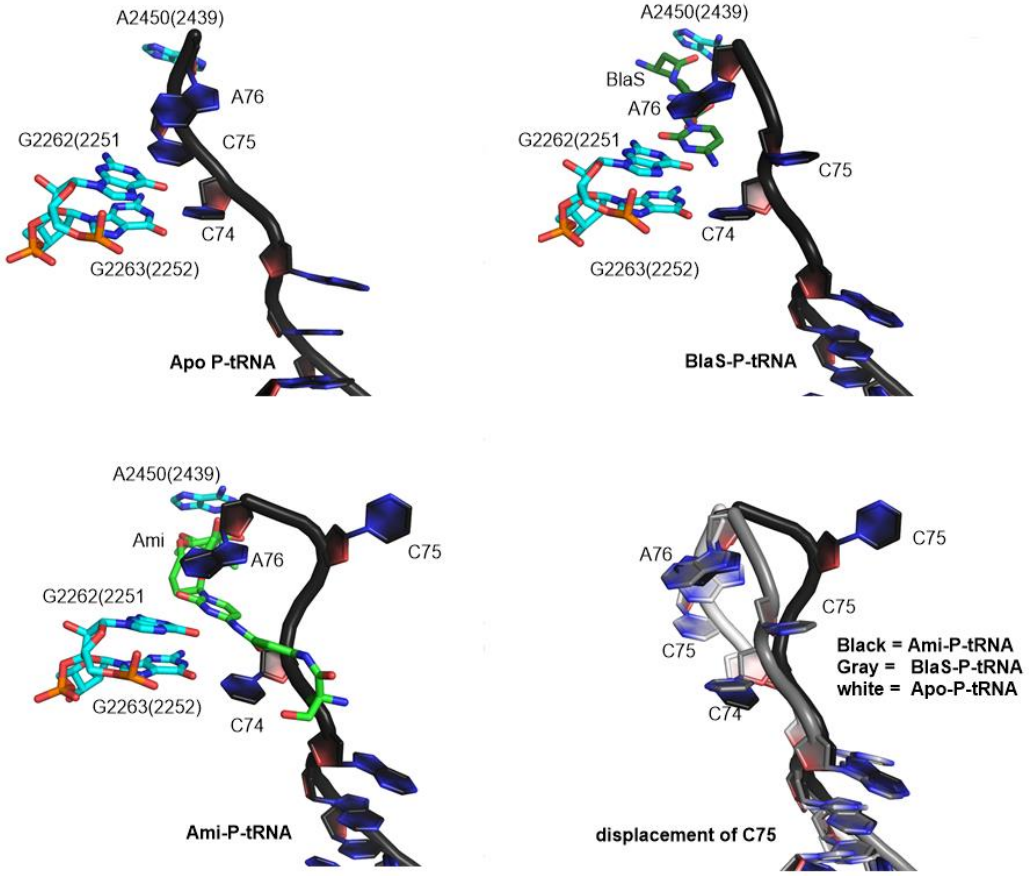

Figure 1.12 Displacement of C75 of 3’ CCA tail of P–tRNA

References

1) Daniel, T. M. History of Tuberculosis. *Resp. Med.* **2006**, *100*, 1862–1870.

2) Cave, A. J. E. The Evidence for the Incidence of Tuberculosis in Ancient Egypt. *Br. J. Tuberc.* **1939**, *33*, 142–52.

3) (a) Jardao, L.; Vieira, O. V. Tuberculosis: New Aspects of an Old Disease. *Int. J. Cell. Bio.* **2011**, *2011*, Article ID 403623, 1–13. (b) Wikipedia. https://en.wikipedia.org/wiki/History_of_tuberculosis (accessed July 30, 2016).

4) Koch, R. Die Aetiologie Der Tuberculose. *Berl. Klin. Wochenschr.* **1882,** *19*, 221–230.

5) Koch, R.; Brock, T. D.; Fred, E. B. The Etiology of Tuberculosis. *Rev. Infect. Dis.* **1982**, *4,* 1270–1274.

6) Cobbett, A. The Role of the Three Types of Tubercle Bacilli in Human and Animal Tuberculosis. The Lancet, **1922**, *199*, 973–983.

7) Lawn, S. D.; Zumla, A. I. Tuberculosis. *Lancet* **2011**, *378*, 57–72.

8) Golden P. M.; Vikram, R. H. Extrapulmonary Tuberculosis: An Overview. *Am. Fam. Physician.* **2005**, *72*, 1761–1768.

9) World Health Organization (WHO) End TB Strategy. http://www.who.int/tb/post2015_strategy/en/ (accessed July 30, 2016).

10) Houben, E. N.; Nguyen, L.; Pieters, J. Interaction of Pathogenic Mycobacteria with the Host Immune System. *Curr. Opin. Microbiol.* **2006**, *9*, 76–85.

11) World Health Organization (WHO) TB Report 2016. http://apps.who.int/iris/bitstream/10665/250441/1/9789241565394–eng.pdf?ua=1 (accessed July 30, 2016).

12) Centers for Disease Control and Prevention (CDC) TB Facts. http://www.cdc.gov/tb/topic/basics/default.htm (accessed July 31, 2016).

13) Centers for Disease Control and Prevention (CDC), Latent Tb and TB Disease. http://www.cdc.gov/tb/topic/basics/tbinfectiondisease.htm (accessed July 31, 2016).

14) (a) Acharjya, B.; Nayak, S. Mantoux Test and its Interpretation. *Indian Dermatol online J.* **2012**, *1*, 2–6. (b) Centers for Disease Control and Prevention (CDC), http://www.cdc.gov/tb/publications/factsheets/testing/skintesting.htm (accessed July 31, 2016).

15) Arlehamn, C. S. L.; Sidney, J.; Henderson, R.; Greenbaum, J. A.; James, E. A.; Moutaftsi, M.; Coler, R.; McKinney, D. M.; Park, D.; Taplitz, R.; Kwok, W. W.; Grey, H.; Peters, B.; Sette, A. Dissecting Mechanisms of Immunodominance to the Common TB Antigens ESAT-6, CFP10, Rv2031c (hspX), Rv2654c (TB7.7) and Rv1038c (EsxJ). *J. Immunol*. **2012**, *10*, 5020-5031.

16) Minnesota Department of Health. Tuberculosis (TB) Blood Test (IGRA). http://www.health.state.mn.us/divs/idepc/diseases/tb/factsheets/igra.html (accessed August 1, 2016).

17) Zhang, Y. The Magic Bullets and Tuberculosis Drug Targets. *Annu*. *Rev*. *Pharmacol*. *Toxicol*. ***2005***. *45*, *529*–64.

18) (a) Old and New TB Drugs: Mechanisms of Action and Resistance http://cdn.intechopen.com/pdfs–wm/28840.pdf (accessed July 31, 2016). (b) TBFACTS.ORG. Information about Tuberculosis. http://www.tbfacts.org/tb–drugs/ (accessed July 31, 2016). (c) Zumla, A.; Nahid, P.; Cole, S. T. Advances in the Development of New Tuberculosis Drugs and Treatment Regimens. *Nat. Rev. Drug Disc.* **2013**, *12*, 388.

19) Centers for Disease Control and Prevention (CDC) TB Facts. http://www.cdc.gov/tb/publications/ltbi/treatment.htm (accessed July 31, 2016).

20) Andrews. J. R.; Noubary. F.; Walensky, R. P.; Cerda, R.; Losina, E.; Horsburgh, C. R. Risk of Progression to Active Tuberculosis Following Reinfection with *Mycobacterium Tuberculosis. Clin. Infect. Dis.* **2012**, *54*, 784–191.

21) Chaisson, R. E.; Churchyard, G. J. Recurrent Tuberculosis: Relapse, Reinfection, and HIV. *J. Infect. Dis.* **2010**, *201*, 653–655.

22) Jurriaan E. M. S.; Gerjo J. K.; Marian T. T. K.; Verbrugha, H. A.; Hernandez–Pandob, R.; Leenenc, P. J. M.; Irma A. J. M.; Woudenberga, B. Relapse of Tuberculosis Versus Primary Tuberculosis; Course, Pathogenesis and Therapy in Mice. *Tuberculosis* **2013**, *93*, 213–221.

23) World Health Organisation (WHO): Global Task Force Outlines Measures to Combat XDR–TB Worldwide. http://www.who.int/mediacentre/news/notes/2006/np29/en/ (accessed July 30, 2016).

24) TB Alliance. https://www.tballiance.org/why–new–tb–drugs/inadequate–treatment (accessed July 30, 2016).

25) Migliori, G. B.; De Iaco, G.; Besozzi, G.; Centis, R.; Cirillo, D. M. First Tuberculosis Cases in Italy Resistant to All Tested Drugs. *Eurosurveillance* **2007**, *12*, 3194.

26) Velayati, A.; Masjedi, M. R.; Farnia, P.; Tabarsi, P.; Ghanavi, J.; Ziazarifi, A.

H.; Hoffner, S. E. Emergence of New Forms of Totally Drug–Resistant Tuberculosis Bacilli. Super Extensively Drug–Resistant Tuberculosis or Totally Drug–Resistant Strains in Iran. *Chest* **2009**, *136*, 420.

27) Udwadia, Z. F.; Amala, R. A.; Ajbani, K. K.; Rodrigues, C. Totally Drug–Resistant Tuberculois in India. *Clin. Infect. Dis.* **2012**, *54*, 579.

28) Mayer, K. H.; Hamilton, C. D. Synergistic Pandemics: Confronting the Global HIV and Tuberculosis Epidemics. http://cid.oxfordjournals.org/content/50/Supplement_3/ S67.full (accessed July 30, 2016).

29) MDR TB Transmission, HIV Coinfection, and Transmission Controle. Addressing the Threat of Drug–Resistant Tuberculosis: A Realistic Assessment of the Challenge: Workshop Summary. https://www.ncbi.nlm.nih.gov/books/NBK45004/ (accessed July 31, 2016).

30) Zumla, A.; Nahid, P.; Cole, S. T. Advances in the Development of New Tuberculosis Drugs and Treatment Regimens. *Nat. Rev. Drug Disc.* **2013**, *12*, 388.

31) Kwara, A.; Flanigan, T. P.; Carter E. J. Highly Active Antiretroviral Therapy (HAART) in Adults with Tuberculosis: Current Status. *Int. J. Tuberc. Lung Dis.* **2005**, *9*, 248–257.

32) Rathbun, R. C.; Liedtke, M. D. Antiretroviral Drug Interactions: Overview of Interactions Involving New and Investigational Agents and the Role of Therapeutic Drug Monitoring for Management. *Pharmaceutics* **2011**, *3*, 745–781.

33) Lopéz–Cortés, L. F.; Ruiz–Valderas, R.; Viciana, P.; Alarcón–González, A.; Gómez–Mateos, J.; León–Jimenez, E.; Sarasanacenta, M.; López–Pua, Y.; Pachón, J. Pharmacokinetic Interactions between Efavirenz and Rifampin in HIV–Infected Patients with Tuberculosis. *Clin. Pharmacokinet.* **2002**, *41*, 681–690.

34) Ribera, E.; Pou, L.; Lopez, R. M.; Crespo, M.; Falco, V.; Ocaña, I.; Ruiz, I.; Pahissa, A. Pharmacokinetic Interaction between Nevirapine and Rifampicin in HIV–Infected Patients with Tuberculosis. *AIDS* **2001**, *28*, 450–453.

35) Burman, W. J.; Jones, B. E. Treatment of HIV–Related Tuberculosis in the Era of Effective Antiretroviral Therapy. *Am. J. Respir. Crit. Care Med*. **2001**, *164*, 7–12.

36) American Thoracic Society Documents. American Thoracic Society/Centers of Disease Control and Prevention/Infectious Diseases Society of America. Treatment of Tuberculosis*. Am. J. Respir. Crit. Care Med.* **2003**, *167*: 603–662.

37) TB Alliance: Global Alliance for TB Drug Development. 2015. http://www.tballiance.org/downloads/Pipeline/TBA%20Pipeline%20Q1%202015

(accessed June 24, 2016).

38) Working Group on New TB Drugs — Discovery Portfolio Drug Pipeline. http://www.newtbdrugs.org/pipeline.php (accessed June 24, 2016).

39) Ma, Z.; Lienhardt, C.; McIlleron, H.; Nunn, A. J.; Wang, X. Global Tuberculosis Drug Development Pipeline: The Need and the Reality. *Lancet* **2010,** *375*, 2100–2109.

40) Sterling, T. R.; Villarino, M. E.; Borisov, A. S.; Shang, N.; Gordin, F.; Bliven–Sizemore, E.; Hackman, J.; Hamilton, C. D.; Menzies, D.; Kerrigan, A.; Weis, S. E.; Weiner, M.; Wing, D.; Conde, M. B.; Bozeman, L.; Horsburgh, C. R. Jr.; Chaisson, R. E. TB Trials Consortium PREVENT TB Study Team. Three Months of Rifapentine and Isoniazid for Latent Tuberculosis Infection. *N. Engl. J. Med.* **2011**, *365*, 2155–2166.

41) Lee, M.; Lee, J.; Carroll, M. W.; Choi, H.; Min, S.; Song, T.; Via, L. E.; Goldfeder, L. C.; Kang, E.; Jin, B.; Park, H.; Kwak, H.; Kim, H.; Jeon, H. S.; Jeong, I.; Joh, J. S.; Chen, R. Y.; Olivier, K. N.; Shaw, P. A.; Follmann, D.; Song, S. D.; Lee, J. K.; Lee, D.; Kim, C. T.; Dartois, V.; Park, S. K.; Cho, S. N.; Barry, C. E. 3rd. Linezolid for Treatment of Chronic Extensively Drug–Resistant Tuberculosis. *N. Engl. J. Med.* **2012**, *367*, 1508–1518.

42) 2014 Pipeline Report: Tuberculosis Drug Development Hobbles Forward. http://www.pipelinereport.org/sites/g/files/g575521/f/201407/TB%20Treatment (accessed June 26, 2016).

43) Food and Drug Administration (U.S.) Press Release. FDA Approves First Drug to Treat Multi– Drug–Resistant Tuberculosis. www.fda.gov/NewsEvents/ Newsroom/PressAnnouncements/ucm333695.htm (accessed Oct 20, 2016).

44) Mahajan, R. Bedaquiline: First FDA–Approved Tuberculosis Drug in 40 years. *Int. J. Appl. Basic Med. Res.* **2013**, *3*, 1–2. (b) Sirturo. https://www.sirturo.com/ (accessed June 20, 2016).

45) European Medicines Agency. Questions and Answers: Positive Opinion on the Marketing Authorisation for Deltyba (Delamanid) – Outcome of Re–examination. http://www.ema.europa.eu/docs/en_GB/document_library/Medicine_QA/human/002552/ WC500155462.pdf. **2013**. (b) TBFACTS.ORG. Information About Tuberculosis. http://www.tbfacts.org/delamanid/ (accessed June 20, 2016).

46) Hoffmann, H.; Kohl, T. A.; Hoffmann–Thiel, S.; Merker, M.; Beckert, P.; Jaton, K.; Nedialkova, L.; Sahalchyk, E.; Rothe, T.; Keller, P. M.; Niemann, S. Delamanid and Bedaquiline Resistance in Mycobacterium Tuberculosis Ancestral Beijing Genotype Causing Extensively Drug–Resistant Tuberculosis in a Tibetan Refugee. *Am. J. Respir. Crit. Care Med*. **2016**, *193*, 337–339.

47) DeBoer, C.; Caron, E. L.; Hinman, J. W. Amicetin, a New *Streptomyces* Antibiotic. *J. Am. Chem. Soc.* **1953,** *75*, 499–500.

48) U of U Screening.

49) Rifampicin –CYP–Induction.

50) DeBoer, C.; Caron, E. L.; Hinman, J. W. Amicetin, a New *Streptomyces* Antibiotic. *J. Am. Chem. Soc.* **1953,** *75*, 499–500.

51) Hinman, J. W.; Caron, E. L.; DeBoer, C. The Isolation and Purification of Amicetin. *J. Am. Chem. Soc.* **1953**, *75*, 5864–5866.

52) McCormick, M. H.; Hoehn, M. M. Isolation of a New Antibiotic from *Streptomyces Fasciculatis* nov. sp. *Antibiot. Chemother.* **1953**, *3*, 718–720.

53) Hinuma, Y.; Kuroya, M.; Yajima, T.; Ishihara, K.; Hamada, S.; Watanabe, K.; Kuchi, K. Antibiotic Substances from Actinomycetes. XXXVI. An Amicetin (Sacromycin) from *Streptomyces* sp. No. 5223. *J. Antibiot.* **1955**, *8A*, 148–152.

54) Haskell, T. H.; Ryder, A.; Frohardt, E. P.; Fusari, S. A.; Jakubowski, Z. L.; Bartz, Q. R. Isolation and Characterization of Three Crystalline Antibiotics from *Streptomyces Plicatus*. *J. Am. Chem. Soc.* **1958**, *80*, 743–747.

55) Tatsuoka, S.; Nakazawa, K.; Inoue, M.; Fujii, S. Antibiotics. V. Extraction and Physicochemical Properties of Allomycin, an Antituberculous Antibiotic, and its Identity with Amicetin. *Yakugaku Zasshi* **1955**, *75*, 1206–1208.

56) Stevens, C. L.; Gasser, R. J.; Mukherjee, T. K.; Haskell, T. H. The Structure of Amicetin. A New Dimethylamino Sugar. *J. Am. Chem. Soc.* **1956**, *78*, 6212.

57) Stevens, C. L.; Nagarajan, K.; Haskell, T. H. The Structure of Amicetin. *J. Org. Chem.* **1962**, *27*, 2991, 3007.

58) Flynn, E. H.; Hinman, J. W.; Caron, E. L.; Woolf, D. O. The Chemistry of Amicetin, a New Antibiotic. *J. Am. Chem. Soc.* **1953**, *78*, 5867–5871.

59) Stevens, C. L.; Blumbergs, P.; Daniher, F. A. Stereochemistry and Synthesis of Amosamine: 4,6–dideoxy–4–dimethylamino–D–glucose. *J. Am. Chem. Soc.* **1963**, *85*, 1552–1553.

60) Stevens, C. L.; Blumbergs, P.; Wood, D. L. Stereochemical Identification and Synthesis of Amicetose and the Stereochemical Identification of Rhodinose and the Sugar from Streptolydigin. *J. Am. Chem. Soc.* **1964**, *86*, 3592–3594.

61) Hanessian, S.; Haskell, T. Configuration of the Anomeric Linkages in Amicetin.

Tetrahedron **1964**, *5*, 2451–2460.

62) Smith, J. L.; Sundaralaingam, M. The Structure of the Antibiotic Amicetin Consisting of Nucleobase, Disaccharide and Amino Acid Moieties. *Acta Crystallogr. Sect. B: Struct. Crystallogr. Cryst. Chem.* **1981**, *B37*, 1095–1101.

63) DeBoer, C.; Caron, E. L.; Hinman, J. W. Amicetin, a New *Streptomyces* Antibiotic. *J. Am. Chem. Soc.* **1953***, 75*, 499–500.

64) Stevens, C. L.; Nagarajan, K.; Haskell, T. H. The Structure of Amicetin. *J. Org. Chem.* **1962**, *27*, 2991, 3007.

65) Bloch, A.; Coutsogeorgopoulos, C. Inhibition of Protein Synthesis by Amicetin, a Nucleoside Antibiotic. *Biochemistry* **1966***, 5*, 3345–3351.

66) Cerna, J.; Rychlik, I.; Lichtenhaler, F. W. The Effect of the Aminoacyl–4–aminohexosyl–cytosine Group of Antibiotics on Ribosomal Peptidyl Transferase. *FEBS Lett.* **1973**, *30*, 147–150.

67) Lichtenhaler, F. W.; Cerna, J.; Rychlik, I. The Effect of Oxamicetin and Some Amicetin Analogs on Ribosomal Peptidyl Transferase. *FEBS Lett.* **1975**, *53*, 184–187.

68) Leviev. I.; Rodriguez–Fonseca, C.; Phan, H.; Garrett, R. A.; Heilek, G.; Noller, H. F.; Mankin, A. S. A Conserved Secondary Structural Motif in 23S rRNA Defines the Site of Interaction of Amicetin, a Universal Inhibitor of Peptide Bond Formation. *Eur. Mol.Biol. Org. J.* **1994***, 13*, 1682–1686.

69) (a) Fox, J. J. Watanabe, K.A.; Bloch, A. Nucleoside Antibiotics. *Prog. Nucleic Acid Res. Mol. Biol.* **1966**, *5*, 251–313. (b) Isono, K. Nucleoside Antibiotics: Structure, Biological Activity, and Biosynthesis. *J. Antibiot.* **1988**, *41*, 1712–1739.

70) (a) Lichtenthaler, F. W.; Trummlitz, G. Structural Basis for the Inhibition of Protein Synthesis by the Aminoacyl–aminohexosyl–cytosine Group of Antibiotics. *FEBS Lett.* **1974**, *38*, 237–242. (b) Barbacid, M.; Vasquez, D. [G–^{3}H] Gougerotin Binding to Ribosomes: Heterogeneity of Eukaryotic Ribosomes. *European Journal of Biochemistry* **1974**, *44*, 445–453. (c) Hansen, J. L.; Moore, P. B.; Steitz, T. A. Structures of Five Antibiotics Bound at the Peptidyl Transferase Center of the Large Ribosomal Subunit. Journal of Molecular Biology **2003**, *330*, 1061–1075. (d) Yukioka, M.; Morisawa, S. Studies on the Mechanism of Action of Gougerotin: (II) Effect of Various Factors on Gougerotin Action. *J. Biochem*. **1969**, *66*, 233–240.

71) (a) Funabashi, Y.; Tsubotani, S.; Koyama, K.; Katayama, N.; Harada, S. A New Anti–MRSA Dipeptide, TAN–1057 A. *Tetrahedron* **1993**, *49*, 13–28. (b) E. Limburg, R. Gahlmann, H. P. Kroll, and D. Beyer. Ribosomal Alterations Contribute to Bacterial Resistance Against the Dipeptide Antibiotic TAN 1057. *Antimicrob.*

Agents Chemother. **2004**, *48*, 619–622.

72) Brock, T. D. Effect of Antibiotics and Inhibitors on M Protein Synthesis. *J. Bacteriol.* **1963**, *85*, 527–531.

73) Coutsogeorgopoulos, C. Aminoacylnucleoside Inhibitors of Protein Synthesis. The Effect of Amino Acyl Ribonucleic Acid on the Inhibition. *Biochemistry* **1967**, *6*, 1704–1711.

74) Pestka, S. Studies on the Formation of Transfer Ribonucleic Acid–Ribosome Complex, XI. Antibiotic Effects on Phenylalanyl–oligonucleotide Binding to Ribosomes. *Proc. Nat. Acad. Sci.* **1969**, *64*, 709–714.

75) Pestka, S. Studies on Transfer Ribonucleic Acid–Ribosome Complexes, X. Phenylalanyl–oligonucleotide Binding to Ribosomes and the Mechanism of Chloramphenicol Action. *Biochem. Biophys. Res. Comm.* **1969**, *36*, 589–595.

76) Tompkins, R. K.; Scolnick, E. M.; Caskey, C. T. Peptide Chain Termination, VII. The Ribosomal Release Factor Requirements for Peptide Release. *Proc. Nat. Acad. Sci.* **1970**, *65*, 702–708.

77) Your Genome Organization. http://www.yourgenome.org/facts/what–is–the–central–dogma (accessed June 30, 2016).

78) Easy Biology Class. http://www.easybiologyclass.com/difference–between–prokaryotic–and–eukaryotic–translation/ (accessed June 30, 2016).

79) Major Differences. http://www.majordifferences.com/2013/10/prokaryotic–vs–eukaryotic–ribosomes–70s.html# (accessed June 30, 2016).

80) Wilson, D. N. Ribosome–Targeting Antibiotics and Mechanism of Bacterial Resistance. *Nature Rev. Microbiol,* **2014**, *12*, 35–48.

81) Hong, W.; Zeng, J.; Xie, J. Antibiotic Drugs Targeting Bacterial RNAs. *Acta. Pharma. Sin. B*. **2014**, *4*, 258–265.

82) Dahlberg, A. E. The Functional Role of Ribosomal RNA in Protein Synthesis. *Cell* **1989**, *57,* 525–529.

83) Mankin, A. S. Ribosomal Antibiotics. *Molecular Biology* **2001**, *33*, 509–520.

84) Palade, G. E. A Small Particulate Component of the Cytoplasm. *J. Biophys. Biochem. Cytol.* **1955**, *1,* 59–68.

85) Poehlsgaard, J.; Dowthwaite, S. The Bacterial Ribosome as a Target for Antibiotics. *Nature Rev*. **2005**, *3*, 870–881.

86) Wilson, D. N.; Nierhaus, K. H. Ribosomal Proteins in the Spot Light. *Crit. Rev. Biochem. Mol. Biol.* **2005**, *40*, 243–267.

87) Yusupov, M. M.; Garber, M. B.; Vasiliev, V. D.; Spirin, A. S. Thermus Thermophilus Ribosomes for Crystallographic Studies. *Biochimie* **1991**, *73*, 887–897.

88) Ban, N.; Nissen, P.; Hansen, J.; Moore, P.B.; Steitz, T. A. The Complete Atomic Structure of the Large Ribosomal Subunit at 2.4 A˚ Resolution. *Science* **2000**, *289*, 905–920.

89) Wimberly, B.T.; Brodersen, D. E.; Clemons Jr, W. M.; Morgan–warren, R. J.; Carter, A. P.; Vonrhein, C.; Hartsch, T.; Ramakrishnan, V. Structure of the 30S Ribosomal Subunit. *Nature* **2000**, *407*, 327–339.

90) Yusupov, M. M.; Yusupova, G. Zh.; Baucom, A.; Liberman, K.; Earnest, T. N.; Cate, J. H.; Noller. H. F. Crystal Structure of the Ribosome at 5.5 A˚ Resolution. *Science* **2001**, *292*, 883–896.

91) Schuwirth, B.S.; Borovinskaya, M. A.; Hau, C. W.; Zhang, W.; Vila–Sanjurjo, A.; Holton, J. M.; Doudna Cate, J. H. Structures of the Bacterial Ribosome at 3.5 A˚ Resolution. *Science* **2005**, *310*, 827–834.

92) Ban, N.; Nissen, P.; Hansen, J.; Moore, P.B.; Steitz, T. A. The Complete Atomic Structure of the Large Ribosomal Subunit at 2.4 A˚ Resolution. *Science* **2000**, *289*, 905–920.

93) Schluenzen, F.; Tocilj, A.; Zarivach, R.; Harms, J.; Gluehmann, M.; Janell, D.; Bashan, A.; Bartels, H.; Agmon, I.; Franceshi, A.; Yonath, A.Structure of Functionally Activated Small Ribosomal Subunit at 3.3 Angstroms Resolution. Cell **2000**, *102*, 615–623.

94) Wimberly, B.T.; Brodersen, D. E.; Clemons Jr, W. M.; Morgan–warren, R. J.; Carter, A. P.; Vonrhein, C.; Hartsch, T.; Ramakrishnan, V. Structure of the 30S Ribosomal Subunit. *Nature* **2000**, *407*, 327–339.

95) Yusupov, M. M.; Yusupova, G. Zh.; Baucom, A.; Liberman, K.; Earnest, T. N.; Cate, J. H.; Noller. H. F. Crystal Structure of the Ribosome at 5.5 A˚ Resolution. *Science* **2001**, *292*, 883–896.

96) Schuwirth, B.S.; Borovinskaya, M. A.; Hau, C. W.; Zhang, W.; Vila–Sanjurjo, A.; Holton, J. M.; Doudna Cate, J. H. Structures of the Bacterial Ribosome at 3.5 A˚ Resolution. *Science* **2005**, *310*, 827–834.

97) Selmer, M.; Dunham, C. M.; Murphy IV, F. V.; Weixlbaumer, A.; Petry, A.; Kelly, A. C.; Weir, J. R.; Ramakrishnan, V. Structure of the 70S Ribosome Complexed with mRNA and tRNA. *Science* **2006**, *313*, 1935–1942.

98) Korostelev, A.; Trakhanov, S.; Laurberg, M.; Noller, H. F. Crystal Structure of a 70S Ribosome–tRNA Complex Reveals Functional Interactions and Rearrangements. *Cell* **2006**,*126*, 1065–1077.

99) Yusupova, G.; Jenner, L.; Rees, B.; Moras, D.; Yusupov, M. Structural Basis for Messenger RNA Movement on the Ribosome". *Nature* **2006**, *444*, 391–394.

100) Noble Prize Organization. https://www.nobelprize.org/nobel_prizes/ chemistry/laureates/2009/ advanced–chemistryprize2009.pdf (accessed July 2, 2016).

101) Polacek, N.; Gomez, M. J.; Ito, K.; Xiong, L.; Nakamura, Y.; Mankin, A. The Critical Role of the Universally Conserved A2602 of 23S Ribosomal RNA in the Release of the Nascent Peptide during Translation Termination. *Mol. Cell*. **2003**, *11*, 103–111.

102) Yamaguchi, H.; Yamamoto, C.; Tanaka, N. Inhibition of Protein Synthesis by Blasticidin S. I. Studies with Cell–Free Systems from Bacterial and Mammalian Cells. *J. Biochem*. **1965**, *57*, 667–677.

103) Hansen, J. L.; Moore, P. B.; Steitz, T. A. Structures of Five Antibiotics Bound at the Peptidyl Transferase Center of the Large Ribosomal Subunit. *J. Mol. Biol*. **2003**, *330*, 1061–1075.

104) Svidritskiy, E.; Ling, C.; Ermolenko, D. N.; Korostelev, A. A. Blasticidin S Inhibits Translation by Trapping Deformed tRNA on the Ribosome. *Proc. Natl. Acad. Sci. USA.* **2013**, *110*, 12283–12288.

105) Serrano, C. M. Synthetic and Biological Studies on Amicetin and its Analogues toward the Development of New Anti–mycobacterial Agents. Ph. D. Dissertation, University of Utah, Salt Lake City, Utah, **2016**.

106) (a) Polikanov, Y. S.; Blaha, G. M.; Steitz, T. A. How Hibernation Factors RMF, HPF, and YfiA Turnoff Protein Synthesis. *Science* **2012**, *336*, 915–918. (b) Winn, M. D.*;* Ballard, C. C.; Cowtan, K. D.; Dodson, E. J.; Emsley, P.; Evans, P. R.; Keegan, R. M.; Krissinel, E. B.; Leslie, A. G. W.; McCoy, A. J.; McNicholas, S. J.; Murshudov, G. N.; Pannu, N. S.; Potterton, E. A.; Powell, H. R.; Read, R. J.; Vagin, A.; Wilson, K. S. Overview of the CCP4 Suite and Current Developments. *Acta Crystallogr., Sect. D: Biol. Crystallogr.* **2011**, *D67*, 235–242. (c) Kabsch, W. Xds. *Acta Crystallog.Sect. D: Biol. Crystallogr*. **2010**, *66*, 125–132.

107) Emsley, P.; Lohkamp, B.; Scott, W. G.; Cowtan, K. D. Features and Development of Coot. *Acta Crystallogr. Sect. D: Biol. Crystallogr.* **2010**, *D66*, 486–501.

108) (a) Adams, P. D.; Afonine, P. V.; Bunkóczi, G.; Chen, V. B.; Davis, I. W.; Echols, N.; Headd, J. J.; Hung, L. W.; Kapral, G. J.; Grosse–Kunstleve, R. W.;

McCoy, A. J.; Moriarty, N. J.; Oeffner, R.; Read, R. J.; Richardson, D. C.; Richardson, J. S. Terwilliger, T. C.; Zwarta, P. H. PHENIX: A Comprehensive Python–Based System for Macromolecular Structure Solution. *Acta Crystallogr. Sect. D: Biol. Crystallogr.* **2010**, *D66*, 213–221. (b) Schuttelkopf, A. W.; van Aalten, D. M. PRODRG: A Tool for High–Throughput Crystallography of Protein–Ligand Complexes. *Acta Crystallogr. Sect. D: Biol. Crystallogr.* **2004**, *60*, 1355–1363.

CHAPTER 2

FIRST GENEREATION ANALOGS

Hydrolytic Stability of Amicetin

Tuberculosis (TB) is a highly contagious airborne bacterial infection and is one of the greatest health threats to the current population as a whole.[1, 2, 3] To address this growing public health issue, the Looper lab launched a campaign of small molecule screening at the University of Utah, and identified a natural product amicetin, a known protein synthesis inhibitor active against drug resistant *Mtb* H37Ra, as a promising lead. Apart from the promicing antimycobacterial activity associated with amicetin, the biggest liabilities are its structural complexicity and hydrolytic stability. Amicetin has also been noted to be highly unstable in acidic and alkaline solutions leading to degradation products cytimidine and cytosamine, respectively, which are 100–fold less potent than amicetin (Figure 2.1).[4, 5, 6] Most notably, due to the presence of highly acid labile cytosine–glycol linkage, amicetin is chemically unstable and remains a poor drug candidate. To confer stability in the gut, oral bioavailability, and synthetic feasibility, redesigning and simplifying the complicated disaccharide portion of amicetin is required. Our quest to increase the potency and therapeutic properties of amicetin and synthesize more potent and synthetically fesible amicetin derivatives stimulated us to design a simplified pharmacophore and develop convergent approach towards their synthesis.

Experimental Design of Simplified Pharmacophore

In an effort to reorganize the disaccharide portion and design a simplified pharmacophore, we note that in a review by Fox and co–workers on nucleoside antibiotics it was stated that “for any aminoacyl nucleosides antibiotics capable of inhibiting protein synthesis will have an accessible amino acid moiety attached to a carrier nucleoside, this in turn attached to another basic center at the end of the molecule.”[7] One basic center is the amine of the amino acid (α–methyl serine), and the other can be a nitrogen of the nucleobase (the dimethyl amino moiety in the disaccharide unit in the case of amicetin).

In addition to Fox’s statement, later in 1973 Lichtenthaler et al. in their studies on structural basis for inhibition of protein synthesis by the cytosine group of antibiotics hypothesized that the spacing of cationic amine of amino acid tethered to the nitrogen of nucleobase by molecular linker (hexose sugar of blasticidin S (BlaS) and gougerotin, and *p*–aminobenzoic acid of amicetin) is important for exhibiting translational inhibitory function.[1, 2, 3] This resulted in an assumption that the accessible amino acid α–methyl serine moiety of amicetin would mimic the sarcosine in gougerotin, *N*–methyl–guanidine unit in BlaS as shown in Figure 2.2. If this overlap were true, it would suggest that cytimidine that constitutes the requisite structural elements except the amine terminus on the other end would be active with a tethered amine (Figure 2.2).[8]

Cytosine–based protein synthesis inhibitors

Most of the cytosine–based antibiotics (amicetin, BlaS, gougerotin) are in agreement with Fox and Lichtenthaler's statement. However, TAN–1057 A–D, a class of translational inhibitors isolated from flexi bacteria, in contradiction to Fox's statement, lacks both a sugar moiety attached to nucleobase and a formal nitrogenous base. TAN 1057 A–B, however, have an isocytosine that mimics cytosine. In partial agreement with Fox's statement, TAN 1057 A–B have two basic centers at either terminus of isocytosine (urea functionality on and an accessible amino acid β–homoarginine).[9]

In perspective of TAN 1057's simple structural features (nonglycosidic linker in particular), compared to other cytosine nucleoside antibiotic agents, we expect that the amicetin analogs with cationic amine attached to a less complex, and more stable alkyl linkers to show translational inhibition properties (Figure 2.3). With the above assumption, we focused our efforts on the design of a simplified pharmacophore model for the analogs synthesis.

To address all the contradictions and assumptions we plan to synthesize simplified amicetin analogs based on hypothetical simplified pharmacophore possessing a basic group (amine) attached via a linker to one side of the nucleobase (cytosine core) which in turn attached to a dipeptide portion (cap region) with an accessible amino acid on the other side of the cytosine (Figure 2.3).

In our approach toward the design and synthesis of amicetin analogs, we planned to safeguard the cytimidine segment of amicetin, which possess the requisite nucleobase (cytosine), and an accessible amino acid (α–methyl serine)

as cationic terminus (cap region). This conceptually prompts an SAR study on the disaccharide portion of amicetin and synthesis of focused library of analogs, re–engineering the sugar moiety and studying their activity against MDR–TB, cytotoxicity and compatibility with ART. We supplanted the disaccharide with non–hydrolysable linkers to investigate conceivable varieties of cationic tails and spacer linkers. Replacing the sugar moiety with an alkyl chain also streamlines potential synthetic challenges.

To test the hypothesis of a simplified pharmacophore, synthesis of dimethyl amino polyethylene glycol (PEG) derivatives of amicetin **11** were designed. PEG linkers (spacers) are the best–known substitutes for disaccharides and have previously been used in antiretroviral and antibacterial chemical entities.[10] Also, the PEG derivatives designed mimic the chain length of disaccharide and position the cationic amine at a similar distance to diamine of the amicetin (Figure 2.4).

Retrosynthetic Analysis of Simplified Amicetin Analogs

A retrosynthetic approach of future designed analogs is depicted in Scheme 2.1. We envisioned two different routes to access the designed amino alkyl cytimidine analogs, the first route being route A; the *N*1–alkylation of cytosine with alkyl halides (linker) followed by a peptide coupling reaction of *N1*– alkylated cytosine (**1**) with PABA derivative (**2**). The PABA derivative could be synthesized via a Buchwald amidation[11] of 4–iodomethyl benzoate and protected α–methyl serine carboxamide (**3**)[11, 12, 13] that in turn would be synthesized from a commercially available serine methyl ester hydrochloride. The alternative method (route B) for the synthesis of amicetin analogs involves the *N1* alkylation of

protected cytimidine (**4**) with requisite alkyl halides / mesylate (linker/spacer). The protected cytimidine can be synthesized by employing a Buchwald–Hartwig amidation reaction of α–methylserine carboxamide (**3**) and aryliodide (**5**). The aryl iodide itself is a peptide coupled product of *p*–Iodobenzoic acid and aminopyrimidine (**6**).[14]

Synthesis of α–methylserine carboxamide

We first focused our efforts on the synthesis of carboxamide **3,** employing Seebach's chemistry and improvising on a reported procedure by Dr. Serrano in the Looper group**.**[12, 13] The carboxamide **3** corresponding to α–methylserine synthesis began with condensation of commercially available L–serine methyl ester hydrochloride (**3a**) with pivaladehyde to form oxazolidine **3b** which was further protected using Boc anhydride to give *N*–Boc oxazolidine **3c** as a single diasteromer. Diastereoselective α–methylation of **3c** employing Seebach's memory of chirality,[11] formed **3d** and subsequent saponification of ester **3d** yielded the acid **3e** in excellent yield and >95:5 *dr***.** The acid **3e** was peptide coupled with ammonium chloride using HATU and DIPEA in DMF to form carboxamide **3** (Scheme 2.2**).**

Synthesis of polyethylene glycol analogs of amicetin

The synthesis of PEG analogs began with the *N*1–pegylation of cytosine with PEG linker **8** (amino PEG chloride), which was formed by chloride displacement in *bis*(2–chloroethoxy) ethane **1a** with dimethyl amine (Scheme 2.3). In another reaction sequence, the peptide-coupling partner (PABA derivative) was

synthesized by a sequence of Buchwald amidation and saponification of the resultant monopeptide. The protected α–methylserine carboxamide **3** was then treated with 4–iodomethyl benzoate under Buchwald–Hartwig amidation conditions to result in the formation of monopeptide **10**.[11] The resultant mono–peptide **10** was saponified to yield acid **11** (Scheme 2.3).

With both alkylated cytosine **9** and acid **11** in hand, we proceeded to setup a peptide coupling reaction to synthesize the dipeptide **12**. The peptide coupling of amine **9** and acid **11** provided protected PEG derivative **12,** which on final global de–protection with trifluoro acetic acid (TFA) yielded the analog **HKR–01–084 (12L)** (Scheme 2.3).

Biological evaluation of PEG analogs of amicetin

Both enantiomers (D and L) of α–methyl serine were successfully synthesized using the similar protocol (Scheme 2.3) and tested for their activity against *Mtb*–H37Ra. The analog of natural enantiomer (*S*)– (–) **HKR–01–084** showed 43% of growth inhibition at 100µg/mL and the other enantiomer (*R*)– (+) **HKR–01–090** showed 49% of inhibition at 100µg/mL. More importantly, both the compounds were more active than cytimidine (inactive at 100 µg/mL) which lacks any kind of substitution on N^1–cytosine. With these encouraging results, our immediate plan was to synthesize similar analogs devoid of amine (cationic tail), and analogs with short linkers to clearly understand the importance of amine and the linker length.

The compounds shown in Figure 2.5 were synthesized using a protocol similar to that shown in Scheme 2.3.

To strengthen our hypothesis of the simplified pharmacophore model, the analog **HKR–01–180** without a pendent amine was inactive (no measurable activity at 100 μg/mL) when tested against *Mtb*–H37Ra. Similarly, the analog **HKR–01–186** where the amine is positioned six atoms (compared to nine atoms in active analog) apart from N^1 of cytosine is slightly less active (34% inhibition compared to 49%), suggesting the importance of cationic amine tether, linker length, and position of amine for biological activity.

Altering the length of the linker in amicetin analogs

At this point, we were unsure about the optimum length for the linker to be an effective protein synthesis inhibitor. Our plan was to synthesize a set of analogs with different linker lengths with different functional groups and investigate their role in biological activity. For quick access to the analogs with a diverse a set of linkers, our strategy was to synthesize the common intermediate cytimidine and exploit the acidic nature of N^1–cytosine proton (pK_a = ~12.2) for alkylations and propargyl cytimidine **12** as a common precursor for diversity generating reactions (A^3 –coupling, and N^1–cytosine alkylations).

Note: All the first generation analogs are synthesized and tested in one lot except **HKR–02–058, HKR–02–059, and HKR–02–061.**

Synthesis of Protected Cytimidine and Propargyl Cytimidine

The protected cytimidine was synthesized through a sequence of reactions on readily available 4–amino–2–chloro pyrimidine. Nucleophilic displacement of 4–amino–2–chloropyrimidine with benzyl alcohol gave 4–amino–2–benzyloxy

pyrimidine **13**. Reaction of **13** with *in situ* generated 4–iodobenzoylchloride resulted in the formation of monopeptide **14,** which was further reacted with carboxamide **3** under Buchwald amidation conditions to form fully protected cytimidine **15**. Careful debenzylation results in protected cytimidine **16**. Propargylation of protected cytimidine **16** with propargyl bromide yielded the common intermediate propargyl cytimidine **17** (Scheme 2.4).[13,15]

Alternate synthetic procedure for protected cytimidine

After gaining a better understanding of the nature and solubility of the cytosine, and cytosine derivatives (propargyl cytosine), the synthesis of the protected cytimidine and propargyl cytimidine was achieved in an expedient and efficient manner using feed stock chemicals with fewer steps by deploying alternative peptide coupling reactions and saponification. The PABA adduct **11** was synthesized via a sequence of peptide coupling reaction of *p*–aminomethyl benzoate and carboxylic acid **3e**, which gives ester **10.** Hydrolysis of **10** produces acid **11**. The propargyl cytosine is prepared from cytosine using tetrabutyl ammoniumhydroxide and propargyl bromide in dichloromethane as shown in Scheme 2.5.[16] The cytosine or propargyl cytosine dissolved in DMSO (only solvent that dissolves cytosine or propargyl cytosine at higher temparatures) is peptide coupled with the α–methylserine coupled PABA adduct (**11**) to form protected cytimidine **16** and propargyl cytimidine **17,** respectively (Scheme 2.5).

A^3–coupling

With the key precursor propargyl cytimidine **17** in hand, we proceeded to explore the utility of **17** to carry out multicomponent coupling reactions, such as A^3– coupling (A^3= alkyne/aldehyde/amine). It is noteworthy that all the efforts to carry out three components coupling reaction using regular protocol by employing (Cu(I)) salts failed with our substrates (alkyl alkyne). Adapted reaction conditions of a reported protocol by Cravotto et al. in their synthesis of umbelliferon aminoalkyl derivatives using $Cu(OAc)_2$ under microwave conditions were successful and resulted in the formation of A^3– coupled products in good yields (Scheme 2.6).[17]

Three component coupling of propargyl cytimidine **17**, paraformaldehyde, and *N,N,N*'–trimethyl ethylenediamine (A^3 –coupling) resulted in the formation of **18** (Scheme 2.5). Global deprotection of A^3 –coupled product **18** using TFA in dichloromethane yielded amino alkyl derivative of amicetin **19** (scheme 2.6)**.** Compounds shown in Figure 2.6 with different tethered amines were synthesized following a protocol similar to that shown in Scheme 2.6.

Synthesis of analogs with increased cLogP

Efforts are being focused on incresing the cLogP and reducing the number of basic amines of the amicetin analogs. We also plan to synthesize tethered carboxylic acids and amines on cytimidine, and derivetize them to peptides as in gougerotin. The next set of analogs synthesized were envisioned to have two basic amines (cationic cap and tail) at either termini of the molecule.

The amide analogs synthesis began with petide bond formation between

Boc–L–proline and bromopropylamine hydrobromide via a carbonic acid anhydride formation on Boc–L–proline, which resulted in tethered alkyl bromide **20**. Cytosine *N*^{1}–alkylation with the resultant alkyl bromide **20** gave alkylated cytosine **21**. Peptide coupling reaction between alkylated cytosine **21** and *N*–acyl PABA **11** resulted in protected tripeptide **22** formation. Global deprotection yields the analog **HKR–02–014 (23)** as trifluoroacetate salt (Scheme 2.7).[18]

The alanyl amide analogs of amicetin (Figure 2.10) was synthesized using a protocol similar to that shown in Scheme 2.7. The synthesized analogs were tested for their protein synthesis inhibition activity.

With the aim of reducing the number of basic amines and having diverse class of linker (length / amine) the amide derivatives of amicetin were targeted and synthesized via alkylation on *N*1 of cytosine in protected cytimidine with an activated alkyl halide methyl bromoactate. It's important to note that the alkylations on protected cytimidine with activated alkyl halides result in better yields with fewer byproducts compared to nonactivated alkyl halides. Also, the unactivated alkyl halides required harsh conditions (heating >80 ^{o}C) which eventually results in unwanted products in the reaction.

The synthesis of targeted analogs began with alkylation of cytimidine with an α–bromo ester followed by saponification of resultant ester **23** afforded the acid **24** in acceptable yields, along with cleaving the base labile amide bond to give byproducts acid **11**, and cytosine acetic acid. The resultant carboxyllic acid was peptide coupled with *N,N',N'*–trimethylethylenediamine resulting in tripeptide **25,** up on global deprotection yielded **HKR–02–019 (25F)** as shown in Scheme 2.8.

Analog **HKR–02–020** was synthesized using the similar protocol shown in **HKR–02–019** (Scheme 2.8), using 3–aminomethyl–Boc–piperidine as peptide coupling partner. Having worked on SAR studies on dibasic (cationic cap and tail regions) amine derivatives and their associated protein synthesis inhibition activities, more efforts are focused on increasing the linker length and cLogP of the analogs limiting the number of basic amines.

For increasing the spacer length consisting of only two basic amines, we thought of synthesizing aryl amides. For the synthesis of aryl amides with pendant amines, the two key reactions employed were peptide coupling and Sonogashira cross coupling using propargyl alcohol.

The targeted analogs synthesis began with a peptide coupling reaction of *p*–iodobenzoic acid with 4–*N*–Boc–amino–piperidine resulting in arylamide **26**, which under Sonogashira cross coupling conditions with propargyl alcohol produced the coupled product alcohol. The alcohol was activated as mesylate **27** and used in the alkylation of the *N1*–of cytosine in protected cytimidine **16** yielded the protected aryl amide **28**, which upon global deprotection produced alkynylaryl amide analog of amicetin as trifluoroacetate salt **HKR–02–056 (28F)** (Scheme 2.9). Prolyl arylamide **HKR–02–057** was synthesized using a similar protocol with the exception of the first step. The 4–iodoaniline was coupled to an activated mixed anhydride of Boc–L–proline to form amide **29** (Figure 2.9).

In view of biological activity of **HKR–02–018**, the synthesis of **HKR–02–059** with tertiary amine as cationic tail was targeted. The amino alkynyl derivatives of amicetin were further reduced to amino alkyl derivatives by careful hydrogenation

of alkyne to alkane to increase the flexibility of the linker and reach of amine cationic tail. The reduced analogs will give an idea of activity of flexible and elongated amicetin derivatives (Scheme 2.10).

Compounds shown in Figure 2.10 were synthesized using a similar protocol to **HKR–02–058** and tested for their proposed biological activity.

Results and Discussion

Advancing with a simplified pharmacophore model, with an emphasis on simplifying the disaccharide portion (linker region) and supplementing it with a methylene group on the cytosine to impart hydrolytic stability, we worked out the SAR on amicetin analogs, which led to the synthesis of a focused library of ~15 compounds.

The compounds synthesized were screened against *Mtb* H37Ra for their antitubercular activity using the MTT assay and translational inhibition activity using the *E. coli S30* extract T/T assay. Out of the 15 analogs tested, the ones lacking an amine tether (cationic tail) did not show any detectable activity at 100 μM (inactive against *Mtb–H37Ra*, inactive in protein synthesis inhibition assay). This result clearly emphasizes the importance of the presence of basic amines at either terminus of the molecule (cationic tail, and cationic cap region) and strengthens our hypothesis of simplified pharmacophore.

The analogs with shorter linker length wherein the basic amine is positioned at distance of ≤ six atoms from N^1 of cytosine, displayed a negligible 10% to 35%) protein synthesis inhibition (on target) activity at 100 μM.

The analogs with longer linker length where the basic amine is positioned

at distance of ≥ ten atoms from N^1 of Cytosine were also shown to have negligible effect on target (protein synthesis inhibition) activity. Most of the analogs with linker length of ≥ ten atoms from N^1 of Cytosine were also dibasic amines. The only dibasic amine–containing analog that showed appreciable activity was **HKR–02–014**, which has the amine positioned at seven atoms distant from *N*1 of Cytosine.

Out of all the 15 analogs, five (Figure 2.7) were active and showed good activity against *Mtb*–H37Ra, and most importantly, they were active against protein synthesis inhibition (on target activity). Interestingly, an observable structure–activity relationship can be drawn based on the set of active compounds.

The five active amicetin analogs possess either a fully saturated alkyl chain (a four–carbon aliphatic *n*–butyl as in **HKR–02–058 / 61** or a three–carbon aliphatic *n*–propyl as in **HKR–02–014**) or an unsaturated alkynyl chain (2–butynyl as in **HKR–02–018 / 59**) as a linker (spacer) between the N^1 of cytimidine and the amine group (cationic tail), which mimics the sugar portion in amicetin. Four among five active analogs are tribasic, whereas the proline substituted amide **HKR–02–014** is dibasic, and is the least active analog among the set of five (80 times less active than amicetin), followed by the alkynes **HKR–02–059** with a tertiary amine as cationic tail, and **HKR–02–018** with a primary amine as cationic tail. The more flexible saturated alkyl amine linker containing compounds are the most potent, with a tertiary amine as a cationic tail as in **HKR–02–061** with an IC_{50} = 7.40 μM against *Mtb*–H37Ra, and the most active analog being **HKR–02–058** consisting of a primary amine as cationic tail with an IC_{50} = 0.98 μM against *Mtb*–H37Ra (Figure 2.11).

As expected and hypothesized, all these analogs were also effective in protein synthesis inhibition (on–target activity) similar to amicetin. They displayed dose dependent protein synthesis inhibition, when evaluated for luciferase expression in the Promega *E. coli* S30 Extract System. Protein synthesis inhibition activity was directly proportional to their antitubercular activity with the most active analog **HKR–02–58** having an IC_{50} = 3.8 μM (amicetin, IC_{50} = 1.6 μM). Analog **HKR–02–058** results in 98% protein synthesis inhibition at 50 μM concentration (compared to amicetin inhibits 100% at 50 μM).

Having seen the antitubercular activity and on–target protein synthesis inhibition activity of these compounds, we wanted to confirm the lack of cytotoxicity. Much to our delight, they exhibited no measurable cytotoxicity against the immuno–compromised CEM/TART T–leukemia cell line up to 100 μM. In addition, the compounds are further tested in Vero cell line cell line (no cytotoxicity observed at 100 μM). Given this lack of toxicity, these compounds were also tested for their effects on cytochrome activation (CYP induction) properties and shown to have no measurable CYP induction at 100 μM (Table 2.1).

The SAR on amicetin analogs and the biological data associated with these analogs supports our initial hypothesis of simplified pharmacophore and simpler scaffolds could preserve the protein synthesis inhibition. The complex disaccharide portion (8–stereo centers) of amicetin can be streamlined with a linear flexible alkyl molecular spacer (0–stereo centers) tethered to a cyclic amine (4–aminopiperidine) that acts as a cationic tail, while maintaining the comparable antitubercular and translation inhibition activities (2–fold less active compared to

amicetin). Noncytotoxicity and non–CYP inducing properties are the significant features of this class of compounds. More importantly, the analogs are synthetically easily accessible compared to amicetin (no reported total synthesis).

Out of 15 analogs synthesized, **HKR–02–058,** which has more flexible alkyl linker and charged amines at either terminii of the molecule and an amine in the linker tether, turned out to be the active in protein synthesis inhibition assays and against MDR–TB/H37Ra. More material was needed for profiling this analog (ADME toxicity testing and *in vivo* studies). Following a convergent synthetic route depicted in Scheme 2.10, we could synthesize enough material for all the biological profiling studies.

The convergent approch begins with *N*1 alkylation of acetylcytosine with 1,4–dibromobutane followed by a S_N2 displacement of the resultant alkylbromide **31** with 4–Boc–aminopiperidine to yield acetylcytosine alkylamine **32**. Deacetylation of **32** using excess ammonium hydroxide followed by a peptide coupling between resultant aminoalkyl cytosine **33** and PABA derivative **11** gave the dipeptide. Global deprotection using methanolic HCl results in **HKR–02–058** as hydrochloride salt. Adopting this convergent protocol, we were able to synthesize (~100 mg) enough material for biological studies (Scheme 2.11).

Similarities in amicetin and its analogs binding interactions to *Tth* 70S ribosome

The Looper group has succeeded in solving the X-ray crystal structures of the natural product amicetin (Ami) (re-expressed, isolated, and purified from the bacteria *Streptomyces vinaceousdrappus* by Dr. Serrano in Looper lab), and two

of the synthesized analogs (**HKR-02-014**, **HKR-02-18)** in complex with the 70S *Thermus thermophiles* ribosome within 3.5 Å resolution, in collaboration with Steitz's lab at Yale University.[19]

Analogs **HKR–02–014** and **HKR–02–018** also bind to the ribosome in a similar fashion as amicetin, involving similar molecular interactions. They share a common binding site in a stretched conformation, albeit with minor disagreements. Each of these structures preserves the WC base pairing of the nucleobase cytosine and guanine G2262 (2251) [*Tth, (E. coli)*]. All three structures have p–aminobenzoate motif positioned to π–stack with A2613 (A2602). The only discrepancies that were seen among the three structures are at the ends of the molecules. The α–methylserine fragment's hydrogen bond interactions in the western portion of the binding pocket of the ribosome vary, and differences in the effectiveness of cation–π interaction of charged terminus with A2450 (2439) are also noted (Figure 2.12 & 2.13).

Differences in binding interactions of HKR–02–014 bound to

Tth 70S ribosome

In the crystal structure of HKR–02–014–70S complex compared to 70S–Ami complex, the propylprolyl amide deviates significantly from amicetin, and extends into the hydrophobic region leading to the exit tunnel, failing to involve in a cation–π interaction with A2450(2439). We assume that the linker length with attached cationic amine (2^o amine in proline) in **HKR–02–014** is short enough to engage in a cation–π interaction with A2439 (A2450). The α–Methylserine in a hydrophilic region anchors the molecule in a binding pocket with two–hydrogen

bonding interaction. First, the carbonyl of the amide interacts with the arginine (R82) of the ribosomal protein L16. Second, the amine of the α–Methylserine hydrogen bonds with the phosphate of G2506 (2495) as shown in Figure 2.9. We assume the lack of cation–π interaction with A2450 (2439) is responsible for the reduced protein synthesis inhibition activity of **HKR–02–014** (Figure 2.12).

Differences in binding interactions of HKR–02–018 bound to *Tth* 70S ribosome

The α–Methylserine surrounded by various polar hydrogen bond donors and acceptors can prompt hydrogen bond formation either through the amine group or via the amide carbonyl or with both as in the case of **HKR–02–018** (see Figure 2.10). Furthermore, the disaccharide region in amicetin protrudes into the helix**,** with the hexose (amicetose) attached to *N*1 of cytosine blocking the exit tunnel through which nascent polypeptide chain egresses into the cytoplasm. In the analog **HKR–02–018** the butynyl amino–piperidine aligns with the amicetine disaccharide and manages to engage in cation–π interactions with A2439(A2450). While the analog **HKR–02–018** has similar binding interactions to Ami, the reduced translation inhibition activity of analog **HKR–02–018** (compared to Ami) could be a result of weaker binding interactions (Figure 2.13).

Conclusion

In summary, amicetin is a ribosomal antibiotic shown to inhibit protein synthesis. This is significantly active against drug resistant strains of TB, non–cytotoxic and compatible with ART. We developed chemistry to build analogs to

reengineer the acid labile disaccharide portion of amicetin and synthesized a library of analogs adopting a simplified pharmacophore. We identified a set of simplified amicetin analogs with comparable antitubercular activity, on–target translational inhibition activity. Lack of cytotoxicity (against mammalian cells) and CYP inducing properties is the best feature of these amicetin analogs. The active analog **HKR–02–058**, is only 4–fold less active against (3–fold more on–target activity), and comparable selectivity ($SI_{RR/E.coli}$ = 125, amicetin SI = 87) compared to the natural product amicetin at the expense of eight less stereo centers.

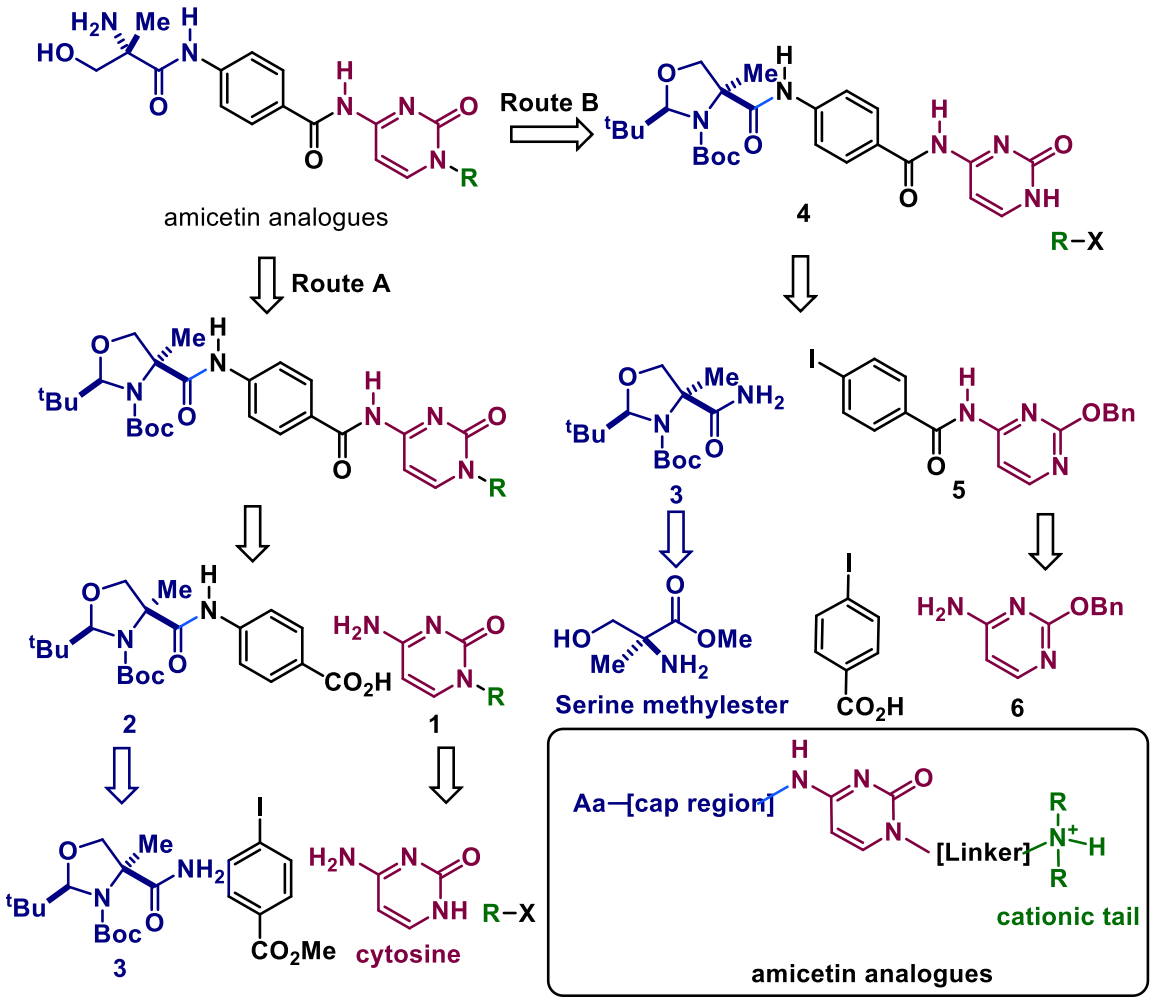

Scheme 2.1 Retrosynthetic analysis of the amicetin analogs

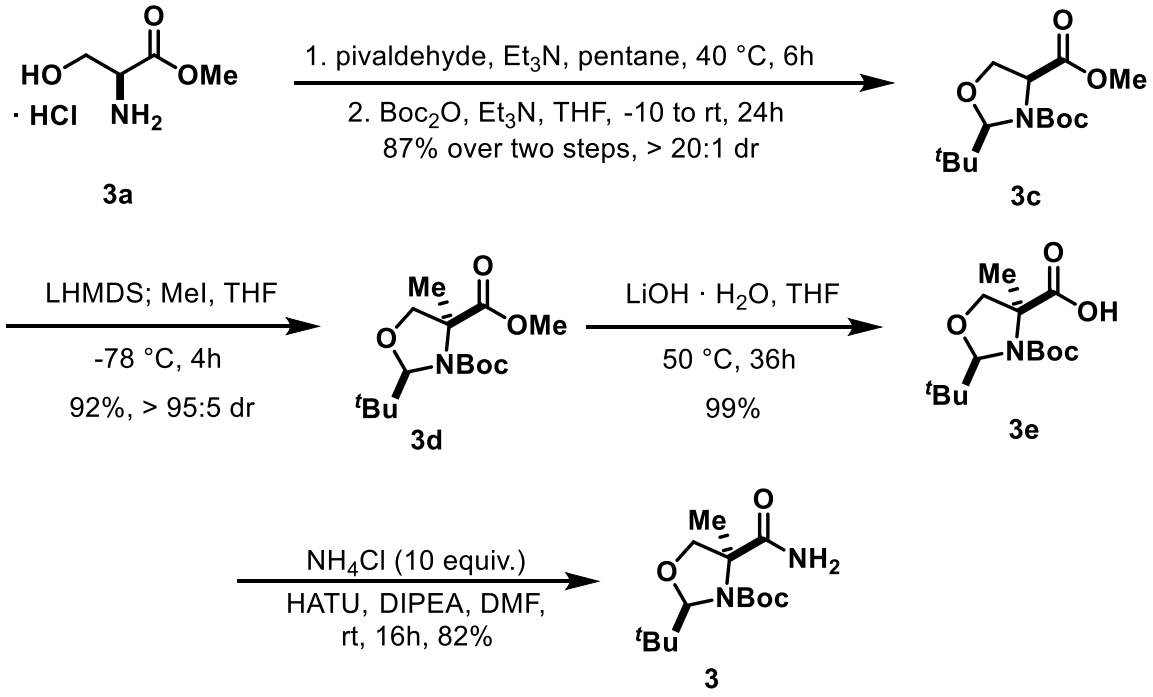

Scheme 2.2 Synthesis of protected α–methylserine carboxamide

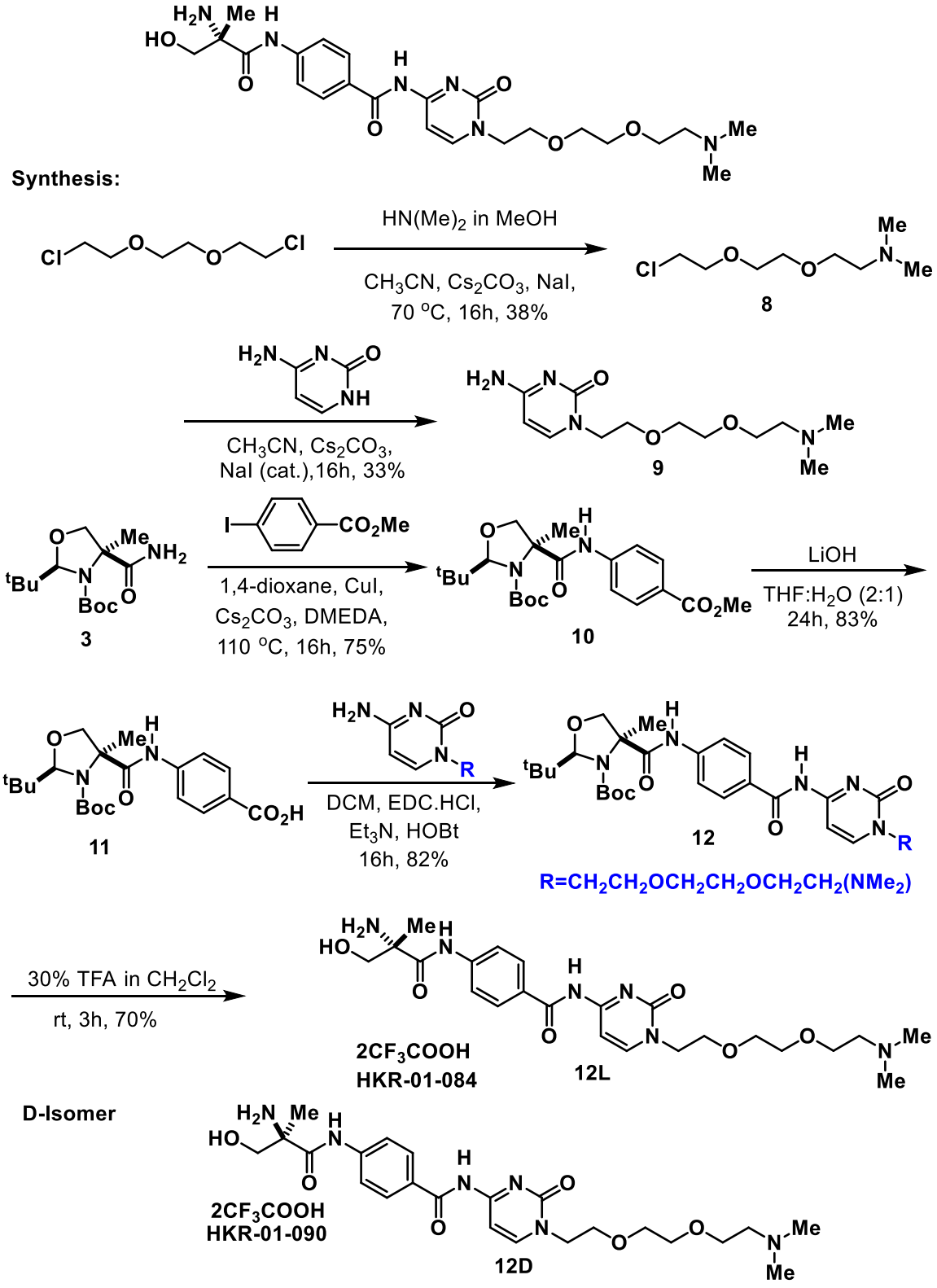

Scheme 2.3 Synthesis of PEG derivatives of amicetin

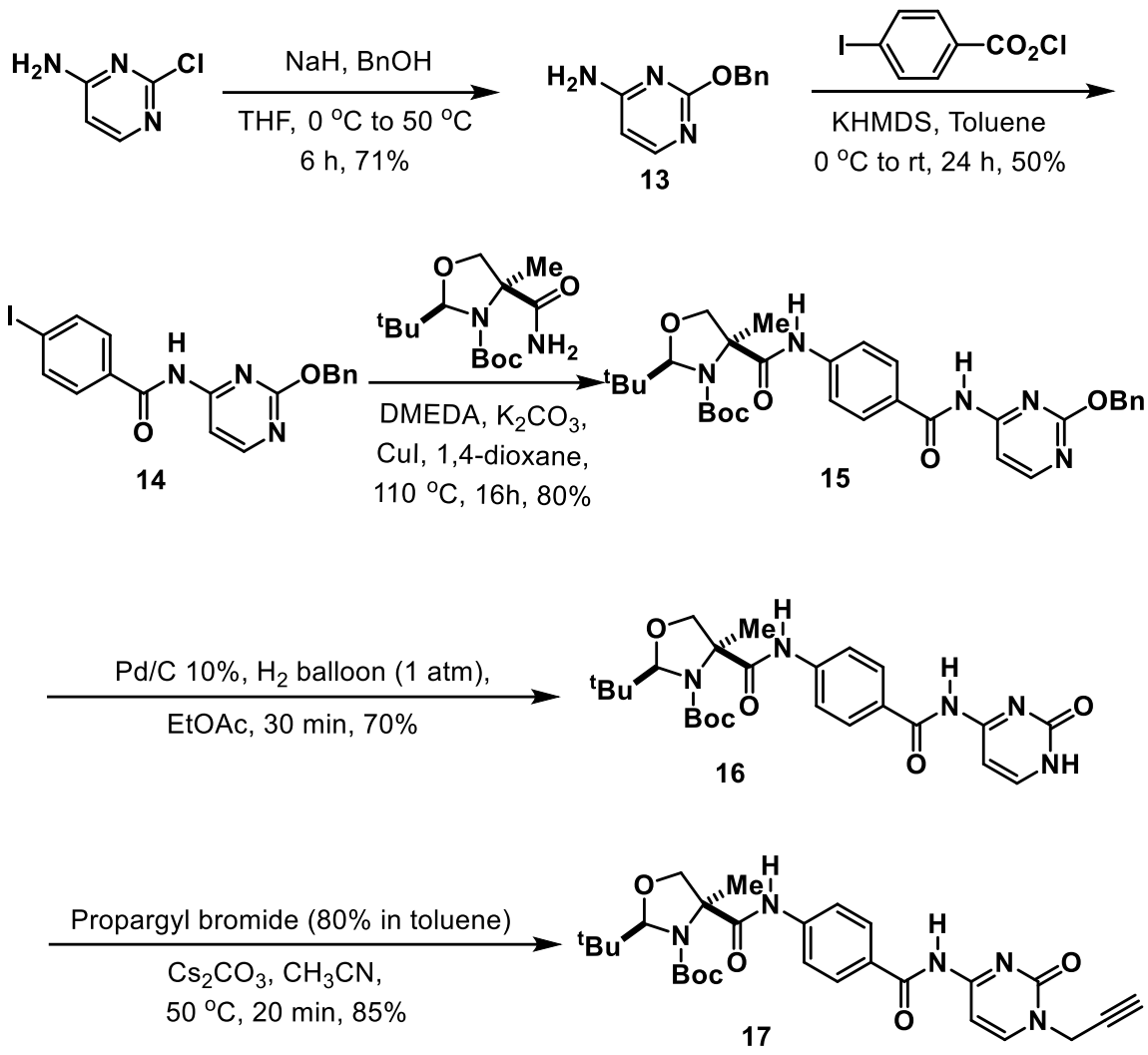

Scheme 2.4 Synthesis of common intermediate propargyl cytimidine

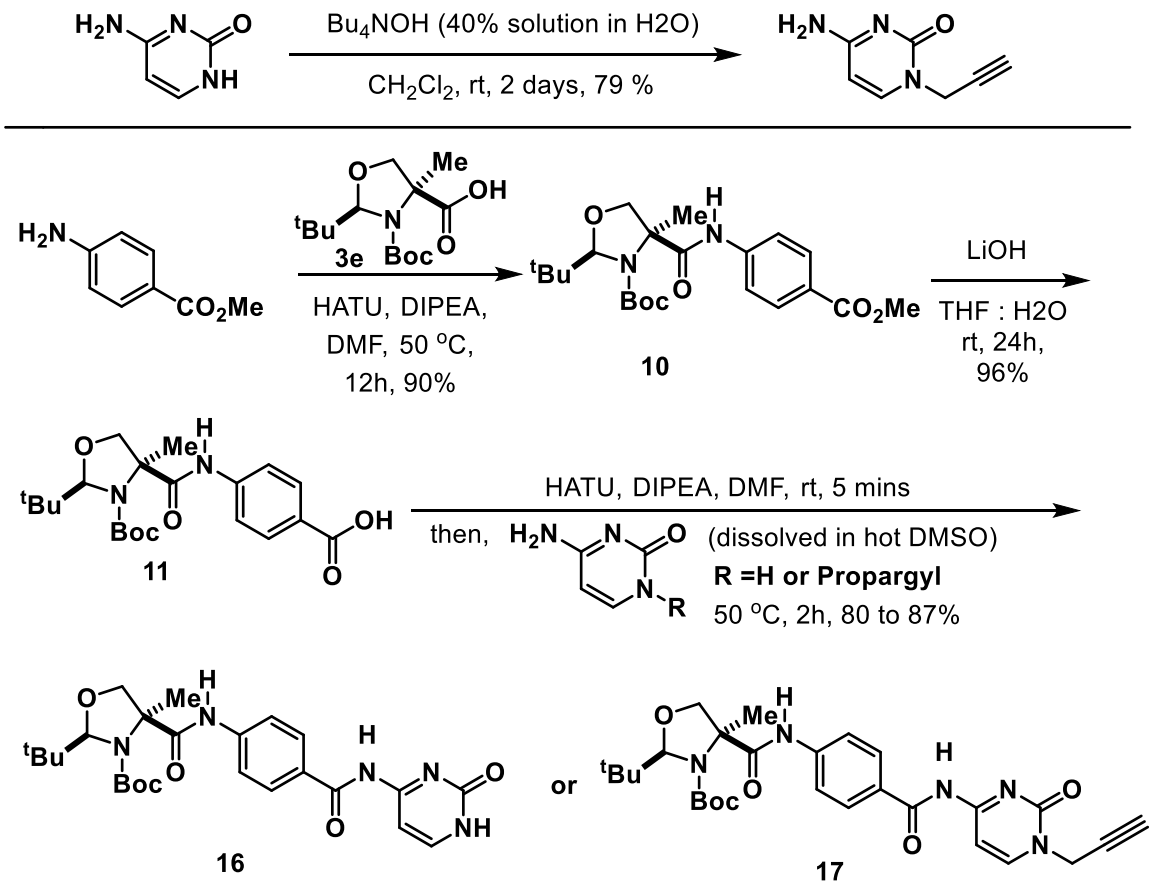

Scheme 2.5 Preparation of protected cytimidine via peptide coupling reactions

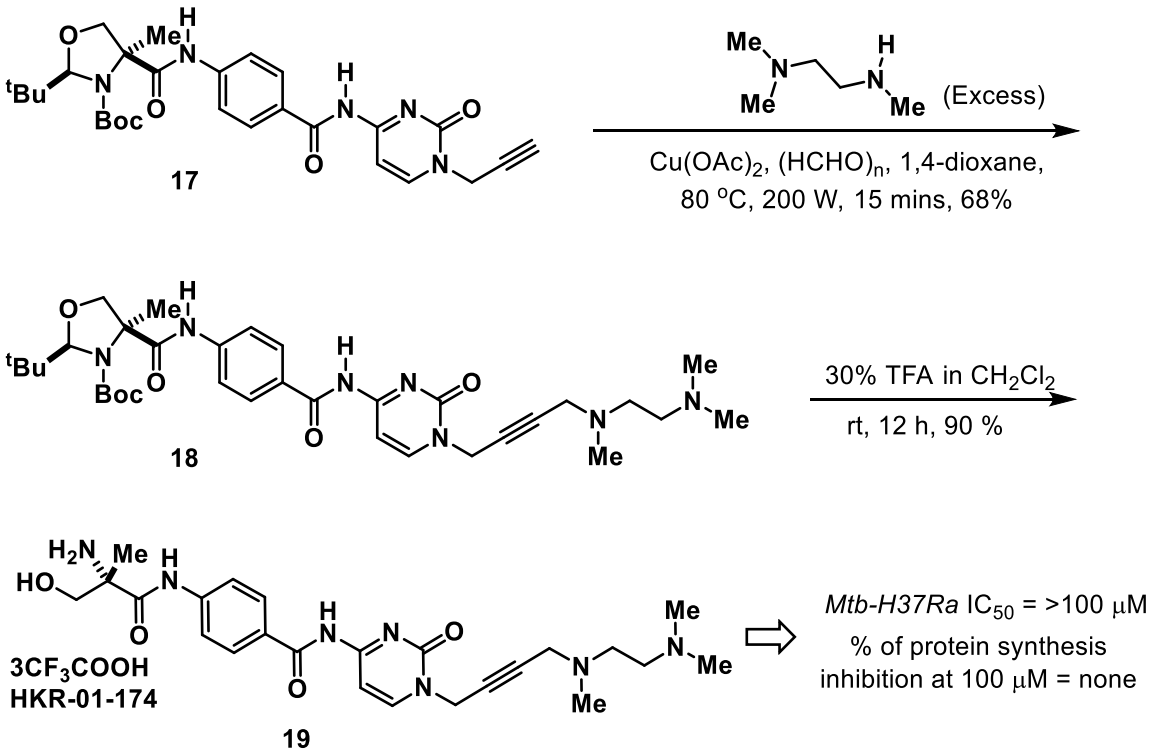

Scheme 2.6 Synthesis of A3–coupled analogs

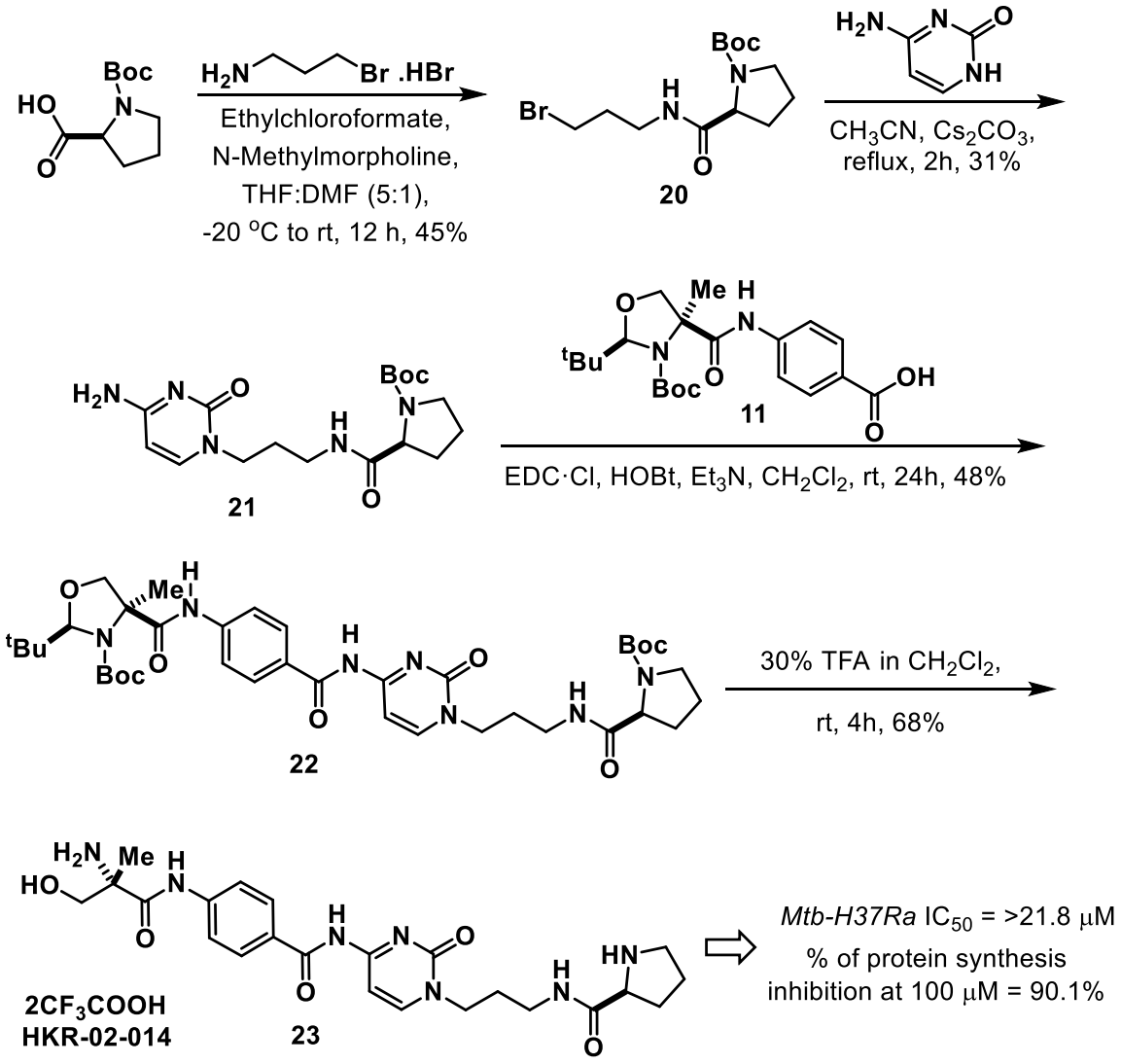

Scheme 2.7 Synthesis of amide analogs of amicetin

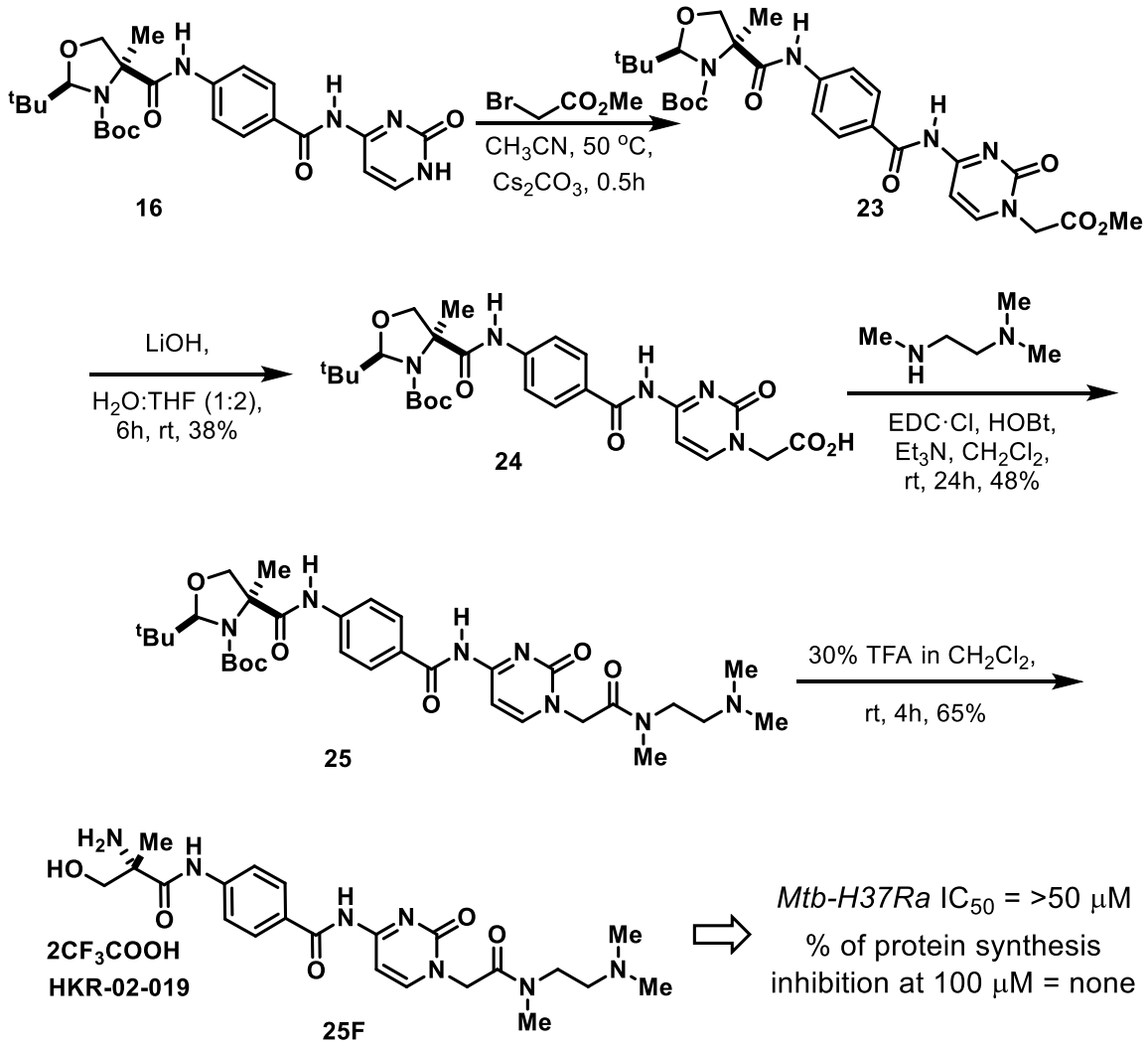

Scheme 2.8 Synthesis of amide analogs of amicetin

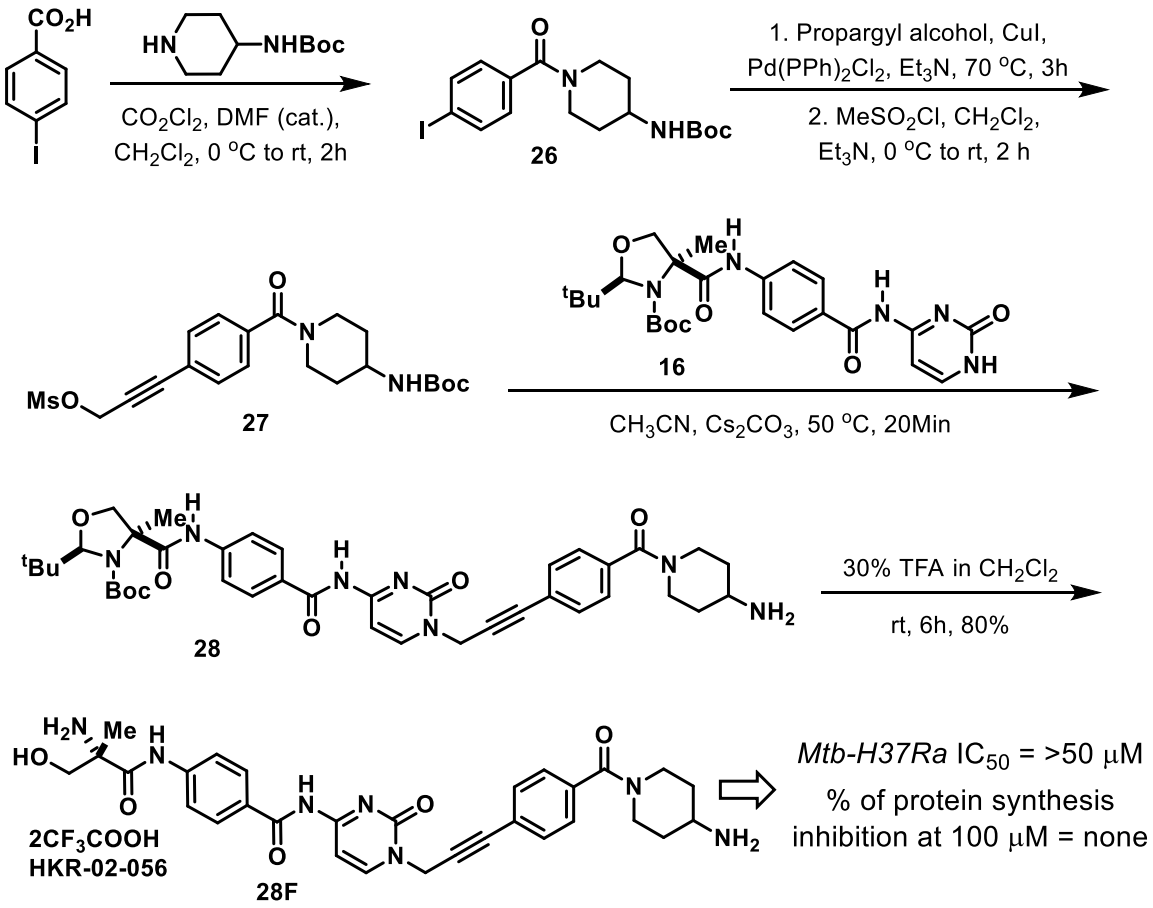

Scheme 2.9 Synthesis of arylamide derivatives of amicetin

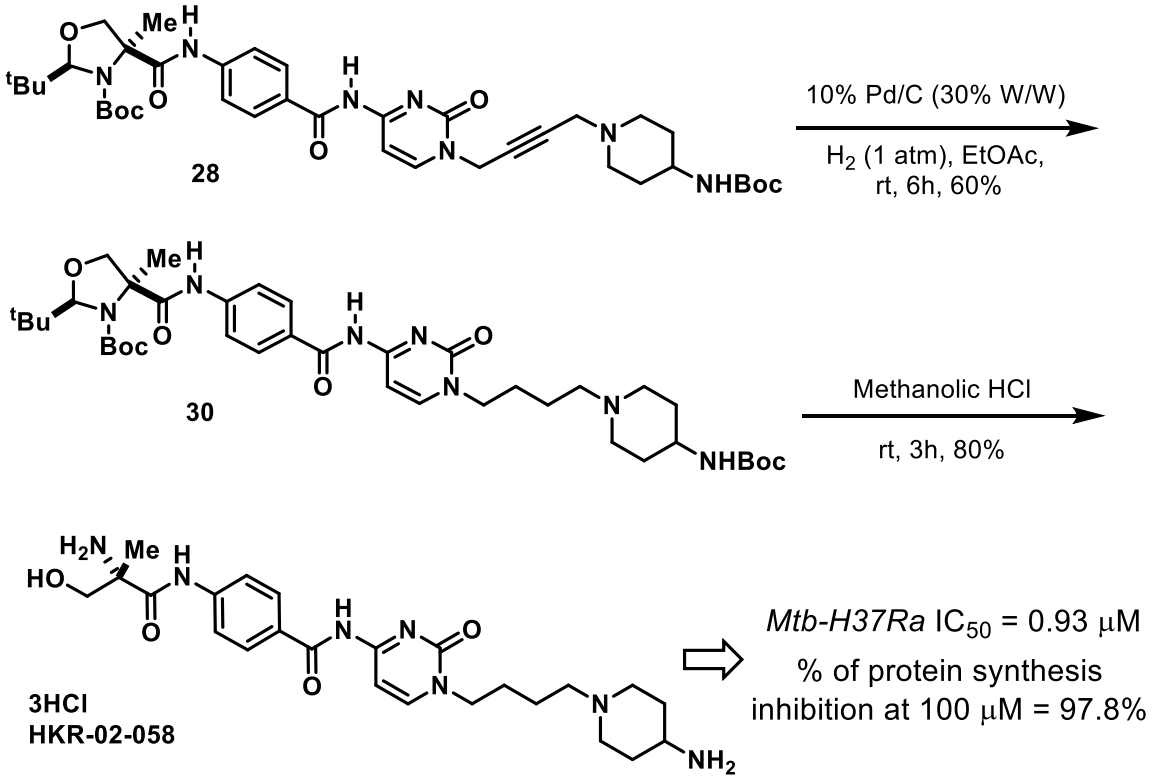

Scheme 2.10 Reduction of alkyne to alkane

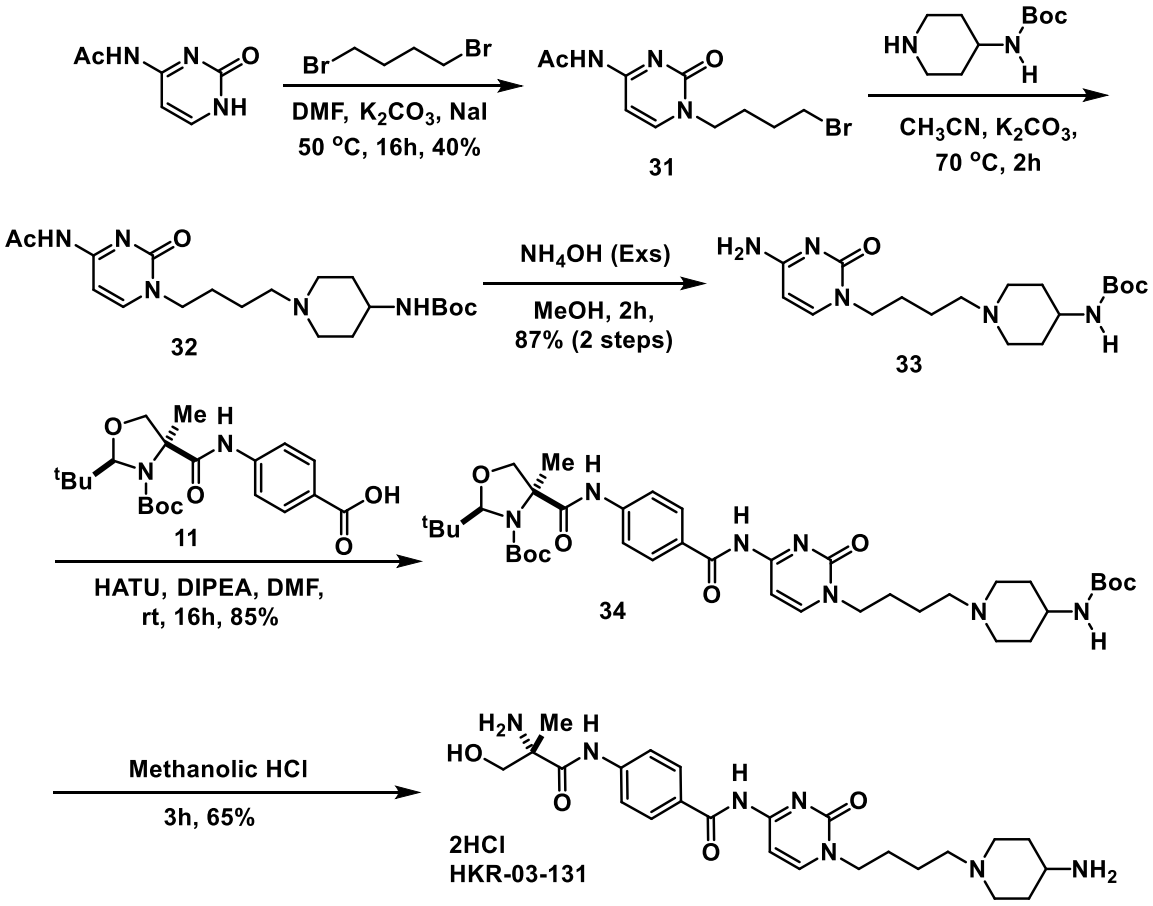

Scheme 2.11 Alternate scale up procedure for HKR–02–058

Table 2.1 Biological data of active analogs

IC_{50} (µM) Compound	*Mtb*– H37Ra	*E. coli* 30S T/T	RR T/T	SI RR/ *E. coli*	CEM – TART	Vero
Amicetin	0.24 ± 1.2	0.82 ± 0.079	71.0 ± 6.5	87	4.40	~70
Cytimidine	>100	—	—	—	>100	>100
HKR–02–014	22.0 ± 1.2	—	—	—	>100	>100
HKR–02–059	19.0 ± 1.2	33.6 ± 3.2	>100	>3	>100	>100
HKR–02–018	8.20 ± 1.2	14.8 ± 3.2	>100	>7	>100	>100
HKR–02–061	7.40 ± 1.2	2.43 ± 0.132	>100	>40	>100	>100
HKR–02–058	0.98 ± 1.2	0.26 ± 0.03	32.7 ± 11.6	125	>100	>100

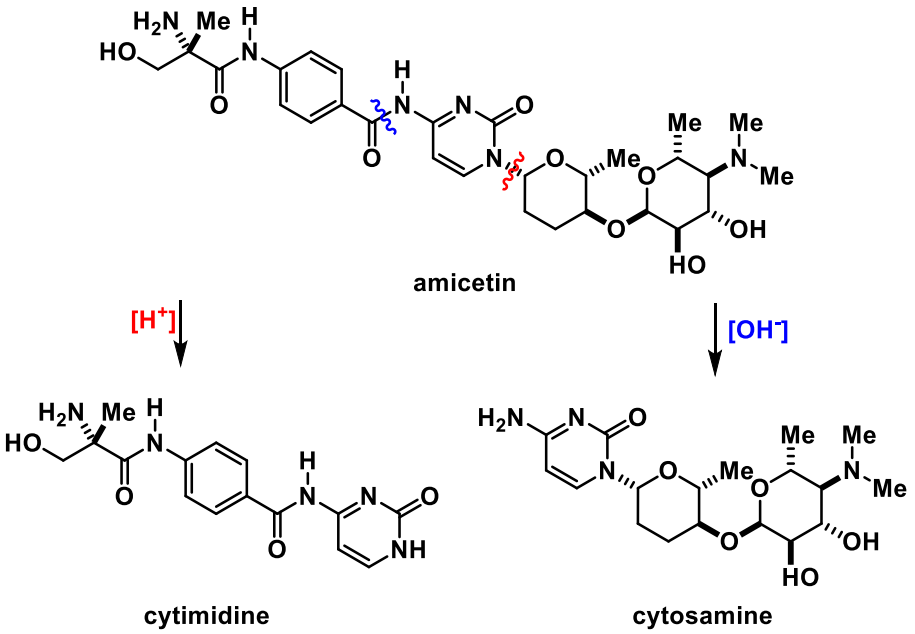

Figure 2.1 Degradation products of amicetin under acidic and basic conditions

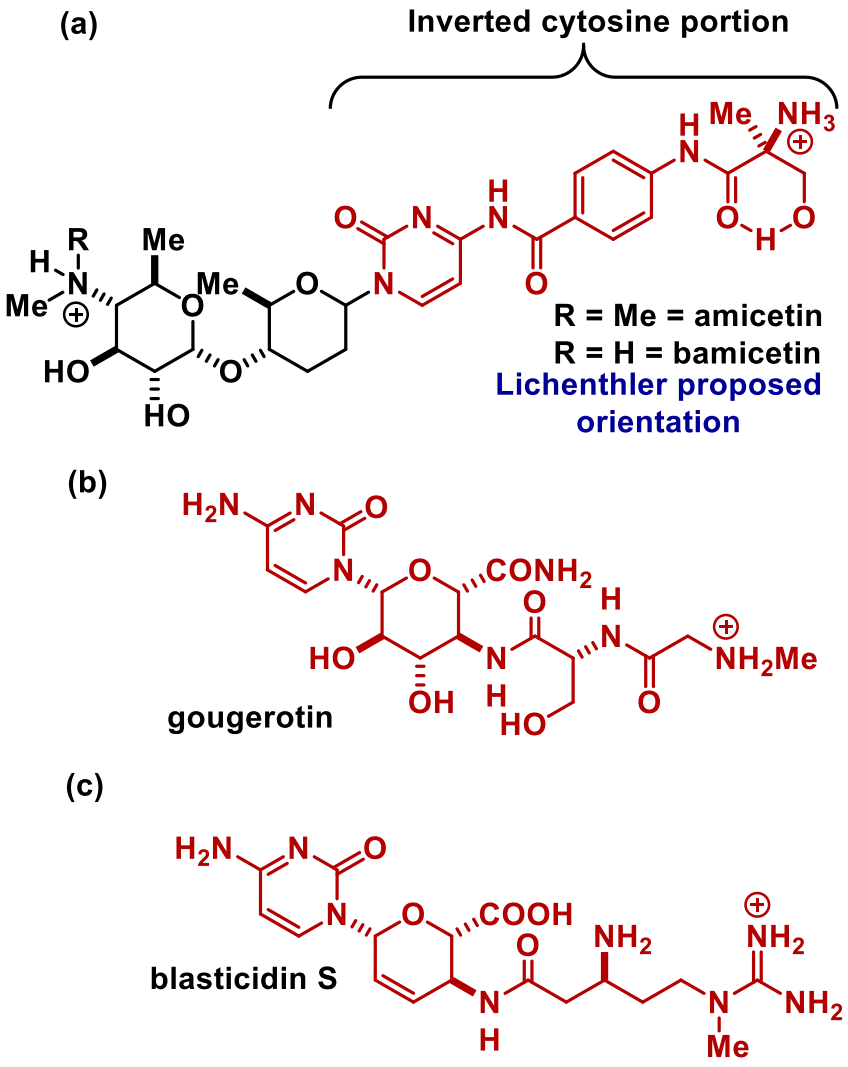

Figure 2.2 Superimposable confirmations of inverted cytosine portion of amicetin and bamicetin with gougerotin and blasticidin S

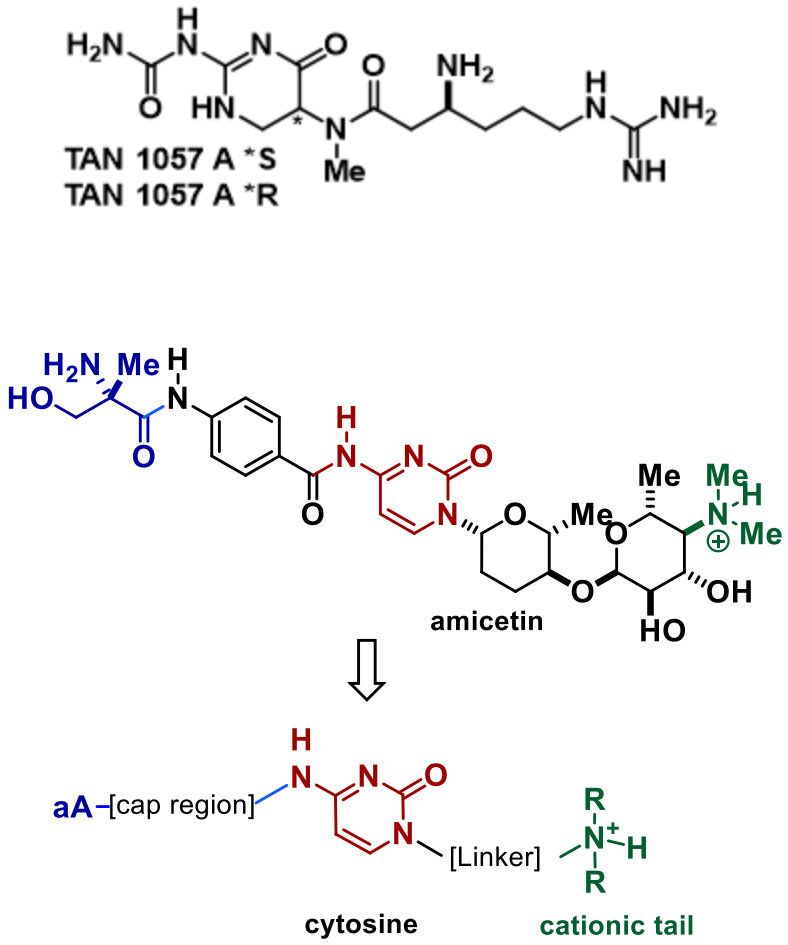

Figure 2.3 Structure of *TAN1057* and a simplified pharmacophore model

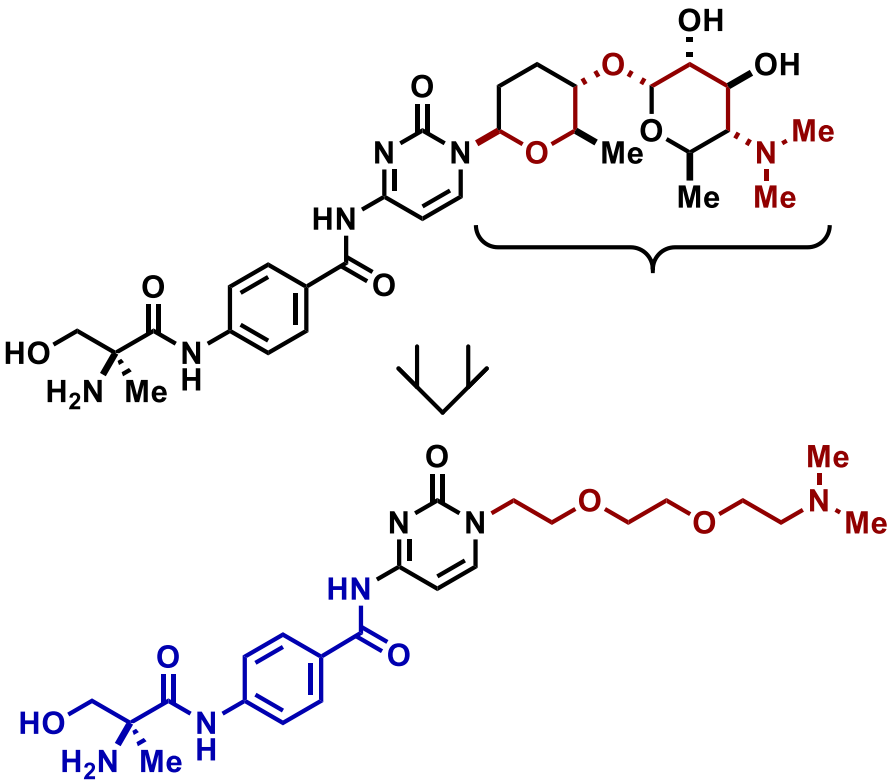

Figure 2.4 Hypothesis for design of polyethylene glycol derivatives of amicetin

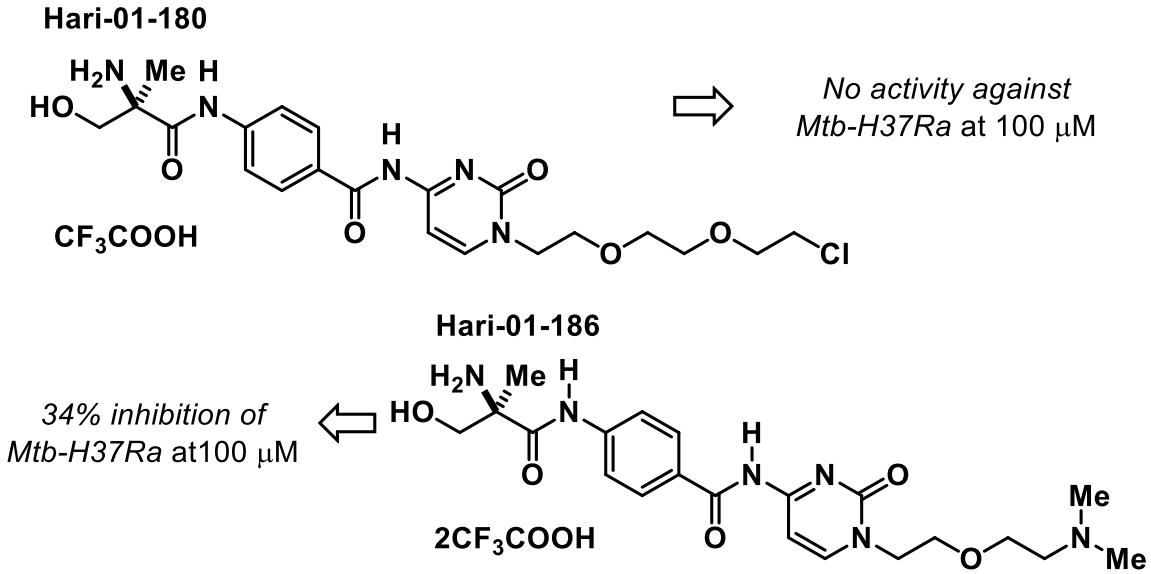

Figure 2.5 Compounds synthesized using a protocol similar to HKR–01–089

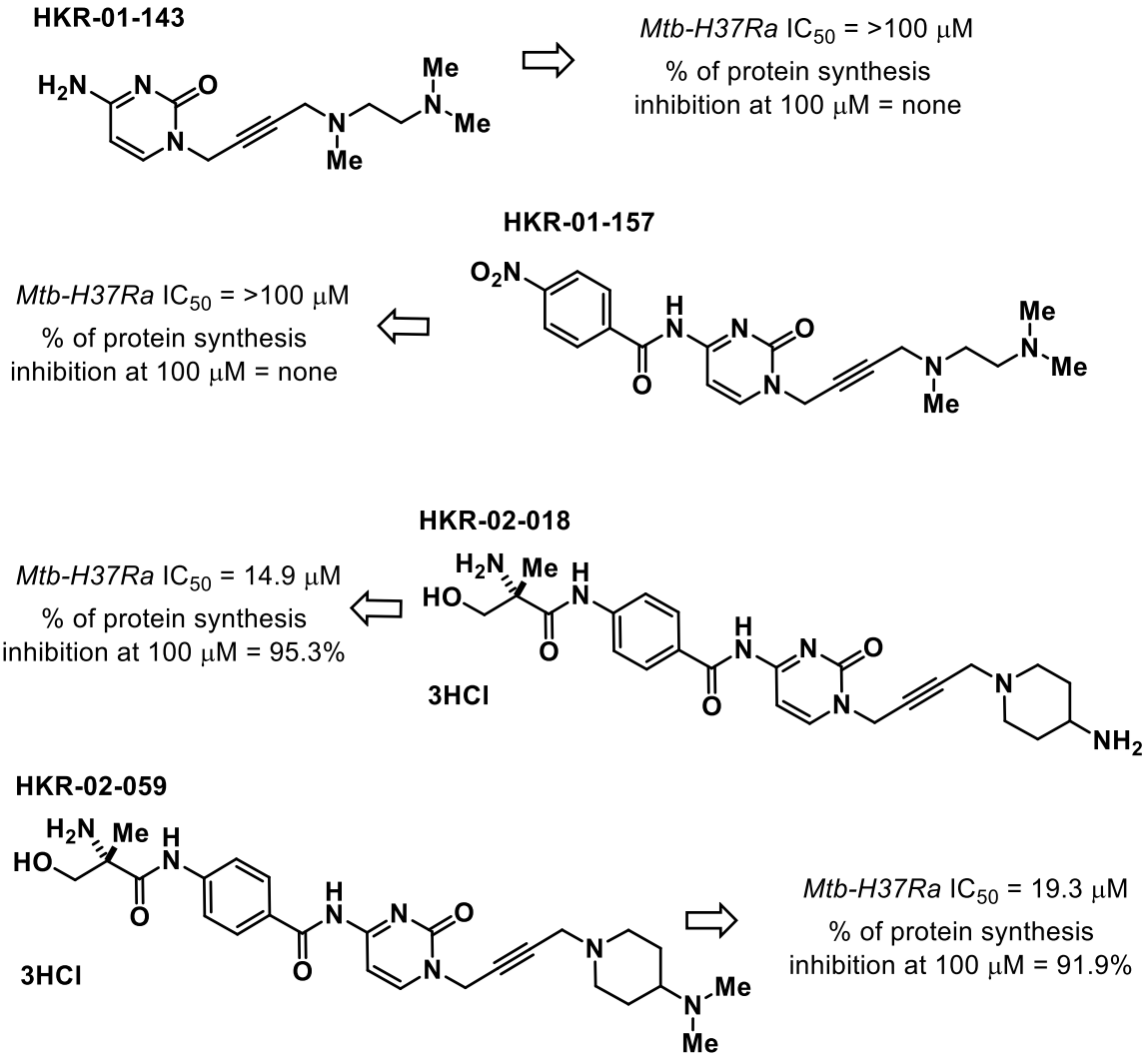

Figure 2.6 Compounds synthesized using a protocol similar to HKR–02–018 and their biological activity

HKR-02-016

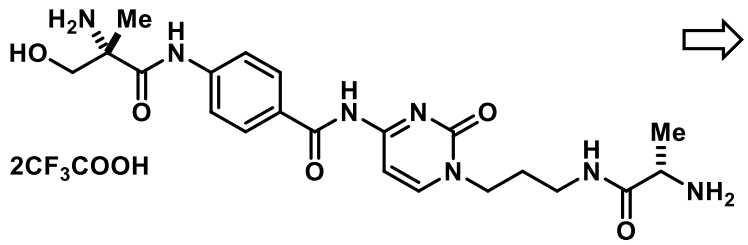

Mtb-H37Ra IC_{50} = >100 μM
% of protein synthesis inhibition at 100 μM = 35%

Figure 2.7 Compound synthesized using a protocol similar to HKR–02–014

HKR-02-020

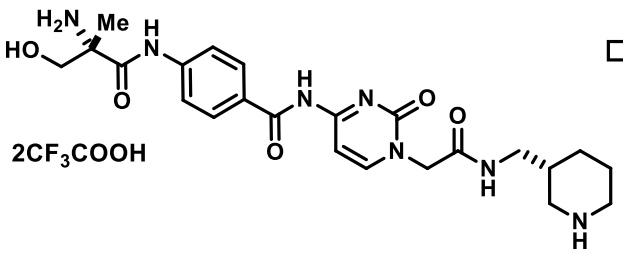

Mtb-H37Ra IC_{50} = >50 μM
% of protein synthesis inhibition at 100 μM = none

Figure 2.8 Compounds synthesized using a protocol similar to HKR–02–019

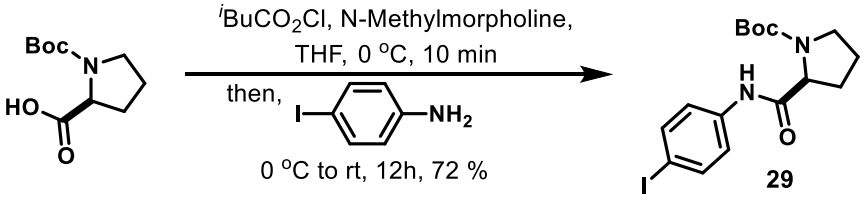

HKR-02-057

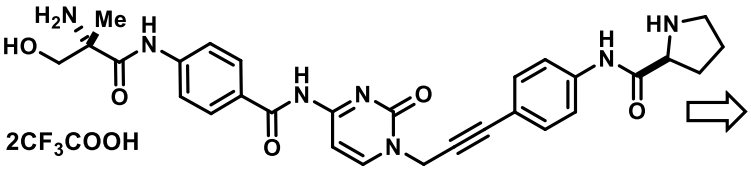

Mtb-H37Ra IC_{50} = >50 μM
% of protein synthesis inhibition at 100 μM = none

Figure 2.9 Compound synthesized using a protocol similar to HKR–02–056

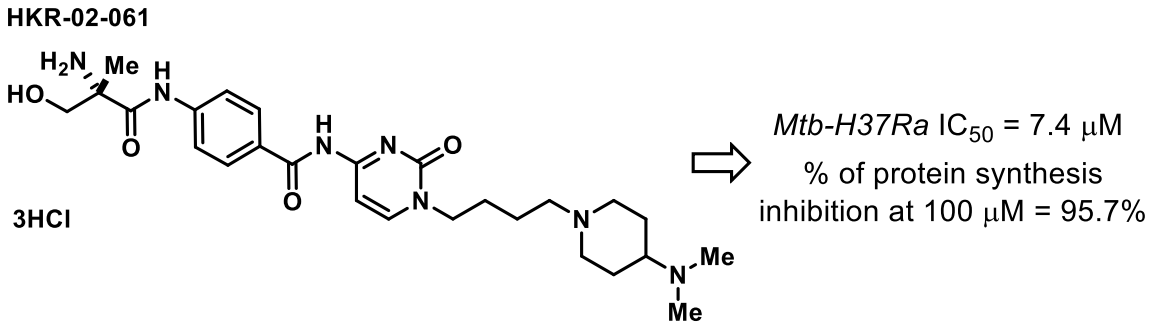

Figure 2.10 Compound synthesized using a protocol similar to HKR–02–058

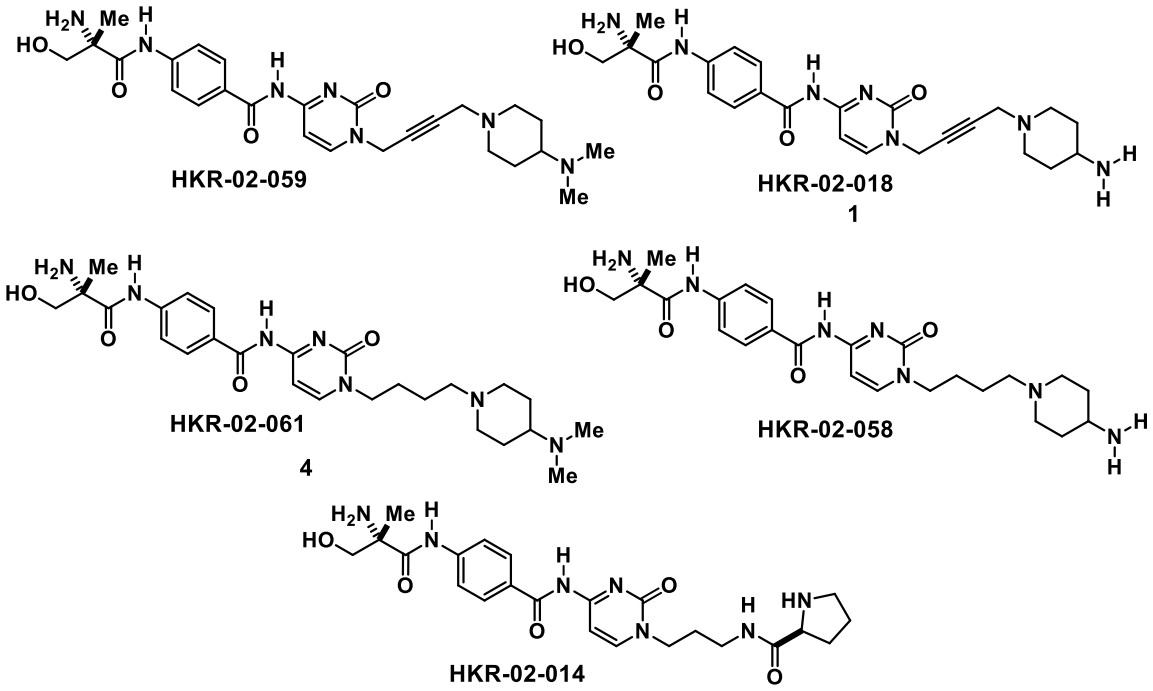

Figure 2.11 Active analogs

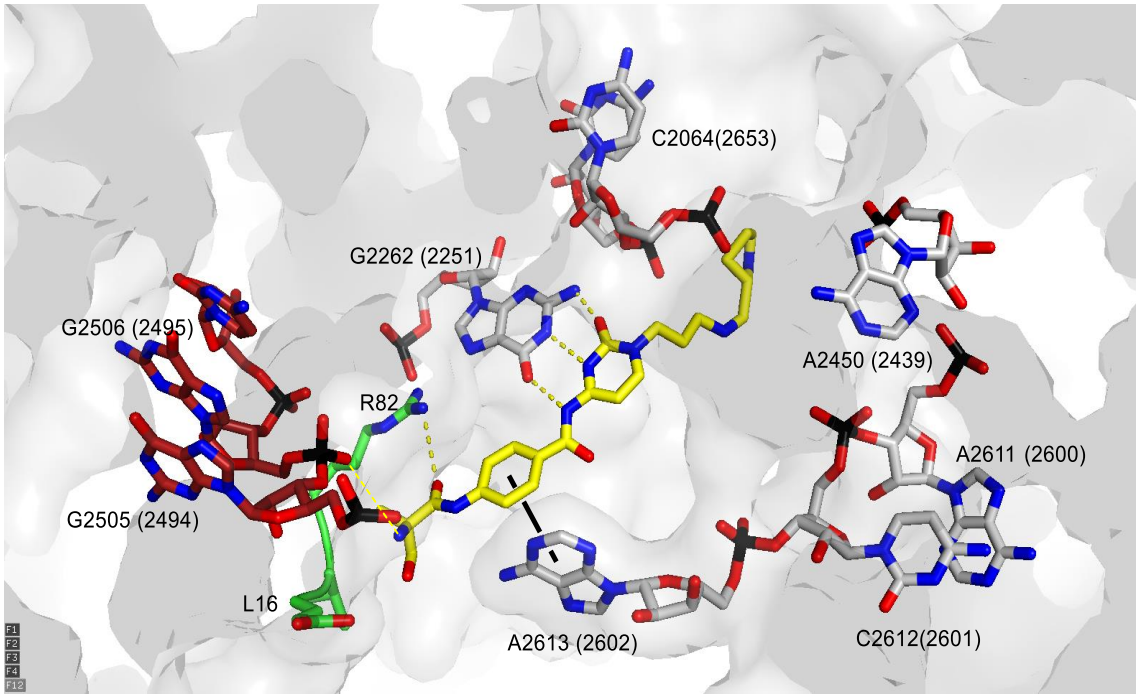

Figure 2.12 Analog HKR–02–014 bound to 70S *Tth* ribosome

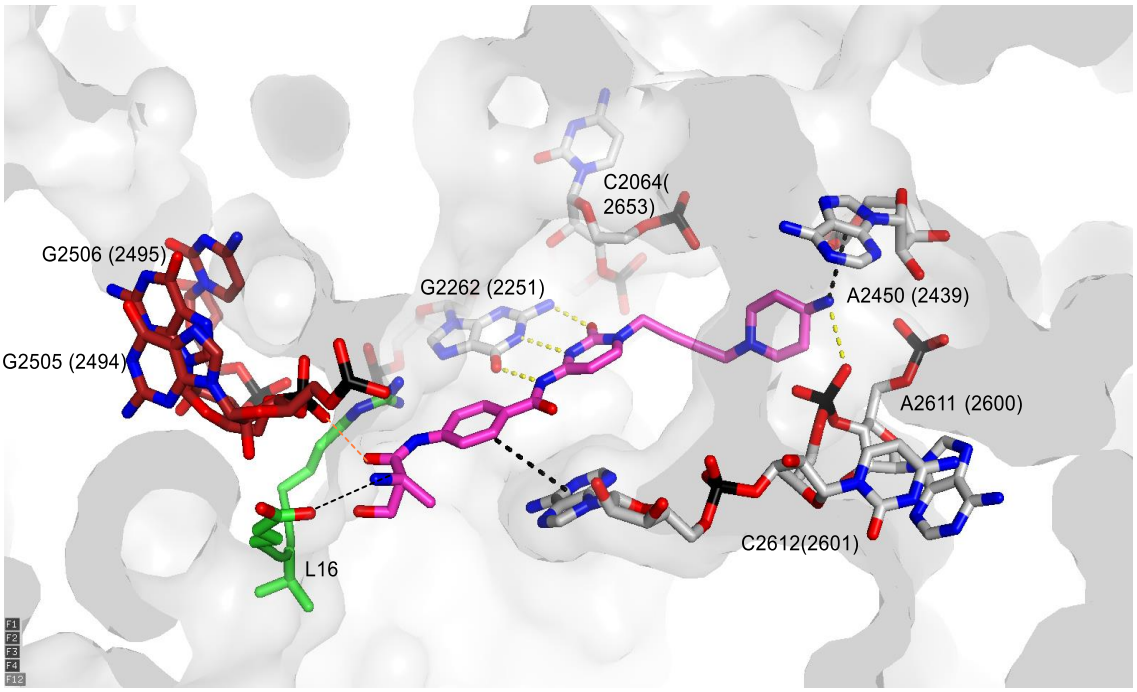

Figure 2.13 Analog HKR–02–018 bound to 70S *Tth* ribosome

References

1) Daniel, T. M. History of Tuberculosis. *Resp. Med.* **2006**, *100*, 1862–1870.

2) Centers for Disease Control and Prevention. http://www.cdc.gov/tb/topic/ basics /default.htm (accessed June 24, 2016).

3) Zhang, Y. The Magic Bullets and Tuberculosis Drug Targets. *Annu*. *Rev*. *Pharmacol*. *Toxicol*. ***2005***. *45*, *529*–64.

4) Stevens, C. L.; Gasser, R. J.; Mukherjee, T. K.; Haskell, T. H. The Structure of Amicetin. A New Dimethylamino Sugar. *J. Am. Chem. Soc.* **1956**, *78*, 6212.

5) Stevens, C. L.; Nagarajan, K.; Haskell, T. H. The Structure of Amicetin. *J. Org. Chem.* **1962**, *27*, 2991, 3007.

6) Flynn, E. H.; Hinman, J. W.; Caron, E. L.; Woolf, D. O. The Chemistry of Amicetin, a New Antibiotic. *J. Am. Chem. Soc.* **1953**, *78*, 5867–5871.

7) (a) Fox, J. J.; Watanabe, K.A.; Bloch, A. Nucleoside Antibiotics. *Prog. Nucleic Acid Res. Mol. Biol.* **1966**, *5*, 251–313. (b) Isono, K. Nucleoside Antibiotics: Structure, Biological Activity, and Biosynthesis. *J. Antibiot.* **1988**, *41*, 1712–1739.

8) (a) Lichtenthaler, F. W.; Trummlitz, G. Structural Basis for the Inhibition of Protein Synthesis by the Aminoacyl–Aminohexosyl–Cytosine Group of Antibiotics. *FEBS Lett.* **1974**, *38*, 237–242. (b) Barbacid, M.; Vasquez, D. [G–^{3}H] Gougerotin Binding to Ribosomes: Heterogeneity of Eukaryotic Ribosomes. *Eur. J. Biochem.* **1974**, *44*, 445–453. (c) Hansen, J. L.; Moore, P. B.; Steitz, T. A. Structures of Five Antibiotics Bound at the Peptidyl Transferase Center of the Large Ribosomal Subunit. *J. Mol. Bio.* **2003**, *330*, 1061–1075. (d) Yukioka, M.; Morisawa, S. Studies on the Mechanism of Action of Gougerotin: (II) Effect of Various Factors on Gougerotin Action. *J. Biochem*. **1969**, *66*, 233–240.

9) (a) Funabashi, Y.; Tsubotani, S.; Koyama, K.; Katayama, N.; Harada, S. A New Anti–MRSA Dipeptide, TAN–1057 A. *Tetrahedron* **1993**, *49*, 13–28. (b) Limburg, E.; Gahlmann, R.; Kroll, H. P.; Beyer. D. Ribosomal Alterations Contribute to Bacterial Resistance against the Dipeptide Antibiotic TAN 1057. *Antimicrob. Agents Chemother*.**2004**, *48*, 619–622. (c) Mallipeddi, R.; Rohan, L. C. Progress in Antiretroviral Drug Delivery Using Nanotechnology. *Int. J. Nanomedicine.* **2010**, *5*, 533–547.

10) Mallipeddi, R.; Rohan, L. C. Progress in Antiretroviral Drug Delivary Using Nanotechnology. *Int. J. Nanomedicine.* **2010**, *5*, 533–547.

11) Klapars, A.; Huang, X.; Buchwald, S. A General and Efficient Copper Catalyst for the Amidation of Aryl Halides. *J. Am. Chem. Soc.* **2002**, *124,* 7421–7428.

12) (a) Seebach, D.; Aebi, J. D. α–Alkylation of Serine with Self–Reproduction of the Center of Chirality*Tetrahedron Lett.* **1984**, *25*, 2545–2548. (b) Brunner, M.; Saakrento, P.; Straub, T.; Rissanen, K.; Koshinen, A. M. P. K. Eur. J. Org. Chem. 2004, 3879. (b) Brunner, M.; Saakrento, P.; Straub, T.; Rissanen, K.; Koshinen, A. M. P. Stereo Controlled α–Alkylation of Fully Protected L–serine. *Eur. J. Org. Chem.* **2004**, 3879–3883.

13) Serrano, C. M.; Looper, R. E. Synthesis of Cytimidine through a One–Pot Copper–Mediated Amidation Cascade. *Org Lett*. **2011**, *13*, 5000–5003.

14) Bronson, J.J.; Ferrara, L. M.; Howell, H. G.; Brodfuehrer, P. R.; Martin, J. C. A New Synthesis of Anti–Herpesvirus Agent (S)–1–[3–hydroxy–2–(phosphonylmethoxy) propyl] Cytosine*. Nucleosides and Nucleotides*. **1990**, *9*, 745–769.

15) Christensen, L.; Hansen, H. F.; Koch, T.; Nielsen, P. E. Inhibition of PNA Triplex Formation by N4–benzoylated Cytosine*. Nuc. Acids Res*. **1998**, *26*, 2735–2739.

16) Greco, E.; Aliev, A. E.; Howell, H. G.; Lafitte, V. G. H.; Bala, K.; Duncan, D.; Pilon, L.; Golding, P.; Hailes, H. C. Cytosine Modules in Quadruple Hydrogen Bonded Arrays. *New J. Chem.* **2010**, *9,* 2634–2642.

17) Cravotto, G.; Balliano, G.; Tagliapietra, S.; Palmisano, G.; Penoni, A. Umbelliferone Aminoalkyl Derivatives, a New Class of Squalene–Hopene Cyclase Inhibitors. *Eur. J. Med. Chem*. **2004**, *39*, 917–924.

18) Reddy, D. N.; Prabhakaran, E. N. Synthesis and Isolation of 5,6–Dihydro–4H–1,3–oxazine Hydrobromides by Autocyclization of *N*–(3–bromopropyl) Amides. *J. Org. Chem*. **2011**, *76*, 680–683.

19) Serrano, C. M. Synthetic and Biological Studies on Amicetin and its Analogues toward the Development of New Anti–mycobacterial agents. Ph. D. Dissertation, University of Utah, Salt Lake City, Utah, **2016**.

Supporting Information

General experimental considerations

All reactions requiring anhydrous conditions were conducted in flame–dried glassware under a positive pressure of either nitrogen or argon. Commercially available reagents were used as received; otherwise, materials were purified according to *Purification of Laboratory Chemicals*.[1] Acetonitrile (CH_3CN), *N,N'*–dimethylformamide (DMF), dichloromethane (CH_2Cl_2), toluene ($PhCH_3$), and tetrahydrofuran (THF) were degassed with nitrogen and passed through a solvent purification system (Innovative Technologies Pure Solv). Dry 1,4–dioxane was purchased from Acros Organics in a Acros Seal™ bottle. Copper iodide (CuI) was purchased from Acros Organics. Microwave reactions were done in CEM Discover System Model 908005.

Melting points were determined using Mel–Temp® Capillary Melting Point Apparatus. Infrared spectra were obtained using Nicolet 380–FT IR spectrometer fitted with a Smart Orbit sample system. Optical rotations were obtained at ambient temperature on a Perkin Elmer Model 343 polarimeter (Na D line) using a microcell with a 1 decimeter path length. Mass spectra were determined on a Micromass Quattro II (ESI/APCI–TOF) for HRMS at the University of Utah Mass Spectrometry Facility. ^{1}H NMR and ^{13}C NMR spectra were recorded at 300 MHz, 400MHz, 500 MHz, and ^{13}C NMR spectra were recorded at 75 MHz, 100 MHz, 125 MHz, respectively. Proton resonances were reported relative to the deuterated solvent peak: 7.26 ppm for $CDCl_3$ and 3.31 ppm (center line signal) for CD_3OD, 4.80 ppm for D_2O using the following format: chemical shift (δ) [multiplicity (s= singlet, bs=

road singlet, d= doublet, dd= doublet of doublet, t= triplet, q= quartet, m= multiplet), coupling constant(s) *J* in Hz, integration].[2] Carbon resonances were reported as chemical shifts (δ) in parts per million, relative to the center line signal of the respective solvent peak: 77.23 ppm for $CDCl_3$ and 49.00 ppm for CD_3OD. All the commercially available chemicals are purchased from Sigma–Aldrich, Acros, TCI America, Combi–Blocks, and Chem–Impex.

References

1. Armarego, W. L. F.; Chai, C. L. L. *Purification of Laboratory Chemicals.* 2003, 5th Ed.

2. Hoye, T.R.; Hansen, P.R.; Vyvyan, J.R. *J. Org. Chem.* **1994,** *59,* 4096–4103

Experimental procedures: Procedure for synthesis of

protected α–methyl serine

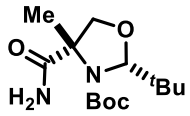

***tert*–butyl(2*R*,4*S*)–2–(*tert*–butyl)–4–carbamoyl–4–methyl–4–methyl–4 –oxazolidine–3–carboxylate** was synthesized according to reported literature. The characterization for this compound was matched as reported in literature.[3]

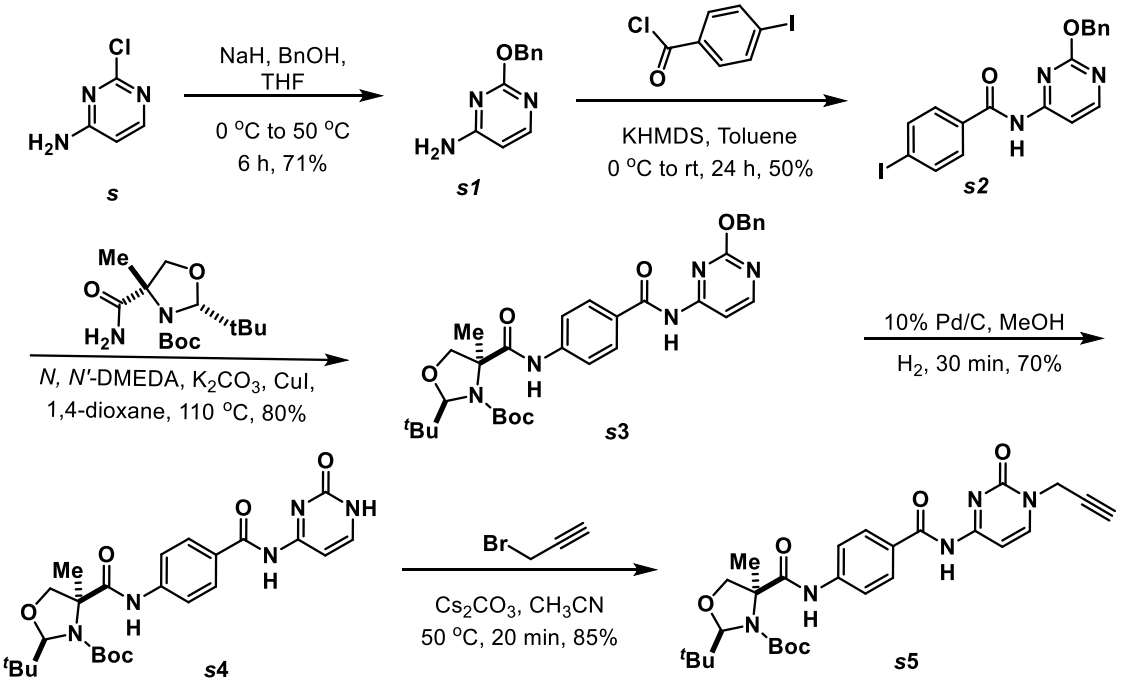

***Scheme* 1. Preparation of propargyl cytimidine.**

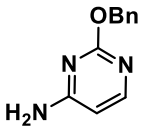

2–(benzyloxy)pyrimidin–4–amine (*S*1). Benzyl alcohol (2.81 mL, 26.0 mmol) was added dropwise to a stirring suspension of 60% NaH in mineral oil (1.0 g, 26 mmol) in dry THF (60 mL) at 0 °C, under a nitrogen atmosphere. The mixture was allowed to stir for a further 30 min until it formed a clear solution. aminochloropyrimidine ***S*** (3.30 g, 25.4 mmol) was dissolved in THF was added dropwise at 0 °C and then was refluxed for 12 hrs. The reaction mixture was concentrated under reduced pressure, and purification using flash chromatography (60% EtOAc/Hexanes) afforded the title compound (3.70 g, 71%) as a white solid.

R*f*= 0.28 (5% MeOH/CH_2Cl_2). M.p. 76–78 °C (lit. 80–81 °C).

^{1}H NMR (400 MHz, $CDCl_3$): δ 7.82 (d, *J*= 5.6 Hz, 1H), 7.36 (d, *J*= 6.8 Hz, 2H), 7.25–7.21 (m, 3H), 5.95 (d, *J*= 5.6 Hz, 1H), 5.89 (brs, 2H), 5.28 (s, 2H). ^{13}C NMR (100 MHz, $CDCl_3$); δ 165.1, 164.7, 156.5, 136.7, 128.2, 127.6, 127.5, 99.7, 68.1 ppm. IR (neat) 3465, 3324, 3034, 3034, 1635, 1559, 1455, 1352, 1292 cm^{-1}. HRMS (ESI) Calculated for $C_{11}H_{12}N_3O$ *m/z* (M^+) 202.0980, Obsd 202.0977.

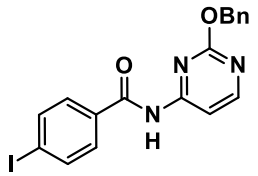

N*–(2–(benzyloxy)pyrimidin–4–yl)–4–iodobenzamide (*S*2).** A 0.5 M solution of KHMDS in toluene (5.95 mL, 2.98 mmol), was added to a stirring solution of the amino pyrimidine ***S1 (0.50 g, 2.48 mmol) in dry toluene (15 mL) at 0 °C under a nitrogen atmosphere. The reaction was left stir for 30 min. In a second flask, 4–iodobenzoic acid (1.85 g, 7.44 mmol) was dissolved in dry CH_2Cl_2 (20 mL) under an atmosphere of nitrogen. The solution was cooled to 0 °C, after which oxalylchloride (0.65 mL, 5.16 mmol) was added drop wise followed by the addition of two drops of DMF. The reaction was allowed to stir for 30 min, until the solution became clear. The acid chloride formed was concentrated and dissolved in a minimum amount (6 mL) of toluene and added dropwise using cannula into the deprotonated amino pyrimidine. The reaction was allowed to warm to room temperature and was stirred overnight. The reaction was quenched with a saturated solution of NH_4Cl (15 mL), extracted with EtOAc (3 x 50 mL). The combined organic fractions were washed with brine (10 mL) and dried over

anhydrous Na_2SO_4, filtered and concentrated under reduced pressure. Purification on silica gel using flash chromatography (10% EtOAc/Hexanes) afforded the title compound (0.54 g, 50%) as a white solid.

R_f= 0.30 (30% EtOAc/hexanes). Mp. 110 –112 °C.

^{1}H NMR (500 MHz, $CDCl_3$); δ 8.50 (d, *J*= 5.2 Hz, 1H), 8.48 (brs, 1H), 7.96 (d, *J*= 6.0 Hz, 1H), 7.88 (d, *J*= 8.0 Hz, 2H), 7.60 (d, *J*= 8.0 Hz, 2H), 7.47 (d, *J*= 7.6 Hz, 2H), 7.38 (t, *J*= 6.8 Hz, 2H), 7.34 (t, *J*= 7.3 Hz, 1H), 5.43 (s, 2H) ppm. ^{13}C NMR (125 MHz, $CDCl_3$); δ 165.4, 164.7, 161.0, 159.2, 138.5, 136.4, 132.8, 128.9, 128.6, 128.2, 128.0, 104.4, 100.6, 69.3 ppm. IR (neat); 3303, 3061, 1695, 1585, 1516, 1402, 1288 cm^{-1}. HRMS (ESI) Calculated for $C_{18}H_{14}N_3O_2NaI$ *m/z* (M+Na) 454.0028, Obsd. 454.0030.

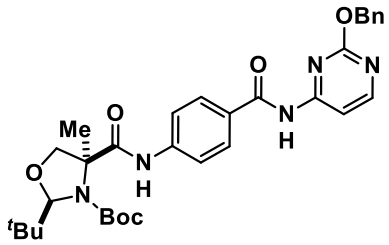

(2R,4S)–tert–butyl4– ((4– ((2– (benzyloxy) pyrimidin–4–yl) carbamoyl) phenyl)carbamoyl)–2–(tert–butyl)–4–methyloxazolidine–3–carboxylate (*S*3). An oven dried pressure tube equipped with a magnetic stir bar was charged with CuI (0.01 g, 0.05 mmol), anhydrous K_2CO_3 (1.44 g, 1.04 mmol), and coupled pyrimidine ***S2*** (0.23 g, 0.52 mmol). The pressure flask was then quickly fitted with a rubber septum. A solution of amide oxazolidine (0.29 g, 0.52 mmol) in dry 1, 4–dioxane (5 mL) was added to the reaction flask via syringe under a positive pressure of nitrogen. The reaction mixture was degassed and purged with nitrogen (this procedure was repeated three times). *N*^{1},*N*^{2}– dimethylethane–1,2–diamine

(20 µL, 0.05 mmol) was then added into the reaction mixture via syringe. The rubber septum was replaced with the sealed tube cap. The reaction was stirred and heated at 110 °C for 24 hrs. The reaction mixture was then diluted with EtOAc (20 mL), filtered through a pad of Celite® and concentrated under reduced pressure. Purification on silica gel using flash chromatography (50% EtOAc/hexanes) afforded title compound (0.25 g, 80%) as a white solid.

R_f= 0.20 (50% EtOAc/hexanes). Mp. 152 – 154 °C. $[\alpha]^{20}_D$ = –53 (*c* = 0.20, $CHCl_3$).

^{1}H NMR (400 MHz, $CDCl_3$); δ 8.48 (t, *J* = 5.6 Hz,2H), 7.98 (d, *J* = 5.4 Hz, 1H), 7.89 (d, *J* = 8.5 Hz, 2H), 7.70 (d, *J* = 8.9 Hz, 2H), 7.48 (d, *J* = 7.4 Hz, 1H), 7.39–7.27 (m, 3 H), 5.45 (s, 2H), 5.22 (s, 1H), 4.82 (d, J = 8.8 Hz, 1 H), 3.82 (d, J = 8.8 Hz, 1H), 1.74 (s, 3H), 1.55 (s, 9H), 0.93 (s, 9H) ppm. ^{13}C NMR (100 MHz, $CDCl_3$); δ 171.7, 165.0, 164.5, 160.5, 159.2, 155.9, 142.5, 136.3, 128.5, 128.4, 128.2, 127.9, 127.8, 119.4, 104.2, 97.9, 82.9, 76.0, 69.0, 68.0, 38.1, 28.1, 26.1, 22.0 ppm. IR (neat); 2967, 2210, 1976, 1691, 1591, 1493, 1460, 1365 cm^{-1}. HRMS (ESI) Calculated for $C_{32}H_{39}N_5O_6Na$ *m/z* (M+Na) 612.2798, Obsd. 612.2809.

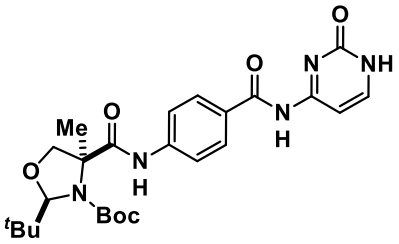

(2R,4S)–tert–butyl–2–(tert–butyl)–4–methyl–4–((4–((2–oxo–1,2–dihydropyrimidin–4–yl)carbamoyl)phenyl)carbamoyl)oxazolidine–3–carboxylate (*S*4). The reaction vessel with the coupled product ***S3*** (0.2 g, 0.34

mmol) was evacuated and backfilled with nitrogen gas, and 10% palladium (Pd) on activated carbon (0.02 g, 10% wt) was transferred into the reaction flask under nitrogen atmosphere. Small amounts of EtOAc (1mL) were added to submerge the Pd/C followed by the careful addition of methanol by creating a stream down the side of the flask wall (8 mL). The reaction mixture was evacuated and purged with hydrogen gas three times, and then the reaction mixture was left to react for 20 min under hydrogen atmosphere, after which, the reaction mixture was filtered through a pad of Celite® and washed with hot methanol. Then the filtrate was concentrated under reduced pressure to yield cytimidine (***S4)*** as white solid (0.12 g, 70%).

R*f*= 0.30 (15% CH_2Cl_2/MeOH). Mp 206 – 208 °C. $[\alpha]^{20}_D$ = –10 (*c* = 0.12, MeOH).

^{1}H NMR (400 MHz, DMSO–d_6): δ 8.03 (d, *J* = 8.20 Hz, 2H), 7.85 (d, *J* = 6.6 Hz, 1H), 7.69 (d, *J* = 8.20 Hz, 2H), 7.17 (brs, 1H), 5.07 (s, 1H), 4.41(d, *J* = 8 Hz, 1H), 4.40 (brs, 1H), 3.85 (d, J = 8 Hz, 1H), 1.64 (s, 3H), 1.46 (s, 9H), 0.90 (s, 9H) ppm. ^{13}C NMR (125 MHz, $CDCl_3$) δ 170.6, 163.7, 154.4, 147.0, 141.9, 129.5, 128.6, 128.4, 119.3, 96.8, 95.5, 81.3, 79.1, 75.8, 67.6, 38.0, 27.7, 25.9, 21.1 ppm. IR (neat) 2972, 1691, 1594, 1493, 1459 cm^{-1}. HRMS (ESI) Calculated for $C_{25}H_{33}N_5O_6Na$ *m/z* (M+Na) 522.2329, Obsd. 522.2333.

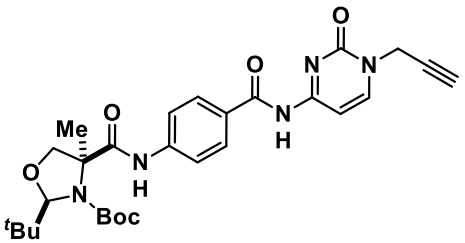

(2R,4S)–tert–butyl–2–(tert–butyl)–4–methyl–4–((4–((2–oxo–1–(prop–

2–yn–1–yl)–1,2–dihydropyri–midin–4–yl) carbamoyl) phenyl) carbamoyl) oxazolidine–3–carboxylate (*S*5). To a solution of ***S*4** (0.04 g, 0.08 mmol) in CH_3CN (2 mL), Cs_2CO_3 (33 mg, 0.10 mmol) and propargylbromide (12 mg, 0.10 mmol) were added under a positive pressure of nitrogen. The reaction mixture was stirred for 0.4 hrs at 50 °C, and then concentrated under reduced pressure. Purification on silica gel using flash chromatography (1.5% CH_2Cl_2/MeOH) afforded the title compound (40 mg, 85%) as a colorless sticky solid.

R_f= 0.30 (5% CH_2Cl_2/MeOH). $[\alpha]^{20}_D$ = –87 (c = 1.00, $CHCl_3$).

^{1}H NMR (400 MHz, $CDCl_3$): δ 8.01(d, *J* = 7.6 Hz, 1H), 7.90 (d, *J* = 8.4 Hz, 2H), 7.69 (d, *J* = 8.4 Hz, 2H), 7.55 (bs, 1H), 5.20 (s, 1H), 4.79 (d, *J* = 9.2 Hz, 1H), 4.72 (d, *J* = 2.8 Hz, 2H), 3.79 (d, *J* = 9.2 Hz, 1H), 2.59 (t, *J* = 2.8 Hz, 1H), 1.71 (s, 3H), 1.53 (s, 9H), 0.90 (s, 9H). ^{13}C NMR (100 MHz, $CDCl_3$) δ 171.7, 162.5, 155.8, 146.6, 142.8, 128.9, 119.3, 97.9, 97.1, 82.9, 76.0, 75.7, 68.0, 44.6, 38.8, 38.1, 28.1, 26.1, 22.0. IR (neat) 3260, 2971, 2130, 1663, 1625, 1597, 1482, 1359 cm–1. HRMS (ESI) Calculated for $C_{28}H_{35}N_5O_6Na$ m/z (M+Na) 560.2485, Obsd. 560.2490.

D. General procedure for three component coupling reaction.

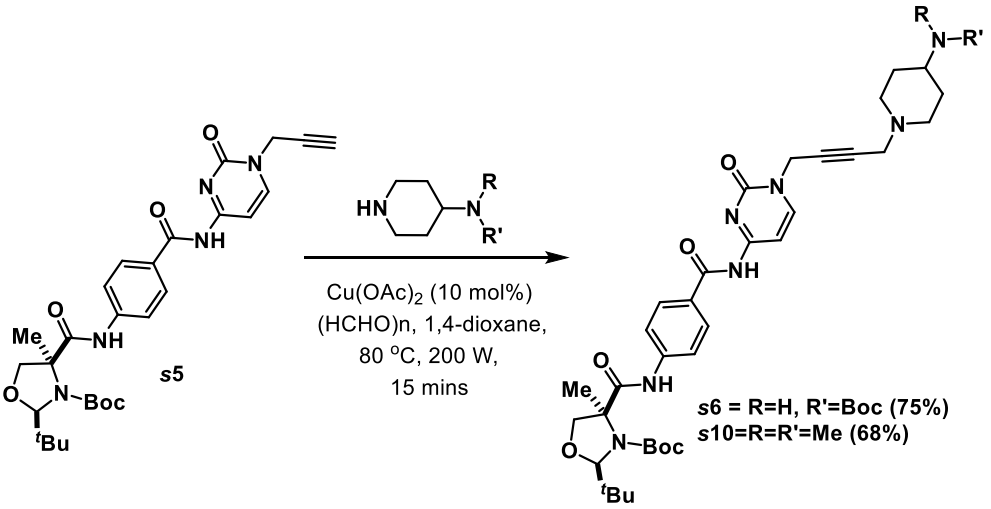

***Scheme* 2. Preparation of A^3–coupled products**

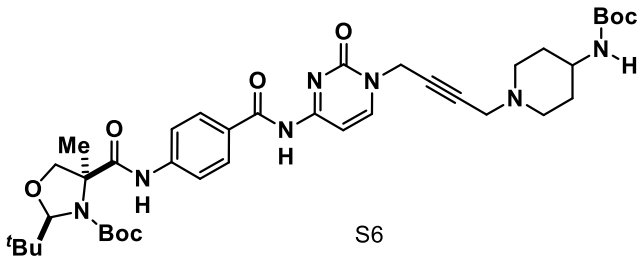

S6

***tert*–butyl(2*R*,4*S*)–4–((4–((1–(4–(4–((*tert*–butoxycarbonyl)amino) piperidin–1–yl)but–2–yn–1–yl)–2–oxo–1,2–dihydropyrimidin–4–yl) carbamoyl)ph-enyl)carbamoyl)–2–(*tert*–butyl)–4–methyloxazolidine–3–carboxylate (*S6*):** In a 10 ml borosilicate glass vessel equipped with a magnetic stir bar the following were added: dry 1,4–dioxane (2.5 mL), paraformaldehyde (15.0 mg, 0.39 mmol, 4.0 equiv.), copper(II) acetate (2.30 mg g, 13.0 µmol, 0.1 equiv.) and the amine (4–NHBoc–aminopiperidine) (27.0 mg, 0.04 mmol 1.1 equiv.). The mixture was irradiated with microwave (200 W) for 10 min at 80 °C, after cooling down to 25 °C, the propargyl cytimidine ***S*5** (70.0 mg, 0.04 mmol, 1.0 equiv.) dissolved in dry 1,4–dioxane (1.0 mL) was added and the mixture was

irradiated further (200 W) for 10 min at 80 °C. The reaction was monitored by TLC using CHCl3/CH3OH (97:3) as eluent. The reaction mixture was diluted with ethyl acetate (5mL x 2) and filtered through a pad of Celite® and concentrated under reduced pressure. Purification on silica gel using flash chromatography (3% MeOH/$CHCl_3$) afforded the A^3–coupled product **S6** (70mg, 75%) as yellow colored solid.

R_f = 0.30 (3% MeOH/CH_2Cl_2). Mp 126 – 128 °C. $[\alpha]^{20}_D$ = –53 ^{o} (*c* = 0.10, $CHCl_3$).

^{1}H NMR (400 MHz, $CDCl_3$) δ 8.01 (d, *J* = 7.2 Hz, 1H), 7.89 (d, *J* = 8.4 Hz, 2H), 7.70 (d, *J* = 8.4 Hz, 2H), 7.58 (d, *J* = 7.2 Hz, 1H), 5.21 (s, 1H), 4.82 (d, *J* = 8.8 Hz, 1H), 4.76 (s, 1H), 4.14 (brs, 1H), 3.82 (d, *J* = 8.8 Hz, 1H), 3.48–3.43 (m, 1H), 3.35 (s, 2H), 2.87 (d, *J* = 10.8 Hz, 2H), 2.26 (t, *J* = 10.8 Hz, 2H), 1.98 (d, *J* = 11.6 Hz, 2H), 1.73 (s, 3H), 1.54 (s, 9H), 1.47 (d, *J* = 11.6 Hz, 2H), 1.44 (s, 9H), 0.92 (s, 9H). ^{13}C NMR (100 MHz, $CDCl_3$); δ 171.5, 166.4, 162.8, 156.0, 155.1, 146.9, 142.3, 131.1, 129.2, 127.8, 118.9, 97.8, 97.1, 83.9, 82.8, 82.6, 79.0, 77.4, 75.9, 67.9, 51.4, 47.1, 39.2, 38.0, 32.0, 28.3, 28.0, 26.0, 21.9. IR (neat) 3258, 2974, 2135, 1696, 1600, 1559, 1489 cm–1. LRMS Calculated for $C_{39}H_{56}N_7O_8$ m/z (M+H) 750.4, Obsd 750.4.

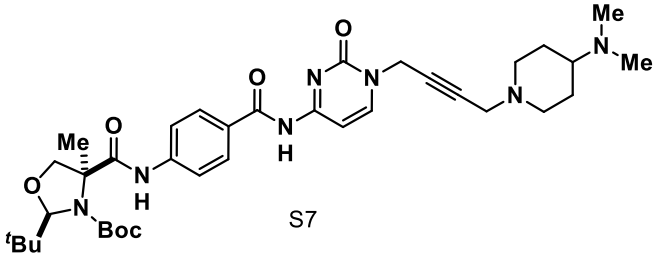

S7

***tert*–Butyl(2*R*,4*S*)–2–(*tert*–butyl)–4–((4–((1–(4–(4–(dimethylamino)**

piperidin–1–yl)but–2–yn–1–yl)–2–oxo–1,2–dihydropyrimidin–4–yl) carbamoyl)phenyl)carbamoyl)–4–methyloxazolidine–3–carboxylate (*S*10): Compound ***S*10** was synthesized following similar procedure as ***S*6** using $Cu(OAc)_2$ (4.00 mg g, 21.3 µmol), paraformaldehyde (34.0 mg, 0.86 mmol), *N*,*N*–dimethylpiperidin–4–amine (27.0 mg, 0.21 mmol), propargylcytimidine (115 mg, 0.21 mmol) and 1,4–Dioxane (2.5 mL) to afford the title compound (98mg, 68%) as colorless solid.

R_f = 0.30 (MeOH/CH_2Cl_2/ NH_4OH (3:7:0.1). Mp 120 – 122 °C. $[\alpha]^{20}_D$ = –39 ^{o} (*c* = 0.10, $CHCl_3$).

^{1}H NMR (400 MHz, $CDCl_3$) δ 8.01 (d, *J* = 7.6 Hz, 1H), 7.87 (d, *J* = 8.4 Hz, 2H), 7.65 (d, *J* = 8.0 Hz, 2H), 7.51 (d, *J* = 7.6 Hz, 1H), 5.17 (s, 1H), 4.77 (d, *J* = 8.8 Hz, 1H), 4.73 (s, 2H), 3.77 (d, *J* = 8.8 Hz, 1H), 3.33 (s, 2H), 2.92 (d, *J* = 11.2 Hz, 2H), 2.26 (s, 6H), 2.15 (t, *J* = 11.6 Hz, 3H), 1.82 (d, *J* = 12.4 Hz, 2H), 1.69 (s, 3H), 1.59–1.50 (m, 2H), 1.49 (s, 9H), 0.89 (s, 9H). 13C NMR (100 MHz, $CDCl_3$); 171.8, 166.0, 162.5, 156.0, 155.2, 147.0, 142.9, 129.0, 128.0, 119.4, 98.0, 97.0, 84.6, 83.1, 76.0, 68.1, 61.7, 52.2, 47.2, 41.6, 39.4, 38.2, 28.2, 28.1, 26.2, 22.1. IR (neat) 3258, 2973, 2131, 1743, 1598, 1412 cm–1. LRMS Calculated for $C_{36}H_{52}N_7O_6$ m/z (M+H) 678.4, Obsd 678.3

E. General procedure for reduction of Alkyne to Alkane

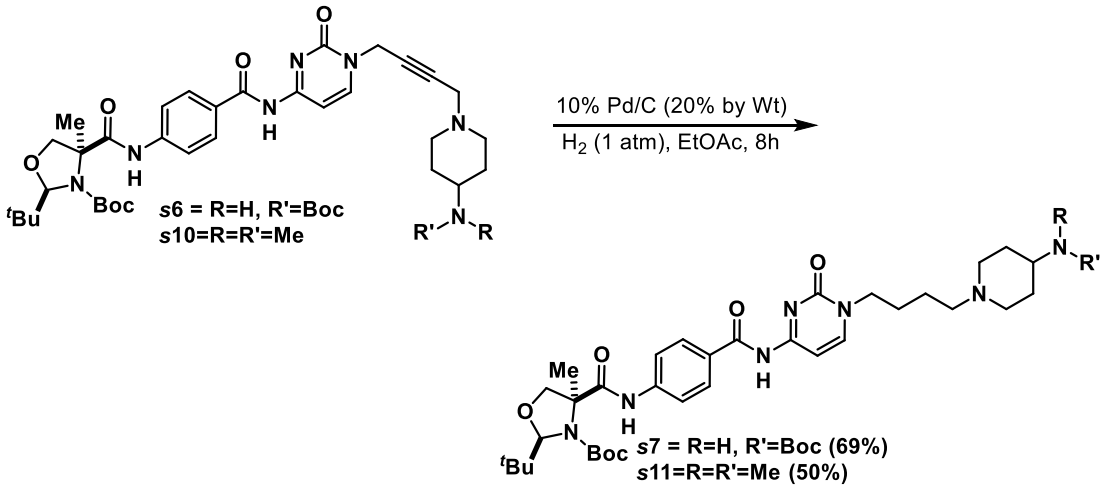

***Scheme* 3. Reduction of Alkynes to Alkanes**

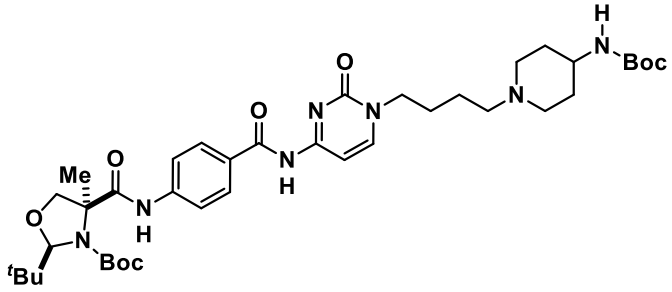

***tert*–butyl(2*R*,4*S*)–2–(*tert*–butyl)–4–((4–((1–(4–(4–(dimethylamino) piperidin–1–yl)butyl)–2–oxo–1,2–dihydropyrimidin–4–yl)carbamoyl)phenyl) carbamoyl)–4–methyloxazolidine–3–carboxylate (*S*8):** A dried round bottom flask equipped with a stir bar was evacuated and backfilled with nitrogen gas, and 10% palladium (Pd) on activated carbon (14 mg, 20% by weight) was transferred into the reaction flask under nitrogen atmosphere. EtOAc (4mL) was added to submerge the Pd/C followed by the addition of alkyne ***S*6** (68 mg, 92.0 µmol, 1.0 equiv.). The reaction mixture was evacuated and purged with hydrogen gas three times, and then the reaction mixture was left to react for 8 hrs under hydrogen atmosphere. The reaction was monitored by TLC using $CHCl_3$/CH_3OH (95:5 to) as

eluent. The TLC shows progressive conversion of alkyne to alkene and then the more polar alkane. The reaction mixture was diluted with ethyl acetate (5mL) and filtered through a pad of Celite® and washed with hot MeOH (3 ml x 2). The solvent was concentrated under reduced pressure affording the reduced products as yellow colored sticky solid. The compound was used in next step without furthur purification.

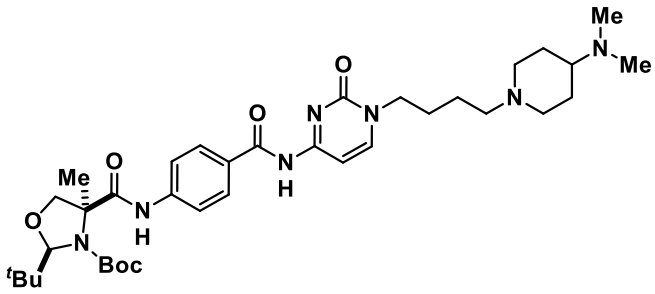

***tert*–butyl–(2*R*,4*S*)–2–(*tert*–butyl)–4–((4–((1–(4–(4–(dimethylamino) piperidin–1–yl)butyl)–2–oxo–1,2–dihydropyrimidin–4–yl)carbamoyl)phenyl) carbamoyl)–4–methyloxazolidine–3–carboxylate (*S12*):** Compound ***S*12** was synthesized following a procedure similar to ***S*8,** using alkyne ***S*10** (70 mg, 93.0 µmol, 1.0 equiv.), Palladium, 10% on activated carbon (14 mg, 20% by weight), and ethyl acetate (3mL) to afford the alkane ***S*12** as yellow colored sticky solid. The compound as such without furthur purification was used in the next step.

F. General procedure for global deprotection

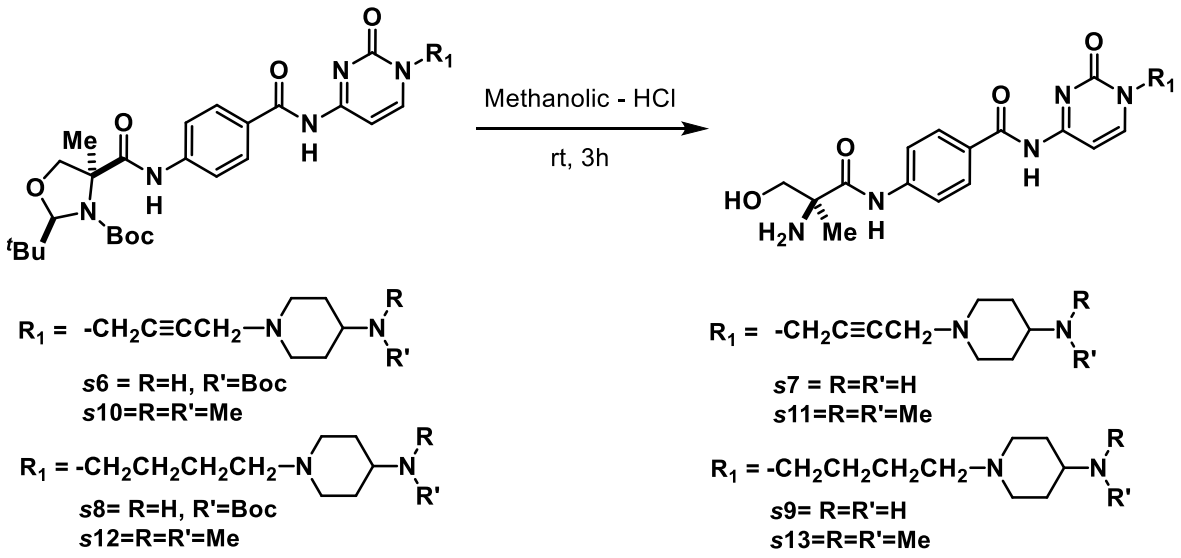

***Scheme* 3. Global deprotection**

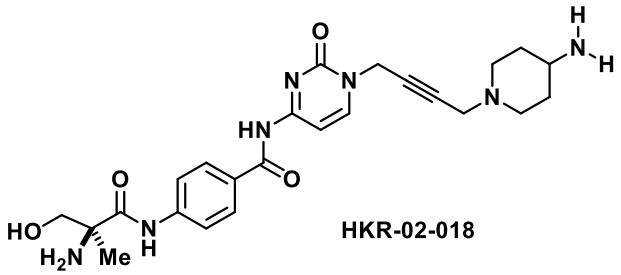

(*S*)–4–(2–amino–3–hydroxy–2–methylpropanamido)–*N*–(1–(4–(4–aminopiperidin–1–yl)but–2–yn–1–yl)–2–oxo–1,2–dihydropyrimidin–4–yl) benzamide (S7): Compound ***S6*** (70 mg, 93.0 µmol) was dissolved in methanolic HCl (3 mL) and stirred at room temperature for three hrs. The reaction mixture was concentrated under reduced pressure. The residue was basified with Et_3N and purified using Isco–Combiflash® and MeOH: $CHCl_3$:NH_4OH (2.8:7:0.2) as eluting solvent to yield the title compound as freebase (31 mg, 69%) as yellow colored solid.

R_f = 0.30 (MeOH: $CHCl_3$: NH_4OH (2.8 :7:.2), Mp 220 – 222

°C(decomposed). $[\alpha]^{20}_D$ = –8 (*c* = 0.10, H_2O).

^{1}H NMR (500 MHz, CD_3OD) δ 8.18 (d, *J* = 7.5 Hz, 1H), 7.94 (d, *J* = 8.5 Hz, 2H), 7.78 (d, *J* = 8.5 Hz, 2H), 7.54 (d, *J* = 7.5 Hz, 1H), 4.76 (s, 2H), 3.95 (d, *J* = 11.0 Hz, 1H), 3.44 (d, *J* = 10.5 Hz, 1H), 3.35 (s, 2H), 2.89 (d, *J* = 12.0 Hz, 2H), 2.70–2.64 (m, 1H), 2.25 (t, *J* = 11.5 Hz, 2H), 1.85 (d, *J* = 11.5 Hz, 2H), 1.47–1.38 (m, 2H), 1.31 (s, 3H). ^{13}C NMR (125 MHz, CD_3OD) δ 177.4, 168.2, 165.0, 157.9, 149.7, 143.9, 130.3, 129.4, 120.4, 98.8, 83.0, 79.4, 69.7, 60.6, 52.2, 47.5, 40.6, 34.8, 23.4. IR (neat) 3726, 3265, 2962, 2138, 1683, 1605, 1546, 1476 cm–1. HRMS (ESI) Calculated for $C_{28}H_{35}N_5O_6Na$ m/z (M+Na)

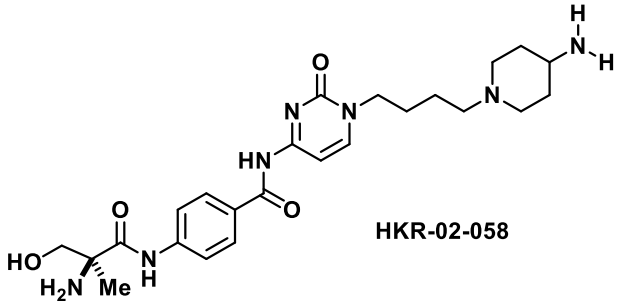

HKR-02-058

(*S*)–4–(2–amino–3–hydroxy–2–methylpropanamido)–*N*–(1–(4–(4–aminopiperidin–1–yl)butyl)–2–oxo–1,2–dihydropyrimidin–4–yl)benzamide (*S*9): Compound ***S*9** was prepared following a procedure similar to **S7** using fully protected **S8** (68 mg, 90.0 µmol) dissolved in methanolic HCl (3 mL) followed by column purification to yield the title compound as free base (18.0 mg, 42%) as yellow colored solid.

R_f = 0.30 (MeOH:CHCl3:NH4OH (2.8:7:0.2), Mp 190 – 192 °C, (decomposed). $[\alpha]^{20}_D$ = –10 (*c* = 0.20, H_2O).

^{1}H NMR (400 MHz, D_2O) δ 8.07 (d, *J* = 7.2 Hz, 1H), 7.97 (d, *J* = 8.8 Hz, 2H), 7.82 (d, *J* = 8.8 Hz, 2H), 7.55 (d, *J* = 7.2 Hz, 1H), 3.97 (brs, 2H), 3.95 (d, *J* = 10.0

Hz, 1H), 3.43 (d, *J* = 10.4 Hz, 1H), 2.92 (d, *J* = 11.6 Hz, 1H), 2.71–2.63 (m, 1H), 2.94 (t, *J* = 10.4 Hz, 2H), 2.05 (t, *J* = 11.6 Hz, 2H), 1.87–1.75 (m, 4H), 1.62–1.54 (m, 2H), 1.49–1.29 (m, 2H) 1,31 (s, 2H). ^{13}C NMR (100 MHz, D_2O) δ 177.5, 168.3, 164.8, 158.8, 151.1, 144.0, 130.3, 129.6, 120.5, 98.5, 79.5, 69.7, 60.6, 58.9, 53.4, 51.7, 34.9, 28.0, 24.7, 23.3. IR (neat) 3847, 2930, 1642, 1482, 1406, 1302, 1242 cm–1. HRMS (ESI) Calculated for $C_{28}H_{36}N_5O_6$ m/z (M+H) 486.2829 Obsd. 486.2830.

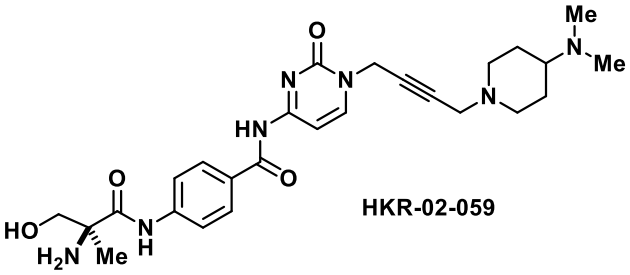

HKR-02-059

(*S*)–4–(2–amino–3–hydroxy–2–methylpropanamido)–*N*–(1–(4–(4–(dimethylamino)piperidin–1–yl)but–2–yn–1–yl)–2–oxo–1,2–dihydropyrimi–din–4–yl)benzamide (*S*11): Compound ***S*11** was prepared following a procedure similar to ***S*7** using fully protected ***S*10** (34 mg, 50 µmol) dissolved in methanolic HCl (2 mL) followed by column purification to yield the title compound as free base. The free base was then dissolved in a minimal amount of MeOH. Then 1M HCl in diethyl ether was added and a solid crashed out. The solid was triturated with diethyl ether and the solvent was decanted. The solid was dried under high vacuum to yield the hydrochloride salt of the title compound as a colorless solid (16 mg, 50%).

R_f = 0.30 (MeOH/$CHCl_3$/NH_4OH (2.8/7.0/0.2), Mp 194 – 196 °C (decomposed). $[\alpha]^{20}_D$ = – 12 ^{o} (*c* = 0.25, H_2O).

^{1}H NMR (500 MHz, D_2O) δ 8.22 (d, *J* = 7.0 Hz, 1H), 7.90 (d, *J* = 7.5 Hz, 2H), 7.63 (d, *J* = 8.0 Hz, 2H), 7.30 (d, *J* = 7.0 Hz, 1H), 4.82 (s, 2H), 4.13 (s, 2H), 4.12 (d, *J* = 12.0 Hz, 1H), 3.89 (d, *J* = 12.0 Hz, 1H), 3.83 (d, *J* = 12.0 Hz, 2H), 3.64–3.55 (m, 1H), 3.22 (t, *J* = 12.0 Hz, 2H), 2.89 (s, 6H), 2.44 (d, *J* = 12.5 Hz, 2H), 2.04–1.98 (m, 2H), 1.66 (s, 3H). ^{13}C NMR (125 MHz, D_2O) δ 171.4, 170.6, 164.5, 156.9, 152.8, 143.1, 131.4, 130.8, 123.6, 100.3, 85.5, 76.1, 66.1, 64.1, 61.6, 52.2, 47.8, 42.5, 42.0, 26.0, 20.0. IR (neat) 3740, 3662, 2945, 2136, 1691, 1600, 1530, 1483, 1246 cm–1. HRMS (ESI) Calculated for $C_{28}H_{35}N_5O_6Na$ m/z (M+Na)

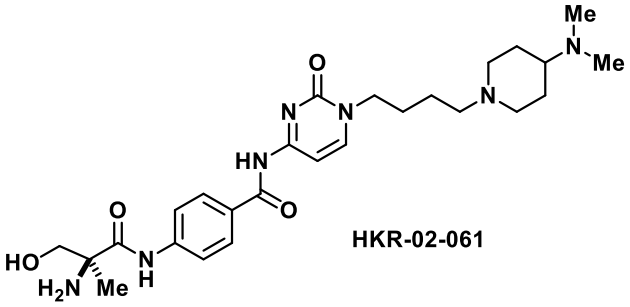

HKR-02-061

(*S*)–4–(2–amino–3–hydroxy–2–methylpropanamido)–*N*–(1–(4–(4–(dimethylamino)piperidin–1–yl)butyl)–2–oxo–1,2–dihydropyrimidin–4–yl) benzamide (*S*13): Compound ***S*12** was prepared following a procedure similar to **S7** using fully protected ***S*12** (34.0 mg, 50 µmol) dissolved in methanolic HCl followed by column purification to yield the title compound as free base. The free base was then dissolved in a minimal amount of MeOH. Then 1M HCl in diethyl ether was added and a solid crashed out. The solid was triturated and the solvent was decanted and residue was dried under high vacuum to yield the title compound as hydrochloride salt (12 mg, 38%).

R_f = 0.30 (MeOH/$CHCl_3$/NH_4OH (2.8/7/0.2), Mp 198 – 200 °C (decomposed). $[\alpha]^{20}_D$ = –9 (*c* = 0.25, H_2O).

^{1}H NMR (500 MHz, D_2O) δ 8.24 (d, *J* = 7.5 Hz, 1H), 7.94 (d, *J* = 8.5 Hz, 2H), 7.66 (d, *J* = 8.5 Hz, 2H), 7.16 (d, *J* = 7.5 Hz, 1H), 4.14 (d, *J* = 12.5 Hz, 1H), 4.00 (brs, 2H), 3.91 (d, *J* = 12.5 Hz, 1H), 3.78 (d, *J* = 12.5 Hz, 1H), 3.64–3.55 (m, 1H), 3.20 (t, *J* = 7.0 Hz, 2H), 3.11 (t, *J* = 12.5 Hz, 2H), 2.89 (s, 6H), 2.41 (d, *J* = 12.5 Hz, 2H), 2.06–1.95 (m, 2H), 1.86–1.75 (m, 4H), 1.67 (s, 3H). ^{13}C NMR (125 MHz, D_2O) δ 169.4, 168.8, 161.0, 153.2, 152.8, 141.4, 129.5, 128.3, 121.6, 97.4, 64.0, 62.1, 59.7, 56.1, 50.6, 50.3, 40.0, 39.9, 25.0, 23.9, 20.6, 17.7. IR (neat) 3723, 3260, 2943, 1692, 1600, 1536, 1486, 1410, 1367, 1245 cm–1. HRMS (ESI) Calculated for $C_{28}H_{35}N_5O_6Na$ m/z (M+Na)

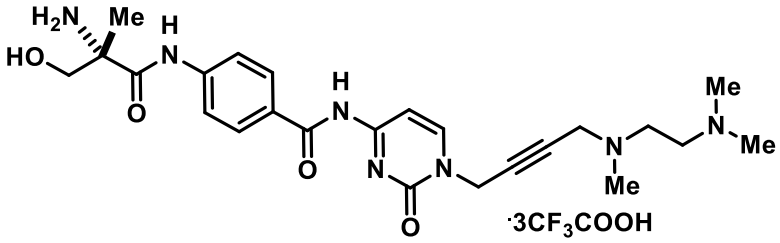

HKR-01-162: (*S*)–4–(2–amino–3–hydroxy–2–methylpropanamido)–*N*–(1–(4–((2–(dimethylamino)ethyl)(methyl)amino)but–2–yn–1–yl)–2–oxo–1,2–dihydropyrimidin–4–yl)benzamide trifluoroacetate salt: Orange colored solid. mp. 108–110 °C, $[\alpha]^{20}_{D}$ = –2.8 (*c* = 2.00, $CHCl_3$). ^{1}H NMR (400 MHz, CDCl3); δ ppm 8.06 (d, *J* = 7.2 Hz, 1H), 7.91 (d, *J* = 8.4 Hz, 2H), 7.71 (d, *J* = 8.4 Hz, 2H), 7.58 (d, *J* = 7.2 Hz, 1H), 4.75 (s, 1H), 4.17 (d, *J* = 10.4 Hz, 1H), 3.48 – 3.44 (m, 3H), 2.56 (t, J_1 = 6.4, J_2 = 7.2 Hz, 2H), 2.42 (t, J_1 = 6.4, J_2 = 7.2 Hz, 2H), 2.33 (s, 3 H), 2.26 (s, 6H), 1.35 (s, 3H) ppm. ^{13}C NMR (100 MHz, $CDCl_3$) δ ppm 175.7, 162.6, 155.5, 146.8, 142.1, 129.1, 127.8, 119.2, 97.2, 84.3, 69.2, 64.2, 59.8, 57.2, 53.6, 46.2, 45.8, 42.2, 39.5, 29.7, 23.7. IR (neat) 2920, 2850, 1733, 1683, 1674, 1653, 1457 cm^{-1}. HRMS (ESI) Calculated for $C_{24}H_{34}N_7O_4Na$ *m/z* 484.2672 (M+H)

Obsd. 484.2676.

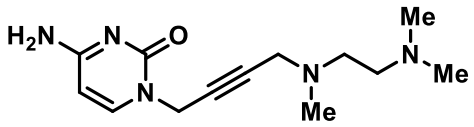

HKR-01-143:4–amino–1–(4–((2–(dimethylamino)ethyl) (methyl) amino) but–2–yn–1–yl)pyrimidin–2(1H)–one

Brick red solid. Mp 150–153 °C. ^{1}H NMR (400 MHz, $CDCl_3$) δ ppm 7.48 (d, *J* = 7.2 Hz, 1H), 5.92 (d, *J* = 6.9 Hz, 1H), 4.54 (bs, 2H), 3.34 (bs, 2H), 2.47 (t, *J* = 6.3 Hz, 2H), 2.34 (t, *J* = 6.3 Hz, 2H), 2.24 (s, 3H), 2.19 (s, 3H). ^{13}C NMR (100 MHz, $CDCl_3$) δ ppm 166.4, 156.4, 143.3, 95.6, 82.3, 78.4, 57.2, 53.4, 46.3, 45.7, 42.2, 38.4.

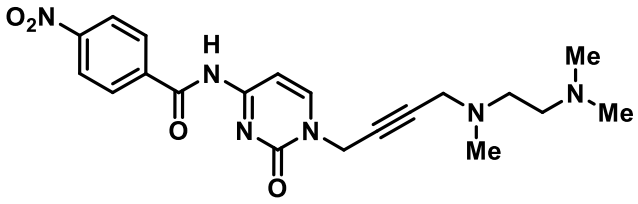

HKR-01-157: N–(1–(4–((2–(dimethylamino)ethyl)(methyl)amino)but–2–yn–1–yl)–2–oxo–1,2–dihydropyrimidin–4–yl)–4–nitrobenzamide

^{1}H NMR (300 MHz, $CDCl_3$) δ ppm 8.26 (d, *J* = 8.7 Hz, 2H), 8.24 (d, *J* = 7.8 Hz, 1H), 8.17 (d, *J* = 8.7 Hz, 2H), 8.01 (d, *J* = 7.8 Hz, 1H), 4.68 (bs, 2H), 3.41 (bs, 2H), 2.49 (t, *J* = 6.9 Hz, 2H), 2.35 (t, *J* = 6.3 Hz, 2H), 2.27 (s, 3H), 2.22 (s, 3H). ^{13}C NMR (100 MHz, $CDCl_3$) δ ppm 167.8, 162.6, 153.9, 150.3, 146.9, 139.4,130.8, 123.9, 98.5, 84.5, 76.7, 57.3, 53.6, 46.3, 45.8, 42.3, 39.4 ppm.

Synthesis of HKR–02–014

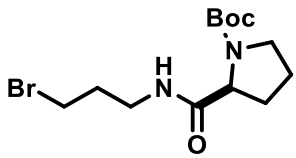

***tert*–butyl(*R*)–2–((3–bromopropyl)carbamoyl)pyrrolidine–1–carboxy-late**: Under a nitrogen atmosphere ethylchloroformate (0.29 mL, 3.11 mmol) was added to a cold (–20 °C) solution of *N*–Boc L–proline (0.64 g, 3.00 mmol) and *N*–Methylmorpholine (0.32 mL, 4.50 mmol) in dry THF (5 mL). After 5 min 3–bromopropylamine hydrobromide dissolved in THF: DMF (1:4 v/v) was added to the above mixture followed by the addition of *N*–Methylmorpholine (0.53 mL, 7.8 mmol). After stirring the mixture at –20 °C for 10 min, it was warmed to room temperature and stirred for 4 hrs. The reaction mixture was diluted with ethyl acetate (25 mL) and washed with water followed by brine. The organic layer was dried over Na_2SO_4 and concentrated under reduced pressure. Purification on silica gel using flash chromatography (30% EtOAc:Hexanes) afforded the desired product (0.60 g, 58%) as a white solid.

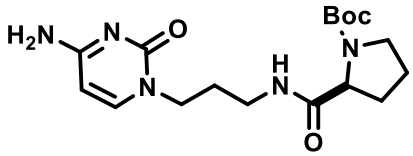

***tert*–butyl(*S*)–2–((3–(4–amino–2–oxopyrimidin–1(2*H*)–yl)propyl) carbamoyl) pyrrolidine–1–carboxylate**: To a stirred solution of cytosine (0.22 g, 2.00 mmol) in CH_3CN (12 mL), Cs_2CO_3 (0.65 g, 2 mmol) and *tert*–butyl (*S*)–2–((3–bromopropyl)carbamoyl)pyrrolidine–1–carboxylate (0.67 g, 2.00 mmol) was added under an atmosphere of nitrogen. The reaction mixture was heated to reflux for 2 hrs. After which, mixture was concentrated under reduced pressure. Purification on silica gel using flash chromatography (10% CH_2Cl_2/MeOH, 1% NH_4OH) afforded the desired product (0.37 g, 51%) as a white colored solid.

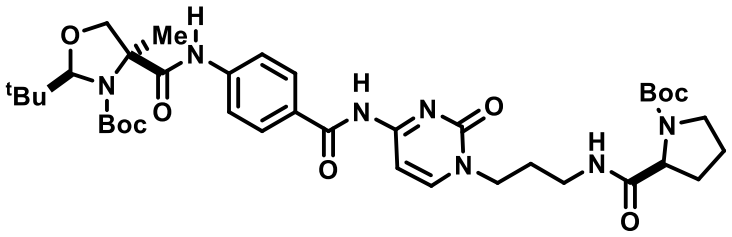

***tert*–butyl(2*R*,4*S*)–4–((4–((1–(3–((*S*)–1–(*tert*–butoxycarbonyl) pyrolidine–2–carboxamido)propyl)–2–oxo–1,2–dihydropyrimidin–4–yl)carbamoyl)phenyl)carbamoyl)–2–(*tert*–butyl)–4–methyloxazolidine–3–carboxylate:** To a solution of 4–((2*R*,4*S*)–3–(*tert*–butoxycarbonyl)–2–(*tert*–butyl)–4–methyloxazolidine–4–carboxamido)benzoic acid (102 mg, 0.25 mmol) in dichloromethane (12 mL), was added EDC.Cl (110 mg, 0.5 mmol), HOBt (70 mg, 0.50 mmol), NEt_3 (137 µL, 1.00 mmol) and stirred at room temperature for 5 min. *tert*–Butyl(*S*)–2–((3–(4–amino–2–oxopyrimidin–1(2*H*)–yl)propyl)carbamoyl)pyrol-edine–1–carboxylate (116 mg, 0.25 mmol) was added to this mixture and stirring continued for an additional 2 hrs. The reaction was quenched with a saturated $NaHCO_3$ (3 mL) aqueous solution and diluted with 3 mL of dichloromethane. The phases were separated and the organic phase was washed with water (2 X 2 mL) followed by a brine wash (1 X 2 mL). The organic layer was dried (Na_2SO_4), filtered and concentrated under reduced pressure. The crude product was purified by flash chromatography (5% MeOH/$CHCl_3$) to afford desired compound (98 mg, 52%) as a white solid.

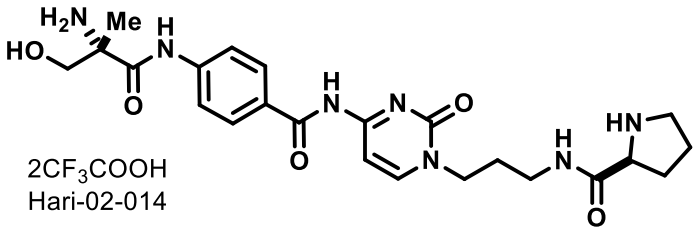

HKR–02–014:(*S*)–*N*–(3–(4–(4–((*S*)–2–amino–3–hydroxy–2–methyl–propanamido) benzamido)–2–oxopyrimidin–1 (2*H*)–yl) propyl) pyrrolidine–2–carboxamide trifluoroacetate salt: *tert*–butyl (2*R*,4*S*)–4–((4–((1–(3–((*S*)–1–(*tert*–butoxycarbonyl)pyrrolidine–2–carboxamido)propyl)–2–oxo–1,2–dihydropyrimidin–4–yl) carbamoyl) phenyl) carbamoyl)–2–(*tert*–butyl)–4–methyloxazolidine–3–carboxylate (76.0 mg, 0.10 mmol) was dissolved in 30% TFA in dichloromethane (4 mL) and stirred at room temperature for 12 hrs. The reaction mixture was concentrated, dissolved in water and washed with ether (2 X 2 mL) to remove the organic impurities. The aqueous layer was diluted with aq. $NaHCO_3$ and the compound was extracted with dichloromethane (2 X 4 mL) dried over anhydrous Na_2SO_4, filtered and concentrated, and the residue was dissolved in 30% TFA in dichloromethane and stirred for 0.5 h. Then, the solvent was evaporated and triturated with diethyl ether followed by filtration affording the title compound **HKR–02–014** (42 mg, 53%).

R_f = 0.30 (MeOH/$CHCl_3$/NH_4OH (2.8/7.0/0.2), Mp 130–132 °C, $[\alpha]^{20}_D$ = – 6 ^{o} (*c* = 0.1, H_2O).

^{1}H NMR (400 MHz, D_2O) δ 8.12 (d, *J* = 7.2 Hz, 1H), 7.98 (d, *J* = 8.0 Hz, 2H), 7.70 (d, *J* = 8.0 Hz, 2H), 7.46 (d, *J* = 7.2 Hz, 1H), 4.38 (t, *J* = 6.8 Hz, 1H), 4.18 (d, *J* = 13.2 Hz, 1H), 4.01 (t, *J* = 6.4 Hz, 2H), 3.95 (d, *J* = 12.8 Hz, 2H), 3.50–3.32 (m, 4H), 2.50–2.43 (m, 1H), 2.12–2.02 (m, 5H), 1.72 (s, 3H). ^{13}C NMR (100 MHz, D_2O) δ 169.4, 162.9, 157.7, 150.9, 140.8, 129.2, 121.9, 117.8, 110.0, 98.5, 64.1, 62.1, 59.8, 48.5, 46.4, 36.7, 29.6, 27.4, 23.7, 17.8 ppm. IR (neat); LC–MS Calculated for m/z [M+H] 486.2, Obsd.486.2.

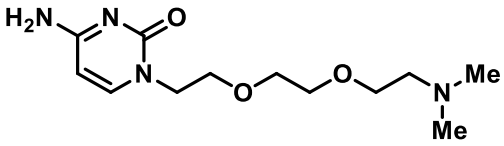

4–Amino–1–(2–(2–(dimethylamino)ethoxy)ethyl)pyrimidin–2(1H)–one: In an oven dried sealed tube, 4–Amino–1–(2–(2–(2–chloroethoxy)ethoxy)ethyl) pyrimidin–2(1H)–one (24 mg, 0.09 mmol), K_2CO_3 (14 mg, 0.09 mmol) and a 2 M solution of dimethylamine in methanol (1 mL) was added under an atmosphere of nitrogen. The reaction mixture was heated for 2 hrs at 70 °C. The solvent was evaporated and the residue was purified on silica gel using flash chromatography (15% CH_2Cl_2/MeOH) affording the desired product (36 mg, 85%) as a colorless oil. ^{1}H NMR (400 MHz, CDCl3); δ ppm 7.37 (d, *J* = 6.8 Hz, 1H), 5.92 (d, *J* = 6.8 Hz, 1H), 3.86 (t, *J* = 4.20 Hz, 2H), 3.62 (t, *J* = 4.2 Hz, 2H), 3.54 (t, *J* = 4.20 Hz, 2H), 3.49 (bs, 6H), 2.70 (t, *J* = 4.2 Hz, 2H), 2.39 (s, 6H). ^{13}C NMR (100 MHz, CDCl3); δ ppm 166.2, 157.1, 146.8, 94.7, 70.3, 70.2, 68.8, 67.8, 58.1, 49.5, 45.1. IR (neat) 3326, 3184, 2867, 1645, 1520, 1489, 1385 cm–1. HRMS (ESI) Calculated for $C_{12}H_{23}N_4O_3$ m/z (M+H) 271.1770, Obsd. 271.1770.

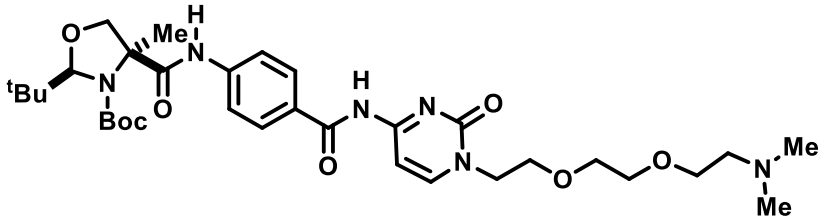

(2*R*,4*S*) –*tert*–butyl2– (*tert* – butyl) –4– ((4– ((1– (2– (2–(dimethylamino) ethoxy)ethyl)–2–oxo–1,2–dihydropyrimidin–4–yl)carbamoyl)phenyl)carbam-oyl)–4–methyloxazolidine–3–carboxylate:

To a solution of 4–((2*R*,4*S*)–3–(*tert*–butoxycarbonyl)–2–(*tert*–butyl)–4

methyloxazolidine–4–carboxamido)benzoic acid (20 mg, 0.04 mmol) in dichloromethane (2 mL), was added EDCI (11 mg, 0.05 mmol), HOBt (7 mg, 0.05 mmol), NEt_3 (20 µL, 0.14 mmol) and stirred at room temperature for 5 min. 4–Amino–1–(2–(2–(dimethylamino)ethoxy)ethyl)pyrimidin–2(1H)–one (12 mg, 0.04 mmol) was added to this mixture, and stirring continued for an additional 2 hrs. The reaction mixture was quenched with a saturated $NaHCO_3$ solution and diluted with 3 mL of dichloromethane. The organic layer was separated and washed with water (2 X 2 mL) followed by a brine wash (1 X 2 mL). The organic layer was dried over anhydrous Na_2SO_4, filtered and concentrated under reduced pressure. The crude product was purified by flash chromatography (5% MeOH/$CHCl_3$, 1% Et_3N) afforded the desired compound (15 mg, 54%) as a yellow sticky solid. $[\alpha]^{20}_D$ = –2.8 (*c* = 2, $CHCl_3$). ^{1}H NMR (300 MHz, $CDCl_3$): δ ppm 7.90 (d, *J* = 9.0 Hz, 2H), 7.82 (d, *J* = 7.2 Hz, 1H), 7.69 (d, *J* = 9.0 Hz, 2H), 7.40 (d, *J* = 7.2 Hz, 1H), 5.21 (s, 1H), 4.82 (d, *J* = 9.6 Hz, 1H), 4.11 (t, *J* = 5.4 Hz, 2H), 3.84 –3.76 (m, 3H), 3.62 – 3.54 (s, 6H), 2.52 (t, *J* = 5.4 Hz, 2H), 2.28 (s, 6H), 1.73 (s, 3H), 1.54 (s, 9H), 0.91 (s, 9H). IR (neat) 2961, 1733, 1683, 1653, 1635, 1598, 1521, 1481 cm^{-1}. HRMS (ESI) Calculated for C33H51N6O8 *m/z* $(M+H)^+$ 659.3768, Obsd. 659.3771.

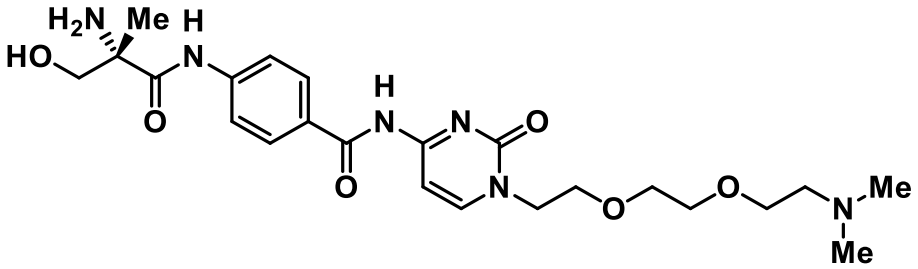

HKR–01–084: (*S*)–4–(2–amino–3–hydroxy–2–methylpropanamido)–*N*–(1–(2–(2–(2–(dimethylamino)ethoxy)ethoxy)ethyl)–2–oxo–1,2–dihydropyri–

midin–4–yl)benzamide trifluoroacetate salt: brick red colored solid. $[\alpha]^{20}_{D}$ = –2.8 (*c* = 2.00, $CHCl_3$). ^{1}H NMR (400 MHz, D_2O); δ ppm 8.10 (d, *J* = 7.2 Hz, 2H), 7.98 (d, *J* = 8.8 Hz, 1H), 7.70 (d, *J* = 8.8 Hz, 2H), 7.47 (d, *J* = 6.8 Hz, 1H), 4.19 (d, *J* = 12.0 Hz, 1H), 4.18–3.94 (m, 2H), 3.93 (d, *J* = 12.0, 1H), 3.90 (t, , *J* = 5.2, 2H), 3.82 – 3.79 (m, 2H), 3.75 – 3.68 (m, 4H), 3.37–3.33 (m, 2H), 2.91 s, 6H), 1.73 (s, 3H) ^{13}C NMR (100 MHz, D_2O); δ ppm.169.5, 168.7, 163.1, 157.8, 151.5, 140.9, 129.2, 121.8, 117.8, 114.9, 98.1, 69.7, 67.5, 63.9, 62.1, 56.7, 50.3, 46.6, 42.7, 22.4, IR (neat) 2924, 2854, 1699, 1669, 1652, 1635, 1558, 1506, 1488cm^{-1}. HRMS (ESI) Calculated for $C_{23}H_{35}N_6O_6$ *m/z* 491.2618 (M^+), Obsd. 491.2628.

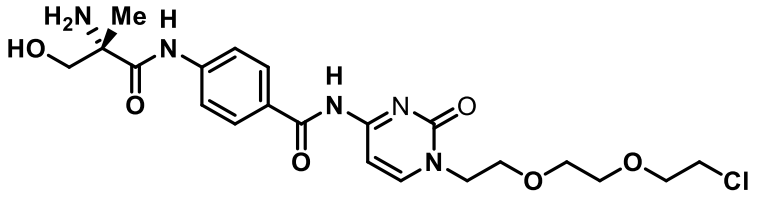

HKR–01–180: (*S*)–4–(2–amino–3–hydroxy–2–methylpropanamido)–N–(1–(2–(2–(2–chloroethoxy)ethoxy)ethyl)–2–oxo–1,2–dihydropyrimidin–4–yl) benzamide trifluoroacetate salt:

White solid. ^{1}H NMR (400 MHz, D_2O); δ ppm 8.04 (d, *J* = 7.2 Hz, 1H), 7.91 (d, *J* = 8.0 Hz, 2H), 7.67 (d, *J* = 8.4 Hz, 2H), 7.37 (d, *J* = 7.2 Hz, 1H), 4.19 (d, *J* = 12.4 Hz, 1H), 4.10 (bs, 2H), 3.97(d, *J* = 12.4, 1H), 3.84 (bs 2H), 3.74 – 3.65 (m, 8H), 1.73 (s, 3H) ^{13}C NMR (100 MHz, D_2O); δ ppm.171.9, 170.6, 165.2, 159.5, 154.4, 143.6, 131.7, 131.4, 123.9, 100.3, 73.3, 72.2, 71.9, 69.8, 66.7, 64.7, 53.0, 45.8, 20.4 ppm.

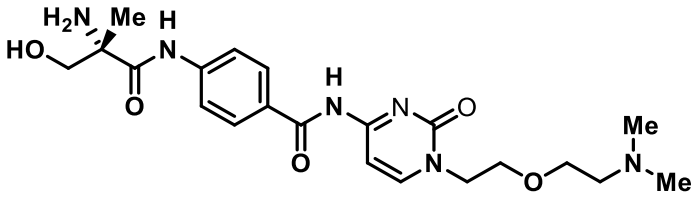

HKR–01–186: (S)–4–(2–amino–3–hydroxy–2–methylpropanamido)–N–(1–(2–(2–(dimethylamino)ethoxy)ethyl)–2–oxo–1,2–dihydropyrimidin–4–yl) benzamide trifluoroacetate salt:

White solid. ^{1}H NMR (400 MHz, D_2O) δ ppm 8.17 (d, *J* = 5.6 Hz, 1H), 8.02 (d, *J* = 6.8 Hz, 2H), 7.74 (d, *J* = 6.4 Hz, 2H), 7.54 (d, *J* = 5.6 Hz, 1H), 4.19 (d, *J* = 12.4 Hz, 1H), 4.16 (bs, 2H), 4.03 (d, *J* = 12.4 Hz, 1H), 3.96 (bs, 2H), 3.88 (bs, 2H), 3.42 (bs, 2H), 2.94 (s, 6H), 1.76 (s, 3H).

CHAPTER 3

SECOND GENERATION AMICETIN ANALOGS

Background

Our first generation analogs were targeted at removal of the acid labile glycosidic (cytosine–acetal) linkage and replacing the complex disaccharide with a stable alkyl group. In doing so, we synthesized ~15 analogs, and identified a set of five simplified analogs that retained activity including our first lead analog **HKR–02–058 / CZ–02–023**.[1] The analog **CZ–02–023** has shown to be active against *Mtb* H37Ra with an IC_{50} of 0.98 μM (amicetin H37Ra IC_{50} = 0.24 μM) only 4–fold less active than the natural product amicetin. Moreover, the analog **CZ–02–023** has 3–fold higher on–target activity (*E. coli S30* IC_{50} = 0.261 μM) compared to amicetin (*E. coli S30* IC_{50} = 0.851 μM), with no measurable cytotoxicity against CEM/TARTs and no CYP induction at 100 μM. One of the biggest assets of the first generation analogs is that they are easily accessible and simple in structure with only one stereocenter, that of the α–methyl serine (compared to amicetin with 9–stereocenters).

Hydrolytic Stability of First Generation Analogs

The biggest concern associated with the first generation analogs is their inherent chemical liability under acidic and basic conditions. The amide bond

formed between cytosine and the *p*–aminobenzoate fragment is not only base labile but also acid sensitive. The Boc–protected first generation analogs under deprotection reaction conditions (TFA or Methanolic–HCl for >4h) result in hydrolysis of the amide bond. The hydrolytic decomposition of purified final compounds largely through the amide bond is seen, when stored in methanol (t1/2 = 72h). The acid sensitivity of these compounds is attributed to the strong electron withdrawing nature of cytosine that results in increased electrophilicity of the carbonyl of the amide thereby making this bond vulnerable to hydrolysis (Figure 3.1. (b)).

Solvolysis and half–life of CZ–02–023

The half–life of CZ–02–023 (both freebase and HCl salt) was determined under different conditions at 25 ^{o}C using proton nuclear magnetic resonance (NMR) spectroscopy. The measured half–life under different conditions are reported in Figure 3.1(b). (See supporting information for experimental procedure).

Replacement of *p*–Aminobenzoate with 2–Aminopyridines

In our second generation analog synthesis, our efforts were focused on optimizing **CZ–02–023** derivatives to improve stability, and potency retaining the selectivity. Advanced SAR on **CZ–02–023** stems from the inputs provided by docking studies of newly designed bi–aryl amine analogs on to the X–ray crystal structure of amicetin bound to the ribosome. The docking studies confirm that the replacement of *p*–amino benzoate with 2–aminopyridines would preserve all the mapping interactions that amicetin has with the ribosome (Figure 3.2).

Accordingly, our next strategy was complete removal of hydrolytically labile *p*–amino benzoate and replacing it with 2–aminopyridine while still preserving the essential structural features (including charged amine termini) to retain amicetin–like ribosomal binding. Presumably, the co–planarity of two aromatic rings in the proposed bi–aryl amine will allow the flanked amine to be able to base pair with G2251, preserving a donor–acceptor–acceptor pattern. The π–π interaction with A2602 involving *p*–amino benzoate will be accomplished by pyridine / phenyl ring in these newly designed analogs. The flexible n–butyl–(4–amino)–piperadinyl linker with primary amine terminus will continue to engage in a cation – π interaction with A2439 and the amine of 1,3–diamine will form a hydrogen bonding interaction with the western portion of binding pocket with the phosphate of G2495 (Figure 3.2).

In this chapter, we describe the synthesis and biological evaluation of different bi–arylamines (pyridyl–cytosine / phenyl–cytosine) with varied charged terminus in the solvent front (western portion of the binding pocket).

Synthesis of Pyridyl–Cytosine Analogs

We envisioned the synthesis of designed bi–aryl amine analogs by employing a Buchwald–Hartwig amination of *N1*–alkylated cytosine **4** and substituted aryl halides **4a**.[2, 3, 4, 5, 6] The synthesis of substituted aryl halides could be achieved from corresponding aldehydes and acids via a reductive amination or peptide coupling with *N*–Boc–1,3–diamino propane, respectively (Figure 3.3).

The forward synthesis of pyridyl–cytosine analogs began with the preparation of substituted aryl halides from their precursors. As shown in Scheme

3.1, the reductive amination of 2–bromo–4–formyl pyridine **2a** with *N*–Boc–1,3–diamino propane and followed by Boc protection of resultant 2^{o} amine afforded di–amino halo pyridine **2**. The amide **3** was synthesized via a peptide coupling reaction of *N*–Boc–1,3–diaminopropane and 2–bromo–pyridine–4–carboxylic acid **3a**. The hydroxy methyl **1a** was protected using TBS and the resultant TBS protected alcohol **1** was used in next step. The prepared substituted 2–halopyridines (**1, 2**, and **3)** were individually reacted in different reaction sequences with an alkylated cytosine **4** under Buchwald–Hartwig amination conditions followed by global deprotection yielded bi–aryl amine analogs as shown in section **D** Scheme 3.1.

The pyridyl–cytosine analogs that we synthesized were tested against *Mtb* H37Ra / *Mtb* H37Rv and for protein synthesis inhibition assays. As expected, the analog with terminal alcohol (no interactions in the western portion of the binding pocket in docking studies) **CZ–02–024** was inactive at 50 μM (MTT assay). The analog with the diamine amine **CZ–02–025** (western half) showed improved activity against *Mtb* H37Ra over the PABA derivatives of amicetin **CZ–02–023** (IC_{50} = 0.98 μM) and is equipotent with amicetin (IC_{50} = 0.24 μM). The 3–pyridylamide substituted analog **CZ–02–026** was 2–fold more active than the natural product amicetin itself. More importantly, both the analogs (**CZ–02–025 / 026**) have shown excellent on–target potency (*E. coli* S30), and are noncytotoxic to mammalian cell line as shown in Table 3.1.

Synthesis of Pyridyl–Cytosine and Phenyl–Cytosine Analogs

The potential biological activities of newly synthesized pyridyl–cytosine analogs encouraged us to synthesize phenyl pyridyl *C4* & *C5*–substidtuted, and *C3* & *C4*–substidtuted 1,3–diamino propane amide and amine variations of biaryl analogs (suggestions from docking studies), and tested for their antitubercular, and protein synthesis inhibition properties.

During the synthesis of phenyl–cytosine derivatives, the general Buchwald–Hartwig amination reaction conditions that worked with activated aryl halides (2–halopyridines) and weak nucleophile (*N1*–alkylated cytosine) did not work for halo benzenes (Bromo benzene or Iodo benzene). Through the screening of various ligands, palladium catalysts and bases we identified a set of optimized reaction conditions with Xantphos/$Pd(dba)_2$/Cs_2CO_3 shown in Scheme 3.2 to couple halo benzene **6** to alkylated cytosine **4**.[2, 3, 4, 5, 6]

Employing optimized amination conditions, we synthesized the phenyl cytosine analogs with substitutions on *C3 & C4* of phenyl ring (amides and amines with 1,3–diaminopropane) as shown in Scheme 3.2. The synthesis of the *C3/C4*–substituted halo benzenes was accomplished in a similar fashion following similar protocols to those described in Scheme 3.1.

Biological Evaluation of Pyridyl–Cytosine and Phenyl–Cytosine Analogs

Biological evaluation of these *meta* or *para* substituted phenyl/pyridyl–cytosine derivatives gave us interesting results. All these analogs are equipotent

or 2– to 3–fold more active than amicetin against *Mtb* H37Ra. As expected, pyridyl–cytosine derivatives were more active than the phenyl–cytosine derivatives (activity is attributed to the planarity of pyridyl–cytosine derivatives). However, the most concerning factor with these new analogs is the loss of selectivity for prokaryotic translation over eukaryotic protein synthesis inhibition. In fact, *m*–substituted pyridyl–cytosine derivatives inhibit eukaryotic translation (Rabbit Reticulocyte Lysate) at lower concentrations than prokaryotic translation (*E. coli* S30) *in vitro.* The *p*–substituted phenyl / pyridyl–cytosine derivatives are slightly selectivity for prokaryotic translation inhibition (Figure 3.2). These compounds show no measurable toxicity to Vero cells (nontoxic, IC_{50}s > 100 μM at 24 hrs). Much to our excitement, the *p*–substituted derivatives **HKR–02–033** / **039** have shown to be active against *Gram* (–) bacteria (whole cell activity) with MIC's 1–8 μg/mL against *E. coli* , WT *K. pneumoniae* (wild type *Klebsiella pneumonia*), CRE *K. pneumoniae* (Carbapenem–Resistant Enterobacteriaceae) and moderately active against *P. aeruginosa* (>64 μg/mL). The broad–spectrum activity of *p*–substituted derivatives opens up new avenues of developing broad spectrum antibiotics (Table 3.2).

Synthesis of RX–P792 for Internal Reference[7]

Encouraged by the activity profiles of *p*–substituted derivatives, and upon further developments, we were hoping to optimize these molecules to create selective and more potent broad spectrum antibiotics. As addressed briefly by Melinta therapeutics in an ASM (American Society for Microbiology) microbe meeting–2011, we learned that they have an active research platform built on

Nobel Prize– winning science. Most importantly, BlaS served as an inspiration for their program to develop novel broad–spectrum pyrrolocytosine containing protein synthesis inhibitors.[7, 8, 9] Toxicity of the pyrrolocytosine class of compounds has been one of the major issues they have yet to address. Before proceeding with further SAR on bi–aryl amine derivatives, we targeted the synthesis of Melinta's active compound **RX–P792** as an internal reference to gain insights into the factors governing the *Gram* (–) penetrance, potency, and toxicity. The convergent synthesis of **RX–P792** was achieved by improvising a reported protocol shown in Scheme 3.3.

Retrosynthetic analysis of RX–P792[7]

The reported convergent synthetic procedure for **RX–P792** employs a key Sonogashira cross–coupling reaction of *N1*–arylated–5–Iodocytosine **9** intermediate with substituted phenyl acetylene **8**, followed by an intramolecular cyclization reaction to produce the pyrrolocytosine. The eastern half of the molecule *N1*–arylated–5–Iodocytosine **9** was synthesized by employing a Chan–Lam coupling reaction of iodo cytosine and boronic acid **11**. The phenyl acetylene **8** is synthesized via a sequence of reactions from fluoro, chloro–substituted aniline **10**. Installation of guanidine on the 1^{o} amine of the eastern half was carried out in the penultimate step of the synthesis. The optimized synthetic route for the western half of the molecule (substituted phenyl acetylene) followed a different synthetic sequence to that of reported procedure.[7]

Reported synthetic procedure of substituted phenylacetylene

The reported synthetic procedure for substituted phenylacetylene **8** involves a six longest–linear step sequence of reactions beginning from a commercially available starting material 4–Chloro–3–fluoroaniline **10**. The 4–Chloro–3–fluoroaniline subjected to *ortho*–iodination followed by *ortho*–bromination using the amine as a strong *o*–directing group, resulted in 2–bromo–4–Chloro–3–fluoro–6–Iodo–aniline **12**. Deamination of the aniline was accomplished by Knoevenagel diazotization followed by 1N NaOH workup to afford 1–bromo–3–Chloro–2–fluoro–5–Iodo–benzene **13**. The reactivity of aryl Iodide was utilized in regio–selective Suzuki–Miyaura cross–coupling reaction with N–cbz–butyl amino boronate to yield alkylated aryl bromide **14**. The reactive bromide was then used in the Sonogashira cross–coupling reaction with trimethylsilyl acetylene, followed by base mediated desilylation of the resultant TMS alkyne **15** to afford the desired product [4–(4–Chloro–3–ethynyl–5–fluoro–phenyl)–butyl]–carbamic acid benzyl ester **8**. The synthetic sequence involves a couple of low yielding steps (47–55%), and also other industrious reaction conditions and expensive reagents as shown in Scheme 3.4.[10]

An efficient convergent synthetic route to **RX–P792** followed an initial synthesis of coupling partners, and late stage installation of guanidine functionality in a regio–selective fashion followed by single step deprotection of Boc and Cbz protecting groups.

Modified synthetic procedure for substituted phenyl acetylene

Our expedient synthesis of the substituted phenyl acetylene (western half) involved a short sequence of three simple steps as shown in Scheme 3.5 (compared to six steps in a reported procedure in Scheme 3.4). The optimized route begins with Iodination of the cheap feedstock chemical 2–Chloro–3–fluoro–benzaldehyde (25G–34$) using aldehyde as the *m*–directing group resulted in 2–Chloro–3–fluoro–5–Iodo–benzaldehyde **16**. The aryl iodide was subjected to Suzuki–Miyaura cross–coupling reaction conditions with *in situ* generated *N*–Cbz–butyl amino boronate to afford alkylated benzaldehyde **17**. The terminal alkyne **18** was generated from aldehyde using Ohira–Bestman reagent in high yields as shown in Scheme 3.5.[7, 11, 12]

Synthesis of *N1–arylated*–5–iodocytosine

The coupling partner to create the pyrrolo–cytosine (*N1*–arylated–5–Iodocytosine) fragment **9** was synthesized following a reported protocol, albeit some modified workup procedures for few reactions. The synthesis commences with iodination of cytosine to give 5–Iodo cytosine as shown in section (E) Scheme 3.6.[13] In another reaction sequence (F), reductive amination of 4–formyl phenylboronic acid with *N*–Boc–1,3–diaminopropane followed by Boc protection of resultant 2^{o} amine produced amino alkyl phenylboronic acid **18**. The resultant phenylboronic acid was oxidatively coupled to 5–iodocytosine under Chan–Lam cross–coupling conditions to form the new N–C bond, resulting in *N1*–arylation of 5–iodocytosine **19**. The amine on aryl iodocytosine **19** was benzoylated using

benzoic anhydride to afford the eastern half **9** of the pyrrolocytosine as depicted in Scheme 3.6.

Regioselective guanylation and synthesis of RX–P792

Having both coupling partners in hand, we went on to synthesize **RX–P792**. The pyroolocytosine **20** was prepared from the Sonogashira cross–coupling reaction of the two coupling partners' phenyl acetylene **8** and iodo cytosine **9**, followed by *in situ* cyclization and debenzoylation. Later, Boc–deprotection of the resultant pyrrolocytosine **20** derivative and subsequent regioselective guanylation of the 1^{o} amine in the presence of the 2^{o} amine in diamine **21** using a bulky guanylating reagent *N, N*–bis–Boc–guanylpyrrazole resulted in the formation of guanidino–pyrrolocytosine **22**. One pot deprotection of Cbz and Boc groups using thioanisole and trifluoroacetic acid followed by column purification afforded desired product **RX–P792** as a yellow colored fluffy solid as illustrated in Scheme 3.7.

Biological Evaluation of RX–P792 and Comparison with CZ–02–039

The compound **RX–P972** was screened for its antibacterial activity and protein synthesis inhibition activity. **RX–P972** was active against a number of *Gram* (+) and *Gram* (–) bacteria with high nanomolar IC_{50}. Though the SAR and synthesis of **RX–P792** are inspired from BlaS, this compound is capable of engaging in a π–π stacking with A2602 like amicetin. We believe the ability of amicetin to π–π stack with A2602 (compared to BlaS) is responsible for the selectivity for prokaryotic translation inhibition over eukaryotic protein synthesis inhibition.

Surprisingly, the compound **RX–P792** showed no selectivity when tested in translational inhibition assays. In fact, it was more potent against eukaryotic translation compared to prokaryotic translation (27 nM vs 37 nM). Both **RX–P972**, and **CZ–02–039** being capable of engaging a π–π stacking interaction with A2602, are nonselective. This observation precludes the role of a π–π stacking interaction with A2602 in selectivity that we witnessed with amicetin and **CZ–02–023**. We assume the guanidine moiety is responsible for the broad-spectrum activity and lack of selectivity of **RX–P792** similar to BlaS. The strong interactions (cation– π) involving guanidine with A2439, and hydrogen bonding interactions with the phosphate backbone of A2439 could contribute to the associated toxicity and non–selective nature of BlaS analogs.

Further, compared to **RX–P792** (37 nM), **CZ–02–039** (52 ± 13 nM) exhibits comparable *E.coli* protein synthesis inhibition, but minimal whole cell activity. We attribute the broad spectrum whole cell activity of **RX–P792** to its high CLogP (3.35 compared to 0.03 of **CZ–02–039**), and maybe the presence of guanidine on 1,3–diamine. Having linked the whole cell activity (partially), and lack of selectivity to guanidine fragment present in RX–P972, we were keen to realize the biological profile of **des–guanyl RX–P792** compared to **RX–P792**. We synthesized **des–guanyl RX–P792** employing a thioanisole, TFA–mediated one pot deprotection of di–Boc amine **20** (Scheme 3.8) and screened for antibacterial and translational inhibition activities. Surprisingly, des–guanyl **RX–P792** continued to display broad spectrum activity, and was moderately selective for prokaryotic translational inhibition (SI = ~6.0, *E. coli* S30 IC_{50}= 30 nM compared to 176 nM for R. ret), and

shown to be cytotoxic against Vero cell line with an IC_{50} of 18 μM (Table 3.3).

These results imply that the lack of cytotoxicity with **CZ–02–039** could be a consequence of its physiochemical properties, restricting both bacterial and mammalian cell wall penetrance. It further suggests that SAR focusing on altering the physiochemical properties (cLogP, tPSA, MWt) of **CZ–02–039** will enhance penetrance and potency. Further, all the three analogs **RX–P972**, des–guanyl **RX–P792,** and **CZ–02–039** have a primary amine as an electrostatic anchor in the western portion of the binding pocket (assuming they bind in a the similar fashion) attached to a 4– and 5–atom linker, respectively. We suspect the flexible linker with an attached primary amine is capable of engaging in off–target interactions, thereby resulting in loss of selectivity.

Strategies for Increasing On–target Potency while Retaining Selectivity

With the inputs provided by **RX–P792**, and **des–guanyl RX–P792** we aim to design our next set of analogs with an increased cLogP (hydrophilicity) for better permeability, and reduced degrees of freedom in the solvated front for selectivity. In addition, we preferred not to have a guanidine in our designed analogs to avoid the general toxicity issues associated with it. Our idea was to synthesize phenyl–cytosine analogs with fluoro–and chloro–substitutions (the similar to RX–P792) on the phenyl rings, and reducing the number of basic amines (replace with a carbon or oxygen) for increasing cLogP.

Synthesis of CZ–02–033 analogs with increased cLogP

All newly proposed analog synthesis involved a penultimate Buchwald–Hartwig amination reaction of two essential coupling partners (amine **4** /aryl halide) followed by a global deprotection using methanolic HCl. The synthesis of designed analogs was pursued with the preparation of requisite western halves, followed by a Buchwald–Hartwig amination reaction using our optimized conditions with the eastern half **4**. The fluoro–chloro–substituted phenyl derivatives were synthesized via an *m*–directed iodination[9] of corresponding carboxylic acid and aldehydes followed by peptide coupling of **23** or reductive amination of **25** with *N*–Boc–1,3–diaminopropane, respectively, to form iodo aryl amide **24** and iodo aryl amine **26** as shown in Scheme 3.9. The amide **24** and amine **26** were reacted individually with alkylated cytosine **4** under Buchwald –Hartwig amination conditions followed by Boc deprotection resulting in **CZ–02–037** and **CZ–02–038,** respectively (Scheme 3.9).

The synthesized analogs screened for their potential biological activities. Surprisingly, the newly synthesized fluoro–chloro– substituted phenyl derivatives have shown a substantial loss in activity across the spectrum (> 32–64 μM) compared to 1–32 μM (except *P. aerugunosa >64*) for unsubstituted counterpart **CZ–02–033**. We were unsure of the reason for the observed loss of activity (Table 3.4).

Since substitutions on the aryl ring did not help us in imparting potency and selectivity, we thought of varying the chain length and the nature of the linker in the next set of analogs. The synthesis of substituted ether linker **30** began with an

S_N2 reaction of a cyclopropyl amine onto 4–bromo–1–butanol, followed by Boc protection of secondary amine **28** resulting in the formation of alcohol **29**. Another S_N2 reaction of the alcohol **29** onto 4– (bromomethyl)–2–bromopyridine afforded bromo pyridine **30**. The western halves with variable alkyl linkers synthesized by employing Suzuki–Miyaura cross– coupling reaction of aryl boronic acid **31** or alkyl borane **37** with aryl halide 1–Bromo–2–fluoro–4–iodobenzene. The alkyl borane was prepared by the hydroboration of the corresponding terminal alkene (**34** or **36**).[7] The alkene **36** was prepared from 1–Boc–4–piperadone via a Wittig olefination reaction as shown in Scheme 3.10.

The western halves synthesized above were reacted with alkylated cytosine **4** under Buchwald–Hartwig amination conditions following a protocol similar to that reported in Scheme 3.9 followed by Boc deprotection resulted in **CZ–02–029** and **CZ–02–040 / 41 / 42**, respectively, as shown in Figure 3.5.

The prepared analogs with diversified linkers in western half targeting increase in cLogP were tested in on–target protein synthesis inhibition assays. The analogs have shown a considerable loss in activity in translational inhibition. They were inactive against *Gram* (–) and *Gram* (+) bacteria and showed good activity against acid–fast *Mycobacterium smegmatis* (4–32 μM). The analogs with ether linkages were shown to be active against the virulent strain of Mtb H37Rv with an IC_{50} of 2 μM, but fail to retain selectivity (Table 3.5).

Synthesis of CZ–02–039 analogs with reduced conformational freedom in linker region

In an attempt to identify a lead compound with on–target potency and selectivity for bacterial translation inhibition, we focused on reducing the conformational freedom of the linker in the western portion of the binding pocket. The rationale for tweaking the amine linker stems from an assumption that the flexible linker engaging in off–target interactions could be the reason for the loss of selectivity. In order to reduce the conformational freedom, we thought of replacing 1,3–diamine with cyclic amines, and chiral tethered amine terminus on western halves. These designed linkers are synthesized from corresponding aldehydes, or acids, via a reductive amination or a peptide coupling reactions respectively as shown in Scheme 3.11. Reductive amination of aldehyde **39** with 2^{o} amine (4–Boc amino piperadine) was achieved under sodium triacetoxy borohydride conditions to give 3^{o} amine **40**, whereas for 1^{o} amines, a conventional $NaBH_4$ reduction was used to access 2^{o} amine followed by Boc protection resulting in amine **41**. To access benzyl amide **42**, the benzyl amine **41** was used as a precursor in peptide couplings with acids (e.g., Boc–Ala), whereas the benzamide **44** was synthesized via a peptide coupling reaction of carboxylic acid **43** and amine (*N*–Boc–azitidine–3–amine) using HATU as the peptide coupling reagent. The synthesis of ether linker **47** was accessed via an S_N2 reaction of alcohol (L–prolinol) on to benzyl chloride **46**. Using the reported protocols in Scheme 3.11, several amines, benzamides, benzyl amides were prepared and used in Buchwald–Hartwig amination reaction followed by global deprotection afforded the bi–aryl

amines with various rigid linkers in the western portion of the binding pocket.

The compounds synthesized were screened for activity against *M. smegmatis* and translational inhibition, and the results are shown in Table 3.6.

Most of these compounds have submicromolar on–target potency and good activity against *M. smegmatis* (2–32 μg/mL). Since *Mtb* is hard and slow to grow *in vitro*, these compounds are tested against *M. smegmatis* (acid–fast bacteria). The activity profile against *M. smegmatis* correlates to *Mtb*. Compounds with MIC's ≤8 against *M. smegmatis* were further screened for activity against the virulent strain of Mtb (H37Rv) in collaboration with NIAID (National Institute of Allergy and Infectious Diseases), as shown in Table 3.7, and on–target protein synthesis inhibition activities but unfortunately none of these analogs retained selectivity.

CZ–02–039 analogs with varied linkers in the

eastern portion of the binding pocket

Compared to amicetin (SI $_{RR/E.Coli}$ = 98), CZ**–02–023** (SI $_{RR/E.Coli}$ = 111), where disaccharide of amicetin is replaced with butylamino piperadine has a better selectivity index. Assuming that the linker portion in the eastern half of the molecule has a role to play in the translational selectivity, we pursued modification in the cation–π region in the eastern portion of the binding pocket. Expanding the optimized route to *N1*–butylaminopiperadine cytosine, we synthesized variable linker substitutions on *N1*–cytosine (eastern fragments) and subjected them to Buchwald–Hartwig amination conditions with the western half of the potent compound (**CZ–02–039**) in the synthesis of bi–aryl amine analogs (Scheme 3.3).

Out of these four analogs of **CZ–02–039** with diverse linkers, the ones with

α–methyl (**CZ–02–084**) and *N*–methyl–4–aminopiperidene (**CZ–02–085**) showed comparable activity. The α–methyl containing analog showed slightly better selectivity (*E. coli* /R. ret = 3.77) compared to **CZ–02–039** (*E. coli* /R. ret = 1.6).

The two analogs were further screened against Mtb H37Rv and the results are shown in Table 3.9.

Conclusion

The second generation analogs synthesized by far replacing the p–amino benzoate with an amine functionality resulted in nonselective broad–spectrum antibacterial compounds (**CZ–02–033, and 039**), and nonselective anti–mycobacterial compounds (**CZ–02–026, 029, 048, 049, 050, 054**) with submicromolar IC_{50}s. The lode of translational selectivity of the second generation analogs has been a major hurdle for progression of this class of compounds.

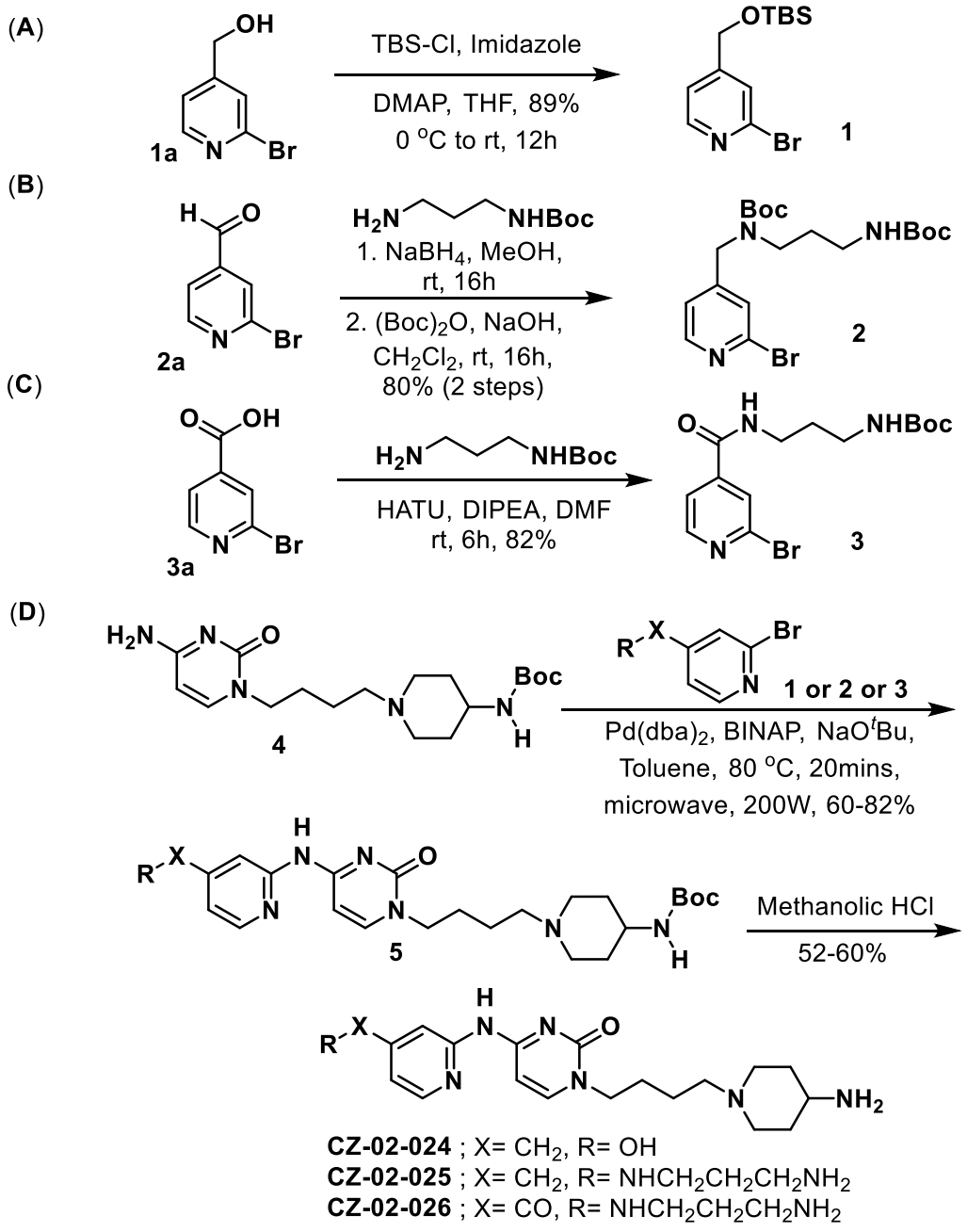

Scheme 3.1 Synthesis of pyridyl–cytosine analogs

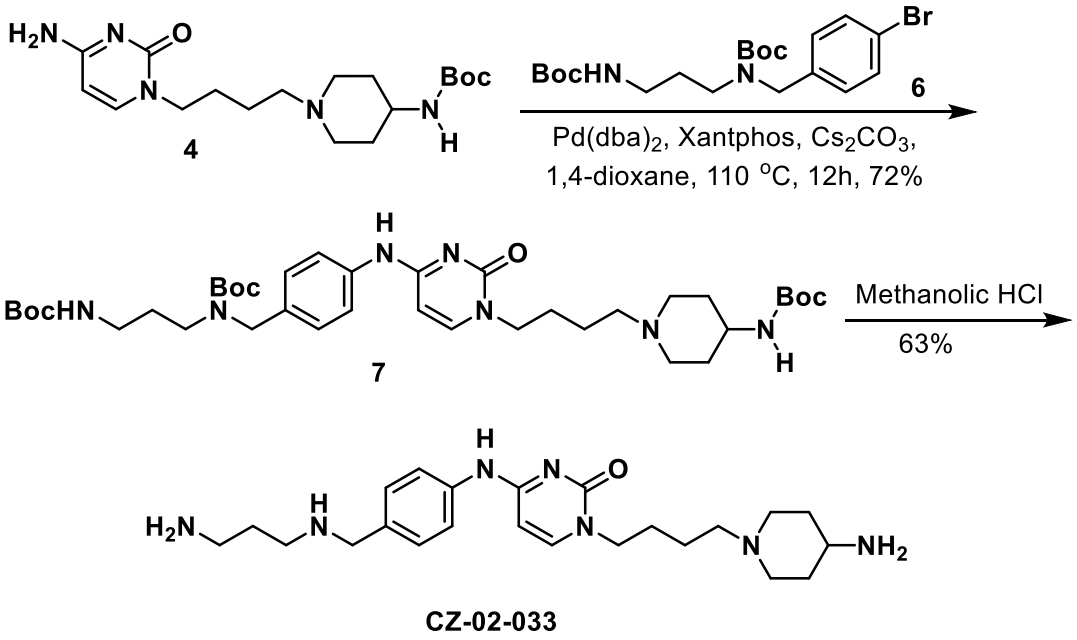

Scheme 3.2 Synthesis of phenyl–cytosine analog **CZ–02–033**

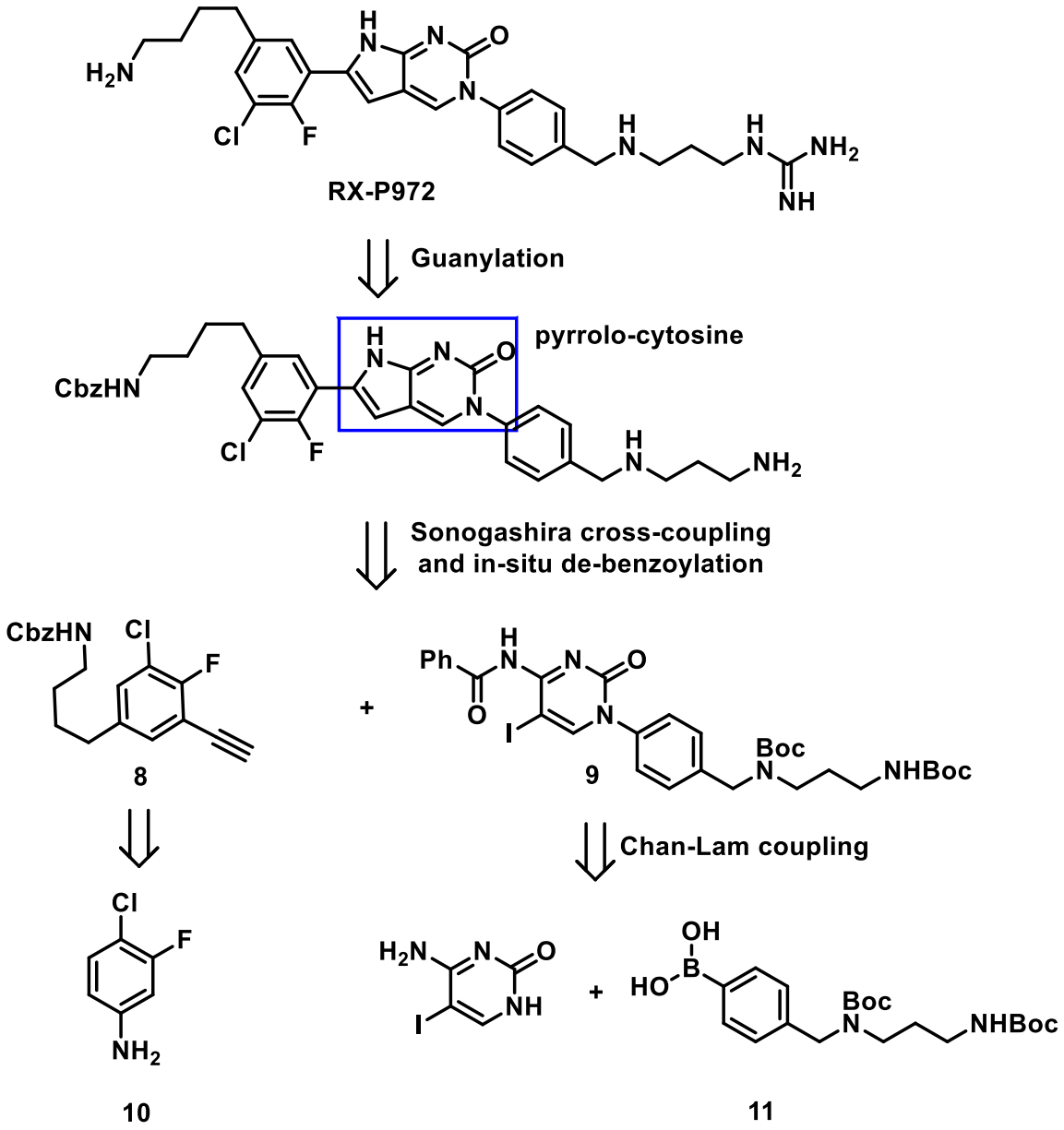

Scheme 3.3 Retrosynthetic analysis of RX–P972

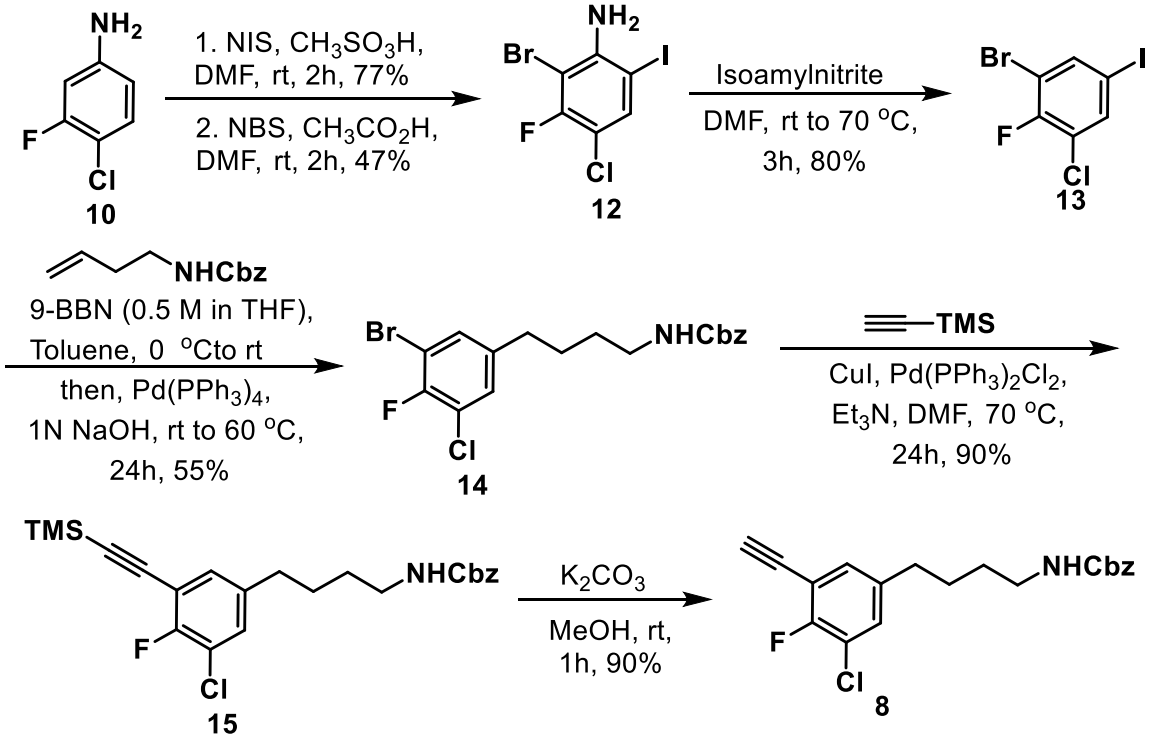

Scheme 3.4 The reported synthetic sequence for substituted phenylacetylene

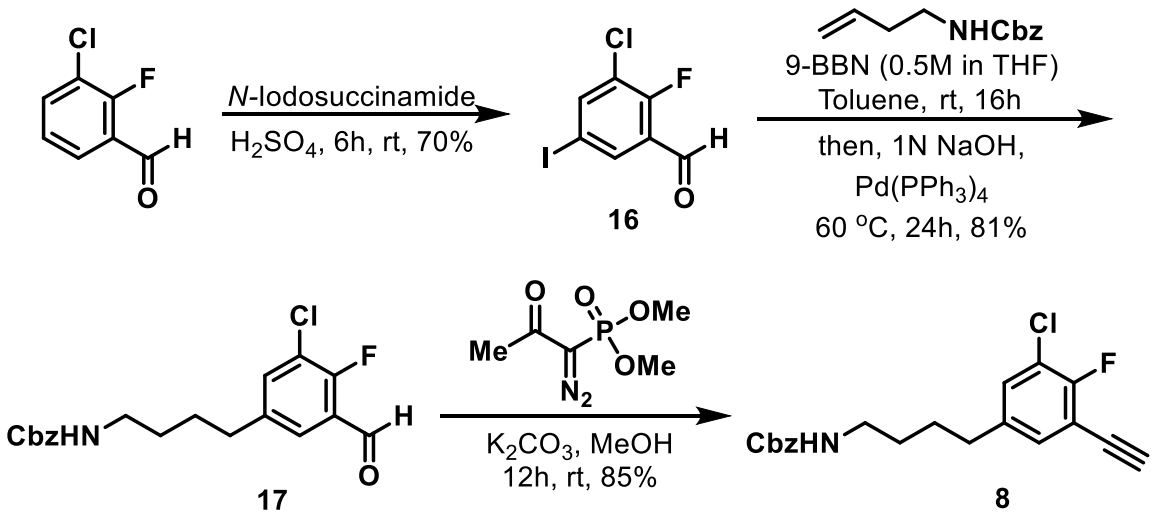

Scheme 3.5 Optimized synthetic route to substituted phenylacetylene

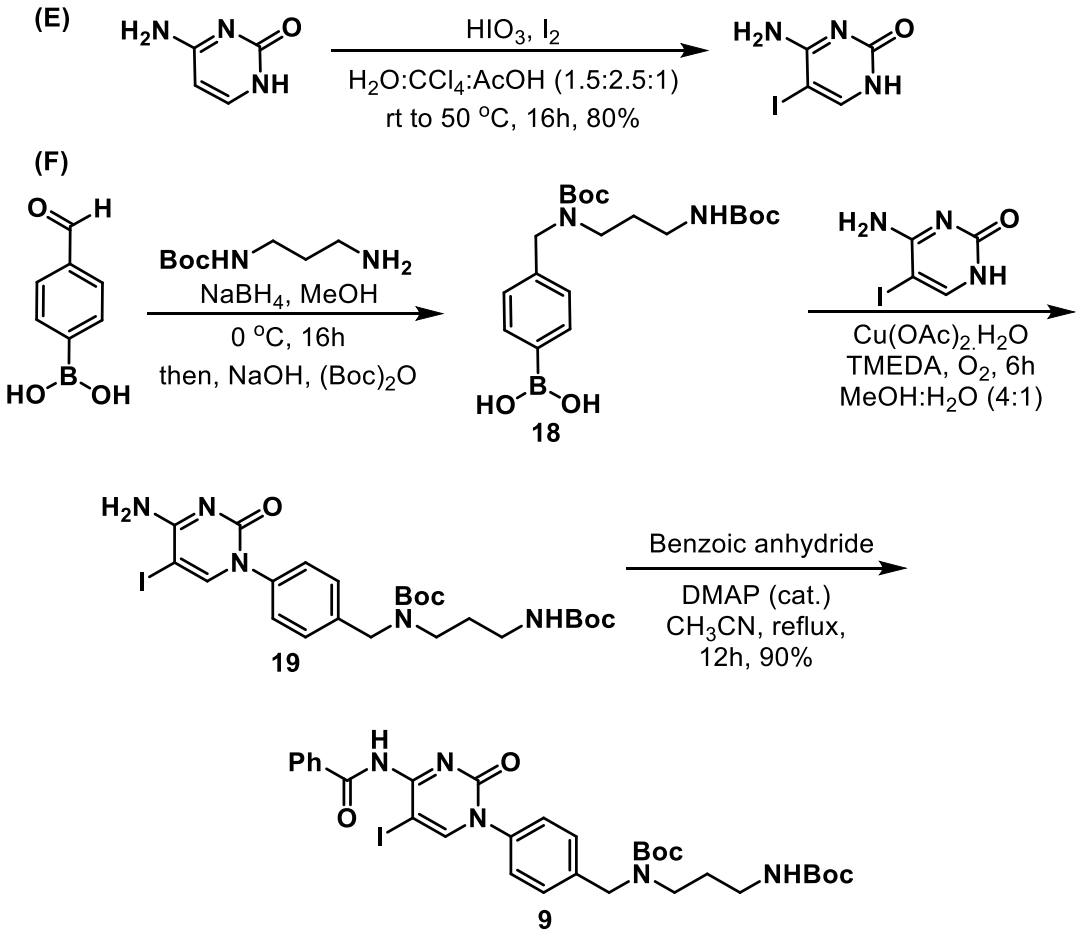

Scheme 3.6 (E) Synthesis of 5–iodocytosine, (F) The synthesis of eastern half (arylated iodocytosine)

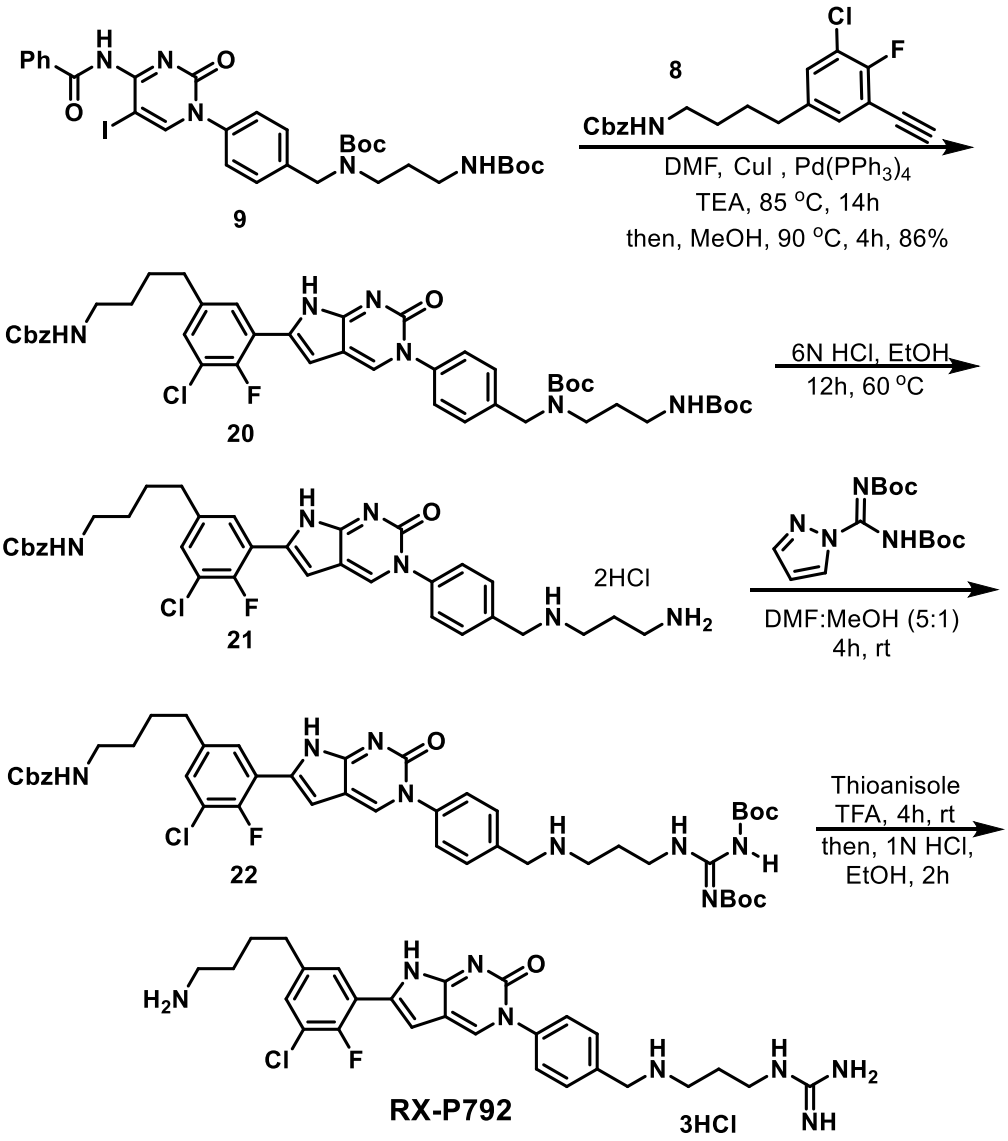

Scheme 3.7 Completion of synthesis of RX–P792

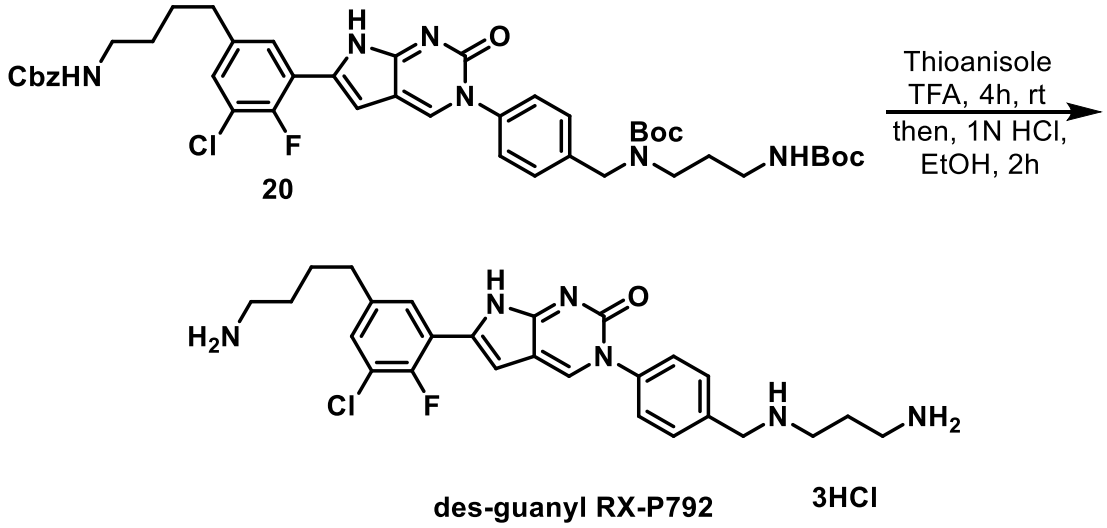

Scheme 3.8 Synthesis of des–guanyl RX–P792

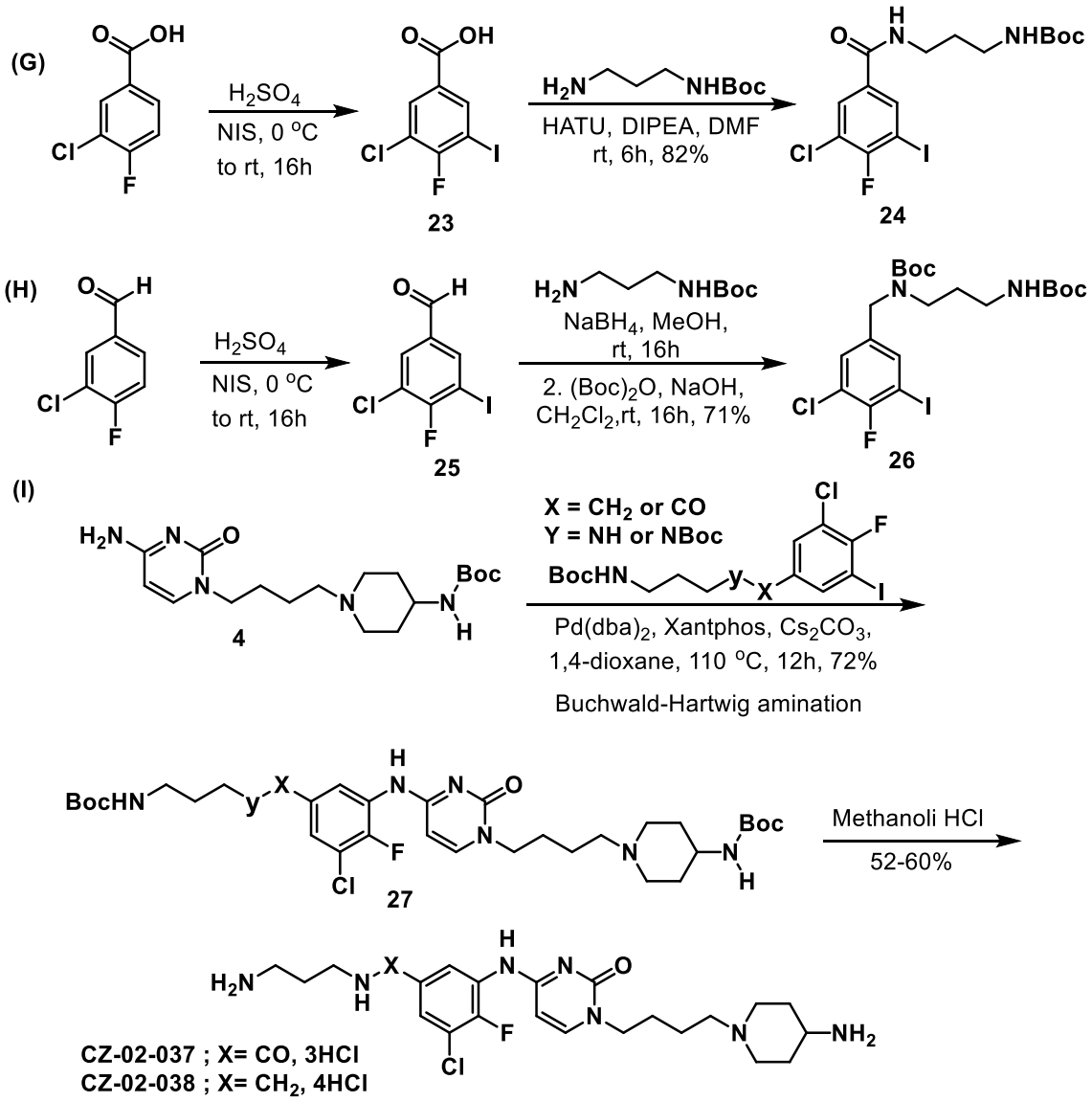

Scheme 3.9 Synthesis of chloro– and fluoro– substituted **CZ–02–033** analogs

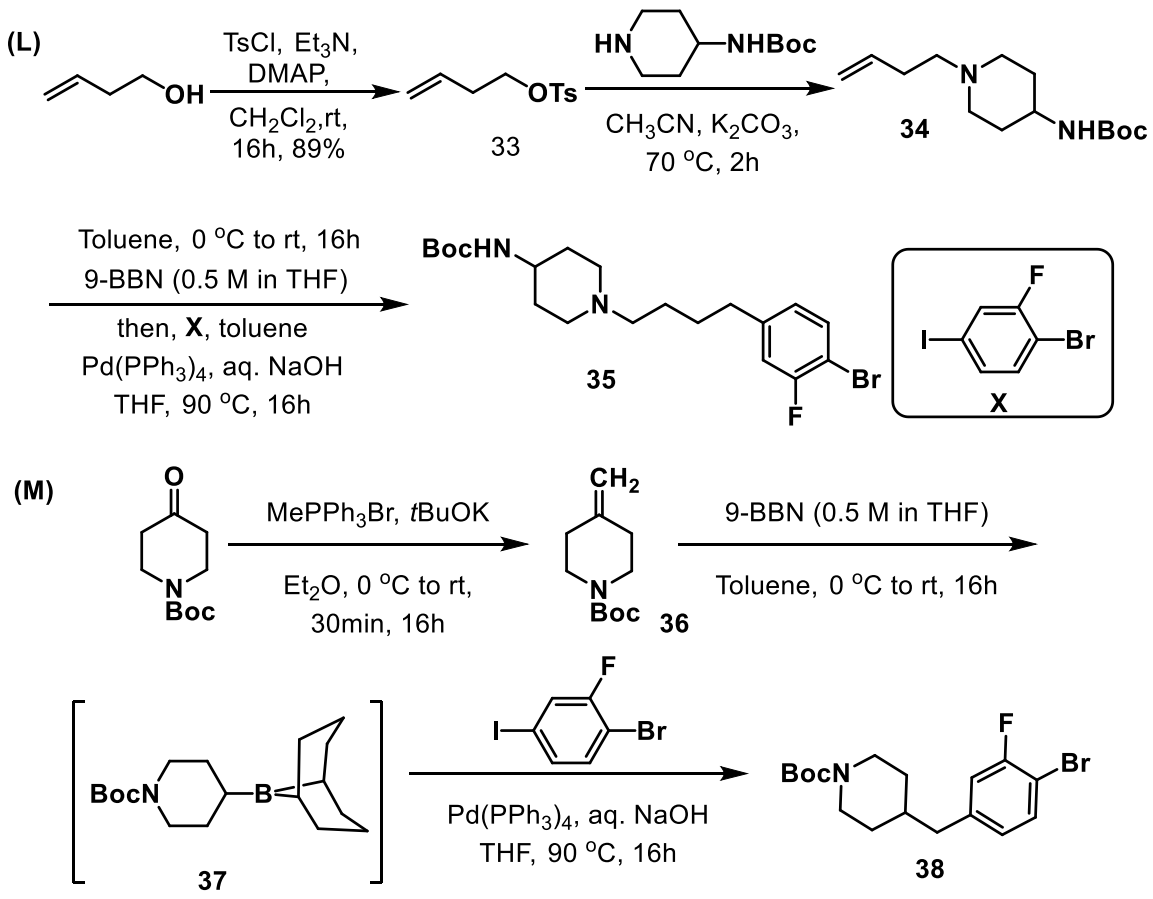

Scheme 3.10 Synthesis of western halves with variable linkers

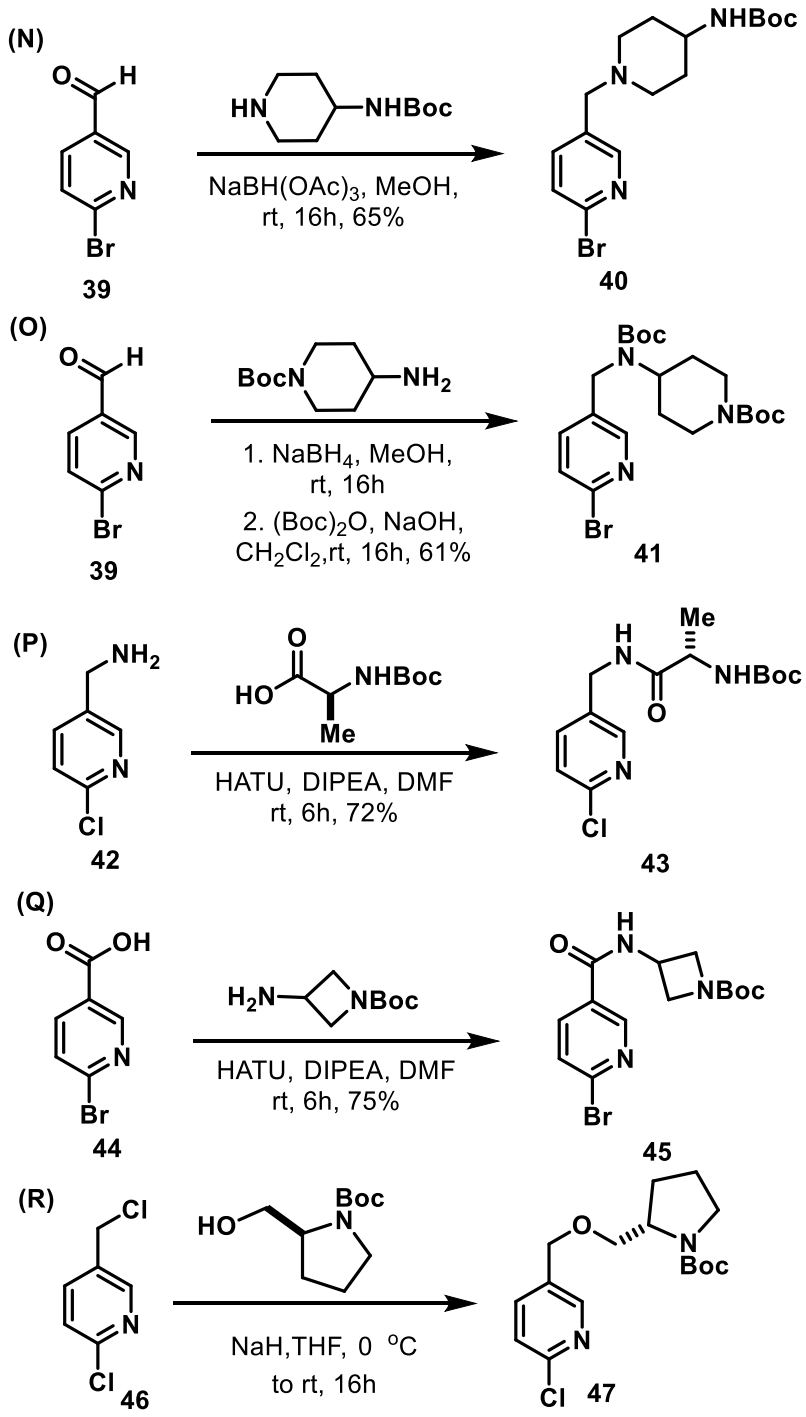

Scheme 3.11 Synthesis of western halves with rigid linkers

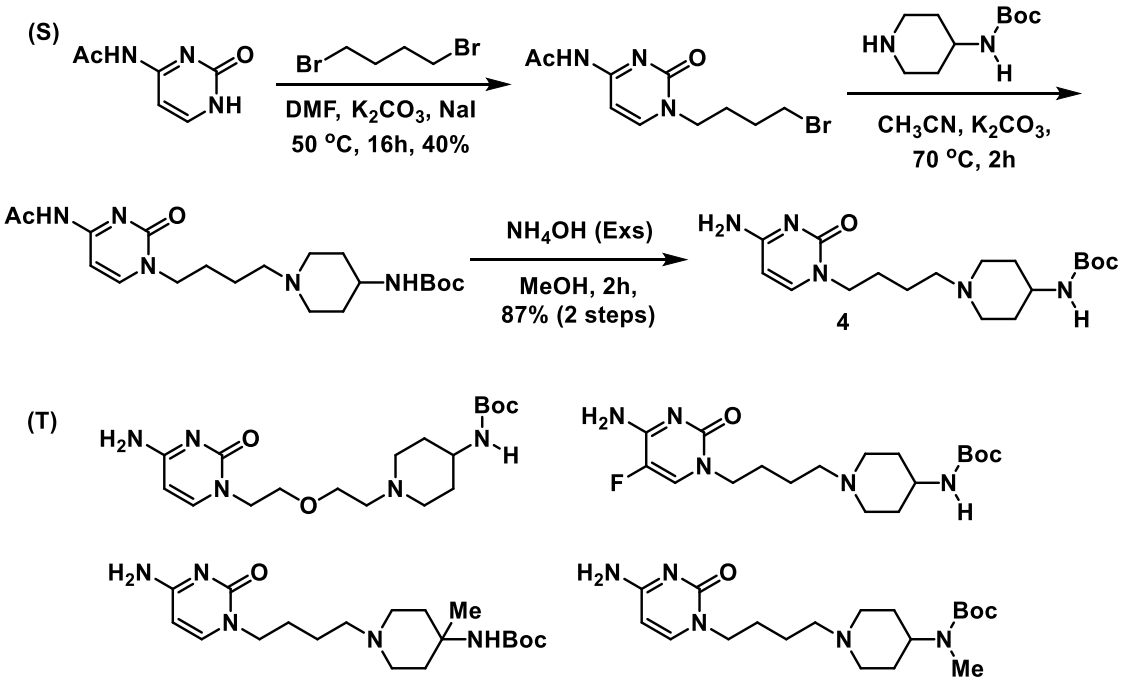

Scheme 3.12 (S) Optimized protocol for cytosine–butyl amino piperadine, and (T) synthesized eastern halves

Table 3.1 Biological evaluation of pyridyl–cytosine analogs.

Compound	CZ-02-024	CZ-02-025	CZ-02-026
Mtb H37 Ra IC_{50} μM	55.4	0.28	0.11
Mtb H37 Rv IC_{50} μM	48.0	0.66	0.22
E. coli S30 IC_{50} μM	1.74 ± 0.26	0.112 ± 0.032	0.027 ± 0.011
M. smeg MIC μg/mL	64	1	4
MRSA MIC μg/mL	--	4-2	8
E. coli MIC μg/mL	--	4	8
Cytotoxicity			
Vero MIC μg/mL	--	>100	>100
HepG2 MIC μg/mL	--	>100	>100

Table 3.2 Biological evaluation of pyridyl–cytosine and phenyl–cytosine analogs

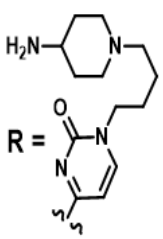	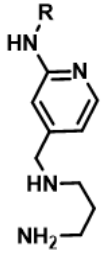	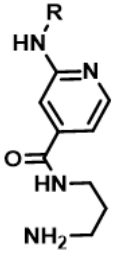	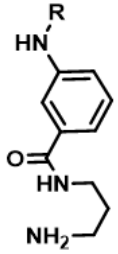	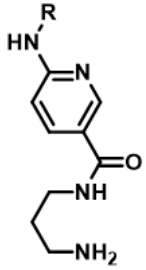	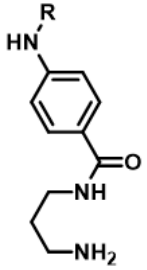	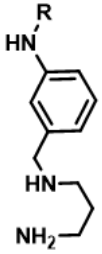	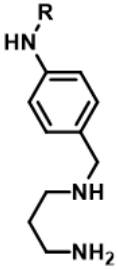	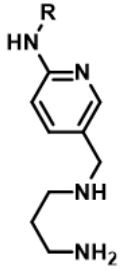
IC50 (μM)	**CZ–02–025**	**CZ–02–026**	**CZ–02–027**	**CZ–02–028**	**CZ–02–030**	**CZ–02–032**	**CZ–02–033**	**CZ–02–039**
E. coli S30	0.112	0.027	23@0.25	1.021	7.891	2.823	0.240	0.052
R. Retic	0.054	0.023	—	0.613	6.448	1.270	0.620	0.082
RR/*E. coli* (SI)	**0.48**	**0.85**	**—**	**0.60**	**0.081**	**0.45**	**2.58**	**1.58**
H37Ra	0.28	0.11					0.37	0.085
H37Rv	0.66	0.22		0.26	1.3	4	0.36	0.69
M. smeg	1	4	64	2	16	8	4	1
MRSA	4	8	>64	>64	>64	16–32	32	16
MIC (μg/mL)								
E.coli	8	8	>64	8–16	>64	16–32	4–8	1–2
CRE *K. pneumo*	>64	>64	>64	>64	>64	>64	4	4
K. pneumo	16	16	>64	—	—	—	2	1–2
P. aeruginosa	>64	>64	>64	>64	>64	>64	>64	>64
Cytotox								
Vero	>100	>100	>100	>100	>100	>100	>100	>100
HepG2	>100	>100	—	—	—	—	>100	>100

Table 3.3 Comparison of CZ–02–039 with RX–P792, and des–guanyl RX–P792

Compound	CZ-02-039	RX-P792	des-guanyl RX-P792
E. coli S30 IC_{50} μM	0.052 ± 0.013	0.020 ± 0.009	0.030 ± 0.009
R. Retic IC_{50} μM	0.082 ± 0.018	0.005 ± 0.003	0.176 ± 0.033
SI (*RR/ E. coli*)	1.6	0.4	6.0
Mtb H37 Ra IC_{50} μM	0.085	0.006	ND
M. smeg MIC μg/mL	1	0.5	<0.5
MRSA MIC μg/mL	32	<0.5	<0.5
E. coli MIC μg/mL	4-8	<0.5	0.5-1
Cytotoxicity			
Vero MIC μg/mL	>100	ND	18
HepG2 MIC μg/mL	>100	ND	ND

Table 3.4 Comparison of CZ–02–033 with CZ–02–037 and CZ–02–038

Compound	CZ-02-033	CZ-02-037	CZ-02-038
Mtb H37 Ra IC_{50} μM	0.37	35% @ 20	51% @ 20
Mtb H37 Rv IC_{50} μM	0.36	---	---
E. coli S30 IC_{50} μM	0.240 ± 0.067	7.3 ± 0.6 @ 0.25	9.2 ± 5.3 @ 0.25
M. smeg MIC μg/mL	4	32	32
MRSA MIC μg/mL	32	>64	>64
E. coli MIC μg/mL	4-8	>64	>64
Cytotoxicity			
Vero MIC μg/mL	>100	>100	>100
HepG2 MIC μg/mL	>100	---	---

Table 3.5 Biologic evaluation of CZ–02–029 / 40 / 41 / 42

Compound	CZ-02-029	CZ-02-040	CZ-02-041	CZ-02-042
Mtb H37 Ra IC_{50} μM	ND	79% @ 20	78% @ 20	55% @ 20
Mtb H37 Rv IC_{50} μM	2.0	57	58	ND
E. coli S30 IC_{50} μM	0.919 ± 0.168	9.9 ± 8.4**	15.4 ± 1.9**	10.3 ± 3.0**
R. retic IC_{50} μM	0.515 ± 0.052	ND	ND	ND
$SI_{RR/E.\ coli}$	0.56	ND	ND	ND
M. smeg MIC μg/mL	4	8	8	32
MRSA MIC μg/mL	>64	64	32	>64
E. coli MIC μg/mL	>64	>64	>64	>64
Cytotoxicity				
Vero MIC μg/mL	>100	>100	>100	>100

** @ 0.25 μM

Table 3.6 Protein synthesis inhibition and MIC evaluation of CZ–02–compounds with conformational rigid linkers

Compound	*E. coli* S30 IC_{50} (μM)	*R. retic* IC_{50} (μM)	*M. smegmatis* MIC μg/mL
CZ-02-048	0.213 ± 0.027	0.101 ± 0.015	2
CZ-02-049	0.153 ± 0.023	0.136 ± 0.053	4
CZ-02-050	23.3 ± 2.3 @ 0.25uM	ND	8
CZ-02-051	39.7 ± 0.7 @ 0.25uM	ND	8
CZ-02-052	0.304 ± 0.058	0.555 ± 0.135	8
CZ-02-054	0.047 ± 0.010	0.055 ± 0.006	2
CZ-02-060	7.7 ± 3.3 @ 0.25uM	ND	16
CZ-02-061	20.8 ± 4.1% @ 0.25uM	ND	4
CZ-02-063	9.2 ± 5.3% @ 0.25uM	79.7 ± 1.5 @ 0.25uM	8
CZ-02-067	1.586 ± 0.371	3.851 ± 0.887	2
CZ-02-069	52.2 ± 4.0 @ 0.25uM	91.0 ± 0.3 @ 0.25uM	32
CZ-02-070	39.4 ± 5.3% @ 0.25uM	ND	16
CZ-02-071	41.4 ± 6.9% @ 0.25uM	ND	16
CZ-02-072	0.369 ± 0.052	0.652 ± 0.031	8

Table 3.7 Activity against *M. tuberculosis* H37Rv under aerobic conditions

Compound	*MIC* (μM)	IC_{50} (μM)	IC_{90} (μM)
CZ-02-048	0.51	0.15	0.55
CZ-02-049	0.9	0.42	2.0
CZ-02-050	2	0.98	2.6
CZ-02-051	2.4	0.87	3.2
CZ-02-053	7.3	2.4	9.4
CZ-02-054	1.9	0.61	2.1
CZ-02-063	4.8	0.93	5.9
CZ-02-067	1.7	0.4	1.9
CZ-02-072	6.4	1.8	7.7

Table 3.8 Biological evaluation of CZ–02–039 analogs with varied linkers in the eastern portion of the binding pocket

Compound	CZ-02-059	CZ-02-083	CZ-02-084	CZ-02-085
Mtb H37 Ra IC_{50} μM	85.0%*	ND	78% @ 20	55% @ 20
Mtb H37 Rv IC_{50} μM	ND	ND	0.29	0.94
E. Coli S30 IC_{50} μM	11.0 ± 6.4**	3.2 ± 12.7%**	0.062 ± 0.016	0.198 ± 0.017
R. Retic IC_{50} μM	ND	45.5 ± 2.4%**	0.234 ± 0.022	0.510 ± 0.037
M. Smeg MIC μg/mL	32	16	2	4
MRSA MIC μg/mL	>64	8	8	4
E. Coli MIC μg/mL	>64	>64	4	4
Cytotoxicity				
Vero MIC μg/mL	>100	ND	>100	>100

** = @ 0.25 μM, * = @ 0.1 μg/mL

Table 3.9 Activity against Mtb H37Rv under aerobic conditions

Compound	*MIC* (μM)	IC_{50} (μM)	*IC_{90}* (μM)
CZ-02-084	0.96	0.29	1.1
CZ-02-085	2.7	0.94	3.2

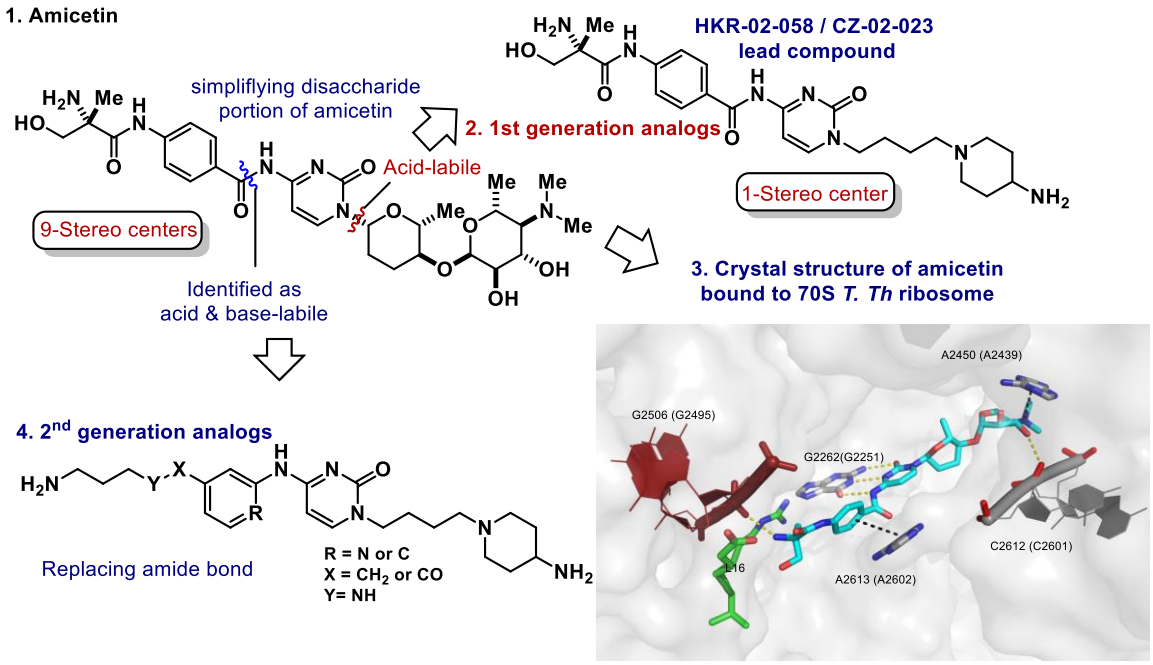

Figure 3.1 Design of second generation amicetin analogs. (a) Strategies. (b) Half–life of CZ–02–023 under different conditions

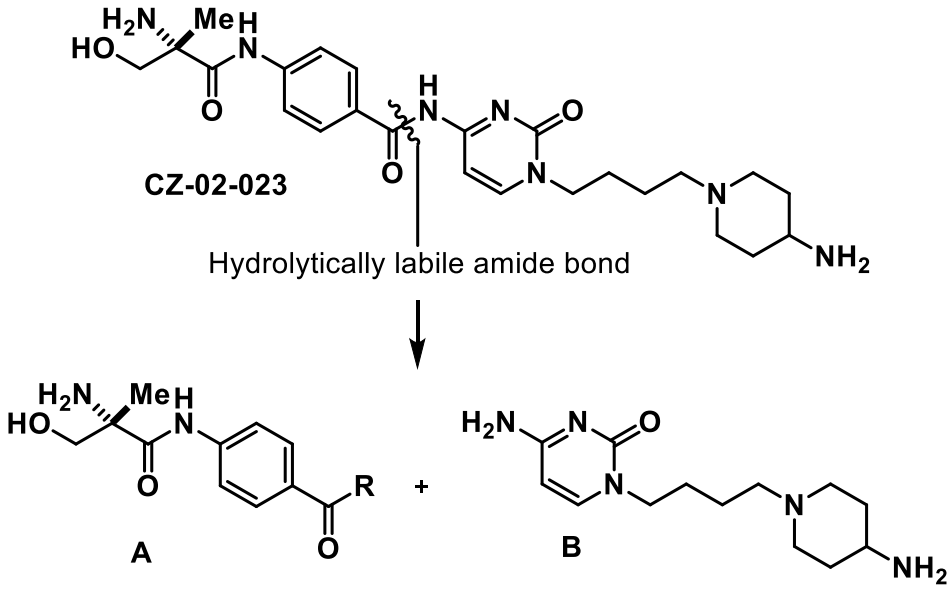

Solvent	Form of amine	Temparature	$t_{1/2}$ in hours
CD_3OD	freebase	25 °C	77
D_2O	HCl Salt	25 °C	66
CD_3OD + 5% TFA	freebase	25 °C	34
CD_3OD + 5% TEA	freebase	25 °C	17

Figure 3.1 Continued

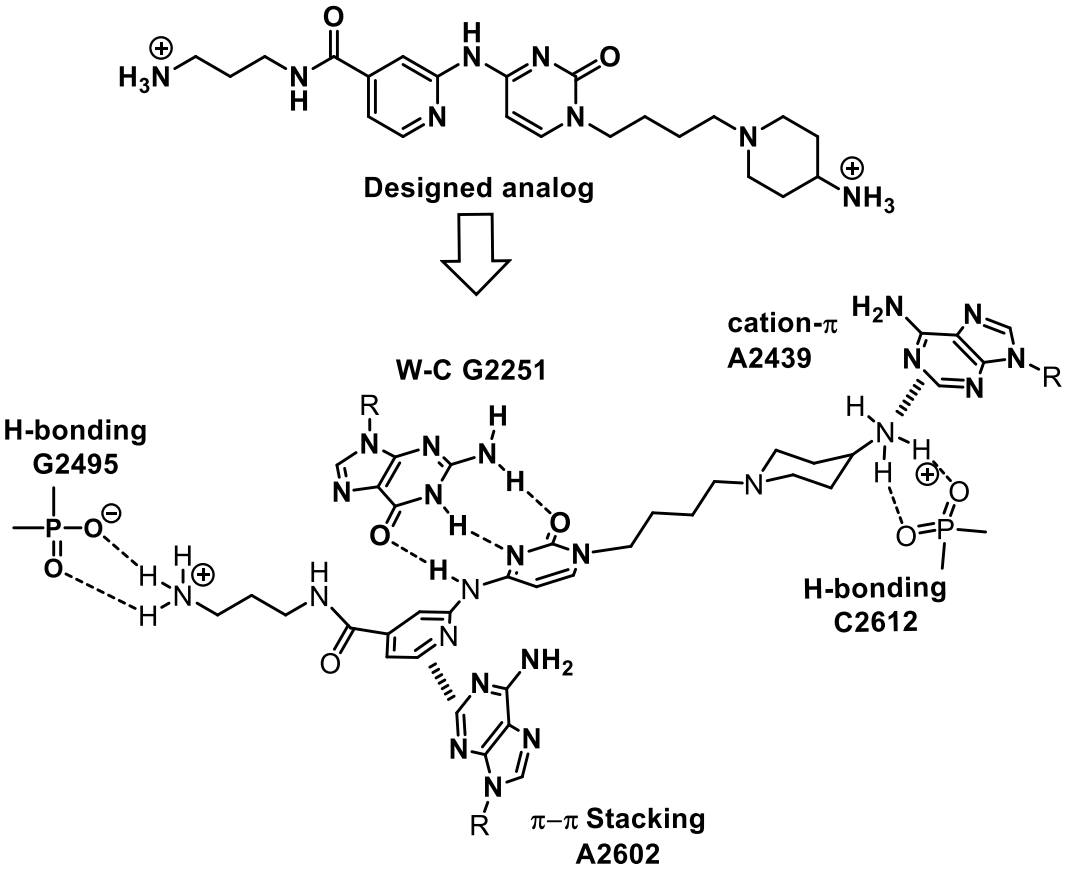

Figure 3.2 Docking interactions of the proposed analogs

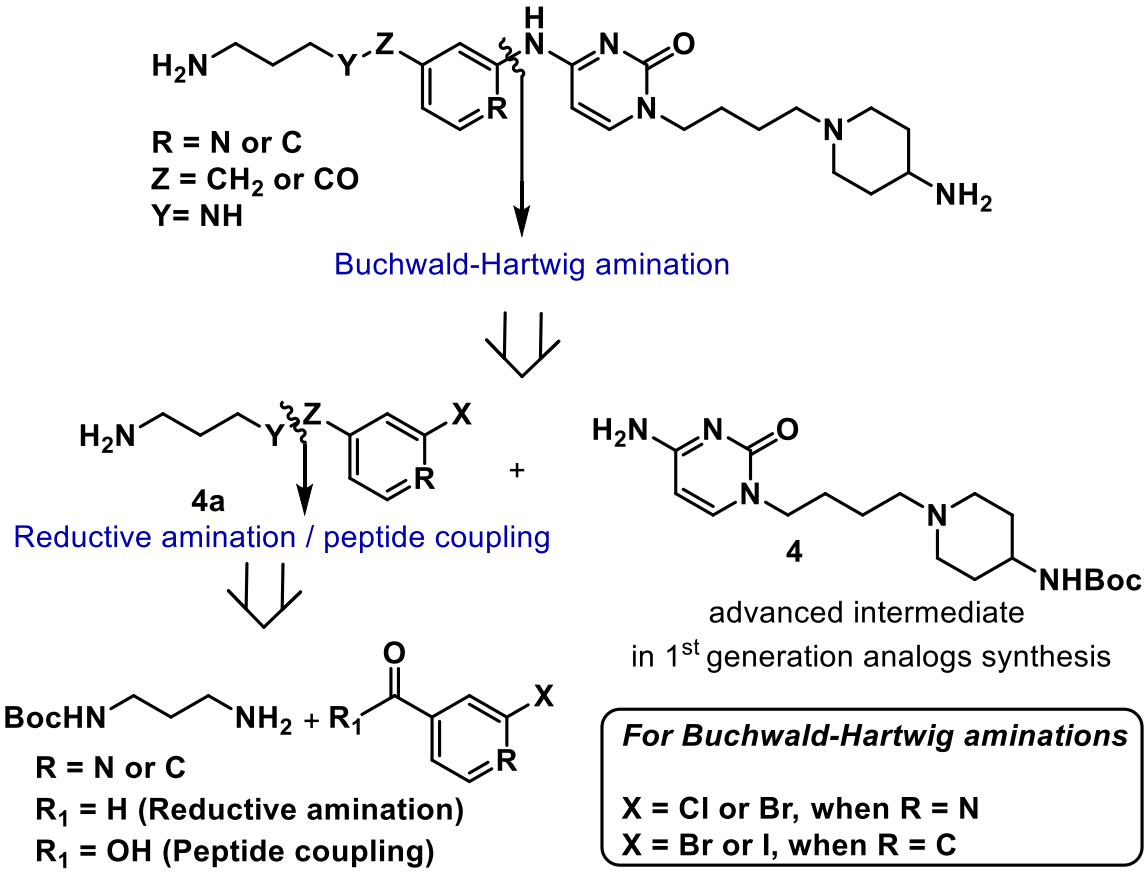

Figure 3.3 Retrosynthetic analysis of second generation amicetin analogs

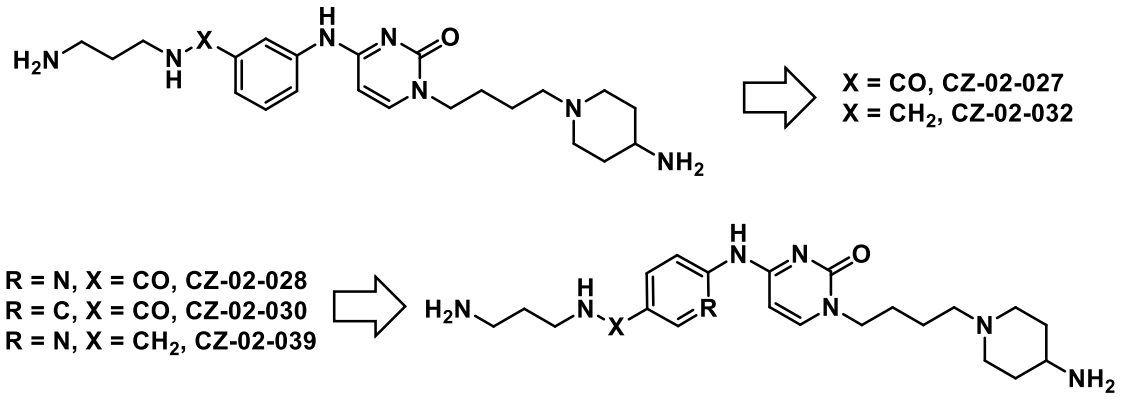

Figure 3.4 Cytosine–pyridyl/phenyl derivatives synthesized using a protocol similar to that shown in Scheme 3.2

CZ-02-029

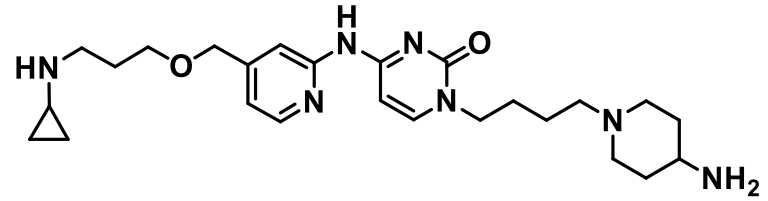

CZ-02-040

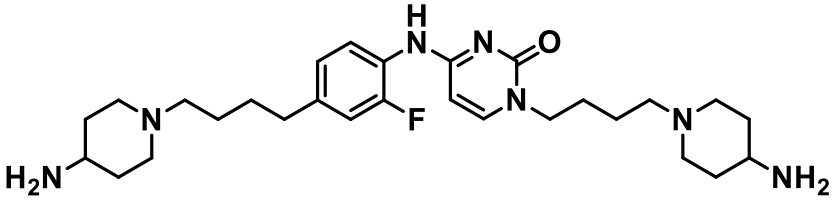

CZ-02-041

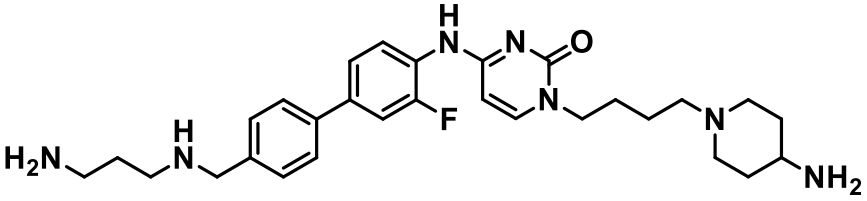

CZ-02-042

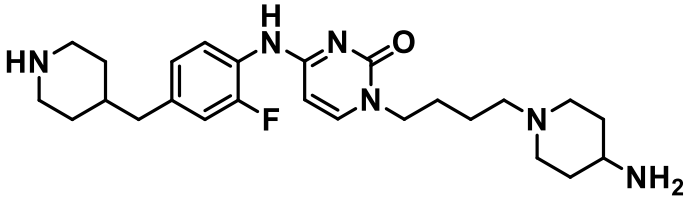

Figure 3.5 Analogs with diversified linker portions in the western half

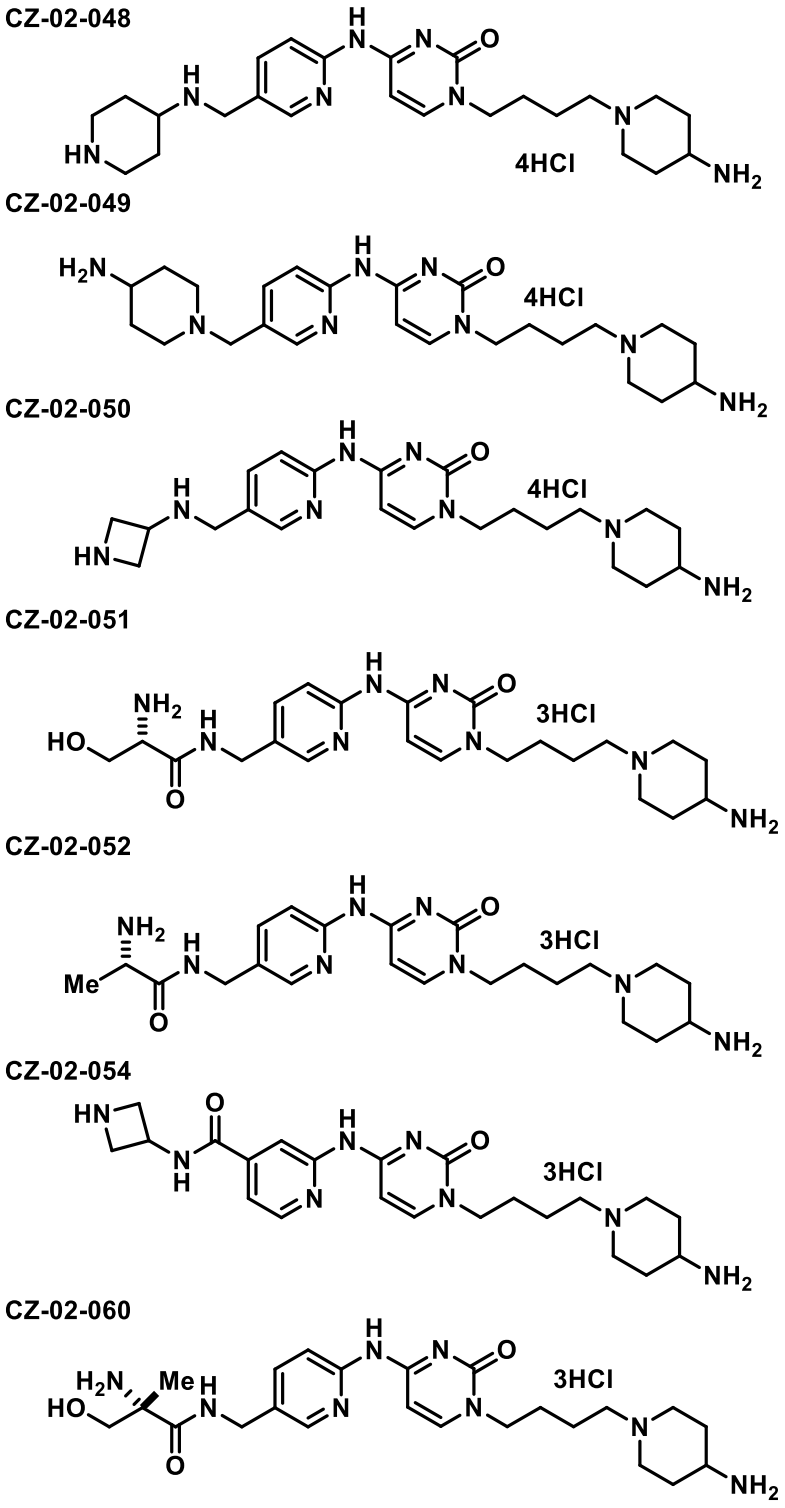

Figure 3.6 Analogs with conformational rigid linkers in the western part of the binding pocket

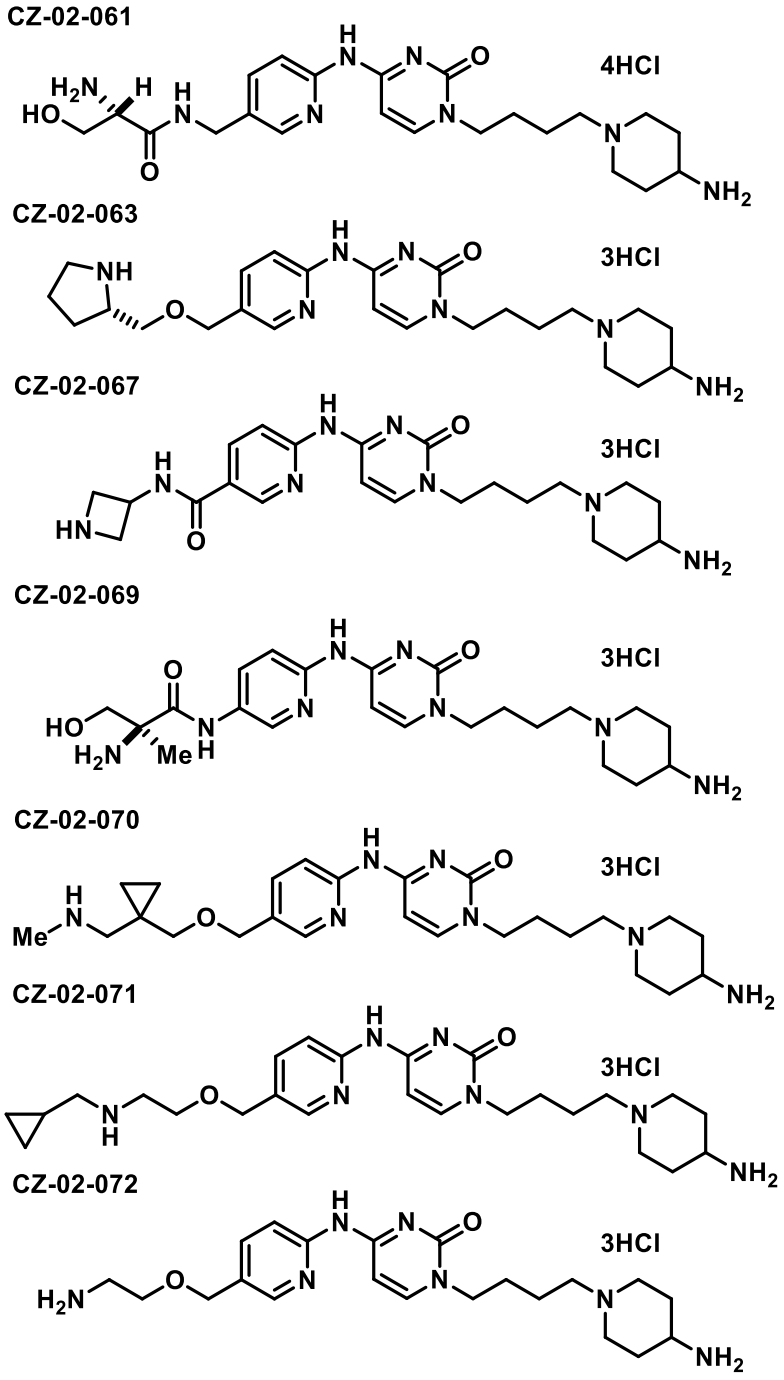

Figure 3.6 Continued

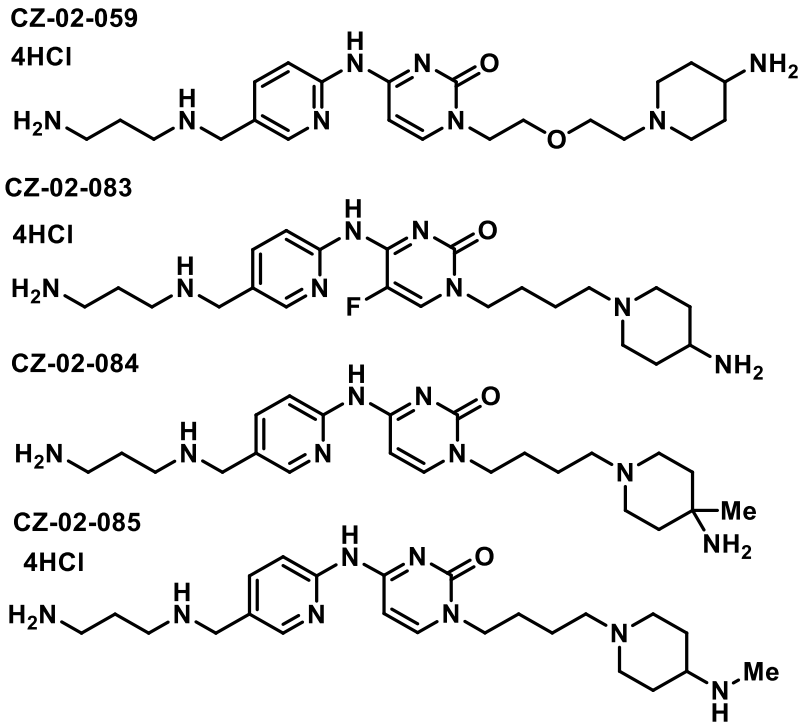

Figure 3.7 Analogs with diversified eastern halves

References

1) Note: CZ stands for Curza; Curza Global, a company based on technology developed at the U of U by Looper and Williams (Research Professor in Orthopedics) Labs. At this point Curza has licensed patents associated with these compounds.

2) Muci, A. R.; Buchwald, S. Practical Palladium Catalysts for C–N and C–O Bond Formation. *Top. Curr. Chem.* **2002**, *219*, 133–209.

3) Hartwig, J. F. Approaches to Catalyst Discovery. New Carbon–Heteroatom and Carbon–Carbon Bond Formation. *Pure Appl. Chem.* **1999***, 71,* 1417.

4) Schlummer, B.; Scholz, U. Palladium–Catalyzed C–N and C–O Coupling–A Practical Guide from an Industrial Vantage Point. *Adv. Synth. Catal.* **2004**, *346,* 1599–1626*.*

5) Wolfe, J. P.; Wagaw, S.; Marcoux, J–F.; Buchwald, S. L. Rational Development of Practical Catalysts for Aromatic Carbon–Nitrogen Bond Formation. *Acc. Chem. Res.* **1998**, *31,* 805–818*.*

6) Hartwig, J. F. Carbon–Heteroatom Bond–Forming Reductive Eliminations of Amines. *Acc. Chem. Res.* **1998**, *31,* 852–860.

7) Duffy, E. M.; Bhattacharjee, A. Pyrrolopyrimidinones as Antimicrobial Agents and Methods of Making and Using the Same. WO2012/173689, **2012**.

8) Hansen, J.L.; Moore, P.B.; Steitz, T.A. Structures of Five Antibiotics Bound at the Peptidyl Transferase Center of the Large Ribosomal Subunit. *J. Mol. Biol.* **2003**, *330*, 1061–1075.

9) Svidritskiy, E.; Ling, C.; Ermolenko, D.N.; Korostelev, A. BlasticidinS Inhibits Translation by Trapping Deformed tRNA on the Ribosome." *Proc. Natl. Acad. Sci. USA.* **2013**, *110*,12283–12288.

10) Housman, S. T.; Sutherland, C.; Nicolau, D. P. *In vitro* Evaluation of Novel Compounds Against Selected Resistant *Pseudomonas Aeruginosa* Isolates. *Antimicrob Agents Chemother.* **2012**, *56*, 1646–1649.

11) Motohide, S.; Hisateru, A.; Masaki, Y.; Masafumi, I.; Hiroshi, K.; Hisashi, S.; Nakamura, H.; Yuji, M.; Shuichi, W. Preparation of 6–(heterocycle–substituted benzyl)–4–oxoquinoline Compounds as HIV Integrase Inhibitors. WO 2007/148780, **2007**.

12) Habrant, D.; Rauhala, V.; Koskinen, A. M. P. Conversion of Carbonyl Compounds to Alkynes: General Overview and Recent Developments. *Chem. Soc. Rev.* **2010**, *39*, 2007–2017.

Supporting Information

General experimental considerations

All reactions requiring anhydrous conditions were conducted in flame–dried glassware under a positive pressure of either nitrogen or argon. Commercially available reagents were used as received; otherwise, materials were purified according to *Purification of Laboratory Chemicals*. Acetonitrile (CH_3CN), *N,N'*–dimethylformamide (DMF), and tetrahydrofuran (THF) were degassed with nitrogen and passed through a solvent purification system (Innovative Technologies Pure Solv). Dry 1,4–dioxane was purchased from Acros Organics in a Acros Seal™ bottle. Microwave reactions were done in CEM Discover System Model 908005.

Melting points were determined using a Mel–Temp® Capillary Melting Point Apparatus. Infrared spectra were obtained using Nicolet 380–FT IR spectrometer fitted with a Smart Orbit sample system. Optical rotations were obtained at ambient temperature on a Perkin Elmer Model 343 polarimeter (Na D line) using a microcell with a 1 decimeter path length. Mass spectra were determined on a Micromass Quattro II (ESI/APCI–TOF) for HRMS at the University of Utah Mass Spectrometry Facility. ^{1}H NMR and ^{13}C NMR spectra were recorded at 300 MHz, 400MHz, 500 MHz and ^{13}C NMR spectra were recorded at 75 MHz, 100 MHz, 125 MHz, respectively. Proton resonances were reported relative to the deuterated solvent peak: 7.26 ppm for $CDCl_3$ and 3.31 ppm (center line signal) for CD_3OD, 4.80 ppm for D_2O using the following format: chemical shift (δ) [multiplicity (s= singlet, bs= broad singlet, d= doublet, dd= doublet of doublet, t= triplet, q= quartet, m=

multiplet), coupling constant(s) *J* in Hz, integration]. Carbon resonances were reported as chemical shifts (δ) in parts per million, relative to the center line signal of the respective solvent peak: 77.23 ppm for $CDCl_3$ and 49.00 ppm for CD_3OD. All the commercially available chemicals are purchased from Sigma–Aldrich, Acros, TCI America, Combi–Blocks, and Chem–Impex.

Half–life of CZ–02–023

CZ–02–023 freebase or salt was dissolved in CD_3OD and D_2O, respectively, (5 mM solution) and an array of proton NMR experiments are run with a 1-hr interval for 72-96 hrs. The solvolysis of CZ–02–023 was monitored by the formation of *N*[1]-alkylated cytosine (fragment B in Figure 3.1(b)). [Note: a distinct peak for cytosine C5-H was seen around δ 6 ppm]. The integral value for newly formed fragment B cytosine C5-H proton was calculated with respect to solvent peak. A plot of ln [Integral cyt-5H] vs Time in hrs gives a straight line, form that the half–life is calculated using the slope of the curve employing the first–order kinetics equation.

$$t_{1/2} = \ln\frac{2k}{slope} \tag{3.1}$$

CZ–02–023 free base in CD_3OD: $t_{1/2} = \frac{0.693}{0.009} = 77$ (3.2)

CZ–02–023 free base in CD_3OD + 5% TFA: $t_{1/2} = \frac{0.693}{0.022} = 31.5$ (3.3)

CZ–02–023 free base in CD_3OD + 5% TEA: $t_{1/2} = \frac{0.693}{0.042} = 16.5$ (3.4)

CZ–02–023–HCl salt in D_2O: $t_{1/2} = \frac{0.693}{0.01} = 66$ (3.5)

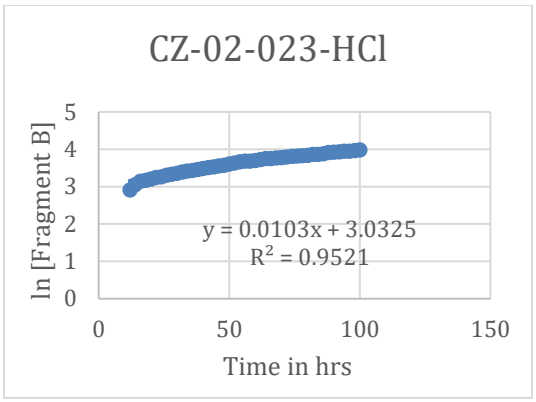

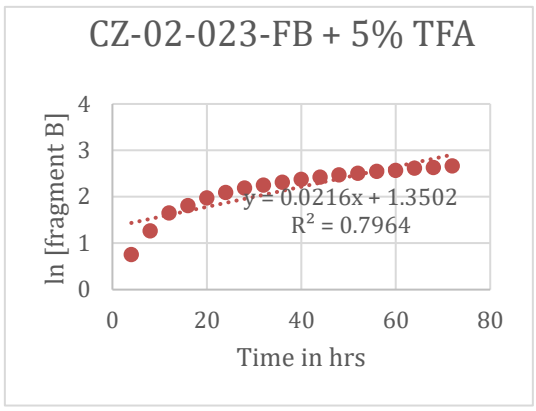

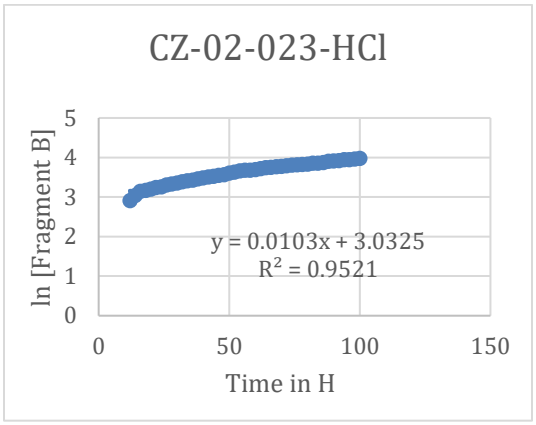

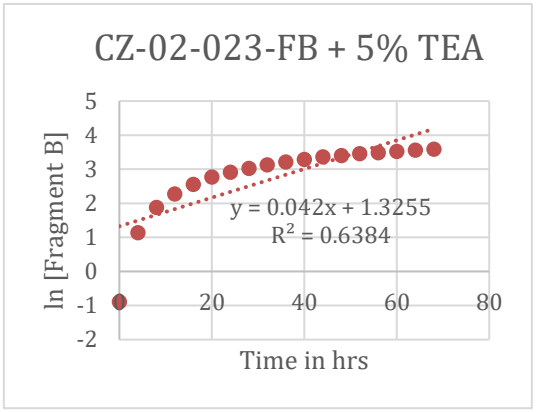

Half–life of CZ-02-023

Experimental procedures

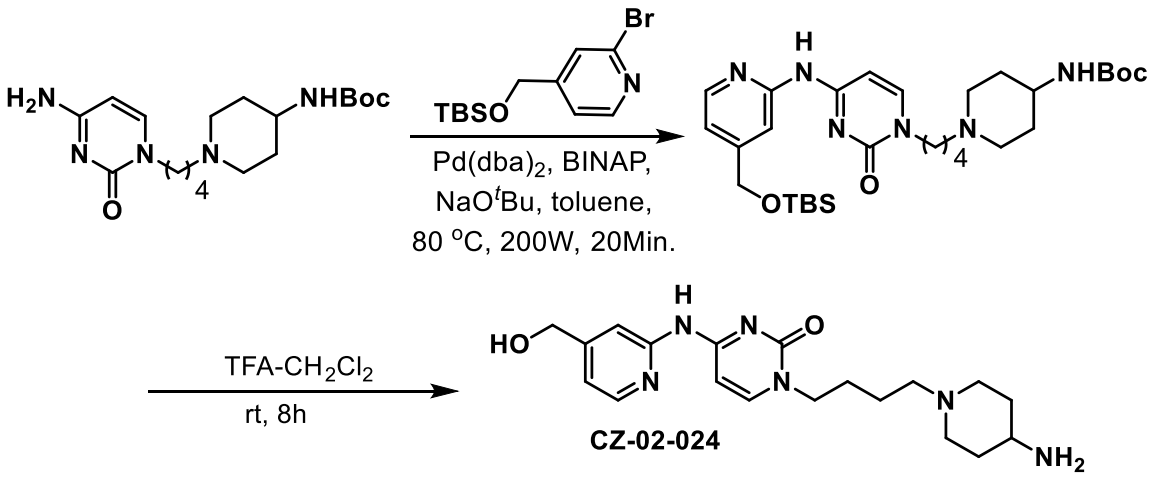

Example for Buchwald-Hartwig amination

Synthesis of CZ–02–024

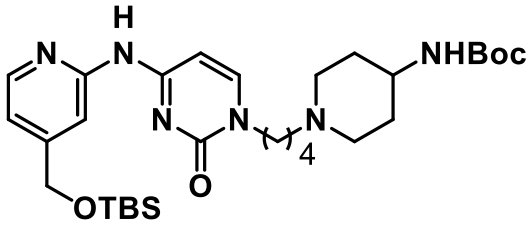

***tert*–butyl (1–(4–(4–((4–(((*tert*–butyldimethylsilyl)oxy)methyl) pyridin–2–yl)amino)–2–oxopyrimidin–1(2*H*)–yl)butyl)piperidin–4–yl)carbamate**; An oven dried microwave reaction tube was charged with 2–bromo–4–(((*tert*–butyldimethylsilyl)oxy)methyl)pyridine (75 mg, 0.25 mmol), *tert*–butyl (1–(4–(4–amino–2–oxopyrimidin–1(2*H*)–yl)butyl)piperidin–4–yl)carbamate (92 mg, 0.25 mmol), NaO^{t}Bu (48 mg, 0.50 mmol), $Pd_3(dba)_2$ (23 mg, 25.0 µmol), *rac*–BINAP (23 mg, 37. µmol) and dry toluene (1 mL). The reaction mixture was degassed and purged with nitrogen three times and stirred and heated in a focused CEM microwave reactor microwave conditions (80 °C 200 W) for 20 min, after which the

reaction mixture was diluted with EtOAc (3 mL) and filtered through a pad of Celite® and concentrated under reduced pressure. Purification on silica gel using flash chromatography (2% MeOH/$CHCl_3$) afforded the desired product (55 mg, 36%) as a yellow colored solid.

CZ–02–024;1–(4–(4–Aminopiperidin–1–yl)butyl)–4–((4–(hydroxyl–methyl)pyridin–2–yl)amino)pyrimidin–2(1*H*)–one

tert–butyl (1–(4–(4–((4–(((*tert*–butyldimethylsilyl)oxy)methyl)pyridin–2–yl)amino)–2–oxopyrimidin–1(2*H*)–yl)butyl)piperidin–4–yl)carbamate (50 mg, 85.0 µmol) was dissolved in 50% TFA in dichloromethane (1 mL) and stirred for 16 hrs at room temperature. The solvent was evaporated and the reaction was neutralized with Et_3N. The compound was purified using MPLC to afford title compound 1–(4–(4–Aminopiperidin–1–yl)butyl)–4–((4–(hydroxymethyl)pyridin–2–yl)amino)pyrami-din–2(1*H*)–one (25 mg, 79%) as a brown colored solid. Mp 174–176 °C.

^{1}H NMR (500 MHz, CD_3OD) δ ppm 8.23–8.19 (m, 2H), 7.75 (d, *J* = 7.0 Hz, 1H), 7.08 (t, J_1 = 1.5, J_1 = 4.5 Hz, 1H), 6.51 (bs, 1H), 4.67 (s, 2H), 3.86 (t, J_1 = 7.0, J_1 = 7.5 Hz, 2H), 2.90 (d, *J* = 12.0 Hz, 2H), 2.65–2.60 (m, 1H), 2.39–2.37 (m, 2H), 2.04–1.98 (m, 2H), 1.83–1.79 (m, 2H), 1.76–1.70 (m, 2H), 1.57–1.51 (m, 2H), 1.44–1.36 (m, 2H). δ ^{13}C NMR (125 MHz, CD_3OD) δ ppm 163.9, 158.9, 155.0, 153.8, 148.7, 147.9, 118.0, 113.7, 97.7, 79.5, 63.8, 59.0, 53.5, 51.1, 35.3, 28.1, 24.7 ppm. HRMS Calculated for m/z, 373.2352 Obsd.373.2350

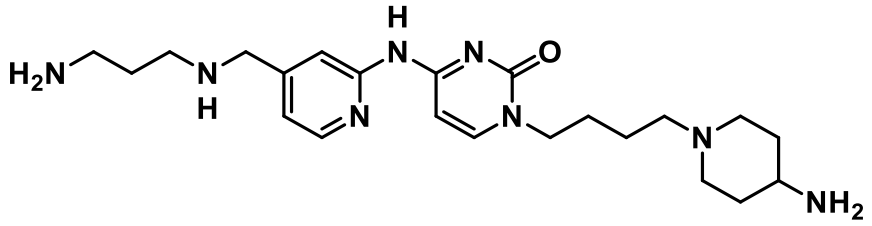

CZ–02–025: Mp 174–176 °C.

NMR (400 MHz, D_2O) δ ppm 8.50 (d, *J* = 6.0 Hz, 1H), 8.13 (d, *J* = 7.6 Hz, 1H), 7.52 (br s 1H), 6.47 (d, J_1 = 6.8, 1H), 4.45 (s, 2H), 4.00 (br s, 2H), 3.73 (d, *J* = 12.8, 2H), 3.61–3.44 (m, 1H), 3.32–3.28 (m, 2H), 3.22 (br s, 2H), 3.17–3.11 (m, 2H), 2.35 (d, *J* = 13.2, 2H), 2.21–2.12 (m, 2H), 1.20–1.92 (m, 2H), 1.90–1.84 (m, 4H). HRMS Calculated for m/z, 429.3090 Obsd.429.3096

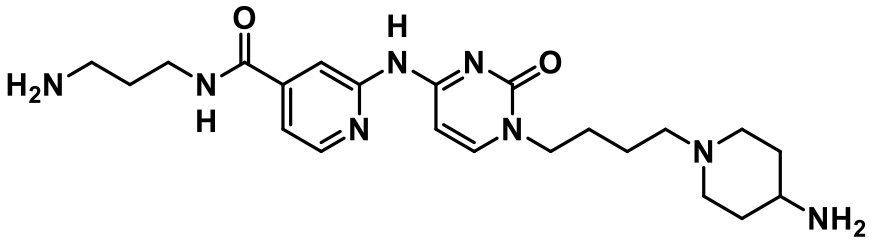

CZ–02–026: Mp 194–196 °C.

^{1}H NMR (500 MHz, CD_3OD) δ ppm 8.59 (br s, 1H), 8.31 (d, *J* = 8.0 Hz, 1H), 7.71 (d, J_1 = 7.5, 1H), 7.37 (d, J_1 = 5.0, 1H), 6.29 (d, J_1 = 4.0, 1H), 3.79 (t, *J* = 7.0, 2H), 3.42–3.38 (m, 2H), 2.82 (d, J_1 = 11.0, 2H), 2.69–2.65 (m, 2H), 2.57–2.51 (m, 1H), 2.29 (t, *J* = 7.5, 2H), 1.93 (t, *J* = 12.0, 2H), 1.76–1.70 (m, 4H), 1.69–1.63 (m, 2H), 1.49–1.43 (m, 2H), 1.36–1.27 (m, 2H). ^{13}C NMR (120 MHz, CD_3OD) δ ppm 167.9, 163.8, 159.0, 154.3, 149.9, 148.1, 144.8, 118.3, 113.0, 97.8, 59.0, 53.5, 51.2, 39.7, 38.4, 35.2, 32.8, 28.2, 28.1, 24.7. HRMS Calculated for m/z, 443.2883 Obsd.443.2884

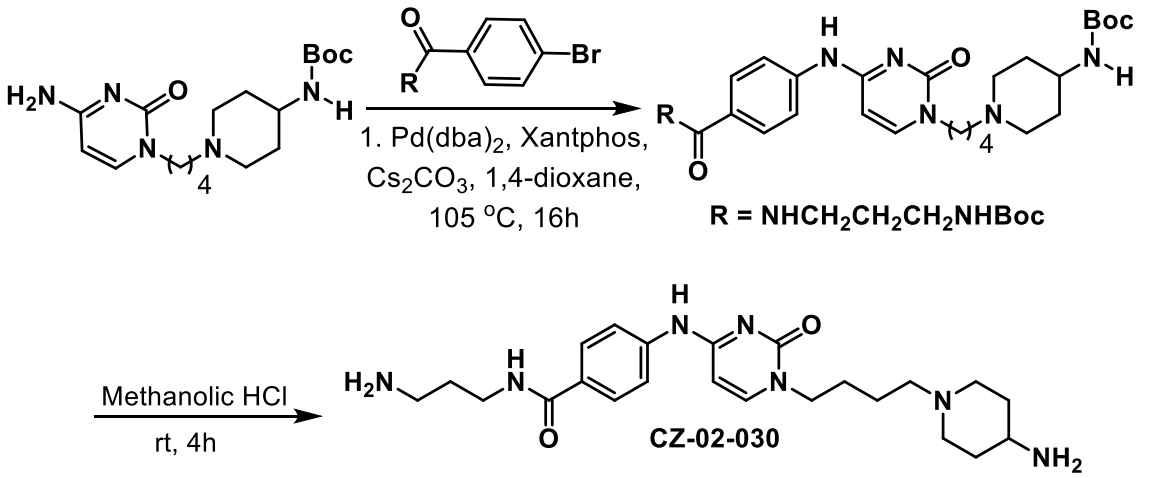

Optimized Buchwald–Hartwig amination procedure

CZ–02–030:**4–((1–(4–(4–aminopiperidin–1–yl)butyl)–2–oxo–1,2–dihydropyrimidin–4–yl)amino)–N–(3–aminopropyl)benzamide**: An oven dried pressure flask was charged with tert–butyl (3–(4–bromobenzamido)propyl)carbamate (1.0 equiv.), *tert*–butyl (1–(4–(4–amino–2–oxopyrimidin–1(2*H*)–yl)butyl)piperidin–4–yl)carbamate (1.01 equiv.), cesium carbonate (2 equiv.), $Pd(dba)_2$ (0.1 equiv.), Xantphos (0.2 equiv.) and dry dioxane (12 mL). The reaction mixture was degassed and purged with nitrogen three times and stirred at 105 °C for 16 hrs, after which the reaction mixture was diluted with $CHCl_3$ (25 mL) and filtered through a pad of Celite® and concentrated under reduced pressure. Purification on silica gel using flash chromatography (2% MeOH/$CHCl_3$) afforded the Boc protected product, which was further dissolved in methanolic HCl and stirred for 4 hrs. The methanol was evaporated after the completion of reaction (monitored by TLC), and the resultant solid was triturated with ether to remove miscellaneous organic impurities and dried over vacuum to yield the desired product as yellow colored solid. Mp 292–294 °C.

^{1}H NMR (500 MHz, D_2O) δ 8.00 (d, *J* = 7.5 Hz, 1H), 7.95 (d, *J* = 9.0 Hz, 2H), 7.60 (d, *J* = 9.0 Hz, 2H), 6.35 (d, *J* = 7.5 Hz, 2H), 3.99 (bs, 2H), 3.79 (d, *J* = 13.0 Hz, 2H), 3.66–3.60 (m, 1H), 3.58 (t, *J* = 7.0 Hz, 2H), 3.27 (bs, 2H), 3.21–3.14 (m, 4H), 2.41 (d, *J* = 13.0 Hz, 2H), 2.10–1.97 (m, 4H), 1.87 (bs, 4H). ^{13}C NMR (125 MHz, D_2O) δ 171.9, 170.0, 158.3, 150.4, 137.0, 133.3, 129.0, 125.0, 94.9, 56.3, 50.8, 49.3, 45.4, 37.1, 36.7, 27.1, 26.7, 25.1, 20.7 ppm. Observed LC–MS $[M+H]^+$ 442.3

.

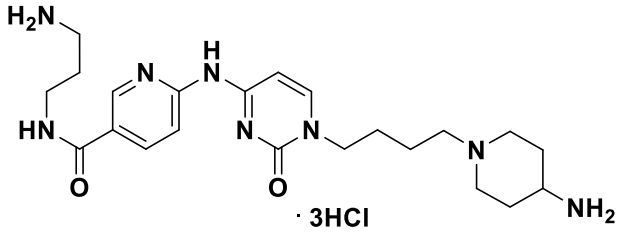

CZ–02–028: Mp 252–254 °C.

^{1}H NMR (500 MHz, CD_3OD) δ 8.77 (d, *J* = 1.5 Hz, 1H), 8.35 (bs, 1H), 8.17 (dd, J_1 = 2.0 Hz, J_2 = 7.5 Hz, 1H), 7.85 (d, *J* = 7.0 Hz, 1H), 6.56 (d, *J* = 3.5 Hz, 1H), 3.89 (t, *J* = 7.0 Hz, 2H), 3.50 (t, *J* = 7.5 Hz, 2H), 2.96 (d, *J* = 12.0 Hz, 2H), 2.92 (t, *J* = 7.0 Hz, 2H), 2.89–2.84 (m, 1H), 2.41 (t, *J* = 8.0 Hz, 2H), 2.07 (t, *J* = 10.0 Hz, 2H), 1.92–1.89 (m, 4H), 1.78–1.70 (m, 2H), 1.59–1.47 (m, 4H). ^{13}C NMR (125 MHz, CD_3OD) δ 168.3, 164.0, 158.9, 156.1, 149.0, 148.6, 138.2, 125.9, 115.1, 98.1, 58.9, 53.1, 51.3, 49.6, 39.0, 37.9, 33.3, 30.7, 28.2, 24.8 ppm. Observed LC–MS $[M+H]^+$ 443.3

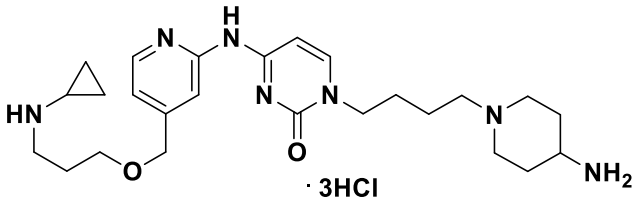

CZ–02–029: Mp 256–258 °C.

^{1}H NMR (500 MHz, D_2O) δ 8.29 (d, *J* = 6.0 Hz, 1H), 8.04 (d, *J* = 7.5 Hz, 1H), 7.42 (d, *J* = 6.0 Hz, 1H), 7.40 (s, 1H), 6.40 (d, *J* = 7.5 Hz, 1H), 4.76 (s, 2H), 3.96 (t, *J* = 6.5 Hz, 2H), 3.75–3.67 (m, 4H), 3.57–3.51 (m, 1H), 3.29 (t, *J* = 7.0 Hz, 2H), 3.19 (t, *J* = 6.5 Hz, 2H), 3.09 (t, *J* = 13.5 Hz, 2H), 2.74 (t, *J* = 6.5 Hz, 2H), 2.32 (d, *J* = 13.5 Hz, 2H), 2.09–2.01 (m, 2H), 1.97–1.87 (m, 2H), 1.80 (bs, 4H). ^{13}C NMR (125 MHz, D_2O) δ 161.9, 158.0, 155.4, 150.1, 148.9, 137.5, 117.7, 112.9, 97.1, 70.0, 68.2, 56.2, 50.6, 50.0, 45.8, 45.3, 30.0, 27.0, 25.4, 25.1, 20.6, 2.9 ppm. Observed LC–MS $[M+H]^+$ 470.3

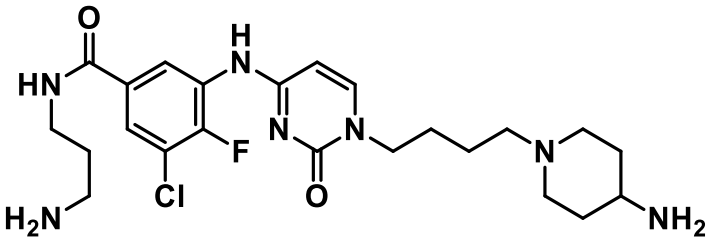

CZ–02–037: Mp 283 °C. (decomposition)

^{1}H NMR (500 MHz, D_2O) δ 8.45 (d, *J* = 3.5 Hz, 1H), 7.63 (d, *J* = 7.0 Hz, 1H), 7.51 (d, *J* = 4.0 Hz, 1H), 6.08 (d, *J* = 7.5 Hz, 1H), 3.69 (t, *J* = 7.5 Hz, 2H), 3.29 (t, *J* = 6.5 Hz, 2H), 2.76 (t, *J* = 10.5 Hz, 2H), 2.71 (d, *J* = 7.0 Hz, 2H), 2.66–2.59 (m, 1H), 2.17 (t, *J* = 10.5 Hz, 2H), 1.88 (t, *J* = 10.5 Hz, 5H), 1.71 (d, *J* = 7.5 Hz, 2H), 1.55 (d, *J* = 7.5 Hz, 2H), 1.38–1.30 (m, 4H). ^{13}C NMR (125 MHz, D_2O) δ 167.8, 164.4, 159.0, 153.1 (d, $J_{C–F}$ = 252.1), 148.2, 131.8, 129.3 (d, $J_{C–F}$ = 10.5), 125.9,

122.9, 122.2 (d, $J_{C–F}$ = 17), 97.4, 58.8, 53.1, 51.5, 49.4, 39.0, 38.2, 33.6, 30.7, 28.1, 24.6 ppm. Observed LC–MS $[M+H]^+$ 494.2

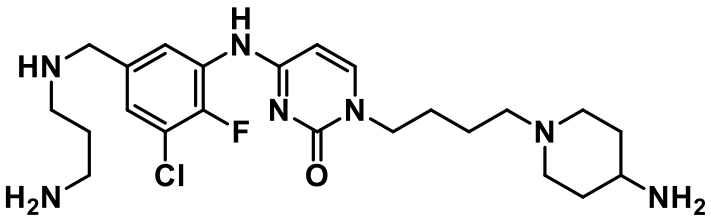

CZ–02–038.

^{1}H NMR (500 MHz, D_2O) δ 7.95 (d, *J* = 7.5 Hz, 1H), 7.76 (bs, 1H), 7.65 (bs, 1H), 6.26 (bs, 1H), 4.29 (s, 2H), 3.91 (bs, 2H), 3.71 (d, *J* = 13.0 Hz, 2H), 3.58–3.53 (m, 1H), 3.32–3.17 (m, 4H), 3.09 (t, *J* = 8.5 Hz, 2H), 2.34 (d, *J* = 13.0 Hz, 2H), 2.15–2.08 (m, 2H), 1.98–1.90 (m, 2H), 1.80 (bs, 4H). ^{13}C NMR (125 MHz, D_2O) δ 160.0, 153.1 (d, $J_{C–F}$ = 250), 149.7, 131.3, 128.0, 127.1, 124.1, 122.6, 122.4, 94.95, 56.2, 50.7, 50.0, 49.4, 46.6, 45.3, 44.2, 36.5, 27.05, 25.03, 23.65, 20.61 ppm. Observed LC–MS $[M+H]^+$ 480.3

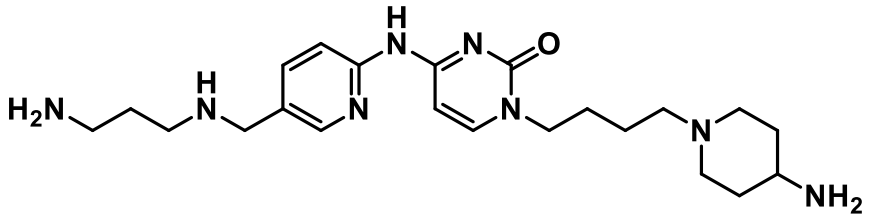

CZ–02–039: Mp 182–184 °C.

^{1}H NMR (500 MHz, CD_3OD) δ 8.26 (s, 1H), 8.23 (bs, 1H), 7.78 (d, *J* = 8.0 Hz, 2H), 6.50 (bs, 1H), 3.87 (t, *J* = 7.0 Hz, 2H), 3.75 (s, 2H), 2.94 (d, *J* = 12.0 Hz, 2H), 2.84 (t, *J* = 7.0 Hz, 2H), 2.75–2.66 (m, 3H), 2.40 (t, *J* = 7.0 Hz, 2H), 2.06 (t, *J* = 12.0 Hz, 2H), 1.86 (d, *J* = 12.0 Hz, 2H), 1.79–1.71 (m, 4H), 1.59–1.53 (m, 2H), 1.50–1.42 (m, 2H). ^{13}C NMR (125 MHz, CD_3OD) δ 164.0, 159.0, 153.0, 149.1,

148.1, 139.8, 131.7, 116.2, 97.9, 59.1, 53.5, 51.3, 51.2, 49.6, 46.7, 40.4, 34.7, 31.3, 28.3, 24.8 ppm. Observed LC–MS $[M+H]^+$ 429.3

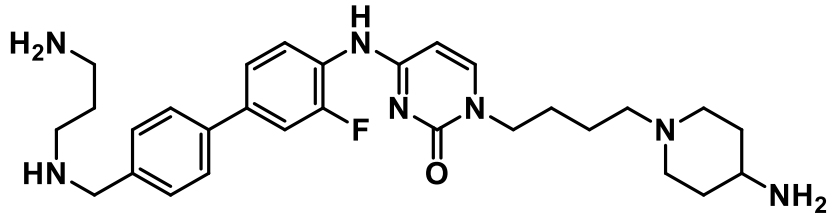

CZ–02–041.

^{1}H NMR (500 MHz, CD_3OD) δ 8.19 (bs, 1H), 7.72 (d, *J* = 7.0 Hz, 1H), 7.60 (d, *J* = 8.0 Hz, 2H), 7.45–7.36 (m, 4H), 6.18 (d, *J* = 7.0 Hz, 1H), 3.83 (t, *J* = 7.0 Hz, 2H), 3.80 (s, 2H), 2.93 (d, *J* = 11.5 Hz, 2H), 2.89 (t, *J* = 7.0 Hz, 2H), 2.80 (p, J_1 = 3.0 Hz, J_2 = 7.0 Hz, 1H), 2.72 (t, *J* = 7.0 Hz, 2H), 2.38 (t, *J* = 7.5 Hz, 2H), 2.05 (t, *J* = 11.5 Hz, 2H), 1.88 (d, *J* = 13.5 Hz, 2H), 1.80 (p, *J* = 7.0 Hz, 2H), 1.71 (p, *J* = 7.0 Hz, 2H), 1.56–1.45 (m, 4H). ^{13}C NMR (125 MHz, CD_3OD) δ 165.0, 159.3, 156.6 (d, $J_{C–F}$ = 247.4 Hz), 147.8, 140.1, 139.6, 130.4, 128.0, 127.0, 126.7 (d, $J_{C–F}$ = 11.4 Hz), 123.6, 114.7 (d, $J_{C–F}$ = 19.9 Hz), 97.2, 59.0, 54.0, 53.2, 51.1, 49.7, 47.6, 40.3, 33.7, 29.7, 28.3, 24.8 ppm. Observed LC–MS $[M+H]^+$ 522.3

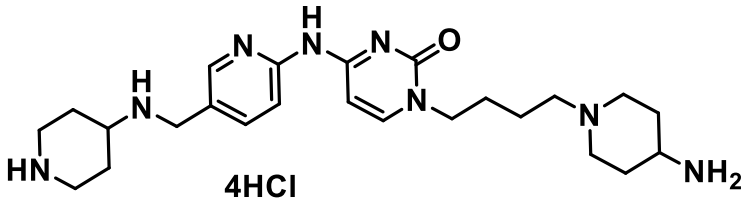

CZ–02–048: Mp 277–279 °C.

^{1}H NMR (500 MHz, D_2O) δ 8.61 (s, 1H), 8.27 (d, J_1 = 8.5 Hz, 1H), 8.17 (d, *J* = 8.0 Hz, 1H), 7.47 (d, *J* = 8.5 Hz, 1H), 6.50 (d, *J* = 7.5 Hz, 1H), 4.49 (s, 2H), 4.04 (t, *J* = 6.5 Hz, 2H), 3.80–3.55 (m, 6H), 3.30–3.11 (m, 6H), 2.53 (d, *J* = 13.0 Hz, 2H), 2.37 (d, *J* = 13.0 Hz, 2H), 2.08–1.79 (m, 8H). ^{13}C NMR (125 MHz, D_2O) δ

158.8, 151.1, 150.9, 144.5, 143.6, 123.9, 116.0, 115.8, 96.2, 56.1, 52.6, 50.7, 50.0, 45.4, 45.0, 42.3, 27.1, 26.9, 25.1, 25.0, 20.6 ppm. Observed LC–MS $[M+H]^+$ 455.3

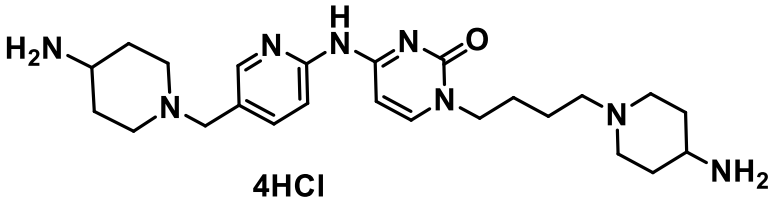

CZ–02–049: Mp 284–196 °C.

^{1}H NMR (500 MHz, D_2O) δ 8.58 (s, 1H), 8.22 (dd, J_1 = 2.0 Hz, J_2 = 8.5 Hz, 1H), 8.16 (d, J = 7.5 Hz, 1H), 7.43 (d, J = 8.5 Hz, 1H), 6.46 (d, J = 7.5 Hz, 1H), 4.48 (s, 2H), 4.00 (t, J = 6.5 Hz, 2H), 3.70 (t, J = 12.5 Hz, 4H), 3.59–3.53 (m, 2H), 3.27–3.20 (m, 4H), 3.12 (t, J = 13.0 Hz, 2H), 2.33 (d, J = 13.0 Hz, 4H), 1.94 (q, J = 13.0 Hz, 4H), 1.83 (bs, 4H). ^{13}C NMR (125 MHz, D_2O) δ 158.5, 151.6, 151.2, 150.2, 146.2, 144.4, 121.7, 115.9, 115.8, 96.2, 56.5, 56.1, 50.7, 50.4, 49.9, 45.4, 45.3, 27.0, 26.9, 25.0, 20.6 ppm. Observed LC–MS $[M+H]^+$ 455.3

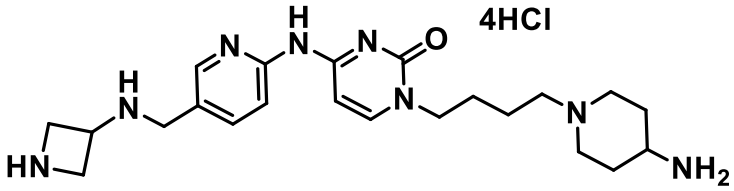

CZ–02–050: Mp 284–286 °C.

^{1}H NMR (500 MHz, D_2O) δ 8.59 (s, 1H), 8.23 (dd, J_1 = 2.0 Hz, J_2 = 8.5 Hz, 1H), 8.17 (d, J = 7.5 Hz, 1H), 7.45 (d, J = 8.5 Hz, 1H), 6.47 (d, J = 7.5 Hz, 1H), 4.62 (p, J = 7.0 Hz, 1H), 4.50 (d, J = 7.0 Hz, 4H), 4.42 (bs, 2H), 4.01 (t, J = 6.5 Hz, 2H), 3.73 (d, J = 13.0 Hz, 2H), 3.61–3.54 (m, 1H), 3.22 (t, J = 6.5 Hz, 2H), 3.14 (t, J = 13.0 Hz, 2H), 2.35 (d, J = 13.0 Hz, 2H), 1.96 (dq, J_1 = 4.0 Hz, J_2 = 13.0 Hz, 2H), 1.85 (d, J = 4.0 Hz, 4H). ^{13}C NMR (125 MHz, D_2O) δ 158.5, 151.4, 151.1,

150.3, 145.0, 143.3, 123.2, 116.0, 96.1, 56.1, 50.7, 49.9, 48.8, 47.5, 45.9, 45.3, 27.0, 25.0, 20.6 ppm. Observed LC–MS $[M+H]^+$ 427.3

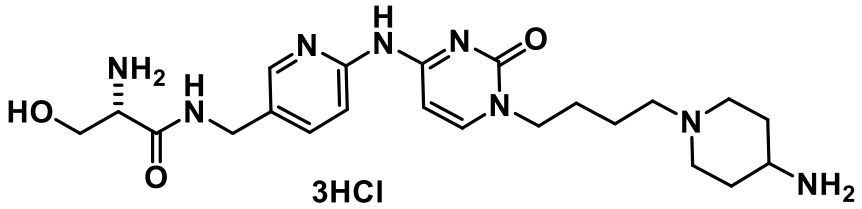

CZ–02–051: Mp 249–251 °C. $[\alpha]^{20}_D$ = –5 (*c* = 0.10, H_2O).

^{1}H NMR (500 MHz, D_2O) δ 8.33 (s, 1H), 8.19 (d, *J* = 8.5 Hz, 1H), 8.09 (d, *J* = 7.0 Hz, 1H), 7.44 (d, *J* = 8.5 Hz, 1H), 6.43 (d, *J* = 7.0 Hz, 1H), 4.56 (d, *J* = 4.5 Hz, 2H), 4.22 (t, *J* = 4.5 Hz, 1H), 4.05–3.97 (m, 4H), 3.73 (d, *J* = 13.0 Hz, 2H), 3.58 (t, *J* = 11.5 Hz, 1H), 3.22 (t, *J* = 8.0 Hz, 2H), 3.14 (t, *J* = 11.5 Hz, 2H), 3.36 (d, *J* = 13.0 Hz, 2H), 2.01–1.92 (m, 2H), 1.84 (bs, 4H). ^{13}C NMR (125 MHz, D_2O) δ 168.1, 160.8, 154.0, 150.3, 148.7, 143.7, 137.8, 130.5, 116.1, 96.8, 60.1, 56.2, 54.5, 50.7, 50.0, 45.4, 39.8, 27.1, 25.1, 20.7 ppm. LC–MS [M+H] 459.3

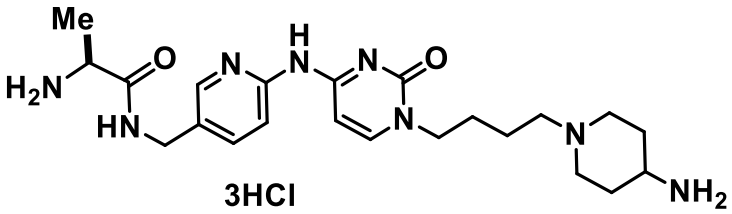

CZ–02–052: Mp 223 – 225 °C. $[\alpha]^{20}_D$ = –6 (*c* = 0.10, H_2O).

^{1}H NMR (500 MHz, D_2O) δ 8.29 (s, 1H), 8.13 (dd, J_1 = 2.0 Hz, J_2 = 8.5 Hz, 1H), 8.05 (d, *J* = 7.5 Hz, 1H), 7.47 (d, *J* = 8.5 Hz, 1H), 6.42 (d, *J* = 7.5 Hz, 1H), 4.72 (s, 2H), 4.15 (q, *J* = 7.0 Hz, 1H), 3.98 (bs, 2H), 3.73 (d, *J* = 13.0 Hz, 2H), 3.58 (t, *J* = 13.0 Hz, 1H), 3.22–3.16 (m, 2H), 3.14 (t, *J* = 13.0 Hz, 2H), 1.96 (q, *J* = 13.0 Hz, 2H), 1.84 (bs, 4H), 1.55 (d, *J* = 7.0 Hz, 3H). ^{13}C NMR (125 MHz, D_2O) δ 171.0,

161.0, 154.3, 150.0, 148.8, 143.1, 138.7, 130.4, 116.1, 96.8, 56.2, 50.7, 49.9, 49.0, 45.4, 39.8, 27.1, 25.1, 20.7, 16.4 ppm. LC–MS [M+H] 443.3

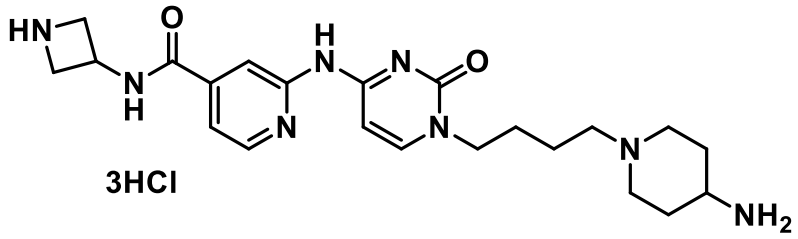

CZ–02–054: Mp 301–303 °C.

^{1}H NMR (500 MHz, CD_3OD) δ 8.72 (bs, 1H), 8.42 (d, *J* = 5.0 Hz, 1H), 7.82 (d, *J* = 7.5 Hz, 1H), 7.47 (d, *J* = 5.0 Hz, 1H), 6.40 (bs, 1H), 4.95–4.89 (m, 1H), 4.00–3.83 (m, 6H), 2.97 (d, *J* = 12.0 Hz, 2H), 2.90–2.85 (m, 1H), 2.42–2.10 (m, 2H), 2.08 (t, *J* = 12.0 Hz, 2H), 1.91 (d, *J* = 13.0 Hz, 2H), 1.78–1.72 (m, 2H), 1.58–1.49 (m, 4H). ^{13}C NMR (125 MHz, CD_3OD) δ 167.7, 164.0, 159.2, 154.4, 150.1, 148.3, 144.5, 118.5, 113.5, 98.0, 58.9, 54.2, 53.1, 51.3, 45.8, 33.2, 28.2, 24.8 ppm. Observed LC–MS $[M+H]^+$ 441.3

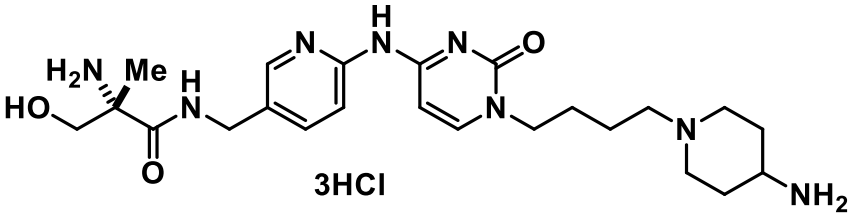

CZ–02–060: Mp 265 – 270 °C. $[\alpha]^{20}_{D}$ = –5 (*c* = 0.10, H_2O).

^{1}H NMR (500 MHz, D_2O) δ 8.37 (d, *J* = 2.0 Hz, 1H), 8.23 (dd, J_1 = 2.0 Hz, J_2 = 8.5 Hz, 1H), 8.15 (d, *J* = 7.0 Hz, 1H), 7.49 (d, *J* = 8.5 Hz, 1H), 6.49 (d, *J* = 7.0 Hz, 1H), 4.61 (s, 2H), 4.07–4.02 (m, 3H), 3.92 (d, *J* = 12.5 Hz, 1H), 3.79 (d, *J* = 13.0 Hz, 2H), 3.64 (p, J_1 = 3.0 Hz, J_2 = 8.0 Hz, 1H), 3.28 (t, *J* = 8.0 Hz, 2H), 3.20 (dt, J_1 = 3.0 Hz, J_2 = 13.0 Hz, 2H), 2.42 (d, *J* = 13.0 Hz, 2H), 2.02 (dq, J_1 = 3.0 Hz,

J_2 = 13.0 Hz, 2H), 1.90 (d, J = 3.0 Hz, 4H), 1.65 (s, 3H). ^{13}C NMR (125 MHz, D_2O) δ 171.1, 160.8, 154.0, 150.3, 148.7, 143.7, 137.8, 130.7, 116.2, 96.9, 64.4, 61.4, 56.3, 50.8, 50.0, 45.5, 40.0, 27.1, 25.2, 20.7, 18.1 ppm. Observed LC–MS $[M+H]^+$ 473.3

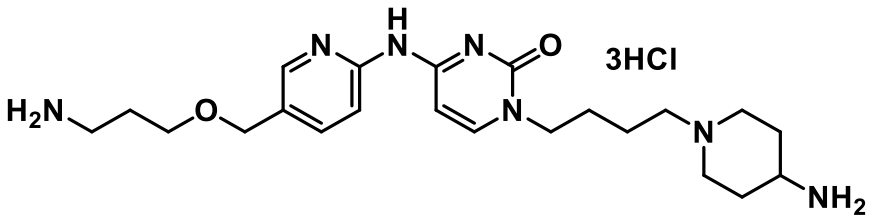

CZ–02–062: Mp 190 – 194 °C.

^{1}H NMR (500 MHz, D_2O) δ 8.36 (s, 1H), 8.26 (d, J = 9.0 Hz, 1H), 8.09 (d, J = 7.0 Hz, 1H), 7.45 (d, J = 9.0 Hz, 1H), 6.42 (d, J = 7.0 Hz, 1H), 4.67 (s, 2H), 3.99 (bs, 2H), 3.73 (t, J = 6.0 Hz, 2H), 3.58 (t, J = 12.5 Hz, 1H), 3.22 (bs, 1H), 3.17–3.10 (m, 4H), 2.35 (d, J = 14.0 Hz, 2H), 2.04–1.92 (m, 4H), 1.84 (bs, 4H). ^{13}C NMR (125 MHz, D_2O) δ 160.9, 154.2, 150.3, 148.9, 144.4, 137.9, 130.3, 116.0, 96.8, 68.5, 67.9, 56.2, 50.7, 50.0, 45.3, 37.4, 27.1, 26.6, 25.1, 20.6 ppm. Observed LC–MS $[M+H]^+$ 473.3

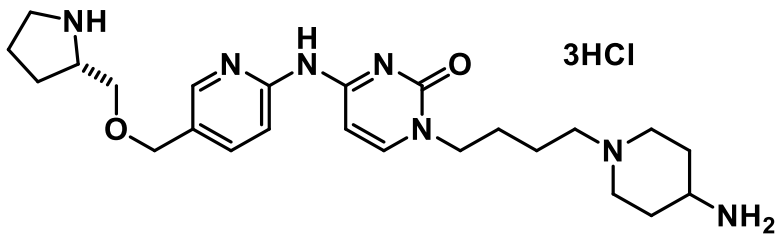

CZ–02–063: Mp 218 – 220 °C. $[\alpha]^{20}_D$ = –5.0 (c = 0.10, H_2O).

^{1}H NMR (500 MHz, D_2O) δ 8.37 (s, 1H), 8.24 (d, J = 8.5 Hz, 1H), 8.05 (d, J = 7.0 Hz, 1H), 7.44 (d, J = 8.5 Hz, 1H), 6.40 (d, J = 7.0 Hz, 1H), 4.69 (s, 2H), 3.96 (bs, 2H), 3.87 (t, J = 7.5 Hz, 2H), 3.70 (d, J = 9.0 Hz, 2H), 3.54 (t, J = 12.5 Hz, 1H),

3.31 (t, *J* = 12.5 Hz, 2H), 3.19 (bs, 2H), 3.10 (t, *J* = 12.5 Hz, 2H), 2.32 (d, *J* = 13.5 Hz, 2H), 2.16–2.05 (m, 2H), 2.04–1.96 (m, 2H), 1.95–1.86 (m, 2H), 1.81 (bs, 4H). ^{13}C NMR (125 MHz, D_2O) δ 160.7, 153.9, 150.0, 148.7, 144.0, 137.6, 129.8, 115.8, 96.6, 68.6, 68.5, 58.9, 55.9, 50.4, 49.8, 45.4, 45.1, 26.8, 25.6, 24.8, 23.0, 20.4 ppm. Observed LC–MS $[M+H]^+$ 456.3

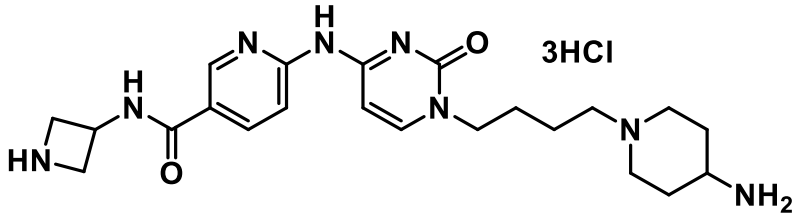

CZ–02–067: Mp 265 – 267 °C.

^{1}H NMR (500 MHz, D_2O) δ 8.84 (d, *J* = 20 Hz, 1H), 8.41 (dd, J_1 = 2.0 Hz, J_2 = 6.5 Hz, 1H), 8.19 (d, *J* = 6.5 Hz, 1H), 7.43 (d, *J* = 8.5 Hz, 1H), 6.49 (d, *J* = 8.5 Hz, 1H), 4.98–4.91 (m, 1H), 4.46 (t, *J* = 11.5 Hz, 2H), 4.37 (t, *J* = 11.5 Hz, 2H), 4.02 (t, *J* = 5.5 Hz, 2H), 3.73 (d, *J* = 13.0 Hz, 2H), 3.60–3.54 (m, 1H), 3.22 (t, *J* = 8.0 Hz, 2H), 3.13 (t, *J* = 13.0 Hz, 2H), 1.20–1.90 (m, 2H), 1.85 (bs, 4H). ^{13}C NMR (125 MHz, D_2O) δ 166.4, 158.5, 152.6, 151.4, 150.1, 143.8, 140.3, 125.9, 115.3, 96.1, 56.2, 52.0, 50.7, 50.0, 45.3, 42.3, 27.1, 25.0, 20.6 ppm. Observed LC–MS $[M+H]^+$ 441.3

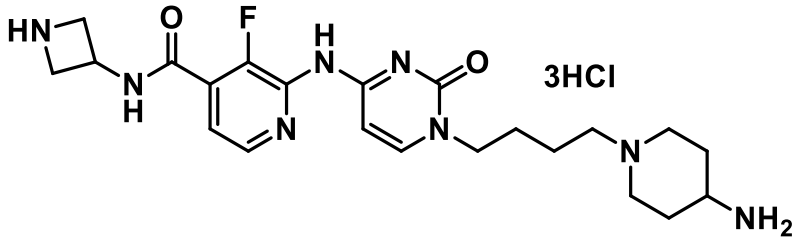

CZ–02–068: Mp 264 °C. (decomposition)

^{1}H NMR (500 MHz, CD_3OD) δ 8.86 (d, *J* = 5.5 Hz, 1H), 8.31 (d, *J* = 7.5 Hz,

1H), 7.84 (d, *J* = 5.5 Hz, 1H), 7.02 (d, *J* = 7.5 Hz, 1H), 4.56 (t, *J* = 10.5 Hz, 2H), 4.50 (t, *J* = 10.5 Hz, 2H), 4.26 (bs, 2H), 3.56 (d, *J* = 10.5 Hz, 2H), 3.74 (t, *J* = 10.5 Hz, 1H), 3.40–3.35 (m, 1H), 3.28–3.20 (m, 4H), 2.34 (d, *J* = 12.5 Hz, 2H), 2.16–2.09 (m, 2H), 1.98 (bs, 2H). ^{13}C NMR (125 MHz, CD_3OD) δ 166.8, 157.6, 152.0, 147.4, 146.3, 140.6, 138.7, 134.0 (d, $J_{C–F}$ = 228.8 Hz), 130.0 (d, $J_{C–F}$ = 12.4 Hz), 123.0, 118.9, 97.4, 57.4, 53.4, 51.9, 50.7, 46.9, 43.4, 28.5, 27.0, 22.0 ppm. Observed LC–MS $[M+H]^+$ 459.3

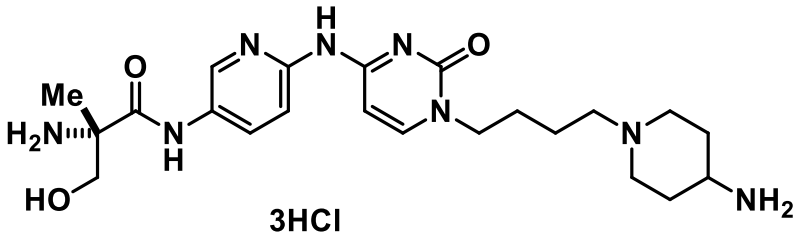

CZ–02–069: Mp 264–266 °C. $[\alpha]^{20}_D$ = –7.0 (*c* = 0.10, H_2O).

^{1}H NMR (500 MHz, D_2O) δ 8.66 (s, 1H), 8.19 (d, *J* = 8.5 Hz, 1H), 8.10 (d, *J* = 7.0 Hz, 1H), 7.37 (d, *J* = 9.5 Hz, 1H), 6.41 (d, *J* = 7.0 Hz, 1H), 4.16 (d, *J* = 12.0 Hz, 1H), 3.99 (bs, 2H), 3.92 (d, *J* = 12.0 Hz, 1H), 3.72 (d, *J* = 13.0 Hz, 2H), 3.57 (t, *J* = 11.5 Hz, 2H), 3.21 (bs, 2H), 3.12 (t, *J* = 12.0 Hz, 2H), 2.34 (d, *J* = 13.0 Hz, 2H), 1.99–1.89 (m, 2H), 1.83 (bs, 4H), 1.70 (s, 3H). ^{13}C NMR (125 MHz, D_2O) δ 169.6, 158.3, 150.7, 150.5, 147.3, 136.3, 135.8, 131.0, 115.8, 96.1, 64.1, 62.1, 56.2, 50.7, 49.8, 45.3, 27.1, 25.0, 20.6, 17.8 ppm. Observed LC–MS $[M+H]^+$ 459.3

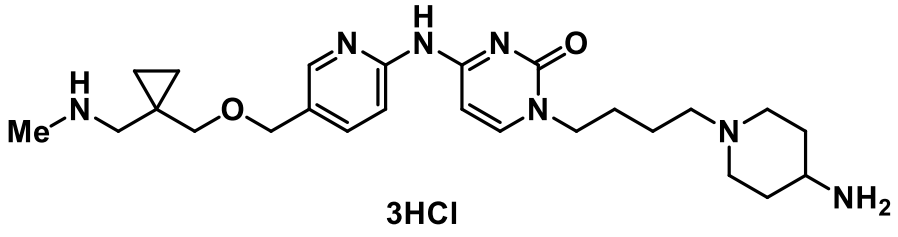

CZ–02–070: Mp 260–262 °C.

^{1}H NMR (500 MHz, D_2O) δ 8.37 (s, 1H), 8.25 (d, *J* = 9.0 Hz, 1H), 8.08 (d, *J* = 7.5 Hz, 1H), 7.45 (d, *J* = 9.0 Hz, 1H), 6.43 (d, *J* = 7.5 Hz, 1H), 4.67 (s, 2H), 3.99 (t, *J* = 6.5 Hz, 2H), 3.72 (d, *J* = 13.5 Hz, 2H), 3.57 (t, *J* = 12.5 Hz, 1H), 3.52 (s, 2H), 3.21 (t, *J* = 7.5 Hz, 2H), 3.13 (d, *J* = 12.5 Hz, 2H), 3.09 (s, 2H), 2.67 (s, 3H), 2.35 (d, *J* = 13.5 Hz, 2H), 1.99–1.88 (m, 2H), 1.83 (d, *J* = 3.5 Hz, 4H), 0.70 (q, J_1 = 8.0 Hz, J_2 = 7.5 Hz, 4H). ^{13}C NMR (125 MHz, D_2O) δ 161.0, 154.2, 150.2, 149.0, 144.3, 137.9, 130.3, 116.1, 96.9, 75.4, 68.5, 56.2, 55.3, 50.7, 50.0, 45.3, 33.3, 27.1, 25.1, 20.6, 17.5, 9.6 ppm. Observed LC–MS $[M+H]^+$ 470.3

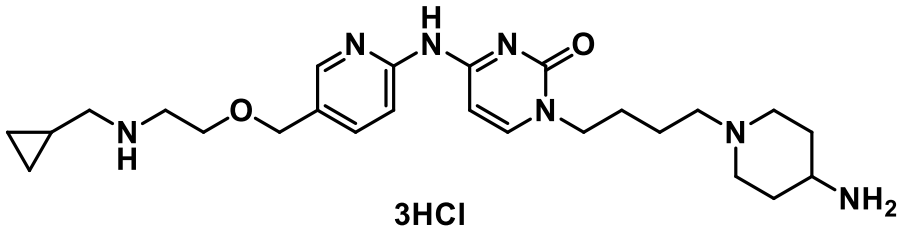

3HCl

CZ–02–071: Mp 226–231 °C.

^{1}H NMR (500 MHz, D_2O) δ 8.39 (d, *J* = 2.0 Hz, 1H), 8.26 (dd, J_1 = 2.0 Hz, J_2 = 6.5 Hz, 1H), 8.07 (d, *J* = 7.5 Hz, 1H), 7.45 (d, *J* = 9.0 Hz, 1H), 6.42 (d, *J* = 7.5 Hz, 1H), 4.70 (s, 2H), 3.98 (t, *J* = 6.5 Hz, 2H), 3.84 (t, *J* = 5.0 Hz, 2H), 3.71 (d, *J* = 13.5 Hz, 2H), 3.56 (p, J_1 = 4.0 Hz, J_2 = 8.0 Hz, 1H), 3.33 (t, *J* = 5.5 Hz, 2H), 3.20 (t, *J* = 7.5 Hz, 2H), 3.14–3.08 (m, 2H), 2.96 (d, *J* = 7.5 Hz, 2H), 2.34 (d, *J* = 13.5 Hz, 2H), 1.98–1.89 (m, 2H), 1.88–1.80 (m, 4H), 1.08–1.04 (m, 1H), 0.66 (q, J_1 = 6.5 Hz, J_2 = 8.0 Hz, 2H), 0.33 (q, J_1 = 5.0 Hz, J_2 = 5.0 Hz, 2H). ^{13}C NMR (125 MHz, D_2O) δ 160.9, 154.1, 150.3, 149.0, 144.3, 138.1, 130.0, 116.1, 96.9, 68.7, 65.1, 56.2, 52.3, 50.7, 50.0, 46.2, 45.3, 27.1, 25.1, 20.6, 6.4, 3.3 ppm. Observed LC–MS $[M+H]^+$ 470.3

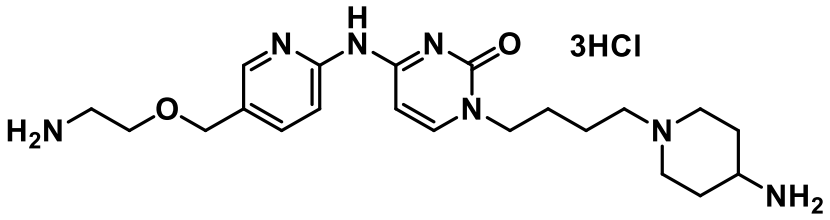

CZ–02–072:

^{1}H NMR (500 MHz, D_2O) δ 8.40 (s, 2H), 8.27 (d, *J* = 8.5 Hz, 1H), 8.07 (d, *J* = 7.5 Hz, 1H), 7.47 (d, *J* = 8.5 Hz, 1H), 6.43 (d, *J* = 7.5 Hz, 1H), 4.72 (s, 2H), 3.99 (bs, 2H), 3.82 (t, *J* = 5.0 Hz, 2H), 3.72 (d, *J* = 13.0 Hz, 2H), 3.60–3.52 (m, 1H), 3.26 (bs, 2H), 3.21 (bs, 2H), 3.12 (t, *J* = 8.0 Hz, 2H), 3.34 (d, *J* = 13.0 Hz, 2H), 1.98–1.90 (m, 2H), 1.83 (bs, 2H). ^{13}C NMR (125 MHz, D_2O) δ 161.0, 154.3, 150.2, 144.2, 138.0, 130.1, 116.1, 96.9, 68.6, 66.0, 56.2, 50.7, 50.0, 45.3, 39.0, 27.1, 25.1, 20.7 ppm. Observed LC–MS $[M+H]^+$ 416.3.

CHAPTER 4

THIRD GENERATION AMICETIN ANALOGS

Background

So far, our efforts to design and synthesize selective prokaryotic translational inhibitors were focused on modifications of eastern (cation–π region) and western halves (solvent front) of bi–aryl analogs. The SAR on bi–aryl analogs (second generation analogs) by synthesizing a wide range of structurally and functionally diverse compounds were unsuccessful in retaining selectivity. We appreciate the fact that these compounds could not advance unless we achieved selective prokaryotic translation inhibition. Initially, during the synthesis of second generation analogs we hypothesized that the ability of Ami to participate in π–π stacking interaction with A2602 and its α–methylserine motif's interaction with L16 ribosomal protein, unlike BlaS (universal translationa inhibitor), is responsible for the observed selectivity of Ami toward prokaryotic translation. However, the second generation Ami analogs synthesized (bi–aryl amines) demonstrated that the ability of engaging A2602 in a π–π stacking interaction and hydrogen bonding interactions in solvent front are not sufficient to confer the selectivity. Inability to identify a selective translational inhibitor, in spite of the considerable number of endeavors leads us to focus on the approaches to mitigate the hydrolytic stability of the amide bond in our first generation analogs (**CZ–02–023**, $SI_{R.\ ret/E.\ coli}$ =112)

by supplanting the amide with a sulfonamide a urea functionality (bio–isostere of amide). Focus on stabilizing the amide bond in **CZ–02–023** series originates from key perceptions of the crystal structures of the ternary complex (amicetin/70S ribosome and P–tRNA) and an in depth analysis of crystal structures of BlaS bound to prokaryotic (70S) and eukaryotic (80S) ribosomes.

X–ray Crystal Structure Inputs for Selectivity and Synthesis of Third Generation Analogs

The X–ray crystal structure of amicetin bound to the ribosome in the presence of P–site tRNA shows two asymmetric ribosome units, each displaying a distinct binding pattern of amicetin (exclusively the α–methyl serine unit) in the solvent front. In one of the structures the α–methyl serine amide rests in *S*–cis confirmation (Figure 4.1, colored in Orange) and exposes the amine to a set of most conserved (both in prokaryotes and eukaryotes) rRNA phosphate backbone which we named the “Ring of Fire” via a hydrogen bonding interaction with the phosphate of G2506, whereas, in the other conformer the α–methyl serine unit of amicetin adopts *S*–*tans* amide (Figure 4.1, colored in gray) positioning the amine away from the ring of fire and toward the tRNA involving in a hydrogen bonding interaction with the C74–phosphate of tRNA. We hypothesize that the conformer, which can place the cationic amine away from the conserved chain of phosphates, will be selective toward prokaryotic translation inhibition (Figure 4.2).[1]

Comparison of both the prokaryotic and eukaryotic ribosomal P-site

To gain further insights into the factors governing the selectivity of amicetin toward prokaryotic translation inhibition, we analyzed the key structural similarities and differences in the prokaryotic 70S ribosome in comparison with the eukaryotic 80S ribosome. Further hypothetical evidence for the selectivity of Ami arises from the docking studies of Ami on to the eukaryotic 80S ribosome.

In the P–site of the prokaryotic ribosome (binding pocket of BlaS, and Ami), the closest distance between the amino acid E80 (where α–methylserine of Ami interacts) of the ribosomal protein L16 and the WC donor G2262 (where is cytosine of Ami, and BlaS binds) is approximately 11.4Å (Figure 4.3), whereas in the eukaryotic ribosome (*saccharomyces cerevisiae)*, the distance between the ribosomal protein L10 (analogous to L16 in prokaryotes) and WC donor G2619 is significantly ~ 3Å shorter (7.8Å) compared to 70S ribosome (Figure 4.4). BlaS (lacking the *p*–aminobenzoate tether attached to cytosine in Ami) being short, can be accommodated both in prokaryotes and eukaryotes hence nonselective. We hypothesize that the shorter binding pocket in eukaryotes fail to accommodate larger compounds like Ami in the binding pocket and hence Ami is selective toward prokaryotic translational inhibition. Both the prokaryotic and eukaryotic ribosomes have a conserved chain of phosphates right above the ribosomal protein. The interaction on compounds with phosphate chain as in second generation analogs fail to confer the selectivity.[2, 3] Advancing with the above hypothesis for selectivity (longer compounds like Ami with tethered pendant amine placed away from the

ring of fire), we identified the piperazinyl ureas as replacements of *p*–aminobenzoate in first generation Ami analogs (Figure 4.5).

Synthesis of Piperazinyl Urea Derivatives of Amicetin

One of the strategies to mitigate the hydrolytic liability of amide bond is to chemically modify it to urea functionality. Most importantly, the opposing dipole moments of carbonyl groups in piperazinyl ureas orients the amine away from the "ring of fire" and toward the C74 phosphate of tRNA. Docking studies of designed piperazinyl ureas onto the crystal structure of ternary complex confirm the anti–conformation of two carbonyls positioning the tethered cationic amine away from the "ring of fire" (Figure 4.5).

As demonstrated in Scheme 4.1, the designed urea analogs synthesis commenced with a peptide coupling reaction of the 3–Boc–amino butyric acid with Cbz–piperazine followed by Cbz de–protection of the resultant amide **50** to afford the piperazine derivative **51**. In another reaction sequence, the reaction of carbonyl di–imidazole (CDI) with alkylated cytosine **4** resulted in an imidazole carboxamide **52**, which was further reacted with the preformed piperazine amide **51** to form the urea **53**. Finally, Boc de–protection of urea **53** using methanolic HCl resulting in the urea derivative.[4]

The *N1*–Phenyl cytosine was synthesized by employing Chan–Lam coupling reaction of cytosine and phenyl boronic acid followed by reductive amination of resultant aldehyde **55** to give 3^{o} amine **56**. The *N1*–aryl cytosine **56** was reacted with carbonyl di–imidazole (CDI) to form imidazole carboxamide **57** as shown in Scheme 4.2. The rest of the reaction sequence to access N^{1}–aryl

cytosine urea derivatives follows the similarly reported protocols in Scheme 14.[5]

Synthesis of *N1*–phenethyl amino cytosine **60** began with an S_N2 reaction of Boc–amino piperadine onto bromoethyl bromo benzene to give bromo benzene **58**. The bromobenzene **58** was converted to boronate ester **59**, which was subsequently reacted with cytosine under Chan–Lam conditions to yield *N1*–phenethyl amino cytosine **60** (Scheme 4.3). The conversion of cytosine **60** to **CZ–02–132** follows the similarly reported protocol in Scheme 4.1.[5]

Using similar procedures listed in Scheme 4.1 and 4.2 following compounds shown in Figure 4.6 were synthesized and tested for translational inhibitory activity.

As shown in Table 4.1, these compounds exhibited a selectivity window of ~34–580 ($SI_{RR/E.\ coli}$). Some of these initial compounds further tested for their antimycobacterial activity and the results are shown in Table 4.2.

Excited with the selectivity window these compounds offer, we decided to work out an SAR on urea derivatives to develop a broad–spectrum and selective translational inhibitor. For quick access to these urea derivatives, our strategy is to develop a unified approach (Scheme 4.4) employing a common intermediate as described in Scheme 4.1.[6]

The synthesis of the common amine intermediate began with the trifluoroacetamide formation of Cbz–piperazine, which upon hydrogenolysis gave the piperazine trifluoroacetamide. The free amine is treated with CDI to produce the Imidazole carboxamide, which is further activated with methyl iodide and reacted with cytosine butyl amino piperadine to yield the urea. Finally, base mediated solvolysis of the trifluoroacetamide resulted in the advanced common

intermediate free amine. We have synthesized ~25 urea derivatives by exploiting the common amine intermediate.

Conclusion

With important learning from the crystal structure of amicetin ternary complex, we were able to develop a class of compounds with high nanomolar on–target potency, and good antimycobacterial activity, modest *Gram (+)* activity and more importantly, retained the translational selectivity (SI $_{34\rightarrow580}$) (**CZ–02–107, 117, 118, 132**). Efforts are being continued to alter the physiochemical properties for improved potency to progress this class of compounds as selective antitubercular compounds.

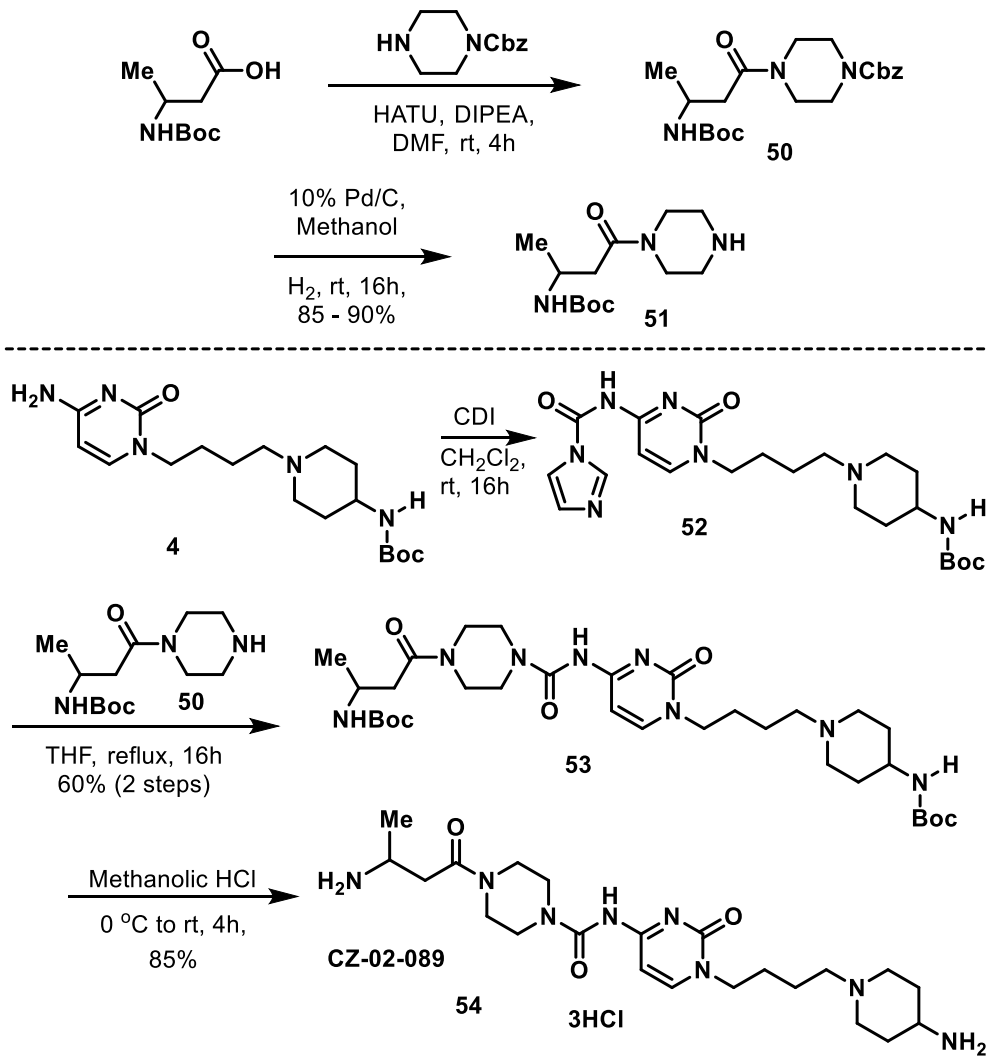

Scheme 4.1 Synthesis of CZ–02–089

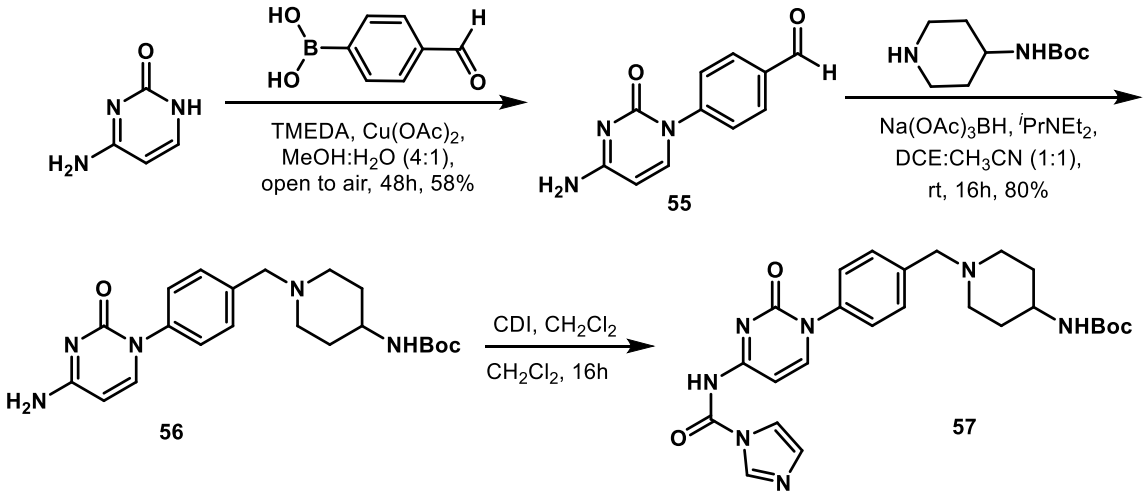

Scheme 4.2 Synthesis of *N1*–aryl cytosine imidazole carboxamide

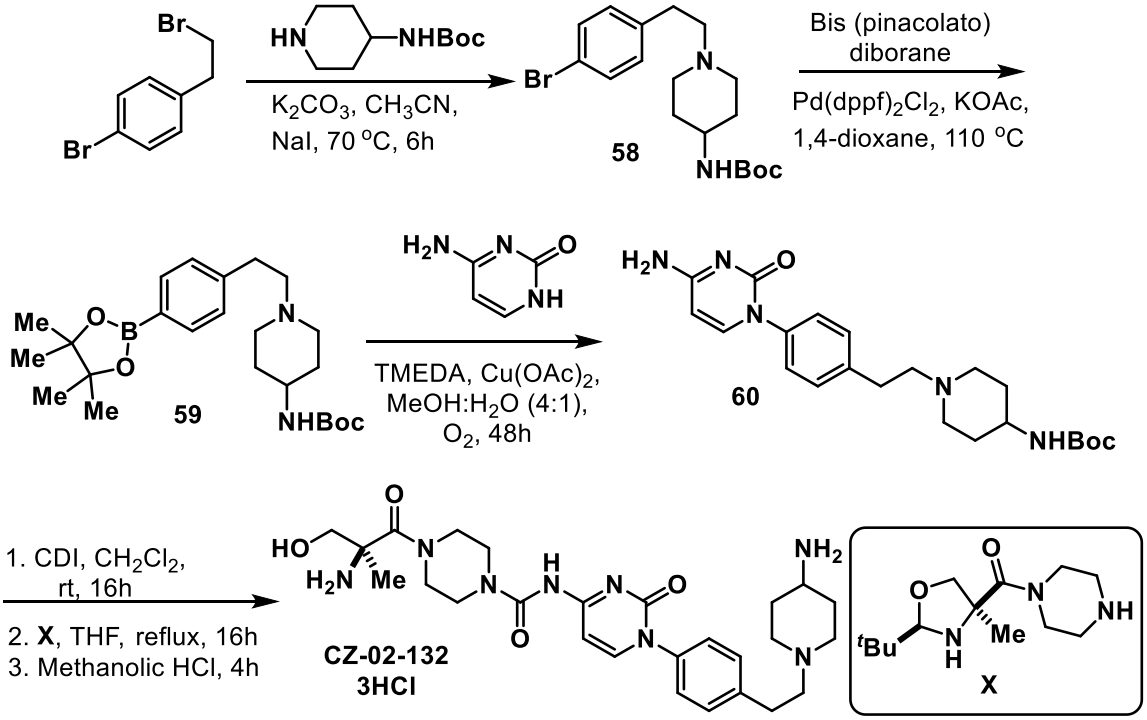

Scheme 4.3 Synthesis of CZ–02–132

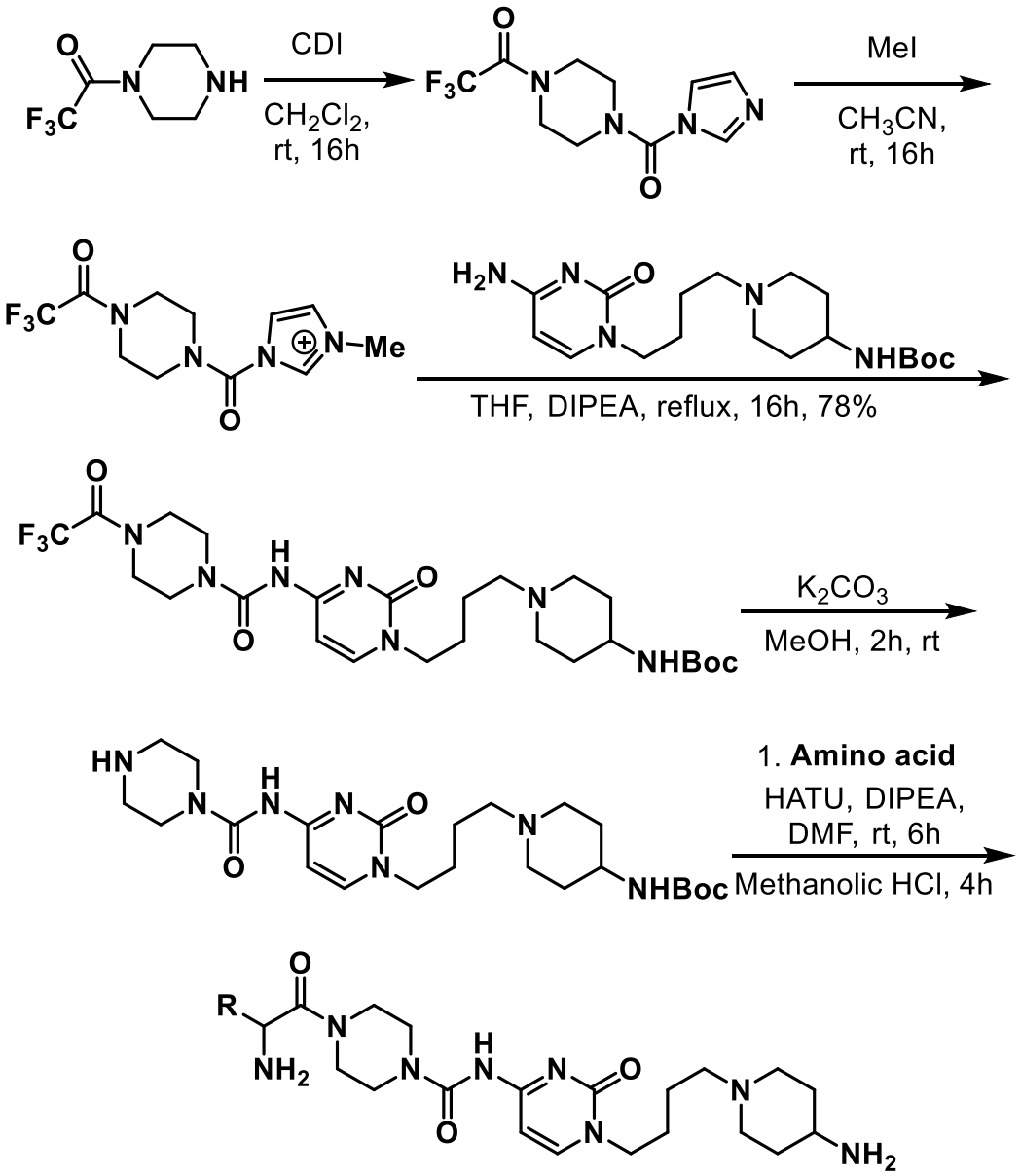

Scheme 4.4 Unified approach to synthesis of Urea derivatives

Table 4.1 Evaluation of piperazinyl ureas in translational inhibition

Compound	*E. coli* S30 IC_{50} (μM)	*R. retic* IC_{50} (μM)	SI *RR/E. coli*
CZ-02-089	0.841 ± 0.200	32.16 ± 2.86	38
CZ-02-090	1.295 ± 0.092	44.02 ± 1.79	34
CZ-02-091	1.223 ± 0.063	44.71 ± 0.56	37
CZ-02-101	1.68 ± 0.24	67.66 ± 8.70	40
CZ-02-103	0.67 ± 0.15	88.6 ± 12.5	132
CZ-02-104	0.35 ± 0.01	25.7 ± 2.0	73
CZ-02-107	0.053 ± 0.011	3.20 ± 0.49	60
CZ-02-117	0.040 ± 0.028	16.22 ± 9.36	406
CZ-02-118	0.165 ± 0.034	16.22 ± 9.36	444
CZ-02-132	0.307 ± 0.02	178.2 ± 30.5	580

Table 4.2 Antimycobacterial activity of piperazinyl ureas

Compound	*M. smegamtis* *MIC* (μg/mL)	*Mtb H37Rv*		
		MIC (μM)	IC_{50} (μM)	IC_{90} (μM)
CZ-02-090	4	4.6	0.94	6.4
CZ-02-091	4	2.2	0.68	2.9
CZ-02-103	2	4.6	1.7	5.4
CZ-02-104	0.5	2.5	0.74	3.2

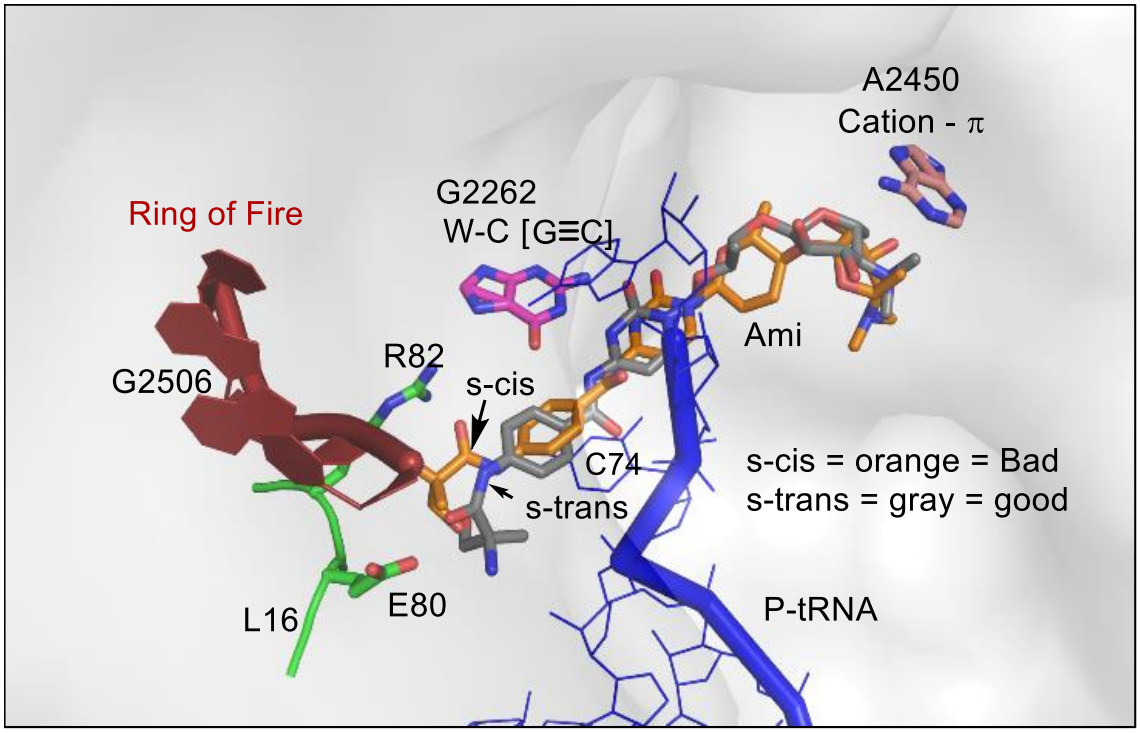

Figure 4.1 Overlay of two conformations of amicetin in Ami–70S–tRNA ternary complex[1–2]

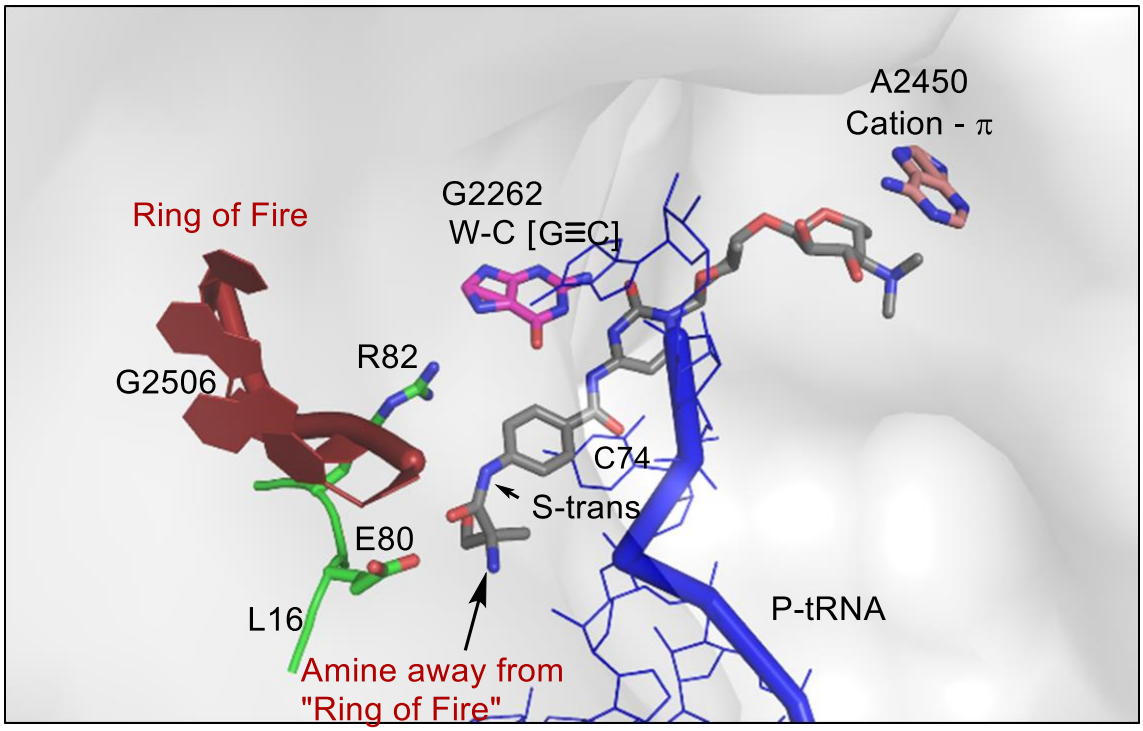

Figure 4.2 *S–trans* amide conformation of amicetin in Ami–70S–tRNA ternary complex[1]

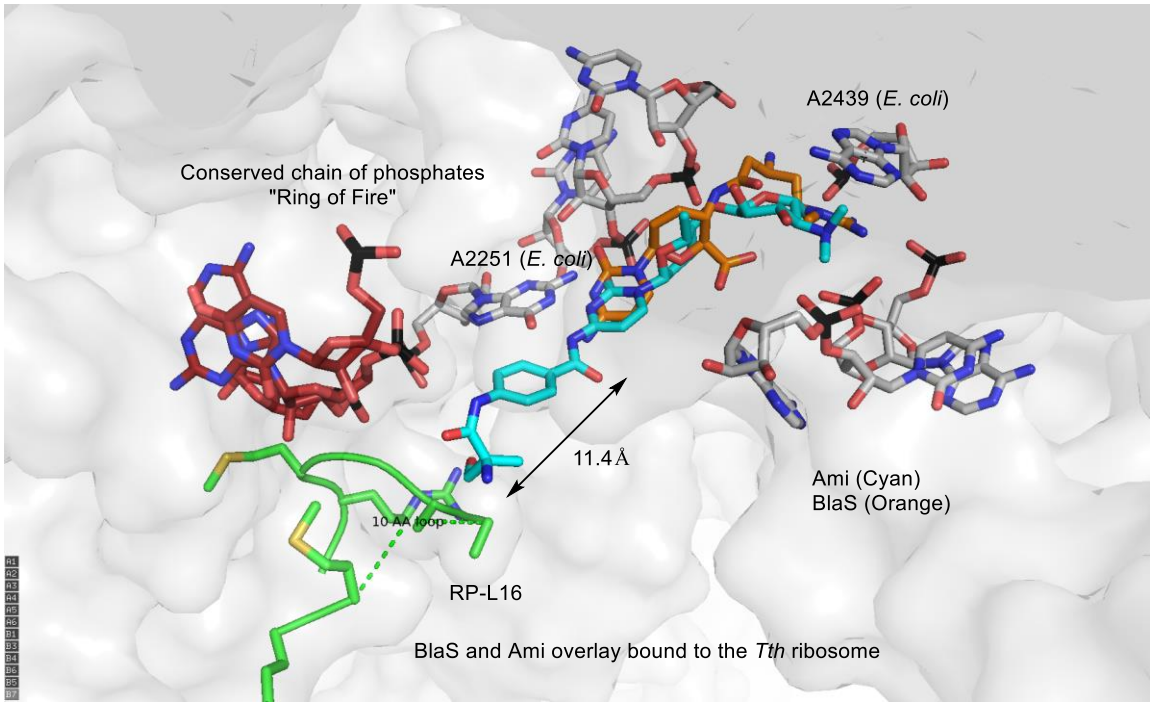

Figure 4.3 Blasticidin S and amicetin overlay in *Tth* 70S ribosome

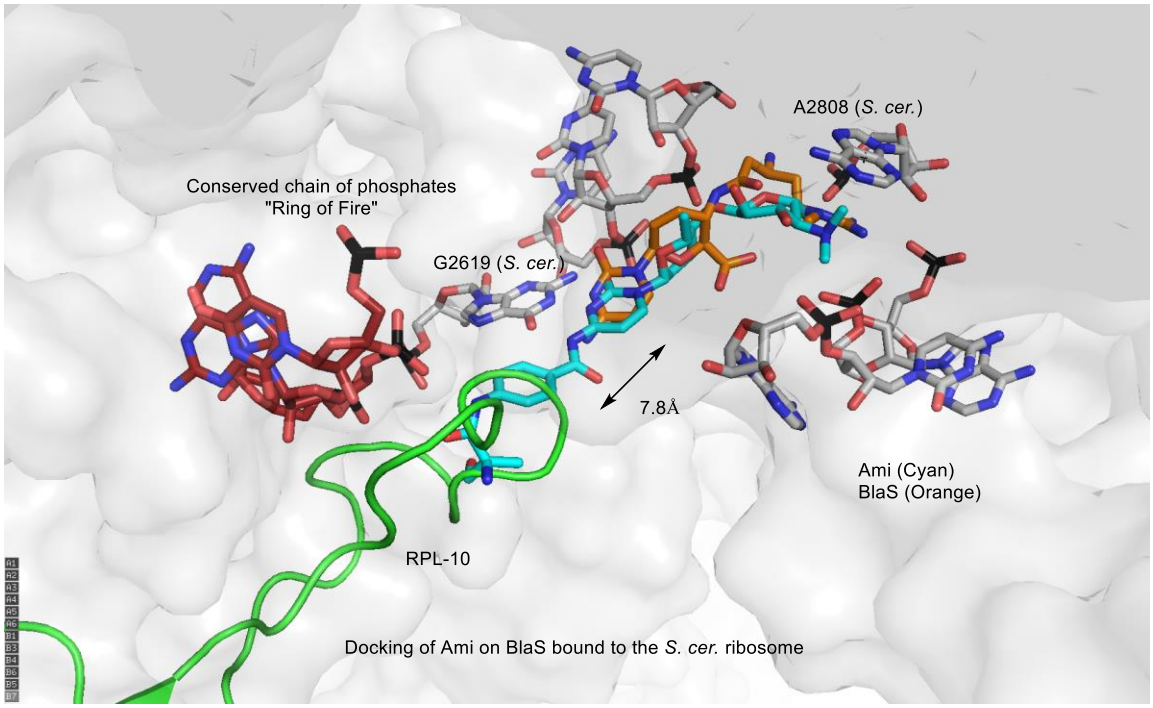

Figure 4.4 Docking of Ami on BlaS bound to the *S. cerevisiae* ribosome

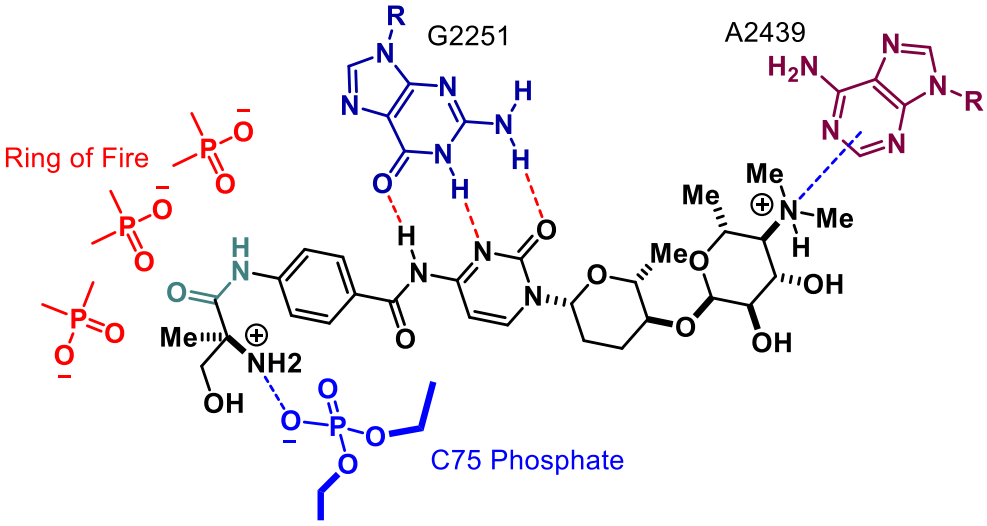

s-trans amide confirmation of Ami in ternary complex (Ami/70S/p-tRNA)

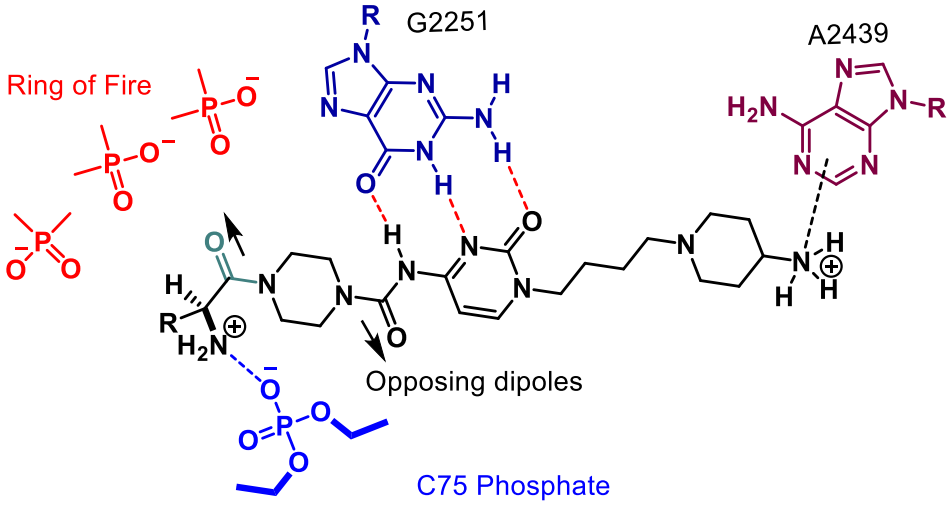

Hypothetical orientation of piperizinyl ureas (anti-conformation of carbonyls).

Figure 4.5 Hypothesis for retaining selectivity

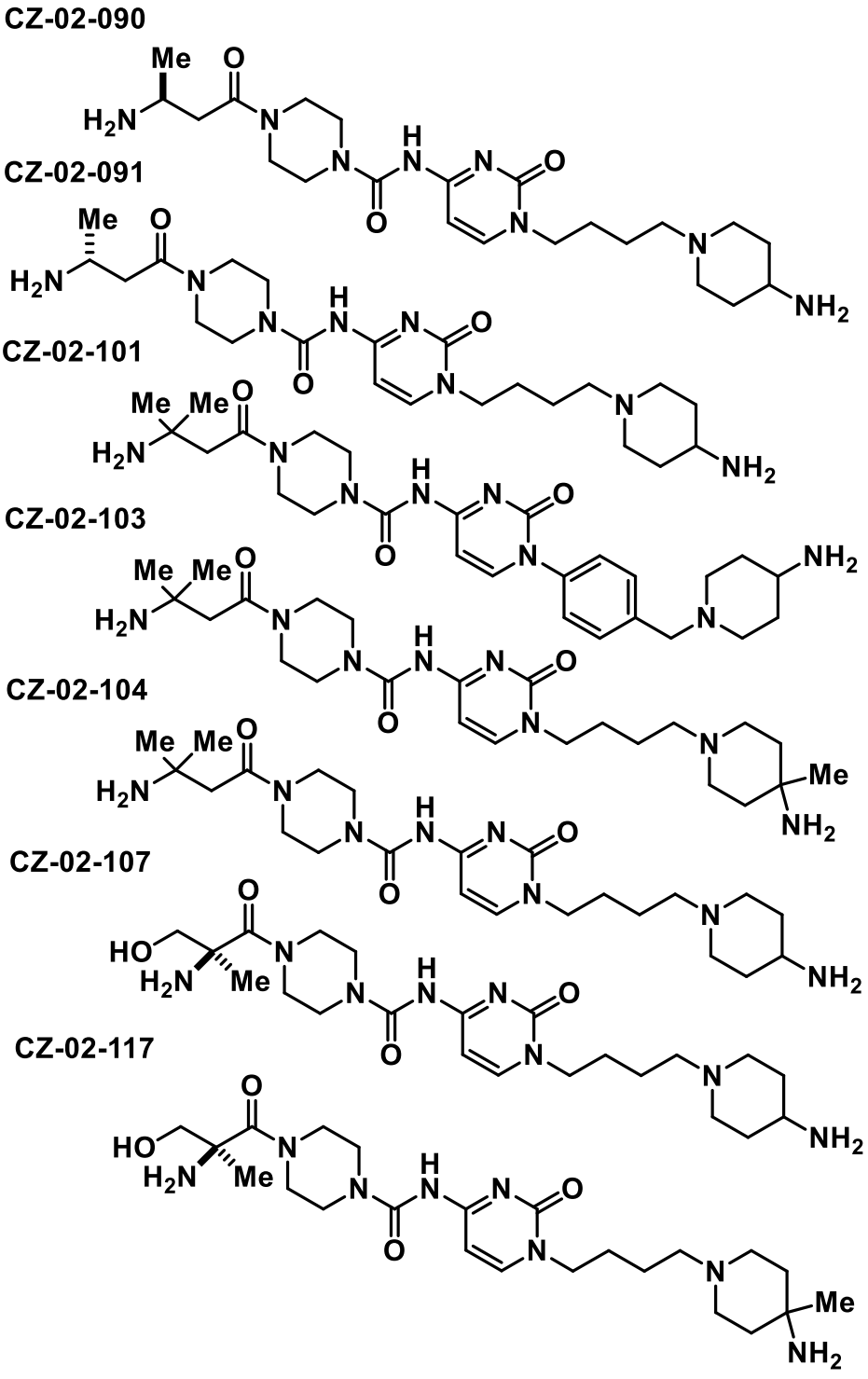

Figure 4.6 Urea derivatives synthesized using a protocol similar to those reported in Scheme 4.1 and Scheme 4.2

References

1) (a) Serrano, C. M. Synthetic and Biological Studies on Amicetin and its Analogues Toward the Development of New Antimycobacterial Agents. Ph. D. Dissertation, University of Utah, Salt Lake City, Utah, 2015. (b) The Looper Group has succeeded in solving the X–ray crystal structures of the natural product amicetin (Ami) (re–expressed, isolated, and purified from the bacteria *Streptomyces vinaceousdrappus* by Dr. Serrano in Looper Lab), in complex with the 70S *Tth* ribosome within 3.5 Å resolution, in collaboration with Dr. Eiler of the Steitz's Lab at Yale University.

2) (a) Svidritskiy, E.; Ling, C.; Ermolenko, D. N.; Korostelev, A. A. BlasticidinS Inhibits Translation by Trapping Deformed tRNA on the Ribosome. *Proc. Natl Acad. Sci*. **2013**, *110*, 12283–12288. (b) Hansen, J. L.; Moore, P. B.; Steitz, T. A. Structures of Five Antibiotics Bound at the Peptidyl Transferase Center of the Large Ribosomal Subunit. *J. Mol. Biol.* **2003**, *330*, 1061–1075.

3) Garreau, N.; Prokhorova, I.; Holtkamp, W.; Rodnina, M. V.; Yusupova, G.; Yusupova, M. Structural Basis for the Inhibition of Eukaryotic Ribosome. *Nature* **2014,** *513*, 517 –522.

4) Lafitte, V. G. H.; Aliev, A. E.; Horton, P. N.; Bursthouse, M. B.; Golding, P.; Hailes, H.C. Quadruply Hydrogen Bonded Cytosine Modules for Supramolecular Applications. *J. Am. Chem. Soc.* **2006**, *128,* 6544–6545.

5) Duffy, E. M.; Bhattacharjee, A. Pyrrolopyrimidinones as Antimicrobial Agents and Methods of Making and Using the Same. WO2012/173689, **2012**.

6) Grzyb, J. A.; Shen, M.; Yoshina–Ishii, C.; Brown, S.; Batey, R. A. Carbamoylimidazolium and Thiocarbamoylimidazolium Salts: Novel Reagents for the Synthesis of Ureas, Thioureas, Carbamates, Thiocarbamates and Amides. *Tetrahedron* **2005**, *61*, 7153–7175.

Supporting Information

General experimental considerations

All reactions requiring anhydrous conditions were conducted in flame–dried glassware under a positive pressure of either nitrogen or argon. Commercially available reagents were used as received; otherwise, materials were purified according to *Purification of Laboratory Chemicals*. Acetonitrile (CH_3CN), *N,N'*–dimethylformamide (DMF), and tetrahydrofuran (THF) were degassed with nitrogen and passed through a solvent purification system (Innovative Technologies Pure Solv). Dry 1,4–dioxane was purchased from Acros Organics in a Acros Seal™ bottle. Microwave reactions were done in CEM Discover System Model 908005.

Melting points were determined using a Mel–Temp® Capillary Melting Point Apparatus. Infrared spectra were obtained using Nicolet 380–FT IR spectrometer fitted with a Smart Orbit sample system. Optical rotations were obtained at ambient temperature on a Perkin Elmer Model 343 polarimeter (Na D line) using a microcell with a 1 decimeter path length. Mass spectra were determined on a Micromass Quattro II (ESI/APCI–TOF) for HRMS at the University of Utah Mass Spectrometry Facility. ^{1}H NMR and ^{13}C NMR spectra were recorded at 300 MHz, 400MHz, 500 MHz and ^{13}C NMR spectra were recorded at 75 MHz, 100 MHz, 125 MHz, respectively. Proton resonances were reported relative to the deuterated solvent peak: 7.26 ppm for $CDCl_3$ and 3.31 ppm (center line signal) for CD_3OD, 4.80 ppm for D_2O using the following format: chemical shift (δ) [multiplicity (s= singlet, bs= broad singlet, d= doublet, dd= doublet of doublet, t= triplet, q= quartet, m=

multiplet), coupling constant(s) *J* in Hz, integration]. Carbon resonances were reported as chemical shifts (δ) in parts per million, relative to the center line signal of the respective solvent peak: 77.23 ppm for $CDCl_3$ and 49.00 ppm for CD_3OD. All the commercially available chemicals are purchased from Sigma–Aldrich, Acros, TCI America, Combi–Blocks, and Chem–Impex.

Experimental procedures

Synthesis of Piperazinyl ureas

Scheme 3

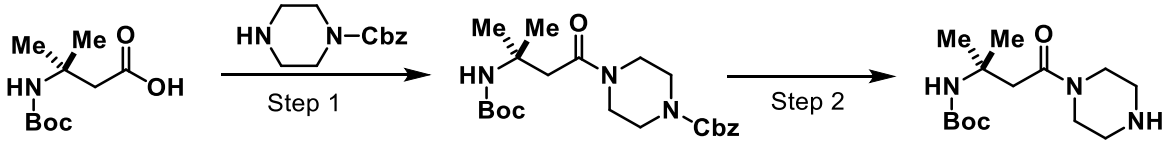

Reagents: Step 1) HATU, DIPEA, DMF, rt, 4h, 2) 10% Pd/C, H2, MeOH, rt, 6h.

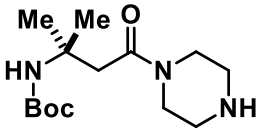

***tert*–Butyl(2–methyl–4–oxo–4–(piperazin–1–yl)butan–2–yl)carbamate**:

Step 1: To a suspension of 3–((*tert*–butoxycarbonyl)amino)–3–methylbutanoic acid (0.96 g, 4.40 mmol) and HATU (2.01g, 5.30 mmol) in dry CH_2Cl_2 (20mL), *N*,*N*–diisopropylethylamine (0.92 ml, 5.30 mmol) was added at room temperature. The suspension was stirred for 10 min. A solution of benzyl piperazine–1–carboxylate (0.97 g, 4.40 mmol) in CH_2Cl_2 (1.5 ml) was added. The solution was stirred at room temperature for 16h and the solvent evaporated under reduced pressure. Water was added to the reaction vessel and the resulting solid was collected by filtration. Purification via flash chromatography yielded benzyl 4–(3–((*tert*–butoxycarbonyl) amino)–3–methylbutanoyl)piperazine–1–carboxylate (1.4 grams, 76%) as a sticky, colorless solid.

Step 2: To a round bottom flask containing benzyl 4–(3–((*tert*–butoxycarbonyl)amino)–3–methylbutanoyl)piperazine–1–carboxylate (1.40 g, 3.33 mmol) and 10% Pd/C (140 mg, 1.3 mmol), was added MeOH (15 mL) and the suspension stirred at room temperature for 12 hrs under an atmosphere of hydrogen. The reaction mixture was filtered through a bed of celite, and the filtrate was concentrated under reduced pressure to afford *tert*–butyl (2–methyl–4–oxo–4–(piperazin–1–yl)butan–2–yl)carbamate (0.795 g, 97%) as a sticky yellow solid.

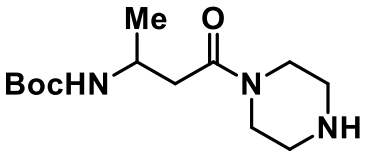

***tert*–Butyl (4–oxo–4–(piperazin–1–yl)butan–2–yl)carbamate:** Prepared as in scheme 1 from 3–Boc–amino butanoic acid (0.50 g, 2.49 mmol) and 1–Cbz–piperazine (0.55 g, 2.49 mmol) to afford the desired product as a tan solid (0.42 g, 62%). ^{1}H NMR (500 MHz, $CDCl_3$): δ 4.94 (br s, 1H), 4.05 (br s, 1H), 2.56 (s, 2H), 1.45 (s, 9H), 1.25 (m, 3H).

Synthesis of CZ–02–104

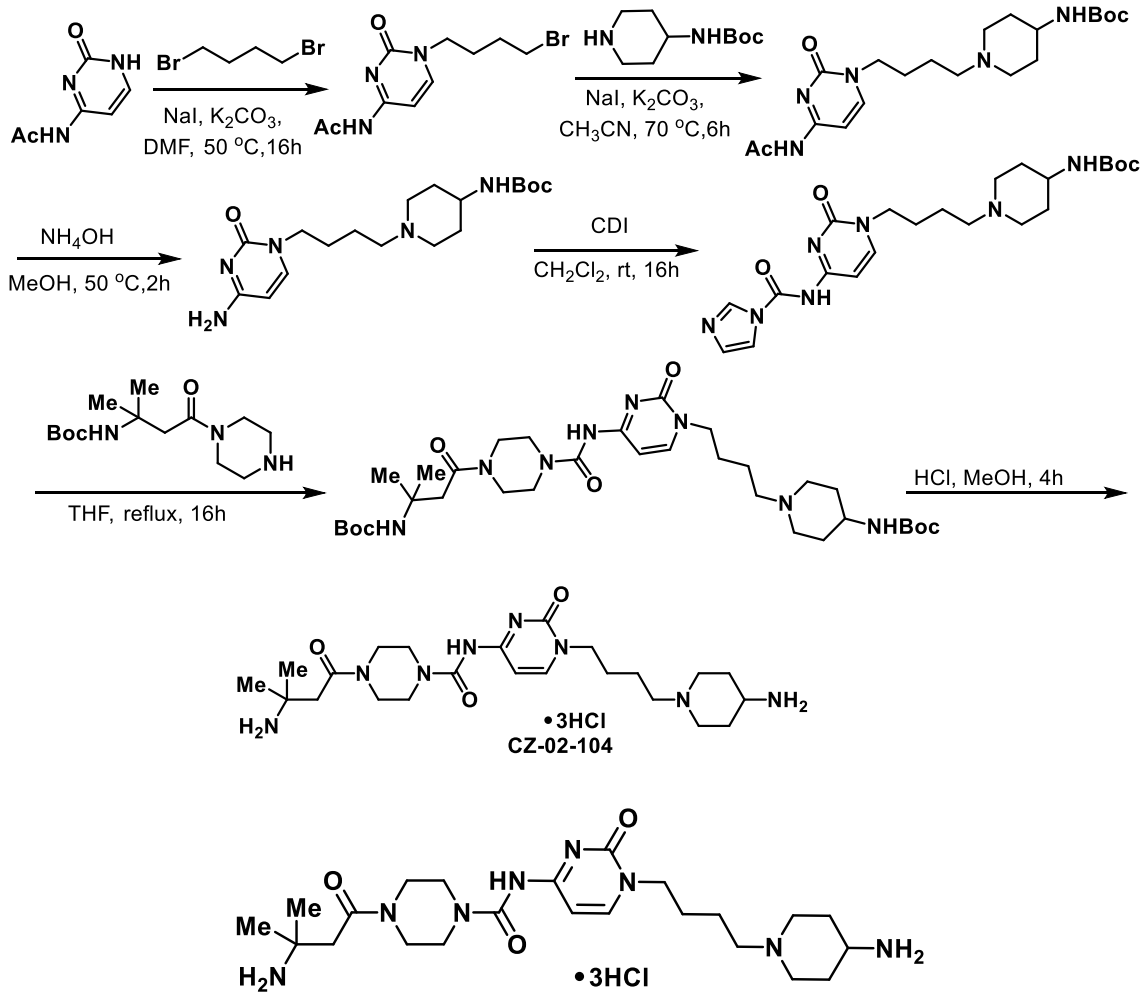

Example 1 CZ–02–104: 4–(3–Amino–3–methylbutanoyl)–*N*–(1–(4–(4–aminopiperidin–1–yl)butyl)–2–oxo–1,2–dihydropyrimidin–4–yl)piperazine–1–carboxamide trihydrochloride salt: Step 1: To a preheated suspension at 50 °C under a nitrogen atmosphere of *N*–(2–oxo–1,2–dihydropyrimidin–4–yl)acetamide (10.0 g, 65.3 mmol), sodium iodide (9.79 g, 65.3 mmol) and potassium carbonate (13.5 g, 98.0 mmol) in dry DMF (150 mL) was added 1,4–dibromobutane (17.0 g, 98.0 mmol). After 16h, the reaction mixture was cooled and filtered. The solvent was removed under reduced pressure and heat (≤55 °C).

Purification via flash chromatography (0–2% MeOH/$CHCl_3$) afforded *N*–(1–(bromomethyl)–2–oxo–1,2–dihydropyrimidin–4–yl)acetamide (7.40 g, 46%) as a colorless solid. ^{1}H NMR (500 MHz, $CDCl_3$): δ 10.50 (s, 1H), 7.60 (d, 1H), 7.42 (d, 1H), 3.90 (q, 2H), 3.18 (t, 2H), 2.29 (s, 3H), 1.89 (t, 2H), 1.85 (t, 2H).

Step 2: A mixture of *N*–(1–(bromomethyl)–2–oxo–1,2–dihydropyrimidin–4–yl)acetamide (4.00 g, 13.9 mmol), 4–(*N*–Boc–amino)piperidine (2.75 g, 13.9 mmol) and potassium carbonate (2.85 g, 20.9 mmol) was suspended in dry CH_3CN (100 mL) at 70 °C under a nitrogen atmosphere. The reaction was stirred 4h before cooling, filtered and washed with chloroform (3 X 15 mL). The filtrate was concentrated under reduced pressure to yield *tert*–butyl (1–(4–(4–acetamido–2–oxopyrimidin–1(2H)–yl)butyl)piperidin–4–yl)carbamate (5.28 g, 93%) as a colorless solid. ^{1}H NMR (400 MHz, $CDCl_3$): δ 9.56 (br s, 1H), 7.64 (d, 1H), 7.39 (d, 1H), 4.51 (s, 1H), 3.89 (t, 2H), 2.92 (s, 2H), 2.46 (m, 2H), 2.29 (s, 3H), 2.17 (m, 2H), 2.96 (d, 2H), 1.78 (m, 2H), 1.57 (m, 2H), 1.44 (s, 12H).

Step 3: *tert*–Butyl(1–(4–(4–acetamido–2–oxopyrimidin–1(2H)–yl)butyl)pip–eridin–4–yl)carbamate (5.26 g, 14.4 mmol) was dissolved in MeOH (100 mL) and ammonium hydroxide (10 mL) was added. The vessel was placed in a preheated oil bath at 50 °C and stirred for 2h. After cooling, the solution was evaporated to dryness under reduced pressure. It was recrystallized from ethanol to yield *tert*–butyl (1–((4–amino–2–oxopyrimidin–1(2H)–yl)methyl)piperidin–4–yl)carbamate (3.26 g, 70%) as a colorless solid.

Step 4: To a 100 mL round bottom flask containing *tert*–butyl (1–((4–amino–2–oxopyrimidin–1(2H)–yl)methyl)piperidin–4–yl)carbamate (0.35 g, 0.82 mmol)

and CDI (0.20 g, 0.84mmol) was added dry CH_2Cl_2 (30 mL) and the mixture was stirred for 16h under a nitrogen atmosphere. The solvent was evaporated under reduced pressure and tert–butyl (1–((4–(1H–imidazole–1–carboxamido)–2–oxopyrimidin–1(2H)–yl)methyl)piperidin–4–yl)carbamate was collected as a colorless solid.

Step 5: To a round bottom flask containing *tert*–butyl (1–((4–(1H–imidazole–1–carboxamido)–2–oxopyrimidin–1(2H)–yl)methyl)piperidin–4–yl)carbamate (0.24 g, 0.48 mmol) and *tert*–butyl (2–methyl–4–oxo–4–(piperazin–1–yl)butan–2–yl)carbamate (0.13 g, 0.48 mmol), was added. dry THF (10 mL). The reaction mixture was heated to reflux and stirred for 16h. The solvent was evaporated under reduced pressure. The residue was dissolved in EtOAc and partitioned between water. The organic layer was washed with water (3X 10 mL), and brine. The organic layer was dried over Na_2SO_4, filtered and concentrated under reduced pressure. Purification via flash chromatography yielded the *tert*–butyl(1–((4–(4–(3–((tert–butoxycarbonyl)amino)butanoyl)piperazine–1–carbox–amido)–2–oxopyrimidin–1(2H)–yl)methyl)piperidin–4–yl)carbamate as a light brown solid.

Step 6: *tert*–Butyl (1–((4–(4–(3–((tert–butoxycarbonyl)amino)butanoyl) piperazine–1–carboxamido)–2–oxopyrimidin–1(2H)–yl)methyl)piperidin–4–yl) carbamate (0.10 g, 0.16 mmol) was dissolved in a solution of methanolic HCl (10 mL, 2 M). The reaction mixture was stirred for 4h. The solvent was removed under reduced pressure. The resultant solid was triturated with diethyl ether and dried under high vacuum to afford 4–(3–aminobutanoyl)–*N*–(1–(4–(4–aminopiperidin–

1–yl)butyl)–2–oxo–1,2–dihydropyrimidin–4–yl)piperazine–1–carboxamide as a color less solid. (67 mg, 90%).

CZ–02–104: ^{1}H NMR (500 MHz, CD_3OD): δ 8.50 (br s, 1H), 6.80 (br s, 1H), 4.08 (s, 2H), 3.98-3.43 (m, 11H), 3.42-3.12 (m, 4H), 2.86 (br s, 2H), 2.31 (br s, 2H), 2.10 (br s, 2H), 1.91 (br s, 4H), 1.45 (s, 6H). ^{13}C NMR (125 MHz, CD_3OD): δ 169.5, 159.8, 153.8, 152.6, 119.2, 94.7, 56.2, 52.5, 49.9, 45.6, 44.8, 40.8, 39.4, 27.2, 25.4, 25.0, 20.9. LC–MS [M+H] 477.3

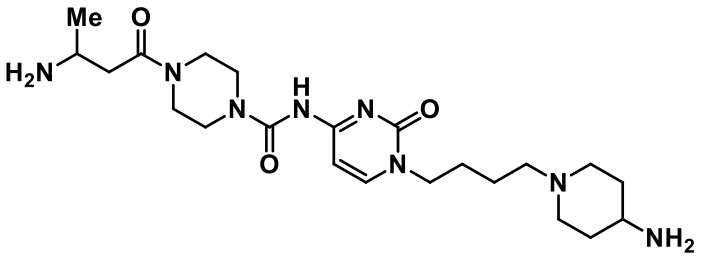

CZ–02–089: ^{1}H NMR (500 MHz, D_2O): δ 8.08 (d, 1H), 6.52 (s, 1H), 3.84 (s, 2H), 3.73–3.47 (m, 10H), 3.20–3.02 (m, 4H), 2.81–2.72 (m, 1H), 2.68–2.57 (m, 1H), 2.04–1.91 (m, 4H), 1.66 (br s, 4H), 1.38 (s, 2H), 1.19 (s, 3H). ^{13}C NMR (125 MHz, D_2O): δ 170.1, 159.4, 152.9, 152.5, 148.9, 95.6, 57.0, 51.6, 51.0, 46.2, 45.5, 45.2, 41.8, 37.0, 28.0, 25.8, 21.5, 18.6. LC–MS [M+H] 463.4.

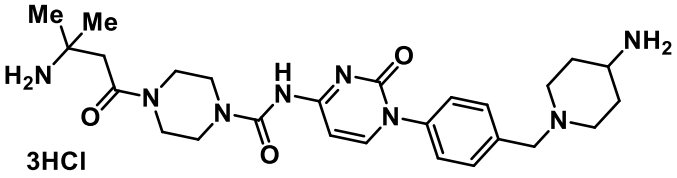

CZ–02–101: ^{1}H NMR (500 MHz, D_2O) δ 8.05 (d, *J* = 7.5 Hz, 1H), 7.55 (d, *J* = 8.0 Hz, 2H), 7.44 (d, *J* = 8.0 Hz, 2H), 7.66 (d, *J* = 7.5 Hz, 1H), 4.28 (s, 2H), 3.56–3.50 (m, 10H), 3.40 (t, *J* = 10.0 Hz, 1H), 3.06 (t, *J* = 13.0 Hz, 2H), 2.70 (s, 2H), 2.16 (d, *J* = 13.0 Hz, 2H), 1.81–1.72 (m, 5H), 1.72 (s, 3H). ^{13}C NMR (100 MHz,

D_2O) δ 170.4, 160.6, 153.3, 151.2, 138.9, 132.6, 130.0, 127.0, 126.9, 96.5, 59.3, 52.5, 50.1, 45.1, 44.4, 40.7, 39.2, 26.7, 24.9. LC–MS [M+H] 511.3

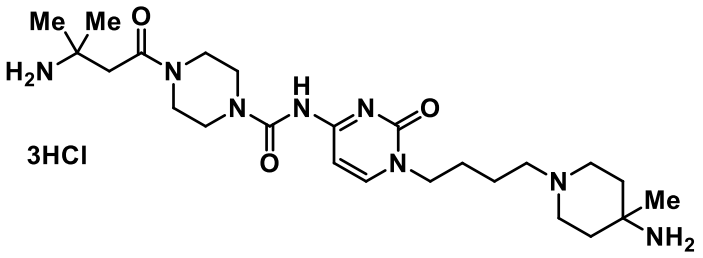

CZ–02–103: ^{1}H NMR (500 MHz, CD_3OD): δ 8.35 (s, 1H), 7.78 (br s, 2H), 7.59 (br s, 2H), 6.79 (s, 1H), 4.44-4.41 (m, 2H), 3.76–3.57 (m, 7H), 3.42 (d, 2H), 3.20 (s, 2H), 2.75 (s, 2H), 2.24–1.95 (m, 4H), 1.49 (s, 2H), 1.34 (s, 8H). ^{13}C NMR (125 MHz, CD_3OD): δ 169.5, 159.7, 153.6, 152.6, 146.6, 94.6, 69.9, 55.8, 52.6, 50.5, 49.8, 44.5, 40.6, 39.3, 32.2, 25.2, 25.0, 20.8, 19.6. LC–MS [M+H] 491.3.

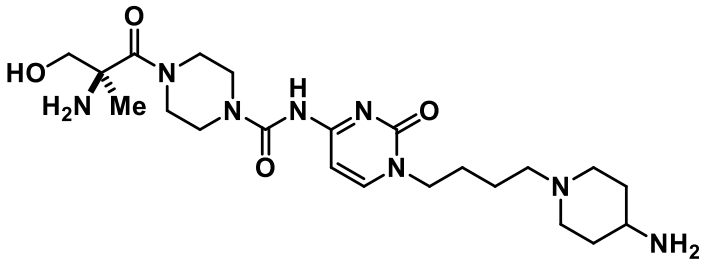

CZ–02–107: ^{1}H NMR (500 MHz, D_2O): δ 8.06 (d, *J* = 7.5 Hz, 1H), 6.50 (br s, 1H), 4.78 (s, 2H), 3.85 (br s, 2H), 3.72 (d, *J* = 13.0 Hz, 1H), 3.63–3.53 (m, 10H), 3.45–3.37 (m, 1H), 3.05 (br s, 2H), 2.97 (t, *J* = 13.0 Hz, 1H), 2.18 (d, *J* = 13.0 Hz, 1H), 1.83–1.65 (m, 2H), 1.67 (br s, 4H), 1.51 (s, 3H). ^{13}C NMR (125 MHz, CD_3OD): δ 169.2, 161.1, 155.7, 153.8, 147.7, 95.8, 65.3, 64.6, 57.5, 52.1, 51.4, 50.0, 47.0, 28.7, 25.0, 22.3, 19.0. LC–MS [M+H] 479.4

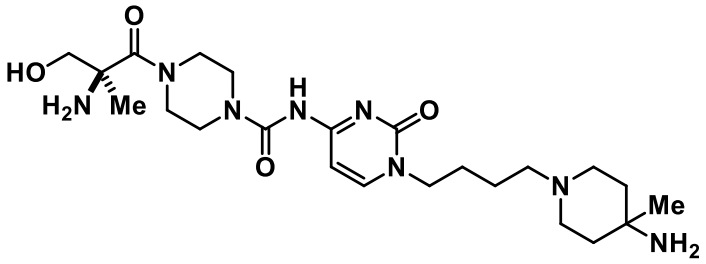

CZ–02–117: ^{1}H NMR (500 MHz, CD_3OD): δ 7.73 (d, *J* = 7.5 Hz, 1H), 6.58 (d, *J* = 7.5 Hz, 1H), 3.91 (br s, 2H), 3.86–3.82 (m, 4H), 3.76 (d, *J* = 11.0 Hz, 1H), 3.64 (br s, 4H), 3.47 (d, *J* = 11.0 Hz, 1H), 2.53 (br s, 2H), 2.44–2.39 (m, 4H), 1.74–1.68 (m, 2H), 1.61–1.54 (m, 6H), 1.33 (s, 3H), 1.14 (s, 3H). ^{13}C NMR (125 MHz, CD_3OD): δ 176.1, 163.0, 159.6, 155.3, 148.0, 99.9, 71.1, 60.8, 59.1, 50.9, 50.7, 50.0, 48.5, 46.2, 45.3, 39.7, 28.2, 24.7, 23.2. LC–MS [M+H] 493.3

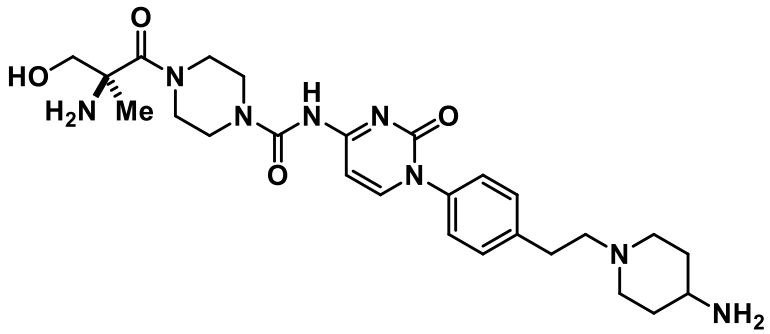

CZ–02–132: ^{1}H NMR (500 MHz, CD_3OD): δ 7.70 (d, *J* = 8.0 Hz, 1H), 7.37 (d, *J* = 8.5 Hz, 2H), 7.34 (d, *J* = 8.5 Hz, 2H), 6.64 (br s, 1H), 3.91 (br s, 2H), 3.89–3.82 (m, 4H), 3.79 (d, *J* = 11.5 Hz, 1H), 3.70–3.64 (m, 4H), 3.50 (d, *J* = 11.5 Hz, 1H), 3.07 (d, *J* = 11.5 Hz, 2H), 2.98–2.93 (m, 1H), 2.89 (t, *J* = 11.5 Hz, 2H), 2.22–2.14 (m, 2H), 1.96 (d, *J* = 11.5 Hz, 2H), 1.62–1.54 (m, 2H), 1.36 (s, 3H), 1.14 (s, 3H). ^{13}C NMR (125 MHz, CD_3OD): δ 175.6, 162.8, 160.1, 154.5, 147.6, 142.5, 139.2, 130.9, 127.7, 100.5, 706, 61.1, 61.0, 53.0, 49.7, 46.2, 45.3, 33.9, 32.8, 30.9, 22.9. LC–MS [M+H] 527.3.

CHAPTER 5

ANTIBIOFILM ANTIMICROBIAL AGENTS

Planktonic Bacteria vs Biofilm

The surface attached aggregate of lively reproducing bacteria encased in a self–produced matrix is referred to as a biofilm, whereas the isolated free–floating bacteria are referred to as planktonic bacteria. The adherent bacteria defend themselves from external threats by constructing an impermeable slimy layer called extracellular polymeric substance (EPS) consisting of their extracellular DNA/RNA, proteins, and polysaccharides around them. The EPS layer anchors, harbors, and shields the bacterial communities and renders bacterial resistance (Figure 5.1).[1]

Phases of Biofilm Life Cycle Attachment

The life cycle of planktonic bacteria's transition into a biofilm phenotype begins with its attachment to a surface via reversible weak Van der Waals forces. This initial attachment stage of life cycle is aided by the slimy material produced and excreted by the bacteria itself. According to J. W. Costerton et al., "Thus, it appears that attachment itself can initiate the synthesis of the extracellular matrix in which the sessile bacteria (biofilm) are embedded."[1] If the pioneer bacteria succeed in initial attachment, then they attach irreversibly using anchor molecules

such as protein surfaces and pili. The anchored bacteria enable the adhesion of other bacteria by providing additional attachment sites (Figure 5.2).[2]

Development of mature biofilm

In the development step, the bacteria adopt two different ways to colonize: a) by bacterial cell division, b) by recruiting other bacteria and starting to produce EPS to embrace the growing biofilm. Throughout the creation of biofilm, the microbes bounded inside the EPS matrix can connect and talk to each other largely through a communication process called “quorum sensing.” Quorum sensing mainly serves as communication network both within single bacterial species and also between distinct bacterial species. A common phenomenon, where typically two different species of bacteria coalesce and live together as one entity, called “mixed–species” biofilms are seen in the lungs of patients with cystic fibrosis (CF) as well as in dental cavities (Figure 5.2). [3]

Another interesting aspect of a matured biofilm is that it is often equipped with water/nutrient channels for nutrient circulation to cells in different regions of biofilm. The bacteria living in deeper regions of biofilm often suffer from oxygen gradient and adapt to live a life of anaerobic bacteria. The biofilm lifestyle of planktonic bacteria helps to evolve and adapt the extreme environmental conditions such as nutrient gradient, pH, oxygen, temperature, and salinity gradient (Figure 5.2).[4]

Disintegration of saturated biofilm

The critical phase of the biofilm life cycle is the spread and dispersal. Once biofilm matures and reaches saturation in density, the planktonic bacteria are forced to come out of EPS periodically, in search of required nutrients. J.W. Costerton refers to this process as “natural pattern of programmed detachment.” The bacteria that come out of biofilms can swiftly multiply, disperse, and invade a new surface and repeat the process of biofilm formation (Figure 5.2).[1, 4, 5]

Biofilm and its Implications in Chronic Infections and Biofouling

Planktonic bacteria are responsible for a majority of acute infections, whereas chronic infections are the consequences of biofilms.[2, 6] The chronic infections caused by biofilm phenotype are tough to treat. Depending on the type of bacteria, the biofilm phenotype can be >10 to 1000-times resistant to trivial antimicrobial agents compared to planktonic bacteria of a similar kind. The EPS around bacterial communities help biofilm to combat innate immune responses of the host system, and also enable resilience to environmental dangers which include chemical attack (conventional antibiotics), thereby causing persistent infections. Also, the proximity of bacteria in biofilms facilitates gene exchange which ultimately leads to mutations and results in the transfer of acquired antibiotic resistance.[1, 7]

The biofilm phenotype is omnipresent and implicated in a number of illnesses such as diabetic foot ulcers, dental plaque, chronic sinusitis, osteomyelitis, chronic prostatitis, Lyme disease, tuberculosis, endocarditis, cystic

fibrosis, and medical devices and implants.[8, 9] The consequences of biofouling, unwanted deposits of biotic substances on surface implants, are also seen in industry settings such as degradation of oil pipes, contamination of drinking water, food processing industry, ship hulls, damaging of the heat exchanging equipment, dairy industry, cooling water plants, and the paper industry. The wet surfaces and nutrient–rich resources in the aforementioned industrial settings promote the formation and fast growth of biofilm.[10, 11, 12] The detrimental biofouling consequences are enormous and cause an estimated financial burden of US$ 200 billion per year to the US alone. Biofilms are responsible for two million chronic infections annually across the globe and result in an estimated health care cost of US $11 billion.[13]

Treatment

Traditional antibiotics are effective in treating acute infections caused by planktonic bacteria. As is evident that the biofilm phenotype is the most preferred mode of living by most bacteria, biofilms are commonly seen in a vast number of clinical settings. For many years, the perception of diagnosis and treatment of biofilm–related infections were done in the wrong way. Clinicians have tried to treat biofilm–related infection by prescribing regular high doses of antibiotics. Unfortunately, the high doses of administered antibiotics were successful in weakening the biofilm temporarily but failed to destroy the biofilm permanently. As a result, some survival bacteria called “persister cells” are capable of regenerating biofilm by efficiently transferring the acquired resistance to other bacteria.[19] The regenerated biofilm is usually antibiotic resistant and is a difficult to impossible

biofilm to destroy. Till today, there are no known clinical antibiotics developed specifically for biofilms, whereas the use of chemical bactericidal agents for treating biofouling in industry settings are bleach and glutaraldehyde, which can kill the bacteria but fail to disrupt the biofilm. [18] The undispersed EPS material will act as the nutrient rich source for the development of new bacterial colonies (biofilm). [14]

Given the implications of biofilm phenotype of different bacteria in industry and healthcare, there is a pressing need to develop new chemical entities (NCE) targeting different phases of biofilm life cycle, like compounds focused on inhibition or dispersion of biofilm formation or disrupting the biofilm and killing the bacteria residing in the biofilm.[14, 15, 16]

Targeting the biofilm phenotype

In vitro studies have demonstrated that it is very easy to treat young biofilms using existing regular antibiotic regimen in contrast with matured biofilm.[17] Therefore, early diagnosis and an aggressive antibiotic prescription are preferred to treat biofilm infections. However, early diagnosis of biofilms is a challenging task, as most of the chronic infections are rooted to a matured biofilm phenotype, which is difficult to treat with existing antibiotics. The two popular, viable targets for the control of biofilm infections are: A) the EPS consisting of poly–anionic polysaccharide alignment; B) The other being “quorum sensing” used by bacteria in biofilms to communicate with each other.[18, 19]

Very little is known and pursued in the field of developing antibiofilm antibiotics. Significant contributions come from Losick, Clardy and coworkers. In

their pivotal studies, they showed that the biogenetic polyamines such as spermidine, and norspermidine are capable of inhibiting biofilm formation. These polyamines are produced at high concentrations (50–80 μM) inside matured biofilms, in response to nutrient gradient and toxic waste accumulation and results in biofilm dispersal. Norspermidine is a better natural inhibitor of biofilm formation with MBIC= ~25 μM (minimum biofilm inhibitory concentration) compared to spermidine MBIC= ~1 mM. In addition, subtle changes in the structure of polyamines (additional methylene unit in spermidine compared to norspermidine) can have a radical impact on activity in biofilm regulation. Further, they have also shown that the addition of exogenous norspermidine has resulted in inhibition of biofilm formation in different bacterial species (*B. subtilis*, *E. coli*, and *S. aureus*). More importantly, this activity difference prompted the possibility of polyamine's role in biofilm functioning. However, the findings from Losick, Clardy et al. are in complete contradiction to the initial reports of Watnick and co–workers, on the role of polyamines in quorum sensing and biofilm physiology.[20, 21, 22] Key findings from their study on *Vibrio Cholera* reveals that protein *NspS*, a polyamine sensor, regulates the biofilm functioning in *V. Cholera* by sensing the presence of norspermidine in particular. Based on their reports norspermidine promotes biofilm formation at lower concentration (10 μM) than spermidine (1mM). [23]

While the role of polyamines in formation or disintegration of the biofilms remain ambiguous, identification of potent antimicrobial agents possessing polyamine motifs in their structures (e.g., squalamine and spermine–squalamine as shown in Figure 5.3) prompted us to develop polyamine containing small

molecules focused on biofilm control.[20, 21, 22] Inspirations for our rational design of polyamine antibiotics stems from structural observations of polyamine frameworks in broad spectrum antimicrobials cationic antimicrobial peptides (AMPs such as meganin, pexiganin, and polymixin B), the ceragenins (cationic steroidal antibiotics such as CSA–13). However, the *in vivo* applications of these small molecules are limited due to their hemolytic properties and cytotoxicity (lack of selectivity for mammalian cell membranes over bacterial cell membranes).[24, 25.]

Design and Synthesis of First Generation Antibiofilm Antibiotics

Acknowledging the significance of polyamines (hydrophilic) attached to a hydrophobic backbone, the Looper group designed and developed compounds by merging these two characteristics. Our hypothesis in the rational design of polyamine containing hydrophobic frameworks attributes to combine the 2–fold "kill" and the "dispersal" properties in a single entity to eradicate biofilms completely. The initial set of compounds has polyamines (charged termini) attached to an aryl (phenyl) hydrophobic backbone. Interesting conclusions can be drawn from the SAR studies carried out on monoaryl polyamine derivatives. Compounds containing a tri–amine separated by three carbons as in norspermidine as a cationic tail are more active than others. *In vitro* activity of some of these compounds against MRSA (methicillin–resistant staphylococcus aureus) is shown in Figure 5.5. The compound **CZ–01–052** (MIC = 4.5 μg/mL) with three norspermidine chains attached off of the benzene ring at 1, 3, 5 positions is more potent than **CZ–01–025** (MIC = 20 μg/mL) with two norspermidine linkers at 1, 3

positions, which in turn is more active than **CZ–01–007** (MIC = >800 μg/mL) consisting of just one norspermidine moiety.[26]

The compounds in the first generation were synthesized using commercially available aldehydes, such as benzaldehyde, substituted benzaldehyde, isopthaladehyde, and benzene–1,3,5–tricarboxaldehyde. Further SAR on the monophenyl backbone is limited by the availability of feed stock chemicals. In future endeavors, we sought to access diversified hydrophobic backbones through chemical synthesis and work out an SAR with identified potent polyamine norspermidine and *N*–alkyl–norspermidine.

Design and Synthesis of Second Generation Antibiofilm Antibiotics

Although**,** the first generation analogs are simple in structure, easy to prepare, and cost effective, the biological activity profile was modest. Further modifications are required to develop these compounds as potent antibiofilm antibiotics. The synthetic procedures involved in first generation analogs preparation lack diversity. To explore further SAR possibilities, we needed a synthetic handle for diversification. In the design of second generation analogs, we intend to maintain the optimal ratio of hydrophilic and hydrophobic properties (charge to grease ratio) in our compounds. To access branched aldehydes, we plan to deploy a Suzuki–Miyaura cross–coupling reaction of 5–bromoisopthaladehyde and a variety of commercially available boronic acids.

We began our efforts to synthesize branched aldehydes by synthesizing 5–bromo–isophthalaldehyde from commercially available isopthalaldehyde **1** using a

reported protocol in the literature.[26] Aromatic *m*–bromination of isopthalaldehyde using Sulfuric acid and NBS resulted in 5–bromo–isophthalaldehyde **2**. The resultant aryl bromide was reacted with phenyl boronic acid under optimized Suzuki–Miyaura cross–coupling conditions to yield 5–Phenyl–isopthalaldehyde **3**.[27, 28] Subsequently, bi–aryl–bis–aldehyde was reductively aminated using Boc–norspermidine to form an alkylated bi–aryal amine. Further, Boc deprotection using Methanolic HCl affords the final compound **CZ–01–058** as the Hydrochloride salt (Scheme 5.1).

Using the optimized sp^2–sp^2 cross–coupling protocol we were able to synthesize a variety of branched aldehydes as shown in Figure 5.6.

The aldehydes synthesized were further used in reductive amination with Boc–norspermidine and *N*–alkyl norspermidines to result in biaryl polyamines. Deprotection of resultant Boc–protected polyamines yielded series of analogs (Figure 5.7) synthesized using a protocol similar to **CZ–01–058** (Scheme 5.1).

Assessment of potency of CZ–01 series of compounds

The potency against planktonic and bacteria in biofilm phenotype (biofilm killing ability) of CZ–01 series of compounds is evaluated using the following methods:

a) Minimum Inhibitory Concentration **(MIC)** against planktonic bacteria is measured as the concentration of the antimicrobial required to attain a 3-log reduction from 10^5 colonies–forming units (CFU)/mL to 10^2 CFU/mL over a 24–hour period as per the (CLSI) guideline M26A.

b) Minimum Biofilm Eradication Concentration **(MBEC)** against moderate biofilms (10^3–10^5) CFU is measured as the concentration of the antimicrobial required to attain a three log reduction from 10^5 CFU/peg to 10^2 CFU/peg for Gram (-) bacteria or one log reduction from 10^3 CFU/peg to 10^2 CFU/peg for Gram (+) bacteria in an MBEC system developed by Innovotech.

c) Effective Biofilm Eradication Concentration (**EBEC**) against heavy biofilms (10^9 CFU) is measured as the concentration required producing a 7-log reduction in the number of biofilm bacteria, grown on the surface of polycarbonate coupons in a CDC biofilm reactor, in 24h.

The compounds synthesized were screened for antimicrobial activity. As shown in Table 5.1, all these bi–aryl polyamines, in particular, **CZ–01–058, 62, 65, 66,** have better activity than the first generation analogs, which supports our hypothesis of adding hydrophobic character to the polyamine tail to increase potency. **CZ–01–062 / 63** with three norspermidine cationic residues on a biphenyl system is more active compared to **CZ–01–058** with two norspermidine chains. It is to be noted that all the four active analogs have three norspermidine chains except **CZ–01–058**. The best among the top four compounds is **CZ–01–065**, with one of the three norspermidines attached at the *para* position. However, none of these compounds showed notable activity (clinical standard) to be selected as a lead compound. Another important thing we observed is, too much hydrophobic character with these compounds does not benefit a great deal to improve the efficacy. This can be seen with analog **CZ–01–070** with two CF_3 groups almost comparable to **CZ–01–066**.

Given the better activity of para–substituted analog, we thought to provide more degrees of freedom for norspermidine chains on both aryl rings. In order to do this, we prepared bi–aryl ether, and alkyl aryl ethereal bis–aldehydes and generate analogs off of these aldehydes. The synthesis of bis–aldehyde biphenyl ether was achieved via a copper acetate mediated oxidative Chan–Lam coupling reaction of 5–Hydroxy–dimethyl isopthalate **4** with phenyl boronic acid followed by a Red–Al reduction of bis–ester **5** to bis–aldehyde **6** as illustrated in Scheme 5.2.[29]

On the other hand, the alkyl–aryl ethereal bis–aldehyde was generated by a nucleophilic substitution reaction (S_N2 reaction) of phenoxide generated from dimethyl–5–hydroxy isopthalate **4** onto benzyl bromide, followed by the Red–Al reduction of resultant ester **7** to aldehyde **8**. The two ethereal bis–aldehydes prepared were treated with Boc–norspermidine under reductive amination conditions to afford protected polyamine derivatives. The final Boc deprotections resulted in polyamines as hydrochloride slats (shown above in Scheme 5.2).

The biological activity of these polyamines with the ether backbone were less potent than the existing analogs. They did slightly better against Gram (–) bacteria compared to their counterpart **CZ–01–058** (Table 5.2). We have made various aryl–alkyl ethereal polyamines with different substitution patterns, but none of them showed a promising enough biological profile. Further, these compounds involve a tedious synthetic procedure compared to the di aryl analogs which makes it difficult to further pursue this series of compounds. We then focused on increasing the hydrophobic nature of these ployamines by adding substitutions off of the amines on cationic tail. Thus far, we have synthesized **CZ–01–058**

derivatives with substitution on the terminal amine of norspermidine at either end.

At the beginning, we started accessing the bis–*N*^{3}–alkylated polyamines via a selective reductive amination of terminal 1^{o} amine of the free bases of final compounds with different aldehydes (e.g., shown in Scheme 5.3A). We observed inconsistencies in biological evaluation with respect to different batches of the synthesized analogs. We attribute this anomaly in biological activity to the impurities formed under the reaction conditions (<5 % –imperceptible through NMR) in synthetic sequence. The issue was addressed by optimizing a linear synthetic route for the side chains used in the preparation of **CZ–01** compounds as shown in Scheme 5.3B.

The side chain synthesis began with reductive amination of amino propanol **9** with isobutaraldehyde to afford *N*–isobutyl amino propanol **10**. The alcohol in **10** was activated to bromide **11** followed by an S_N2 reaction with 1,3–diaminopropane resulted in pure *N*^{1}–isobutyl norspermidine **12** after the excess 1,3–diaminopropane was distilled under vacuum. The final CZ compounds were prepared by using the alkylated norspermidines synthesized by the above protocol, resulting in better purity and fewer byproducts (Scheme 5.3C).

Analogs pertaining to **CZ–01–058** series were synthesized using different alkylated norspermidines by employing similar reaction sequence mentioned above in Scheme 5.3B and 5.3C. Interesting biological activity profiles were observed when the synthesized *bis*–N3–alkylated polyamines were screened for their proposed antibiotic activity. All these compounds did well against MRSA with MIC's <5 μg/mL, except **CZ–01–086** (batch variation), and **CZ–01–112**

(hydrophobic with extra methyls) with MIC's >10 μg/mL. All of these *N*–alkylated polyamine containing compounds were more active against *Gram* (–) bacteria compared to their unsubstituted counterpart **CZ–01–058** analog.

Having seen their biological activity (Table 5.3), we were excited to see the activity profiles of tris–aldehydes with three substituted norspermidines. We synthesized the **CZ–02–062** series of compounds with three substituted norspermidine chains on bi–aryl backbone.

The bi–aryl polyamines substituted with three units of *N*–alkylated norspermidine have shown impressive activity profiles, particularly **CZ–01–122** with N–octyl norspermidine which showed broad spectrum activity with MIC's of 2 μg/mL aginst Gram (+) MRSA and 3.5 μg/mL against Gram (–) *P. aeruginosa.* Analogs with **CZ–01–140 / 127** have better activity against MRSA compared to P. *aeruginosa.* **CZ–01–099** with *N*–isobutyl norspermidine cation linker is not active against *Gram* (–) bacteria, and shows moderate efficacy against MRSA as depicted in Table 5.4**.**[26]

The notable clinically relevant broad–spectrum activity of some of these compounds has prompted us to pursue further biological profiling. ADME–toxicity studies of these compounds using the international standard ISO 10993 L929 fibroblast cell lysis assay confirmed the *in vitro* efficacy of these compounds is related to their associated cytotoxicity. The potency and cytotoxicity are often associated with the hydrophobicity (increased cLogP) of the compounds. Also, polyamines are notoriously responsible for causing hemolysis and toxicity. Therefore, **CZ–01–128** consisting of longer *N*–octyl substitution on norspermidine

is possibly more potent as well as cytotoxic by virtue of its higher cLogP (polarity; hydrophilicity and hydrophobicity of the compounds, calculated theoretically from the structures using maestro–11 Schrödinger software and Chemdraw software). All the three compounds except **CZ–01–099** scores a score of 4 at 12.5 µg/mL or 50 µg/mL (score of 0, 1, or 2 is a pass, and 3, or 4 is a fail). Surprisingly, **CZ–01–099** shown to be noncytotoxic (score of 0 even at 1000 µg/mL), thus translating to a therapeutic window of ~500.

Since the beginning of the synthesis of bi–aryl polyamines, we wanted to synthesize the derivatives using tetra–aldehyde. Our Initial attempt to access the bi–phenyl tetra–aldehyde failed, and ended up isolating the proto–de–boralated / proto–de–brominated by product (i.e., isopthalaldehyde, 30%) from the reaction mixture. We might have lost the desired product in column purification in the first attempt, owing to its insoluble nature (insoluble in any known solvent). Taking into account the therapeutic index of **CZ–01–099**, and with intent to synthesize tetra–substituted version of **CZ–01–099**, we revisited the reaction sequence and accomplished the synthesis of **CZ–01–189**, tetra–aldehyde and eventually bi–phenyl derivative with four isobutyl norspermidine chains attached.

The pursuit began with the conversion of 5–bromoisopthalaldehyde to pinacol boronate ester, followed by a Suzuki–Miyaura cross–coupling with resultant boronate ester and 5–bromoisopthalaldehyde gave bi–phenyl tetra–aldehyde. The solid crashed out in the reaction mixture was filtered and washed with water and subsequently with ethyl acetate, to remove organic and inorganic impurities. The aldehyde (solid) was taken as such and suspended in dry methanol

and reacted under reductive amination conditions with isobutyl norspermidine to give the final product **CZ–01–189** as hydrochloride salt upon treatment with Methanolic HCl as depicted in Scheme 5.4. When tested for biological activity, **CZ–01–189** had comparable MIC's with **CZ–01–099**. However, it was shown to be cytotoxic.

Biological Profiling of CZ–01–099

The selectivity index of **CZ–01–099** has opened new avenues for this project. Efforts were focused on further modifications of side chain substitutions and the bi–phenyl backbone itself. Further, it also inspired the synthesis of terphenyl, and tri–aromatic systems and their amine conjugates with various substituted polyamines. As further SAR studies on **CZ–01–099** series is in progress, we carried out detailed biological profiling of **CZ–01–099**.

Biofilm dispersal abilities of CZ–01–099

When screened against various *Gram* (+) and *Gram* (–) planktonic as well as biofilm phenotype, **CZ–01–099** showed appreciable activity against *Gram* (+) bacteria (*MRSA, B. subtilus, S. aureus, L. monocytogenes)* except *M. tuberculosis*, and not active against gram (–) ve bacteria. Further, in qualitative biofilm dispersal assays, **CZ–01–099** is tested in comparison with glutaraldehyde, and vancomycin for its ability to disperse well established biofilm grown on stainless steel titanium plates. It was confirmed through scanning electron microscopy (SEM) imaging technique that the **CZ–01–099** is a more effective biofilm disperser compared to vancomycin. **CZ–01–099** performs better (disperses >90% biofilm) than

vancomycin (a known first line antibiotic commonly used in treating MRSA related infections), and the existing biocidal agent glutaraldehyde (as positive control, ineffective in dispersing the biofilms) as seen in Figure 5.10.

Applications of CZ–01–099 as topical medication

Considering the biofilm dispersal abilities of **CZ–01–099**, and its lack of cytotoxicity, we advanced to investigate its *in vivo* biocidal efficacy profile in a topical wound model using Yorkshire pigs. Using 1 cm biopsy punch a total 24 (12 each side and in 4 sections of 6) second degree burn wounds were created on a pig back. Twelve wounds on one side were inoculated with MRSA planktonic bacteria, and the twelve wounds on the other side with well–established MRSA biofilm phenotype. After elevn days of infection development, the two sections of wounds (six wounds with planktonic MRSA and six wounds with MRSA biofilm) were left untreated, and the other two sections were treated with 2% of **CZ–01–099** along with 200 ppm $AgNO_3$ for 14–day period. The pig was mercy killed after the treatment period, and the culture swabs from each wound were streaked on CHROM–agar (used to diagnose MRSA) plates (Figure 5.10).

As can be seen in Figure 5.10, the wounds inoculated with planktonic MRSA both treated with **CZ–01–099** (top right), and untreated (top left) do not show the growth of MRSA in agar plates. This means **CZ–01–099** can kill planktonic MRSA, and similarly pigs' immune system can take care of infections related to planktonic MRSA, whereas, the MRSA growth can be seen (bottom left) in the plates streaked with culture swabs of MRSA biofilm related wounds, but not from the wound treated with **CZ–01–099**+**$AgNO_3$** (bottom right). In fact, all the wounds treated with **CZ–**

01–099+$AgNO_3$ had re–epithelialized by day 25. In contrast, the untreated wounds inoculated with established biofilms have developed signs of chronic infection such as irregular wound borders and early growth of necrotic tissue. This topical wound study clearly demonstrates the ability of **CZ–01–099** to kill the bacteria in biofilm phenotype.

Resistance development assay

One of the serious global health threats in the present–day world is antibiotic resistance. Bacteria have come up with strategies to combat the current antibiotic regimen. Bacteria develop drug resistance to all the available antibiotics over a period, but a lower frequency of mutation is an ideal characteristic of a promising lead compound. The clinical isolates of MRSA were subjected to sub-MIC levels of **CZ–01–099**, and the persisting cells were grown in fresh media and resubjected to sub–MIC levels. This process was repeated, and the MRSA isolates were passed through a series of 19 passages. The MIC and MBC of **CZ–01–099** was consistent at 6 μg/mL throughout 19 passages albeit with minimal changes. In fact, the isolates after the 15^{th} passage started growing at a slower rate on an agar plate, indicative of the ability of **CZ–01–099** to weaken the isolates of MRSA. On the other hand, MIC stayed constant, but MBC of vancomycin faded after the 12^{th} passage. The cultures were withdrawn and disposed of fearing a danger of generating a vancomycin–resistant MRSA isolate (Figure 5.12).

Conclusion

Through the synthesis second generation analog aimed at modifying the hydrophobic backbone of poly cationic amines, we developed a novel class of anti–biofilm antibiotics. We identified **CZ–01–099** as a potential lead and further biological profiling under progress. This series of compounds has demonstrated broad spectrum activity, and biofilm dispersal properties. Further SAR on **CZ–01–099**, aimed at increasing potency while maintain noncytotoxic properties, is under progress.

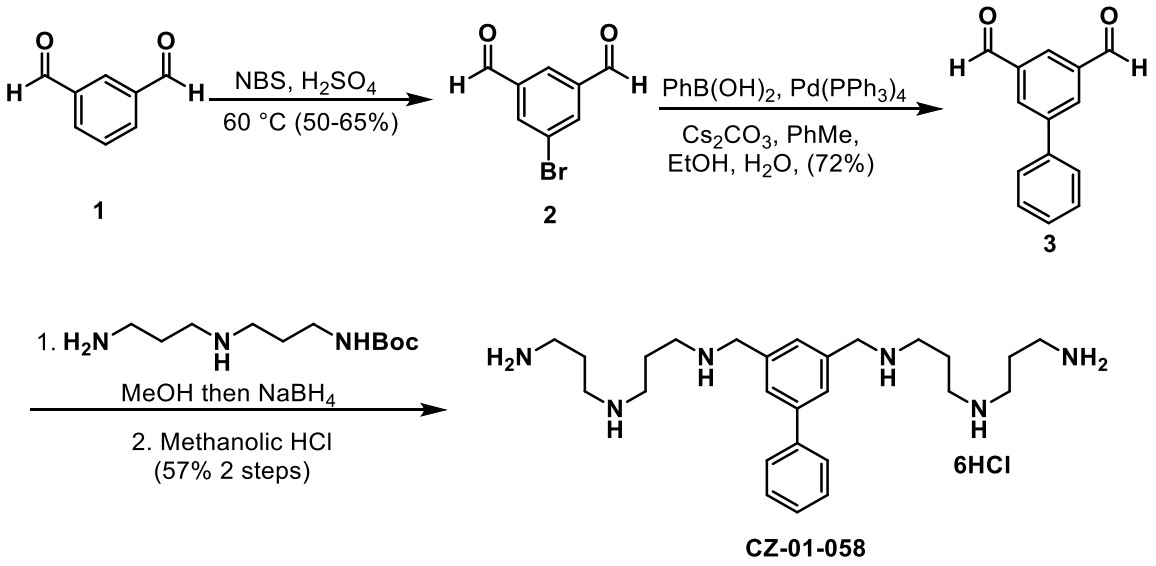

Scheme 5.1 Synthesis of CZ–01–058

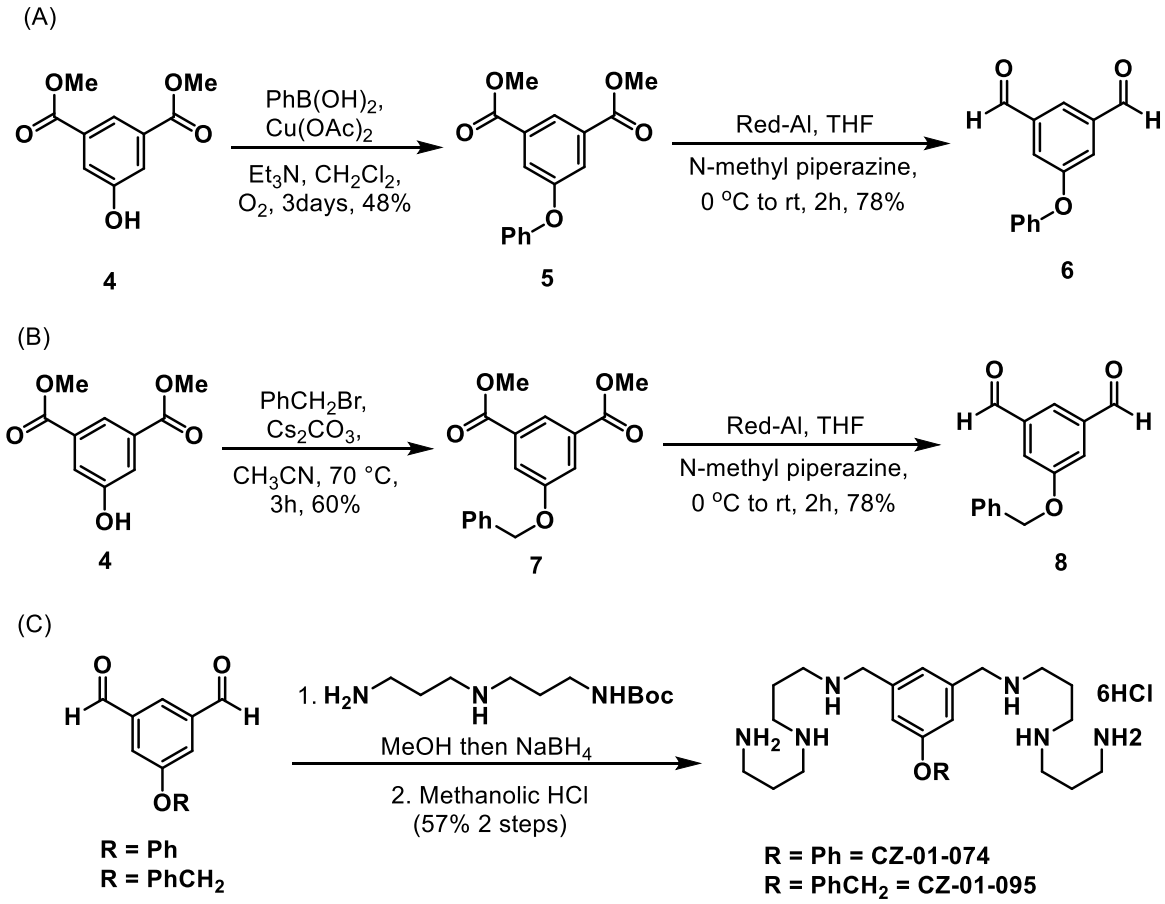

Scheme 5.2 Synthesis of compounds with aryl–alkyl etherial linkage. A) Synthesis of biphenyl bis–aldehyde. B) Synthesis of benzyl phenyl bis–aldehyde. C) Reductive amination and deprotection of Boc groups.

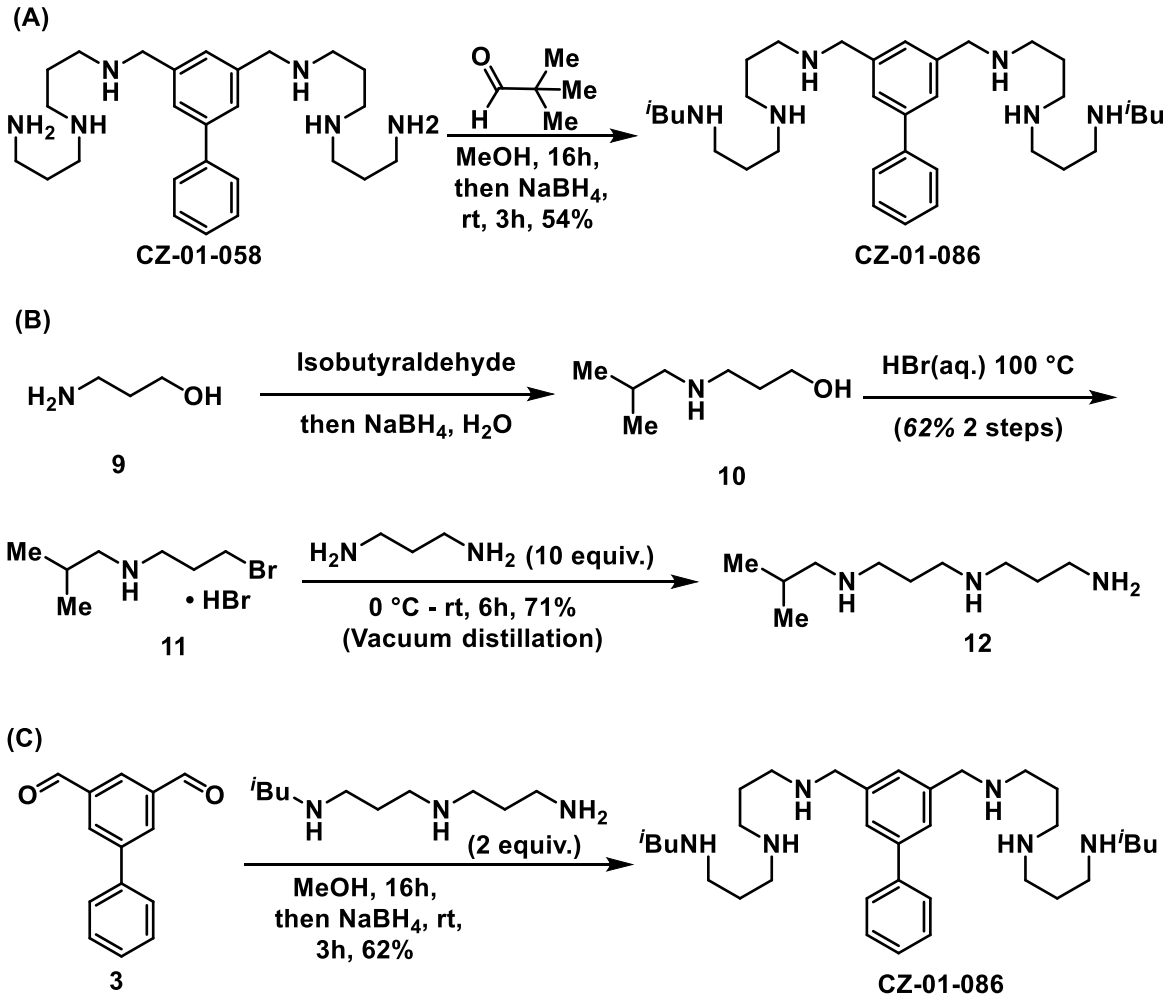

Scheme 5.3 Optimized protocol for the synthesis of CZ–01–086. (A) Initial protocol for the synthesis of CZ–01–086. (B) Reaction sequence for the preparation of Isobutyl norspermidine side chain. (C) Reductive amination of bis–aldehyde with alkylated norspermidine.

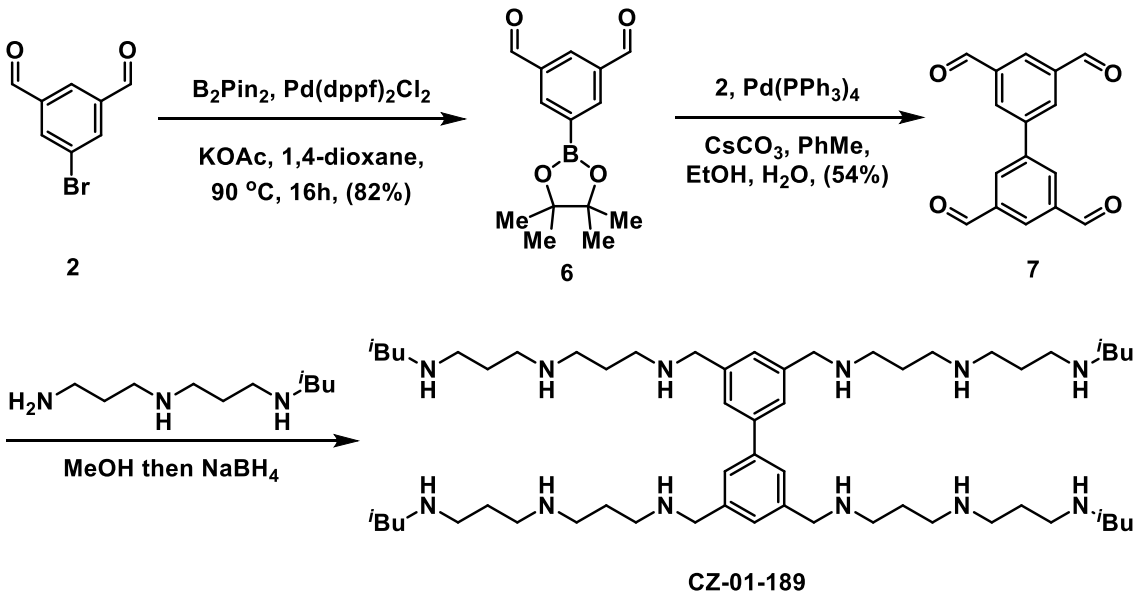

Scheme 5.4 Synthesis of tetra–substituted bi–aryl amine CZ–01–189

Table 5.1 *In vitro* antibacterial activity of CZ–01 series second generation analogs against *MRSA* and *pseudomonas aeruginosa.*

Compound	MIC–MRSA (µg/mL)	MIC– *P.* aeruginosa (µg/mL)
CZ–01–058	7.3 (n=9)	50
CZ–01–062	4.64	18
CZ–01–065	2	14.5
CZ–01–066	5.1	19.3
CZ–01–067	NT	NT
CZ–01–069	>10	>20
CZ–01–070	>5	20
CZ–01–071	>5	20

Table 5.2 Comparison of antibacterial activity of CZ–01–074 and CZ–01–095 to their counterpart CZ–01–058

Compound	MIC–MRSA (µg/mL)	MIC– *P.* aeruginosa (µg/mL)
CZ–01–058	7.3 (n=9)	50
CZ–01–074	8	>25
CZ–01–095	10	>25

Table 5.3 Comparison of antibacterial activity of *N–alkylated* derivatives of CZ–01–058 series of analogs

Compound	MIC–MRSA (µg/mL)	MIC– *P.* aeruginosa (µg/mL)
CZ–01–058	7.3 (n=9)	50
CZ–01–086	8.1±4.1 (n=10)	25
CZ–01–092	2	10.0
CZ–01–096	2	30
CZ–01–111	5	10
CZ–01–112	10	>30
CZ–01–114	1	10
CZ–01–118	1	10

Table 5.4 Comparison of antibacterial activity of *N–alkylated* derivatives of CZ–01–062 series of analogs

Compound	MIC–MRSA (µg/mL)	MIC– *P.* aeruginosa (µg/mL)	cLogP
CZ–01–065	2	14.5	1.01
CZ–01–099	5.8	200	7.29
CZ–01–127	3	18	10.9
CZ–01–128	2	3.5	14.0
CZ–01–140	2	40	10.9

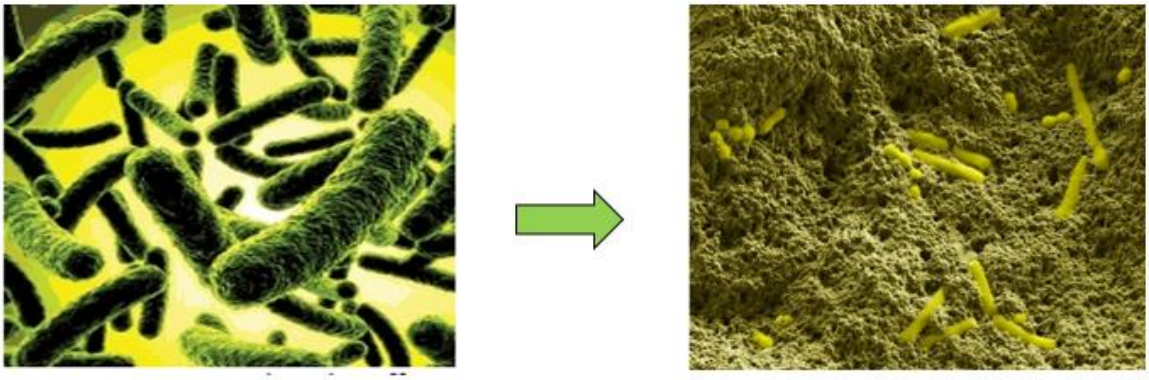

Figure 5.1 Cryo–scanning electron microscope images of planktonic bacteria and biofilm phenotype[4–5]

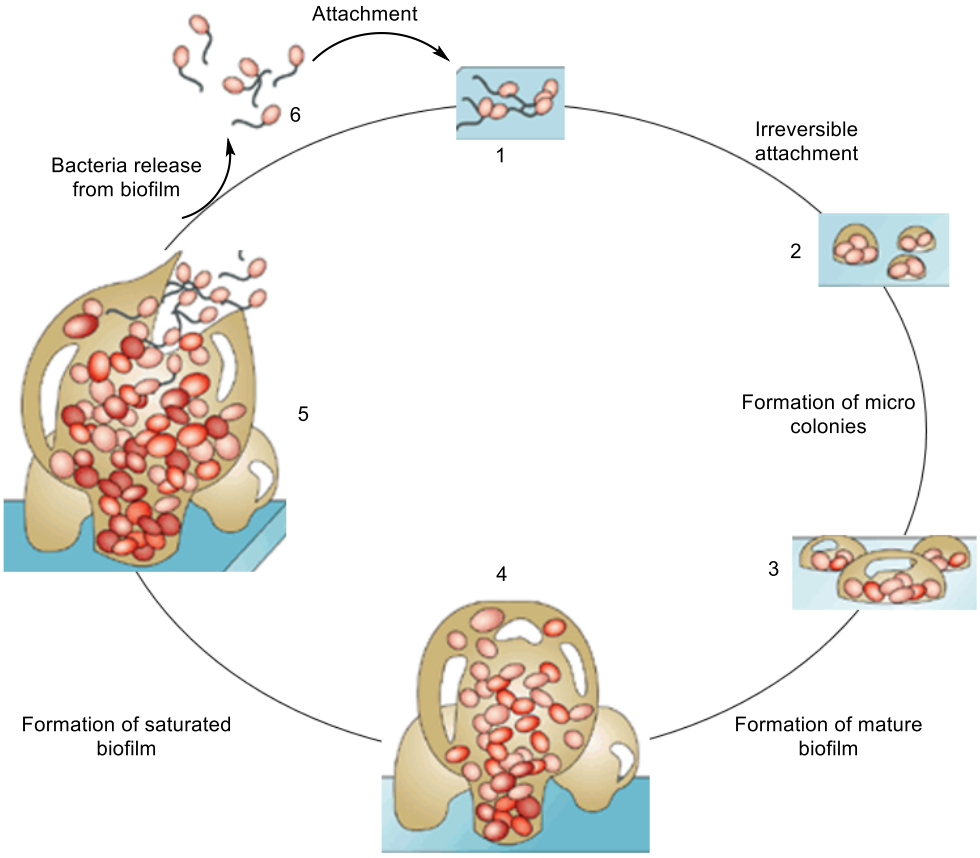

Figure 5.2 Life cycle of a biofilm: 1) Attachment of planktonic bacteria to a surface 2) EPS secretion and irreversible attachment 3 and 4) Formation of a matured biofilm 5) Biofilm disintegration and release of bacteria 6) Planktonic bacteria finding a new surface for attachment[8]

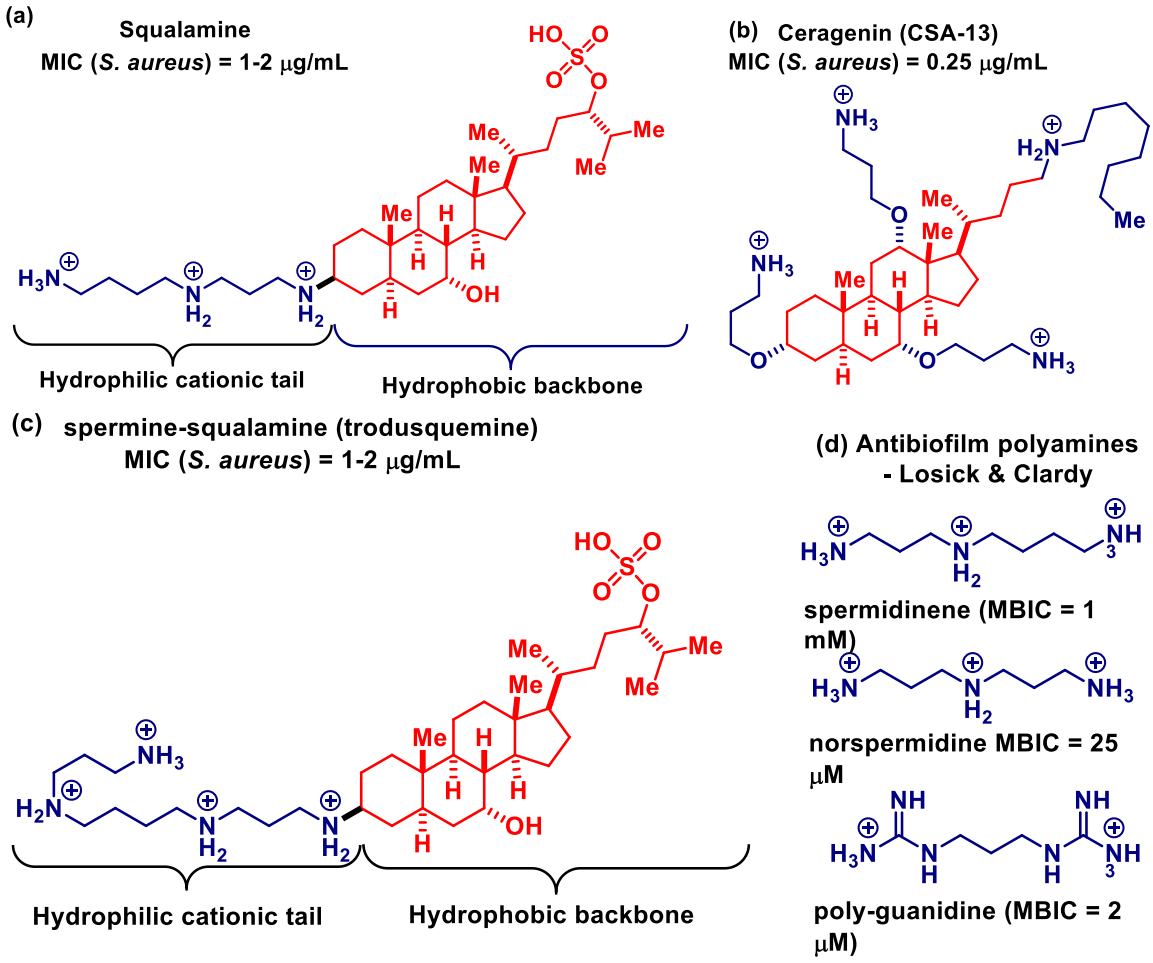

Figure 5.3 Compounds with polyamine tail attached to a hydrophobic backbone. (a) Squalamine with spermidine polyamine tail attached to a steroidal backbone (b) Cationic steroidal antibiotic aka. Ceragenin's – CSA–13 (c) Trodusquemine (d) Antibiofilm polyamines

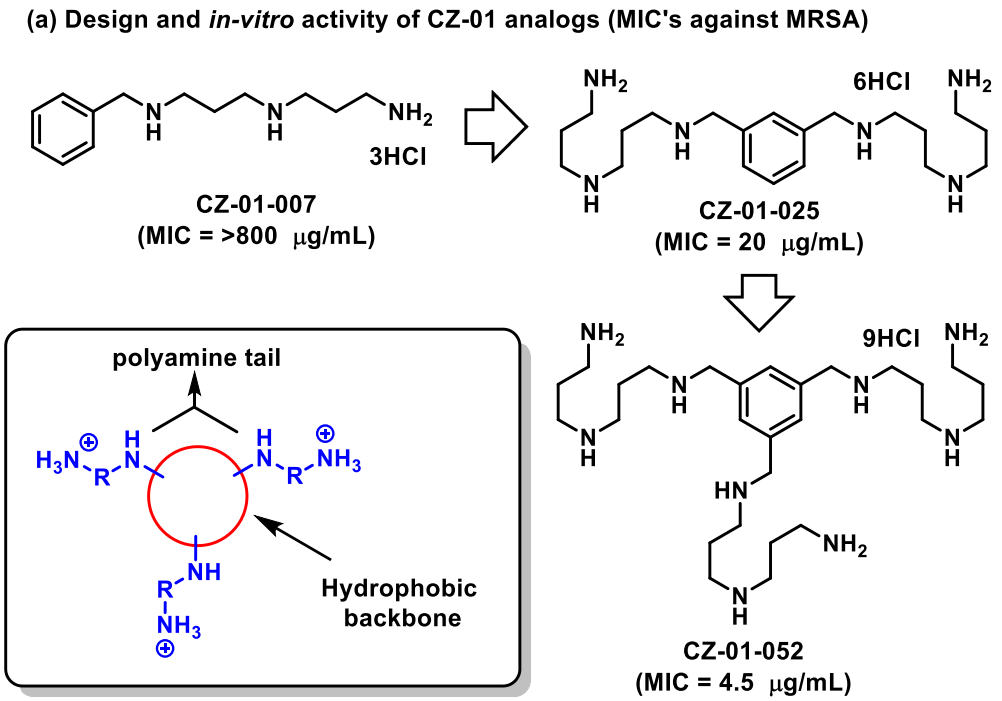

Figure 5.4 Design and antibacterial activity of CZ–01–analogs

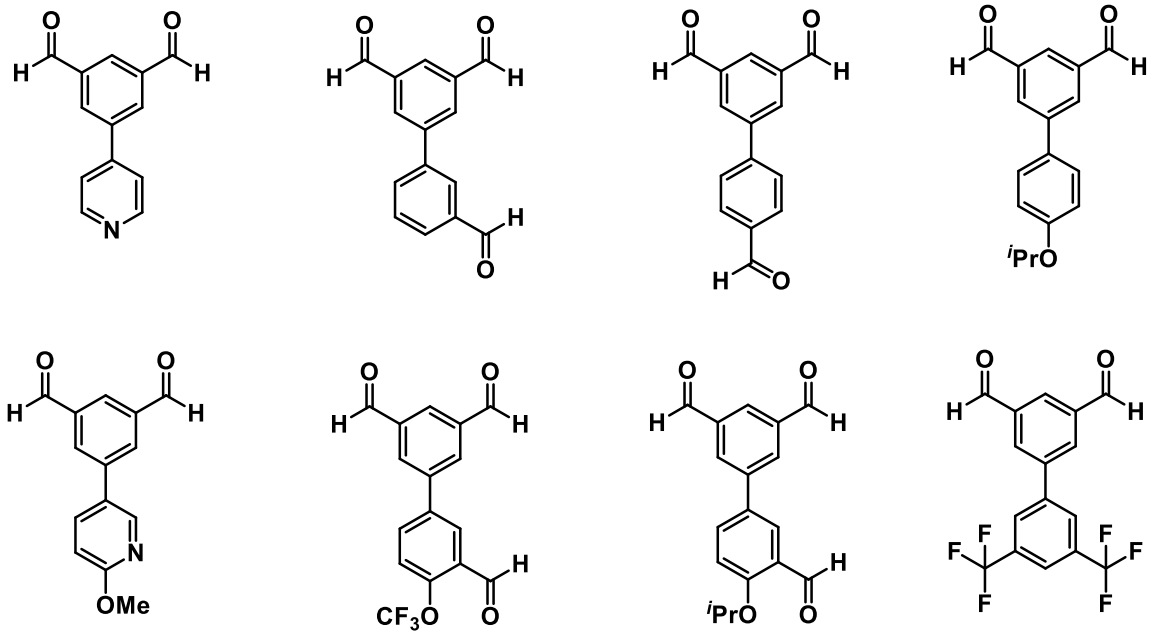

Figure 5.5 Aldehydes synthesized employing a Suzuki–Miyaura cross coupling

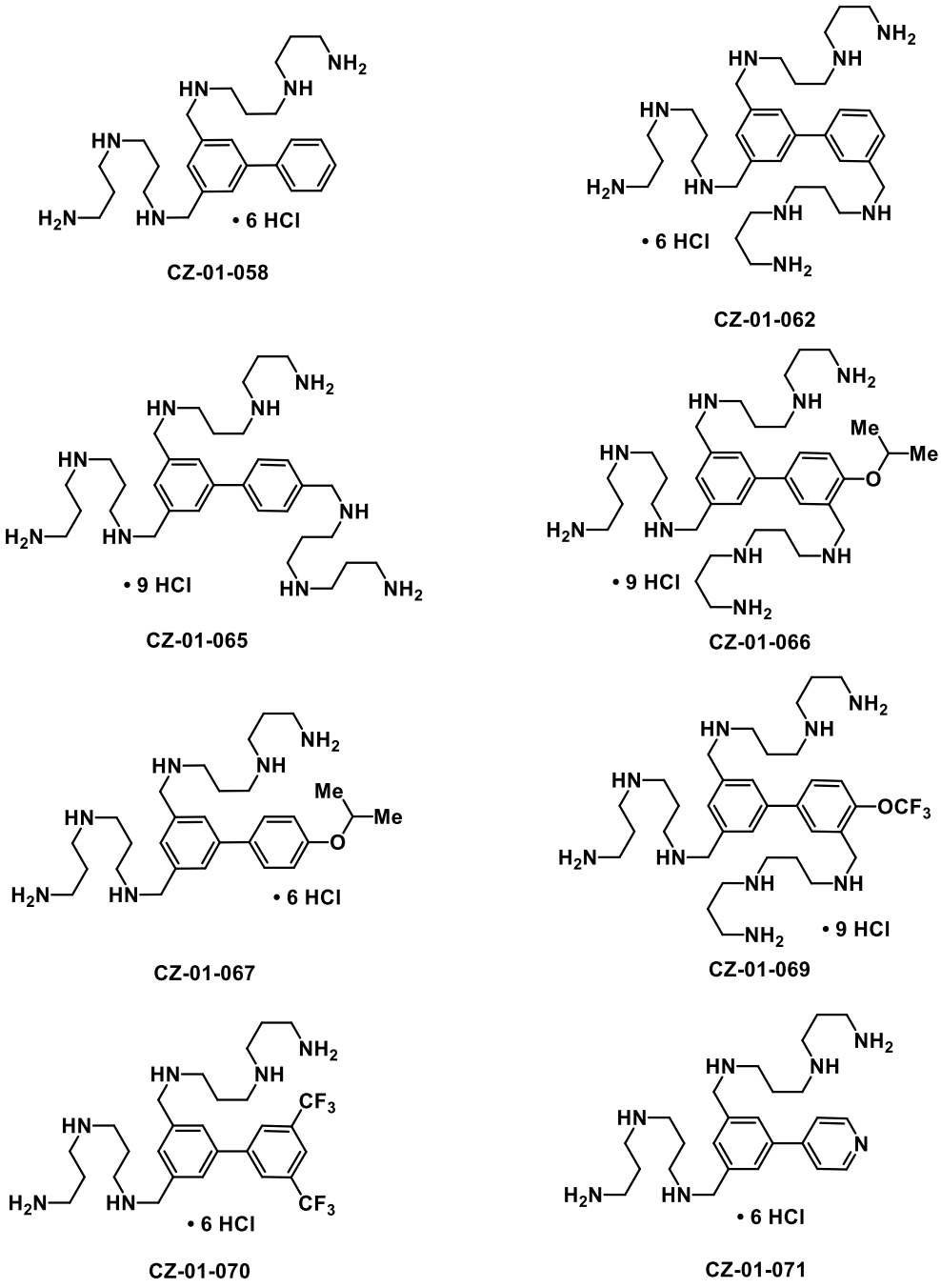

Figure 5.6 Compounds synthesized using a protocol similar to CZ–01–058

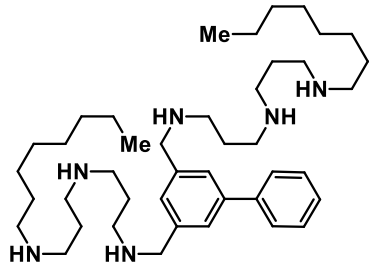

N-octyl-norspermidine
CZ-01-92

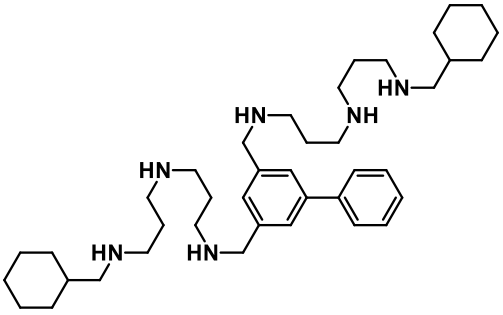

N-cyclohexylmethyl-norspermidine
CZ-01-96

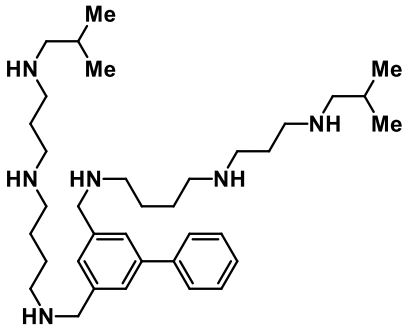

N-isobutyl spermine
CZ-01-111

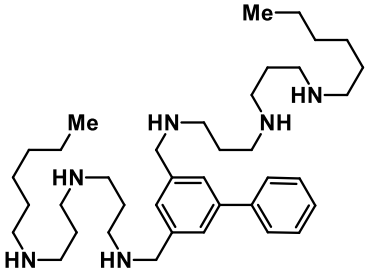

N-hexyl-norspermidine
CZ-01-114

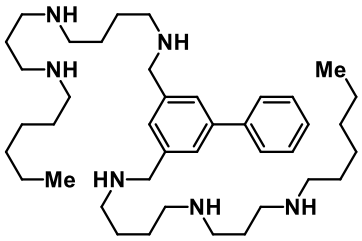

N-hexyl-spermine
CZ-01-118

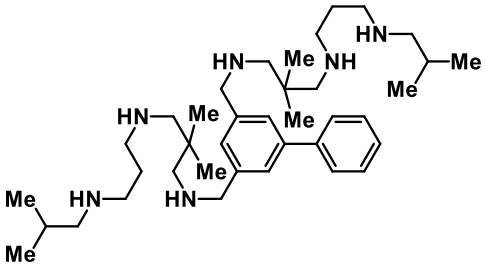

N-isobutyl-3-(2,2-dimethylpropylamino)-
1,3-diaminopropane
CZ-01-112

Figure 5.7 N–alkylated polyamine derivatives of CZ–01–058

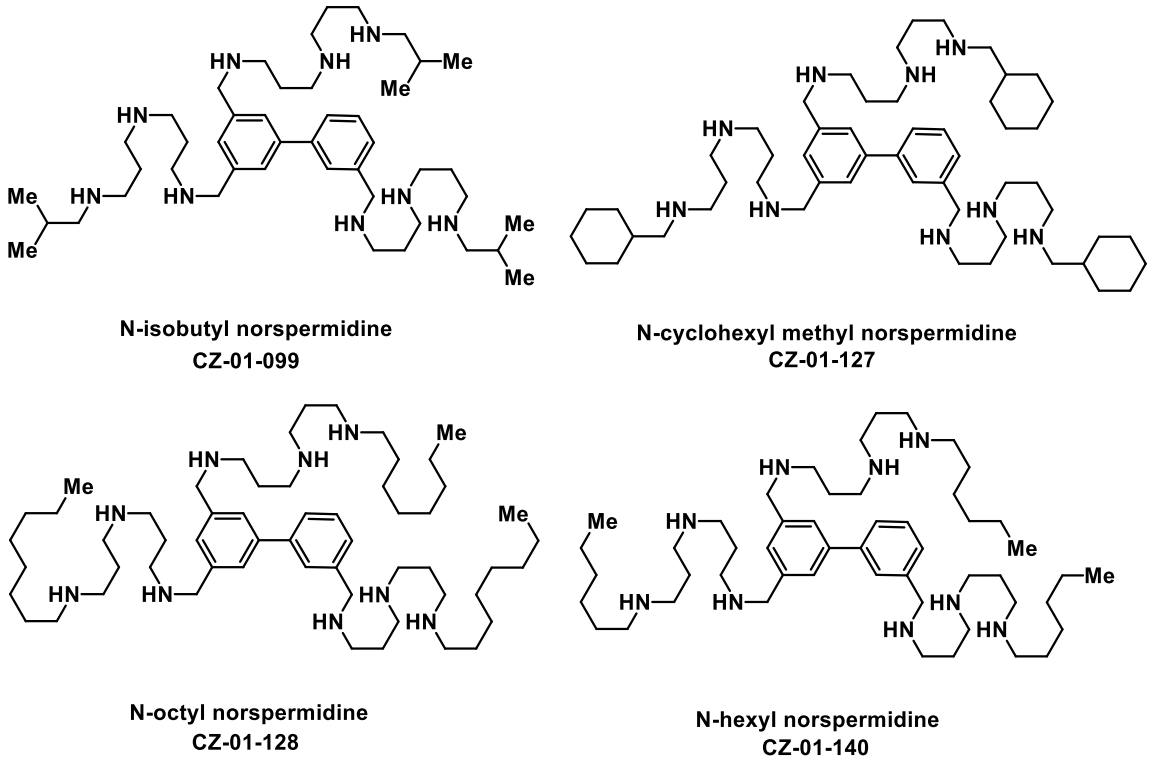

Figure 5.8 CZ–01–062 series of compounds with *N*–substituted norspermidine

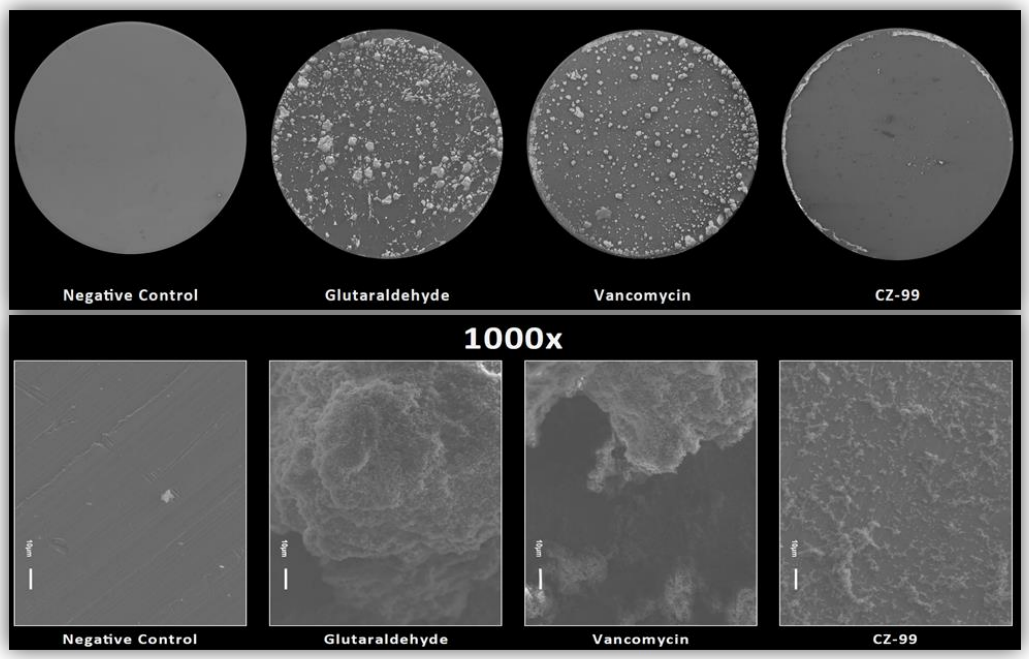

Figure 5.9 SEM images confirming CZ–01–099 as effective biofilm disperser

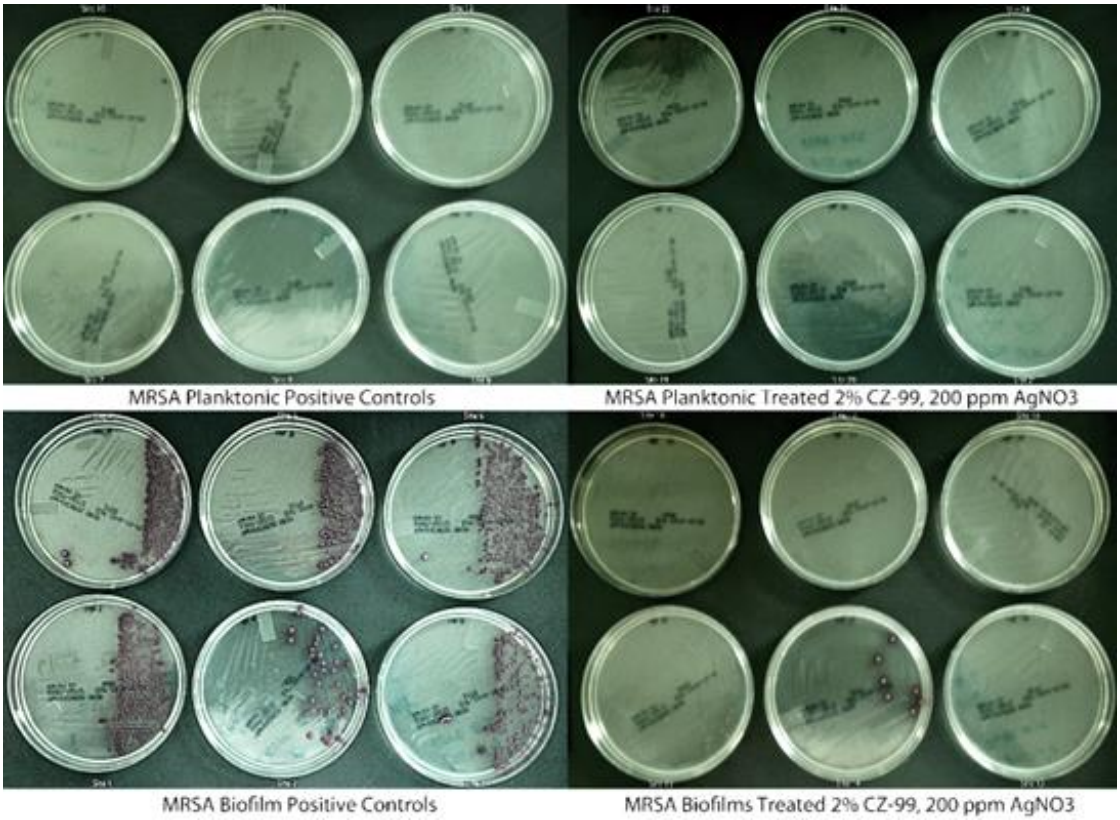

Figure 5.10 Topical wound model, swab cultures grown on CHROM–agar plates

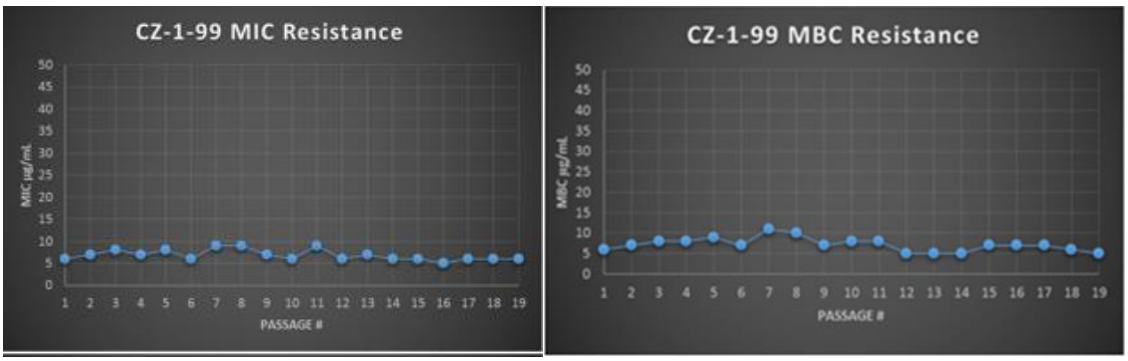

Figure 5.11 Serial passage assay for diagnosis of resistance development

References

1) (a) Costerton, J. W.; Geesey, G. G.; Cheng, K. J. How Bacteria Stick. *Sci. Am*. **1978**, *238*, 86–95. (b) Costerton, J. W.; Stewart, P. S.; Greenberg, E. P. Bacterial Biofilms: A Common Cause of Persistent Infections. *Science* **1999**, *284*, 1318–1322. (c) Costerton, J. W.; Cheng, K. J.; Geesy, G. G.; Ladd, T. I.; Nickel, J. C.; Dasgupta, M.; Marrie, T. J. Bacterial Biofilms in Nature and Disease. *Ann. Rev. Microbiol.* **1987**, *41*, 435–464.

2) Seneviratne, C. J.; Wang, Y.; Jin, L.; Wong, W.; Sarah, S.; Herath, T. D. K.; Samaranayake, L. P. Unraveling the Resistance of Microbial Biofilms: Has Proteomics been Helpful. *Proteomics* **2012**, *12*, 651–665.

3) (a) Rickard, A. H.; Palmer, R. J. Autoinducer 2: A Concentration–Dependent Signal for Mutualistic Bacterial Biofilm Growth. *Mol. Microbiol.* **2006**, *60*, 1446–1456. (b) Elias, S.; Banin, E. Multi–Species Biofilms: Living with Friendly Neighbors. *FEMS Microbiol. Rev.* **2012**, *36*, 990–1004.

4) Ben–Ari. E. T. Not Just Slime: Beneath the Slippery Exterior of a Microbial Biofilm Lies a Remarkably Organized Community of Organisms. *Bio Science* **1999**, *49, 689–695.*

5) Solano, C.; Echeverz, M.; Lasa, I. Biofilm Dispersion and Quorum Sensing. *Curr. Opin. Microbiol.* **2014,** *18,* 96–104.

6) Bjarnsholt, T. The Role of Bacterial Biofilms in Chronic Infections. *APMIS,* **2013**, *121,* 1–58.

7) Jensen, P.; Givskov, M.; Bjarnsholt, T.; Moser, C. The Immune System vs Pseudomonas Aeruginosa Biofilms. *FEMS Immunol. Med. Microbiol,* **2010,** *59,* 292–305.

8) Lebeaux, D.; Ghigo, J–M.; Beloin, C. Biofilm–related Infections: Bridging the Gap between Clinical Management and Functional Aspects of Recalcitrance toward Antibiotics. *Microbiol Mol Biol Rev.* **2014**, *3*, 510–543.

9) Garett, T. R.; Bhakoo, M.; Zhang, Z. Bacterial Adhesion and Biofilm on Surfaces*. Prog. Nat. Sci.* **2008,** *18,* 1049–1056.

10) (a) Dufour, D.; Leung, V.; Lévesque, C. M. Bacterial Biofilm: Structure, Function, and Antimicrobial Resistance. *Endod. Topics* **2012**, *22*, 2–16. (b) Costerton, J. W.; Cheng, K. J.; Geesy, G. G.; Ladd, T. I.; Nickel, J. C.; Dasgupta, M.; Marrie, T. J. Bacterial Biofilms in Nature and Disease. *Ann. Rev. Microbiol.* **1987**, *41*, 435–464.

11) Beech, I. B.: Sunner J. A.; Hiraoka, K. Microbe–surface Interactions in

Biofouling and Biocorrosion Processes. *Int. Microbiol.* **2005**, *8*, 157–168.

12) Flemming, H. C. Microbial Biofouling: Unsolved Problems, Insufficient Approaches, and Possible Solutions. *Biofilm Highlights* **2011**, *5*, 81–110.

13) Biofilm and Biofouling: Cost and Effect on Drinking Water Quality for Human Development. https://www.researchgate.net/publication/274139244 (accessed October 15, 2016).

14) Bacteriality. Understanding Chronic Disease. http://bacteriality.com/2008/05/biofilm/#footnote_0_190 (accessed November 3, 2016).

15) Creamer, M. Biofilm Impact on Food Industry. *Food Magazine*. http://www.foodsafetymagazine.com/magazine–archive1/junejuly–2012 (accessed June 28, 2016).

16) Agricultural and Food Development Authority. https://www.teagasc.ie/food/food–chemistry—technology/national–food–imaging–centre/the–equipment/ecectron–microscopy/ (accessed June 30, 2016).

17) McGinley, H. R. ASI Adhesives and Sealants Industry. Glutaraldehyde Uses and Counterfeits. http://www.adhesivesmag.com/articles/91766-glutaraldehyde-uses-and-counterfeits (accessed October 20, 2016).

18) Lewis, K. Persister Cells, Dormancy and Infectious Disease. *Nature Rev. Microbiol*. **2007***, 5*, 48–56.

19) Hett, E. C.; Hung, D. T. Targeting Multiple Biofilm Pathways. *Chem. Biol.* **2009,** *16*, 1216–1218.

20) Kolodkin–Gal, I. Cao, S.; Chai, L.; Bottcher, T.; Kolter, R.; Clardy, J.; Losick,R. A Self–produced Trigger for Biofilm Disassemby that Targets Exopolysaccharide. *Cell* **2012**, *149*, 684–92.

21) Bottcher, T.; Kolodkin–Gal, I.; Kolter, R.; Losick, R.; Clardy, J. Synthesis and Activity of Biomimetic Biofilm Disruptors. *J. Am. Chem. Soc.* **2013**, *135*, 2927–2930.

22) Moore, K. S.; Wehrli, S.; Roder, H.; Rogers, M.; Forrest, J. N.; McCrimmon, D.; Zasloff, M. Squalamine: An Aminosterol Antibiotic from the Shark. *Proc. Natl. Acad. Sci. U.S.A.* **1993***, 90*, 1354–1358.

23) Karatan, E.; Duncan, T. R.; Watnick, P. I. NspS, a Predicted Polyamine Sensor, Mediates Activation of Vibrio Cholerae Biofilm Formation by Norspermidine. *J. Bacteriol.* **2005**, *187*, 7434–7443.

24) (a) Li, C.; Budge, L. P.; Driscoll, C. D.; Willardson, B. M.; Allman, G. W.; Savage, P. B. Incremental Conversion of Outer–Membrane Permeabilizers into Potent Antibiotics for Gram–Negative Bacteria. *J. Am. Chem. Soc.* **1999**, *121*, 931–940. (b) Lai, X.; Feng, Y.; Pollard, J.; Chin, J. N.; Rybak, M. J.; Bucki, R.; Epand, R. F.; Epand, R. M.; Savage, P. B. Ceragenins: Cholic Acid–based Mimics of Antimicrobial Peptides. *Acc. Chem. Res.* **2006**, *41*, 1233–1240. (c) Ding, B.; Taotofa, U.; Orsak, T.; Chadwell, M.; Savage, P. B. Synthesis and Characterization of Peptide–Cationic Steroid Antibiotic Conjugates. *Org. Lett.* **2004**, *6*, 3433–3436.

25) Drewry, J. A.; Burger, S.; Mazouchi, A.; Duodu, E.; Ayers, P.; Gradinaru, C. C.; Gunning, P. T. Src Homology 2 Domain Proteomimetics: Developing Phosphopeptide Selective Receptors. *Med. Chem. Comm.* **2012**, *3*, 763–770.

26) Haussener, T. J. The Design and Synthesis of Novel Antibiofilm Antibiotics and Efforts Toward the Total Synthesis of the Complex Aminocyclopentanol Pactamycin. Ph. D. Disseration, University of Utah, Salt Lake City, Utah, **2016**.

27) Muci, A. R.; Buchwald, S. L. Pratical Palladium Catalysts for C–N and C–O Bond Formation. *Top. Curr. Chem.* **2002**, *219*, 131–209.

28) Miyaura, N.; Suzuki, A. Palladium–Catalyzed Cross–Coupling Reactions of Organoboron Compounds. *Chem. Rev.* **1995**, *95*, 2457–2483.

29) Shin, W. K.; Kang, D.; An, D. K. Partial Reduction of Esters to Aldehydes Using a Novel Modified Red–AL Reducing Agent. *Bull. Korean Chem. Soc.* **2014***, 35,* 2169–2171.

Supporting Information

For supporting information and spectral data please see Haussener, T. J. The design and synthesis of novel anti-biofilm antibiotics and efforts toward the total synthesis of the complex aminocyclopentanol pactamycin. Ph. D. Disseration, University of Utah, Salt Lake City, Utah, **2016**.[26]

APPENDIX A

^{1}H, ^{13}C SPECTRA FOR CHAPTER 2

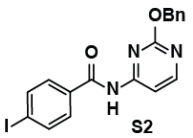
OBn
O
N
N
N
H
I
S2

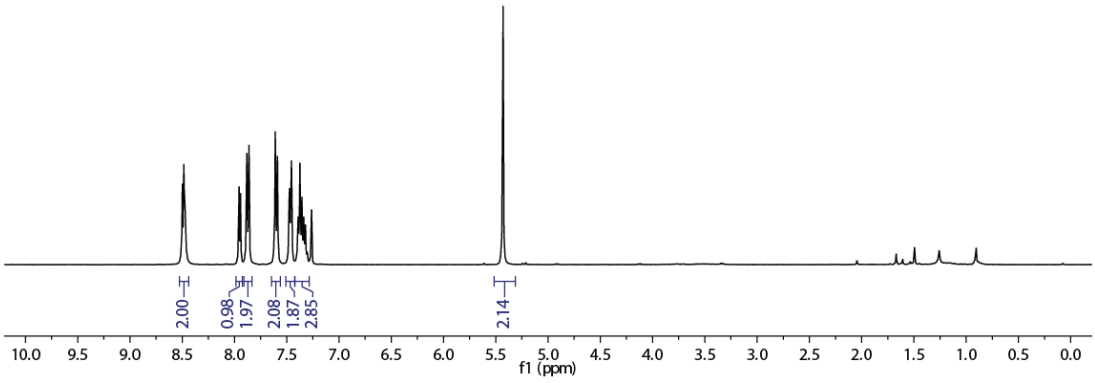
2.00
0.98
1.97
2.08
1.87
2.85
2.14
10.0 9.5 9.0 8.5 8.0 7.5 7.0 6.5 6.0 5.5 5.0 4.5 4.0 3.5 3.0 2.5 2.0 1.5 1.0 0.5 0.0
f1 (ppm)

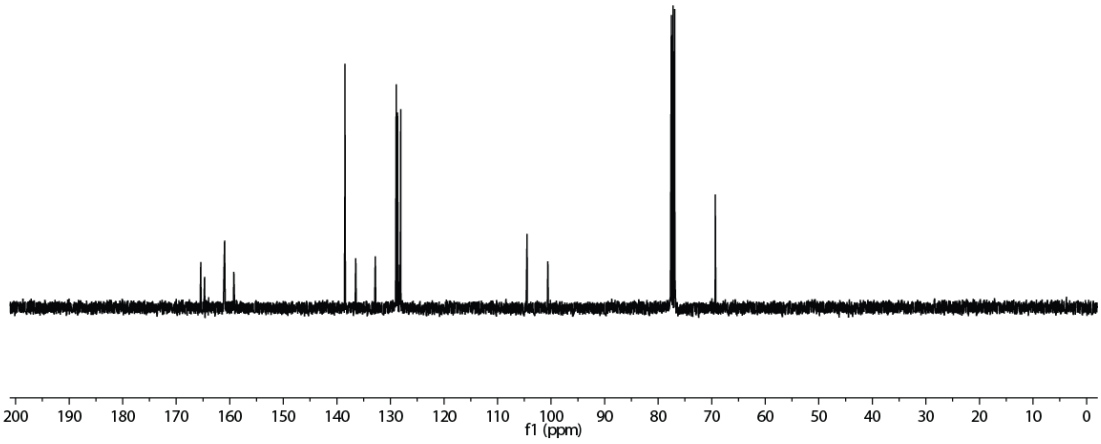
200 190 180 170 160 150 140 130 120 110 100 90 80 70 60 50 40 30 20 10 0
f1 (ppm)

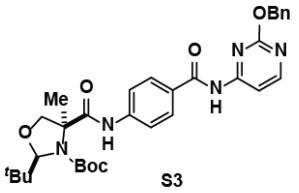
OBn
N
N
O
N
H
Me
O
O
N
H
N
Boc
tBu

S3

1.90
0.89
2.00
1.92
2.03
2.86
2.00
0.93
0.84
0.96
3.10
9.47
9.50
10.0 9.5 9.0 8.5 8.0 7.5 7.0 6.5 6.0 5.5 5.0 4.5 4.0 3.5 3.0 2.5 2.0 1.5 1.0 0.5 0.0
f1 (ppm)

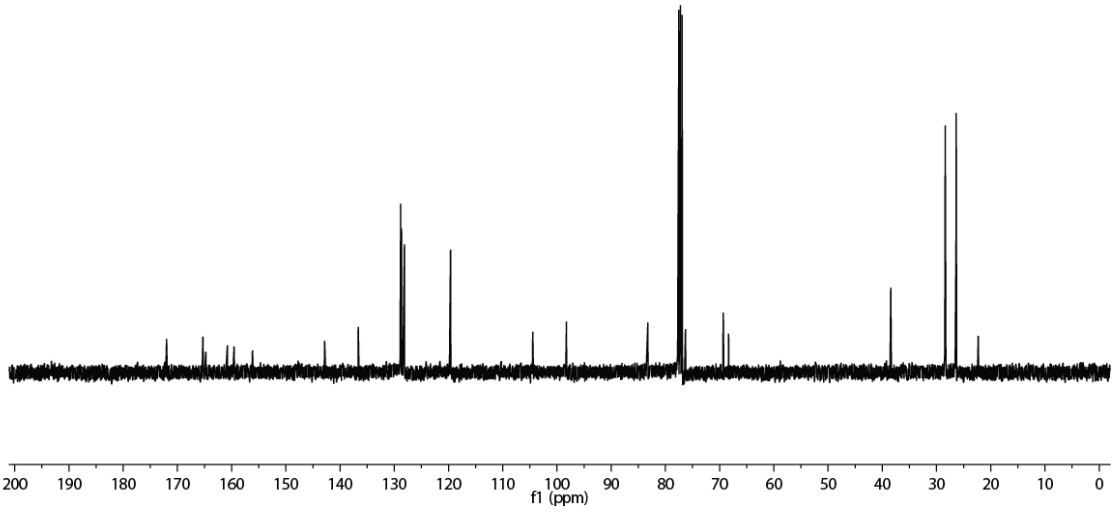
200 190 180 170 160 150 140 130 120 110 100 90 80 70 60 50 40 30 20 10 0
f1 (ppm)

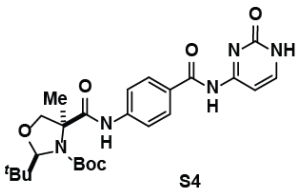
Me
O
N
H
O
N
H
O
N
NH
O
N
Boc
tBu

S4

2.00
0.97
1.97
0.66
0.91
0.81
0.92
3.10
9.60
9.41
10.0 9.5 9.0 8.5 8.0 7.5 7.0 6.5 6.0 5.5 5.0 4.5 4.0 3.5 3.0 2.5 2.0 1.5 1.0 0.5 0.0
f1 (ppm)

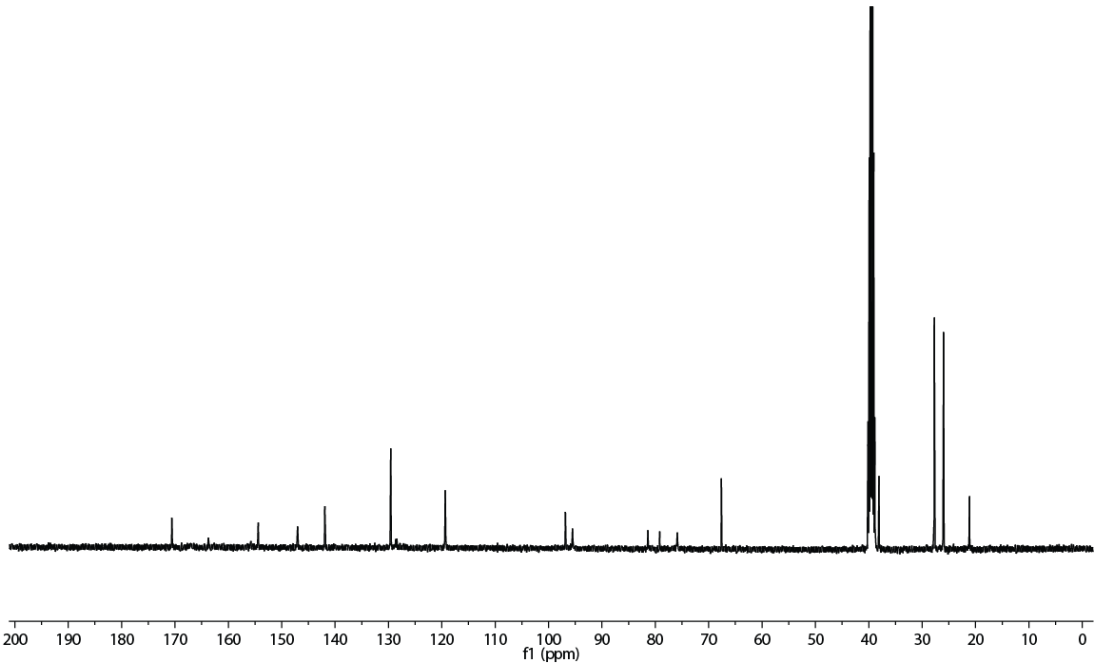
200 190 180 170 160 150 140 130 120 110 100 90 80 70 60 50 40 30 20 10 0
f1 (ppm)

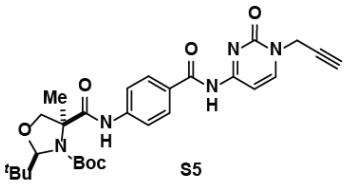
Me
O
O
N
H
O
N
H
N
N
O
Boc
tBu

S5

1.00
2.12
2.14
0.90
1.17
1.10
2.22
1.21
0.77
3.56
9.74
9.87
10.0 9.5 9.0 8.5 8.0 7.5 7.0 6.5 6.0 5.5 5.0 4.5 4.0 3.5 3.0 2.5 2.0 1.5 1.0 0.5 0.0
f1 (ppm)

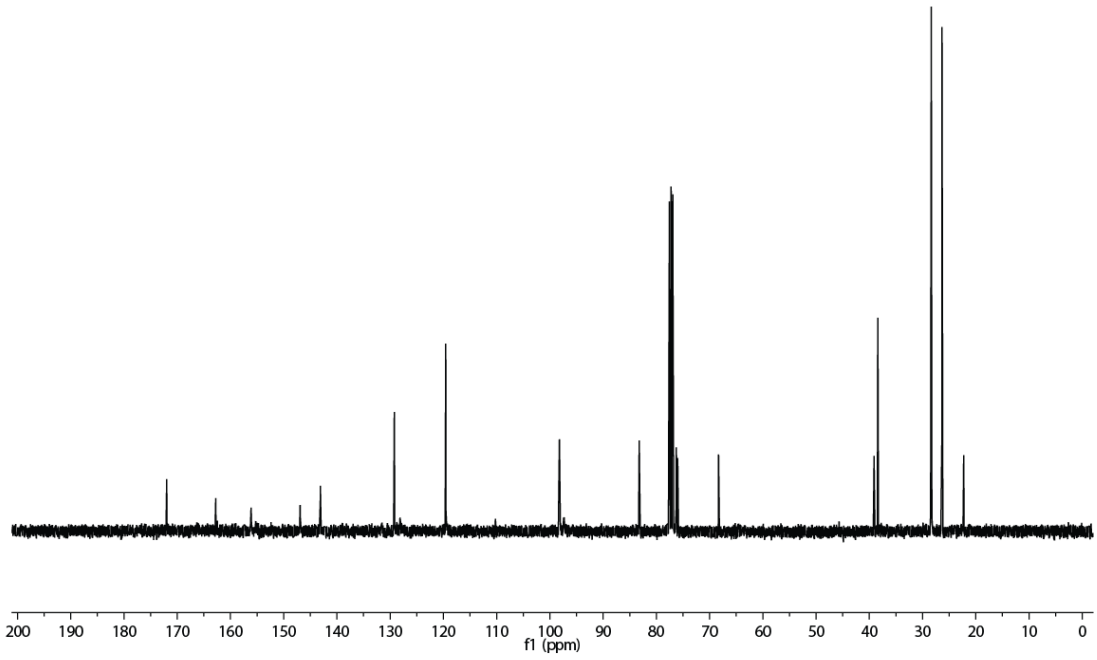
200 190 180 170 160 150 140 130 120 110 100 90 80 70 60 50 40 30 20 10 0
f1 (ppm)

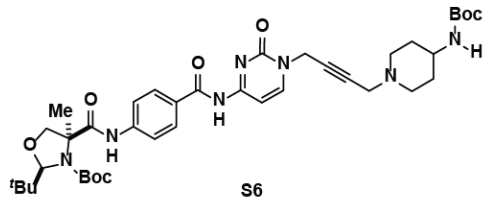
Boc
N
H
O
N
N
O
N
H
O
Me
O
N
H
O
N
Boc
tBu

S6

1.20
2.50
2.63
1.07
1.23
1.21
2.48
1.00
1.32
1.86
2.66
2.49
2.53
2.63
3.64
11.10
11.10
11.06
10.0 9.5 9.0 8.5 8.0 7.5 7.0 6.5 6.0 5.5 5.0 4.5 4.0 3.5 3.0 2.5 2.0 1.5 1.0 0.5 0.0
f1 (ppm)

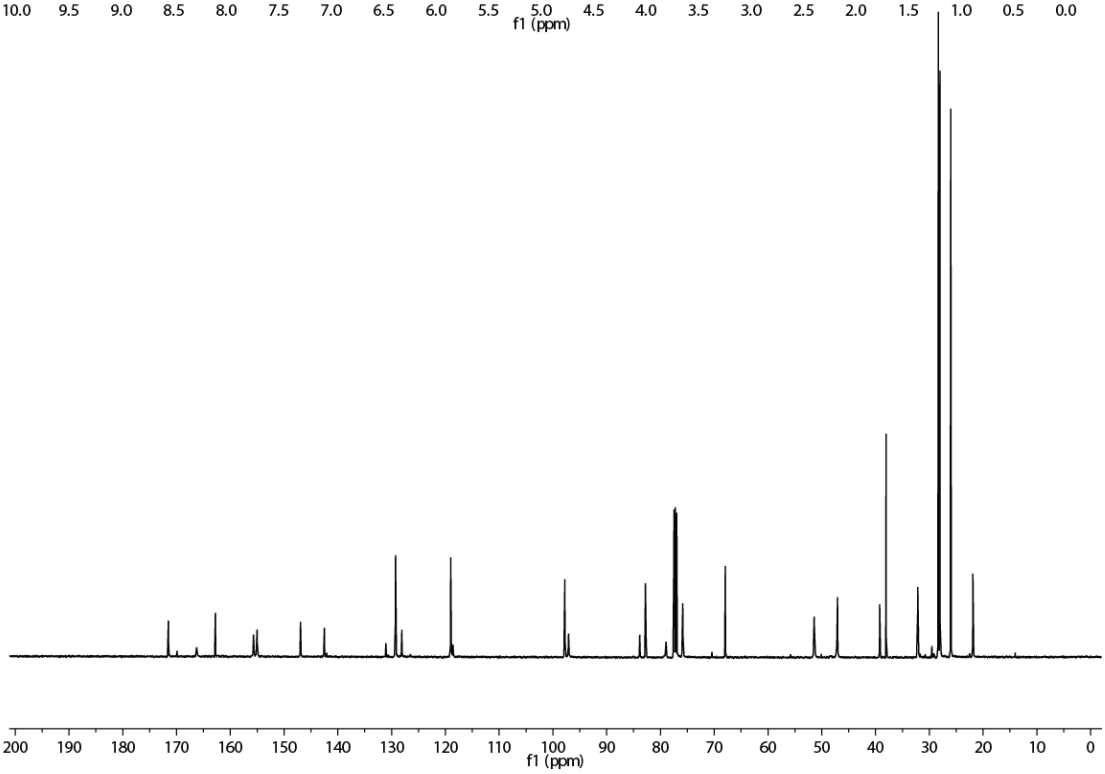
200 190 180 170 160 150 140 130 120 110 100 90 80 70 60 50 40 30 20 10 0
f1 (ppm)

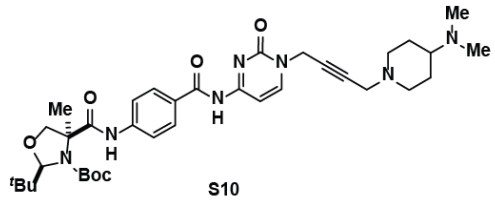
Me
O
N
H
O
Me
N
Boc
tBu
O
N
N
H
O
N
N
Me
Me

S10

1.00
2.26
2.28
1.03
1.06
3.29
1.03
2.26
2.16
6.17
3.36
2.25
3.21
13.54
9.77
10.0 9.5 9.0 8.5 8.0 7.5 7.0 6.5 6.0 5.5 5.0 4.5 4.0 3.5 3.0 2.5 2.0 1.5 1.0 0.5
f1 (ppm)

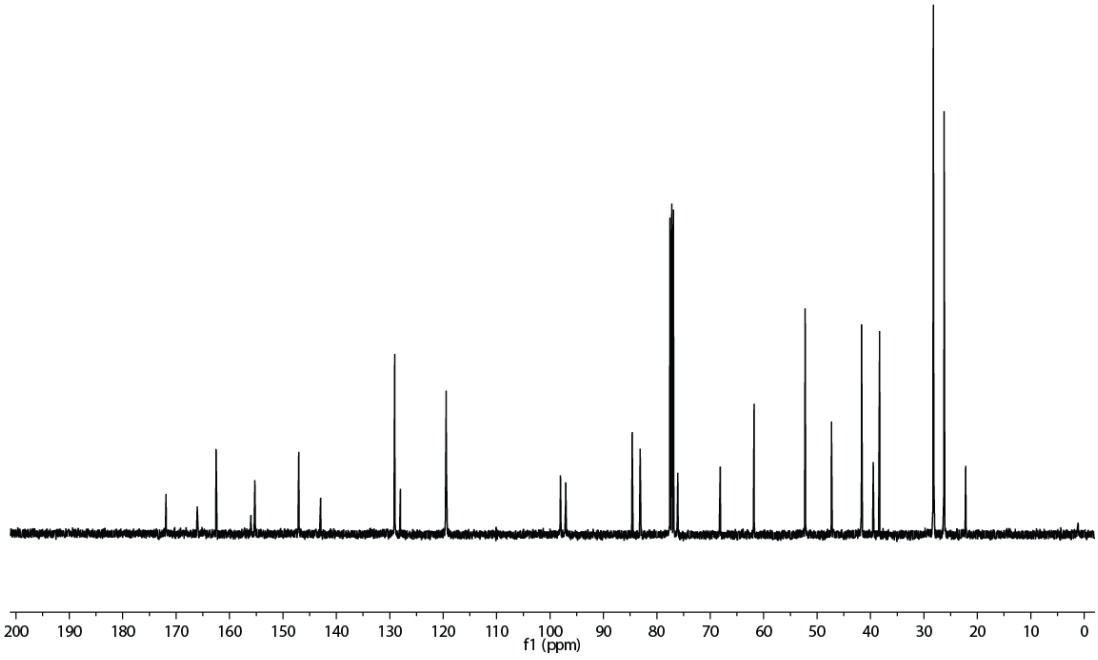
200 190 180 170 160 150 140 130 120 110 100 90 80 70 60 50 40 30 20 10 0
f1 (ppm)

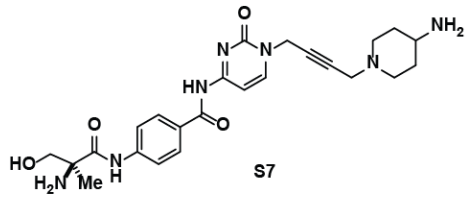
O
N
N
NH2
HN
N
O
O
HO
N
H
H2N
Me

S7

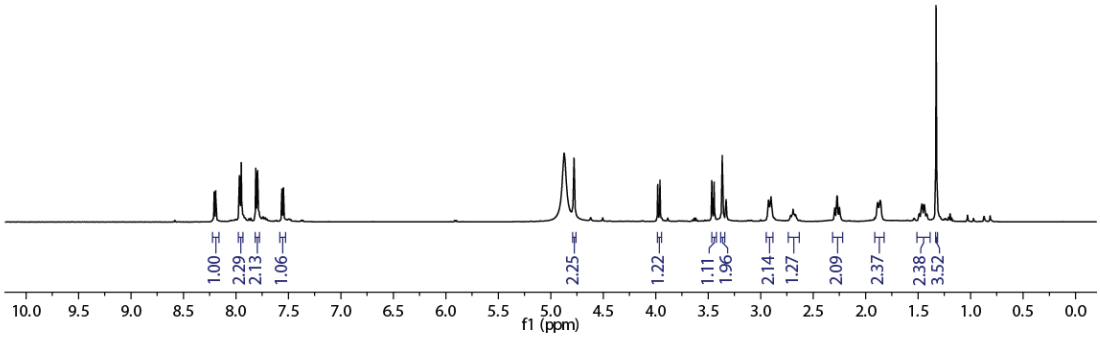
1.00
2.29
2.13
1.06
2.25
1.22
1.11
1.96
2.14
1.27
2.09
2.37
2.38
3.52
10.0 9.5 9.0 8.5 8.0 7.5 7.0 6.5 6.0 5.5 5.0 4.5 4.0 3.5 3.0 2.5 2.0 1.5 1.0 0.5 0.0
f1 (ppm)

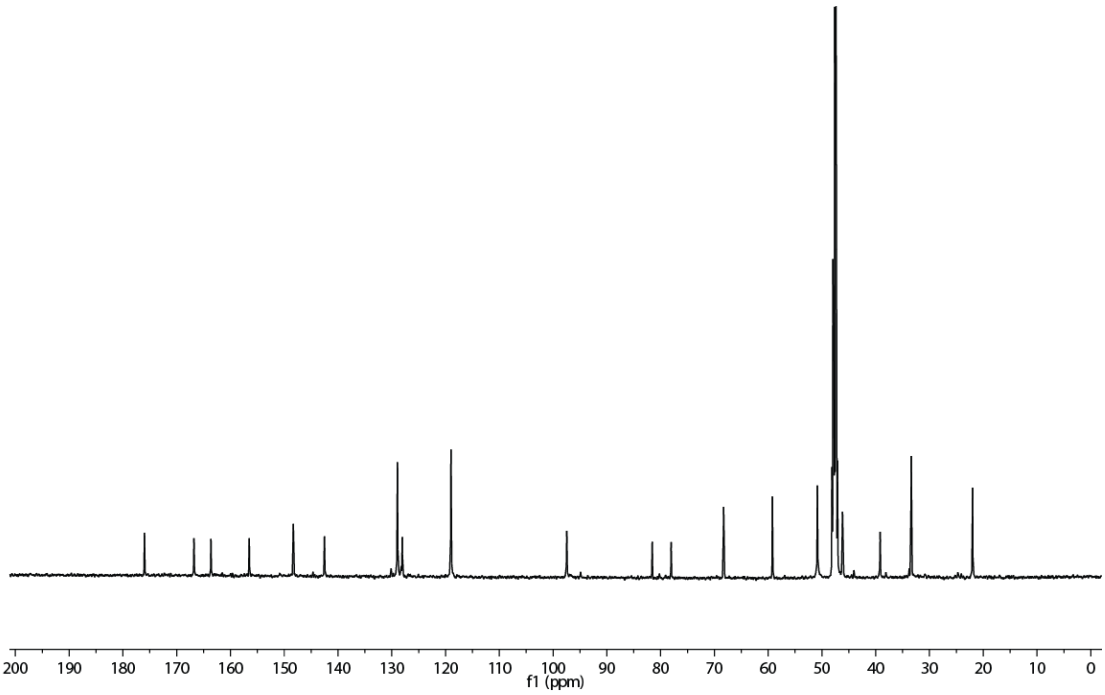
200 190 180 170 160 150 140 130 120 110 100 90 80 70 60 50 40 30 20 10 0
f1 (ppm)

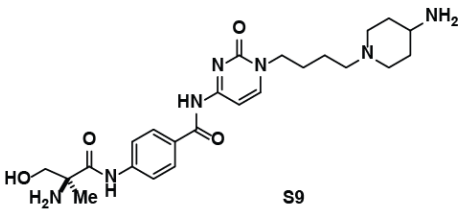
NH2
O
N
N
N
HN
O
O
HO
N
H
H2N
Me

S9

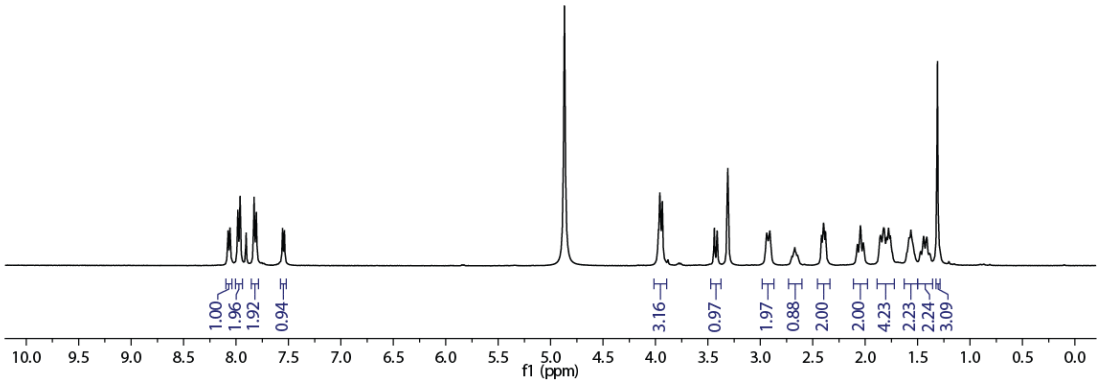
1.00
1.96
1.92
0.94
3.16
0.97
1.97
0.88
2.00
2.00
4.23
2.23
2.24
3.09
10.0 9.5 9.0 8.5 8.0 7.5 7.0 6.5 6.0 5.5 5.0 4.5 4.0 3.5 3.0 2.5 2.0 1.5 1.0 0.5 0.0
f1 (ppm)

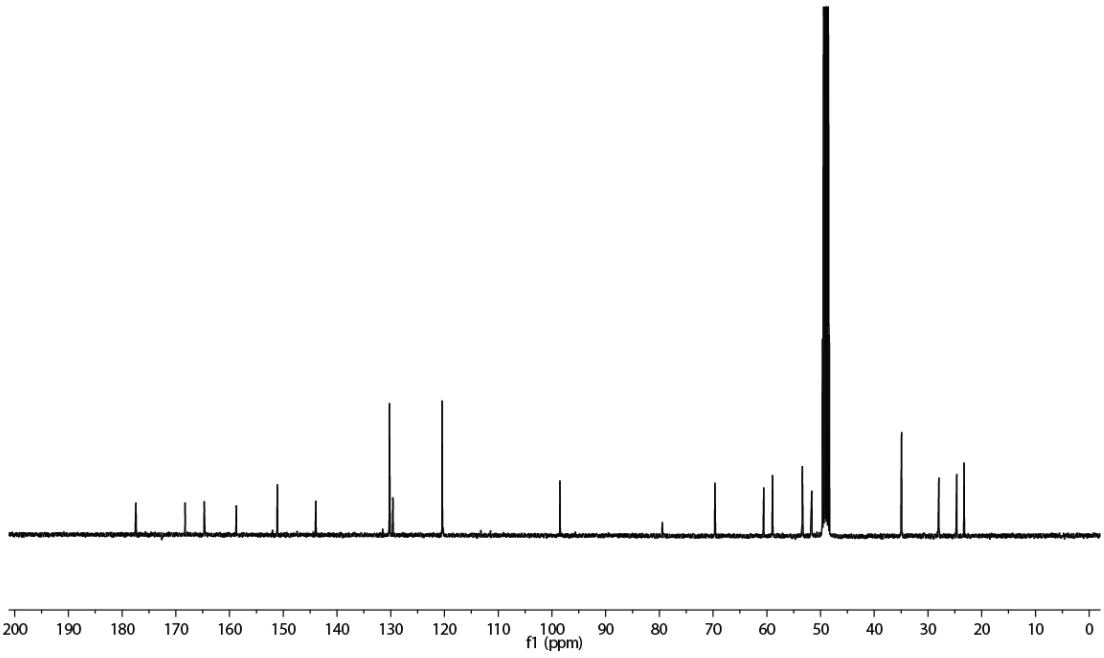
200 190 180 170 160 150 140 130 120 110 100 90 80 70 60 50 40 30 20 10 0
f1 (ppm)

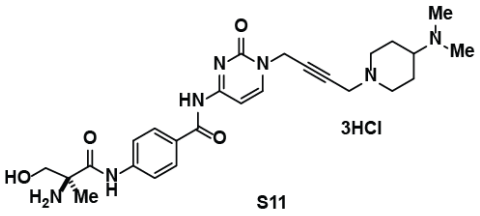
O
N
N
HN
O
Me
N
Me
N
3HCl
O
HO
N
H
H2N
Me

S11

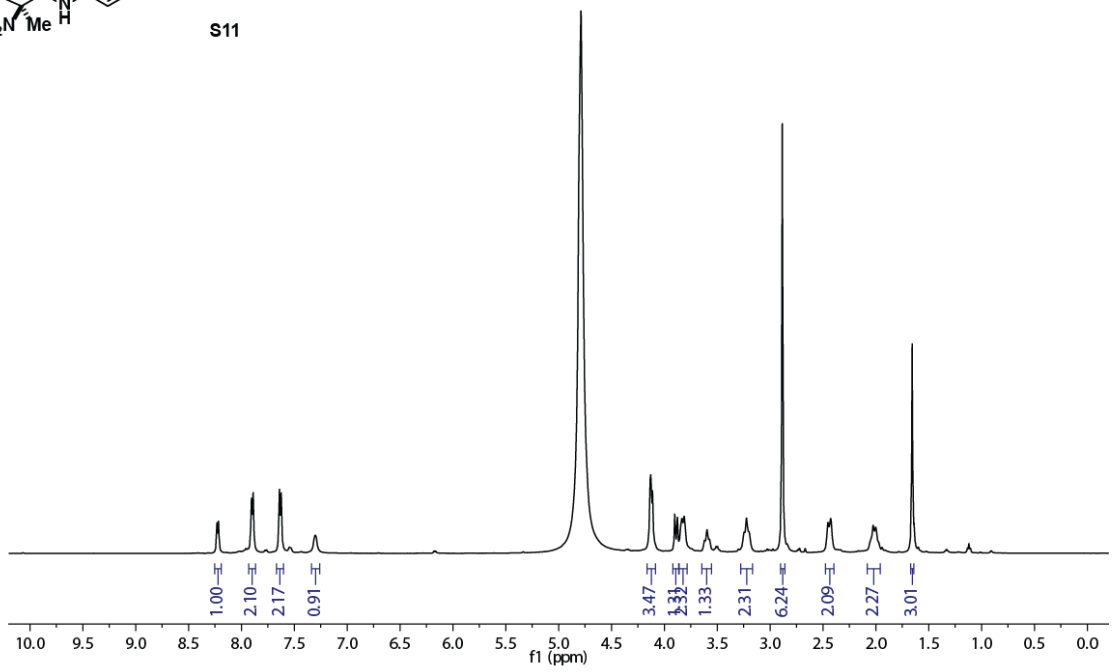
1.00
2.10
2.17
0.91
3.47
1.33
2.31
6.24
2.09
2.27
3.01
10.0 9.5 9.0 8.5 8.0 7.5 7.0 6.5 6.0 5.5 5.0 4.5 4.0 3.5 3.0 2.5 2.0 1.5 1.0 0.5 0.0
f1 (ppm)

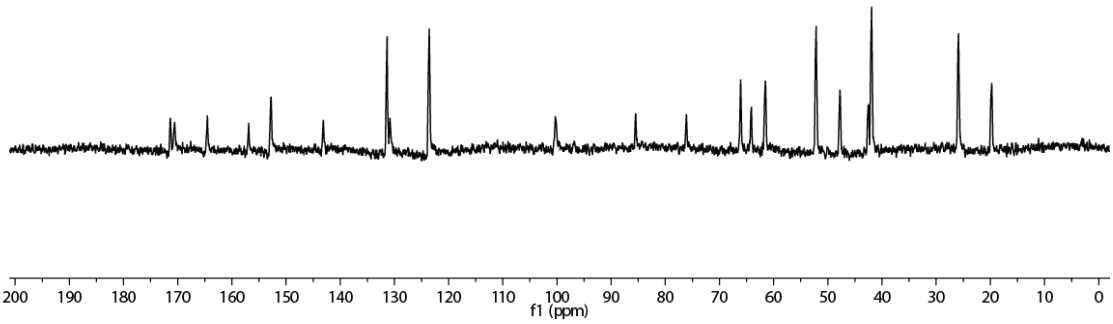
200 190 180 170 160 150 140 130 120 110 100 90 80 70 60 50 40 30 20 10 0
f1 (ppm)

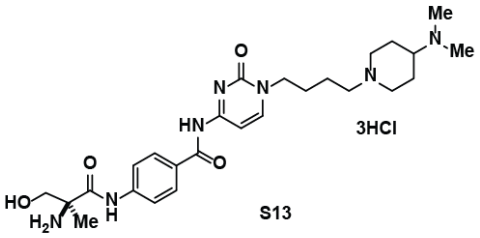
Me
N
Me
O
N
N
N
HN
3HCl
O
O
HO
N
H
H2N
Me

S13

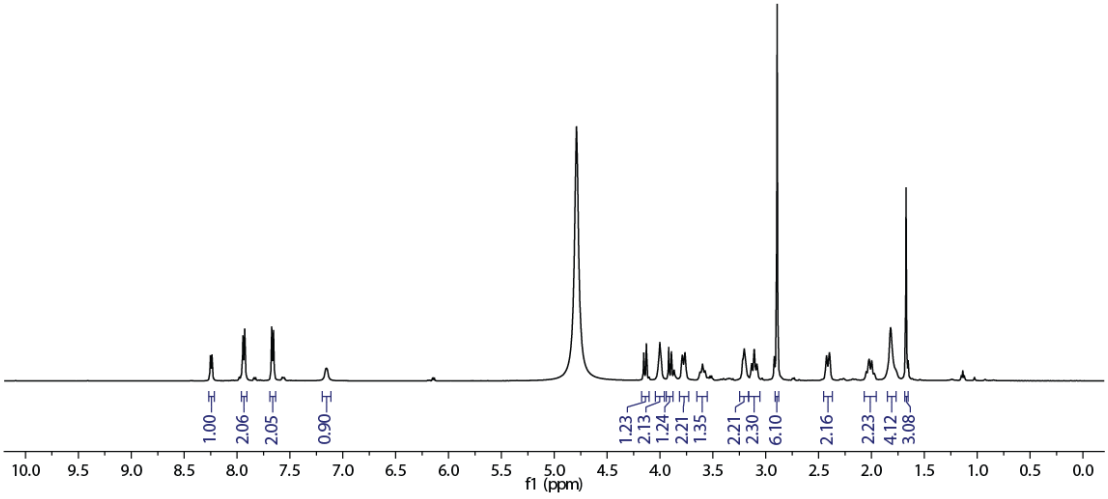
1.00
2.06
2.05
0.90
1.23
2.13
1.24
2.21
1.35
2.21
2.30
6.10
2.16
2.23
4.12
3.08
10.0 9.5 9.0 8.5 8.0 7.5 7.0 6.5 6.0 5.5 5.0 4.5 4.0 3.5 3.0 2.5 2.0 1.5 1.0 0.5 0.0
f1 (ppm)

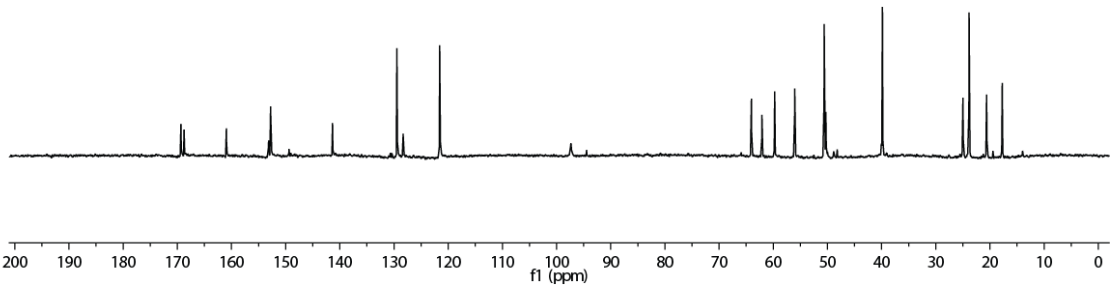
200 190 180 170 160 150 140 130 120 110 100 90 80 70 60 50 40 30 20 10 0
f1 (ppm)

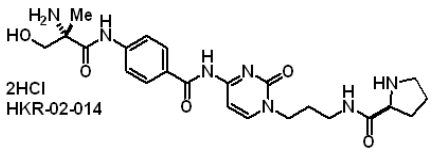
2HCl
HKR-02-014

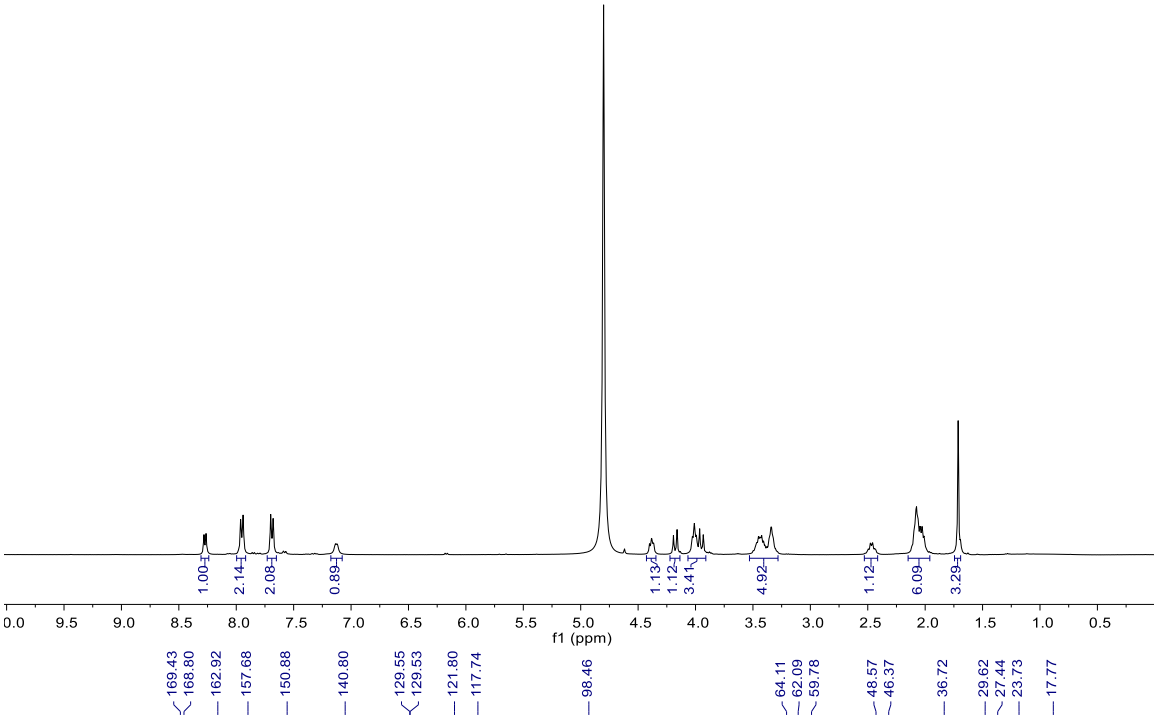
1.00
2.14
2.08
0.89
1.13
1.12
3.44
4.92
1.12
6.09
3.29
f1 (ppm)
169.43
168.80
162.92
157.68
150.88
140.80
129.55
129.53
121.80
117.74
98.46
64.11
62.09
59.78
48.57
46.37
36.72
29.62
27.44
23.73
17.77

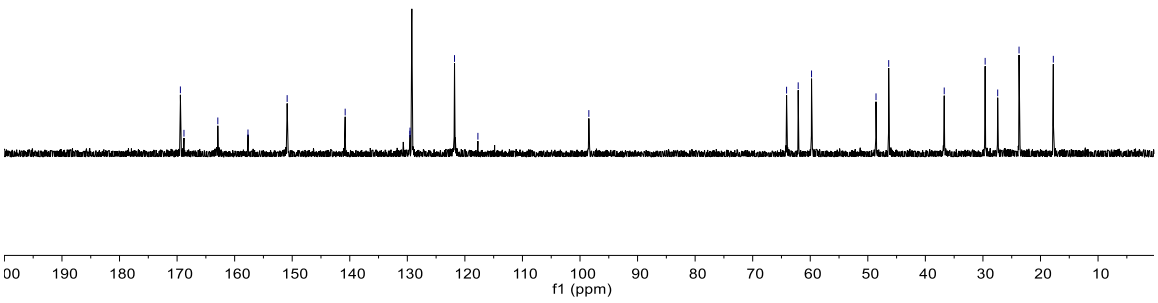
f1 (ppm)

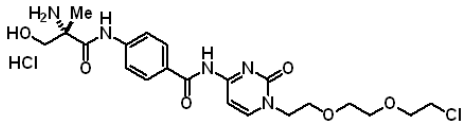
H2N
Me
H
HO
HCl
O
N
H
N
O
N
O
O
N
O
O
Cl

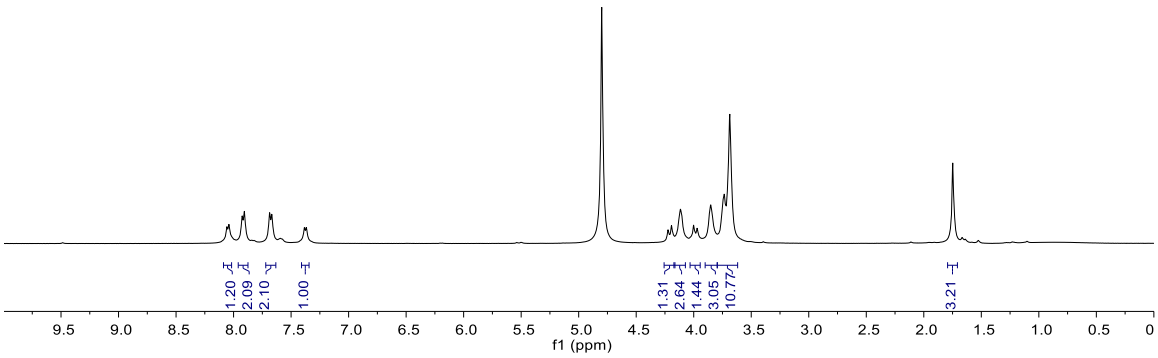
1.20
2.09
2.10
1.00
1.31
2.64
1.44
3.05
10.77
3.21
9.5 9.0 8.5 8.0 7.5 7.0 6.5 6.0 5.5 5.0 4.5 4.0 3.5 3.0 2.5 2.0 1.5 1.0 0.5 0
f1 (ppm)

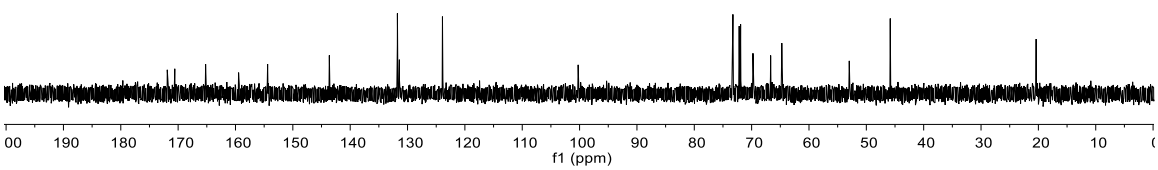
00 190 180 170 160 150 140 130 120 110 100 90 80 70 60 50 40 30 20 10
f1 (ppm)

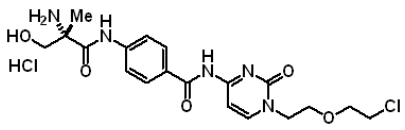
H2N
Me
H
N
HO
HCl
O
H
N
N
O
O
N
O
O
Cl

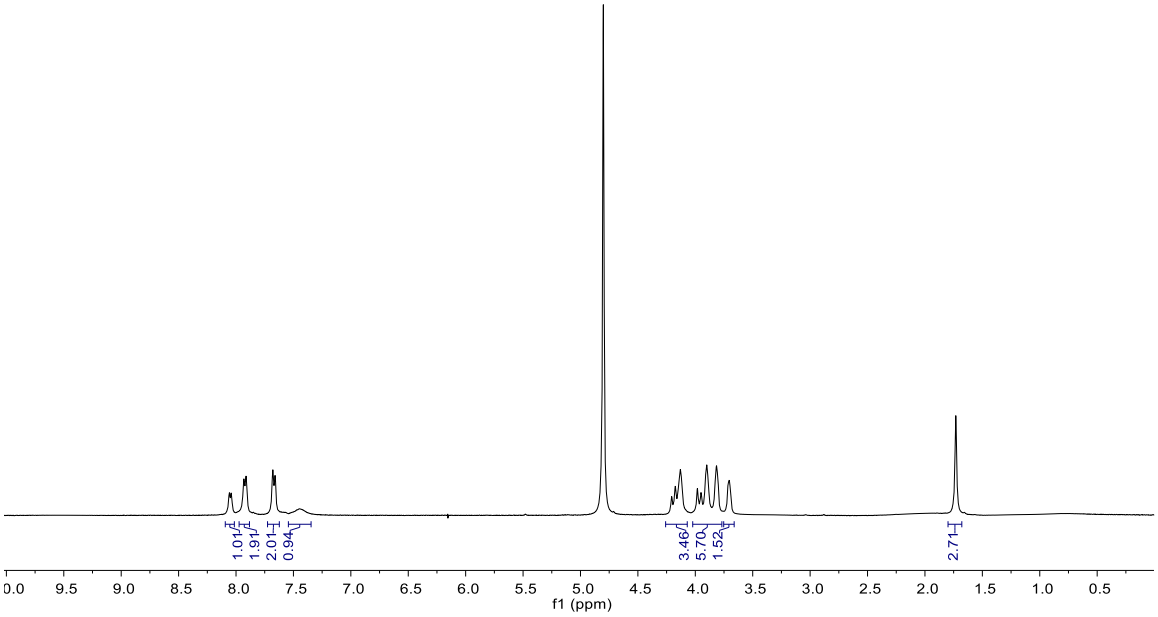
1.01
1.91
2.01
0.94
3.46
5.70
1.52
2.71
f1 (ppm)

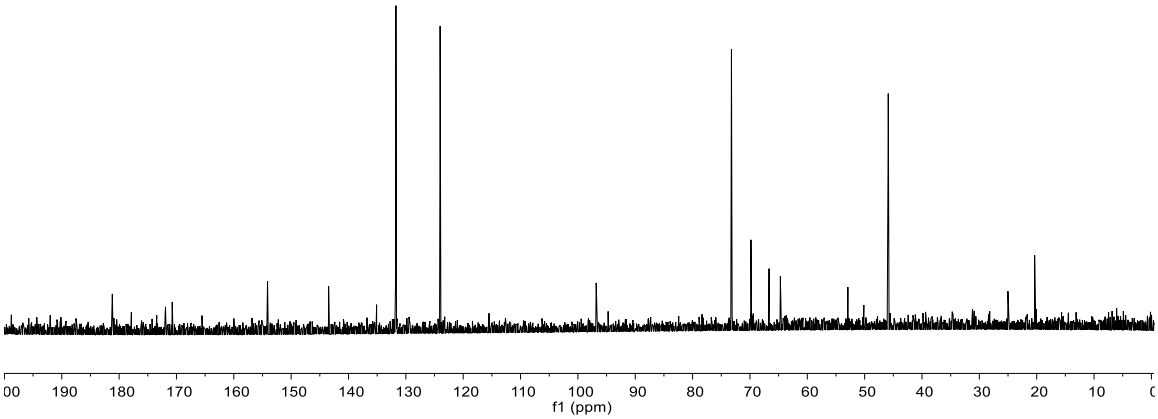
f1 (ppm)

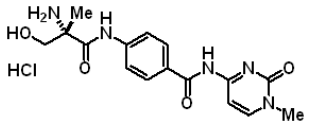

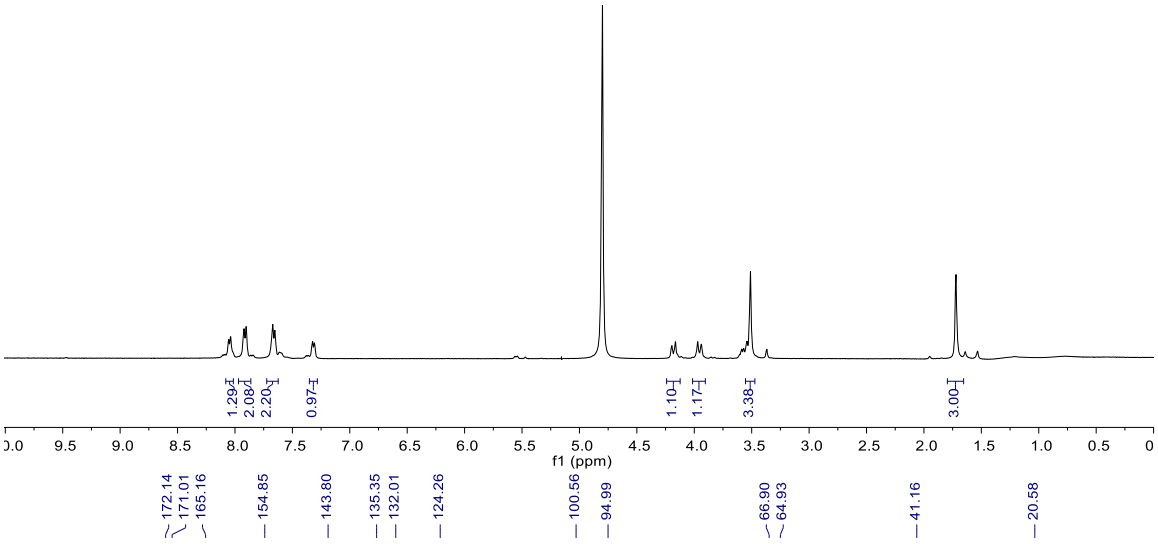

172.14
171.01
165.16
154.85
143.80
135.35
132.01
124.26
100.56
94.99
66.90
64.93
41.16
20.58

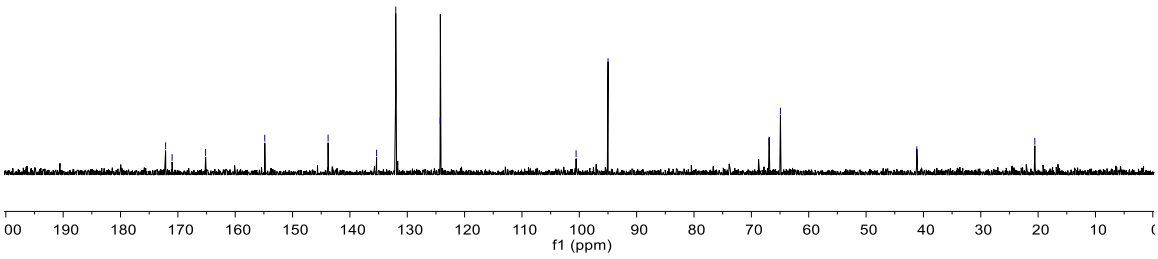

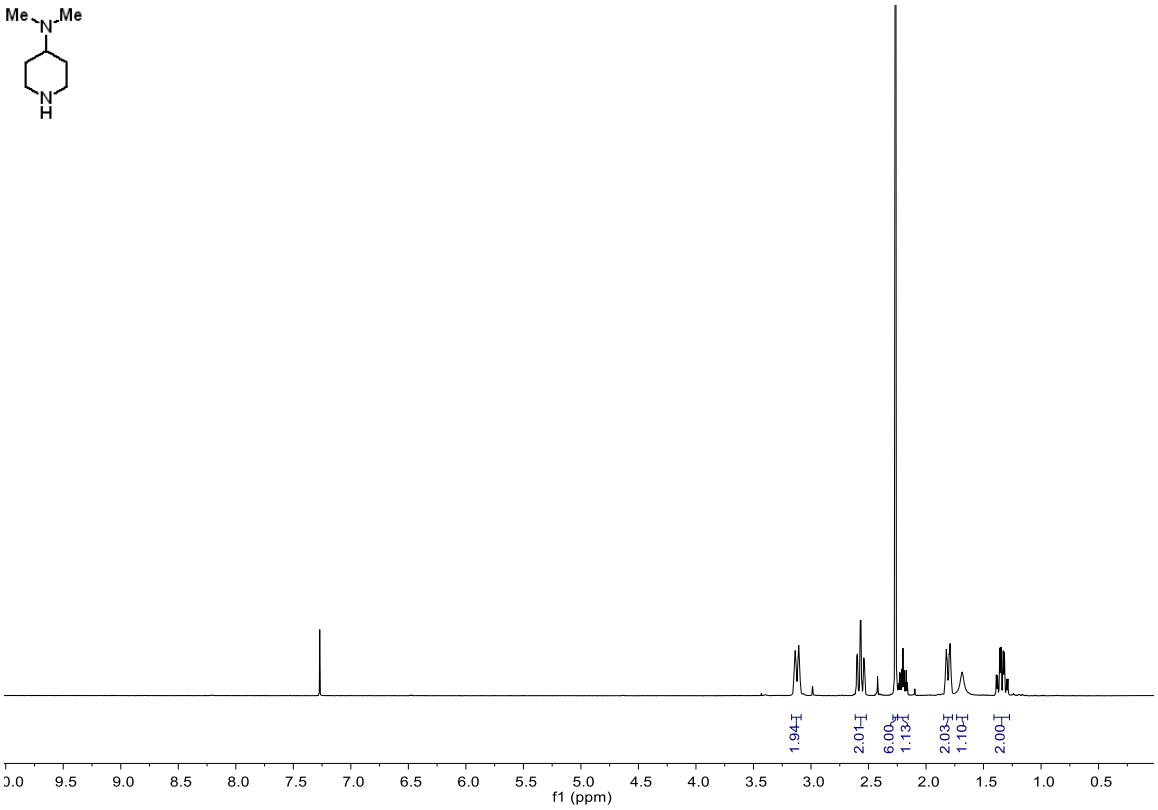
Me
N
Me
N
H
1.94
2.01
6.00
1.13
2.03
1.10
2.00
f1 (ppm)

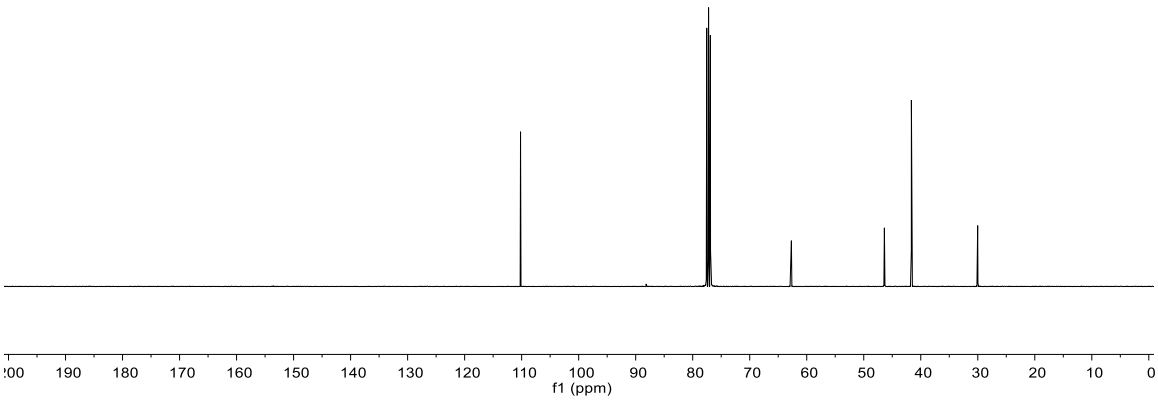
f1 (ppm)

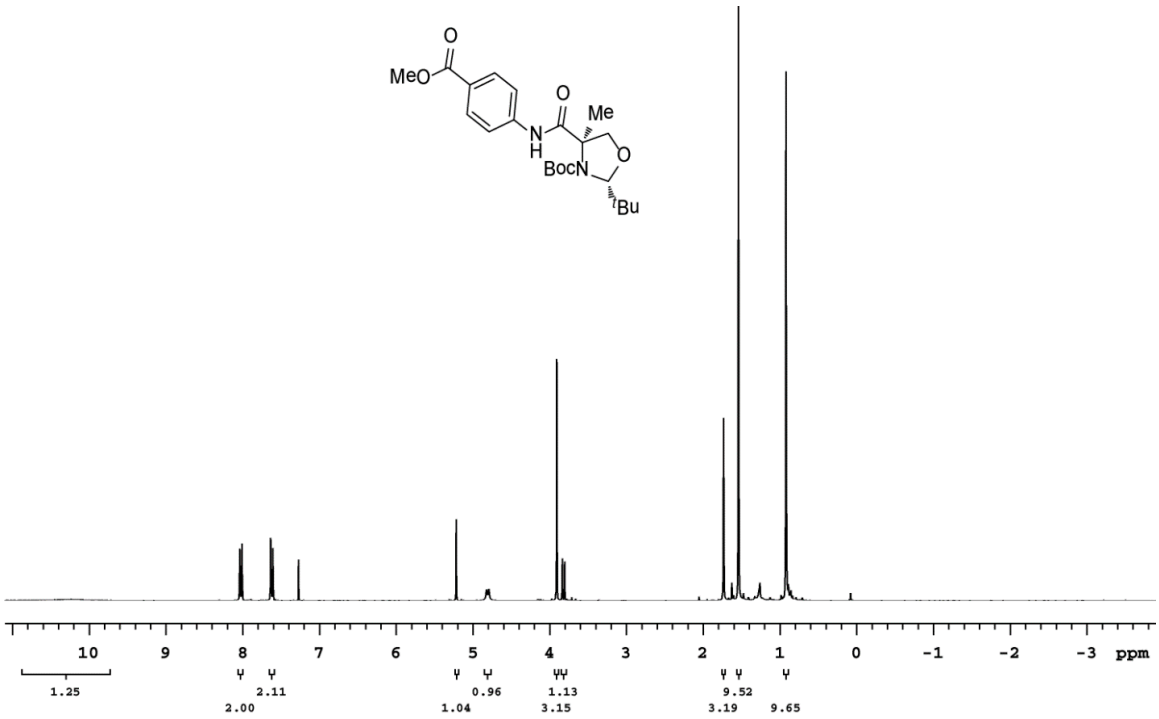
MeO
O
O
N
H
Me
BocN
O
tBu
10
9
8
7
6
5
4
3
2
1
0
-1
-2
-3
ppm
1.25
2.00
2.11
1.04
0.96
3.15
1.13
3.19
9.52
9.65

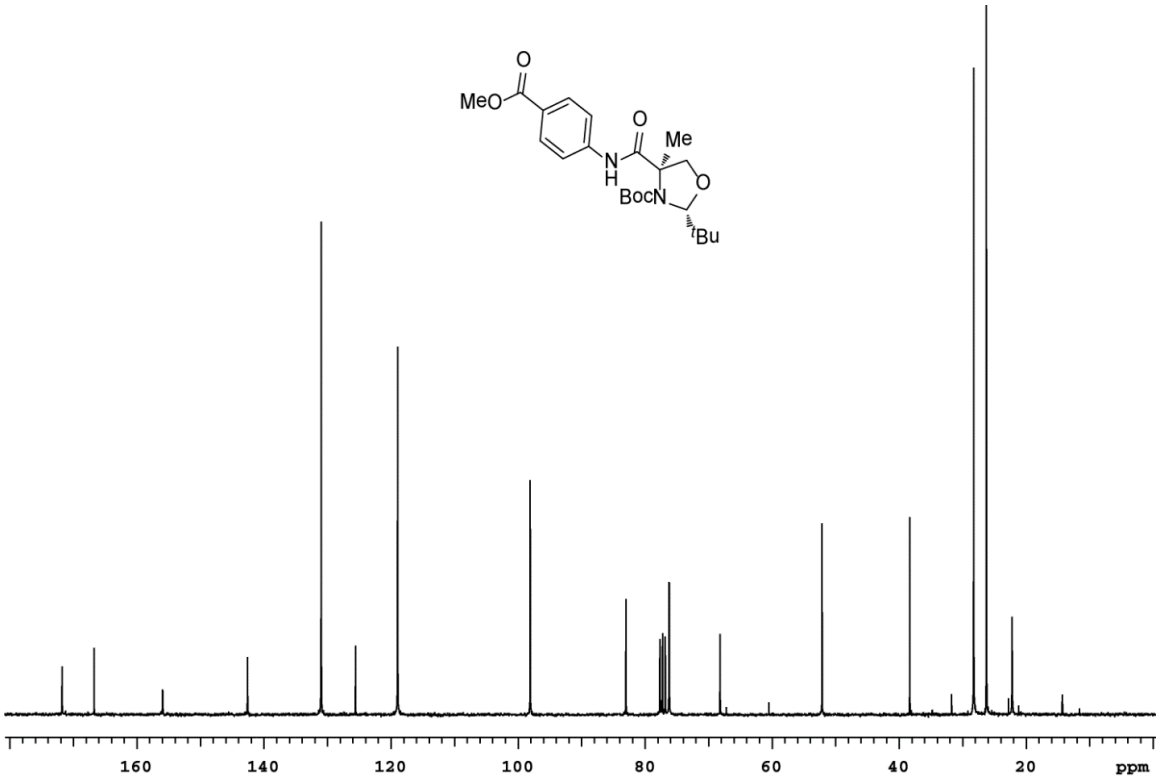
MeO
O
O
N
H
Me
BocN
O
tBu
160
140
120
100
80
60
40
20
ppm

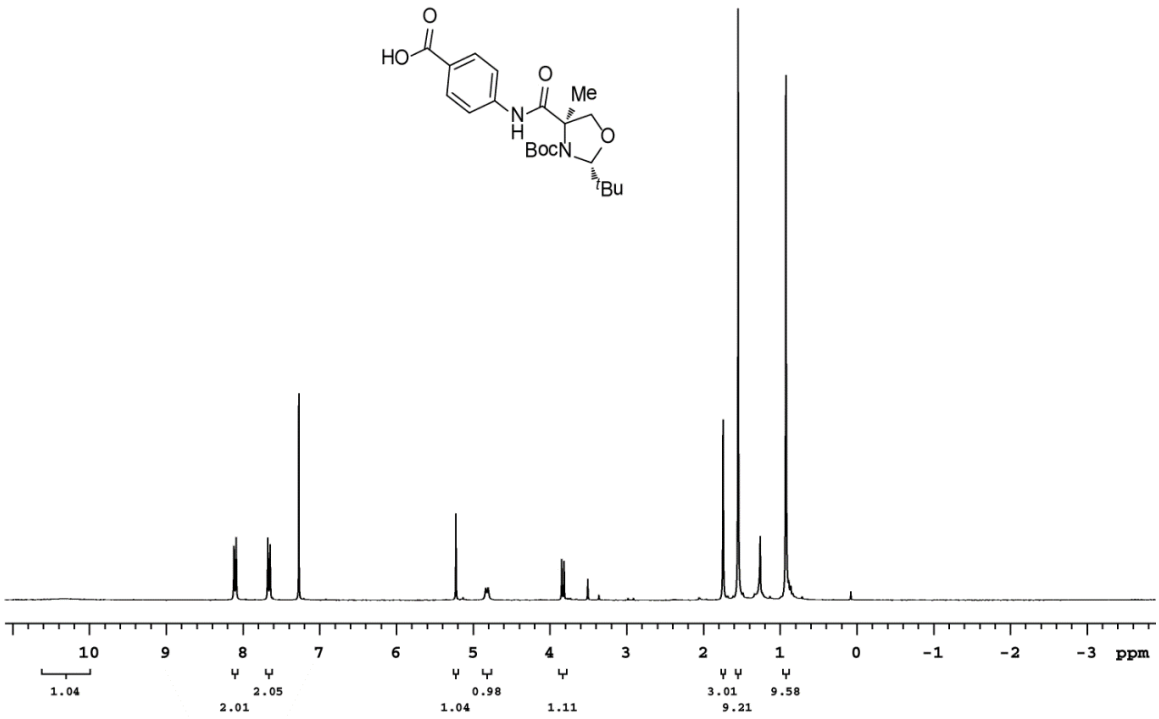
HO
O
N
H
O
Me
BocN
O
tBu
10
9
8
7
6
5
4
3
2
1
0
-1
-2
-3
ppm
1.04
2.01
2.05
1.04
0.98
1.11
3.01
9.21
9.58

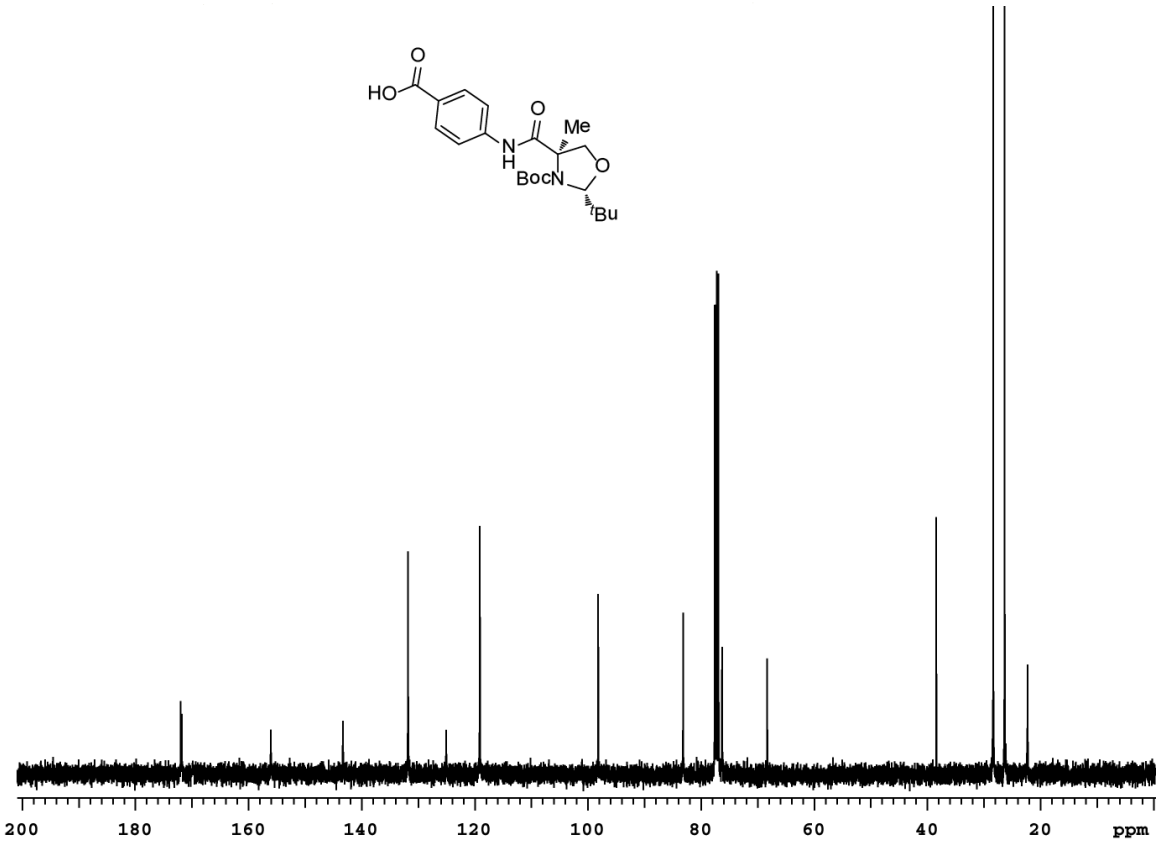
HO
O
N
H
O
Me
BocN
O
tBu
200
180
160
140
120
100
80
60
40
20
ppm

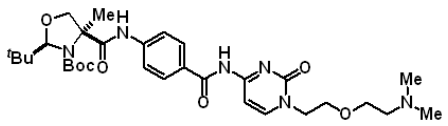
Me
H
N
O
tBu
N
Boc
O
H
N
N
O
O
N
Me
O
N
Me

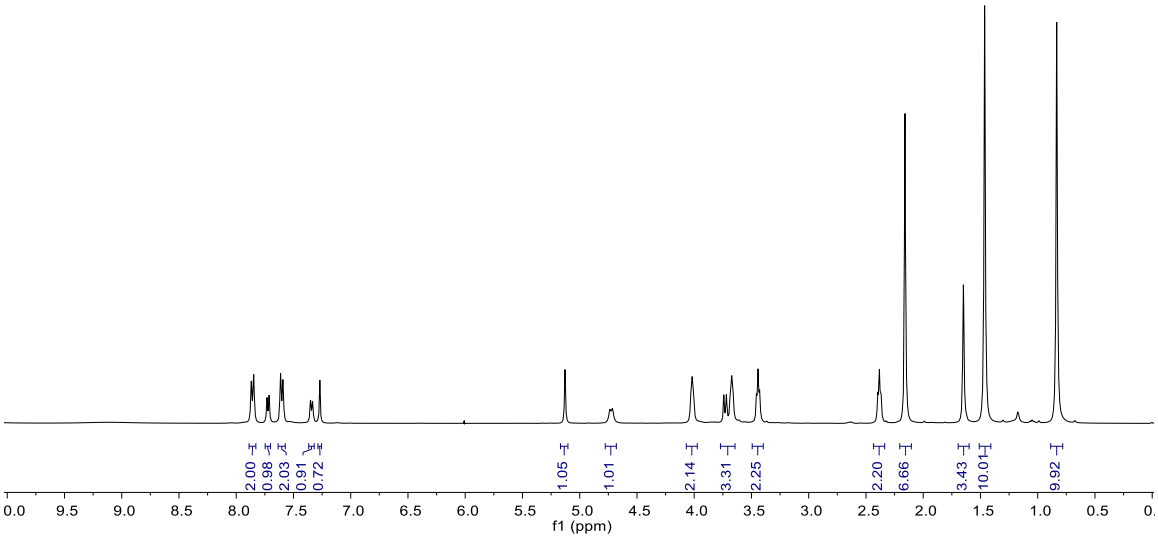
2.00
0.98
2.03
0.91
0.72
1.05
1.01
2.14
3.31
2.25
2.20
6.66
3.43
10.01
9.92
f1 (ppm)

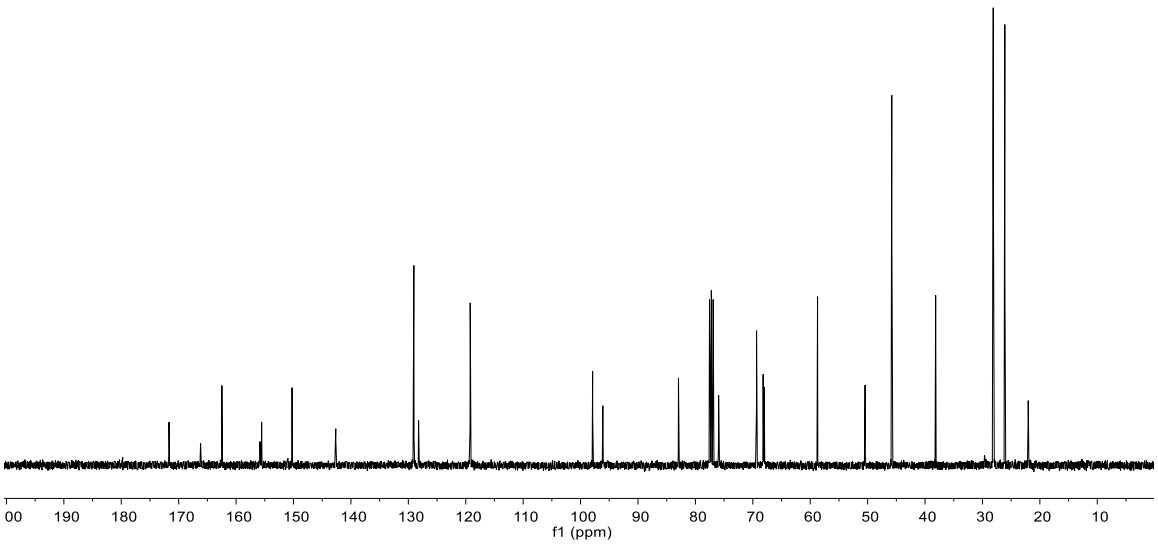
f1 (ppm)

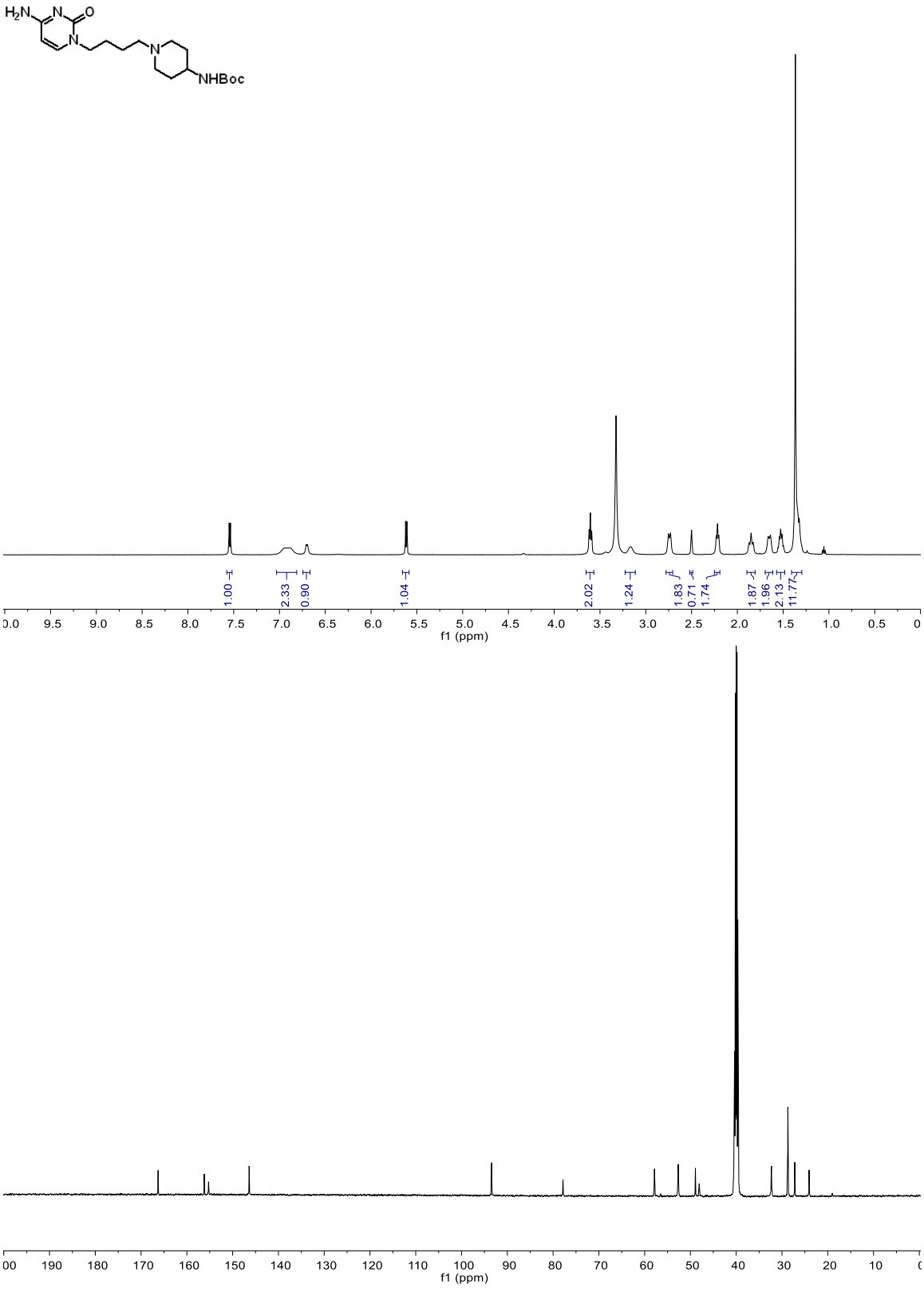
NHBoc
1.00
2.33
0.90
1.04
2.02
1.24
1.83
0.71
1.74
1.87
1.96
2.13
11.77
f1 (ppm)
f1 (ppm)

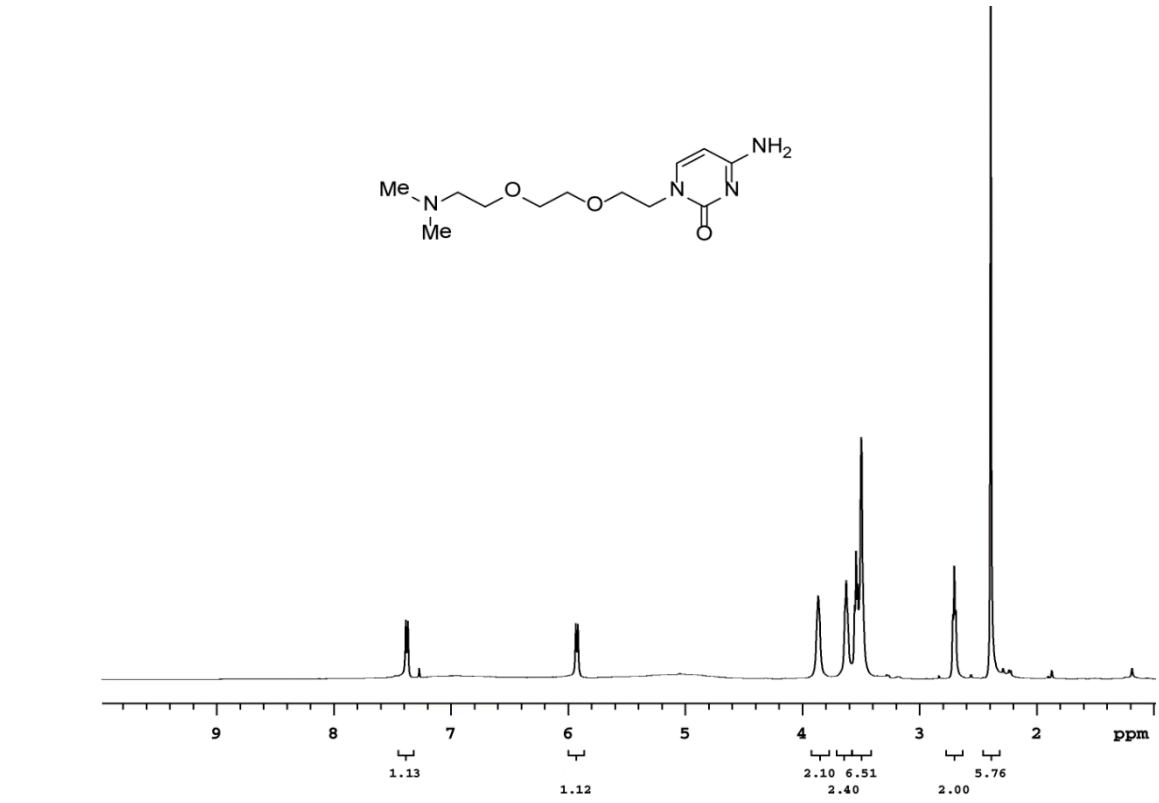
NH2
Me
N
Me
O
O
N
N
O
9
8
7
6
5
4
3
2
ppm
1.13
1.12
2.10
6.51
2.40
2.00
5.76

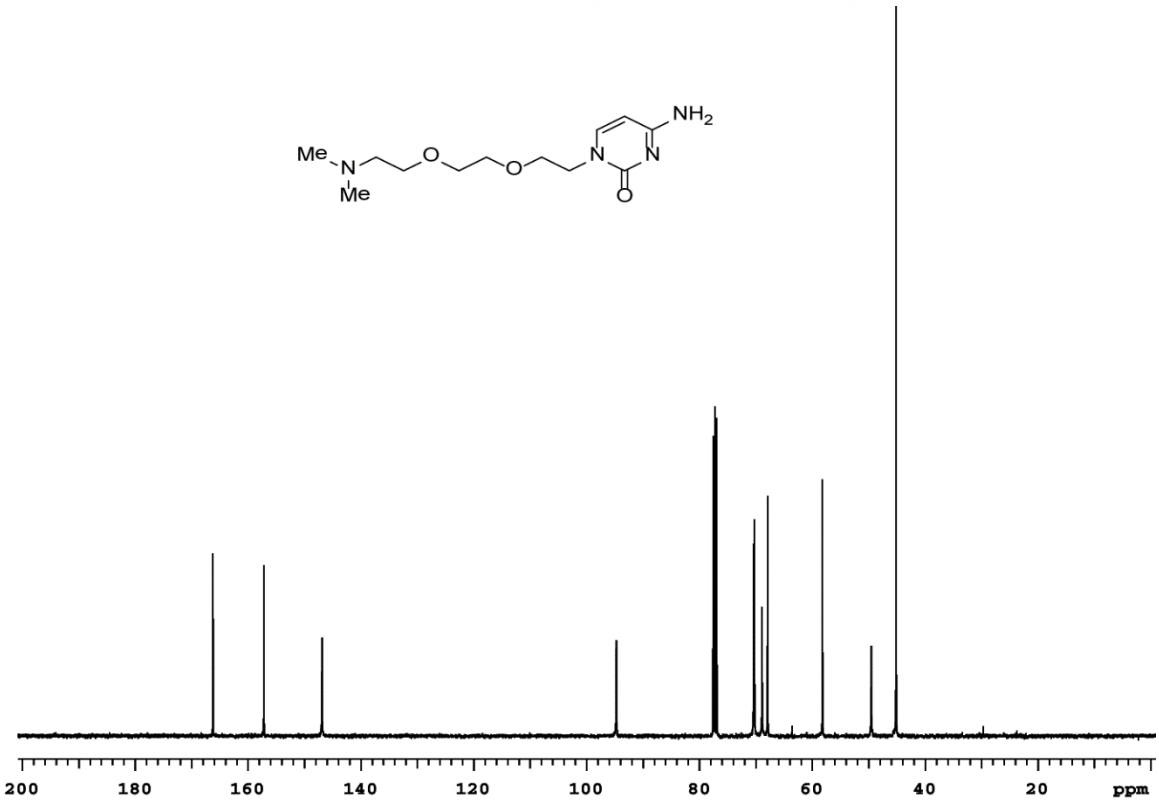
NH2
Me
N
Me
O
O
N
N
O
200
180
160
140
120
100
80
60
40
20
ppm

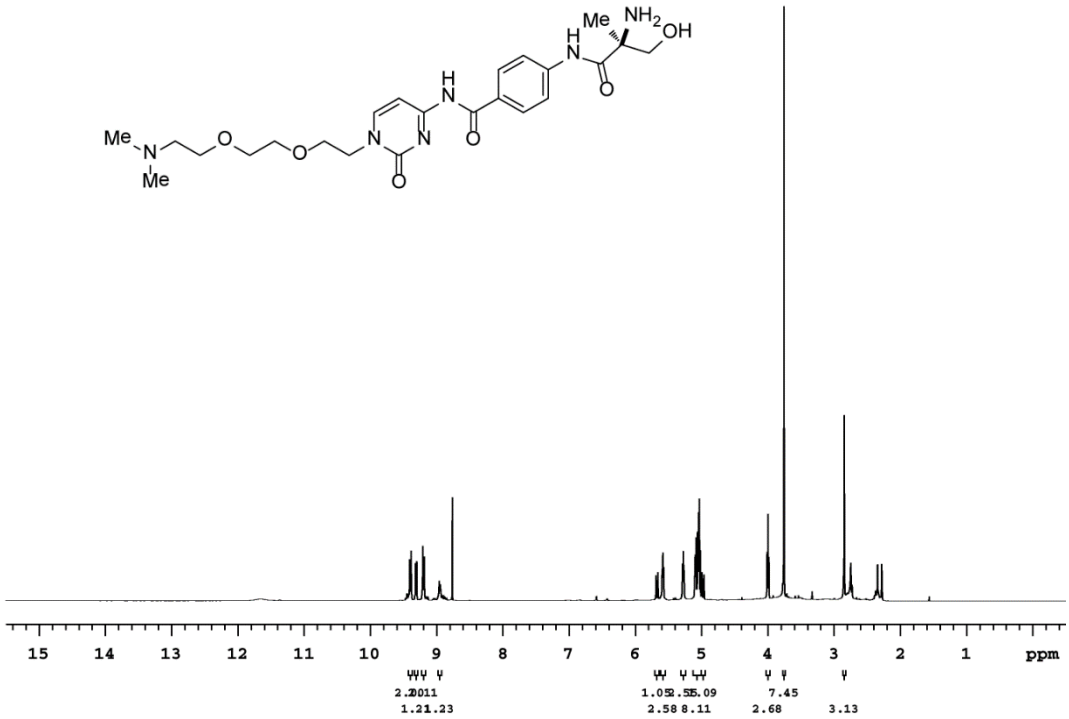
Me
NH2
OH
H
N
O
Me
N
Me
O
O
N
N
H
N
O
O
15 14 13 12 11 10 9 8 7 6 5 4 3 2 1 ppm
2.20 11 1.21 1.23
1.05 2.55 5.09
2.58 8.11
7.45
2.68
3.13

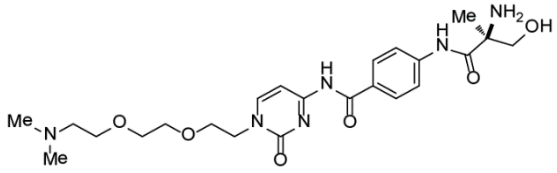
Me
NH2
OH
H
N
O
Me
N
Me
O
O
N
N
H
N
O
O

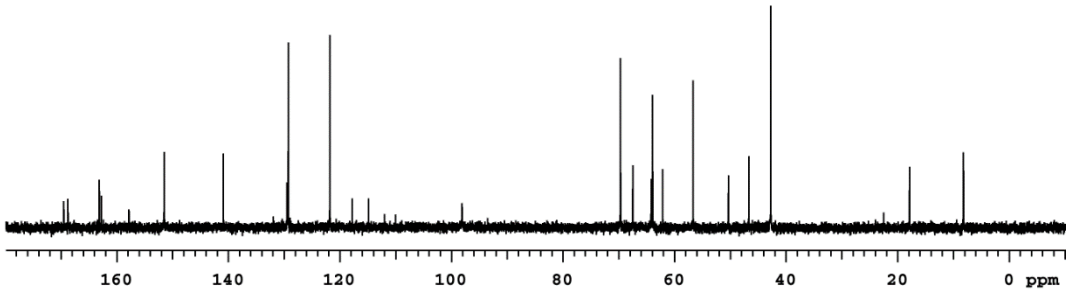
160 140 120 100 80 60 40 20 0 ppm

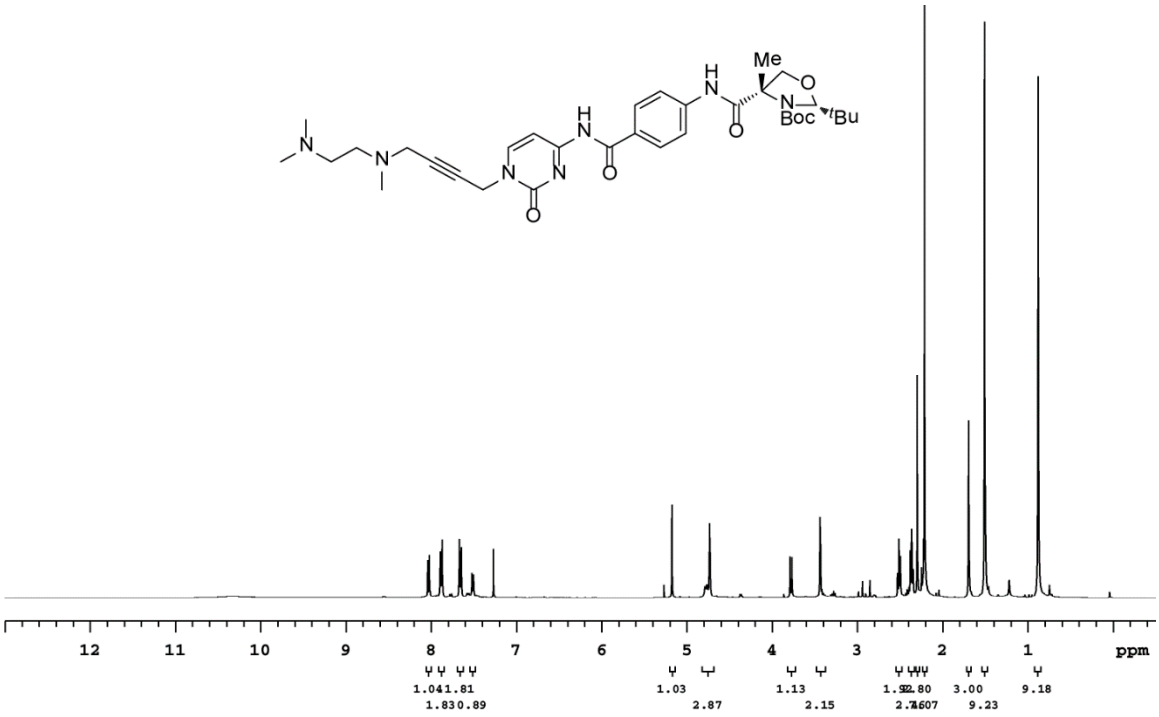
Me
H
N
O
N
Boc
tBu
H
N
O
N
N
O
N
N
12
11
10
9
8
7
6
5
4
3
2
1
ppm
1.04
1.81
1.83
0.89
1.03
2.87
1.13
2.15
2.80
3.00
9.18

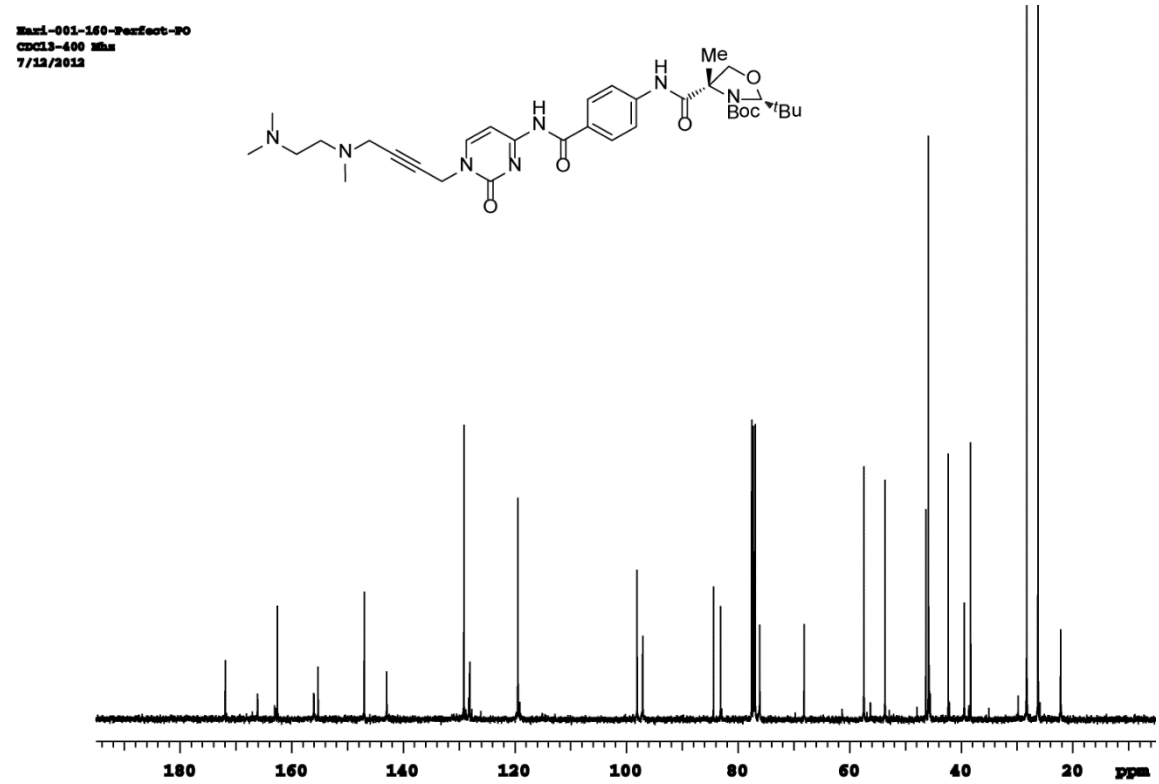
Hari-001-160-Perfect-PO
CDCl3-400 Mhz
7/12/2012
Me
H
N
O
N
Boc
tBu
H
N
O
N
N
O
N
180
160
140
120
100
80
60
40
20
ppm

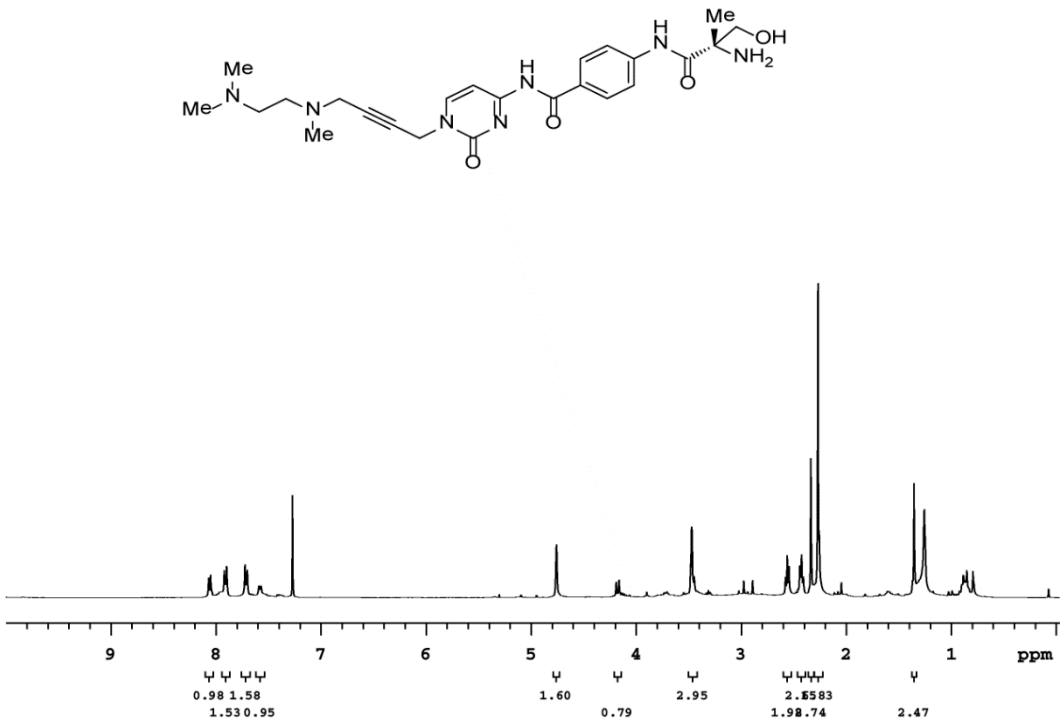
Me
OH
NH2
Me
N
Me
N
Me
H
N
H
N
N
N
O
O
O
9
8
7
6
5
4
3
2
1
ppm
0.98 1.58
1.53 0.95
1.60
0.79
2.95
1.98 8.74
2.47

APPENDIX B

^{1}H, ^{13}C SPECTRA CHAPTER 3

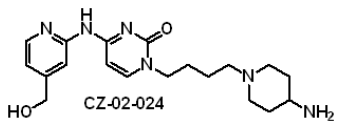
HO
CZ-02-024
NH2

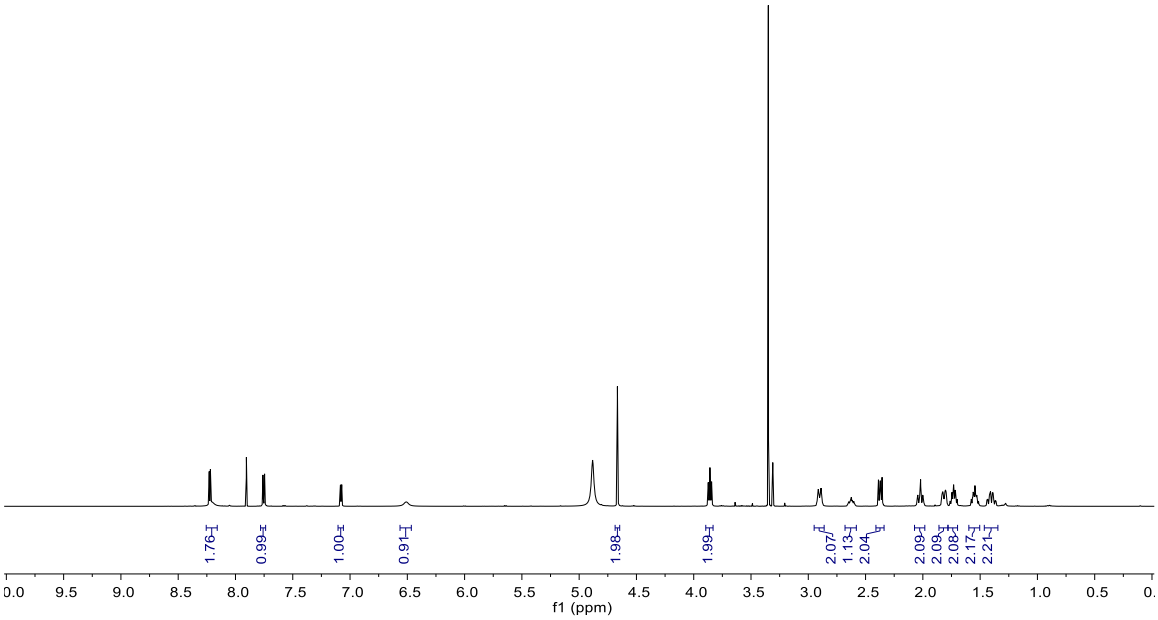
1.76
0.99
1.00
0.91
1.98
1.99
2.07
1.13
2.04
2.09
2.09
2.08
2.17
2.21
f1 (ppm)

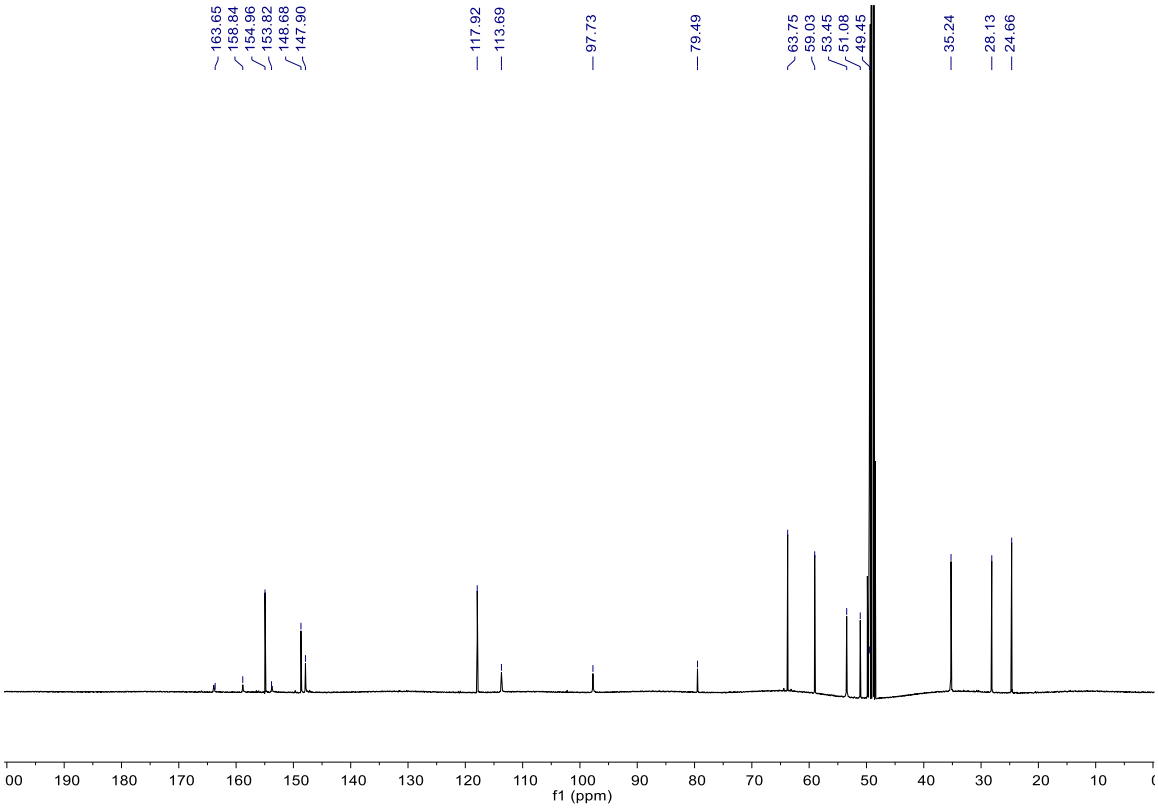
163.65
158.84
154.96
153.82
148.68
147.90
117.92
113.69
97.73
79.49
63.75
59.03
53.45
51.08
49.45
35.24
28.13
24.66
f1 (ppm)

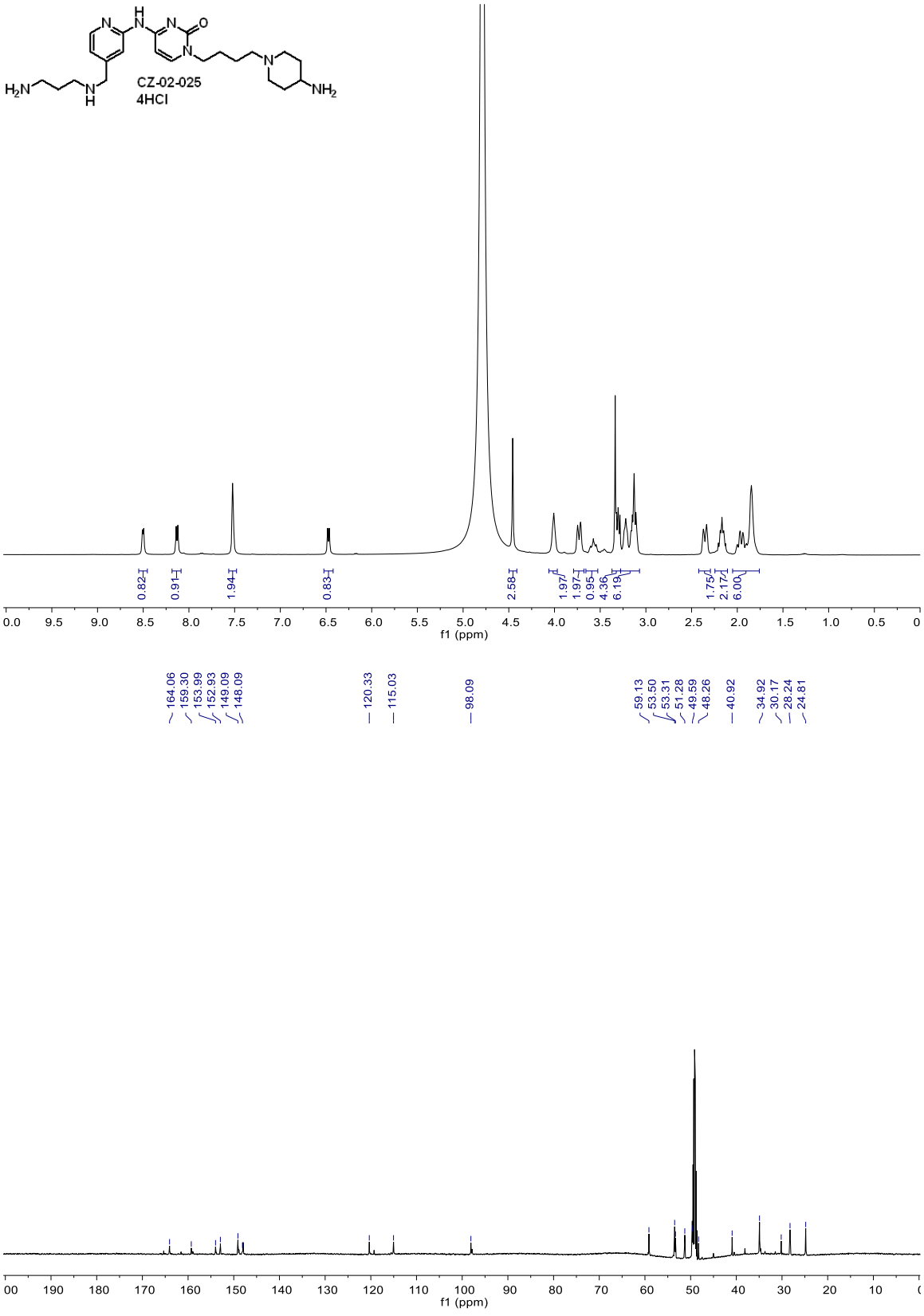
CZ-02-025
4HCl
0.82
0.91
1.94
0.83
2.58
1.97
1.97
0.95
4.36
6.19
1.75
2.17
6.00
f1 (ppm)
164.06
159.30
153.99
152.93
149.09
148.09
120.33
115.03
98.09
59.13
53.50
53.31
51.28
49.59
48.26
40.92
34.92
30.17
28.24
24.81
f1 (ppm)

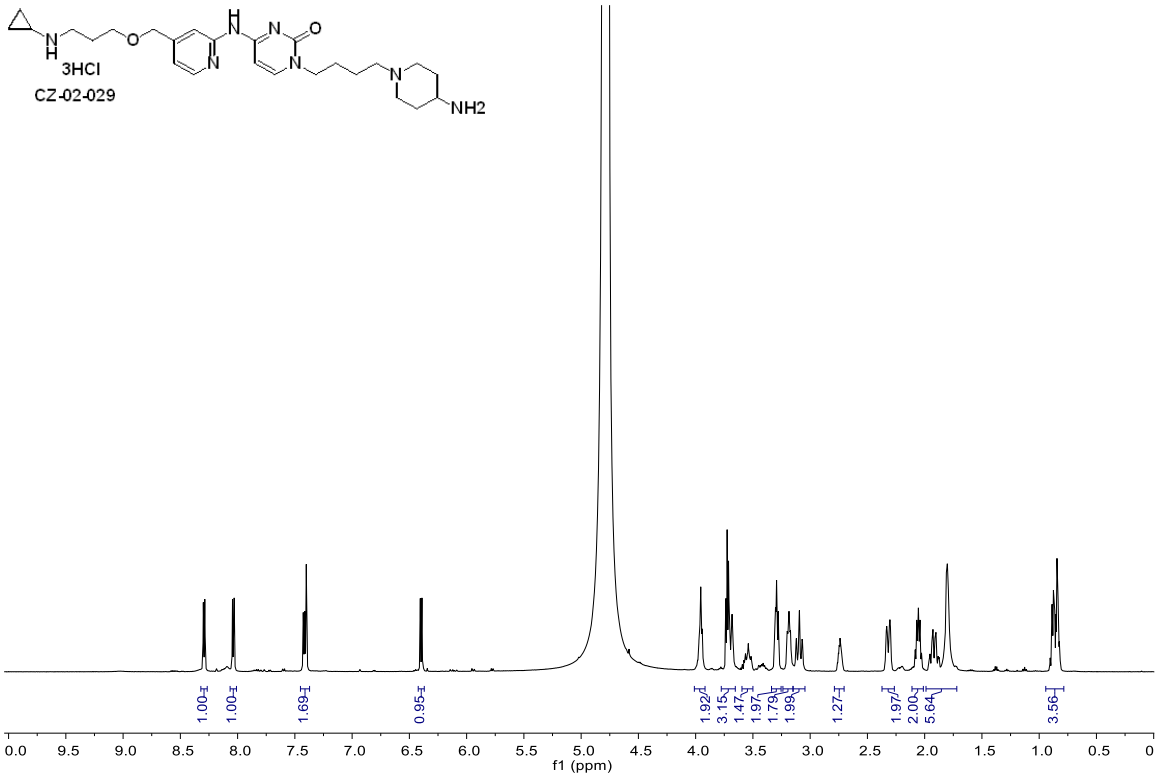
3HCl
CZ-02-029
NH2
1.00
1.00
1.69
0.95
1.92
3.15
1.47
1.97
1.79
1.99
1.27
1.97
2.00
5.64
3.56
f1 (ppm)

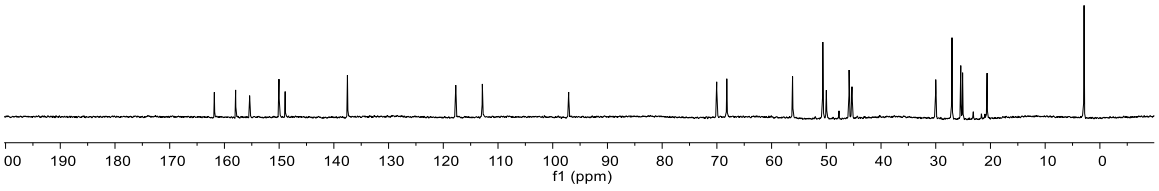
f1 (ppm)

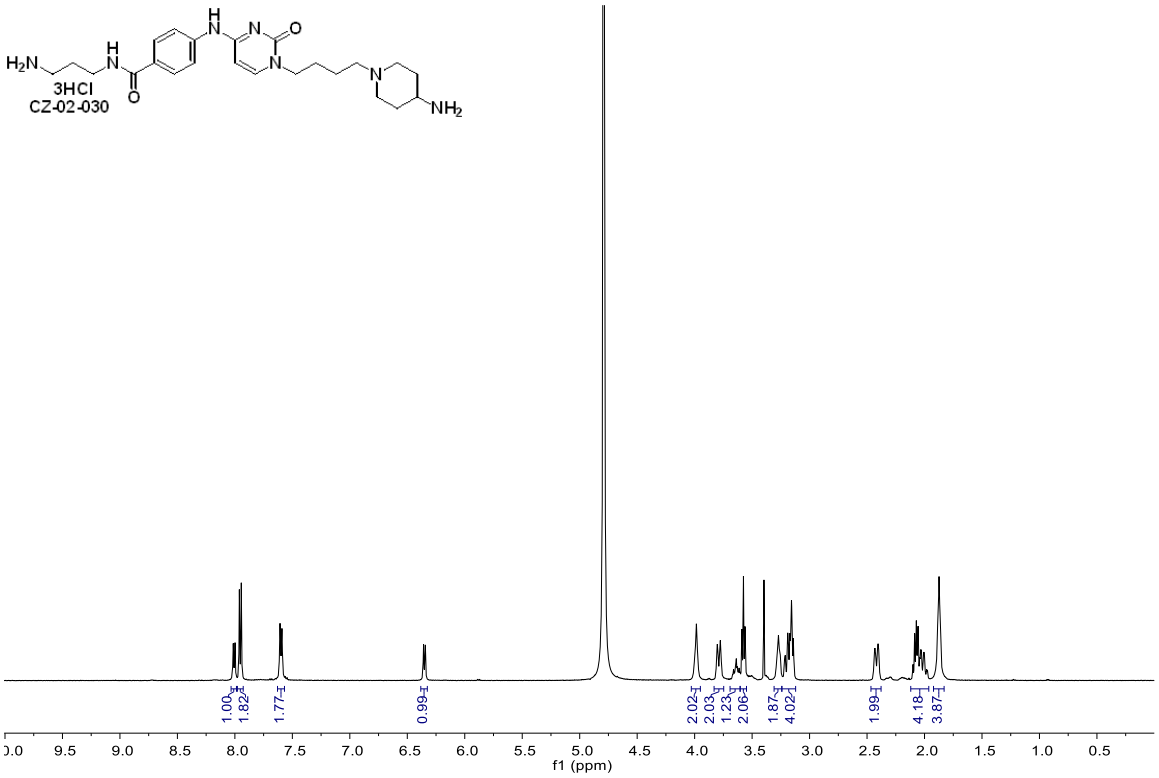
3HCl
CZ-02-030
1.00
1.82
1.77
0.99
2.02
2.03
1.23
2.06
1.87
4.02
1.99
4.18
3.87
f1 (ppm)

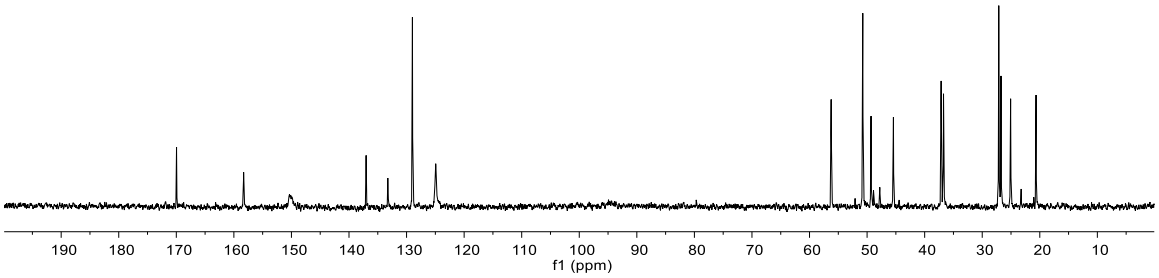
f1 (ppm)

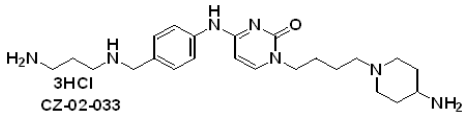
3HCl
CZ-02-033

2.86
2.03
1.00
2.21
1.80
1.29
2.08
1.94
2.90
2.13
2.16
2.20
4.11
2.26
2.33
f1 (ppm)

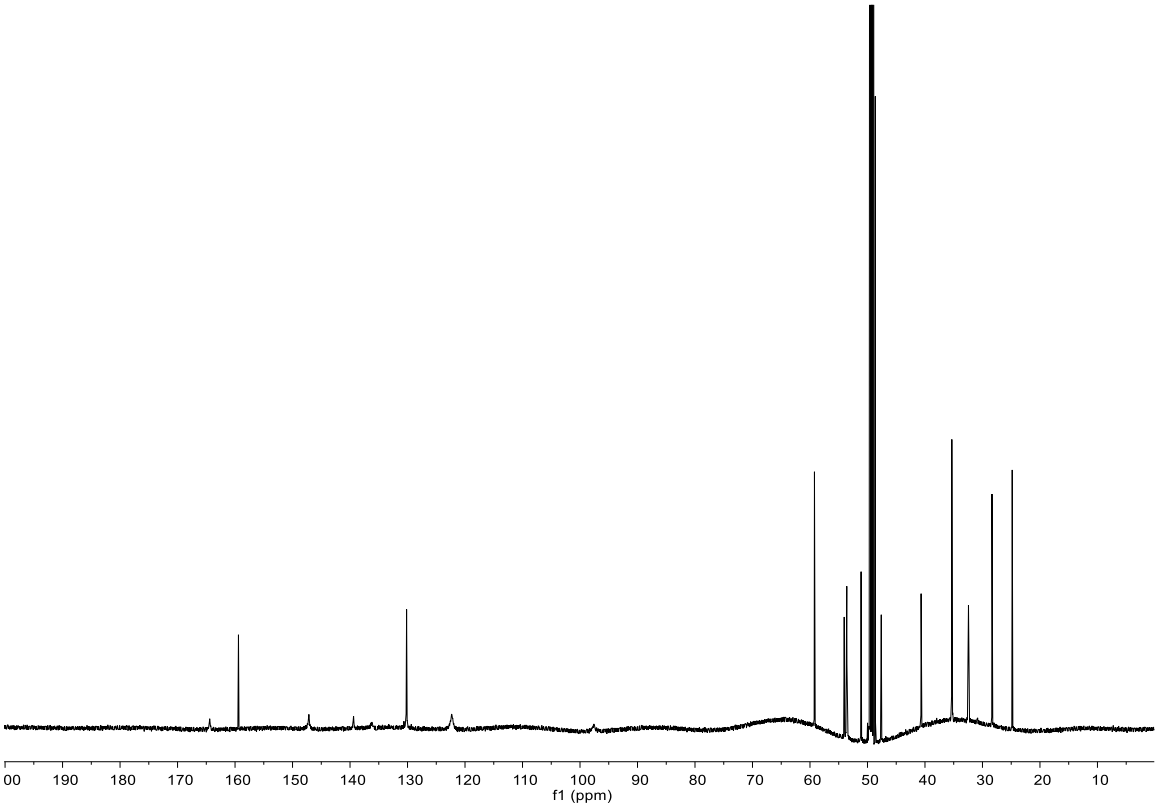
f1 (ppm)

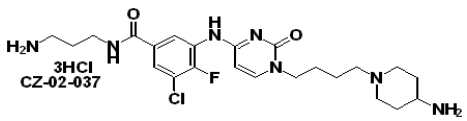
3HCl
CZ-02-037

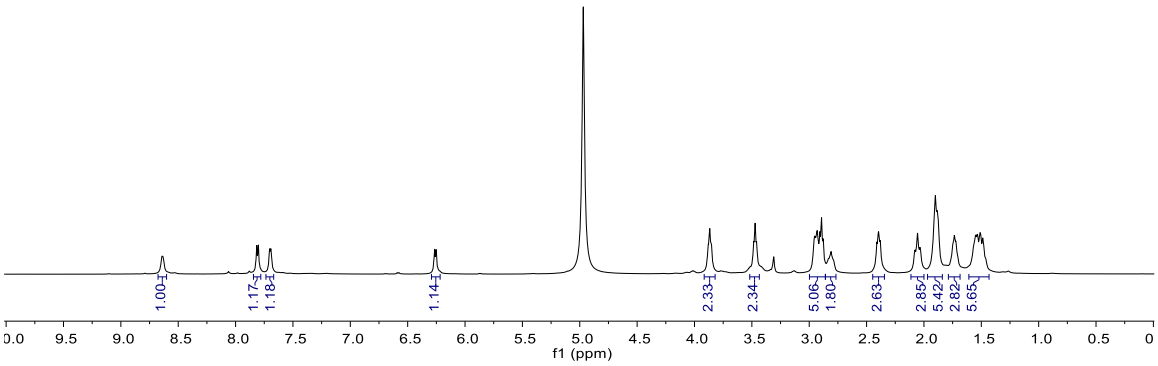
1.00
1.17
1.18
1.14
2.33
2.34
5.06
1.80
2.63
2.85
5.42
2.82
5.65
f1 (ppm)

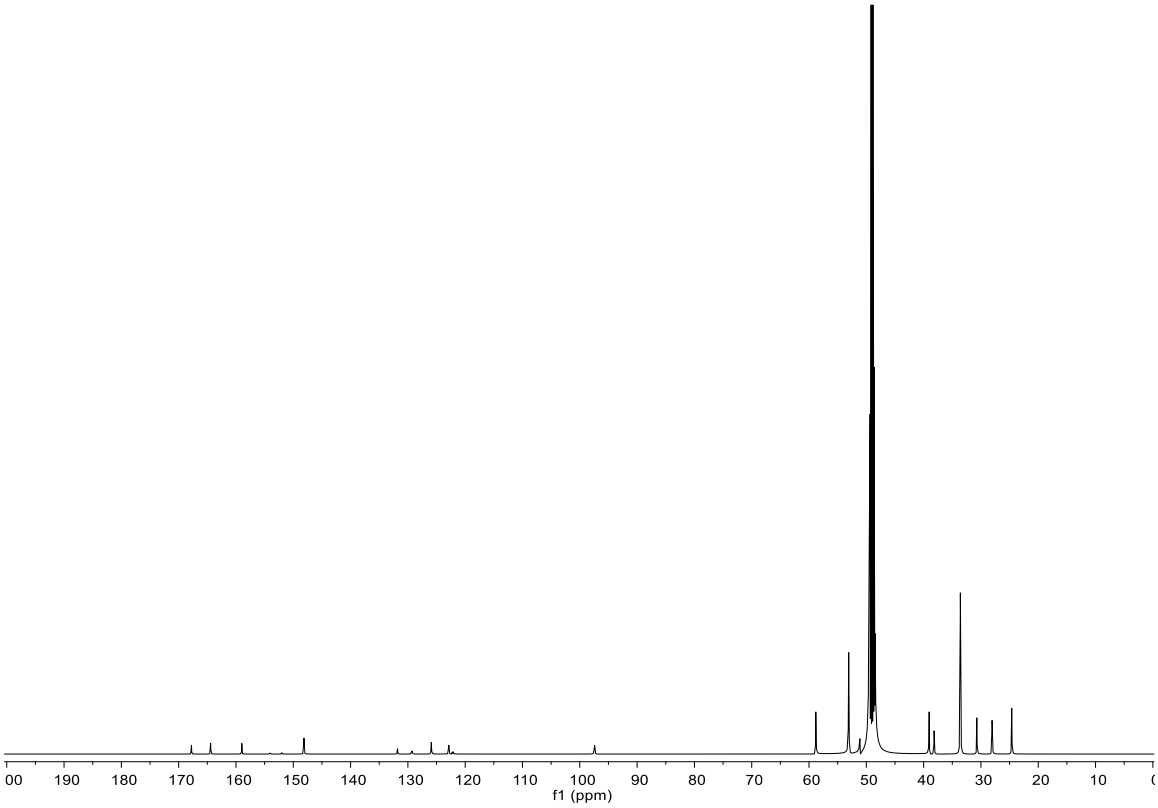
f1 (ppm)

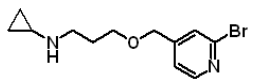
N
H
O
Br
N

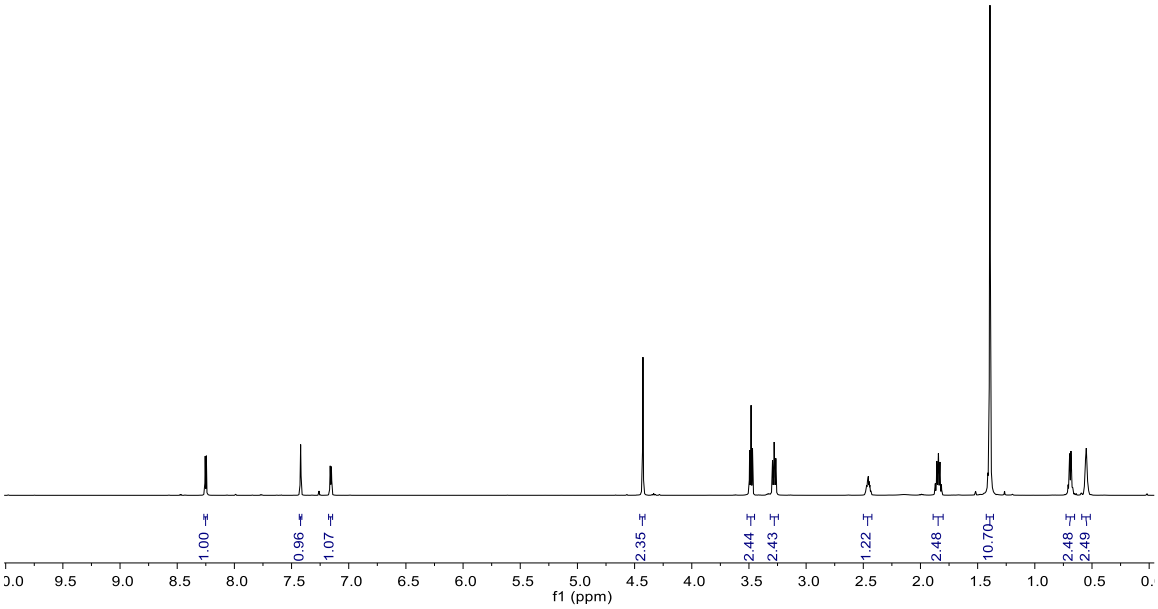
1.00
0.96
1.07
2.35
2.44
2.43
1.22
2.48
10.70
2.48
2.49
9.5 9.0 8.5 8.0 7.5 7.0 6.5 6.0 5.5 5.0 4.5 4.0 3.5 3.0 2.5 2.0 1.5 1.0 0.5
f1 (ppm)

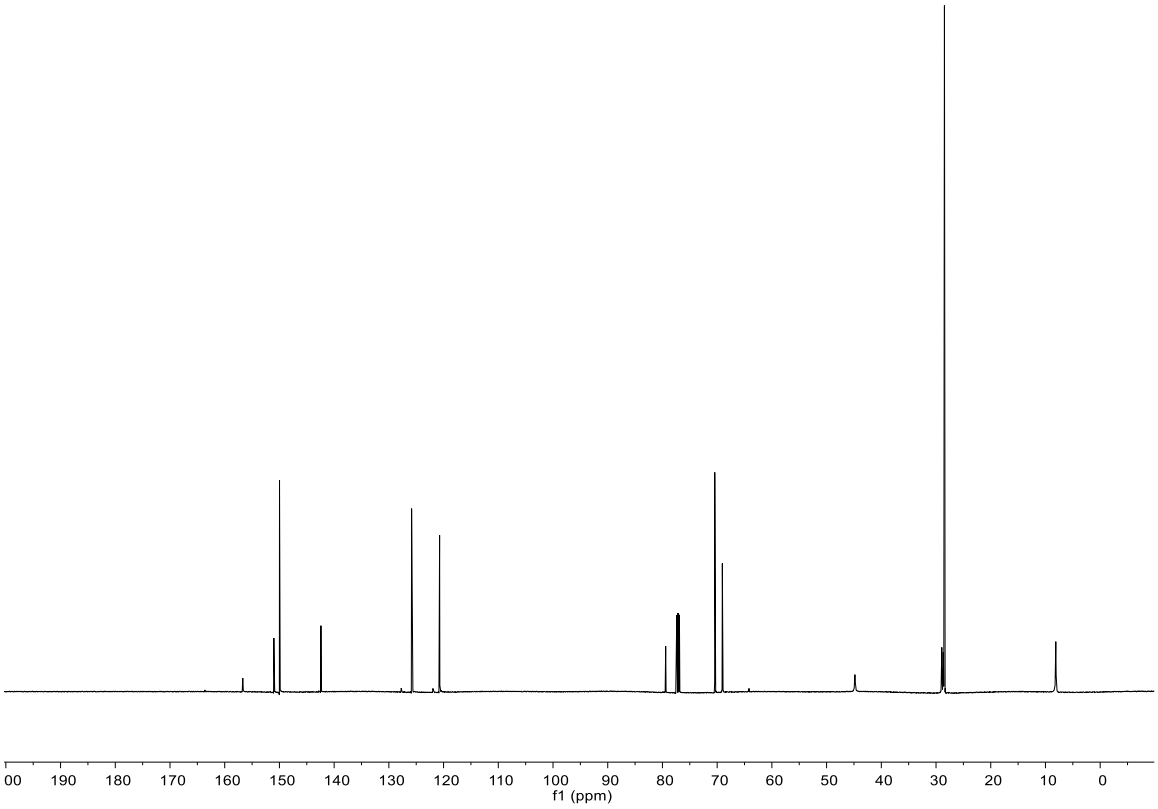
190 180 170 160 150 140 130 120 110 100 90 80 70 60 50 40 30 20 10 0
f1 (ppm)

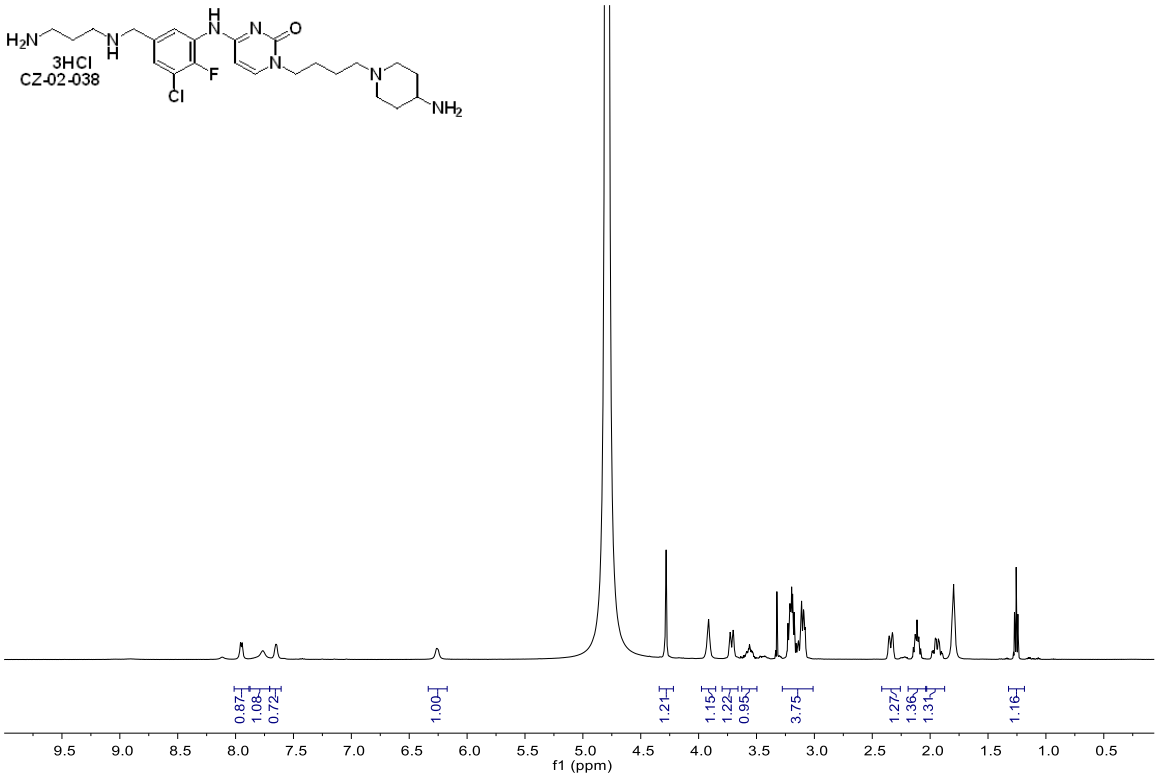
3HCl
CZ-02-038
0.87
1.08
0.72
1.00
1.21
1.15
1.22
0.95
3.75
1.27
1.36
1.31
1.16
f1 (ppm)

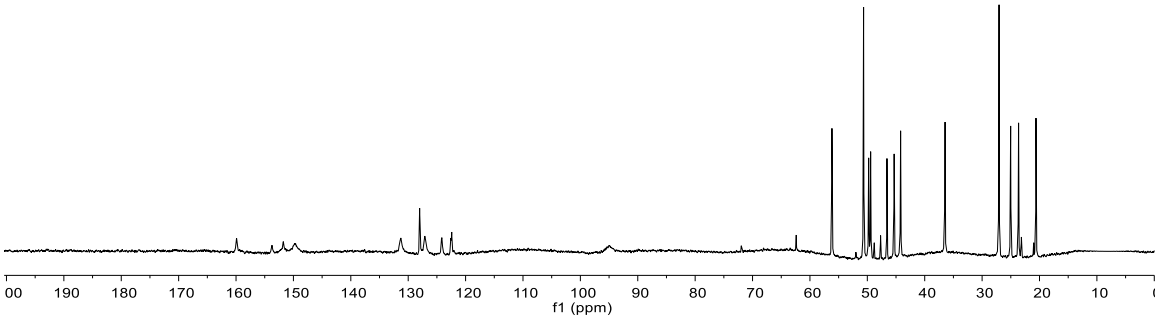
f1 (ppm)

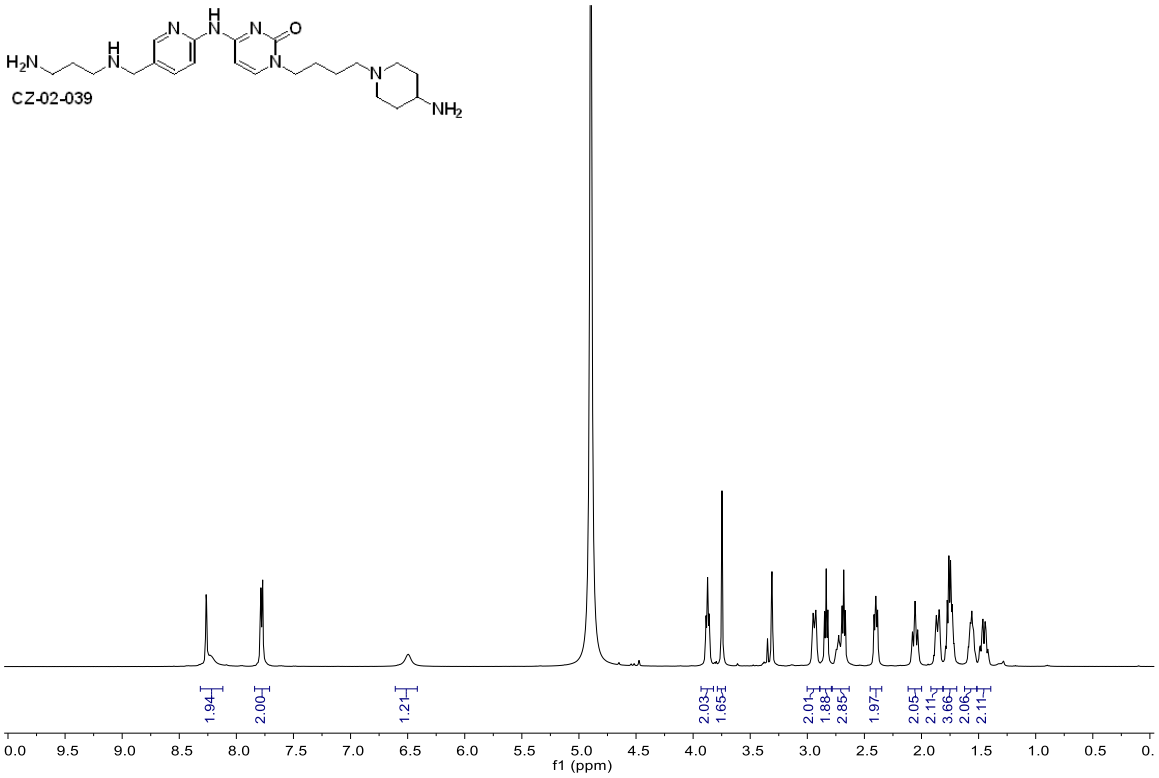
CZ-02-039
1.94
2.00
1.21
2.03
1.65
2.01
1.88
2.85
1.97
2.05
2.11
3.66
2.06
2.11
f1 (ppm)

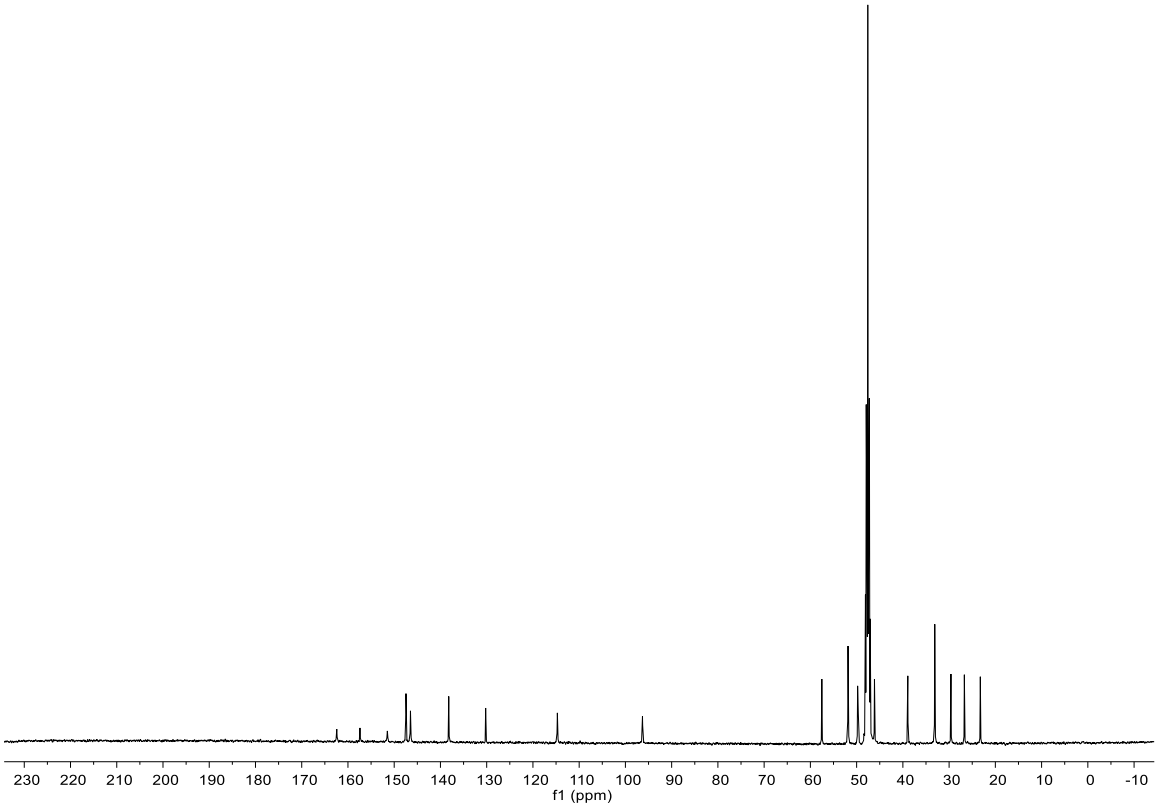
f1 (ppm)

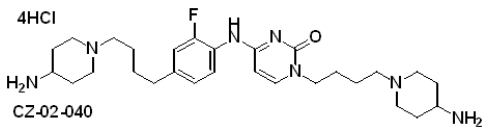
4HCl
F
H
N
N
O
N
N
H_2N
NH_2
CZ-02-040

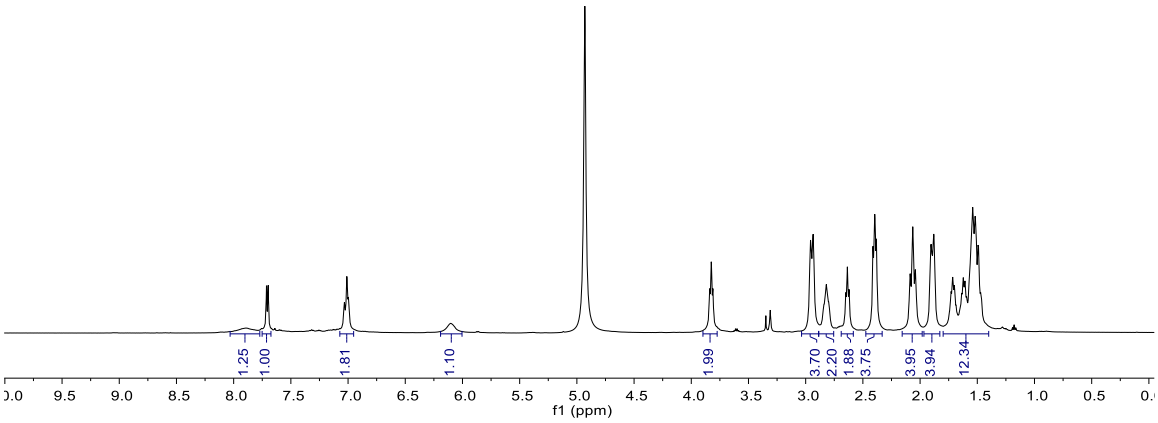
1.25
1.00
1.81
1.10
1.99
3.70
2.20
1.88
3.75
3.95
3.94
12.34
f1 (ppm)

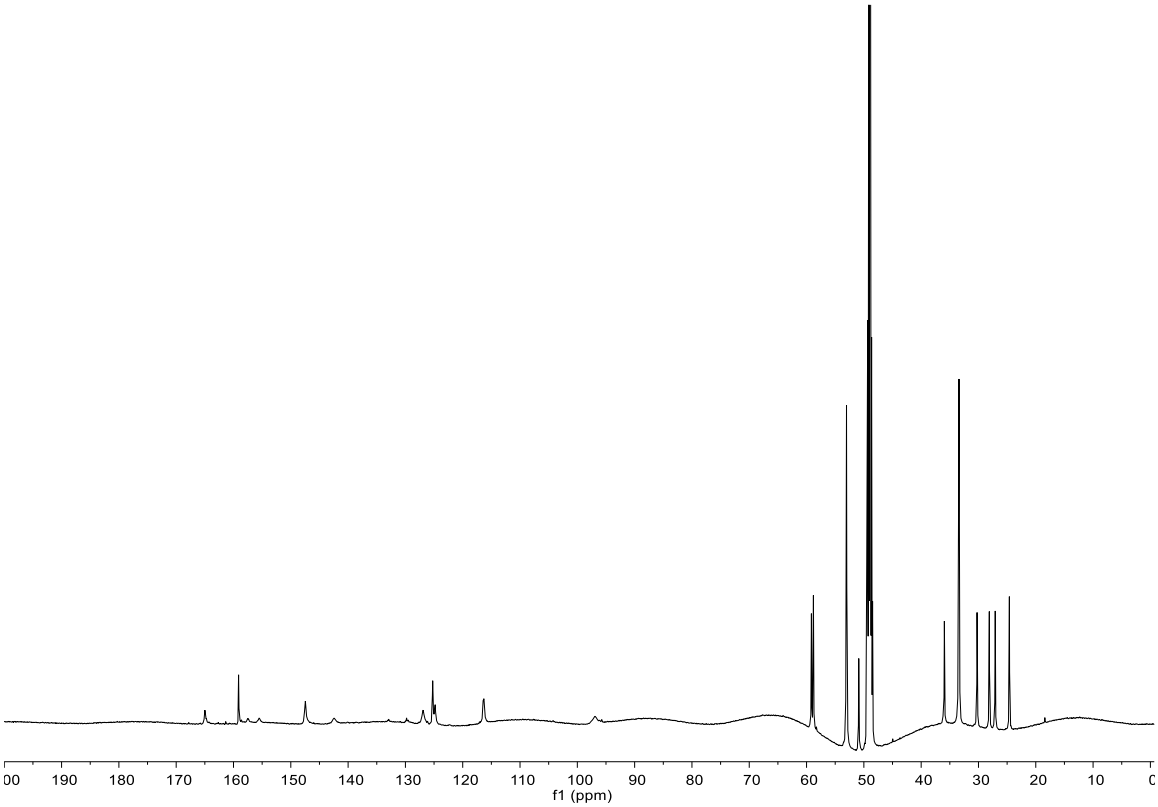
f1 (ppm)

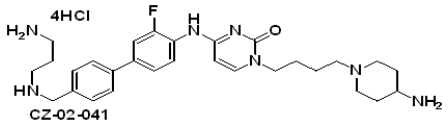
4HCl
F
H
N
N
O
N
N
HN
NH2
CZ-02-041

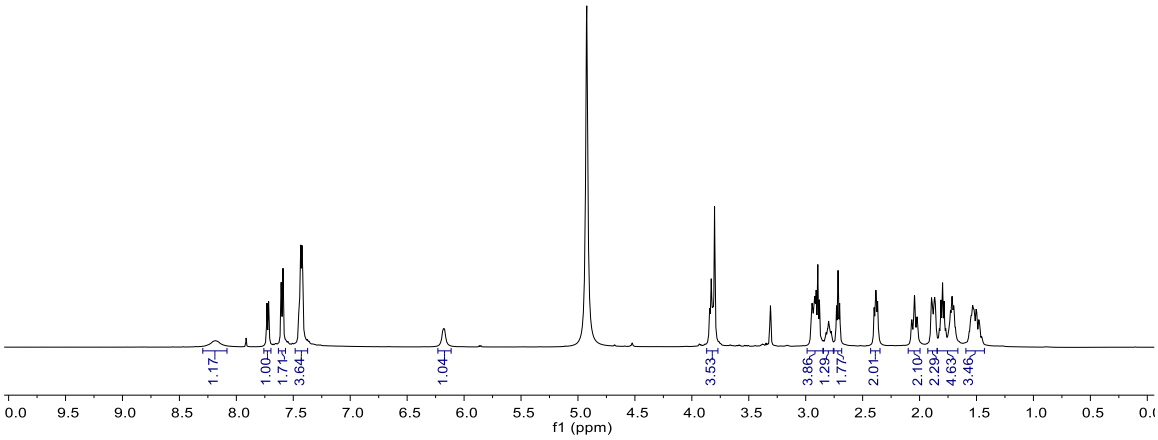
1.17
1.00
1.71
3.64
1.04
3.53
3.86
1.29
1.77
2.01
2.10
2.29
4.63
3.46
f1 (ppm)

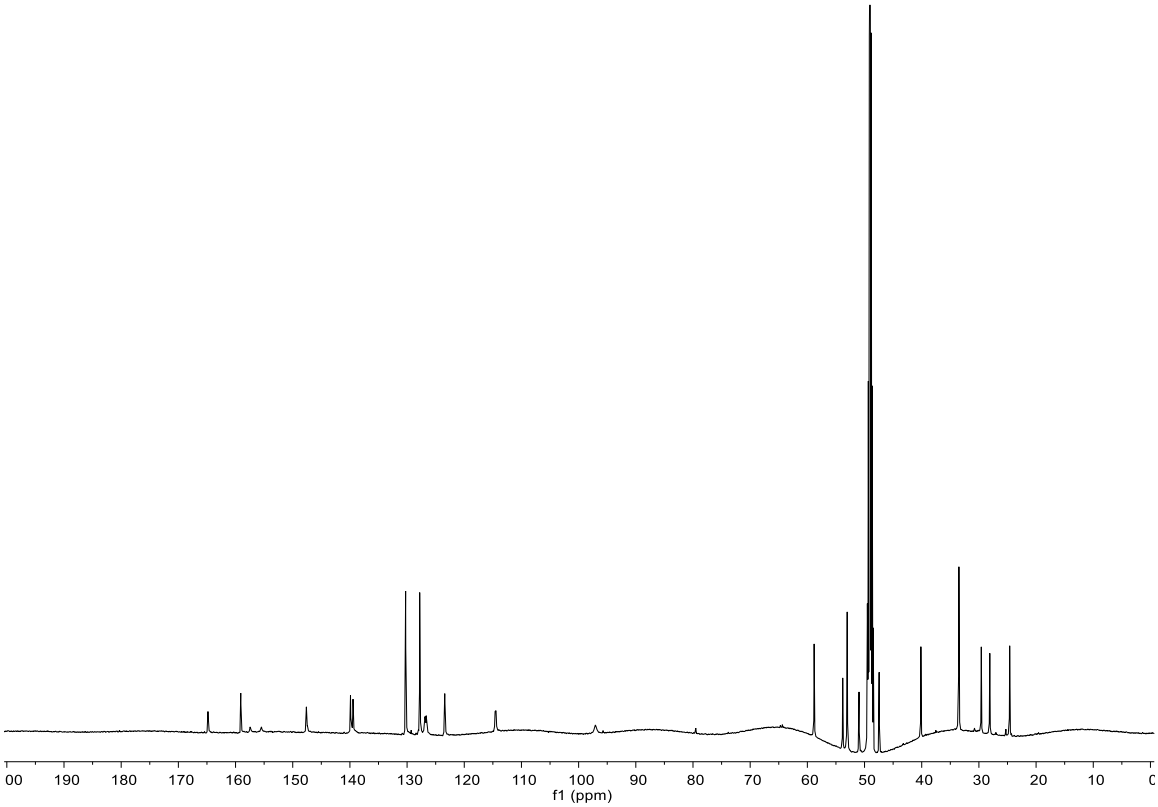
f1 (ppm)

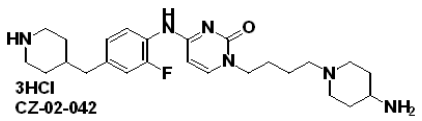
HN
H
N
N
O
F
N
N
NH2
3HCl
CZ-02-042

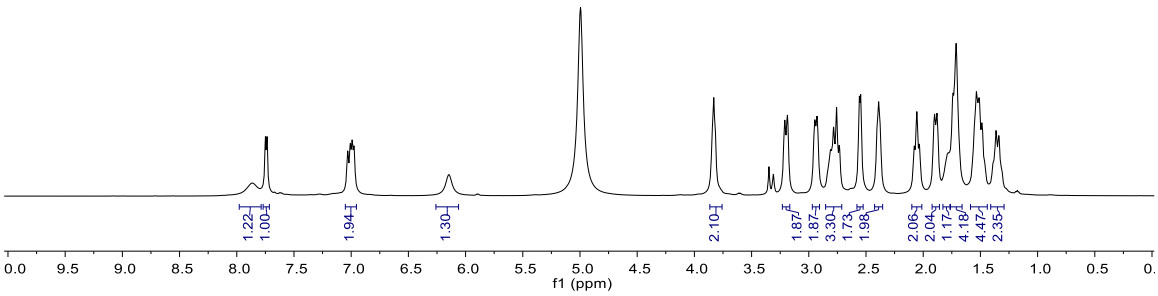
1.22
1.00
1.94
1.30
2.10
1.87
1.87
3.30
1.73
1.98
2.06
2.04
1.17
4.18
4.47
2.35
f1 (ppm)

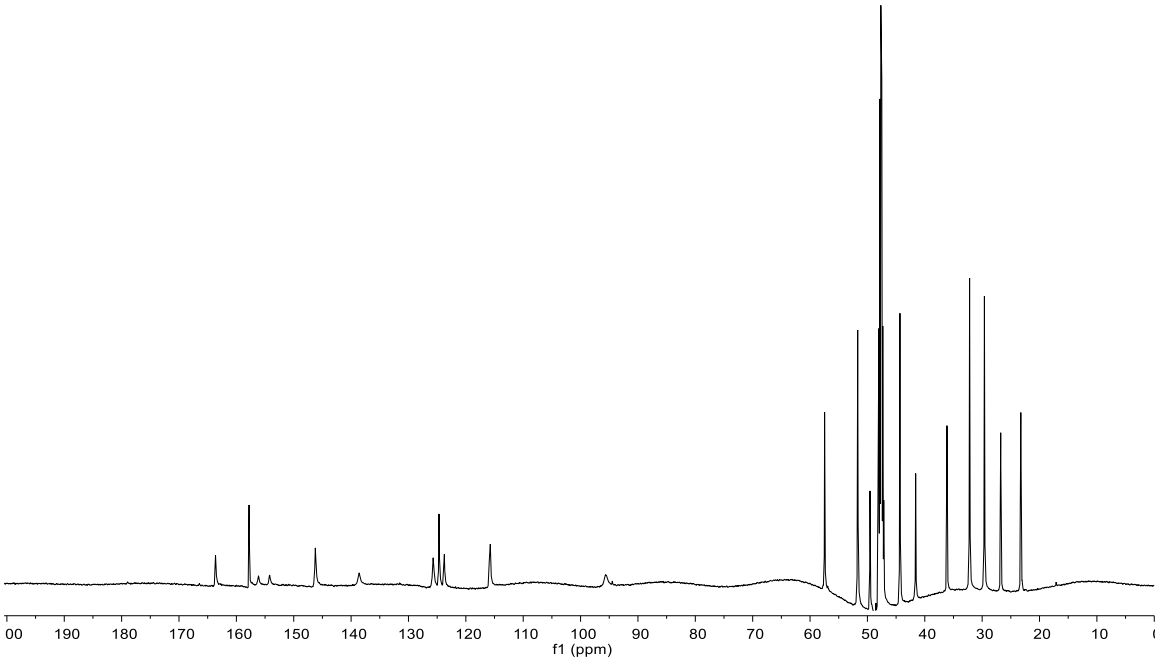
f1 (ppm)

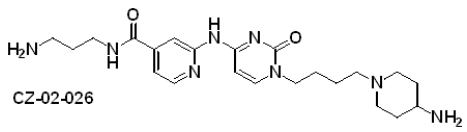
H2N
O
N
H
H
N
N
N
O
N
N
NH2

CZ-02-026

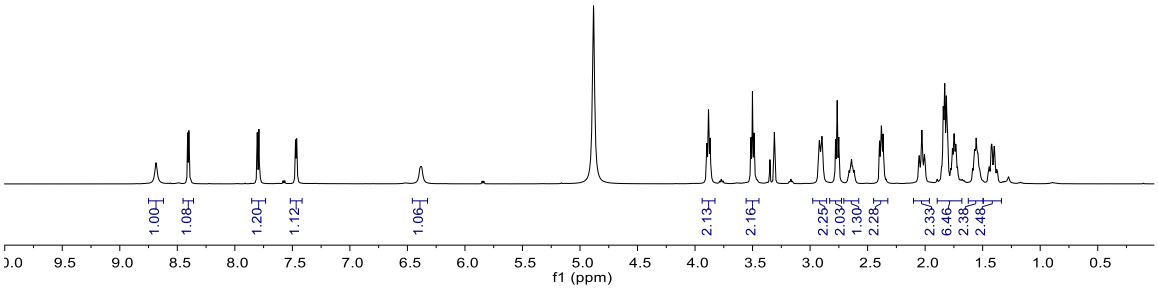
1.00
1.08
1.20
1.12
1.06
2.13
2.16
2.25
2.03
1.30
2.28
2.33
6.46
2.38
2.48
f1 (ppm)

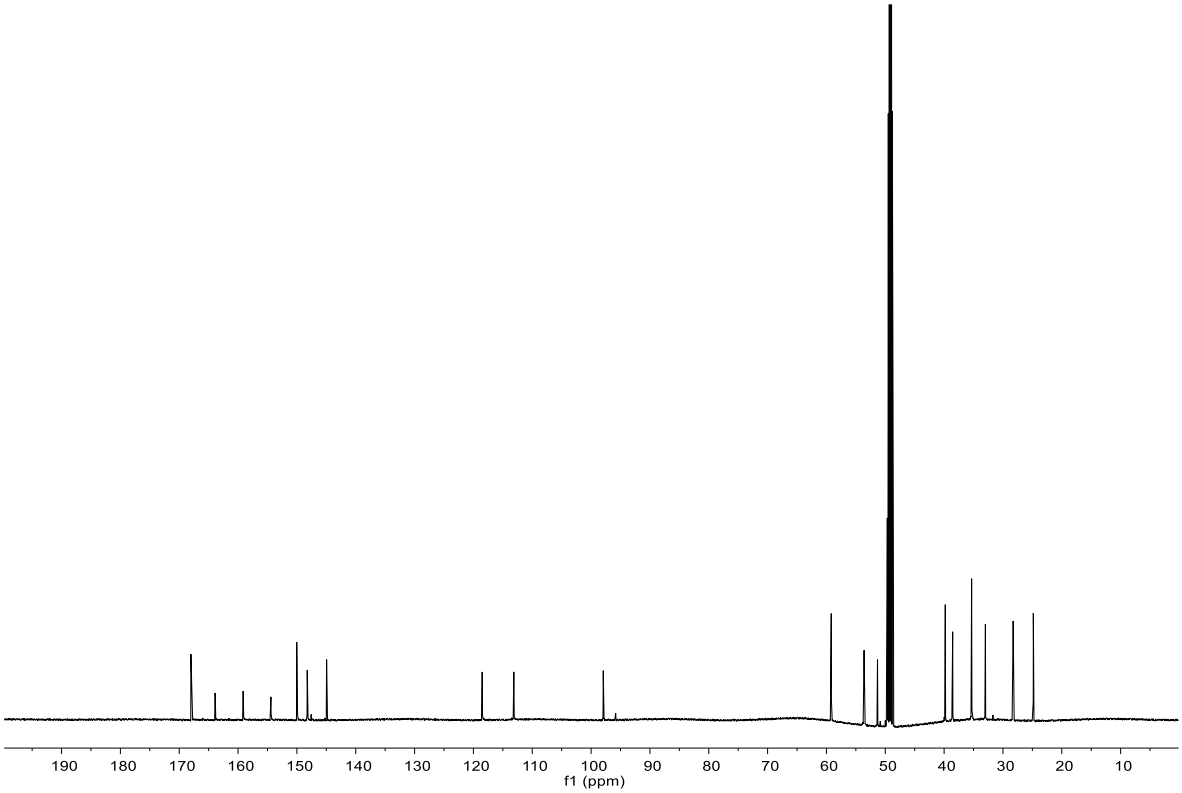
f1 (ppm)

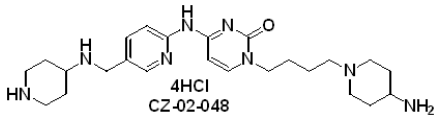
4HCl
CZ-02-048

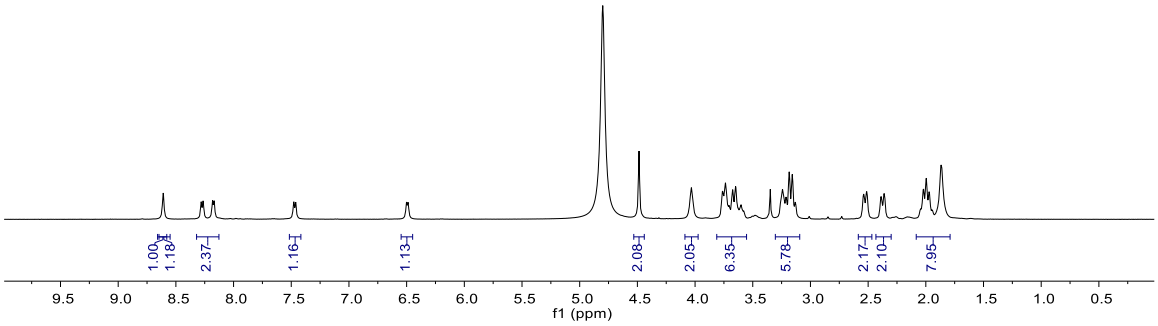
1.00
1.18
2.37
1.16
1.13
2.08
2.05
6.35
5.78
2.17
2.10
7.95
f1 (ppm)


158.81
151.07
150.82
144.49
143.55
123.86
115.97
115.83
96.24
56.18
52.67
50.71
49.96
45.38
44.97
42.26
27.06
25.11
25.00
20.63

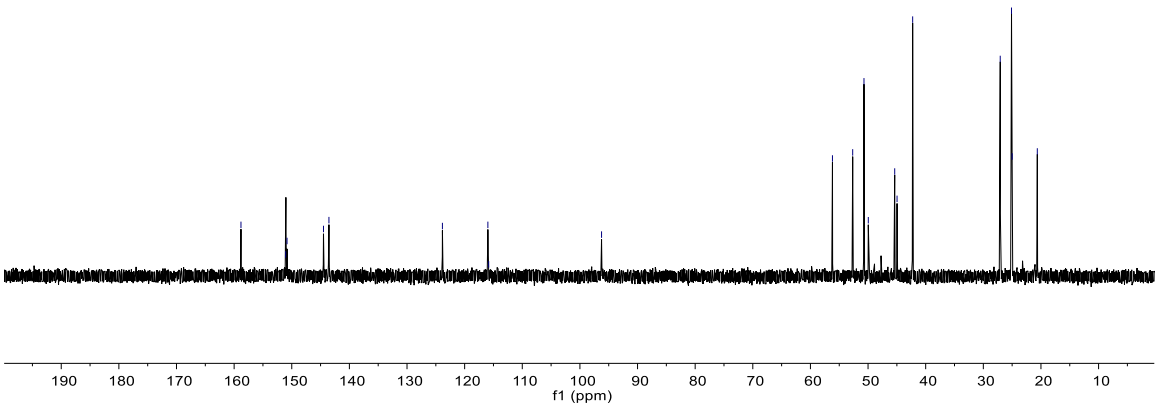
f1 (ppm)

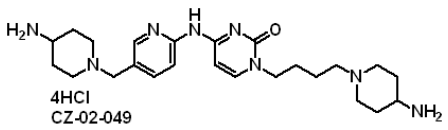
4HCl
CZ-02-049

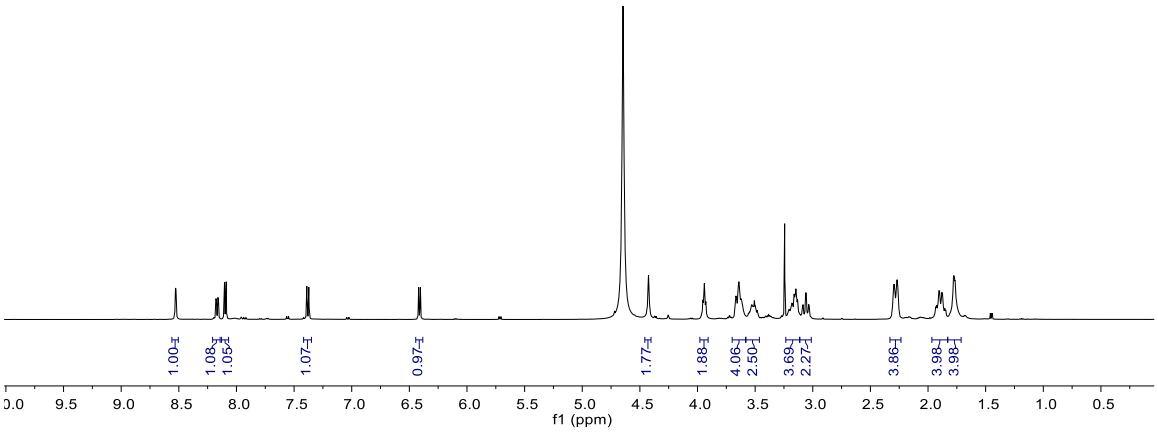
1.00
1.08
1.05
1.07
0.97
1.77
1.88
4.06
2.50
3.69
2.27
3.86
3.98
3.98
f1 (ppm)

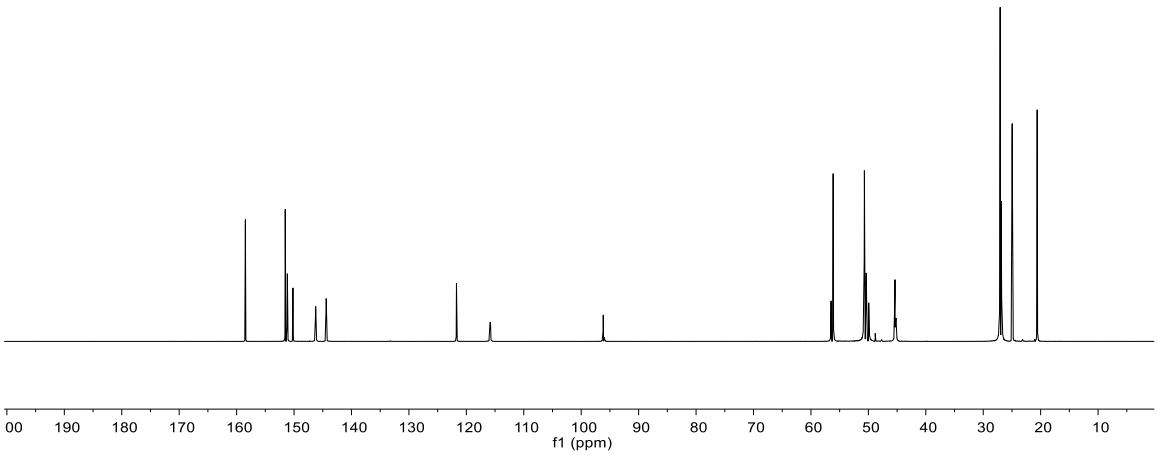
f1 (ppm)

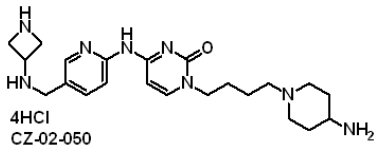
4HCl
CZ-02-050

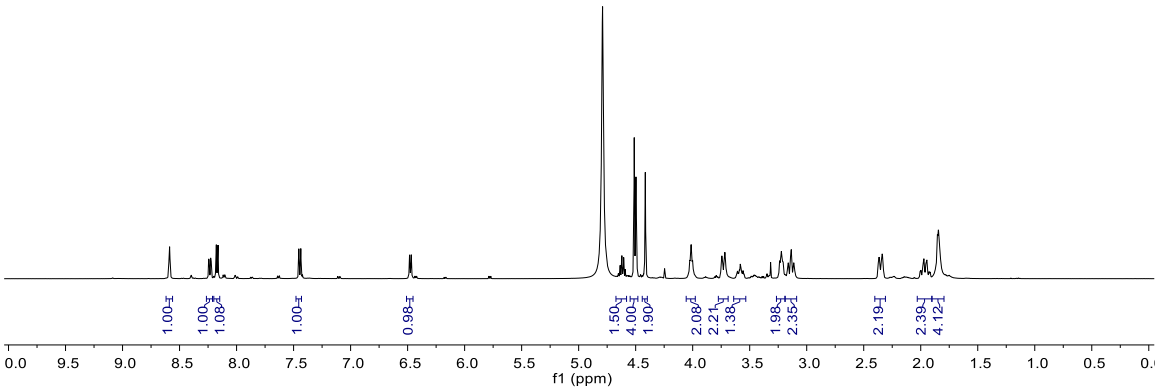
1.00
1.00
1.08
1.00
0.98
1.50
4.00
1.90
2.08
2.21
1.38
1.98
2.35
2.19
2.39
4.12
f1 (ppm)


158.50
151.35
151.14
150.28
144.97
143.29
123.19
116.04
96.16
96.07
56.14
50.70
49.95
48.80
47.48
45.95
45.33
27.05
24.97
20.62

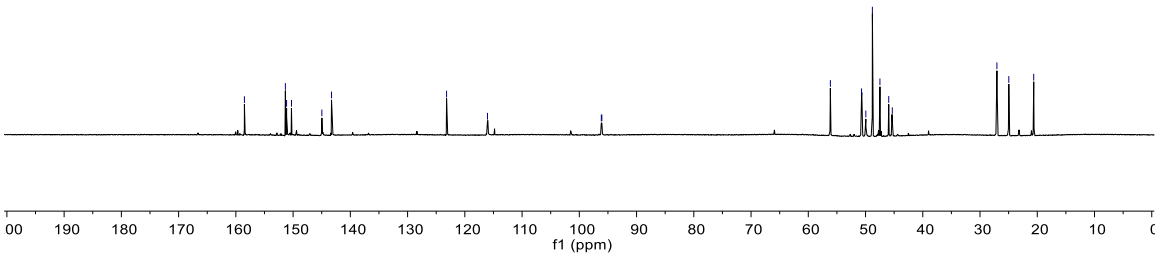
f1 (ppm)


3HCl
CZ-02-051
1.00
1.07
1.06
1.05
1.05
1.77
1.08
3.85
2.19
1.39
1.96
2.24
2.10
2.33
4.07
f1 (ppm)

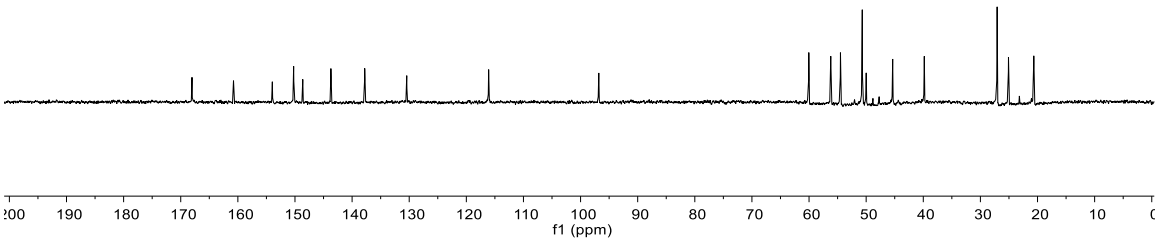
f1 (ppm)

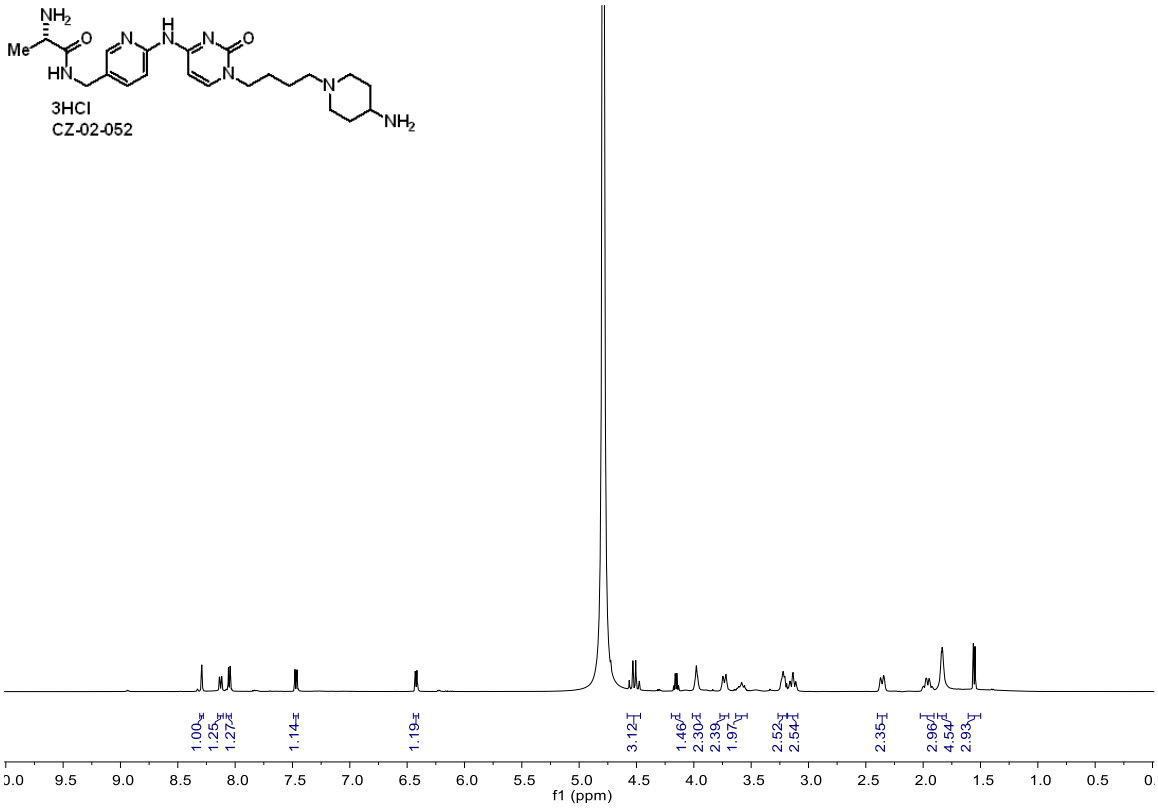
3HCl
CZ-02-052
f1 (ppm)

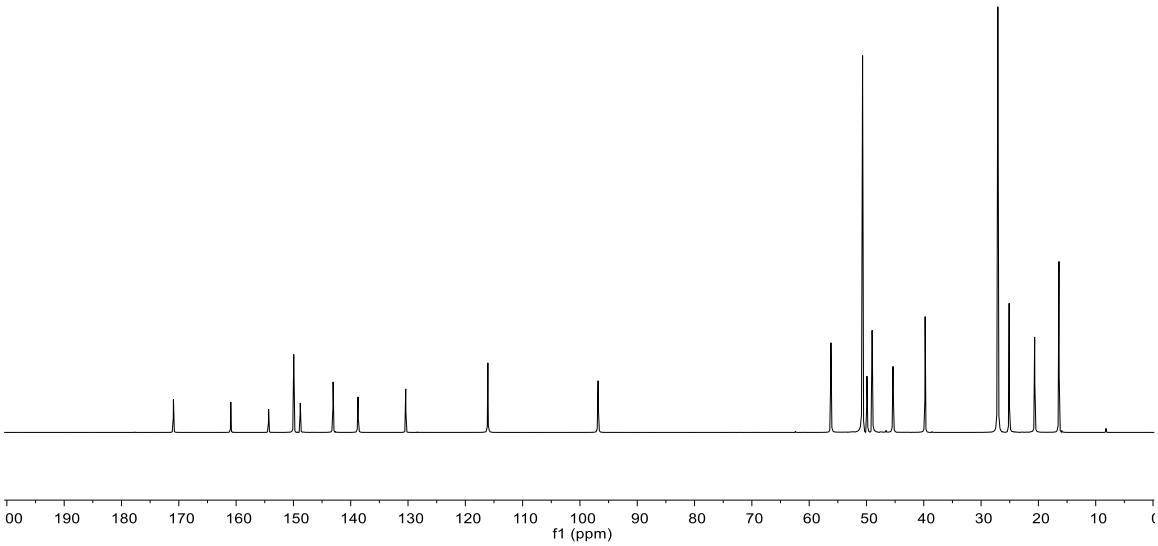
f1 (ppm)

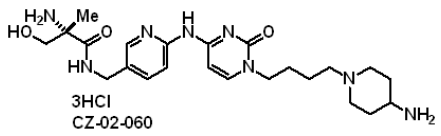
3HCl
CZ-02-060

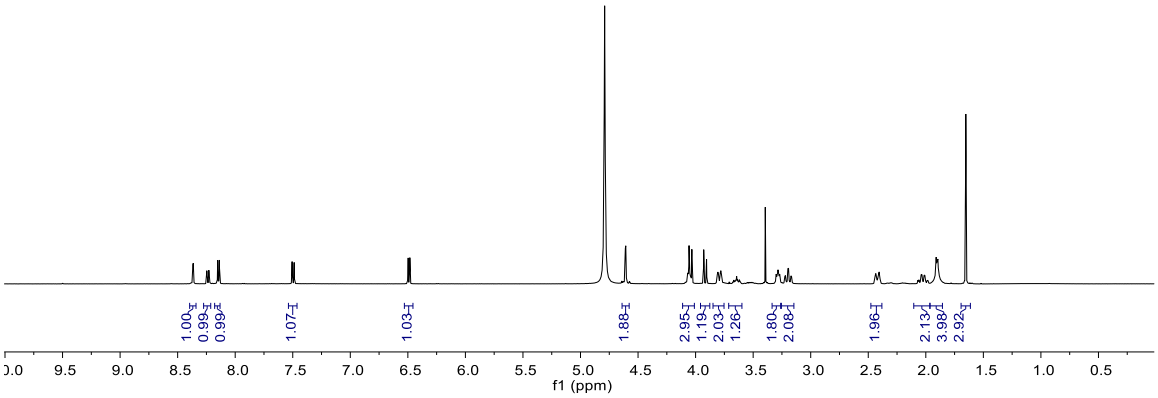
1.00
0.99
0.99
1.07
1.03
1.88
2.85
1.19
2.03
1.26
1.80
2.08
1.96
2.13
3.98
2.92
f1 (ppm)

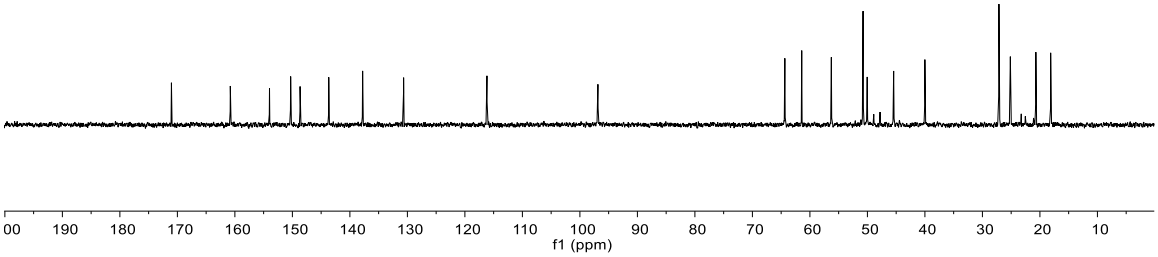
f1 (ppm)

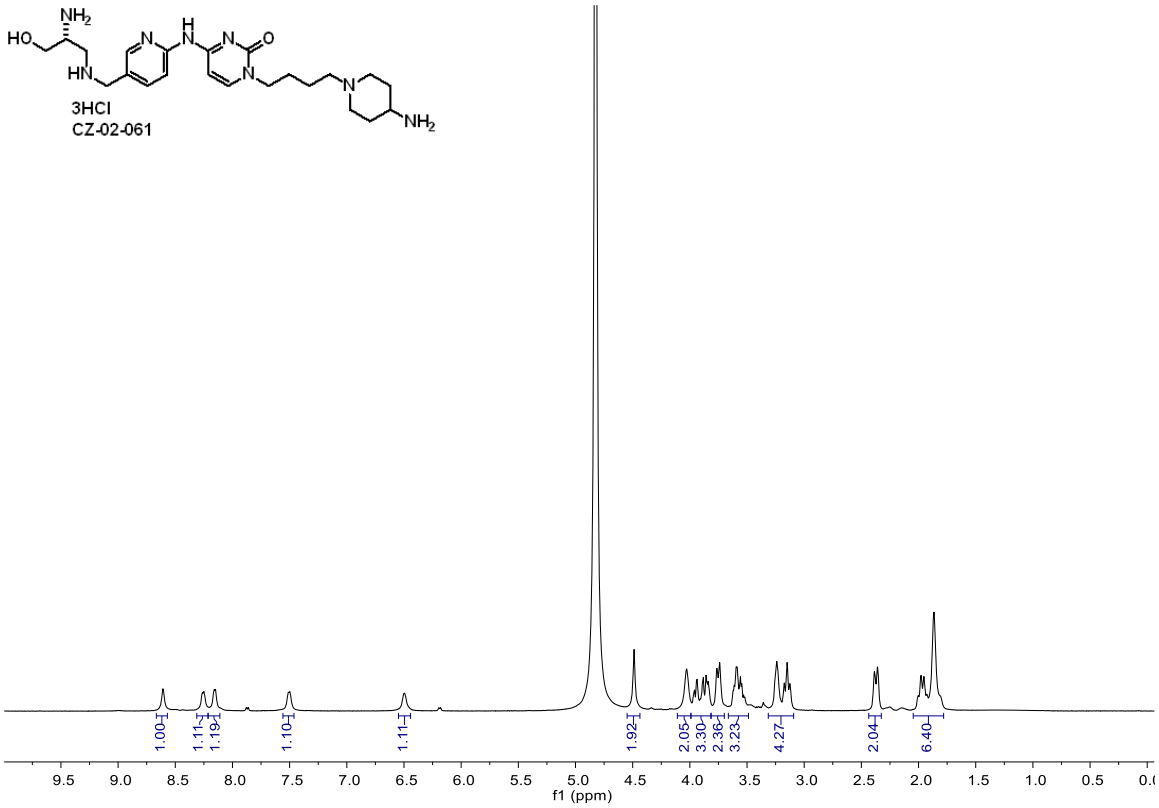
3HCl
CZ-02-061
1.00
1.11
1.19
1.10
1.11
1.92
2.05
3.30
2.36
3.23
4.27
2.04
6.40
f1 (ppm)

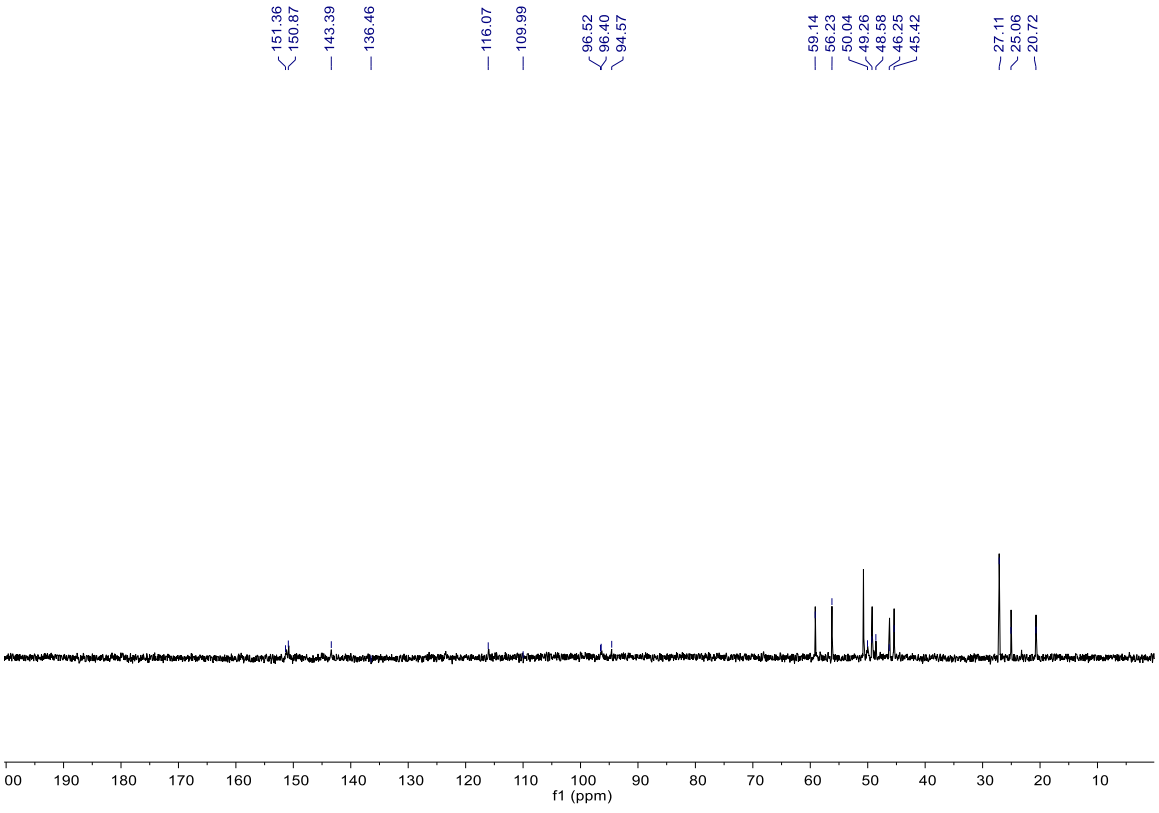
151.36
150.87
143.39
136.46
116.07
109.99
96.52
96.40
94.57
59.14
56.23
50.04
49.26
48.58
46.25
45.42
27.11
25.06
20.72
f1 (ppm)

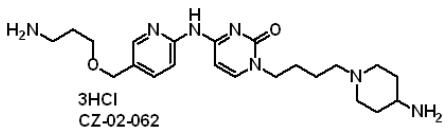
3HCl
CZ-02-062

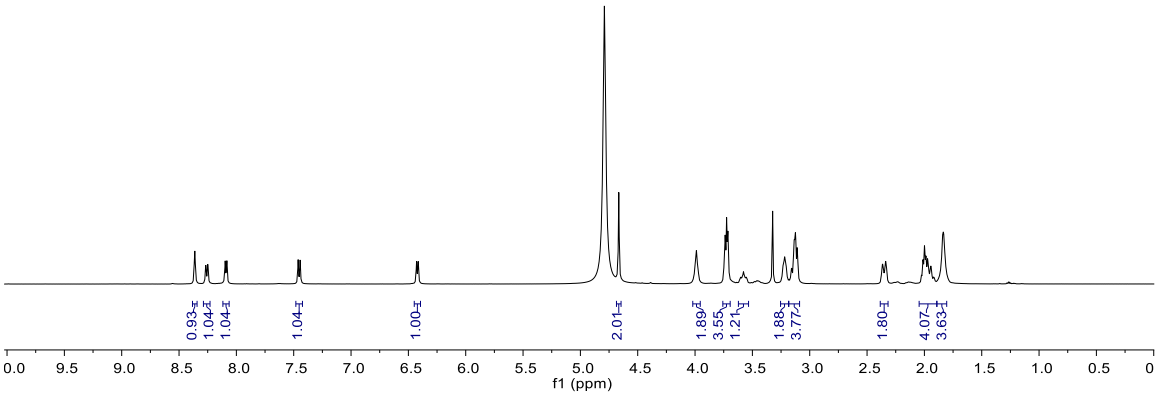
0.93
1.04
1.04
1.04
1.00
2.01
1.89
3.55
1.21
1.88
3.77
1.80
4.07
3.63
f1 (ppm)

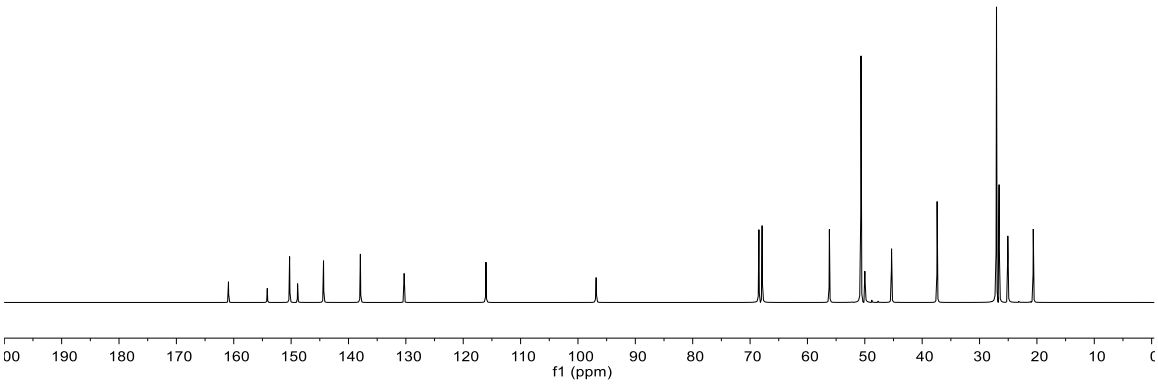
f1 (ppm)

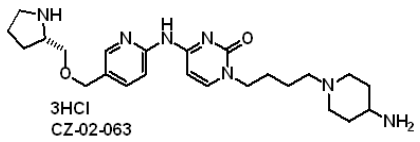

3HCl
CZ-02-063

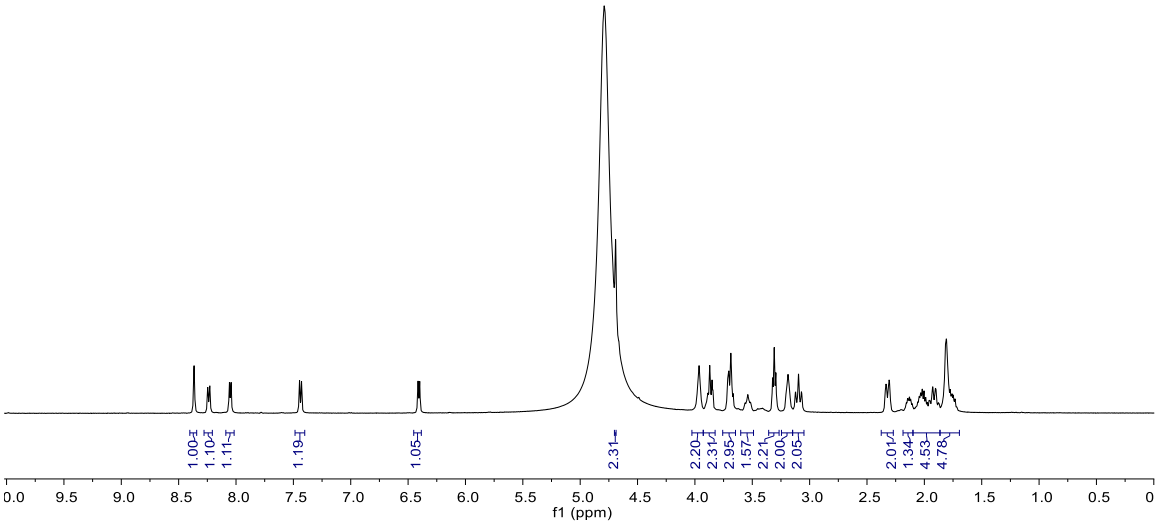

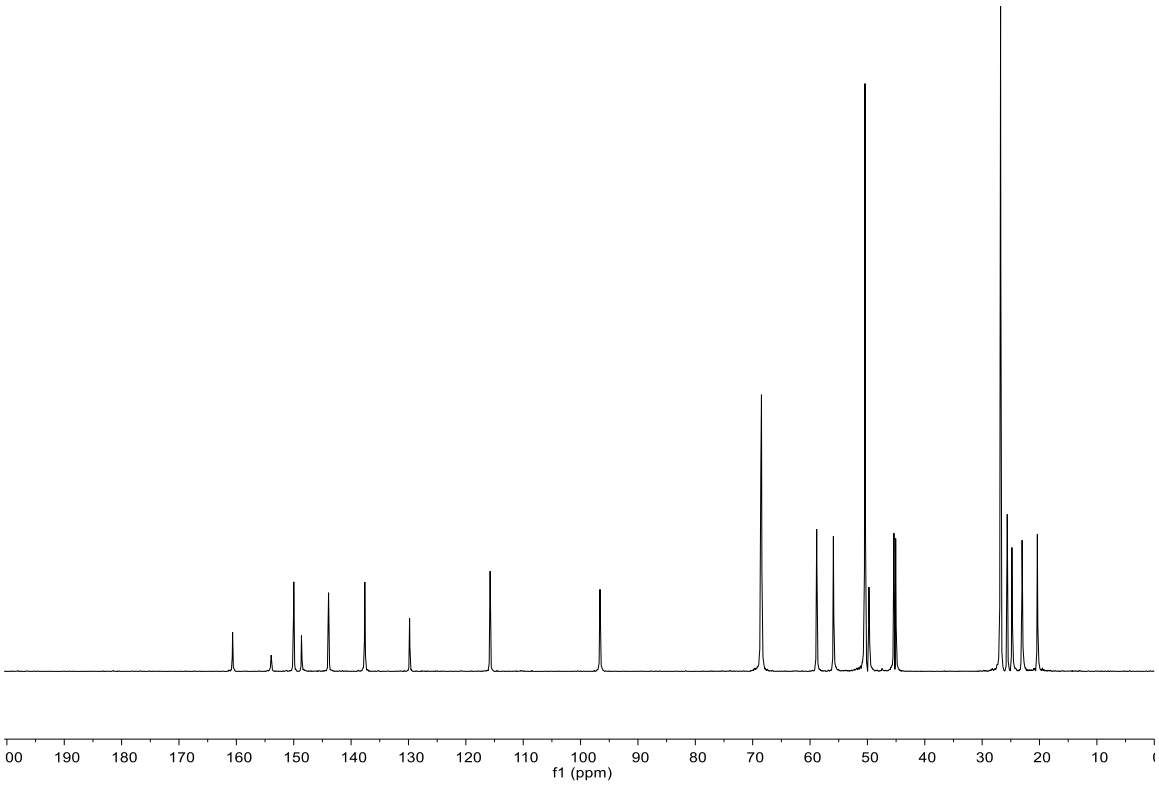

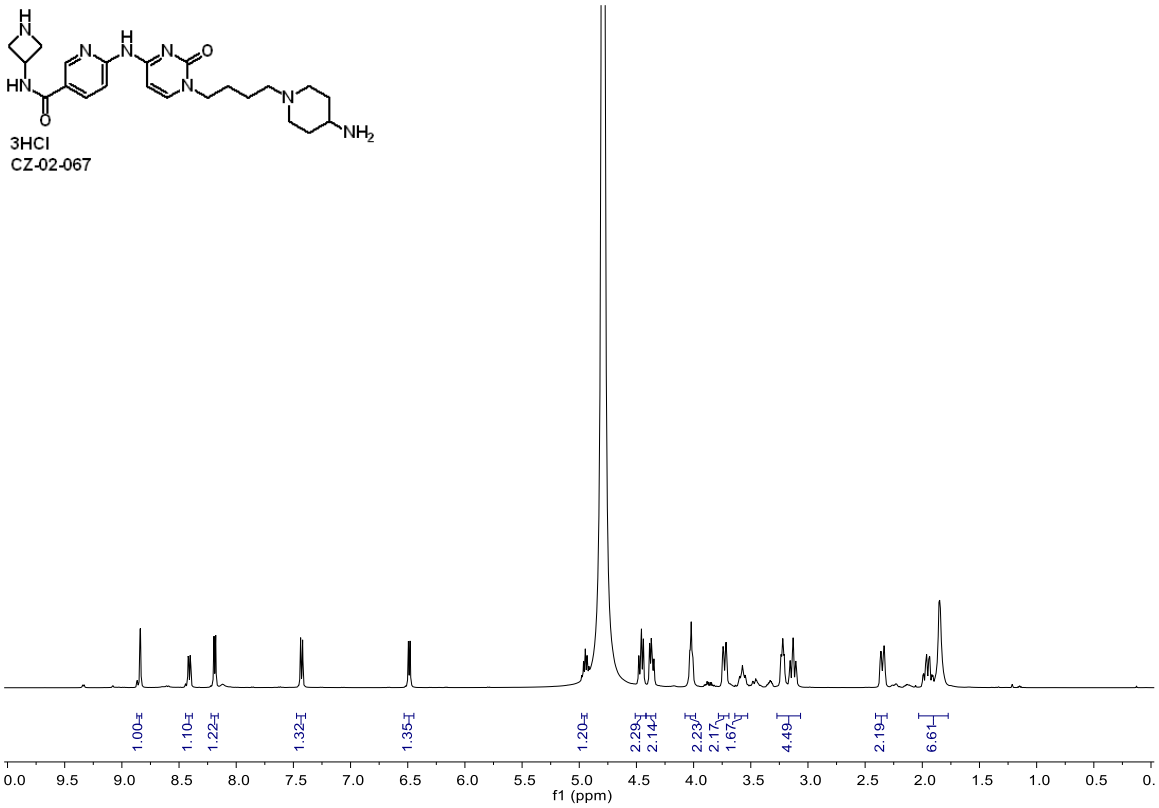
3HCl
CZ-02-067
1.00
1.10
1.22
1.32
1.35
1.20
2.29
2.14
2.23
2.17
1.67
4.49
2.19
6.61
f1 (ppm)

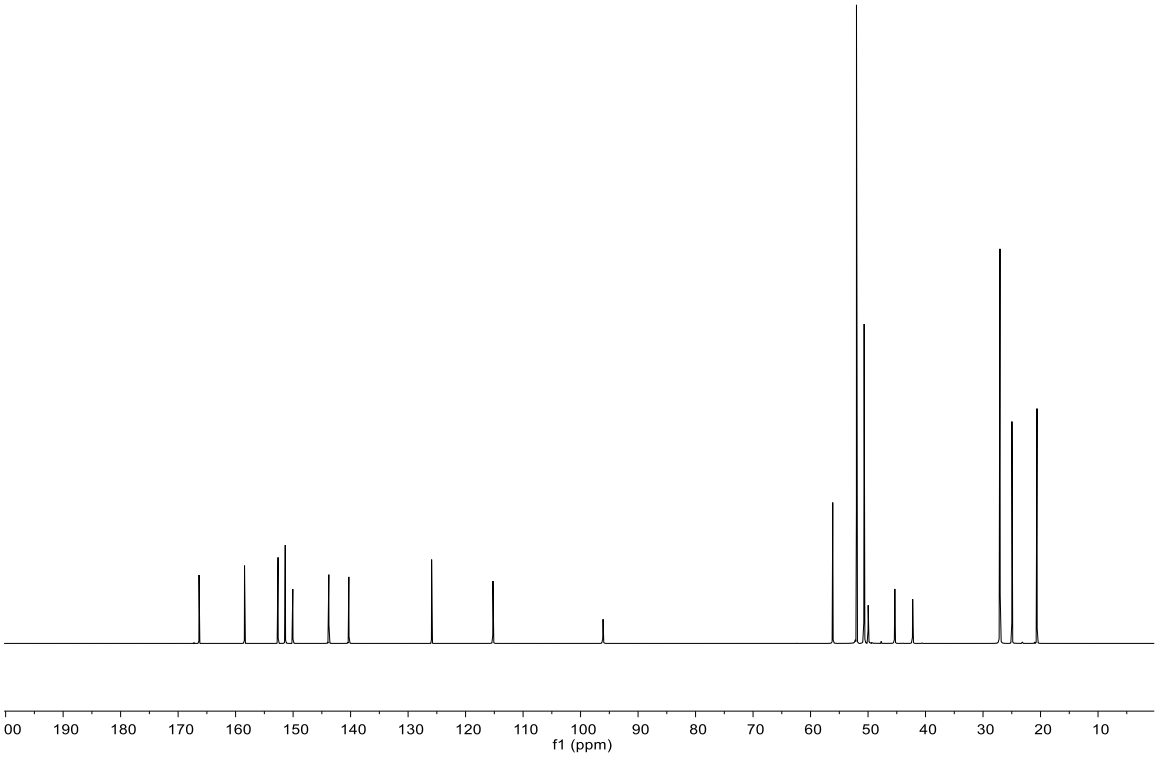
f1 (ppm)

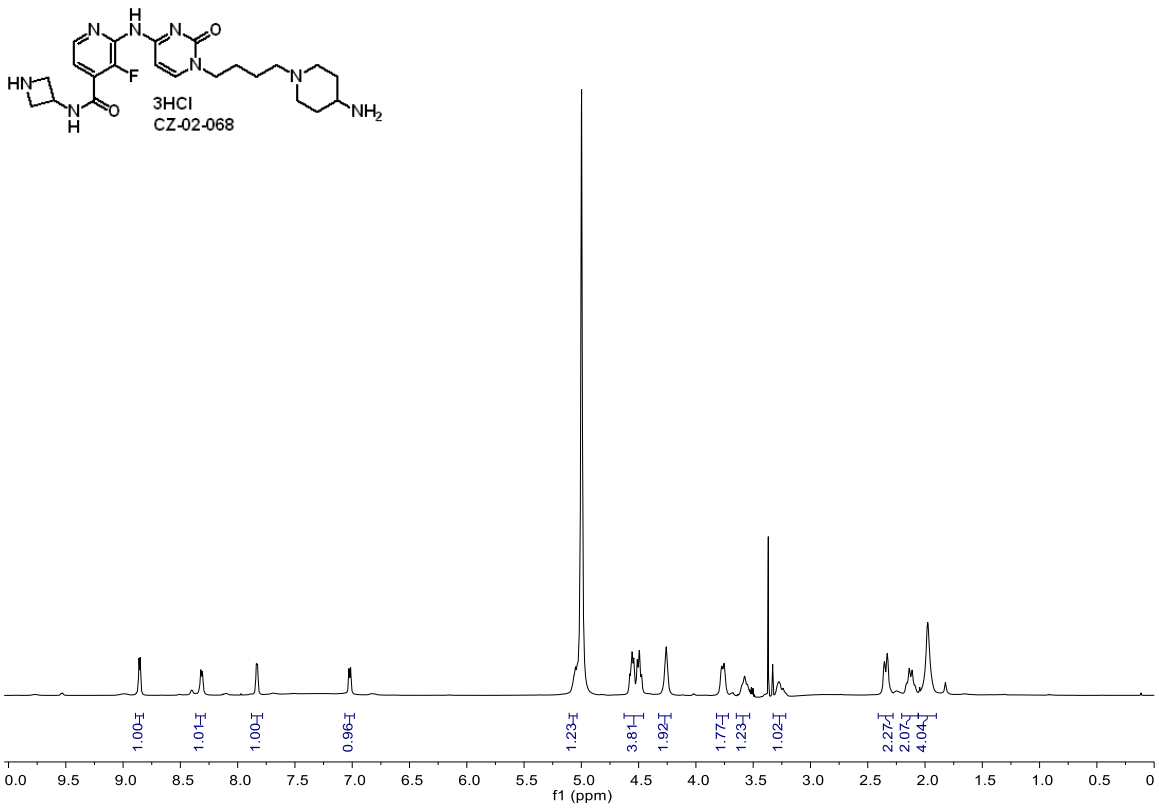
3HCl
CZ-02-068
1.00
1.01
1.00
0.96
1.23
3.81
1.92
1.77
1.23
1.02
2.27
2.07
4.04
f1 (ppm)

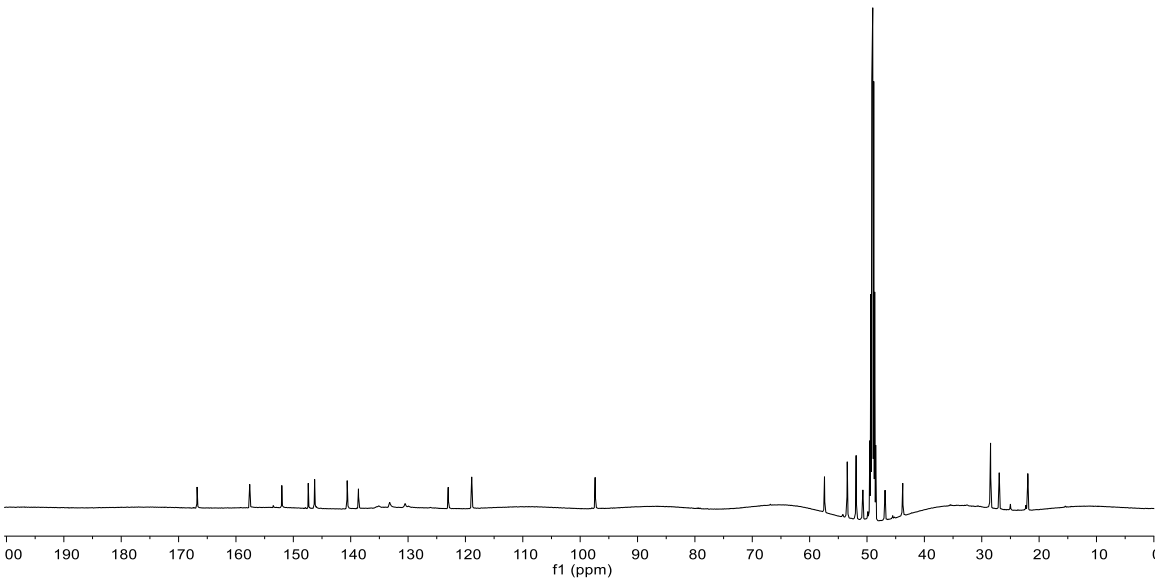
f1 (ppm)

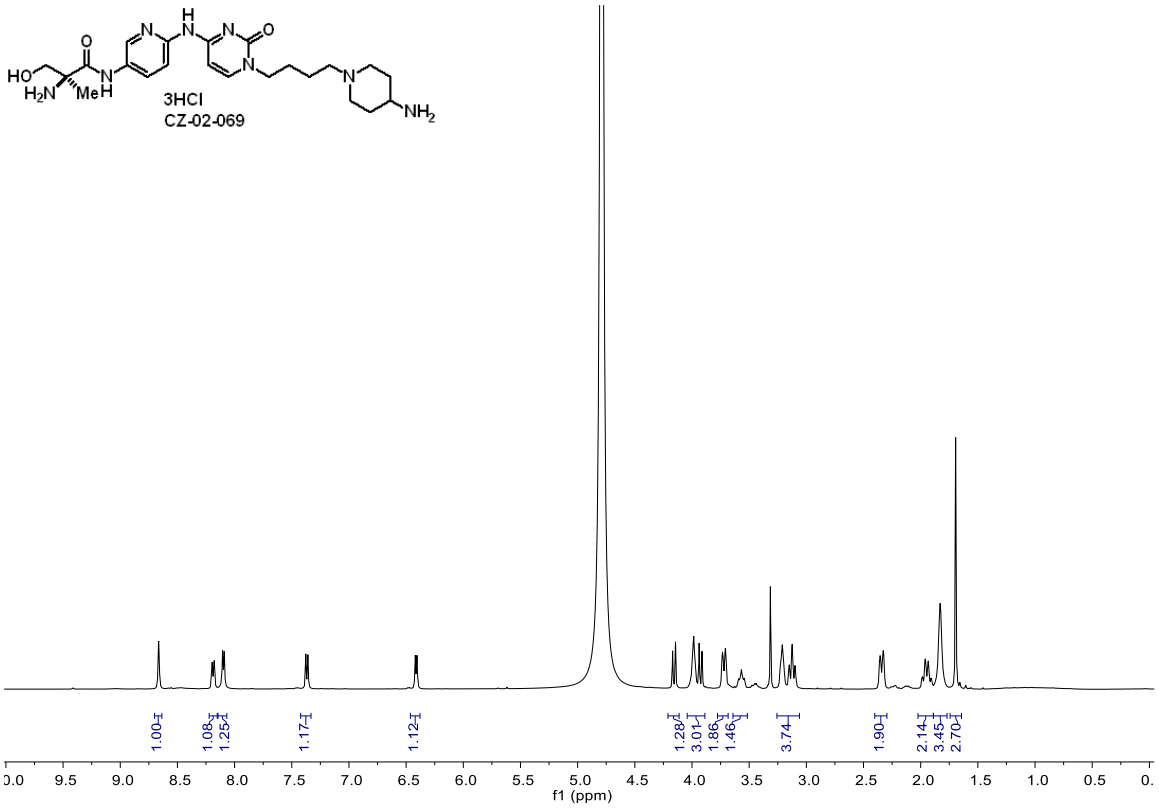
3HCl
CZ-02-069
1.00
1.08
1.25
1.17
1.12
1.28
3.01
1.86
1.46
3.74
1.90
2.14
3.45
2.70
f1 (ppm)

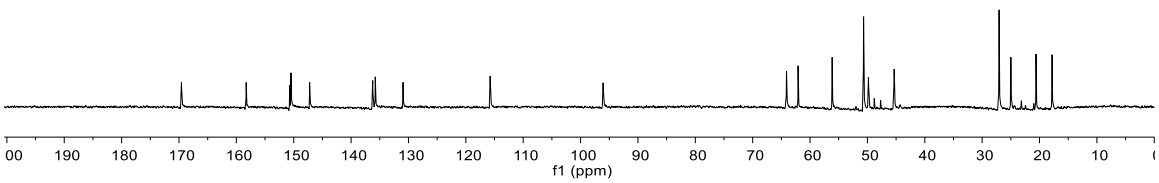
f1 (ppm)

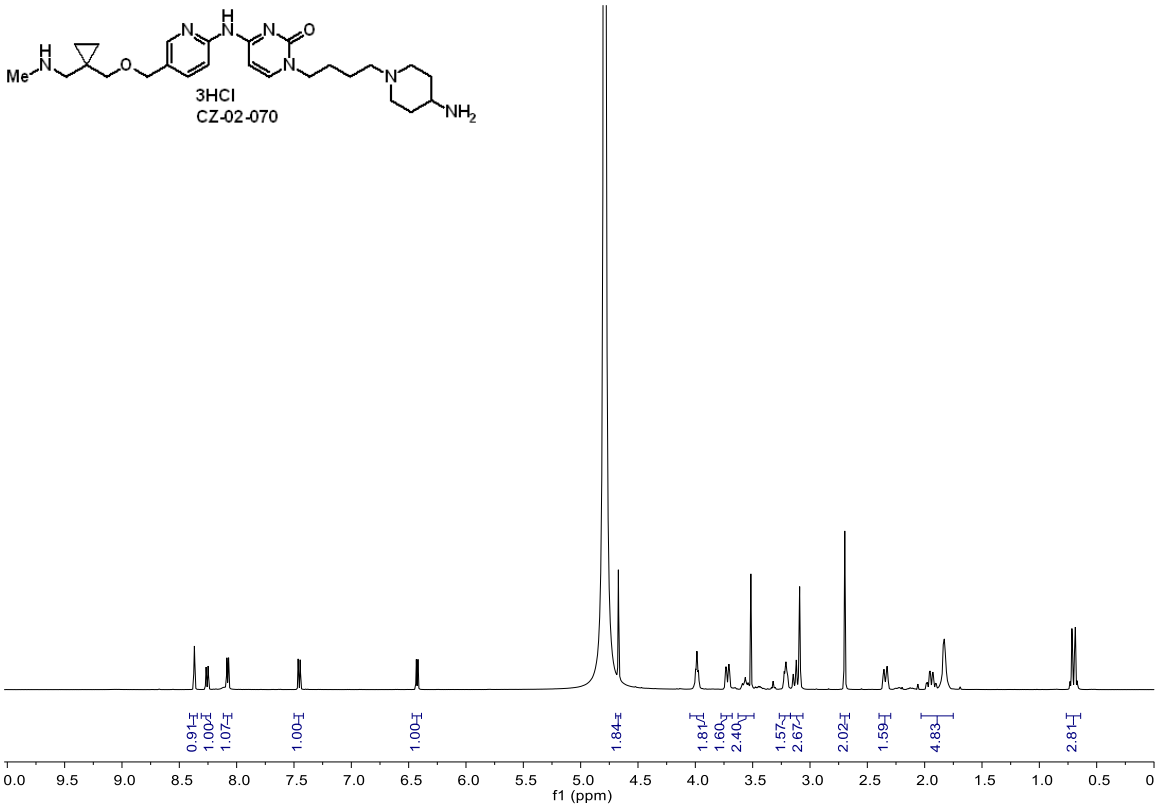
3HCl
CZ-02-070
0.91
1.00
1.07
1.00
1.00
1.84
1.81
1.60
2.40
1.57
2.67
2.02
1.59
4.83
2.81
f1 (ppm)

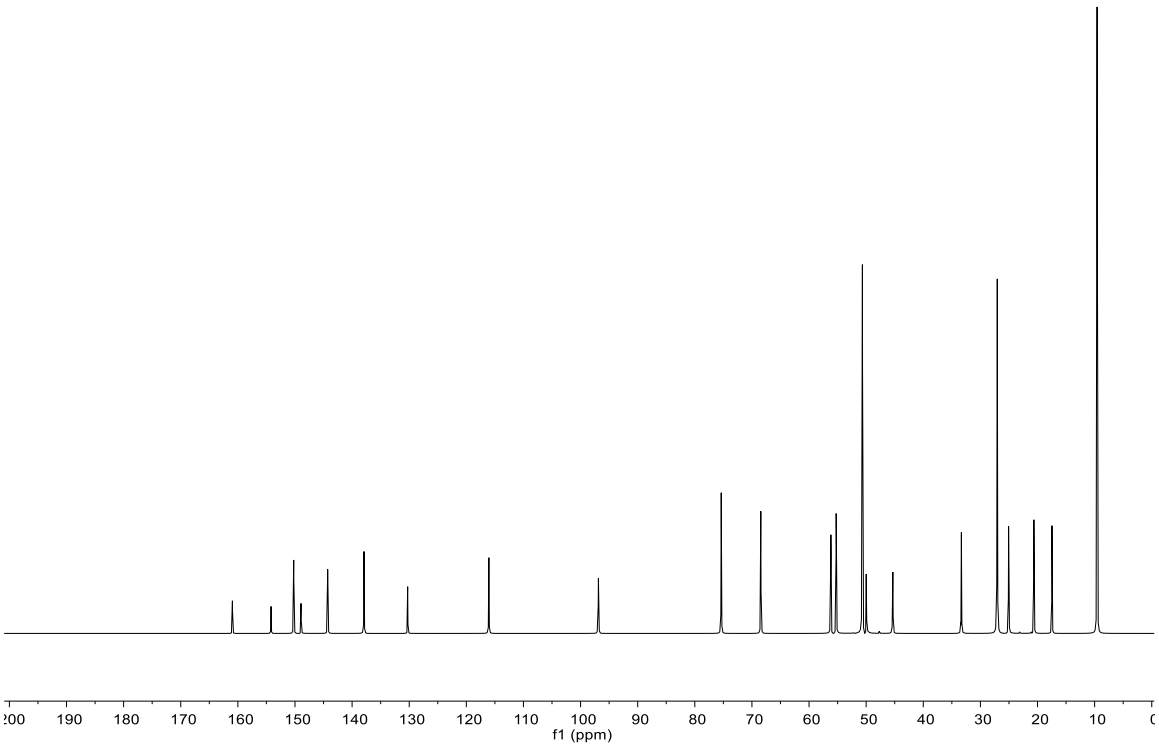
f1 (ppm)

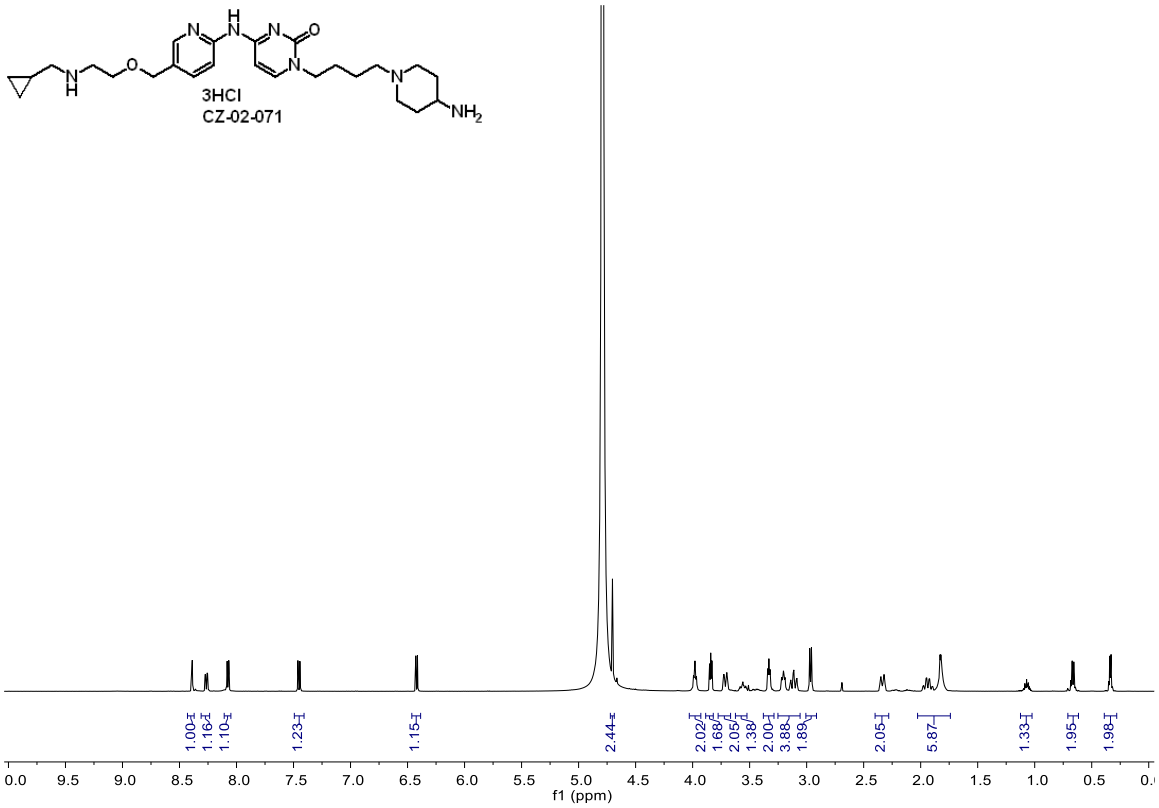
3HCl
CZ-02-071
1.00
1.16
1.10
1.23
1.15
2.44
2.02
1.68
2.05
1.38
2.00
3.88
1.89
2.05
5.87
1.33
1.95
1.98
f1 (ppm)

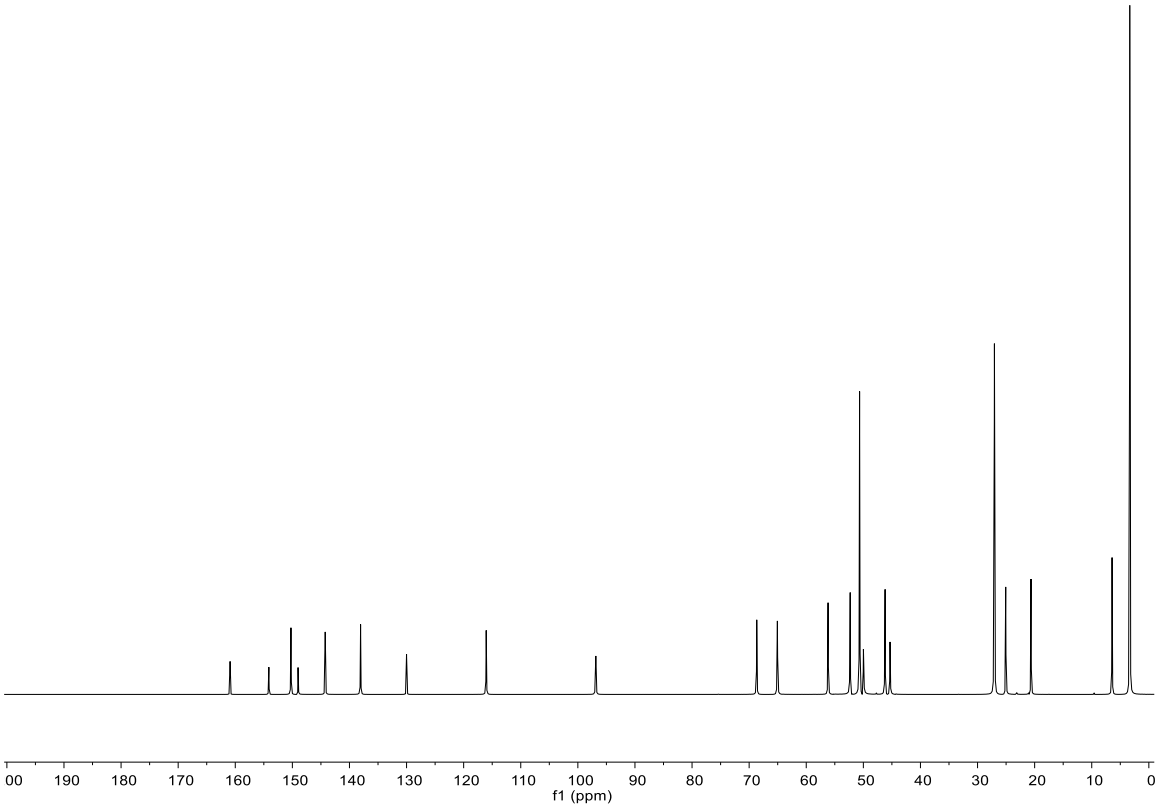
f1 (ppm)

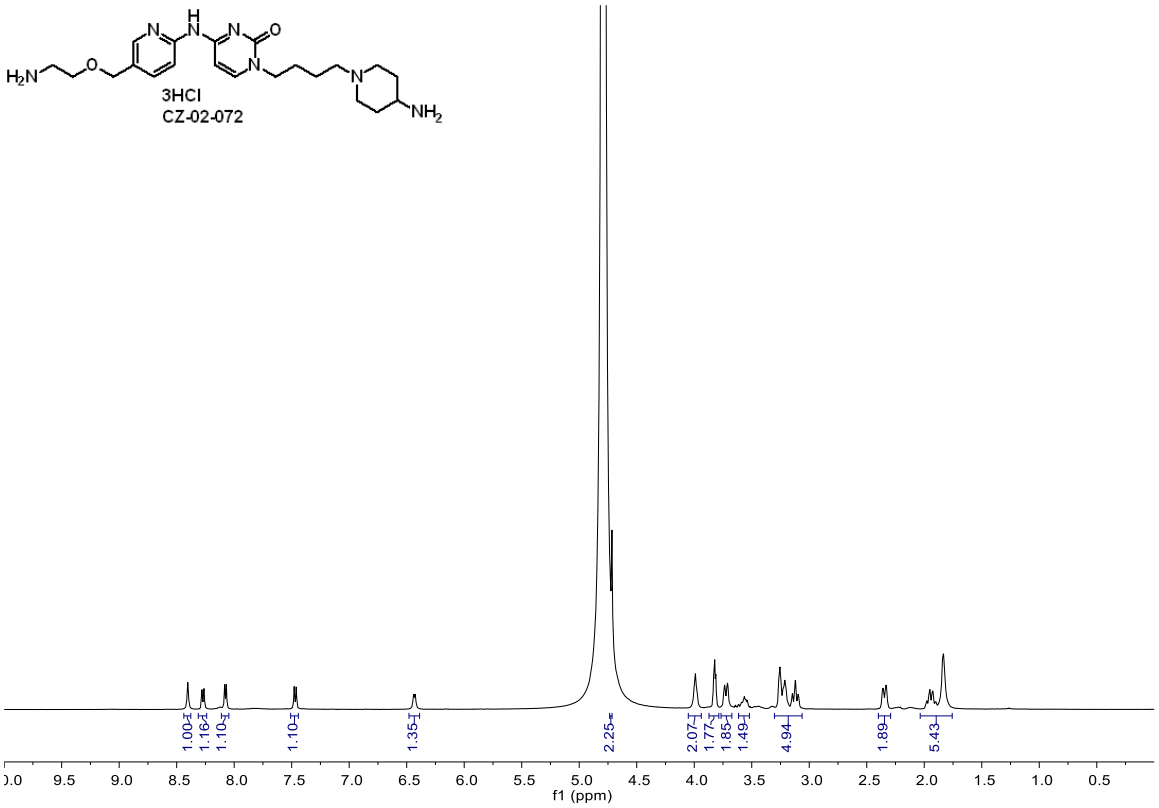
3HCl
CZ-02-072
1.00
1.16
1.10
1.10
1.35
2.25
2.07
1.77
1.85
1.49
4.94
1.89
5.43
f1 (ppm)

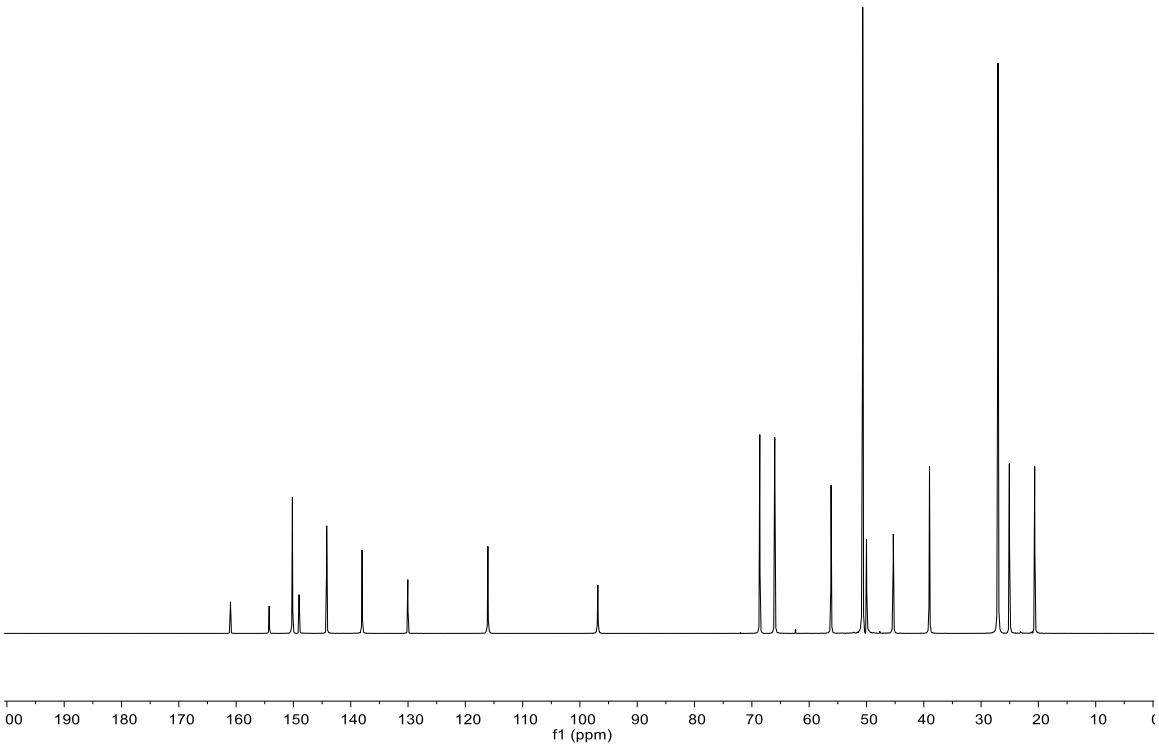
f1 (ppm)

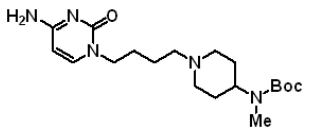
H2N
N
O
N
N
Boc
N
Me

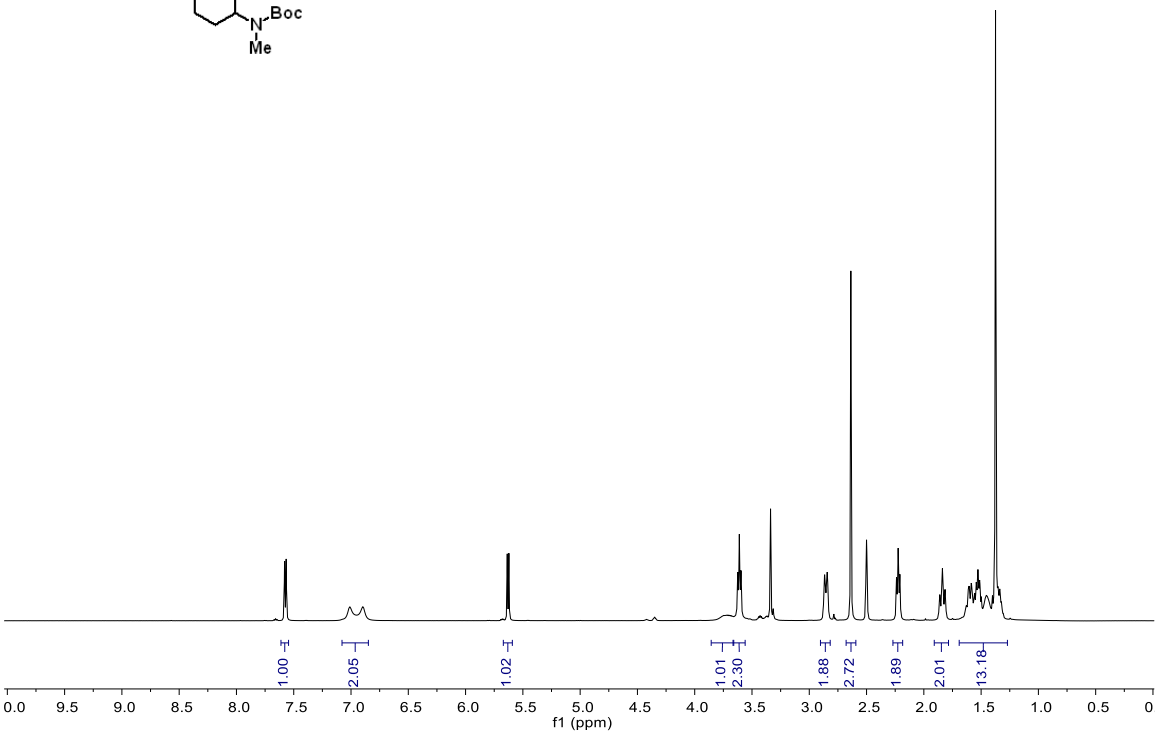
1.00
2.05
1.02
1.01
2.30
1.88
2.72
1.89
2.01
13.18
0.0 9.5 9.0 8.5 8.0 7.5 7.0 6.5 6.0 5.5 5.0 4.5 4.0 3.5 3.0 2.5 2.0 1.5 1.0 0.5 0
f1 (ppm)

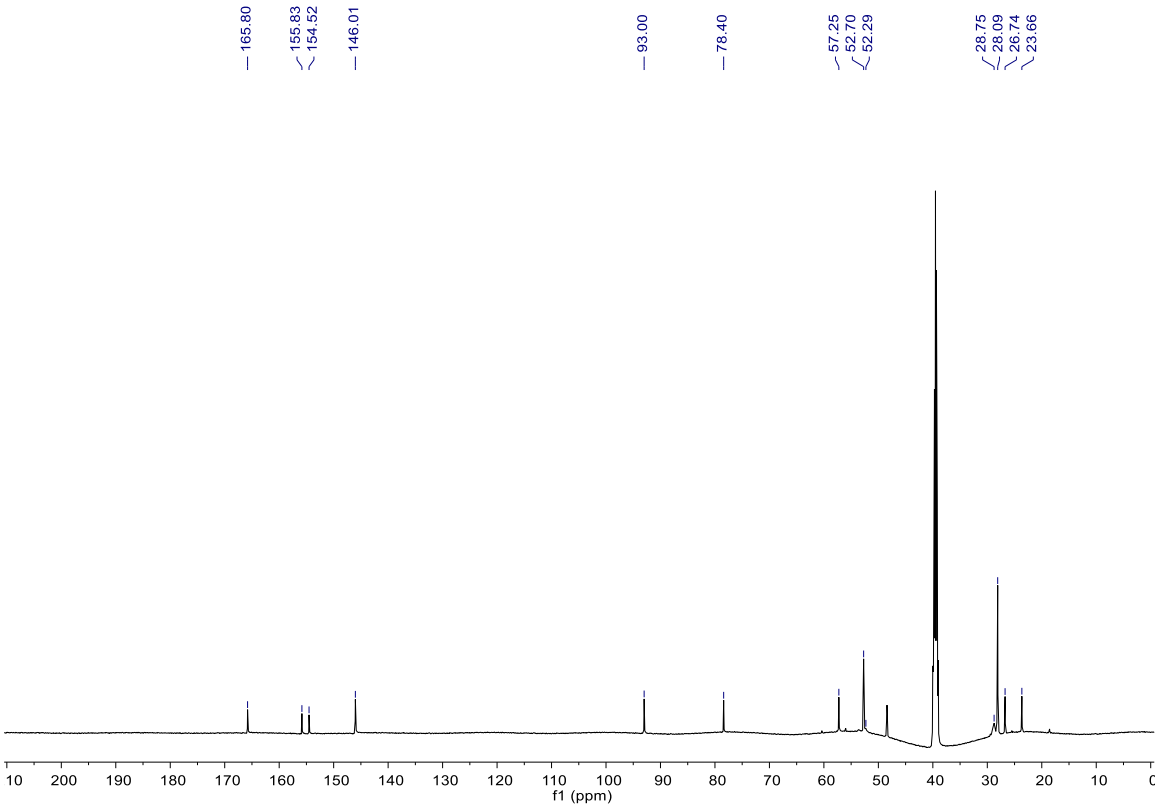
165.80
155.83
154.52
146.01
93.00
78.40
57.25
52.70
52.29
28.75
28.09
26.74
23.66
10 200 190 180 170 160 150 140 130 120 110 100 90 80 70 60 50 40 30 20 10 0
f1 (ppm)

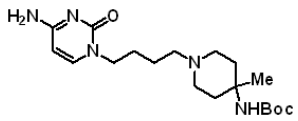
H2N
N
O
N
N
Me
NHBoc

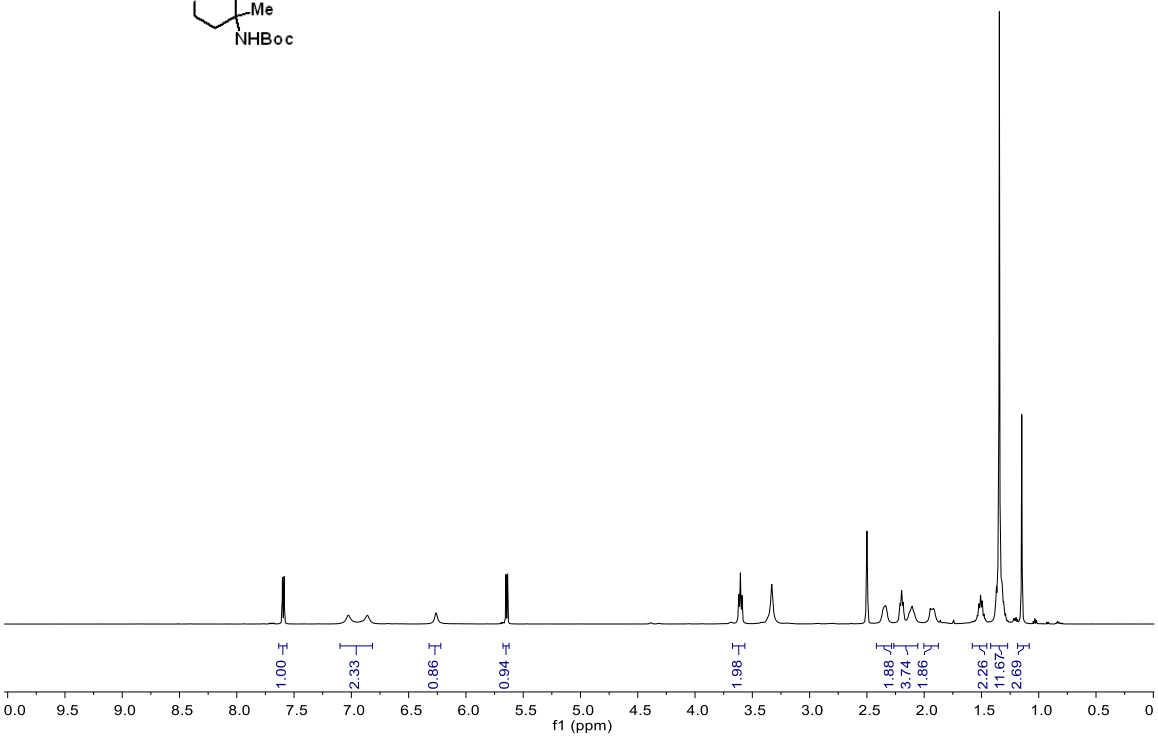
1.00
2.33
0.86
0.94
1.98
1.88
3.74
1.86
2.26
11.67
2.69
f1 (ppm)

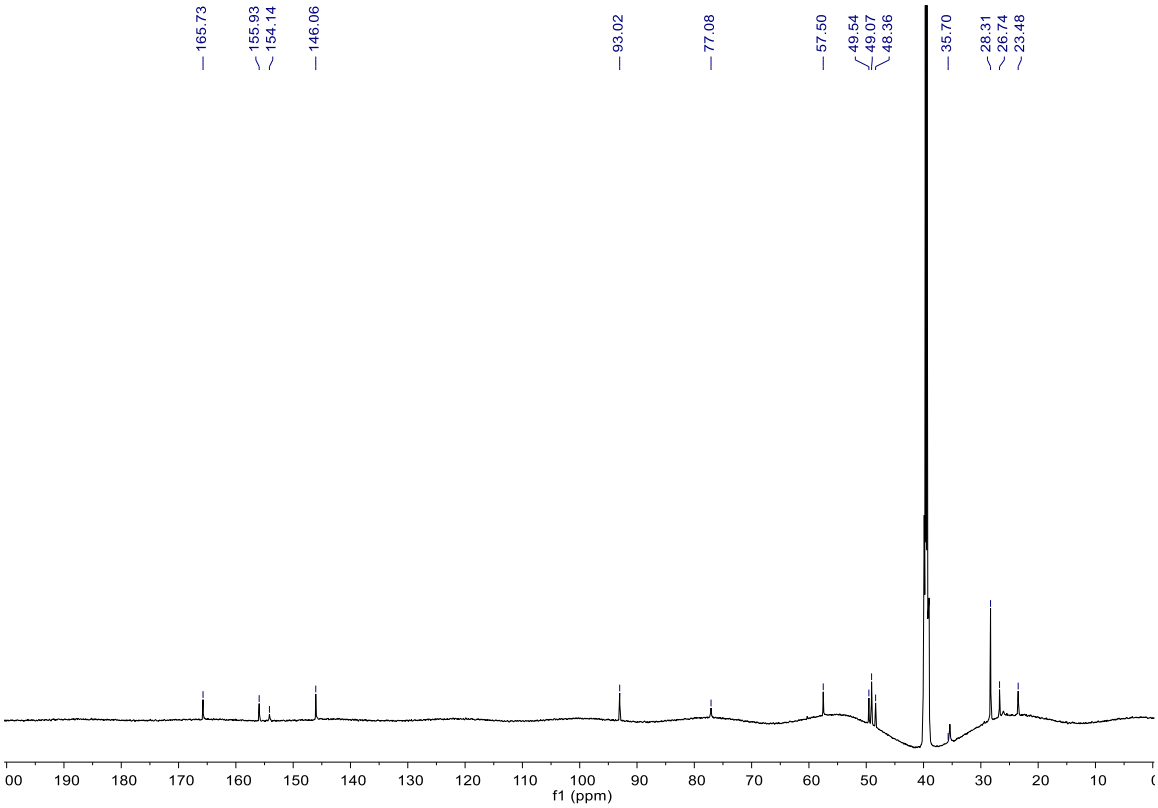
165.73
155.93
154.14
146.06
93.02
77.08
57.50
49.54
49.07
48.36
35.70
28.31
26.74
23.48
f1 (ppm)

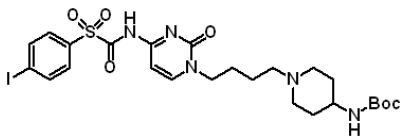

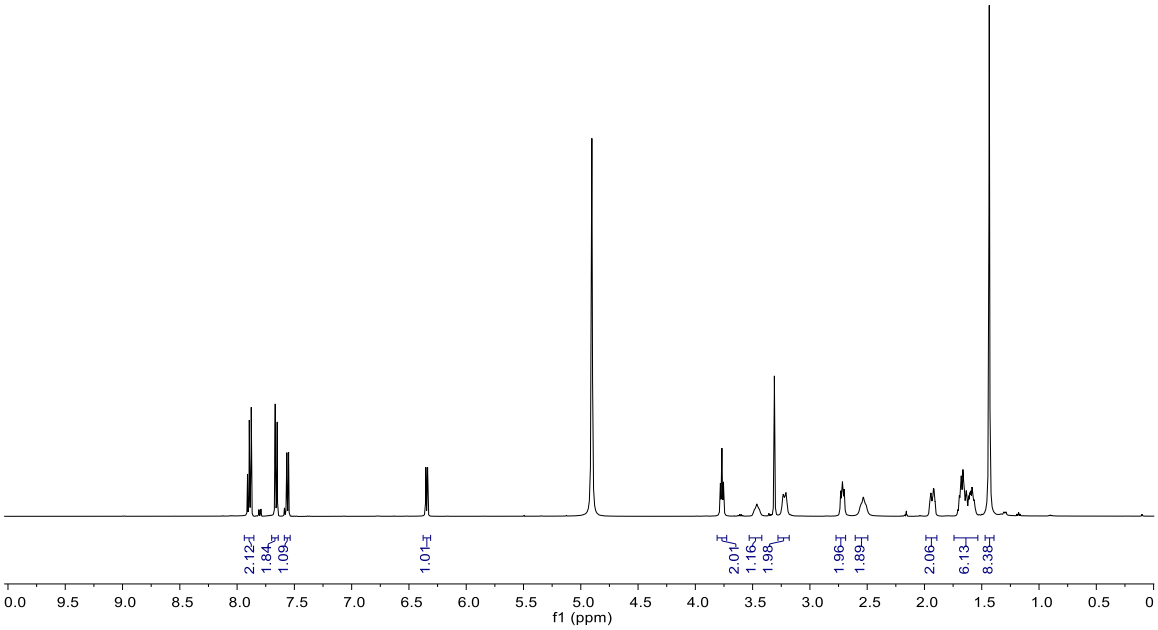
2.12
1.84
1.09
1.01
2.01
1.16
1.98
1.96
1.89
2.06
6.13
8.38
f1 (ppm)

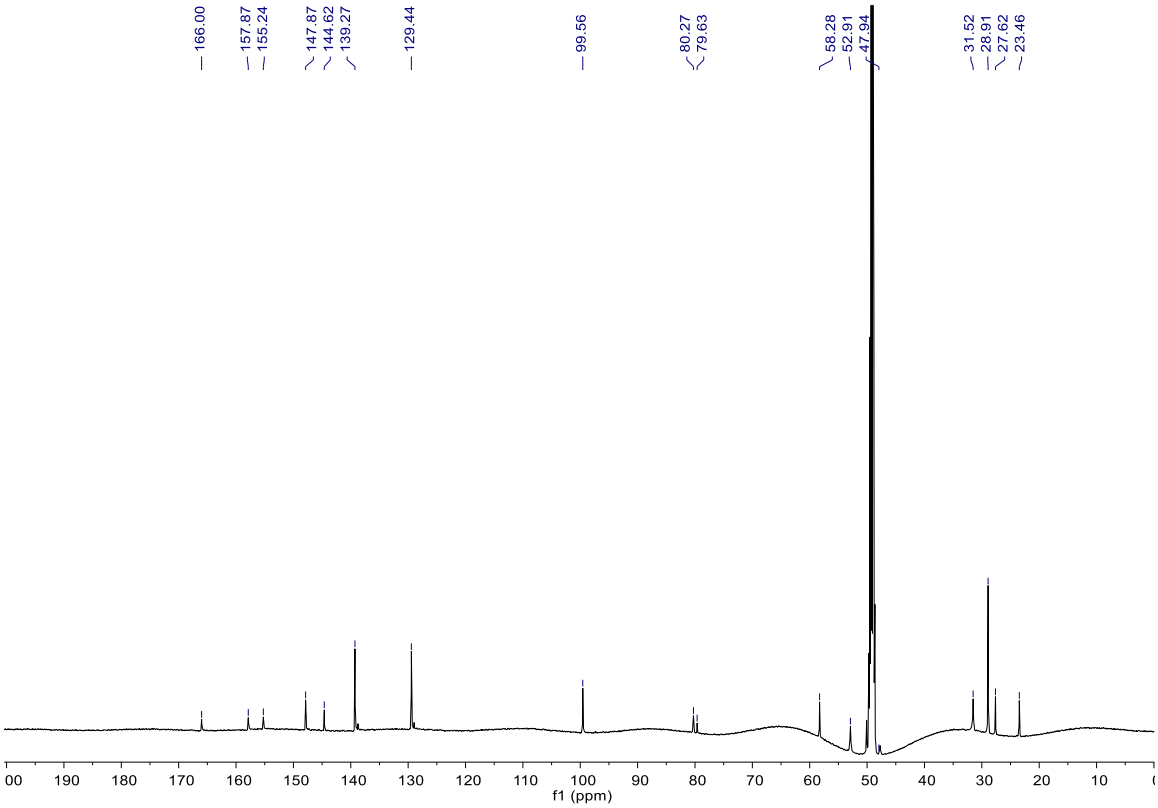
166.00
157.87
155.24
147.87
144.62
139.27
129.44
99.56
80.27
79.63
58.28
52.91
47.94
31.52
28.91
27.62
23.46
f1 (ppm)

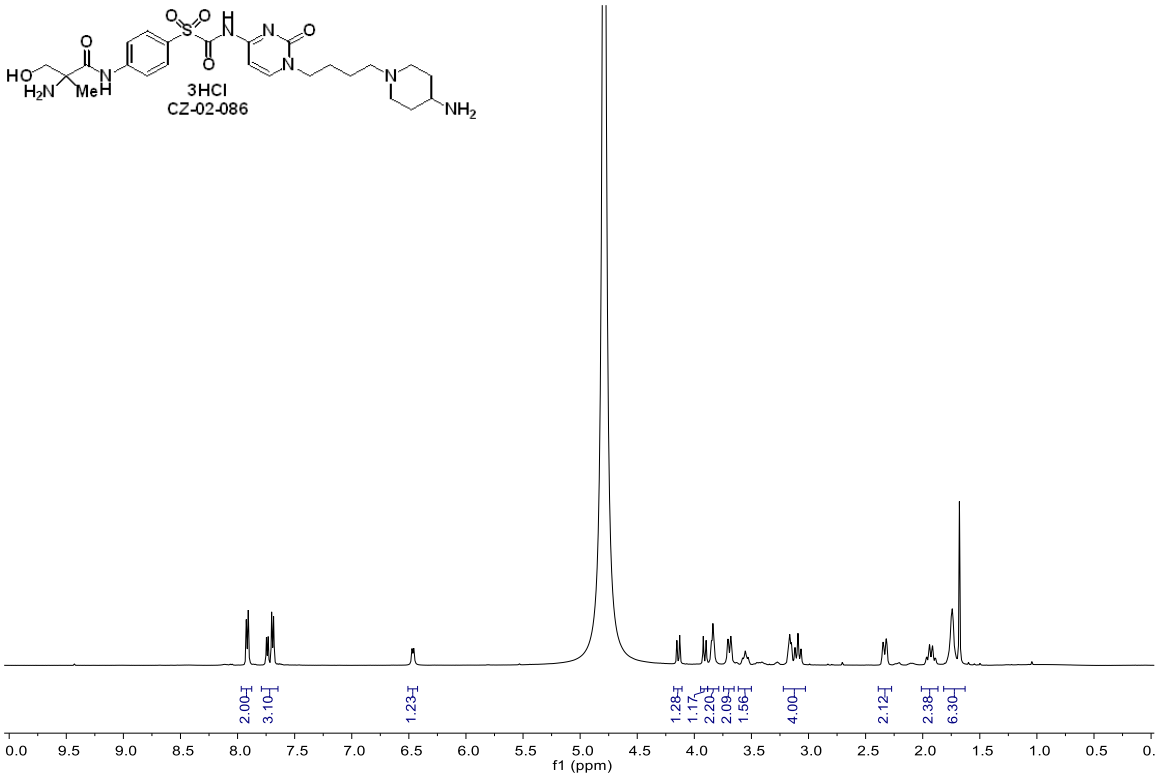
3HCl
CZ-02-086
2.00
3.10
1.23
1.28
1.17
2.20
2.09
1.56
4.00
2.12
2.38
6.30
f1 (ppm)

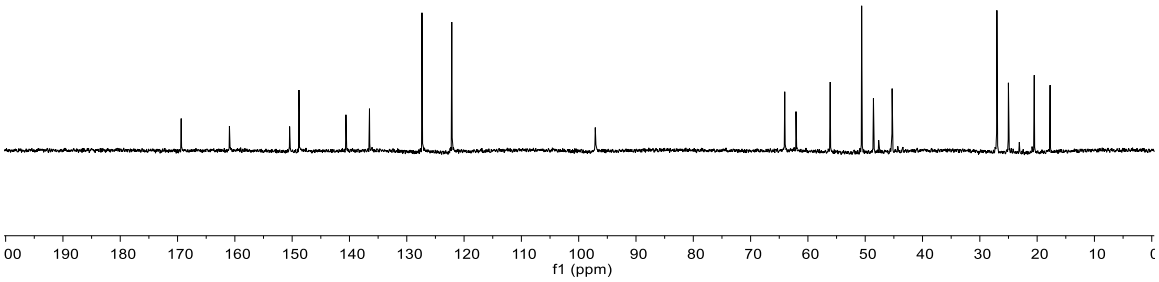
f1 (ppm)

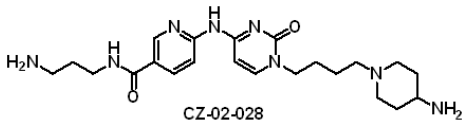
CZ-02-028

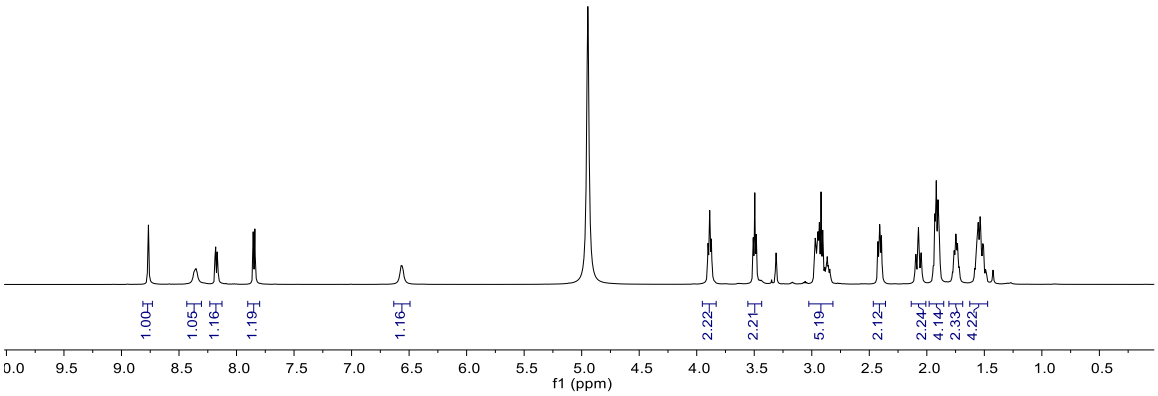
1.00
1.05
1.16
1.19
1.16
2.22
2.21
5.19
2.12
2.24
4.14
2.33
4.22
f1 (ppm)

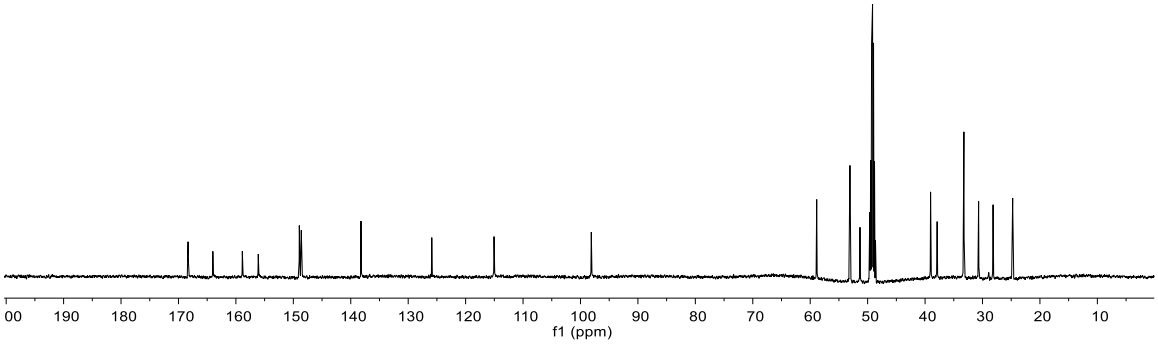
f1 (ppm)

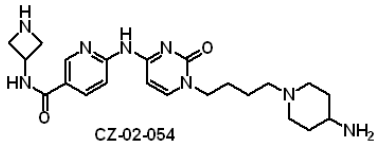
H
N
HN
O
H
N
N
O
N
N
NH2

CZ-02-054

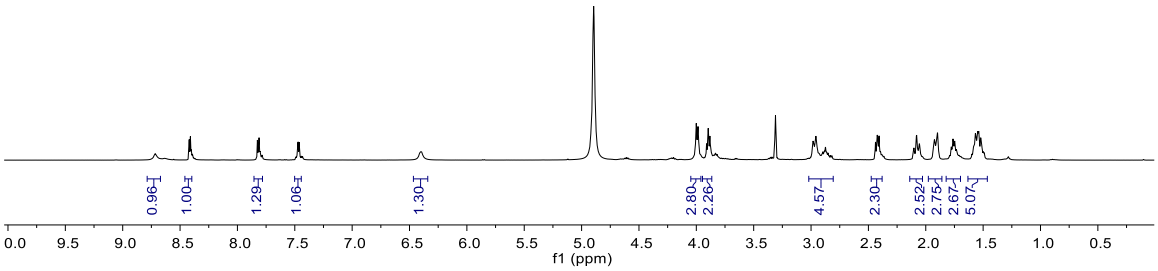
0.96
1.00
1.29
1.06
1.30
2.80
2.26
4.57
2.30
2.52
2.75
2.67
5.07
0.0 9.5 9.0 8.5 8.0 7.5 7.0 6.5 6.0 5.5 5.0 4.5 4.0 3.5 3.0 2.5 2.0 1.5 1.0 0.5
f1 (ppm)

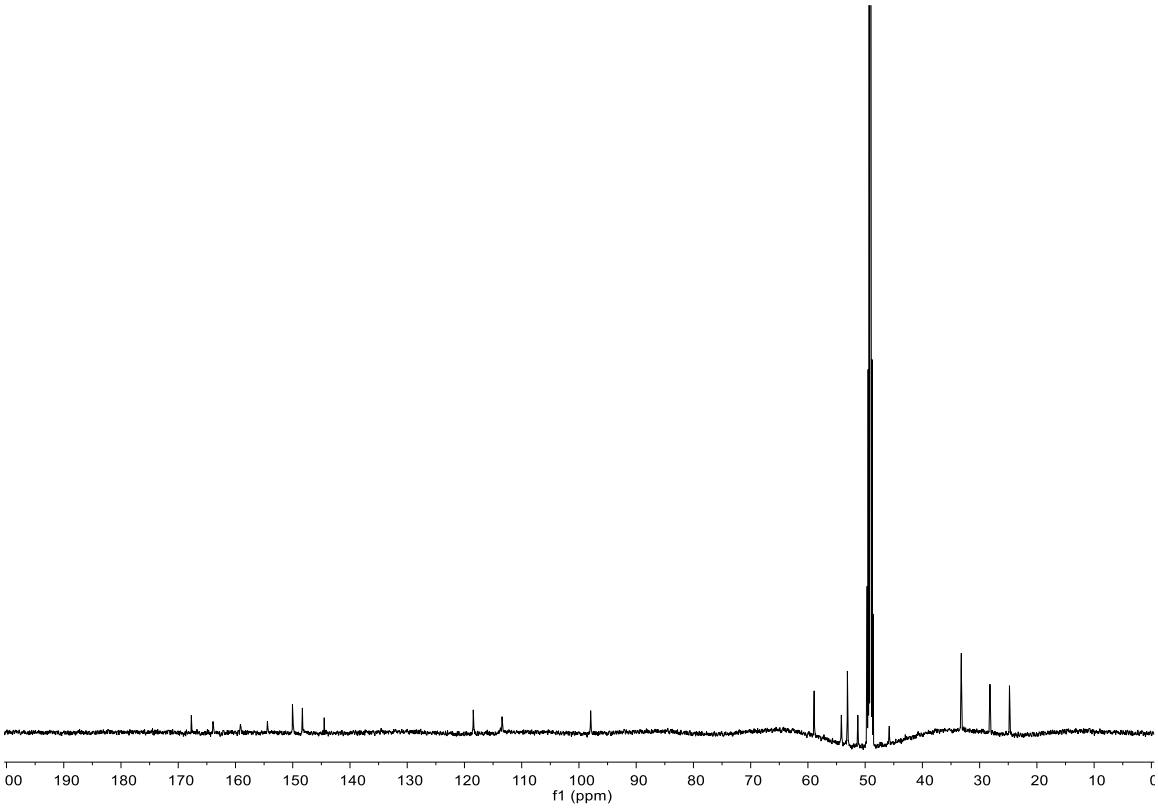
00 190 180 170 160 150 140 130 120 110 100 90 80 70 60 50 40 30 20 10
f1 (ppm)

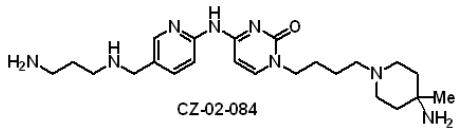
H2N
H
N
N
H
N
N
O
N
Me
NH2

CZ-02-084

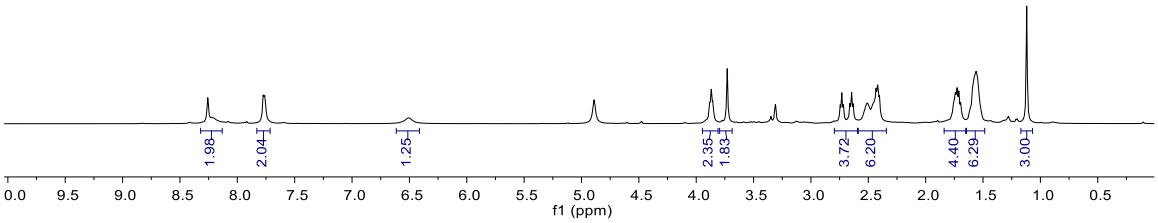
1.98
2.04
1.25
2.35
1.83
3.72
6.20
4.40
6.29
3.00
0.0 9.5 9.0 8.5 8.0 7.5 7.0 6.5 6.0 5.5 5.0 4.5 4.0 3.5 3.0 2.5 2.0 1.5 1.0 0.5
f1 (ppm)

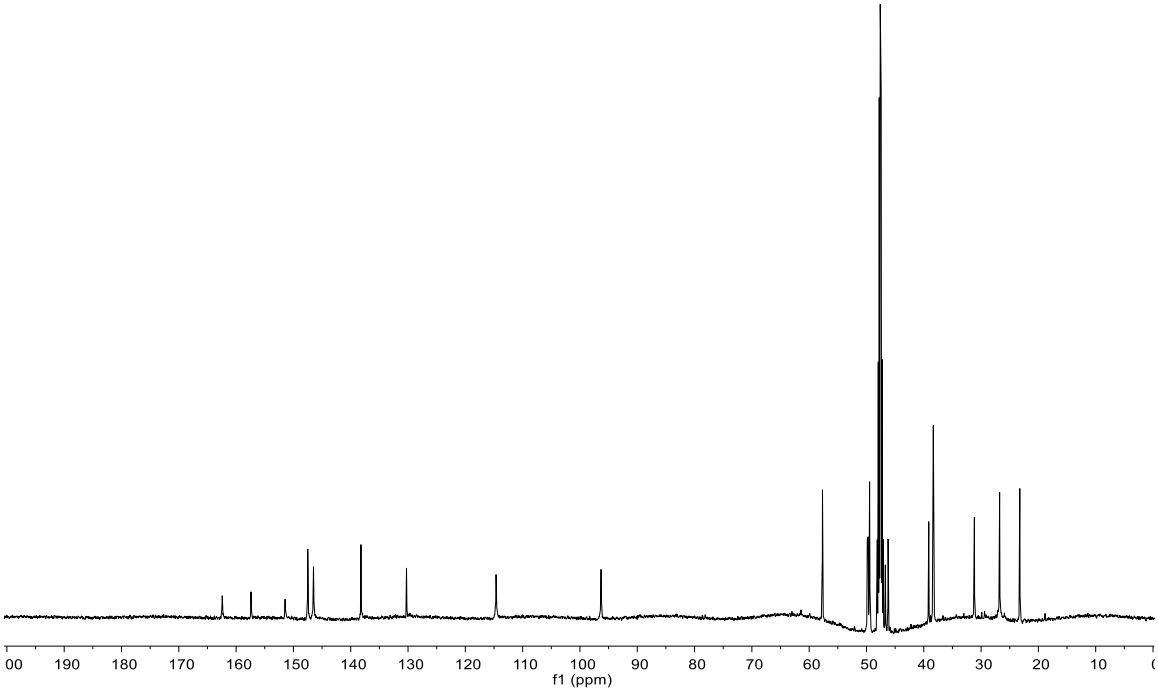
00 190 180 170 160 150 140 130 120 110 100 90 80 70 60 50 40 30 20 10
f1 (ppm)

APPENDIX C

^{1}H, ^{13}C SPECTRA CHAPTER 4

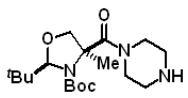
O
O
N
Me
tBu
N
Boc
NH

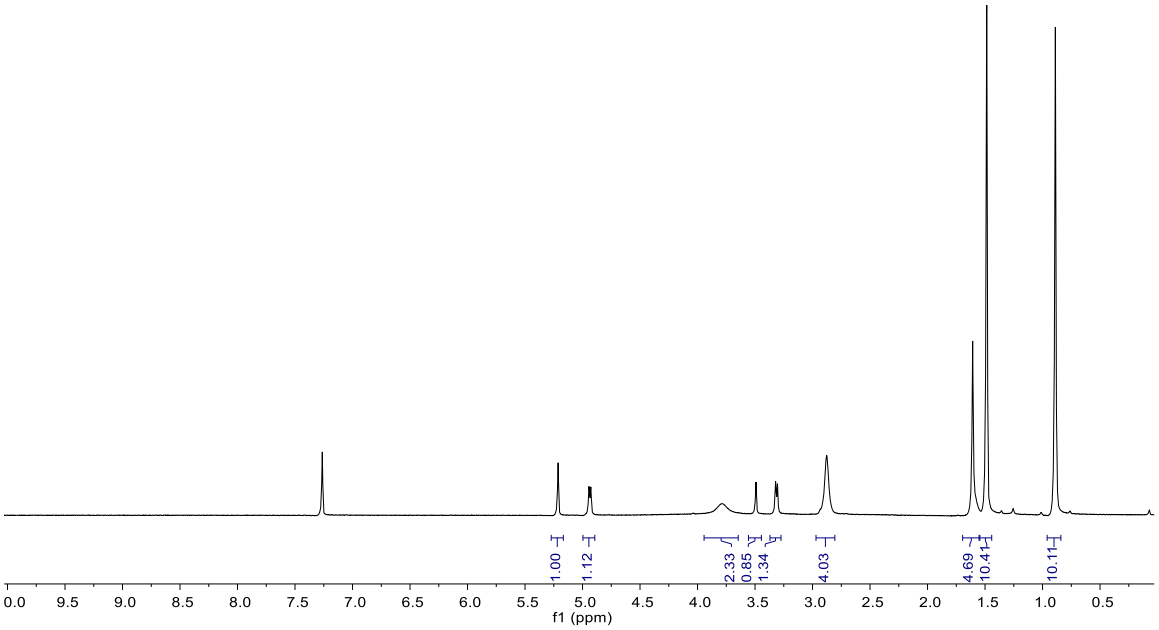
1.00
1.12
2.33
0.85
1.34
4.03
4.69
10.41
10.11
0.0 9.5 9.0 8.5 8.0 7.5 7.0 6.5 6.0 5.5 5.0 4.5 4.0 3.5 3.0 2.5 2.0 1.5 1.0 0.5
f1 (ppm)

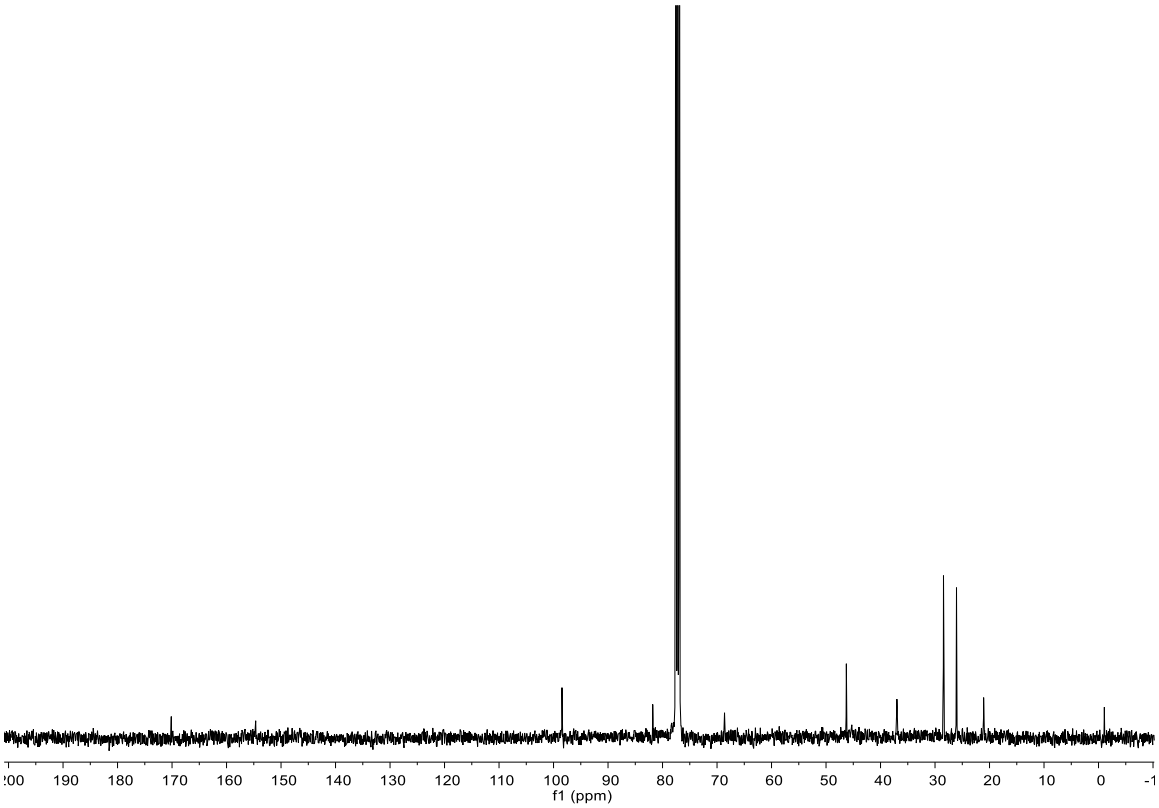
200 190 180 170 160 150 140 130 120 110 100 90 80 70 60 50 40 30 20 10 0 -1
f1 (ppm)

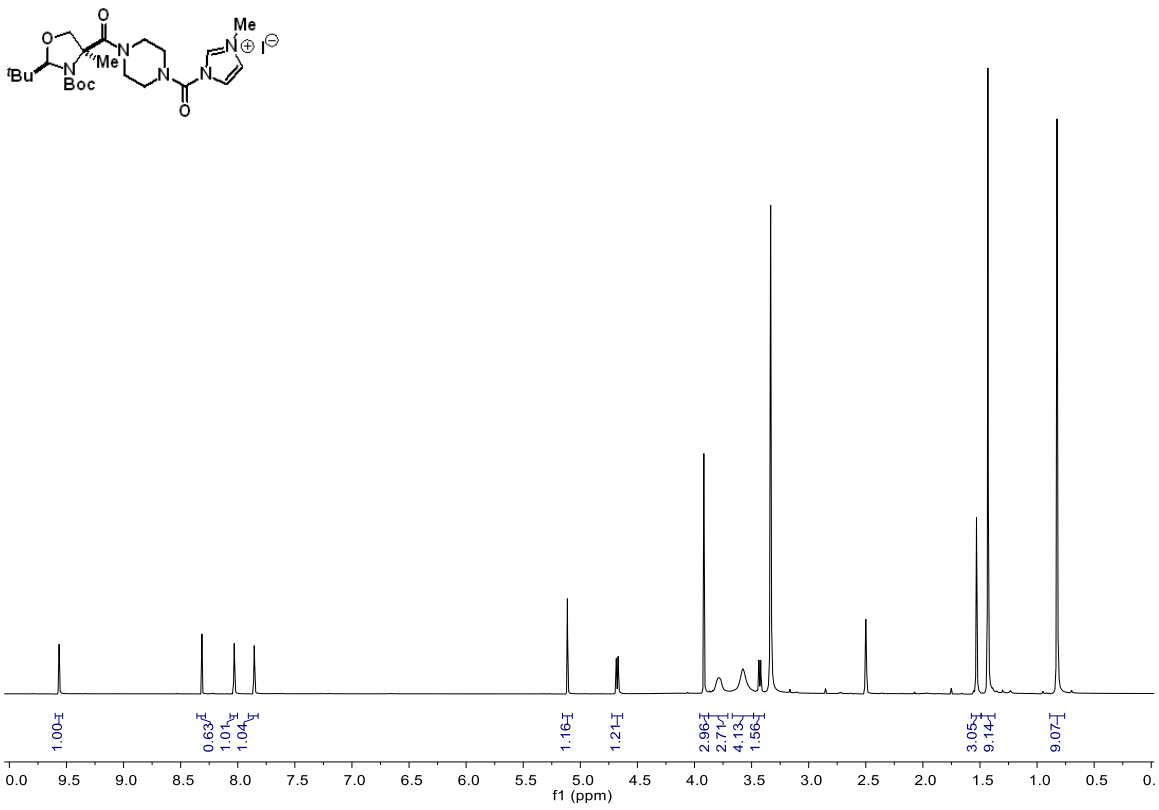
Me
I
tBu
Boc
1.00
0.63
1.01
1.04
1.16
1.21
2.96
2.71
4.13
1.56
3.05
9.14
9.07
f1 (ppm)

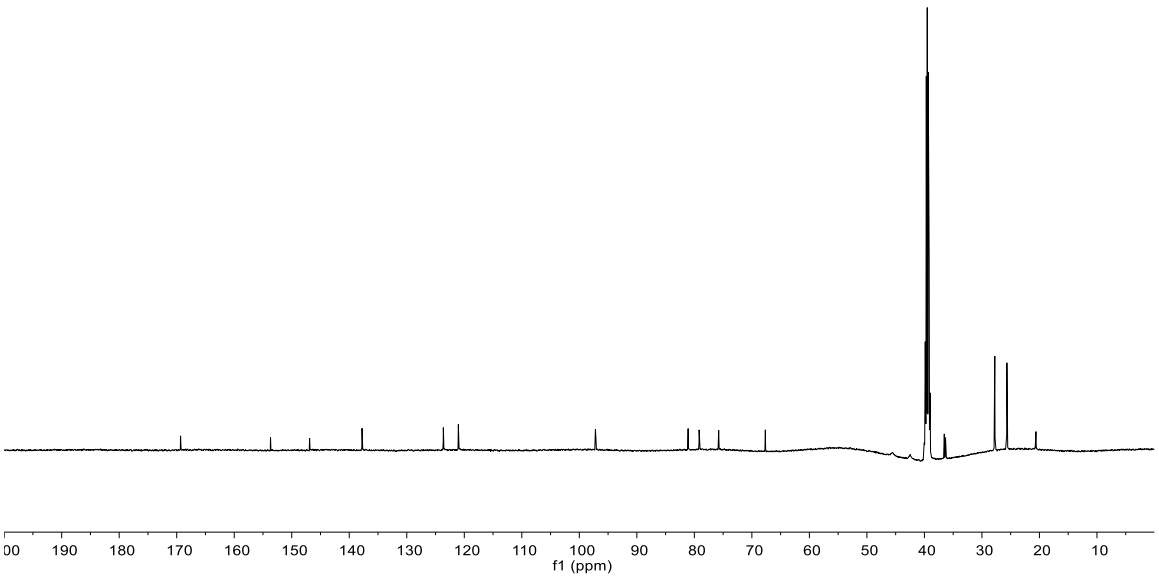
f1 (ppm)

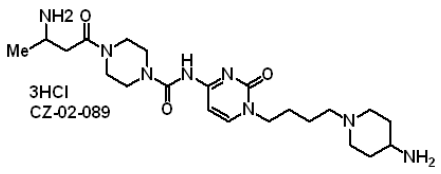
NH2
O
Me
N
N
H
N
N
O
O
N
N
NH2
3HCl
CZ-02-089

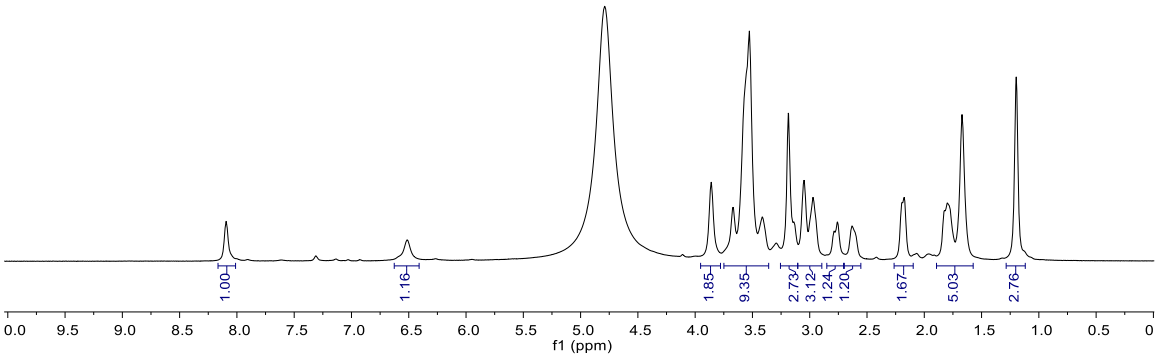
1.00
1.16
1.85
9.35
2.73
3.12
1.24
1.20
1.67
5.03
2.76
0.0 9.5 9.0 8.5 8.0 7.5 7.0 6.5 6.0 5.5 5.0 4.5 4.0 3.5 3.0 2.5 2.0 1.5 1.0 0.5 0
f1 (ppm)


171.23
160.31
153.88
149.57
96.62
56.97
51.54
46.20
45.54
45.15
43.67
41.79
36.99
27.95
25.77
21.48
18.58

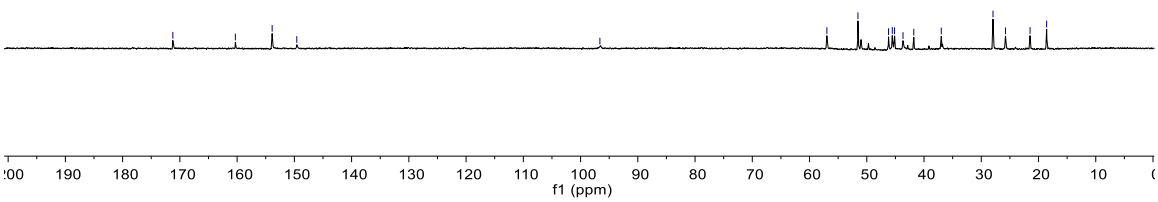
190 180 170 160 150 140 130 120 110 100 90 80 70 60 50 40 30 20 10
f1 (ppm)

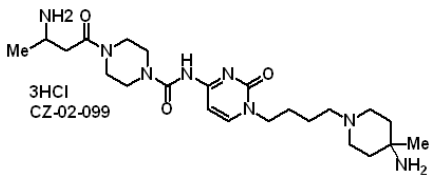
NH2
O
Me
N
N
H
N
N
O
O
N
N
Me
NH2
3HCl
CZ-02-099

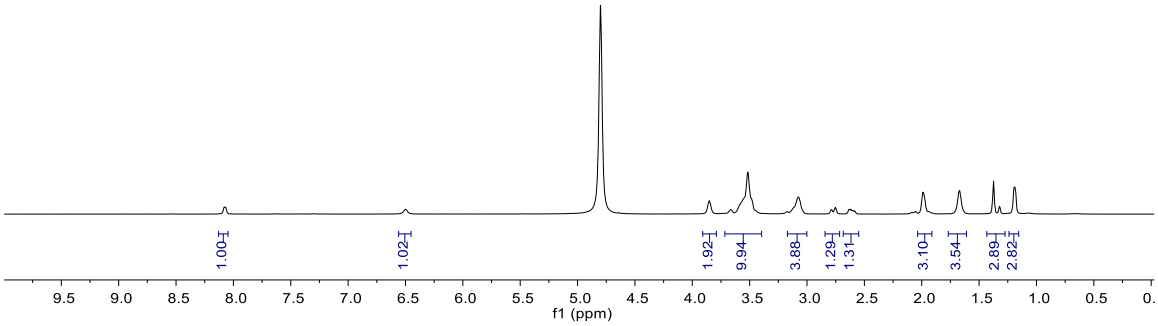
1.00
1.02
1.92
9.94
3.88
1.29
1.31
3.10
3.54
2.89
2.82
9.5 9.0 8.5 8.0 7.5 7.0 6.5 6.0 5.5 5.0 4.5 4.0 3.5 3.0 2.5 2.0 1.5 1.0 0.5 0.
f1 (ppm)


170.13
159.41
152.93
152.53
148.95
95.52
55.70
50.30
49.84
48.21
44.42
44.05
40.69
35.86
31.84
24.69
20.44
19.37
17.46

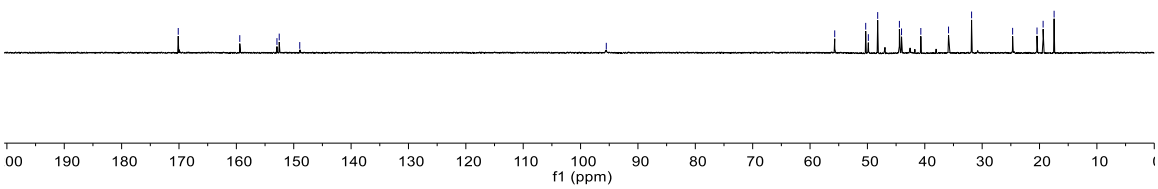
00 190 180 170 160 150 140 130 120 110 100 90 80 70 60 50 40 30 20 10
f1 (ppm)

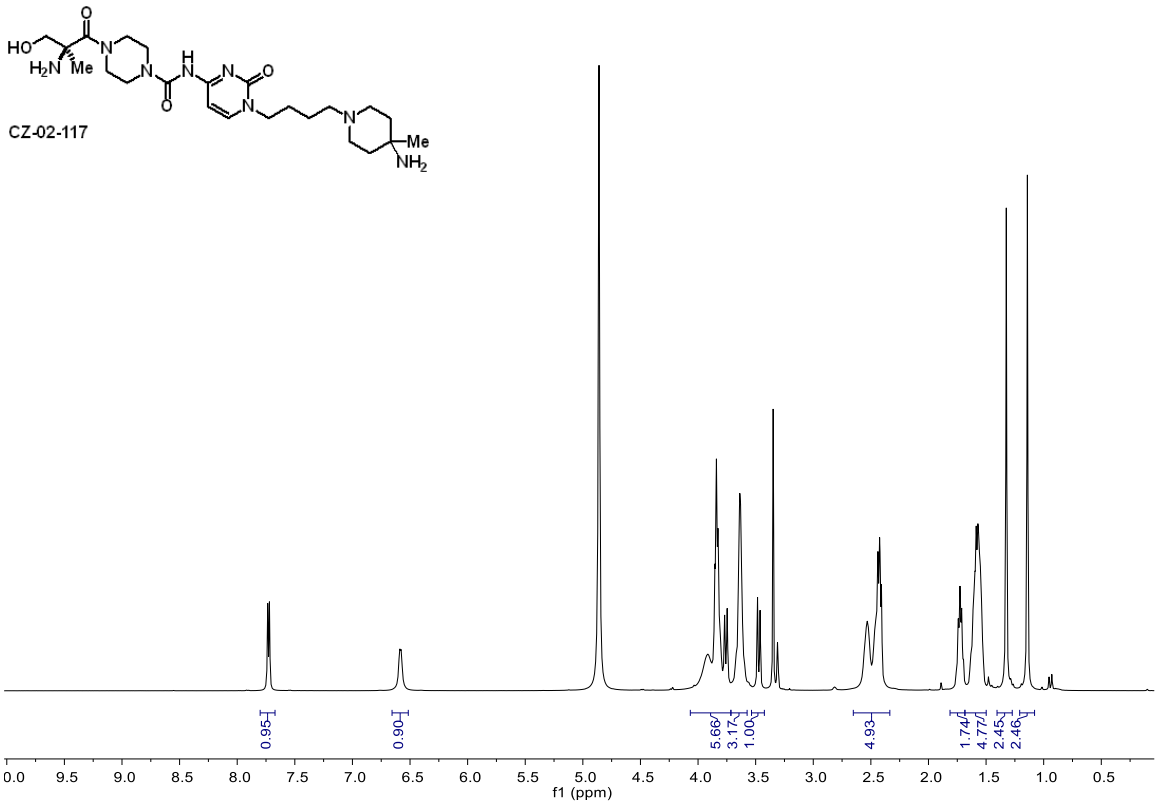
CZ-02-117
0.95
0.90
5.66
3.17
1.00
4.93
1.74
4.77
2.45
2.46
f1 (ppm)

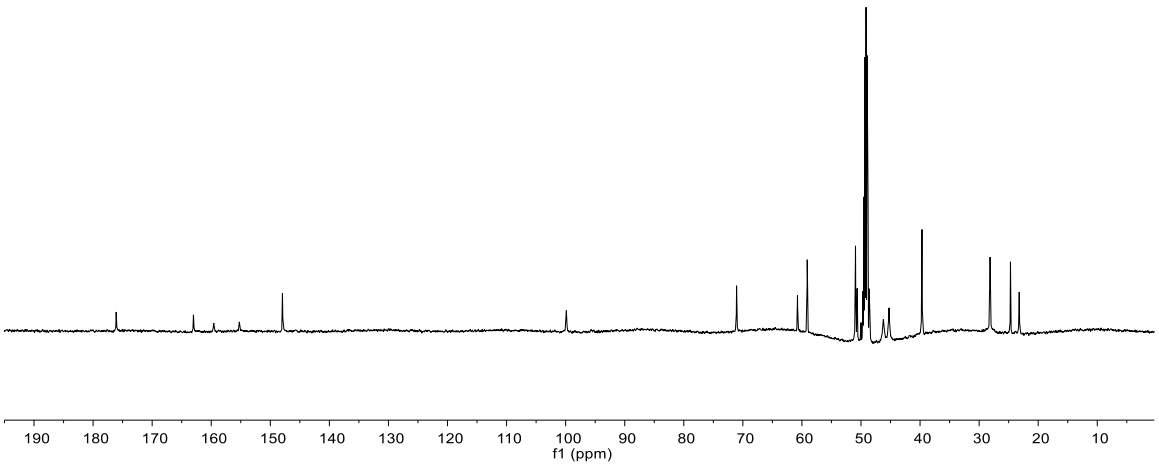
f1 (ppm)

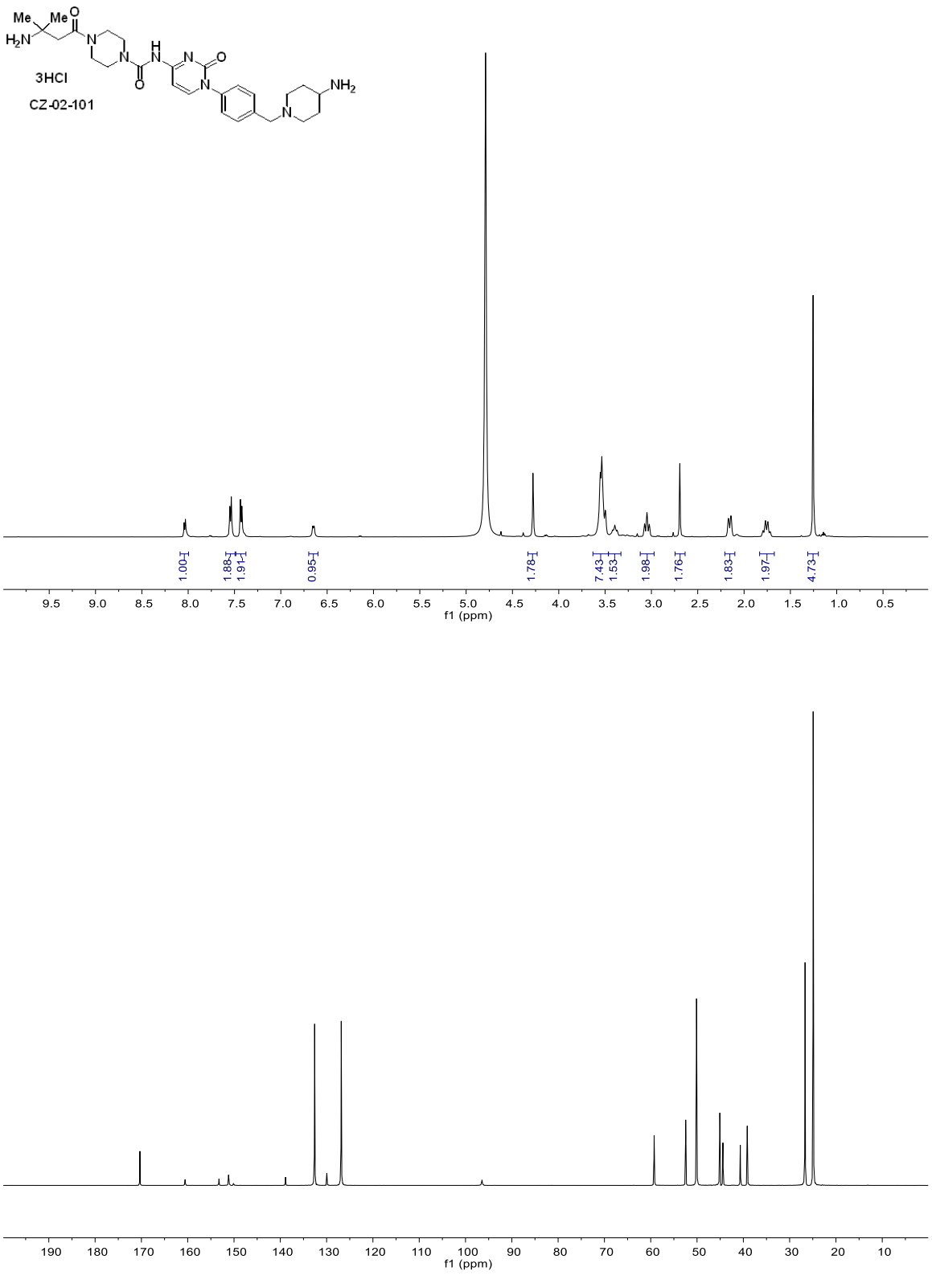
3HCl
CZ-02-101
1.00
1.88
1.91
0.95
1.78
7.43
1.53
1.98
1.76
1.83
1.97
4.73
f1 (ppm)
f1 (ppm)

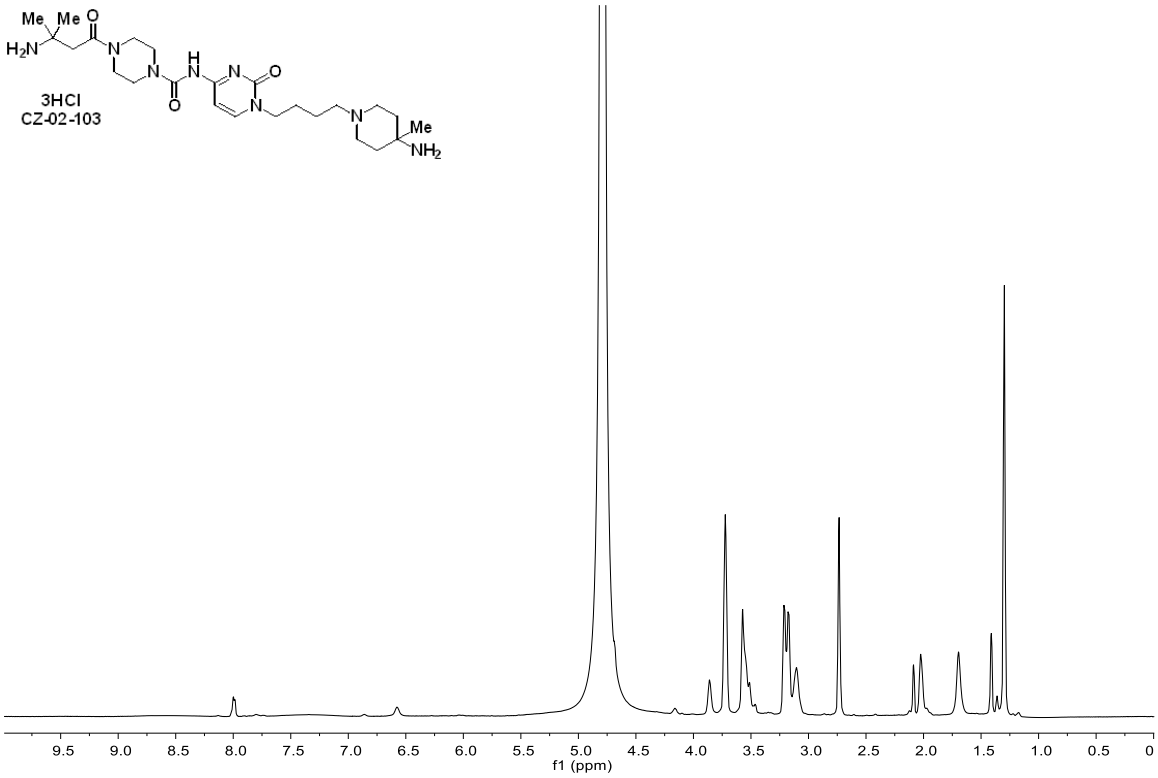
3HCl
CZ-02-103
f1 (ppm)

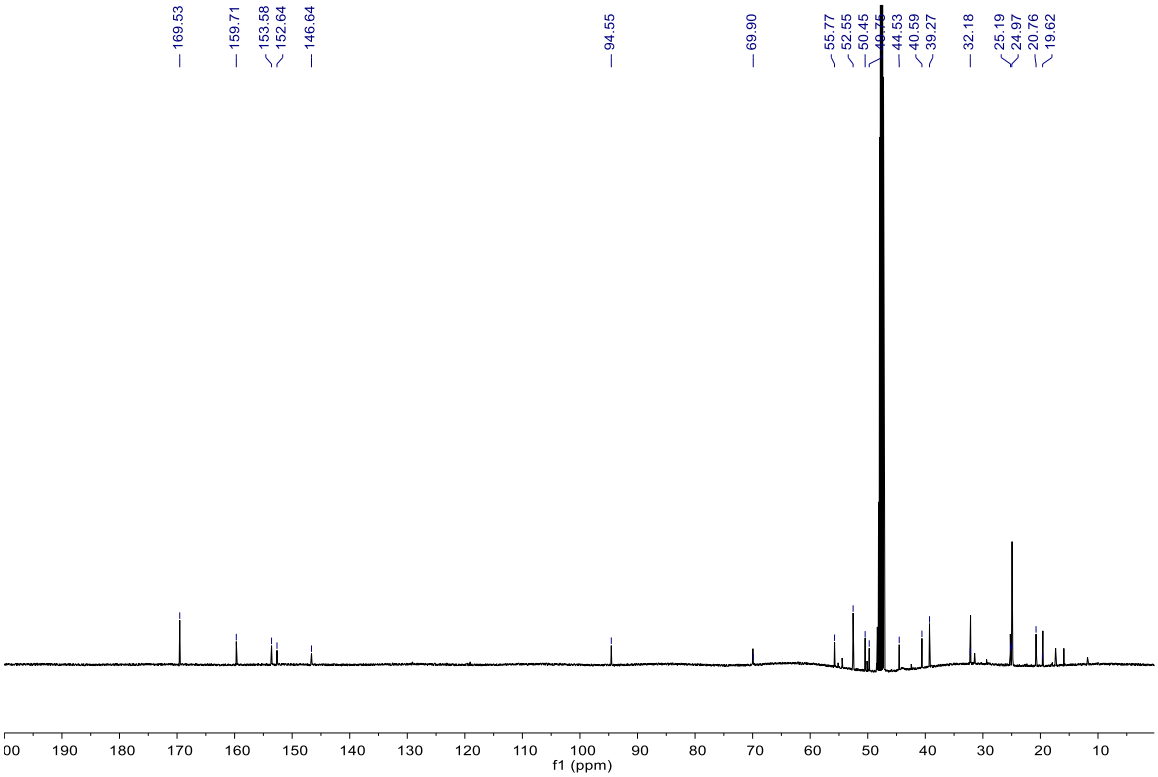
169.53
159.71
153.58
152.64
146.64
94.55
69.90
55.77
52.55
50.45
44.53
40.59
39.27
32.18
25.19
24.97
20.76
19.62
f1 (ppm)

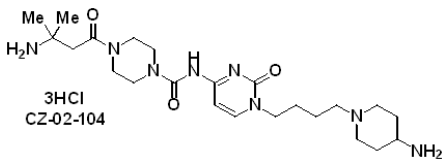
Me
Me
O
H2N
N
N
H
N
N
O
O
N
3HCl
CZ-02-104
NH2

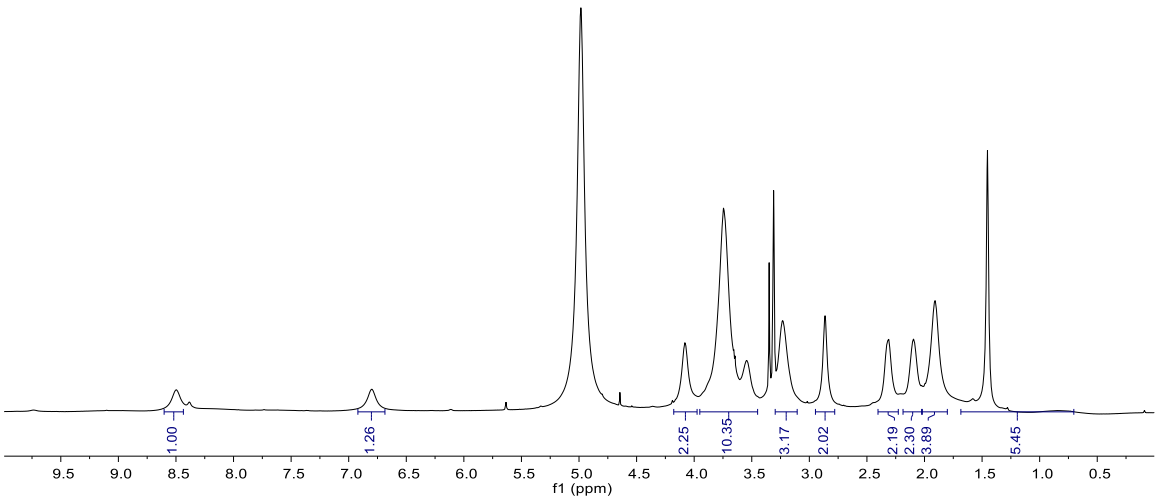
1.00
1.26
2.25
10.35
3.17
2.02
2.19
2.30
3.89
5.45
9.5 9.0 8.5 8.0 7.5 7.0 6.5 6.0 5.5 5.0 4.5 4.0 3.5 3.0 2.5 2.0 1.5 1.0 0.5
f1 (ppm)

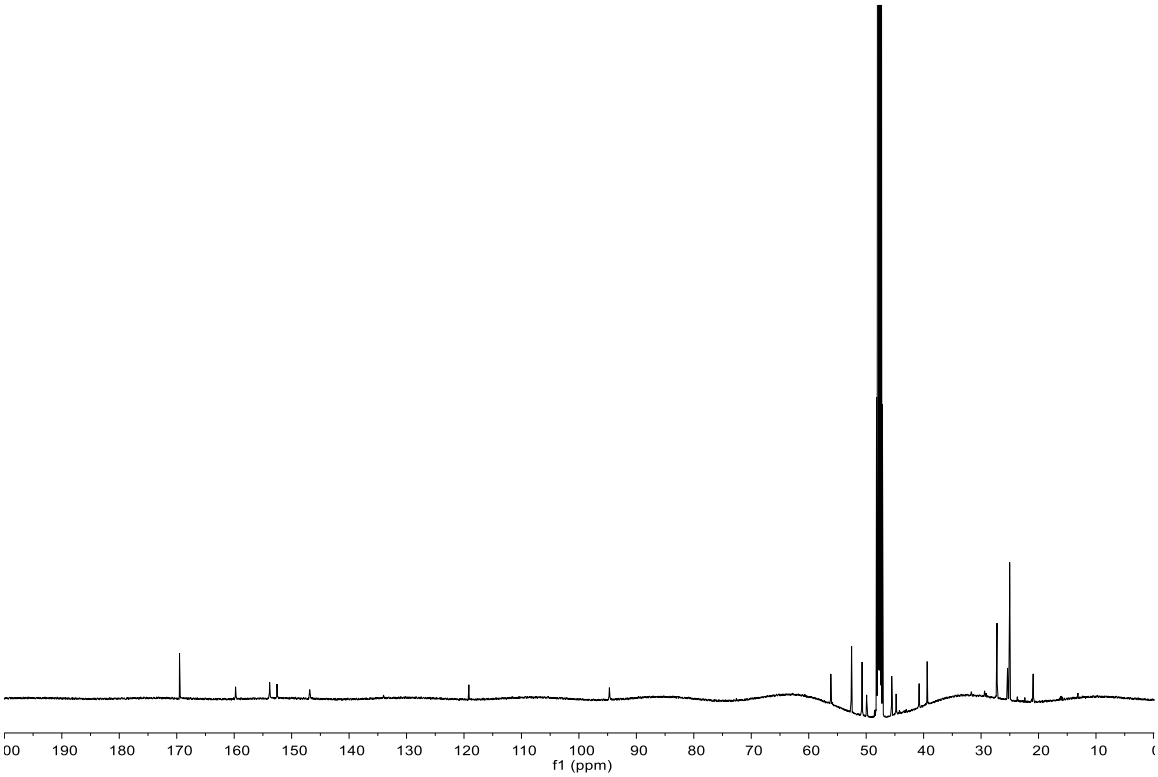
00 190 180 170 160 150 140 130 120 110 100 90 80 70 60 50 40 30 20 10
f1 (ppm)

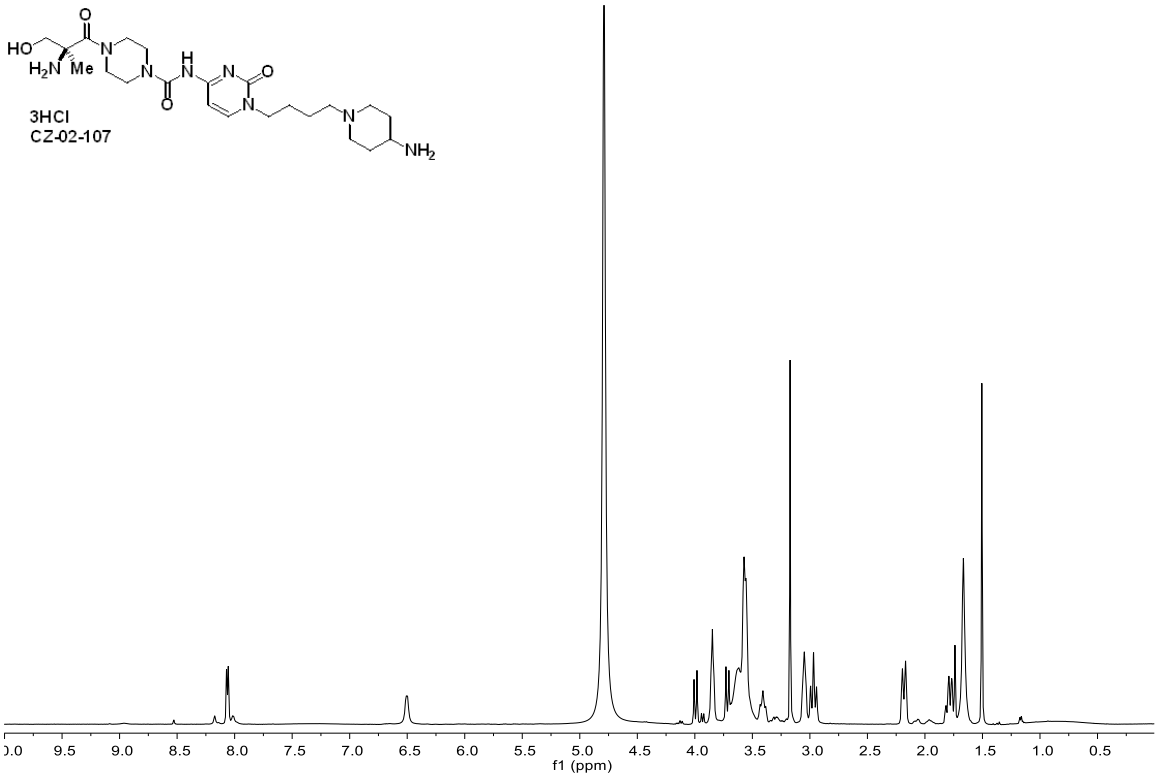
3HCl
CZ-02-107
f1 (ppm)

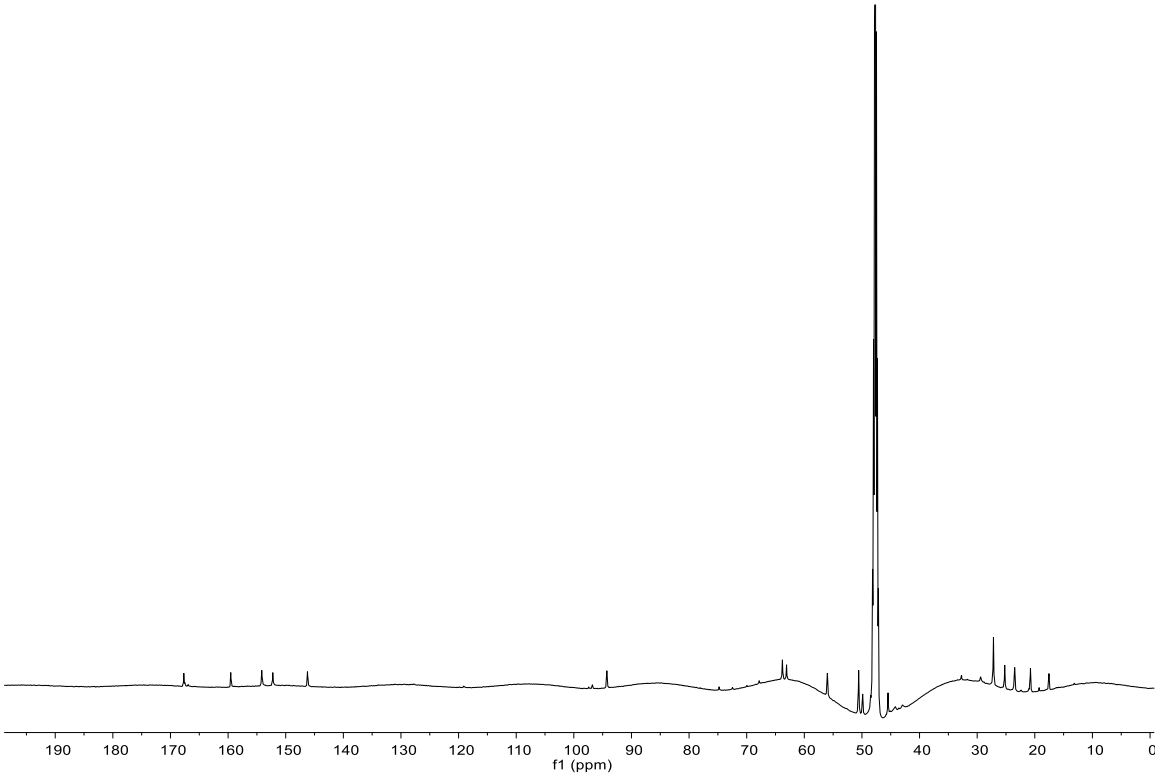
f1 (ppm)

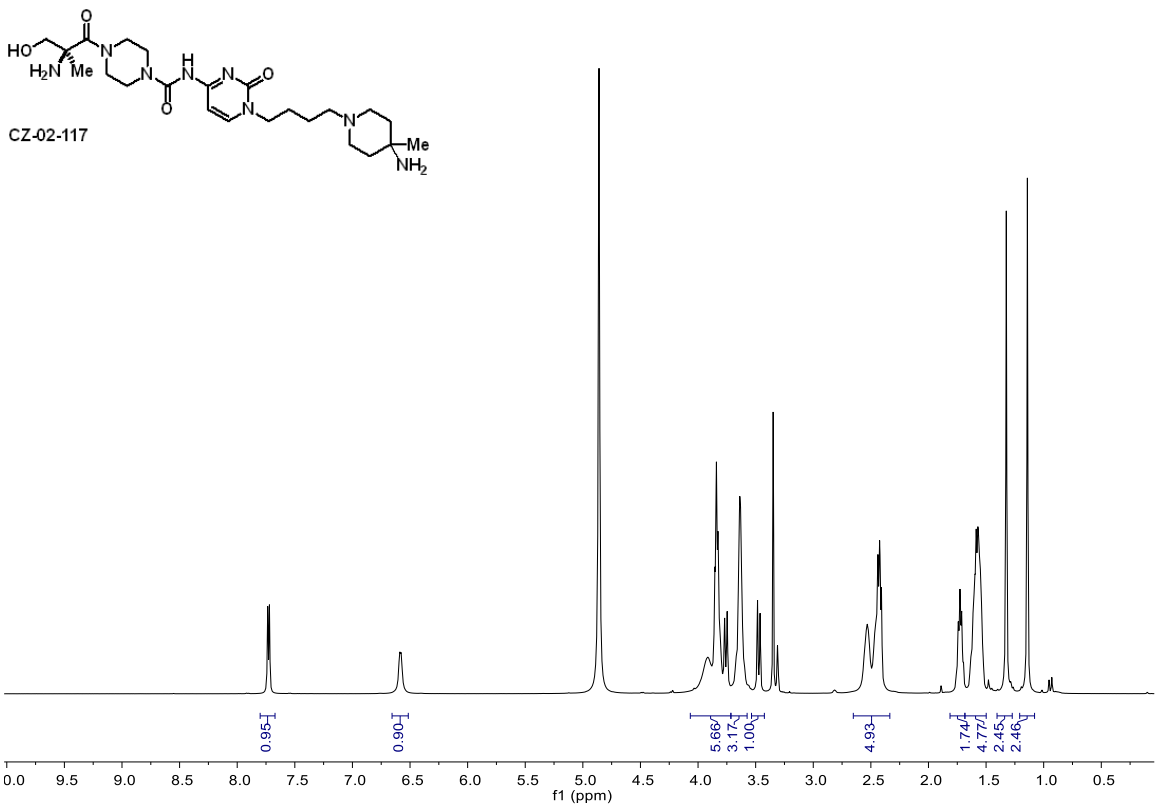
CZ-02-117
0.95
0.90
5.66
3.17
1.00
4.93
1.74
4.77
2.45
2.46
f1 (ppm)

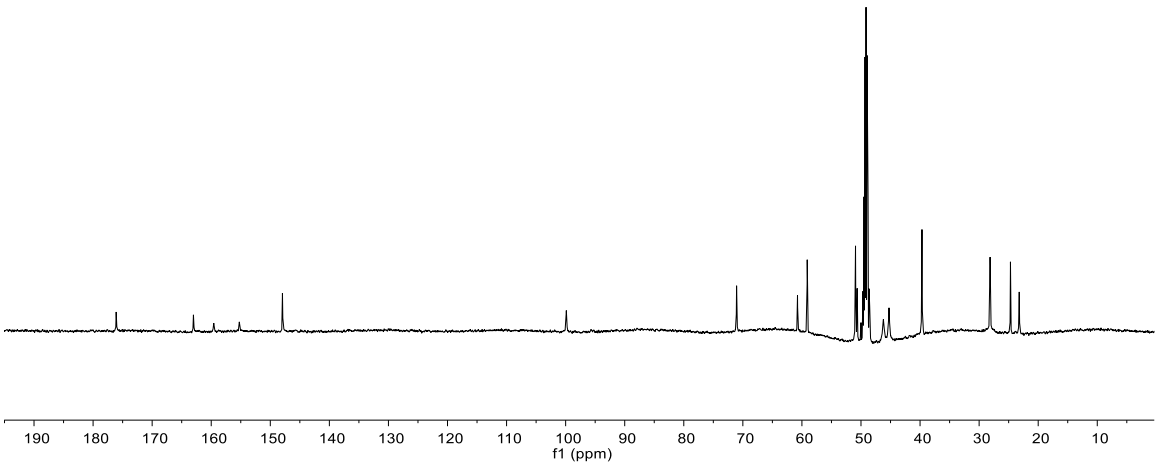
f1 (ppm)

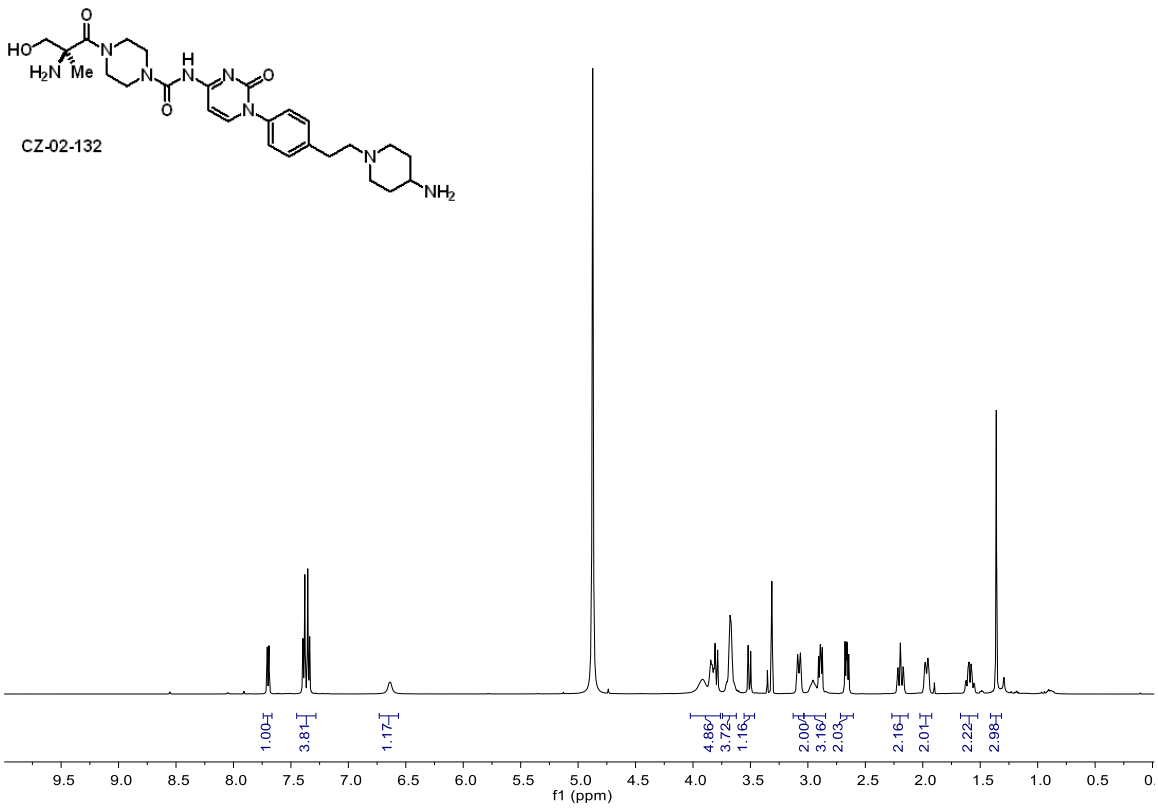
CZ-02-132
1.00
3.81
1.17
4.86
3.72
1.16
2.00
3.16
2.03
2.16
2.01
2.22
2.98
f1 (ppm)

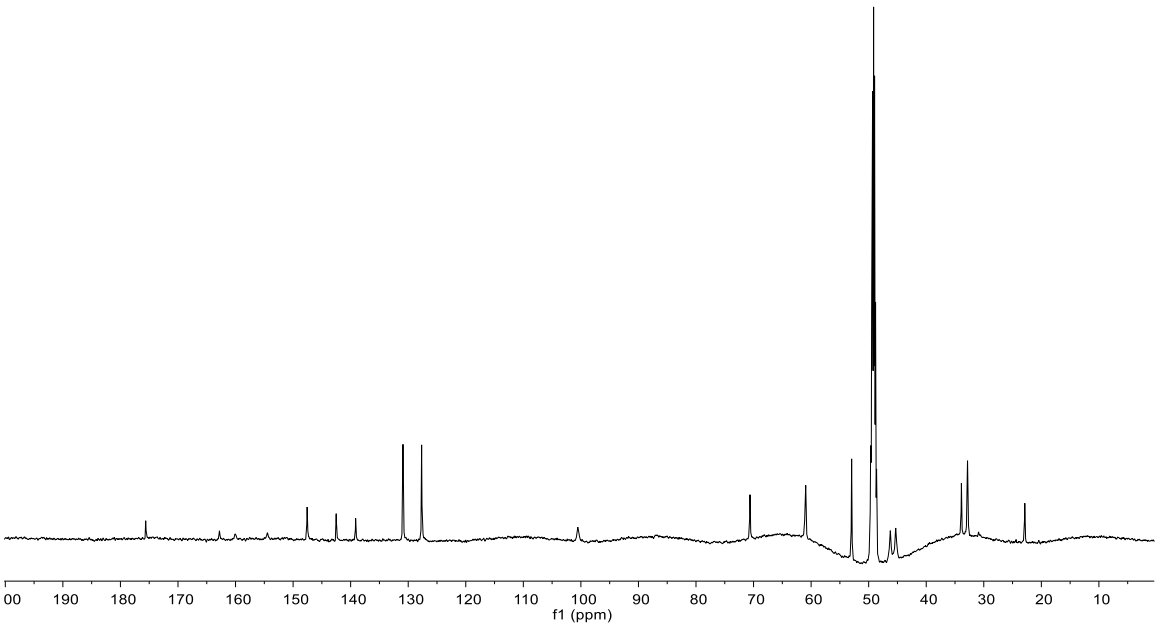
f1 (ppm)